

University of Nottingham
UK | CHINA | MALAYSIA

Development and Application of the Antigen Microarray for the Detection of Autoantibodies in Hepatocellular Carcinoma Patients

By

Afrakoma Afriyie-Asante

BSc, MSc

Thesis submitted to the University of Nottingham for the degree of Doctor of Philosophy (PhD)

May 2019

Abstract

Hepatocellular carcinoma (HCC) is a primary liver cancer characterised by mutations in the cellular machinery, which induces the liver cells to replicate at a higher rate. It is the fifth most common cancer and the third most common cause of cancer-related deaths worldwide. The extensive prevalence of this malignancy carries a significant economic burden on a country. HCC occurs within the background of cirrhosis and chronic liver diseases, where hepatitis B virus (HBV), hepatitis C virus (HCV) infections and alcoholism are regarded as the most frequent risk factors of the disease. However, current diagnostic tools are sensitive only at the advanced stages, which hugely contribute to the grave prognosis and compromised effective curative treatment, resulting in poor 5-year patient survival. With the continuous devastating effect of this malignancy, there is an urgent need for an efficient tool, which could detect the malignancy at both the early and late stages.

Recently, an increasing number of studies have shown that cancer patients produce detectable serological biomarkers in the form of IgG autoantibodies, which appear five years even before clinical manifestation of the disease. This evidence has recently generated opportunities for immune system exploitation as source of cancer biomarkers. Autoantibodies are elicited by the release of tumour-associated antigens (TAAs) during tumour development, making the autoantibody signature an effective approach for the early diagnosis of HCC. They could also represent as novel tools for prognosis, monitoring and prediction of response for chemotherapy. It is therefore crucial to design a non-invasive, high-throughput and robust screening system that would allow autoantibodies to be detected early in HCC and high-risk patients.

In recent times, the antigen microarray, which is a new generation probing technique, has emerged as a promising tool for the examination of humoral immune responses in cancer in a multiplexed and high-throughput manner. This technology is adapted as an alternative approach to the already existing Enzyme Linked Immunosorbent Assay (ELISA). In Antigen Microarrays, the recombinant TAAs are spotted robotically on a glass slide and probed with sera after which signals are amplified and quantified through fluorescence. The technology has the advantage of quantifying serum autoantibodies to hundreds of TAAs simultaneously and further providing a form of

protein analysis at a scale beyond that which is achievable by traditional immunological techniques.

This thesis documents the development, validation and application of the in-house Antigen Microarray platform to detect and characterise specific anti-TAA IgG autoantibodies to a panel of TAAs in the sera of HCC and underlying liver disease patients.

Important parameters associated with the antigen microarray such as slide surface chemistry, target humidity, printing buffer, blocking buffer and antigen concentration were optimised to improve the accuracy and precision of the technology for this early biomarker detection. Secondly, the validity of the developed technology was further assessed using guidelines drawn by the Food and Drug Administration for pharmacokinetic assay validation. Additionally, we opted to produce a panel of eight recombinant TAAs in a mammalian expression system, to be sure of the quality and purity of antigens generated. The suitability of in-house TAAs were also tested on the microarray assay to reveal precision of the assay. Lastly, serum anti-TAA autoantibody levels were measured in HCC (n=183), liver cirrhosis (n=90), chronic hepatitis patients (n=133) as well as healthy groups (n=46), over a wide range of in-house (KRAS, HRAS, HDGF, CDKN2A, RALA, P62, P53, Gankyrin) and commercial TAAs produced both in mammalian (KRAS, HRAS, HDGF, CDKN2A, RALA, P62, P53, Gankyrin) and *E. coli* expression systems (KRAS, HRAS, HDGF, RALA, P62, APCN, AFP, IMP1, GRP78, Gankyrin).

Validation studies showed high reproducibility as precision values were within the acceptable limits, namely, intra (within) and inter (across days) coefficient of variation were less than 15% and 20% respectively. Eight highly expressed Flag-tagged recombinant TAAs (KRAS, HRAS, HDGF, CDKN2A, RALA, P62, P53, Gankyrin) in lysates were produced and evaluated by western blotting.

Preliminary studies conducted to investigate whether heat treatment reduces or elevates autoantibody levels in sera revealed no significant effect ($P>0.05$) of heat inactivation on the detectability of autoantibodies to TAAs. There was a significant difference ($p<0.05$) in the distribution of specific anti-TAA autoantibody responses across the four cohorts with highest responses detected in HCC patients followed by chronic hepatitis and liver cirrhosis patients. This suggests that high anti-TAA autoantibody levels are

strongly associated with the cancer. Poor correlation ($r<1$) was observed between autoantibody responses and the gender or age of HCC patients. Positive autoantibody frequency to the three TAA categories in HCC patients varied from 3.0% to 23% with highest frequencies observed in responses to P62 (18%), HRAS (20%) and HDGF (21%). Elevated autoantibody prevalence to HRAS (19.5%-25%) and P53 (9.7%-10.5%) were also detected in pre-malignant liver conditions (chronic liver hepatitis) suggesting malignant transition to HCC is related with increased responses to cellular proteins which might play a role in the cancer.

Our study has explored the development of a simple blood test which has the potential to offer a competitive benefit over present HCC diagnostic tools as it is easy to use, portable, non-invasive and inexpensive. It could also be applicable as an annual check in General Practice (GP) surgery to provide reports of greater relevance that could be used for effective curative treatment strategies.

Declaration

I declare that this thesis is an original report of my research, has been written by me and has not been submitted for any previous degree. The experimental work is entirely my own work which was performed between 2014 and end of 2017. Contributions and advice have been clearly indicated and acknowledged. Due references have been provided on all supporting literatures and resources.

Afrakoma Afriyie-Asante

May 2019

Acknowledgements

Firstly, I would like to express my deepest appreciation and praise to the Almighty God for His grace, mercies and strength throughout the PhD journey. He has indeed been the bedrock of all the successes attained during these years. Working as a PhD student was a challenging and magnificent experience and many people have played an instrumental role in shaping my academic career. It would have been difficult to thrive in my doctoral work without the massive support from the following personalities.

I would like to thank my supervisor, Dr. Lucy Fairclough for giving me the opportunity to undertake this interesting research project. Her valuable guidance, consistent encouragement, enthusiasm and friendly nature helped me to complete my research in a respectable manner. I would like to convey deep regards to Dr. Patrick Tighe for introducing me into the world of 'robotics' and providing me with extensive support in understanding the complex microarray and statistical analysis. I am also very grateful to Dr. Ian Todd for his valuable input in my PhD.

Special thanks to Professor John Robertson for providing me with economic support for my living expenses as I was able to fully focus on my research without financial anxiety. Many thanks to Professor William Irving, Patrick McCullough and the Centre of Excellence for Autoimmunity in Cancer (CEAC) for their clinical input and supplying us with serum samples as well *E. coli* generated tumour-associated antigens. This work would not have materialised without the Vice chancellor's Scholarship for Research Excellence offered by the University of Nottingham as it entirely funded the project.

Additionally, I would like to acknowledge my internal assessor and personal tutor Dr. Alex Tarr and Dr. Luisa Martinez-Pomares respectively for their helpful suggestions and countless counselling throughout my PhD. I would also like to extend my gratitude to Dr. Ola Negm, Elizabeth Abbott, Colin Nicolson and to all the members in the MBTI research group for their friendship, expertise and comments when I joined the group as it enabled me to adjust quickly and stay focused on my laboratory work.

Many thanks to all my friends Osman, Philemon, Christine, Milly, Georgina, Kwadwo, Dennis, Ade, Yemisi as well as my Nottingham church family for their love, friendships and endless laughter. These have really made all the difference.

Finally, no amount of words can express my heartfelt and earnest gratitude to my husband and best friend Meshach Asare-Werehene. I am indeed privileged to have you in my life as you have been my mentor, counsellor, motivator, understanding my emotions and praying immensely for me throughout as these kept me going especially during difficult times. You also fortified me to take advantage of the many opportunities that came my way during this journey. Thank you from the bottom of my heart. I would also like to acknowledge my mum Hannah Okyere-Boateng and my aunt Naomi Ampadu for their love and emotional support as these helped to keep my head up.

I hope I made all of you proud.

Table of Contents

Abstract ..... *i*

Declaration ..... *iv*

Acknowledgements ..... *v*

List of Abbreviations ..... *xvii*

Conferences Attended and Awards ..... *xxiii*

Chapter One: Introduction ..... *- 1 -*

1.1 Introduction to Cancer ..... **- 1 -**
1.1.1. The Global burden ..... - 1 -
1.1.1.2 Cancer Statistics in the United Kingdom ..... - 3 -
1.1.1.3 Cancer Predictions ..... - 3 -
1.1.2 Molecular Hallmarks of Cancer ..... - 4 -
1.1.3 How is Cancer Staged? ..... - 7 -
1.1.4 Who is at Risk? ..... - 9 -
1.1.5 Hidden Costs of Cancer ..... - 9 -

1.2 The Liver and Hepatocellular Carcinoma ..... **- 11 -**
1.2.1 Anatomy and Physiology of the Liver ..... - 11 -
1.2.2 Hepatocellular Carcinoma: Demographics and Epidemiology ..... - 13 -
1.2.3 Major Risk Factors of Hepatocellular Carcinoma ..... - 19 -
1.2.4 Mechanism of Hepatocarcinogenesis ..... - 27 -

1.3 Introduction to the Immune System ..... **- 32 -**
1.3.1 Tumour-Associated Antigens (TAAs) and Tumour Specific Antigens (TSAs) in Hepatocellular Carcinoma ..... - 33 -
1.3.1.1 Overexpressed Tumour-Associated Antigens (TAAs) ..... - 33 -
1.3.1.2 Mutated Tumour-Associated Antigens ..... - 37 -
1.3.1.3 Altered Expression of Tumour-Associated Antigens ..... - 38 -
1.3.1.4 Post-translational modifications of Tumour-Associated Antigens ..... - 39 -
1.3.2 Immune response and Hepatocellular Carcinoma ..... - 41 -

1.4 Diagnosis, Prevention and Management of Hepatocellular Carcinoma ..... **- 69 -**
1.4.1 Clinical Diagnosis of Hepatocellular Carcinoma ..... - 69 -
1.4.2 Prevention ..... - 73 -
1.4.3 Management and Treatment of Hepatocellular Carcinoma ..... - 75 -

1.5 Aims and Objectives ..... **- 80 -**
1.5.1 Aim ..... - 80 -
1.5.2 Specific Objectives ..... - 80 -

Chapter Two: Materials and Methods ..... *- 82 -*

2.1 Materials (Antigen Microarray Technology) ..... **- 82 -**
2.1.1 Chemicals and Reagents ..... - 82 -
2.1.2 Substrate for array printing (Slide Surfaces) ..... - 84 -
2.1.3 Antibodies used for the Microarray Assay ..... - 84 -
2.1.4 Commercial Tumour-Associated Antigens (TAAs) ..... - 85 -
2.1.5 In-house Recombinant Tumour-Associated Antigens ..... - 87 -
2.1.6 Quality controls used for the Antigen Microarray Assay ..... - 88 -
2.1.7 Acquisition of Human Serum Specimens: Permission and Collection ..... - 88 -

2.2 Methods (Antigen microarray) ..... **- 90 -**
2.2.1 Plate Preparation and Storage of Plates ..... - 90 -

2.2.2 Microarray Printing ..... - 90 -
2.2.3 Initial Protocol for the Antigen Microarray Assay without Amplification ..... - 93 -
2.2.4 Antigen Microarray Assay with Amplification ..... - 95 -
2.2.5 Initial Protocol for Quantification of specific anti-TAA IgG levels in serum samples using HCC His-tagged Tumour-associated antigens ..... - 97 -
2.2.6 Optimising the Antigen Microarray Assay Using Different Microtiter Volumes. ..... - 98 -
2.2.7 Optimising the Antigen Microarray Assay using different Blocking Buffers ..... - 99 -
2.2.8 Optimising the Antigen Microarray Using Different Printing Buffers and Arrayers ..... - 100 -
2.2.9 Optimising the Antigen Microarray Using Different Slide surfaces ..... - 100 -
2.2.10 Optimising the Print Position of Antigens in the Microarray Assay ..... - 100 -
2.2.11 Optimising Monoclonal mouse anti-His_6 antibody and Biotinylated anti-mouse antibody dilutions in Antigen microarray Assay ..... - 101 -
2.2.12 Finalised Antigen Microarray Assay Protocol for different categories of Tumour-Associated Antigens (Commercial and In-house) ..... - 101 -
2.2.13 Scanning of Microarray Slides ..... - 103 -
2.2.14 Generation of Genepix Array List Files (GAL) for Axon Genepix Pro Software ..... - 104 -
2.2.15 Statistical Analysis ..... - 105 -
2.2.17 Microarray Validation ..... - 106 -

2.3 Materials (Production of In-House HCC TAAs) ..... - 107 -
2.3.1 Media, reagents, solutions ..... - 107 -
2.3.2 Plasmids ..... - 108 -
2.3.3 Expression Systems ..... - 109 -
2.3.4 Culture media, Reagent and buffers ..... - 109 -
2.3.5 Transfection reagent ..... - 110 -
2.3.6 Antibiotics ..... - 110 -
2.3.7 Growth Conditions and Storage ..... - 111 -

2.4 Methods (Production of In-House HCC TAAs) ..... - 112 -
2.4.1 Transfection of cDNA clones into HEK 293 cells ..... - 112 -
2.4.2 Generation of Stable Cell line (Selective Pressure) ..... - 112 -
2.4.3 Preparation of Cell Lysate ..... - 113 -
2.4.4 Protein Buffer Exchange, Concentration and Quantification ..... - 114 -
2.4.4.3 Protein Detection ..... - 115 -

Chapter Three: Development of the Antigen Microarray Technology for Autoantibody detection in Hepatocellular Carcinoma Patients ..... - 123 -

3.1 Introduction ..... - 123 -

3.2 Materials and Methods ..... - 137 -

3.3 Results ..... - 141 -
3.3.1 Validation Assessment of the In-House Antigen Microarray Assay ..... - 141 -
3.3.2 Assessing the reproducibility of signal intensities using HCC tumour-associated antigens ..... - 148 -
3.3.3 Optimisation of the Antigen Microarray Technology ..... - 151 -
3.3.4 Determining the Optimal Relative Humidity and Microtiter Volumes for Printing ..... - 152 -
3.3.5 Optimisation of Printing Buffers ..... - 163 -
3.3.6 Assessing the Position of Print on a Slide ..... - 166 -
3.3.7 Testing different Slide Surface Chemistries ..... - 168 -
3.3.8 Testing different blocking Buffers ..... - 175 -
3.2.9 Optimisation of Monoclonal Primary and Secondary Antibodies ..... - 178 -
3.3.10 Re-validation of the Antigen Microarray Technology ..... - 182 -
3.2.11 Testing the Validity of the Microarray platform with HCC patients sera ..... - 187 -

3.3 Discussion ..... - 192 -

Chapter Four: ..... *- 198 -*

Production and Purification of a Panel of Recombinant Tumour-Associated Antigens in Hepatocellular Carcinoma ..... *- 198 -*

4.1 Introduction ..... **- 198 -**
4.1.1 Tumour Antigens ..... - 198 -
4.1.2 Recombinant Protein Expression Systems ..... - 200 -
4.1.3 Mammalian Cell Transfection Platforms ..... - 204 -
4.1.4 Purification systems for expressed recombinant proteins ..... - 207 -

4.2 Materials and Methods ..... **- 210 -**
4.2.1 Materials and reagents ..... - 210 -
4.2.2 Transfection and Flow Cytometry ..... - 210 -
4.2.3 Selection of Resistant Cells ..... - 211 -
4.2.4 Cell lysate preparation and BCA assay ..... - 211 -
4.2.5 SDS-PAGE and Immunoblot ..... - 212 -

4.3 Results ..... **- 217 -**
4.3.1. Preliminary Expression of Recombinant Flag-tagged proteins in HEK 293 cells ..... - 217 -
4.3.2 In Vitro expression of KRAS, HRAS and CDKN2A proteins in HEK 293 Cell Extracts ..... - 220 -
4.3.3. Recombinant Flag-tagged Protein Detection by Dot Blot Analysis. ..... - 221 -
4.3.4 Affinity Pull-Down of Flag-tagged Recombinant Proteins Using Anti-FLAG® M2 Affinity Gel ..... - 223 -
4.3.5 Purification of Flag-Tagged Recombinant Proteins using Anti-Flag® M2 Magnetic Beads ..... - 224 -
4.3.6 Analysis of the expression of eight Recombinant Flag-tagged proteins with an Anti-Flag antibody. ..... - 226 -
4.3.7 Purification of Flag-tagged Recombinant proteins from HEK 293 cells transfected with Eight Myc-DDK cDNA clones ..... - 229 -
4.3.8 Detection of HCC recombinant TAAs in Cell Lysates using Anti-Myc and Antigen specific antibodies (anti-KRAS and anti-P53) ..... - 233 -
4.3.9 Purification of Myc-DDK tagged proteins using Myc®Trap MA Magnetic Beads ..... - 235 -
4.3.10 Quality Assessment of Commercial HCC Tumour-associated Antigen Panel ..... - 240 -

4.4 Discussion ..... **- 244 -**

Chapter Five: ..... *- 251 -*

Testing In-house and Commercial TAAs on Microarray platform ..... *- 251 -*

5.1 Introduction ..... **- 251 -**

5.2 Materials and Methods ..... **- 255 -**

5.3 Results ..... **- 258 -**
5.3.1 Establishment of Optimal Conditions for Printing In-house Recombinant TAAs ..... - 258 -
5.3.2 Optimising Printing Buffers for In-house Recombinant Tumour-Associated Antigens - 259 -
5.3.3 Effect of Stringent Washing condition Prior to Slide Processing ..... - 261 -
5.3.4 Simultaneous Print of In-house and Commercial HCC Tumour -Associated Antigens on the Microarray Platform. ..... - 265 -
5.3.5 Validation of Twenty-Two In-house and Commercial Recombinant Tumour-associated antigens using random serum samples ..... - 270 -

5.4 Discussion ..... **- 278 -**

Chapter Six: ..... *- 280 -*

Clinical Utility of the Microarray Platform for the Detection of Autoantibodies in Hepatocellular Carcinoma Patients ..... - 280 -

6.1 Introduction ..... - 280 -

6.2 Materials ..... - 282 -

6.2.1 Tumour-associated antigens (TAAs) ..... - 282 -

6.2.2 Patients samples ..... - 282 -

6.3 Methodology ..... - 283 -

6.3.1 Detection of autoantibody reactivity using Antigen Microarray ..... - 283 -

6.3.2 Statistical Data Analysis ..... - 284 -

6.4 Results ..... - 286 -

6.4.1 Effect of Heat Treatment of Human Serum on Autoantibody Measurement in HCC patients - 286 -

6.4.2 Characterisation of Research Subjects in the Study ..... - 291 -

6.4.3 Measurement and Comparison of Autoantibody Responses against TAAs across Different Cohorts ..... - 293 -

6.4.4 Autoantibody Responses between Commercial and In-house Tumour-Associated Antigens in All Cohorts ..... - 302 -

6.4.5 Prevalence of Autoantibody Positivity to Individual TAAs across different Cohorts ..... - 305 -

6.4.6 Correlation in Autoantibody Measurement between Commercial and In-house generated TAAs. ..... - 309 -

6.4.7 Effect of Age on Autoantibody Response in Hepatocellular Carcinoma ..... - 311 -

6.4.8 Effect of Gender on the development of Hepatocellular Carcinoma ..... - 316 -

6.5 Discussion ..... - 318 -

Chapter Seven: General Discussion ..... - 325 -

7.1. Epidemics and Fatality of Hepatocellular Carcinoma ..... - 325 -

7.2 Development of the New Antigen Microarray Platform ..... - 326 -

7.3 Generation of Recombinant TAAs for the Microarray Assay ..... - 329 -

7.4 Development of the Antigen Microarray Technology for TAAs expressed in Lysates ..... - 332 -

7.5 Application of the developed Antigen Microarray Platform for Autoantibody Detection ..... - 333 -

7.6 Conclusions ..... - 337 -

7.8 Future Directions ..... - 338 -

References ..... - 341 -

APPENDIX ..... - 374 -

List of Figures

Figure 1: The growing menace of cancer.. - 2 -
Figure 2: Most commonly diagnosed cancers in the world (left) and most common causes of cancer deaths (right) worldwide. - 3 -
Figure 3: Global cancer cases predictions by 2035. - 4 -
Figure 4: Six main hallmarks of cancer.. - 7 -
Figure 5: The costs of cancer - 10 -
Figure 6: An anatomical illustration of the liver and gall bladder (Left) and a nuclear medicine scan of the abdomen (Right) revealing the liver and the gall bladder (Right) - 12 -
Figure 7: Microscopic anatomy of the liver showing the basic components such as hepatocytes, lobules, ducts and blood vessels - 12 -
Figure 8: Incidence and mortality of Hepatocellular carcinoma worldwide - 14 -
Figure 9: Age specific HCC incidence rates per 100,000 population among males and females in the UK, 2013-2015 - 15 -
Figure 10: The incidence of Hepatocellular carcinoma in both males and females worldwide. Higher incidences are recorded in Sub-Saharan African countries and Asia - 17 -
Figure 11: Risk factors of hepatocellular carcinoma. - 19 -
Figure 12: Stages of development of hepatocellular carcinoma - 26 -
Figure 13: A schematic diagram comparing a healthy liver to hepatocellular carcinoma. - 27 -
Figure 14: Molecular mechanisms inducing hepatocellular carcinogenesis at the cirrhosis stage - 31 -
Figure 15: Major signalling transduction pathways implicated in hepatocellular carcinoma - 32 -
Figure 16: Hepatocellular carcinoma tumour markers. - 40 -
Figure 17: Immune response in hepatocellular carcinoma.. - 46 -
Figure 18: The functions of immune cells become dysregulated as the liver disease progresses from cirrhosis to hepatocellular carcinoma.. - 48 -
Figure 19: Proposed integration for biomarkers into HCC treatment - 49 -
Figure 20: T cell dependent B cell activation. - 55 -
Figure 21: Structure of an Immunoglobulin (Antibody). - 60 -
Figure 22: Technologies used for TAA and autoantibody identification in Hepatocellular carcinoma. - 66 -
Figure 23: An example of Protein Microarray Technology.. - 68 -
Figure 24: Photograph of the Biorobotics Microgrid II arrayer. - 92 -
Figure 25: Illustrates A) microarray printing B) Proteins arrayed onto glass slides. - 92 -
Figure 26: Schematic representation showing quality control antigens, Candida albicans and Tetanus (ten replicates) and a two-fold serial dilution of purified human IgG (quadruplicates) on a single (approximately 5x5mm) microarray grid. - 94 -
Figure 27: Schematic diagram showing the main processes in the initial antigen microarray assay.. - 95 -
Figure 28: Schematic diagram showing Tyramide signal amplification in the antigen microarray assay.. - 96 -
Figure 29: Annotated diagram showing the print pattern of His-tagged tumour-associated antigens on antigen microarray assay. - 97 -
Figure 30: Green and red streptavidin conjugated cy5 dyes prepared in three different microtiter volumes (10 µl, 15 µl and 20 µl) in a 384 microtiter well plate. - 99 -
Figure 31: Photograph of the Genepix 4200AL Microarray Scanner. - 103 -
Figure 32: Principle Model of Microarray Scanning. - 104 -

Figure 33: An example of a plate map (Left) and the alignment of a resultant Genepix Array List (GAL) file grid onto corresponding spots on a TIFF image (right) to obtain the median fluorescence per each spot.. - 105 -
Figure 34: Statistical softwares and workflow used in the analysis and interpretation of Microarray data. - 107 -
Figure 35: Schematic diagram outlining the main procedures involved in generating Hepatocellular carcinoma (HCC) recombinant tumour associated antigens using HEK 293 cells. - 113 -
Figure 36: Schematic diagram showing the processes involved in Ultracentrifugation... - 114 -
Figure 37: The diagram above shows the processes involved in protein quantification using the BCA assay kit. - 115 -
Figure 38: Diagram showing the processes involved in Flag-tag affinity chromatography.. - 119 -
Figure 39: Diagram showing the processes involved in anti-Flag® M2 bead protein chromatography - 121 -
Figure 40: Enzyme Linked Immunosorbent Assay (ELISA) vs Protein microarray..... - 125 -
Figure 41: Slide surface chemistries for protein microarrays.. - 128 -
Figure 42: Microarray printing. The figure above shows (**A)** contact printing, where the solid pin makes direct contact with the surface to dispense proteins while (**B)** in non-contact microarray, the solid pin does not contact the slide surface as it drops proteins unto the slide surface by the ink-jet method. - 130 -
Figure 43: Schematic diagram showing the various steps involved in the Method Validation Assay. - 132 -
Figure 44: Diagram elucidating the intra-assay variability (CV%) for ten and four spot replicates of Candida antigen and human IgG serial dilution standard respectively. - 134 -
Figure 45: Diagram showing the inter assay variability (CV%) for ten 10 spot replicates of human IgG serial dilution standard respectively. - 135 -
Figure 46: Schematic diagram outlining the various processes involved in the development of the Antigen Microarray Technology, for the detection of autoantibodies in HCC patients. - 136 -
Figure 47: The figure above shows the acceptable level of signal uniformity and regularity of spots required for statistical analysis of microarray data. - 140 -
Figure 48: Morphological differences in spots of control antigens.. - 142 -
Figure 49: Differences in arbitrary fluorescence in response to quality control antigens across different days.. - 143 -
Figure 50: Intra- and inter- assay precision of arbitrary fluorescence. - 145 -
Figure 51: Human IgG standard curves across three consecutive days.. - 146 -
Figure 52: Intra- and inter- assay precision after normalisation with human IgG standard curve.. - 147 -
Figure 53: Morphological appearance of HCC His-tagged tumour-associated antigen spots on Poly-L-lysine slides. - 149 -
Figure 54: Difference in signal intensities to HCC tumour-associated antigens between two days.. - 150 -
Figure 55: Schematic diagram showing the effect of inadequate relative humidity on appearance of antigen spots.. - 153 -
Figure 56: Deposition of samples unto glass slides. - 153 -
Figure 57: Testing different microtiter volumes for microarray printing.. - 154 -
Figure 58: Spot morphology of Cy3 and Cy5 Streptavidin dyes on a Poly-L-lysine slide printed from three different microtiter volumes.. - 157 -
Figure 59: Effect of different microtiter volumes on intra spot variation.. - 162 -

Figure 60: Effect of different microtiter volumes on diameter of spots.. ..... - 163 -
Figure 61: Spot morphology of HCC antigens when tested with different printing buffers and arrayers.. ..... - 165 -
Figure 62: Testing the effect of printing buffers and arrayers on assay variability.. - 166 -
Figure 63: Image to show the print positions of HCC antigens on a slide.. ..... - 167 -
Figure 64: Morphology of spots on different slide surfaces. ..... - 171 -
Figure 65: Analysis of diameter and signal intensities of AFP on different slide surfaces. - 172 -
Figure 66: Analysis of diameter and signal intensities of Gankyrin on different slide surfaces.. ..... - 173 -
Figure 67: Evaluation of different blocking buffers for antigen microarrays.. ..... - 177 -
Figure 68: Scanned morphology of TAAs tested with different dilutions of monoclonal mouse anti-His_6 and anti-mouse antibodies. ..... - 180 -
Figure 69: Arbitrary fluorescence of HCC TAAs tested with monoclonal mouse anti-His_6 and anti-mouse antibodies.. ..... - 181 -
Figure 70: Investigating the precision of arbitrary fluorescence across different dilutions of anti-His_6 and anti-mouse antibodies used on the microarray. ..... - 182 -
Figure 71: Morphological appearance of HCC antigen spots across different days. - 184 -
Figure 72: Signal intensities in response to HCC antigens ..... - 185 -
Figure 73: Intra and Inter-assay precision of Anti-His_6 antibody responses to HCC antigens. ..... - 186 -
Figure 74: Spot morphology of HCC antigen probed with control sera.. ..... - 188 -
Figure 75: Arbitrary fluorescence of antibody responses to HCC antigens. ..... - 189 -
Figure 76: Intra-assay precision of arbitrary fluorescence.. ..... - 190 -
Figure 77: Intra-assay precision after normalising with human IgG.. ..... - 191 -
Figure 78: Inter-assay precision before and after normalising with human IgG. ..... - 191 -
Figure 79: Protein expression systems. ..... - 201 -
Figure 80: Workflow of transfection in mammalian cells. ..... - 205 -
Figure 81: Common methods of transfecting mammalian cells.. ..... - 207 -
Figure 82: Outline of the procedures involved in the expression, detection and purification of Myc-DDK(Flag-tagged) recombinant tumour-associated antigens in HCC ..... - 216 -
Figure 83: Preliminary expression of Flag-tagged recombinant proteins in HEK 293 cells.. ..... - 220 -
Figure 84: Analysis of recombinant HDGF over-expression with anti-Flag antibody - 221 -
Figure 85: Dot blot analysis of KRAS, HRAS, HDGF and CDKN2A overexpressed in HEK 293 cells.. ..... - 222 -
Figure 86: Dot blot analysis of the elution, filtrate, flow through and wash fractions of Flag-tagged recombinant proteins after purification with anti-Flag® M2 agarose beads. ..... - 223 -
Figure 87: Anti-Flag® M2 magnetic bead purification of flag-tagged proteins from HEK 293 cell lysates.. ..... - 225 -
Figure 88: Analysis of the expression of eight recombinant Flag-tagged proteins with anti-Flag antibody… - 228 -
Figure 89: Affinity Purification of Flag-tagged Recombinant proteins from HEK 293 cell lysates on anti-Flag® M2 magnetic bead chromatography. ..... - 232 -
Figure 90: Recombinant HCC TAAs in lysates detected by anti-Myc, anti-P53 and anti-KRAS antibodies. ..... - 234 -
Figure 91: Recombinant Myc-DDK tagged protein purification using Myc Trap MA Magnetic Beads. ..... - 239 -

Figure 92: Representative analysis of a panel of eukaryotic and E. coli generated HCC TAAs.. ..... - 243 -
Figure 93: Schematic diagram outlining the processes involved in the Antigen Microarray Assay (lysates).. ..... - 257 -
Figure 94: Reveals spot morphology of in-house TAAs probed with different sera... - 259 -
Figure 95: Determining the optimal print buffer for in-house TAAs...... - 261 -
Figure 96: Comparing spot morphology when the slide was rigorously washed prior to and after processing.. ..... - 265 -
Figure 97: Immobilisation of in-house and commercial HCC TAAs simultaneously onto an Aminosilane slide surface.. ..... - 268 -
Figure 98: Testing the performance of different sets of TAAs on the microarray with serum samples...... - 269 -
Figure 99: Heat Map showing signal intensities of total IgG levels in 15 serum samples.. - 272 -
Figure 100: Precision of signal intensities before normalisation.. ..... - 275 -
Figure 101: Precision after normalisation of signal intensities...... - 277 -
Figure 102: Effect of heat treatment on autoantibody measurement in HCC and non-HCC subjects...... - 291 -
Figure 103: Differences in anti-TAA responses in subjects with HCC, non-HCC cirrhosis (liver cirrhosis only), non-HCC non-cirrhosis (chronic liver hepatitis) and healthy groups: Kras-A, Kras-B, Kras-C, Hras-A, Hras-B, Hras-C, HDGF-A, HDGF-B, HDGF-C, P16-A, P16-C, RALA-A, RALA-B, RALA-C, P62-A, P62-B, P62-C, P53-A, P53-C, Gankyrin-A, Gankyrin-B, Gankyrin-C, IMP-B, AFP-B, GRP78-B, APCN-B(A-Z, respectively)..... - 301 -
Figure 104: Box plots showing autoantibody responses amongst the three categories of TAAs (A, B, C) in HCC, non-HCC cirrhotic, non-HCC non-cirrhotic and healthy subjects.. ..... - 304 -
Figure 105: Correlation between "age" and autoantibody responses to KRAS-A, KRAS-B, KRAS-C, HRAS-A, HRAS-B, HRAS-C, HDGF-A, HDGF-B, HDGF-C, P16-A, P16-C, RALA-A, RALA-B, RALA-C, P62A, P62B, P62C, P53A, P53-C, Gankyrin-A, Gankyrin-B, Gankyrin-C, IMP-B, AFP-B, GRP78. ..... - 316 -

List of Tables

Table 1: The TNM staging of Cancers. - 8 -
Table 2: Overexpressed TAAs in hepatocellular carcinoma. - 36 -
Table 3: Classes of immunoglobulins and their respective properties.. Error! Bookmark not defined.
Table 4: Different subclasses of Immunoglobulin G (IgG). - 62 -
Table 5: The Barcelona Clinic-Liver Cancer (BCLC) staging system of HCC. - 76 -
Table 6: Composition of printing buffers tested for arraying proteins onto glass slides. - 82 -
Table 7: Different blocking buffers tested. - 83 -
Table 8: Different types of slide surfaces tested. - 84 -
Table 9: Antibodies used for Antigen Microarray Assay. - 85 -
Table 10: Commercial recombinant tumour-associated antigens arrayed onto glass slides. - 86 -
Table 11: In-house recombinant tumour-associated antigens (TAAs) arrayed onto glass slides. - 87 -
Table 12: A selection of quality controls used in the antigen microarray assay. - 88 -
Table 13: Information on clinical sample cohort. - 89 -
Table 14: List of C-Terminal Myc-DDK (Flag) tagged human TrueORF cDNA clones used in the study. - 108 -
Table 15: List of growth media, reagents and buffers used in cell culture. - 110 -
Table 16: List of antibiotics used. Antibiotics were stored at -20ºC. - 111 -
Table 17: Intra slide variation of AFP, Gankyrin and MAGE spot signals within and across eight blocks on the Poly-L-lysine slides when probed with (A) anti-His6 antibody and (B) control serum on two consecutive days. - 151 -
Table 18: Intra-slide variability (CV%) of the signals and diameter of (A) first fifty (B) second fifty and (C) third fifty Cyanine (Red and Green) spots from three microtiter volumes. - 158 -
Table 19: Effect of print positions of antigens on the precision off an assay. The tables below show the coefficient of variation of signal intensities and diameter of **(A)** AFP and **(B)** Gankyrin spots within and across blocks when printed at the edge and centre positions on a Poly-L-lysine slide in a 16-pad format. - 168 -
Table 20: Effect of different Slide Surfaces on Assay Precision. The tables below show the variation of signal intensities and diameter of AFP and Gankyrin spots within and across blocks when printed on Poly-L-lysine, Aminosilane, Epoxysilane and Nitrocellulose slide surfaces. - 174 -
Table 21: Different tumour-associated antigens discovered in patients with hepatocellular carcinoma patients since 1993. - 199 -
Table 22: Affinity tags used in purification of recombinant proteins expressed in mammalian cells. - 209 -
Table 23: Clinical Characterisation of Research Subjects from three datasets. - 292 -
Table 24: Information on clinical samples and related aetiologies. - 293 -
Table 25: 95th percentile of specific anti-TAA autoantibody responses in healthy controls. - 295 -
Table 26: Kruskal-Wallis statistical tests of the distribution of anti-TAA autoantibody responses across the four sample cohorts (HCC, non-HCC cirrhotic, non-HCC, non-cirrhotic and Healthy controls). - 296 -
Table 27: Frequency of positive autoantibody responses to set A tumour-associated antigens. - 306 -

Table 28: Frequency of positive autoantibody responses to set B tumour-associated antigens.- 307 -
Table 29: Frequency of positive autoantibody responses to set C tumour-associated antigens.- 308 -
Table 30: Correlation between autoantibody responses to commercial and in-house TAAs produced in HEK 293 cells. .....- 310 -
Table 31: Correlation between autoantibody responses to commercial TAAs produced in HEK 293 cells and E. coli.....- 311 -
Table 32: Correlation between Gender and Autoantibody responses in HCC.....- 317 -

List of Abbreviations

Ab- Antibody

ADCC- Antibody Dependent Cell Cytotoxicity

AFB_1-Aflatoxin B1

AFP-Alpha Feto Protein

AFU-Arbitrary Fluorescent Unit

Ag- Antigen

AIDS-Acquired Immune Deficiency Syndrome

AIF-Apoptotic Inducing Factor

ALD- Alcohol Liver Disease

ALKM1-Anti-liver kidney microsome-1

ANA-Anti-nuclear autoantibodies

APC- Antigen presenting cells

BCA- Bicinchoninic acid assay

BCLC- Barcelona Clinic Liver Cancer

BCR-B cell receptor

Bet- Betaine

Bregs- B regulatory cells

BSA- Bovine Serum Albumin

CD4- Cluster of Differentiation 4

CD8- Cluster of Differentiation 8

CDK4- Cyclin Dependent Kinase 4

CDKN2A- Cyclin-Dependent Kinase Inhibitor 2A

cDNA- Complementary Deoxyribonucleic acid

CEAC- Centre of Excellence for Autoimmunity in Cancer

CENPF- Centromere Protein F

CEUS-Contrast Enhanced Ultrasound

C_H-Constant heavy chain

CHO- Chinese Hamster Ovary cells

C_L-Constant light chain

CT- Computed Tomography

CV%- Coefficient of Variation %

Cy3- Cyanine 5

Cy5- Cyanine 3

DC- Dendritic Cells

DMEM- Dulbecco's Modified Eagle's Media

DMSO- Dimethyl Sulfoxide

DNA- Deoxyribonucleic Acid

DTT- Dithiothreitol

E. coli- Escherichia coli

ECL- Enhanced Chemiluminiscence

EDTA- Ethylenediaminetetraacetic acid

EGF- Epidermal Growth Factor

EGFR- Epidermal Growth Factor Receptor

EIF2- Eukaryotic Initiation Factor

ELISA- Enzyme Linked Immunosorbent Assay

EP1-Expanded Programme of Immunisation

Fab-Antigen-binding fragment

FBS- Fetal Bovine Serum

FDA- Food and Drug Administration

Fc-Fragment crystallizable fragment

FNA-Fine Needle Aspiration

FOXP3- Fork head box protein 3

GAL- Genepix Array List

GFP- Green Fluorescent Protein

GPR- Genepix Results

GRP78- Glucose Regulated Protein 78

GTPase- Guanosine Triphosphate Pases

H- Healthy

HBV- Hepatitis B Virus

HCC- Hepatocellular Carcinoma

HCL- Hydrochloric acid

HCV- Hepatitis C Virus

HDGF- Hepatoma Derived Growth Factor

HDV- Hepatitis D Virus

HEK- Human Embryonic Kidney

HER2-Human Epidermal Growth Factor 2

HI-Heat Inactivated

HIV- Human Immunodeficiency Virus

HPV- Human Papilloma Virus

HRAS- Harvey Rat Sarcoma Viral Oncogene Homolog

HRP- Horseradish Peroxidase

HSP60- Heat Shock Protein 60

IFN- Interferon

IFN-γ: Interferon gamma

IgA- Immunoglobulin A

IgD- Immunoglobulin D

IgE- Immunoglobulin E

IgG- Immunoglobulin G

IgM- Immunoglobulin M

IL- Interleukin

IL-β- Interleukin β

IL-12- Interleukin 12

IL-6- Interleukin 6

IR-Insulin Resistance

JAK- Janus Kinases

JNK- C Jun N Terminal Kinases

KRAS- Kirsten Rat Sarcoma Viral Oncogene Homolog

MAC-Membrane Attack Complex

MAGE4- Melanoma Antigen Family A, 4

MAPK- Mitogen-Activated Protein Kinase

MDM2- Mouse Double Minute 2 Homolog

MHC- Major Histocompatibility Complex

MMP- Matrix Metalloproteinase

MRI- Magnetic Resonance Imaging

mRNA- Messenger Ribonucleic Acid

mTOR- Mammalian Target of Rapamycin

MWCO-Molecular weight cut-off

MyD88- Myeloid Differentiation Primary Response 88

N-Number

NaCl- Sodium Chloride

NAFLD- Non-Alcoholic Fatty Liver Disease

NASH- Non-Alcoholic Steatohepatitis

NF-KB- Nuclear Factor Kappa β

NHC- Non-Hepatocellular Carcinoma Cirrhosis

NHNC- Non-Hepatocellular Carcinoma Non-Cirrhosis

NHS- National Health Service

NK- Natural Killer Cells

NO- Nitric Oxide

NS3- Non-Structural Protein 3

NS5A- Non-Structural Protein 5A

ORF- Open Reading Frame

P13K- Phosphatidylinositol-4,5-bisphosphate 3-kinase

PBP-Prostate Binding Protein

PBS-Treh- Phosphate Buffered Saline-Trehalose

PBS-Treh-Tw-Betain- Phosphate Buffered Saline-Trehalose-Tween-Betaine

PBST-Phosphate Buffered Saline-Tween

PCR- Polymerase Chain Reaction

PD1-Programmed Cell Death Receptor 1

PEI-Percutaneous Ethanol Injection

PI- Isoelectric point

PMT- Photo Multiplier Tube

PSMD10- Proteasome Non-ATPase Regulatory Subunit

PVDF- Polyvinylidene Fluoride

Ras- Rat Sarcoma Viral Oncogene Homolog

RIPA- Radioimmunoprecipitation

RNA- Ribonucleic Acid

ROS- Reactive Oxygen Species

Rpm- Revolutions per minute

RPPA- Reverse Phase Protein Array

RT-Room Temperature

S. cerevisiae- Saccharomyces cerevisiae

SDCCAG8- Serologically Defined Colon Cancer antigen 8

SDS-PAGE- Sodium Dodecyl Sulphate Polyacrylamide Gel Electrophoresis

SEREX- Serological analysis of recombinant tumour cDNA expression libraries

SERPA- Serological Proteome Analysis

SF9- Spodoptera frugiperda

sIgG- Specific Immunoglobulin G

SMA-Smooth muscle autoantibodies

SNP-Single Nucleotide Polymorphisms

SOCS3- Suppressor of Cytokine Signalling 3

SPSS- Statistical Package for Social Sciences

STATS- Signal Transducer and Activator of Transcription

SV40- Simian Virus 40

T1D- Type 1 Diabetes

TA-Tyramide Amplification

TAA- Tumour-Associated Antigens

TBS- Tris Buffered Saline

TBST- Tris Buffered Saline $Tween_{20}$

TGF-β- Tumour Growth Factor β

Th1-T helper 1 cells

Th2- T helper 2 cells

Th22-T helper 22 cells

TNF-α- Tumour Necrosis Factor Alpha

TNM- Tumour Node Metastasis

TP53- Tumour Protein 53

TRAIL-Tumour Necrosis Factor Related Apoptosis Inducing Ligand

Tregs- T regulatory cells

TSA-Tumour-Specific Antigens

Tw- Tween20

VEGF- Vascular Endothelial Growth Factor

V_H-Variable heavy chain

V_L-Variable light chain

WB-Western Blot

WHO-World Health Organisation

Conferences Attended and Awards

This work was presented in either oral or poster sessions in the following meetings:

2nd Immunology Research Showcase, (University of Nottingham, 2015)

3rd Immunology Research Showcase, (University of Nottingham, 2016)

Federation of Clinical Immunology Scientists, (United States, 2016)

British Society for Immunology Conference, (BSI Liverpool, 2016)

Life Sciences Postgraduate Symposium (University of Nottingham, 2017)

LINK17 Postgraduate Research Conference (University of Nottingham, 2017).

Three Minutes Thesis Competition, (University of Nottingham, 2017

Postgraduate Research Showcase, (University of Nottingham, 2017)

Life Sciences Postgraduate Symposium (University of Nottingham, 2017)

L'Oréal-UNESCO for Women in Science 2018 Conference (London, UK, 2018)

Peoples' Choice Award, Universitas 21 Three Minutes Thesis Competition, 2017

Winner, University of Nottingham Tri-Campus Three Minutes Thesis Competition, 2017

People's Choice Award, East Midlands Doctoral Research Three Minutes Thesis

Competition, 2017

Early Researcher Award for Excellence (University of Nottingham, 2017)

Winner, Three Minutes Thesis Competition, (University of Nottingham, 2017)

Runner Up, LINK17 Postgraduate Research conference (University of Nottingham, 2017)

Top ten finalist, L'Oréal-UNESCO for Women in Science 2018 poster competition, (London, UK, 2018)

In Process Publication: Development and Application of the Antigen Microarray as a Diagnostic Platform for Hepatocellular Carcinoma

Chapter One: Introduction

1.1 Introduction to Cancer

1.1.1. The Global burden

Cancer continues to be a major health threat worldwide (1), despite great effort and resources provided to research the aetiology, molecular basis, host-tumour interface and treatments options for the disease (1). Cancer now causes more deaths than common diseases such as coronary heart disease, stroke, tuberculosis, HIV/AIDS and malaria (1). In fact, one in seven deaths in the world are as a result of cancer. It also ranks the second leading cause of deaths in high income countries while it stands as the third leading cause of deaths in low- and middle-income countries (2). In 2012, 8.2 million cancer related deaths were recorded worldwide, of which 57% were males and 43% were females (3, 4). 12.7 million new cases of cancer were recorded in 2008 (**Figure 1**), of which 5.6 million occurred in developed countries and 7.1 million in developing countries (3). It is also estimated that 170 million years of healthy lives were lost because of cancer in 2008 (5). Specifically, 44% of cancer cases and 53% of cancer deaths occur in countries at low or a medium level of human developmental index (2). This represents an increase of 68% compared with 2012. More than half of all cancer deaths each year are due to liver cancer, lung cancer, stomach cancer, colorectal cancer and breast cancers combined (2). As such, extensive efforts into early detection of cancer are taking place in order to minimise its global burden.

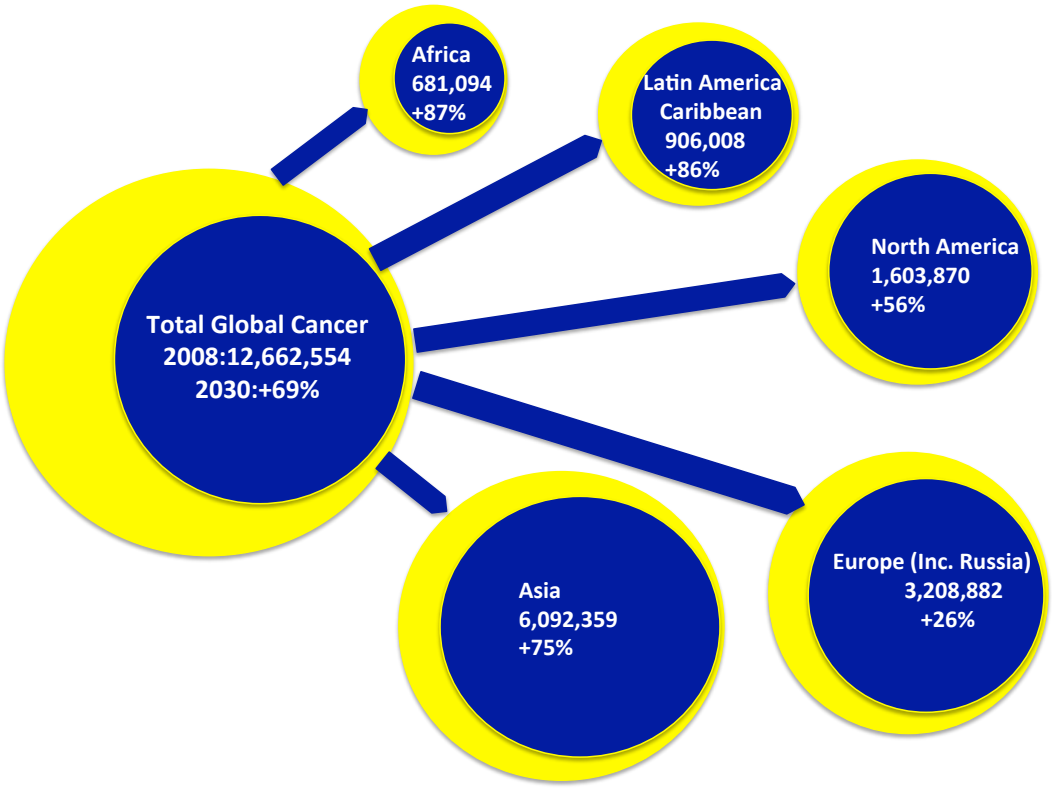


Figure 1: The growing menace of cancer. 12.7 million cases of cancer and 7.6 million deaths were recorded in 2008. In 2030, more than 21 million cancer cases are predicted to be recorded with 13 million deaths occurring. Adapted from (1).

Reports from Cancer Research UK in 2011, show that there are over 200 types of cancers and certain types have been shown to commonly cause cancer deaths worldwide (**Figure 2**) (6). These include cancers of the lung, liver, stomach, breast, bowel, oesophagus, prostate, cervix, ovary, kidney, uterus and bladder (6). Lung cancer is considered as the most common cancer in the world causing 1.6 million deaths due to its high fatality rates. Breast cancer is the second most common cancer with 1.7 million cases but ranks fifth in cancer deaths (522,000). On the other hand, 1.4 million cases of colorectal cancers are recorded causing 694,000 deaths. 307,000 deaths result from prostate cancer while, stomach cancers result in 600,000 deaths. Lastly, liver cancer results in 745,000 deaths.

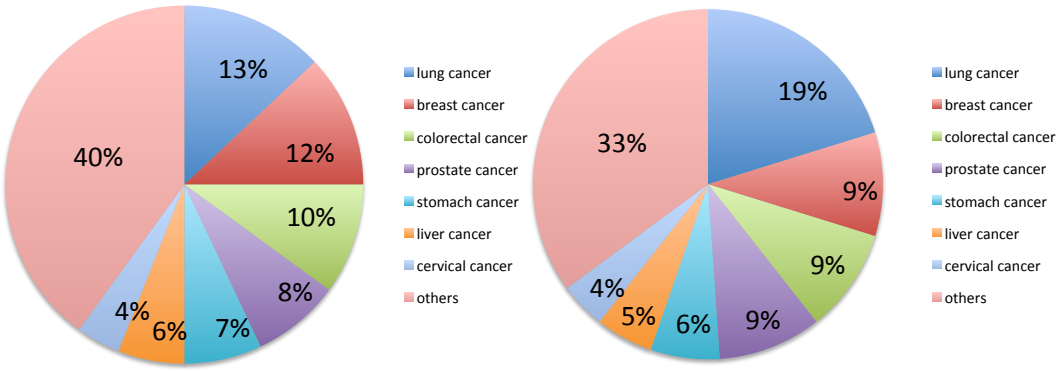


Figure 2: Most commonly diagnosed cancers in the world (left) and most common causes of cancer deaths (right) worldwide. Adapted from (7).

1.1.1.2 Cancer Statistics in the United Kingdom

In 2011, over 331,000 people in the UK were diagnosed with cancer (5). Subsequently, 352,000 new cases were recorded in 2013, with 960 cases diagnosed daily (5). 173,000 cases were diagnosed in females while 179,000 were recorded in males the same year. Around 163,000 cancer deaths were seen in 2014, with 450 deaths every day (5). This shows the devastating effect of cancer in Britain. It has been estimated that in every two minutes someone is diagnosed with cancer while someone dies from it in every four minutes. Since the 1970s, incidence rates for all cancers combined have increased by almost a 30% (5). It has been predicted that every 1 in 3 people will develop cancer at some time in their life (5).

1.1.1.3 Cancer Predictions

The burden of cancer is expected to rise to 23.6 million each year by 2035 (**Figure 3**) (3, 4). However, a combination of screening and treatment is increasingly effective in reducing the mortality of some cancers. As such, basic prevention through environmental and lifestyle intervention could be the best remedy for reducing the global burden worldwide (8).

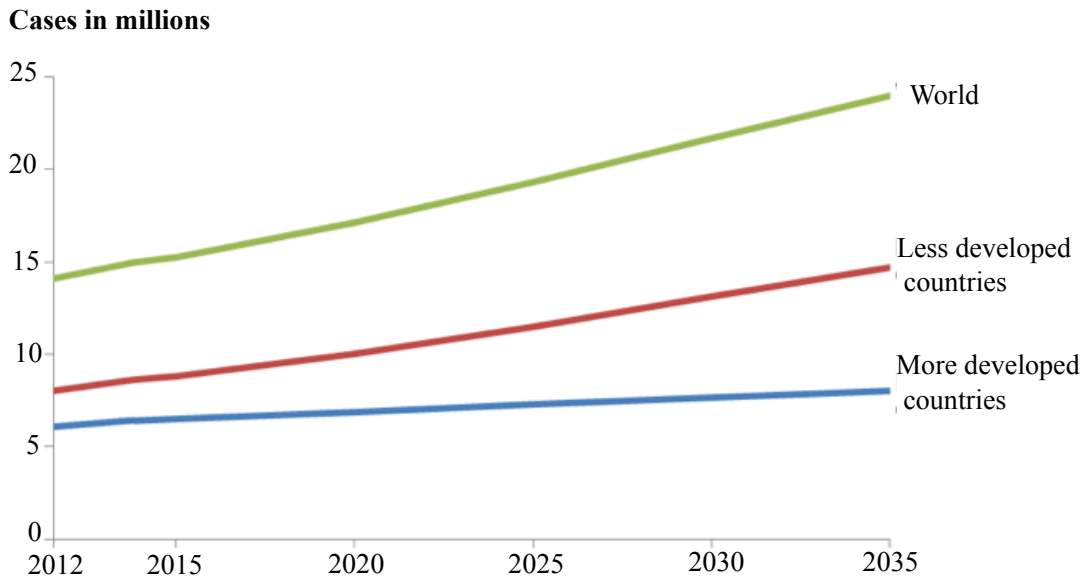


Figure 3: Global cancer cases predictions by 2035. Figure taken from (4).

1.1.2 Molecular Hallmarks of Cancer

Cancer is associated with an accelerated or abnormal growth of cells: the cells undergo different behavioural and metabolic changes causing them to excessively proliferate in order to escape surveillance and elimination by the immune system and spread to distant parts of the body (9). This process is also characterised by the mutation of oncogenes and tumour suppressor genes, activation of growth signalling pathways or loss of growth regulatory pathways (10). According to Floor *et al*, there are certain recognised basic characteristics of cancer (10). These characteristics are categorised into six biological capabilities and are acquired during the development of tumours (**Figure 4**) (11). First of all, there is evasion of apoptosis, a condition where the mechanisms of cell death are inhibited. Secondly, there is activation of metastasis and invasion, where primary tumour cells move from tumour masses and invade adjacent tissues (10). Moreover, there is induction of angiogenesis further stimulating the secretion of growth factors, which activate the signalling pathways to induce tumour vascularisation (10). There is also insensitivity to anti-growth signals, limitless replication is activated and

finally, self-sufficiency in growth signals (10). Alteration in the functions of these genes, for instance in the case of the tumour suppressor genes, leads to the disruption of the apoptotic signalling pathways leading to more immortal cells being created (12).

The basic characteristic of cancer cells involves their ability to maintain consistent chronic proliferation. Normal tissues control the release of growth signals, which ensure normal tissue architecture, and functions are maintained (11). Cancer cells develop the capability to maintain proliferative signalling in several ways; for example they produce ligands themselves, which induce autocrine proliferative stimulation (11). These cells may also send signals to activate normal cells within tumour-associated stroma and reciprocate by providing cancer cells with growth factors (13).

DNA sequence analyses of genomes of cancer cells have shown somatic mutation in certain human tumours, which predicts the activation of signalling pathways, usually triggered by activated growth factor receptors. Studies have shown that about 40% of human melanomas contain activating mutations affecting the MAP kinase pathway (14) and P13 kinase isoforms. Negative feedback loops have been shown to dampen several types of signalling. However, defects in feedback mechanisms have the ability of enhancing proliferative signalling. This instance is evidenced in Ras oncoprotein in that the oncogenic effects of Ras is not from hyperactivation of its signalling power but due to oncogenic mutations affecting Ras genes, which compromise Ras GTPase activity. This acts as an intrinsic negative feedback mechanism ensuring that active signal transmission is transitory (11). The study of oncogenic action has encouraged the idea that ever-increasing expression of cancer genes manifested in their protein products would result in correspondingly increased cancer cell proliferation, leading to tumour growth. Increased signalling by oncoproteins such as Ras, Myc and Raf induce the induction of cell senescence. Cells exhibiting features of senescence, such as enlarged

cytoplasm and absence of proliferation markers, are abundant in tissues of mice engineered to overexpress certain oncogenes (15) and are prevalent in some cases of human melanoma (16). Many tumour suppressors that function in various ways to reduce cell growth and proliferation have also been identified through their characteristic inactivation in animal or human cancers. Changes in these genes and regulatory pathways could result from DNA damage and viral transformations (12). There are two groups of genes affected:

- Proto-oncogenes are group of genes that cause normal cells to become cancerous when they are mutated. Mutations in these genes are usually dominant in nature and their mutated version is referred to as oncogene. Proto-oncogenes encode proteins that inhibit cell differentiation, stimulate cell division and halt cell death. However, oncogenes show increased production of these proteins causing increased cell division, decreased cell differentiation and inhibition of cell death. Examples of proto-oncogenes include HER2 gene, which codes for transmembrane tyrosinase kinase receptor called Human Epidermal Growth factor receptor (17).
- Tumour-suppressor genes are usually involved in the regulation of cellular proliferation. These genes encode for proteins that are involved in inhibiting the proliferation of cells, which is vital to normal cell development and differentiation. Due to this ability, these genes can act to stem the uncontrolled growth of cancer cells. Mutations in these genes give rise to the development of cancerous tumour. An example is TP53, which encodes a protein called TP53 (17).

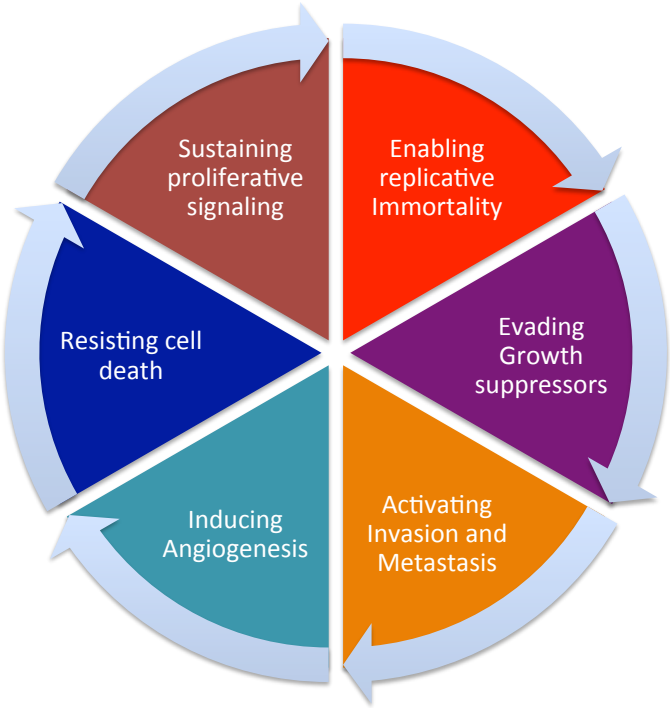


Figure 4: Six main hallmarks of cancer. Adapted from (11).

1.1.3 How is Cancer Staged?

The staging of cancer helps to determine the extent of the cancer in order to provide clinicians with the means to quantify prognosis and therapy for patients. This is usually done when a patient is firstly diagnosed before treatment (18). In addition, it enables descriptive and statistical analysis of the tumour registry data and this is important for looking at trends over time. The main types of staging cancer include clinical and pathological staging (18). Clinical staging is focused on estimating the extent of cancer based on physical examination as well as laboratory diagnosis such as blood tests, tumour biopsies and imaging. On the other hand, pathologic staging is focused on determining the extent of cancer spread during surgeries (18). Various staging systems are used to classify cancer. This involves the Tumour Node Metastasis (TNM) and number staging systems. However, the American Joint Committee on cancer and the International Union of Cancer Control, maintain the TNM system as the tool for doctors to stage different cancers (**Table 1**). In the TNM staging, each cancer is assigned a letter

to describe the tumour, node and metastasis. Thus, T denotes the size and growth of tumour, N informs whether the cancer has reached the lymph nodes while M represents the cancer spread to different parts of the body (18).

Table 1: The TNM staging of Cancers (18).

TNM STAGING	DESCRIPTION
TX	Tumour cannot be evaluated
T0	No primary evidence of primary tumour
Tis	Cancer cells are only growing in superficial layer of tissues
T1-T4	Size and Extent of primary tumour
NX	Lymph nodes cannot be evaluated
N0	Lymph nodes do not have cancer
N1-N3	Cancer spread to lymph nodes
M0	No cancer spread
M1	Cancer has spread to distant parts of the body such as tissues and organs

1.1.4 Who is at Risk?

Anyone can develop cancer although the risk of being diagnosed with it increases with age. Reports have shown that 58% of newly diagnosed cancer cases occur usually at 65 years of age or older compared with 48% in developing countries. For most cancer types, the risk is higher with a family history of the disease. Cancer can be caused by a number of external factors such as continued exposure to ionising and non-ionising radiations, ultraviolet radiations and asbestos (19). Tobacco smoking by far is the largest contributing cause of cancer followed with risk percentage of 25-30% and 30-35% respectively, as well as excessive intake of alcohol, poor diet, physical inactivity and exposure to environmental pollutants (19). Viral infections caused by Hepatitis B virus (HBV), Hepatitis C virus (HCV) and Human Papilloma virus (HPV) have been reported to be risk factors for cancer occurrence (20). 5%-10% of cancers are attributed to genetic defects inherited from parents (21). Hormones such as the Insulin-like growth factors (IGFs) play a vital function in accelerating the proliferation of these cancer cells (20). However, treatment options, such as surgery, radiation, chemotherapy and immunotherapy have been developed to manage people affected (6). With the growing complexity of cancer, there is the need for more comprehensive, integrated and robust treatment options while minimised toxicity is maintained.

1.1.5 Hidden Costs of Cancer

Reports have indicated that the financial cost of cancer is substantial. This involves expenditures for treatment, care and rehabilitation related to the illness. Secondly, indirect cost involves the loss of economic output due to premature death (7). The exact costs of global cancer are not really known but thought to be in the hundreds of billions of dollars per year. Cancer costs the world more than any other disease (**Figure 5**). It cost $895 billion annually as compared to heart disease and diabetes, which costs $753

billion and £204 billion respectively (22). People suffering from cancer face financial stress due to loss of income while having to deal with other costs such as hospital travel, increased fuel bills and gloomy economic climate (22). About four in five cancer patients in the UK are hit with average costs of £570 a month as a result of their illness (23). One in three persons with cancer in the UK lose £860 per month in earnings because they are unable to work or have cut down their hours (23). The biggest financial impact in terms of loss of life and productivity in which cancer accounts for 1.5% of global gross domestic product losses (23).

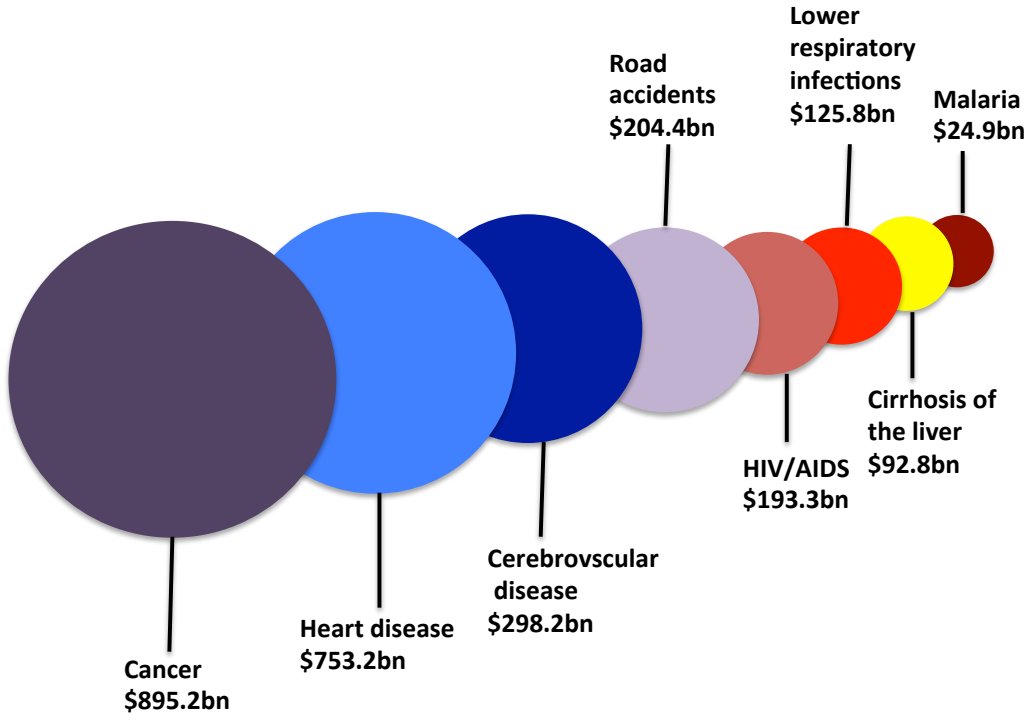


Figure 5: The costs of cancer. Cancer costs outweigh the costs from other ill health such as heart diseases, cerebrovascular diseases, HIV/AIDS, road accidents, lower respiratory infections and malaria. Adapted from (7).

1.2 The Liver and Hepatocellular Carcinoma

1.2.1 Anatomy and Physiology of the Liver

The liver is a reddish brown wedge-shaped organ, which lies below the diaphragm and at the upper right quadrant of the abdominal cavity (**Figure 6**) (24). It is regarded as the largest internal gland in the body weighing between 1.44kg to 1.66kg. The liver is covered in a serous coat derived from the peritoneum and has an inner fibrous coat to which it is firmly adhered. This organ is linked to a number of blood vessels, namely the hepatic artery, portal vein and the hepatic vein. Blood rich in digested nutrients are carried from the gastrointestinal tract, spleen and pancreas to the liver via the hepatic portal vein, while oxygen rich blood is carried from the aorta by the hepatic artery. The hepatic vein carries deoxygenated blood from the liver to the inferior vena cava of the heart. The liver usually consists of microscopic functional units called the lobules (25). These lobules are made up of millions of hexagonal hepatocytes radiating from the acentral vein (**Figure 7**) (26). These carry out the main functions of the liver such as removing exogenous and endogenous materials from the blood and also involved in a number of metabolic processes, such as metabolism of carbohydrate, protein and lipids, production of bile, urea, enzymes, albumin, and clotting factors (25). Other units of the liver include Kupffer and Stellate cells which act as macrophages to clear pathogens and store vitamin A respectively. The bile ductile collects blood secreted by the hepatocytes while the sinusoids are enlarged capillaries through which blood from the hepatic portal vein enters via the portal triads and then drains to the central vein (**Figure 27**). The liver emerges from a ventral mesogastrium and only the upper posterior surface is outside the structure (27). It is smooth and featureless on the diaphragm and presents with a number of indentations on the visceral surface where it connects the

adrenal glands, stomach and the kidney (27, 28). This shows how vital this organ is to the human body and hence a defect could result in fatal complications leading to death. The risk of hepatocellular carcinoma accelerates significantly in the presence of an established liver disease.

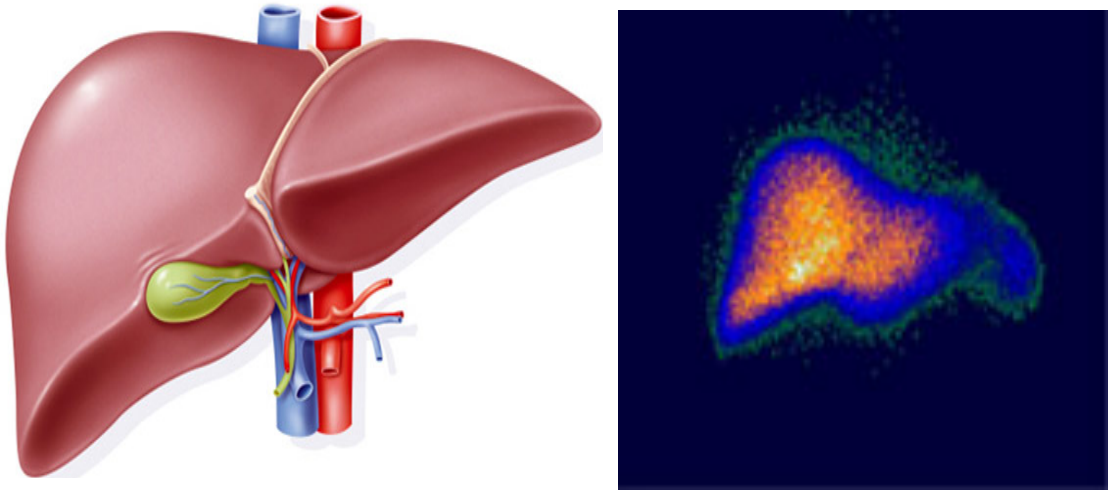


Figure 6: An anatomical illustration of the liver and gall bladder (Left) and a nuclear medicine scan of the abdomen (Right) revealing the liver and the gall bladder (Right). Figure taken from (24).

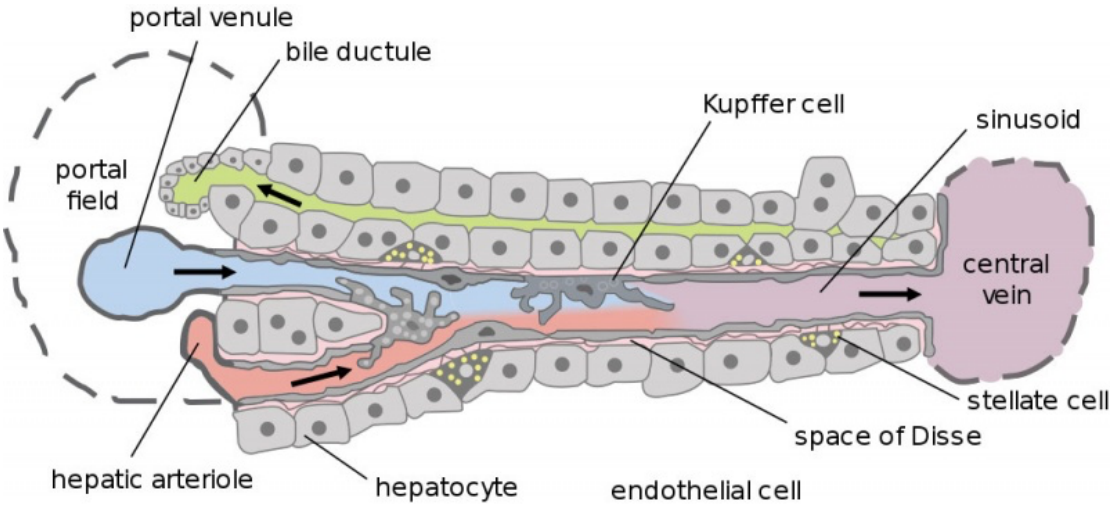


Figure 7: Microscopic anatomy of the liver showing the basic components such as hepatocytes, lobules, ducts and blood vessels. Figure taken from (26)**.**

1.2.2 Hepatocellular Carcinoma: Demographics and Epidemiology

1.2.2.1 Incidence, Mortality and Geographical Distribution

Hepatocellular carcinoma (HCC) also referred to as malignant hepatoma, is a primary liver cancer which is reported as the fifth most common cancer and the third most common cause of cancer-related deaths worldwide, resulting in 600,000 deaths each year (29, 30). More than 800,000 new cases of HCC are diagnosed yearly (29). The incidence of HCC has tripled since 1980; from 2004 to 2013 (29). This shows the aggressive nature of the cancer. Epidemiological studies have revealed that Eastern Asia and sub-Saharan Africa have increased incidence of HCC where China accounts for over 50% of cases in the world (31), while a decreased incidence is recorded in Europe, South and Northern America (31). For example, the incidence is 99 per 100,000 in Mongolia, 49 per 100,000 in Korea, 35 per 100,000 in China (**Figure 8**). Other regions in Africa that raises more concerns are Gambia, Guinea, Mali and Mozambique. Despite the fact that the incidence is low in the developed world, USA and Japan are slowly falling victim to the burden of HCC (32). The incidence is gradually increasing in the Great Britain, where between 1975 and 2009, HCC rates increased from 1.4 to 4.7 per 100,000 populations and 3,800 liver cancers deaths were recorded in 2010 (33). The HCC mortality rates have drastically increased in some European countries such as Italy and France over the past 40 years by 85% in an assessment undertaken from 1970-2010 (34). The aggressive nature of HCC demands a careful and cutting-edge research into its microenvironment to investigate the mechanisms of escape and resistance. This could provide a well-tailored knowledge on novel antigenic targets for personalised treatment.

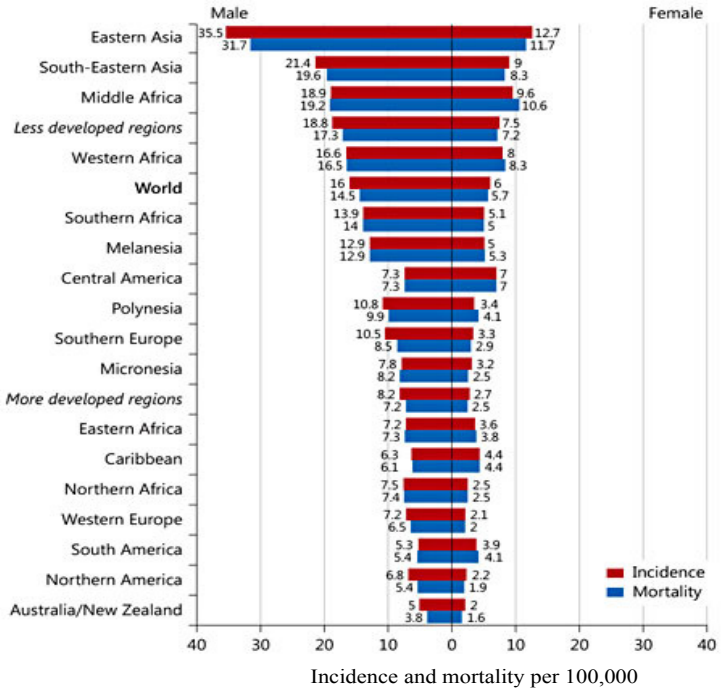


Figure 8: Incidence and mortality of hepatocellular carcinoma worldwide. Figure taken from (7).

1.2.2.2 Predisposing conditions to Hepatocellular Carcinoma

1.2.2.2.1 Age

HCC incidence is strongly associated with age and gender, with the highest incidence occurring in older males than females. Studies have shown that global age distribution of HCC varies by region, incident rate, sex and aetiology (3). However, a shift in incidence of HCC in younger individuals has been reported for at least two decades (35). Female rates peak in the age group 5 years older than the peak age group for males. Mortality rates in low-risk populations, such as United Kingdom (**Figure 9**), are higher amongst the elderly (namely 75 years or older (36). These different age specific patterns are likely to be related to differences in the dominant hepatitis virus in population that can lead to the development of HCC, or the age at viral infection. Most male HCC deaths occurred between the ages of 70 and 74 in the UK in 2007, whereas most deaths

in females occurred at age of 85 years and above. In contrast, in Japan, the peak age is between 70 and 79 years, where chronic hepatitis C virus (HCV) infection is the most important risk factor for HCC. On the other hand, in Europe and North America, most patients are between 60 and 65 years old at diagnosis (37).

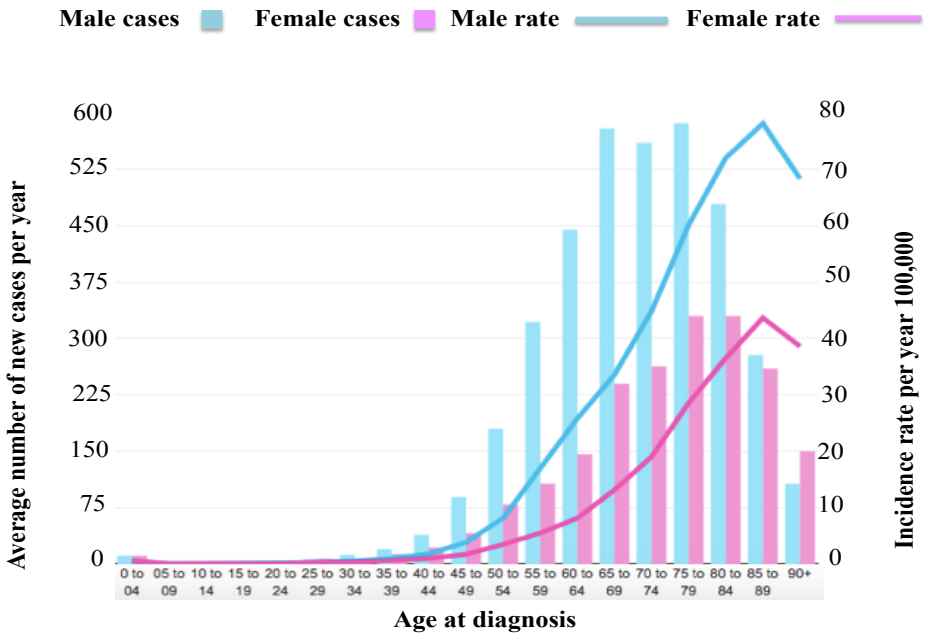


Figure 9: Age specific HCC incidence rates per 100,000 population among males and females in the UK, 2013-2015. Figure taken from (36).

1.2.2.2 Gender

HCC occurrence varies with gender (**Figure 10**), where males reportedly show a higher rate of liver cancers than females (38). Most male: female ratios range between 2:1 and 4:1. HCC is considered as the fourteenth most common cancer in males. This is evident in a study where the occurrence of HCC was two to four times more in males than females (39). This could be attributed to the fact that men are at a higher risk of HCV and HBV infection, they consume more cigarettes and alcohol and have an increased iron store (40). Elevated androgen levels have also been demonstrated to enhance HCC progression (41). In 2013, 5,413 new cases of liver cancer were recorded in the UK, of

which 3,491 were males (which represents 64%) and 1922 were females (which represents 36%). The high rate in males could be also be attributed to sex specific differences in exposure to risk factors (5). An experiment undertaken in mice revealed a two to eight fold increase in HCC development in male mice (42). A study conducted by Yeh *et al*, affirms that due to the stimulatory effect of androgen and the protective effects of eostrogen men tend to have higher HCC incidence than females (43). Androgens act as tumour promoters by inducing DNA damage and oxidative stress (44). Yeh *et al*, further conducted a study in which a knockout of androgen receptor expression in hepatocytes, delayed development of N'N'diethylnitrosamine induced HCC. Further studies show that oestrogen protects the hepatocytes from malignant transformation via downregulation of Interleukin 6 (IL-6) release from Kupffer cells, which is highly dependent on MyD88 (43). Factors such as high body mass index and higher levels of androgenic hormones can also affect males' risk (45).

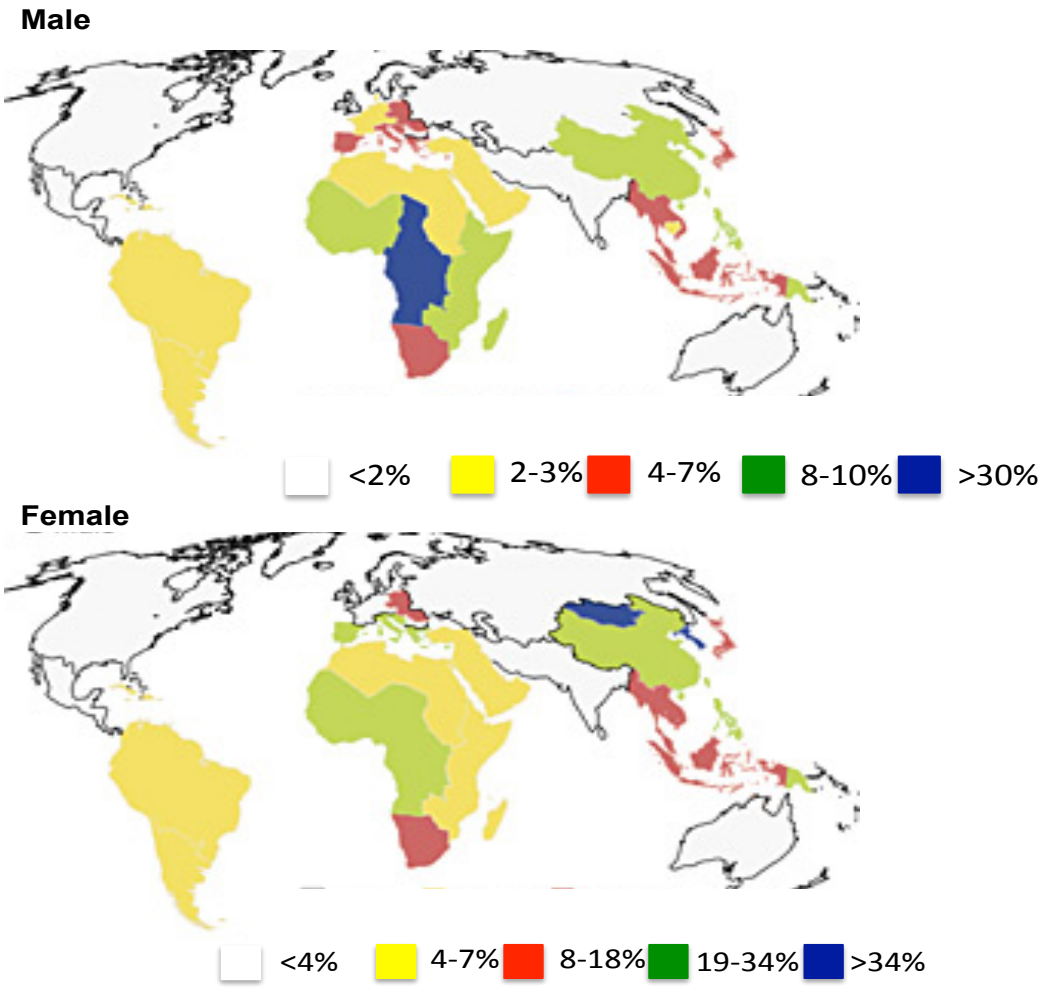


Figure 10: The incidence of hepatocellular carcinoma in both males and females worldwide. Higher incidences are recorded in Sub-Saharan African countries and Asia. Figure taken from (46).

1.2.2.3 Ethnicity

The incidence of this cancer varies among race and ethnicity as the rate of HCC is two times greater in Asians than Americans and Africans (3). Ethnicity has an adverse impact on the incidence of HCC as well as patients' response to treatment. The reason behind the ethnic variability is attributed to the differences in prevalence and acquisition time as the major risk factors for liver disease such as HBV and HCV are more endemic in South-east Asia and Sub-Saharan Africa (47). The incident rates vary among different populations within a particular region. For instance, Chinese, ethnic Indian and Malay populations of Singapore had age-adjusted rates ranging from

21.21/100000 among Chinese males to 7.86/100000 among Indian males (3). HCC is more common among the Asians and African Americans with chronic hepatitis C virus than Caucasians in the United States. A case control study of 464 patients with Hepatitis C and cirrhosis (207 cancer patients and 257 controls) was conducted from four San Francisco Bay medical centers in order to examine ethnicity as a potential HCC risk factor in patients with chronic hepatitis. After the medical records and pathology were examined, a cancer risk was significantly increased in Asians and African American men compared with Caucasians (48). Consequently, the incidence of HCC was consistently low in Caucasian whites, while rates gradually rise in Black, Hispanic white, Japanese, Chinese, Korean and Filipino (48).

Wong *et al,* further revealed that the incidence of HCC among Asians was the highest, thus double that of white Hispanics and four times higher than that of Caucasians (49). The mortality rates from cirrhosis of the liver and primary liver cancer were examined among first generation migrants to England and Wales. Results showed a two-fold rise in mortality from cirrhosis among men from East Africa, Bangladesh and India. There was also a significant increase in mortality amongst Bangladeshi and African-Caribbean migrants (50).

Artinyan *et al*, investigated the relationship between race, ethnicity and socioeconomic status on the survival of HCC patients. Black and low-income individuals had the poorest long-term survival as compared to Asians and Hispanics who had the best survival. These outcomes were despite the fact that the appropriate and equivalent treatment was administered to these groups of patients. This means that the significant racial and ethnic disparities in the outcome of HCC patients persist despite the receipt of comparable treatment. This indicates that genetic differences would have a greater bearing on patient survival (51). Chen and his co-workers conducted a spatial analysis

to determine the geographic variation of liver cancer and its relationship with immigration in Ontario. Risk factors such as alcohol, drinking, smoking, obesity and diabetes mellitus were found to be insignificant in elucidating the significant variation detected. It was noticed that the rise of African and Asian immigrants was the explanation for the clustering of liver cancer in Ontario (52).

1.2.3 Major Risk Factors of Hepatocellular Carcinoma

HCC occurs within the background of cirrhosis. Cirrhosis is a liver condition which develops after long periods of fibrosis of the liver (large amount of scar tissues replacing normal healthy tissues). This provides the environment for the cancer cells to develop. There are several risk factors associated with HCC (**Figure 11**). However HBV and HCV infections are regarded as the most frequent risk factor of HCC (53). Chronic infections caused by HBV and HCV account for 75% of all HCC cases whereas metabolic disorders, genetic and alcohol account for less than 25% (54).

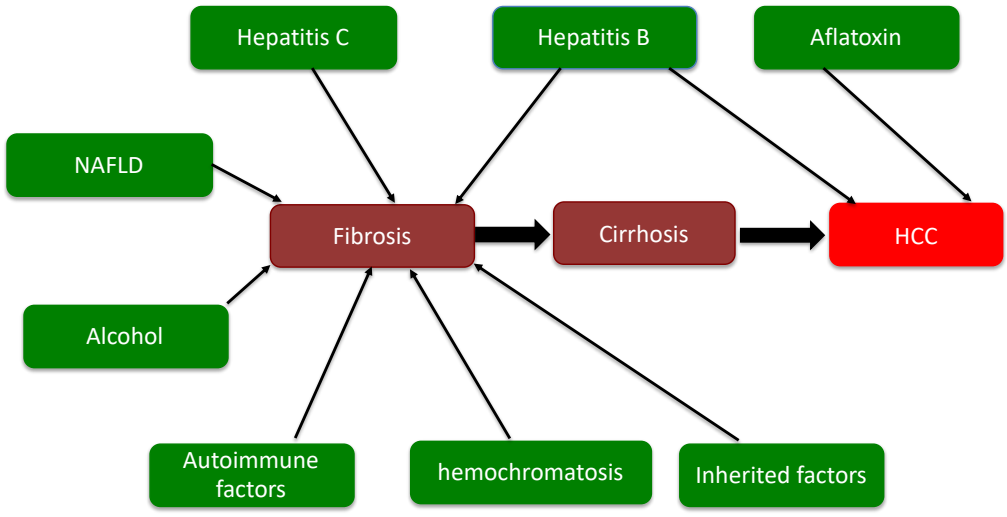


Figure 11: Risk factors of hepatocellular carcinoma. Hepatitis B and C viruses, excessive alcohol intake, Aflatoxins, Non-Alcoholic Fatty Liver Disease (NAFLD), hemochromatosis influence a normal healthy liver to develop into Hepatocellular carcinoma. Adapted from (55).

1.2.3.1 Hepatitis B Virus (HBV)

Globally, HBV is considered as the most frequent risk factor of HCC, causing 320,000 deaths every year (56). HBV infection is associated with most cases of cirrhosis in high-risk countries as well as 80% of the HCC cases. The majority of the cases of HBV are in Africa, Asia and Western Pacific region (56). Previous works have shown that there is a 5 to 15-fold increased risk of developing HCC in chronic HBV carriers compared with the general population and this usually occurs at HBV endemic areas (57, 58). About 70% and 90% of HBV-related HCCs occur in patients with cirrhosis although in some cases occur in the absence of cirrhosis (47).

HBV belongs to the Hepadnaviridae family and it is a partially double-stranded DNA containing virus. The virus is usually transmitted from mother to child. However, this is different in areas with low HCC incidence rates, where HBV is acquired in adulthood through sexual intercourse with more than 90% of acute infections resolving spontaneously (47). Certain factors have been shown to accelerate the risk of HCC among HBV carriers including males, older age, Asian or African race; cirrhosis; family history of HCC; exposure to aflatoxin, alcohol, or tobacco; or co-infection with HCV or hepatitis D virus (HDV). Persons who are immune to HBV infection have a substantially lower risk of acquiring HCC.

Hepatitis B vaccination is widely recognised as the most effective measure to prevent HBV infection. The first evidence that HCC is preventable via effective vaccination was revealed in a study undertaken in Taiwanese children (59). Ten years after the initiation of the immunisation program, the incidence of HCC among 6- to 14-year-olds in Taiwan declined dramatically (59). The average incidence of HCC declined from 0.7 per 100,000 children from 1982 to 1986 to 0.36 from 1990 to 1994. Goldstein *et al*, used mathematical modeling to estimate that there were 620,000 persons who died from

HBV related causes worldwide: 580,000 from chronic infection related cirrhosis and HCC. The model estimated that 64.8 million people would become HBV infected while 1.4 million would die from HBV related diseases without vaccination. Routine infant hepatitis B vaccination, with 90% coverage and the first dose administered at birth, would prevent 84% of global HBV-related deaths (60).

The impact of HBV infection on the progression of HCC is reflected by the correlation between increased HCC incidences in patients with high HBV DNA in serum (61). The HBV DNA integrates into the host genome and induces chromosomal instability (62). It encodes viral proteins such as HBx that modulates gene transcription and regulates cell response to protein degradation and cell stress (63). It further enhances the carcinogenic process interfering with DNA repair mechanisms by altering the expression of cell cycle control genes such as JNK, ERK, REF, Ras and P53 (64).

1.2.3.2 Hepatitis C Virus (HCV)

Chronic HCV infection is also a major risk factor for HCC development. The rising incidence of HCC is linked to the epidemic of chronic HCV (65). Recent studies have shown that chronic HCV infection affects about 71 million people globally (66, 67), where 20% of chronic HCV cases lead to liver cirrhosis (**Figure 12**) and 2.5% result in HCC (68). HCV infected patients are at about a 17%-fold increased risk of developing HCC (69). In Japan about 80% to 90% of HCC cases are due to HCV while in Italy and USA, it is responsible for 40% to 60% cases (70). Africa and Asian countries tend to have a high prevalence of HCV-associated HCC (71). The risk of acquiring HCV-associated HCC actually depends on the severity of underlying liver disease (72). Recent studies have indicated that about 80% of people infected with HCV do not successfully eliminate the virus and hence progress to the chronic stage (73). Gradual

inflammation due to hepatitis leads to chromosomal damage and HCC progression (73). HCV-contaminated blood and hemophiliacs have been observed to contain the highest incidence rates for cirrhosis and HCC. However, lowest rates of developing HCC have been reported in women who received a one-time contaminated anti-D immune globulin treatment (70). The likelihood of the development of HCC among HCV-infected persons is difficult to determine due to the scarcity of adequate long-term cohort studies. However, the best estimate is from 1% to 3% after 30 years.

HCV belongs to the Flaviviridae family (62). Unlike HBV, HCV is an RNA virus and cannot integrate into the host genome. It usually localises at the outer membranes of the endoplasmic reticulum and mitochondrion as part of its replication process and cause oxidative stress, which further enhances pro-inflammatory cytokine production (73). This mechanism leads to the activation of P38-MAPK and Nuclear Factor Kappa Beta (NF-KB) signalling pathways and therefore altering the apoptotic pathways and accelerating tumour formation (74). NS3 and NS5A are non-structural proteins of HCV and alter the P53 regulatory pathway responsible for controlling cell survival and cell cycle progression (75, 76). Furthermore, it has been deduced that HCV together with co-infection with HBV and excessive alcohol intake further increases risk of HCC development (77). HCC risk has been shown to be increased by 17-fold in HCV infected patients compared with HCV negative controls in a meta-analysis of 21 case-control studies where second-generation enzyme immunoassay tests for anti-HCV were used (69).

1.2.3.3 Alcohol

The World Cancer Research Fund and the American Institute concluded alcohol consumption for Cancer Research as probably a direct cause of cancer in 2007 (78).

Excessive ethyl alcohol or ethanol intake, namely ingestion of more than 50–70 g/day for prolonged periods, is regarded as a frequent contributing factor to HCC development (**Figure 12**). There is an established evidence for a synergistic effect of heavy alcohol ingestion with HCV. These factors seemingly function together to increase HCC risk by promoting cirrhosis. However, with the presence of HCV infection, there was an additional 2-fold increase in HCC risk over that which was observed with alcohol use alone (69).

High alcohol intake induces the production of proinflammatory cytokines via monocyte inactivation (79). It also causes the induction of higher concentration of circulating endotoxin activating Kupffer cells (79). These cells release many cytokines and chemokines such as Tumour Necrosis Factor α (TNFα), Interleukin 1β, Interleukin-6 and prostaglandin E2 (79). These have massive effect on the hepatocyte survival. Excessive alcohol intake damages the liver by oxidation thus, ethanol accelerates injury to the mitochondrion by enhancing reactive oxygen species production and hepatic glutathione production in the liver (79). This mechanism contributes to HCC development by enhancing cirrhosis and fibrosis progression (80). Reports have also shown that oxidative stress enhances the accumulation of oncogenic mutations (81). Some case control studies have shown that alcohol independently causes an induction of cirrhosis (82) and HCC (69) although a higher prevalence is seen with HBV and HCV infection. A case control study showed that synergistic relationship between alcohol intake and hepatitis virus infection significantly increased the risk of liver cancer (69). These findings were confirmed by Yamanaka *et al,* where cirrhotic patients with heavy alcohol intake and HCV infection are at a higher risk of developing HCC than those with alcoholic cirrhosis (83).

1.2.3.4 Aflatoxin B1

Aflatoxin B1 (AFB_1) is a mycotoxin produced by Aspergillus, which is a powerful hepatocarcinogen in increasing the risk of HCC (84). In Africa and Asia, the climate and storage techniques support the growth of this fungus on contaminated grains, corn and legumes, hence increased incidence of Aflatoxin B1-associated HCC in these regions (64). AFB_1 was classified as a powerful hepatocarcinogen by the International Agency for Research on Cancer based on experiments undertaken in animals (47). Short-term prospective studies in Shanghai, China showed that interaction between AFB_1 exposure and chronic HBV infection increases one's risk of having HCC. Aflatoxin is regarded as a mutagen since it has been shown to cause mutations in P53 (85). This mutation has been observed in 30%–60% of HCC tumors in aflatoxin-endemic areas (86). Once the aflatoxin is absorbed into the human body, it metabolises to an active intermediate AFB1-exo-8, 9 epoxide that binds to DNA and induces mutation of the codon 249 in P53 tumour suppressor gene (87). This up-regulates insulin-like growth factor II which subsequently decreases apoptosis (47).

1.2.3.5 Non-Alcoholic Fatty liver disease (NAFLD)

Nonalcoholic fatty liver disease is regarded as the most common liver disorder in western countries (88) and occurs in the absence of alcohol use, although the hepatic histology appears consistent with alcoholic hepatitis (89). NAFLD has been shown to be closely linked with metabolic syndrome, particularly type 2 diabetes mellitus and obesity (90), where NAFLD occurs mostly among diabetic patients who are morbidly obese (91). NAFLD together with multiple components of the metabolic syndrome is thought to accelerate the risk for developing chronic liver disease, cirrhosis, and HCC (90). Studies show that 20% of the individuals with NAFLD present with

steatohepatitis, while the majority only have steatosis (92). The risk for developing HCC is more in Hepatitis B than in NAFLD but due to the increasing prevalence, NALFD and non-alcoholic steatohepatitis (NASH) are gradually becoming identified as underlying risk factors in patients with newly diagnosed HCC (93).

Insulin resistance (IR) is considered as an established driver of NAFLD. IR is described as a pathological condition where cells fail to respond normally to insulin and it is closely associated with obesity (91). IR causes increased peripheral lipolysis and increases circulating fatty acids that are taken up by the liver leading to accumulation of hepatic triglyceride in the liver or fatty liver. Accelerated intrahepatic fatty acid levels are also thought to provide a source of oxidative stress, which is vital in the development from steatosis to steatohepatitis (94). Hepatic mitochondria produce reactive oxygen species (ROS), which oxidize fat deposits to discharge lipid peroxidation products, and in turn causes oxidative damage to the mitochondrial genome (95). ROS and lipid peroxidation products enhance the production of proinflammatory cytokines, including TNF-α, Tumour Growth factor (TGF)-β, and Fas ligand as well as inducing pro-oncogenic signals, and epigenetic changes (96, 97). These activate stellate cells and further drive the development of fibrosis (98).

A study conducted by Calle *et al*, revealed that amongst 900,000 individuals the risk of HCC was found to be 4.5 times higher in males with a high body mass index than those with normal BMI (99). Another study reported a doubling in HCC incidence in patients with diabetes mellitus (DM) (53). However, studies undertaken found some contrasting outcome as there was no increased risk of HCC from obesity and diabetes mellitus (DM) in HBV/HCV endemic population, thus confirming that NAFLDs association with cirrhosis related HCC is far from straight forward (100).

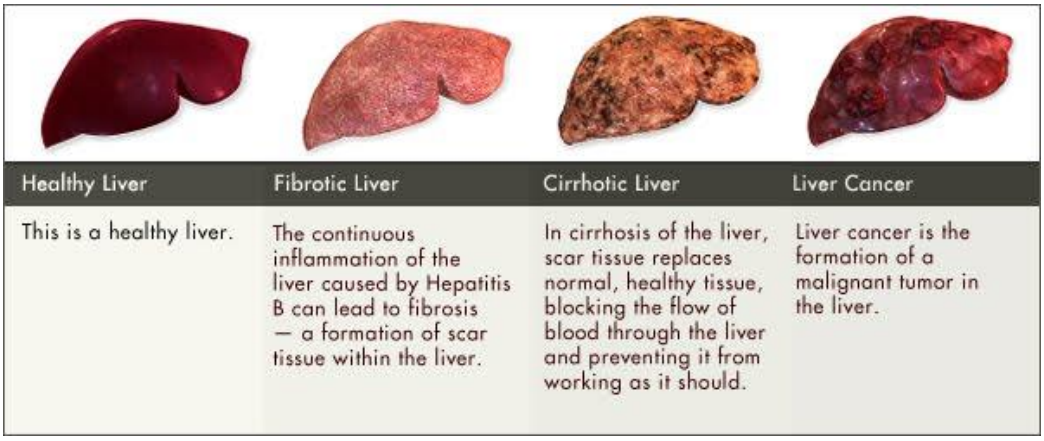


Figure 12: Stages of development of hepatocellular carcinoma. The above diagram shows the progression of a normal healthy liver to hepatocellular carcinoma as result of factors such as HCV, HBV, excessive alcohol intake, aflatoxins obesity, NAFLD, tobacco, hemochromatosis, etc. Figure taken from (101).

1.2.3.6 Other Risk Factors

There are other risk factors, such as older age (especially over 75 years), tobacco use, poor diet, (102, 103), overdose of oral contraceptives, hemochromatosis, vinyl chloride (104) as well as co-infection with HIV and diabetes. With respect to Hemochromatosis, the progressive accumulation of iron leads to fibrosis and cirrhosis and promotes the development of HCC (92). Patients who are affected have a 20-fold higher risk to develop HCC. An overdose of oral contraceptives have been shown to contain high levels of oestrogen and progesterone and these promote the formation of liver tumours in animals (41). These hormones cause liver neoplasia by increasing rates of spontaneous mutations (105, 106). 20% to 30% of cirrhotic patients have overt diabetes and impaired glucose tolerance. A study conducted by El Serag *et al*, showed significantly increased risk of HCC with diabetes (107). A low vegetable intake diet increases HCC risk in patients with HBV, in that some vegetables contain components such as Chlorophyllin, which has anti-cancer properties by inactivating carcinogens

(108). Moreover, low levels of selenium have also been reported to increase HCC progression (109).

1.2.4 Mechanism of Hepatocarcinogenesis

Hepatocellular carcinogenesis usually does not occur in a healthy liver during normal aging but the risk of acquiring the cancer is increased in response to chronic liver injury at the cirrhosis stage (54). Hepatocellular carcinoma develops when there is mutation in the cellular machinery and causes the cells to replicate at a higher rate (**Figure 13**) (110). Cirrhosis is a condition highly associated with hepatocarcinogenesis, which occurs after long latencies (20-40yrs) of chronic liver disease although the risk of HCC is quite low during chronic liver disease stage (110). This is attributed to the fact that at the cirrhotic stage, the liver's regenerative capacity is exhausted (111). The process of Hepatocarcinogenesis is quite complex involving the accumulation of epigenetic and genetic changes, as well as alterations in signalling pathways that occur during the initiation and progression stages of the disease (111). A number of mechanisms occurring at the cirrhosis stage of the liver accelerate the formation of cancers.

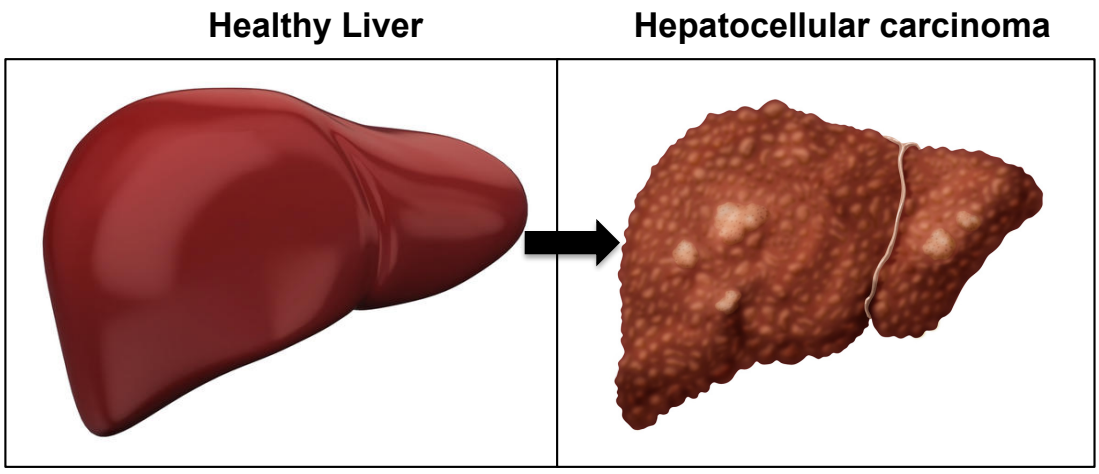


Figure 13: A schematic diagram comparing a healthy liver to hepatocellular carcinoma. Adapted from (111).

The telomerase plays a very important role in maintaining telomere length and chromosomal stability (112). During the cirrhotic stage, there is dysfunction of this enzyme, which leads to the shortening of the telomeres (113) which results in the accumulation of senescent hepatocytes (113). Acceleration of telomere shortening during the cirrhotic stage induces chromosomal uncapping leading to DNA damage signals, cell cycle arrest, senescence and apoptosis (**Figure 14**) (114). Telomere shortening increases the initiation of liver tumours in telomerase deficient mice in response to carcinogen treatment and supports the fact that telomere dysfunction enhances HCC formation (115). Recent studies have reported that dysfunction of the telomere at the cirrhotic stage drives the activation of DNA repair pathways leading to chromosomal fusions hence, cells with fused chromosomes tend to enter the cell cycle (116). This results in chromosomal translocations in daughter cells hence, initiating the formation of liver tumours (115). The decrease in proliferation of the hepatocyte at the cirrhosis stage itself enhances cancer formation. This was demonstrated in a rat model where administration of hepatocarcinogenic compounds (Aflatoxin B1, diethyl nitrosamine and N-hydroxy-2-acetylaminofluorene), which limited hepatocyte proliferation, enhanced liver tumour formation (117).

During cirrhosis there is the activation of stellate cells which induce the production of extracellular matrix proteins, cytokines and oxidative stress products (118). These tend to impair hepatocyte proliferation and initiate tumour formation (119). A study conducted in a cholestasis hepatitis mouse model showed that deletion of NF-KB impaired HCC progression (120). Another study showed that the deletion of suppressor of cytokine signalling-3 (SOCS3), a negative regulator of interleukin-6-related cytokine promotes hepatocarcinogenesis in mice (121). This informs the impact of inflammatory immune response on HCC progression. According to Wiemann *et al*, there is increased

expression of MDM2 and Gankyrin during cirrhosis, which abrogates cell cycle checkpoints P53 and Rb/16 (122). P53 and Rb/16 limit cell survival and proliferation in response to telomere shortening and cause cell cycle arrest during oncogene activation (122). Impairment of these genes at the cirrhosis stage leads to proliferation of more hepatocytes with dysfunctional telomeres and therefore increasing chromosomal instability and initiating HCC (115). Mutations in the P53 gene can occur as a result of oxidative stress. Mutations in P53 could also impair the expression of other cyclin dependent kinase inhibitors such as P14AR7 and p27, which contributes to HCC progression (123). A study conducted by Plentz *et al*, showed increased expression of ID1, an inhibitor of P16 in HCC patients (124). In more than 80% cases of HCC, Rb, P16 and P15 checkpoints are rendered dysfunctional (124). Heterozygosity loss in the Insulin Growth Factor receptor 2 (IGFR2) locus is considered as a very frequent and early event in hepatocarcinogenesis (125). This receptor alters proliferation of cells by promoting degradation of Insulin-like Growth Factor 2 mitogen and enhancing the activation of TGF-β signalling (126). Aging on the other hand, has been shown to promote hepatocarcinogenesis. This is evident in a study where aging impaired hepatocyte proliferation in mice by inducing CCAAT/ enhancer binding protein α mediated expression of E promoter binding factor (127).

Activation of certain oncogenic pathways during the cirrhotic stage induces HCC progression. Pathways such as the Wnt/β-catenin pathway (**Figure 15**) are regulated tightly during early liver development (128). This pathway is responsible for cell proliferation, differentiation, motility and apoptosis (128). Activation of this pathway occurs in mouse and human HCC, which involves somatic mutations (129). Alcoholic liver cirrhosis and infections with HBV/HCV induce mutations in β-catenin and adenomatous polyposis coli, which in turn activate the Wnt signalling pathway,

initiating HCC (128, 130). Mitogen activated protein kinase (MAPK) signalling pathway is implicated in processes such as cell survival, proliferation and differentiation (**Figure 15**) (130). It is targeted and activated by HCV E2 protein produced during HBV/HCV infections and therefore promoting tumour formation (131). The pathway is also activated by mutations in Ras proteins induced by chemicals such as nitrosamine (132). Further signal transducers and activators of transcription such as Janus Kinase (JAK) and Signal Transducer and Activator of Transcription (STATS) (**Figure 15**) are activated by hormones and cytokines, which initiate formation of tumours (133). Activation of P13K/Akt signalling (**Figure 15**) at the cirrhotic stage is implicated in 40% to 60% of human HCC (134). Activation of these pathways limit apoptosis induced by TGF-β and growth inhibitory activity of CCAAT/enhancer binding protein which in effect promote tumour formation. Stress conditions induce Heat Shock proteins (HSP) to undergo phosphorylation, which initiates HCC (135). During cirrhosis, inflammatory conditions assist in HCC progression where NF-KB signalling pathway is activated by cytokines or interleukins such as IL-6 and TNF-α that enhance survival of pre-cancerous hepatocytes. Proinflammatory cytokines released from macrophages and lymphocytes induce angiogenetic effects which stimulate the growth of cancer cells (136). Loss of liver function and liver cell mass during cirrhosis stimulates these conditions that leads to tumour formation (137).

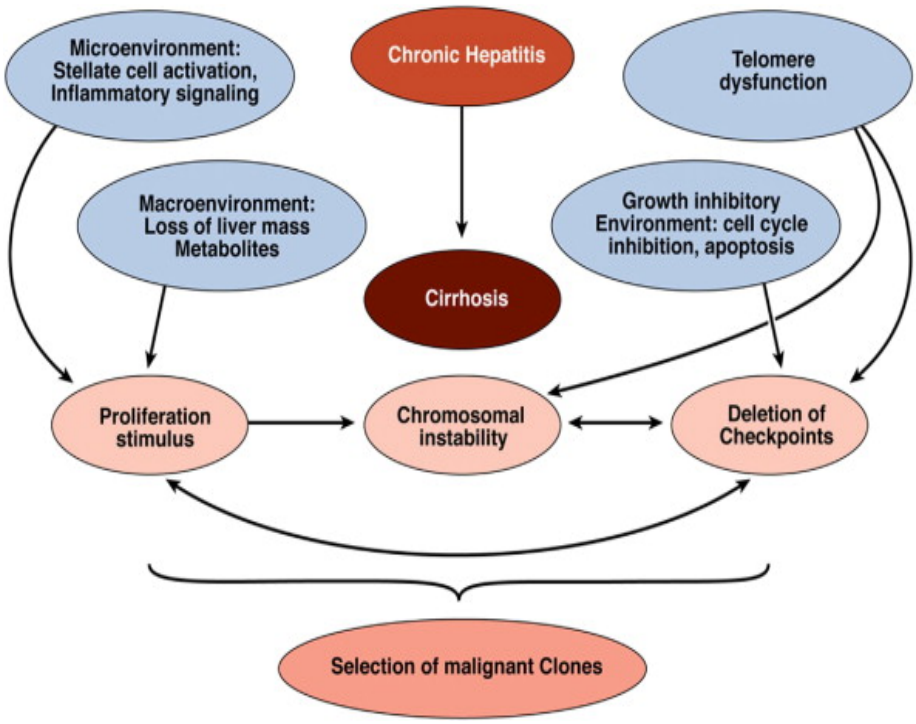


Figure 14: Molecular mechanisms inducing hepatocellular carcinogenesis at the cirrhosis stage. The mechanisms that accelerate cancer risk at the cirrhotic stage are summarised above. There is shortening of the telomere, which results in the activation of cell cycle and apoptosis checkpoints and limits the proliferative capacity of the liver cells. This further induces instability of chromosomes, which can be accelerated by loss of checkpoint function. Cirrhosis induces changes in the microenvironment including altered secretion of cytokine from activated stellate cells as well as inflammatory signalling from infiltrating immune cells. The reduction of liver function could increase toxic metabolites in the blood serum resulting in alteration of the macroenvironment. Both the changes in the macroenvironment and microenvironment induce the proliferation of hepatocytes thus leading to selection of genetically altered malignant clones and hence the occurrence of hepatocellular carcinoma. Figure taken from (47).

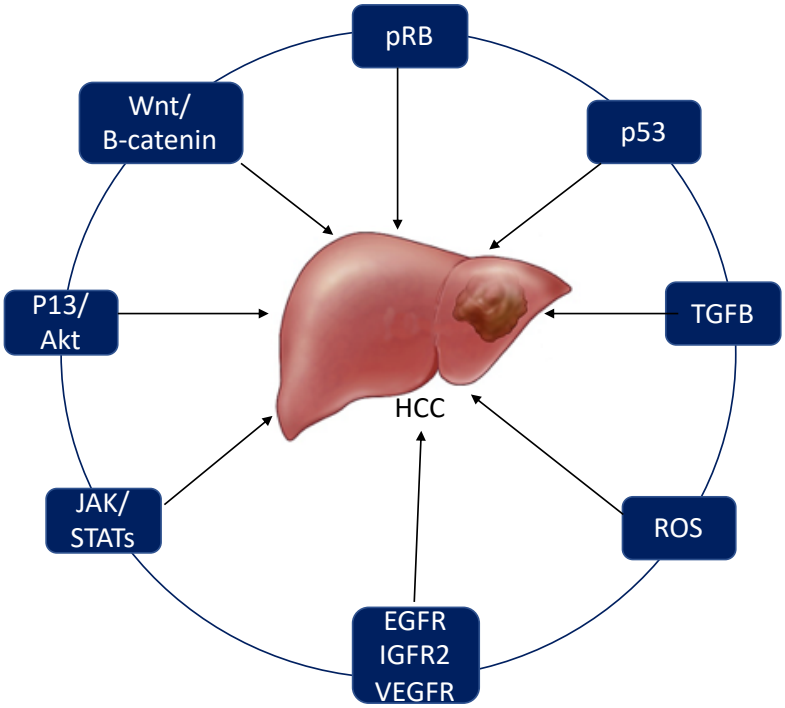


Figure 15: Major signalling transduction pathways implicated in hepatocellular carcinoma pathogenesis. Wnt/βcatenin, PI3K-AKT, JAK/STATs, TGF-β and many others are highly disrupted during HCC tumorigenesis. Adapted from (138).

1.3 Introduction to the Immune System

The immune system, which is a network of different cells, lymphoid organs and mediators, defends the host against infections and diseases (139). The system is categorised into innate and adaptive immunities, which are involved in generating acute and chronic inflammatory responses (140). The innate immunity serves as the first line of defence and usually consists of cell populations such as epithelial cells, monocytes, macrophages, dendritic cells, polymorphonuclear cells, natural killer cells as well as humoral factors such as complement proteins, lysozymes and cytokines (139). The adaptive or acquired immunity on the other hand, which is the second line of defence, consists of T lymphocytes which express antigen specific receptors and stimulate B cells to produce antibodies against the antigen (139). Together, the components of the immune system generate mechanisms to remove foreign agents in the body that are

considered as non-self (140). Although the precise immune response to HCC has not been fully elucidated, it is known that tumours are immunogenic and cancer is caused by a variety of defective genes that encode proteins involved in cell growth (141). The host immune system can identify a number of antigens produced by HCC cells. Studies have revealed that liver carcinogenesis is induced by chronic inflammation and decreased recognition of malignant cells (142). Dysregulation of the immune system, such as changes in cytokine levels and alterations in the immune system function, promotes progression of HCC (54).

1.3.1 Tumour-Associated Antigens (TAAs) and Tumour Specific Antigens (TSAs) in Hepatocellular Carcinoma

Tumours produce antigens that elicit a specific host immune response (143) that is absent in normal individuals making them useful biomarkers in detecting tumours (143). Tumour antigens are either overexpressed, mutated, misfolded, truncated, improperly glycosylated or aberrantly degraded (143). Tumour antigens with respect to HCC are classified into tumour specific antigens (TSA) and tumour associated antigens (TAA), the latter which are usually found on both tumour and normal cells (144).

1.3.1.1 Overexpressed Tumour-Associated Antigens (TAAs)

Calreticulin is resident in the endoplasmic reticulum of most cells and it is regarded as a high capacity Ca^{2+} binding protein. It is a vital component of the Major Histocompatibility Complex class 1 (MHC1) loading complex. It is responsible for chaperoning and regulating Ca^{2+} homeostasis and signalling (145). Calreticulin plays an essential role in the identification of tumour cells and has been implicated as a biomarker in liver, pancreatic and colorectal cancers (146). In addition, IgA and IgG

anti-calreticulin autoantibodies are detected in the sera of HCC, colorectal and pancreatic cancer patients (147). Other studies have also revealed that Calreticulin elicits a humoral response in HCC with a reactive epitope appearing in a mutated form (CRT32) (148).

Gankyrin is a component of the 19S regulatory cap of the proteasome and is required for cytosolic pathogen degradation prior to loading onto MHC Class I. It is a 25kDa protein, which is highly conserved in mammals. It encodes seven ankyrin repeats (149) and it is highly overexpressed in cancers such as HCC, oesophageal squamous cell carcinoma, pancreatic and colorectal cancers (150). Gankyrin usually links with ubiquitin ligase MDM2 and promote P53 degradation and ubiquitylation (151). RAL A belongs to the Ras family of GTpases. It has been reported to be involved in cell morphology, vesicle trafficking, transcriptional activation and human oncogenesis (152). It is usually involved in carcinogenesis of the liver as well as other cancers such as bladder (153), lung, prostate and pancreatic (154).

Hepatoma Derived Growth Factor (HDGF) is regarded as a heparin-binding growth factor, which was purified originally from media conditioned with human hepatoma cell line HUH7 (155). HDGF is highly expressed in foetal tissues and responsible for the development of lungs, muscle, liver and kidney, gut and cardiovascular system (156). Reports have indicated that HDGF expression is associated with poor prognosis in cancer patients (157). Hence, it not surprising to see them overexpressed in tumours such as HCC, melanoma, pancreatic, gastric, oral ad oesophageal (158).

Glucose regulated-protein 78 (GRP78), also referred to as the Binding Immunoglobulin protein, is an endoplasmic reticulum (ER) chaperone protein, which belongs to the heat shock protein 70 family. It is importantly involved in protein biosynthesis and it is

induced by environmental and physiological stress such as nutrient deprivations (159) and hypoxia in cancer (160). They are located on the surface of cancer cells such as prostate, ovarian, HCC, breast, stomach, colon adenocarcinoma, lung adenocarcinoma and neuroblastoma (161, 162). Their expression is associated with tumourigenic abilities of cancer cells and particularly promotes the invasion of HCC (163). Studies have revealed the presence of anti-GRP78 autoantibodies in ovarian cancer patients (164), prostate (165), gastric (166) and HCC (167) and stands as a potential biomarker for these cancers.

C-myc is a proto-oncogene, which is involved in growth control, apoptosis and differentiation. It is expressed in a large percentage of human tumours (168). Autoantibodies against C-myc are found in the serum of patients with breast, lung, colorectal, gastric, pancreatic and liver cancers. It has also been tested as a panel of TAA in HCC (169). Other overexpressed TAAs are outlined in the table below.

Table 2: Overexpressed TAAs in hepatocellular carcinoma.

Overexpressed TAAs	**Function**	**Reference**
Glypican 3 (Figure 16**)**	It is a cell surface heparin sulphate proteoglycan which controls cell division and growth regulation	(170, 171)
Cyclin B1	It is responsible for controlling the G2/M transition phase in cell cycle	(172)
Cytokeratin 8	It modulates cell attachment, protein synthesis and G1/S transition in the cell cycle	(173)
L-Myc	It regulates cell growth and cell cycle	(174)
Wnt1	It is implicated in oncogenesis including regulation of cell fate	(175)
SOX2	It regulates embryonic development and cell fate	(176)

1.3.1.2 Mutated Tumour-Associated Antigens

P53 tumour suppressor protein which is usually referred to as the "guardian of the genome" (177) is found in the nucleus of a normal cell and prematurely arrests cell cycle progression at the G1 stage, by inhibiting DNA synthesis upon detection of DNA damage. It is regarded as one of the most extensively studied TAA's (144) and has a wide range of mutational hot spots located over 11 exons. Missense point mutations often lead to the accumulation of relatively high levels of stabilised P53 protein in the nucleus. Aberrations in the P53 gene are the most common genetic changes in human malignancies. This often leads to the production of P53 autoantibodies as part of humoral immune response (178). Autoantibodies to this tumour antigen were first reported in 1982 (179) and serve as specific markers for patients with malignancy (180). About 3.5%-30% of patients with different cancers have serum anti-P53 autoantibodies, especially women with ovarian carcinoma (181). Anti-P53 autoantibodies and P53 missense point mutations have been detected in hepatocellular, ovarian, breast, gastric, oesophageal cancers in addition to others (182). Initially, it was understood that only tumours with missense p53 mutations leading to P53 overexpression could induce anti-P53 autoantibodies. However, these autoantibodies have been detected in the sera of patients lacking P53 overexpression. This might be as a result of unusual presentation of large amount of wild type P53 from necrotic tumours (183).

HRAS is also known as the transforming protein 21 and it belongs to the Ras gene family (184). However, mutations in the HRAS gene are found in most human cancers (185). The expression of oncogenic HRAS promotes tumourigenesis (186) and it is a key player in several signal transduction pathways. Moreover, it is implicated in the tumourigenicity and apoptosis of bladder and liver cancers (184).

KRAS belongs to the Ras superfamily or the Ras-like GTPases. It usually engages the Raf and P13 kinases upon activation. Mutations in the KRAS gene are very frequent in several human cancers such as adenocarcinomas of the colon, pancreas and the lung (187), liver, bladder, cervical, endometrial breast and myeloid leukaemia (188). Reports show that about 7% of human liver cancers carry activating mutations in the KRAS oncogene (48).

P16 is a tumour suppressor protein and a member of the INK family (189). It is associated with CDK4 kinase and usually inactivates retinoblastoma protein (190). Its expression is repressed by HBV X protein and down regulated during liver tumorigenesis (191). P16 mutations are seen in oropharyngeal (192), breast, colon (193), renal (194), bladder (195), cervical (196) and liver (197) cancers.

β-catenin protein plays an important role in the generation and differentiation of tissues and it is implicated in cell-to-cell adhesion (198). β-catenin is a key regulator in the Wnt/β catenin-signalling pathway and this pathway is very crucial in the development of HCC. In HCC, there is a mutation in the posttranslational modification site of β-catenin. It is also deregulated in other cancers, such as gastric, breast and colon cancers (199).

1.3.1.3 Altered Expression of Tumour-Associated Antigens

Many TAAs often show differentiated or altered patterns of expression in cancer. Survivin is an inhibitor of apoptosis gene that is implicated in the suppression of apoptotic cell death (200). The expression of Survivin is normally elevated in human cancers of epithelial and hematopoietic origin such as lung, breast colon and gastric cancers, though it is usually restricted to embryonic development. Its expression is

usually linked with poor prognosis in patients (201). Survivin is considered an important target for the development of immunotherapeutic strategies because its overexpression may provide a survival benefit for tumour cells as well as their increased expression is entirely limited to malignant tissues (201).

Another antigen with an altered expression is the NYESO-1. NYESO-1 belongs to the cancer testis family and its expression is limited to the ovary and testes however, it is seen in various cancers such as lung, ovarian and oesophageal cancers. It is regarded as the most important of all cancer testes antigens and has become an attractive target for vaccine development in cancer. Stockert *et al*, reported autoantibody responses to NYESO-1 in ovarian carcinoma patients (202).

Alpha Fetoprotein (AFP) (**Figure 16**) is a glycoprotein which is produced in early fetal life by the liver and a variety of tumours such as HCC and gastrointestinal cancers. High levels of AFP are usually found in 70% of HCC patients and therefore it is considered as the most widely used tumour antigen in the early detection of HCC (203).

1.3.1.4 Post-translational modifications of Tumour-Associated Antigens

Some TAAs are subjected to aberrant posttranslational modifications such as glycosylation, oxidation, phosphorylation and peptidoglycan cleavage. This may induce a neo-epitope with affinity for the induction of an immune response. HCC1/CAPER has been shown to regulate calcitonin, Vascular Endothelial Growth Factor (VEGF) gene expression (204), as well as modulates oncogenic activity of Rel/NF-κB (205). It is a co-activator of activated protein 1 (AP-1) and other oestrogen receptors (206). P62/IMP2, a member of the IGF-2 mRNA binding protein was first identified when screening the sera of HCC patients (144). It is an oncofetal protein,

which disappears soon after birth and reappears during malignancies (144). It binds and regulates the translation of insulin growth factor 2 mRNA (205). It has also been shown to stabilise C-myc and regulate its post-transcriptional expression (207). Reports have indicated that this tumour antigen is present in about 21% of HCC patients but not in liver cirrhosis and chronic liver hepatitis (144).

P90/CIP2A was first identified in liver and gastric cancers and its main function is to regulate C-myc stability (208). According to Shi *et* al, the cancer testis antigen has been detected in HCC, though previous reports had identified its expression in gametogenic tissues (209).

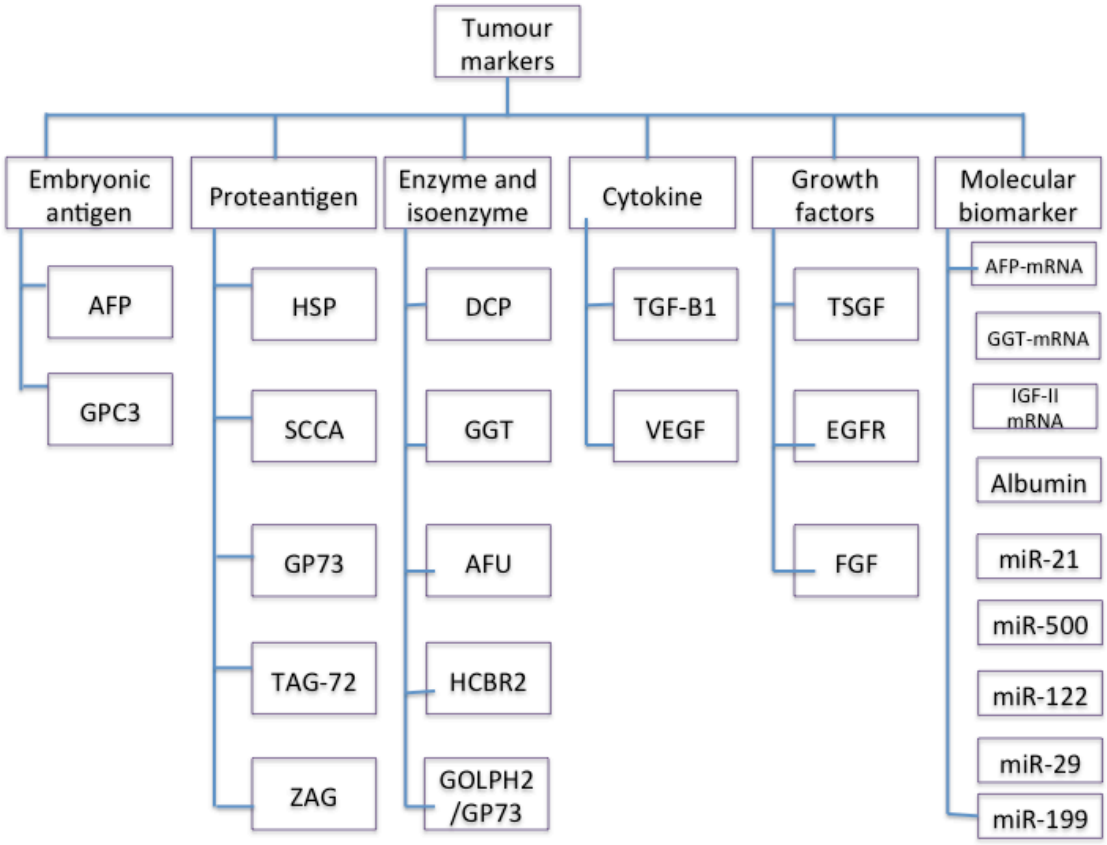


Figure 16: Hepatocellular Carcinoma tumour markers. Adapted from (210).

1.3.2 Immune response and Hepatocellular Carcinoma

Mounting an effective recognition, processing and presentation of tumour antigens by antigen presenting cells such dendritic cells (DCs) are fundamental for a successful immune response against tumours. Tumour antigens are recognised by pattern recognition receptors on DCs after which they are processed and presented by the DCs to naïve T-cells via Major Histocompatibility Complex (MHC)-T-cell receptor interaction. Thus, MHC proteins are found on the surface of antigen presenting cells while T cell receptor is found on naive T cells (**Figure 17**). MHC class I presents epitopes of tumour antigens to naïve CD8 T-cells while MHC class II presents epitopes to naïve CD4 T-cells (211). Firstly, DCs present tumour antigens to naïve CD4 T cells (**Figure 17**). However, full activation and differentiation of these immature T-cells require a second stimulus which is generated through the interaction between co-stimulatory molecules, CD80/86 present on antigen presenting cells and CD28 on T cells (211). Activated $CD4^+$ T-cells express CD40 ligand which binds CD40 on DCs resulting in the production of Interleukin 12 (IL-12) from DCs as well as differentiation of activated $CD4^+$ T-cells to IFN-γ producing Type 1 helper T-cells (212). These help DCs to present tumour antigens to CD8 T cells which then become activated to $CD8^+$ cytotoxic T cells (**Figure 17**). Subsequently, the activated $CD8^+$ cytotoxic T cells move through the blood stream to the tumour microenvironment, where they recognise tumour antigens presented by MHC class I on these tumour cells and begin to destroy them (**Figure 17**). Activated T cells are $CD8^+$ cytotoxic and $CD4^+$ T helper cells which play important roles in impeding and killing tumour cells (213). Thus, when $CD8^+$ cytotoxic T cells are activated, they induce cytolytic and apoptotic effects on the tumour cells by producing Granzyme B and Perforin (**Figure 17**). On the other hand, $CD4^+$

helper T cells play a vital role in the maintenance of the adaptive immune response. $CD4^+$ helper 1 T-cells produce cytokines such as Interferon (IFN)-γ and TNF-α which provide sustained mediation for $CD8^+$ cytotoxic T-cells and further recruit cytotoxic macrophages to destroy tumour cells (214). These cytokines also activate antigen presenting cells to produce molecules such as LMP2, LMP7 and MHC class I in order to increase presentation to cytotoxic T cells. For tumours expressing MHC class II directly, $CD4^+$T-cells directly kill them through conventional MHC dependent recognition. Thus, producing CD4 responses against carbohydrate epitopes (214). Furthermore, a subset of $CD4^+$ T cells referred to as the T-follicular helper cells help to produce opsonising antibodies by aiding B-cells to induce isotype switching and affinity maturation. These antibodies tend to be specific for the tumour antigens (141).

Tumour cells express specific antigens especially within the MHC class I and II molecules. However, they cannot fully active T cell responses (T-cell anergy) because they have reduced expression of co-stimulatory molecules, CD80/86 (141). Maturation defects such as reduced endocytosis, allostimulation, IL-12 secretion and a decreased expression of MHC class I molecules often result in failed HCC-associated antigen presentation (215) (**Figure 18**). HCC patients with HCV and HBV infections have functional defects in peripheral DCs (216). Cytotoxic T-lymphocyte-associated protein (CTLA)-4^+ DCs, a newly identified regulatory subset of DCs which express inhibitory molecular-like CTLA4 and programmed death receptor 1 (PD-1), were seen in the peripheral blood and tumour masses of HCC patients (217). These cells secrete IL-10 and Indoleamine 2,3, dioxygenase leading to the suppression of the $CD4^+$ T-cell immune response, thereby aiding tumour immune escape and progression. Neutrophils are a common inflammatory infiltrate in tumours that could provide a prediction of poor survival in HCC patients, since their numbers correlates positively with the stage of

cancer. Kuang *et al*, showed that peritumoral stromal cells were fortified with neutrophil populations under the influence of Th17 cells through chemokines, like CXCL8 (218). Proteases, like matrix metalloproteinase-9 in HCC tissues, produced by neutrophils promote angiogenesis thus, these cells provide a connection between immune cells and angiogenesis as well as promoting tumor growth (218).

Macrophages play an important role by recruiting other kinds of immune cells as well as presenting antigens to T-cells. Macrophages present in cancerous tissues are referred to as Tissue Associated Macrophages (TAMs) (212). TAMs in the presence of T helper 1 cytokines such as IFN- γ, produce inflammatory cytokines such as IL-1β, IL-6, TNF-α, reactive oxygen species (ROS) as well as nitric oxide (NO), which are involved in pro-inflammatory responses. Moreover, TAMs cause cytotoxicity of cancer cells which is essential for anti-cancer immune response. These types of TAMs are referred to as M1 Macrophages (212). In contrast, an anti-inflammatory immunity is generated by macrophages in the presence of T helper 2 cytokines such as IL-4 and IL-13. These are called the M2 macrophages and they produce immunosuppressive cytokines such as TGF-β, IL-10 which cause wound healing and tissue remodelling (212).

The cytolytic population of Natural Killer (NK) cells serve as an immune monitor in the liver microenvironment (219). These cells are cytotoxic and control the activity of other immune cells through the cytokines they release (220). Their effect could be helpful to the host depending on the extent of the cytokines produced. NK cells facilitate their function in the liver under normal physiological conditions via the production of "cytolytic granules" which contain perforin, granzymes, tumor necrosis factor-related apoptosis-inducing ligand (TRAIL) and IFN-γ (56). The function of NK cells is quite similar to $CD8^+$ cytotoxic T-cells but they react faster during immune responses. Also,

they recognise cancer cells with missing MHC class on their surface. However, in case of many cancers, such as HCC, their functions are not completely reported. A significantly lower proportion of these NK cell subsets exhibited reduced levels of IFN-γ (141). A study conducted by Gao *et al*, revealed that in HCC patients, there is a significant decrease of CD56dim NK subsets in the peripheral blood as compared to healthy subjects (221). CD56dim NK subsets account for 90% of human cells and are usually cytotoxic against tumour cells. Another study conducted by Berzofsky *et al*, showed NK cell levels were increased in HCC patients with a gradual rise from the blood through the liver to the tumour (222). Several mechanisms have been put in place to explain the decreased functioning of NK cells and their association with cancer and cirrhosis of the liver (47) as well as phagocytic uptake of NK cells by activated hepatic stellate cells found between the hepatocytes and small blood vessels of the liver.

Another set of immune cells in the adaptive immune response is Regulatory T cells (Tregs). This cohort of cells tends to express CTLA-4 unlike the normal T cells which express CD28. CTLA-4 acts as a repressive receptor to CD80/CD86 and inhibits T-cell activation. They also express CD25 on their surface along with intracellular transcription factor Forkhead box P3 (FoxP3) (223). These cells have been reported to play a crucial role in carcinogenesis. They supress autoimmune reactions and sustain immunological tolerance. Tregs express several cytokines such as TGF-β and Interleukin 35 (IL-35) which exert suppressive effects on proliferation of T-cells. Granzyme B produced by Tregs causes apoptosis of effector T-cells (**Figure 18**). A subset of these cells, called induced Tregs, are elevated in the infiltrating lymphocytes and peripheral blood of HCC patients (223). The number of Tregs correlates with the severity of the disease, in that patients with advanced HCC stages tend to have a higher percentage of FoxP3 intrahepatic regulatory T cells in comparison to patients who are

at the initial stages. This means that elevated levels of tumour infiltrating Tregs serve as important prognostic markers in HCC patients. Moreover, Tregs downregulate NK cell expression and hence dampen NK cell responses, which lead to progression of HCC (224). T-Helper (Th) 17 are a subset of pro-inflammatory T-helper cells, which are defined by their production of interleukin 17 (IL-17). These cells are elevated in HCC tissues than non-tumour tissues (225). There is a positive correlation of Th17 cells with reduced survival HCC cases, although the role in this type of cancer is not completely defined.

Cytokines, such as IL-2, have direct correlation with HCC prognosis as high levels of IL-2 is associated with elevated number of CD8 T cells (226). These cytokines can change the functional abilities of NK and $CD8^+$ cytotoxic T cells thereby controlling carcinogenesis if only they are alterated (227). T helper 22 (Th22), which is a subset of $CD4^+$ helper T-cell produces Interleukin 22 (IL-22), which has been found to be significantly increased in patients with HCC (228). The production of higher levels of IL-1β may assist to elevate the production of cytokines such as IL-6 and TNF-α, which stimulate complex immunological processes to eradicate viruses in the case of hepatitis induced HCC. Moreover, IL-1β has also been shown to induce the growth of $CD8^+$ T-cells in many HCC cell lines, hence, contributing to tumour evasion (24). IL-10 in conjunction with other T helper 2 (Th2) cytokines, correlate with HCC progression. In addition, IL-6 is found to be linked with poor prognosis in HCC patients (229), since its expression is elevated in HCC contributing to tumour progression.

B-cells are regarded as another category of lymphocytes in the adaptive immune response. They are responsible for regulating immune response to cancer. First of all, they serve as antigen presenting cells when DCs fail to recognise tumour antigens effectively. This contributes to the survival and proliferation of tumour-infiltrating T

cells. They express cytokines which promote $CD8^+$ cytotoxic T cells to exert direct tumouricidal effect on cancer cells and further assist in the priming of $CD4^+$ and $CD8^+$ T-cells (230). B-cells become activated by Th1 and Th2 cells via the production of CD40 ligand and IL-4 respectively, which causes them to proliferate. These further differentiate into antibody secreting plasma cells which then produce tumour-reactive antibodies (230-232). Studies have shown that B-cells are associated with HCC survival (233). Controversially, a current study undertaken by the same group revealed that a subset of B-cells referred to as B-regulatory cells (Bregs) are downregulated in HCC patients indicating their protective roles in enhancing HCC progression via the CD40/CD40 ligand signalling pathways (233). Bregs can also directly or indirectly minimise Th1 and Th2 cytolytic T-cell responses (231).

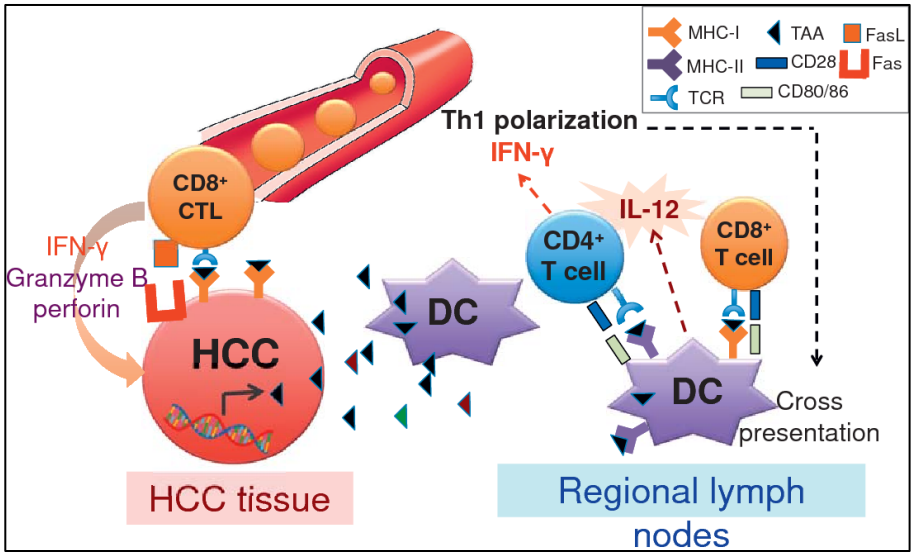


Figure 17: Immune response in hepatocellular carcinoma. Dendritic cells (DCs) become activated via the uptake and recognition of tumour antigens. Activated DCs express co-stimulatory molecules CD80/86 and IL-12 and migrate to the regional lymph nodes where they present tumour antigens to naïve $CD4^+$ T-cells. These become activated and differentiate into $CD4^+$ Type 1 helper cells. These cells help DCs to present tumour antigens via MHC class I to CD8 T-cells and this induces the development of $CD8^+$ cytotoxic T-cells. These exert their anti-cancer effects by producing granzyme B and perforin. Figure taken from (212).

1.3.2.1 Immune Evasion Strategies

Tumour cells have devised several mechanisms of avoiding detection by the immune system (234). The tumour load could be very high for the immune system to mount an effective immune response (234). It has also been shown that the tumour could modulate tumour antigens expressed on their surface by transferring them into the cytoplasm and hence rendering them immunologically not visible (234). Other strategies include altering the cell adhesion molecule expression, which hinders stable contact with cytotoxic cells (235). Tumour antigens could also be coated with sialomucins and mucoproteins, which are proteins considered as self and hence cannot be recognised by the immune system.

Despite the presence of tumour specific immune responses, tumours progress in HCC patients. This means that HCC escapes several immune mechanisms by generating cells with immune suppressor functions including myeloid derived suppressor cells, inhibitory macrophages. These cells mask immune responses specific for the tumour (234). In HCC, there is also a down regulation of the MHC class molecules and CD80/86 co-stimulatory molecules which results in the impairment of the processing and presentation of tumour associated antigens (TAAs) (236). Other studies have shown inadequate CD4 T cell help and hence leads to exhaustion of CD8 T cell responses (237). Others have shown suppression of CD4 and CD8 T cell responses by T regulatory cells in HCC (238). The immune system is induced by the tumour cells to produce blocking antibodies (IgG_3 and IgG_4 subtype) which are unable to activate the complement system, hence, efficient lysis of tumour cells cannot take place (234). Moreover, the tumour produces soluble components such as IL-10, TNFβ, TGFβ and vascular endothelial growth factor (VEGF) which supress the immune system.

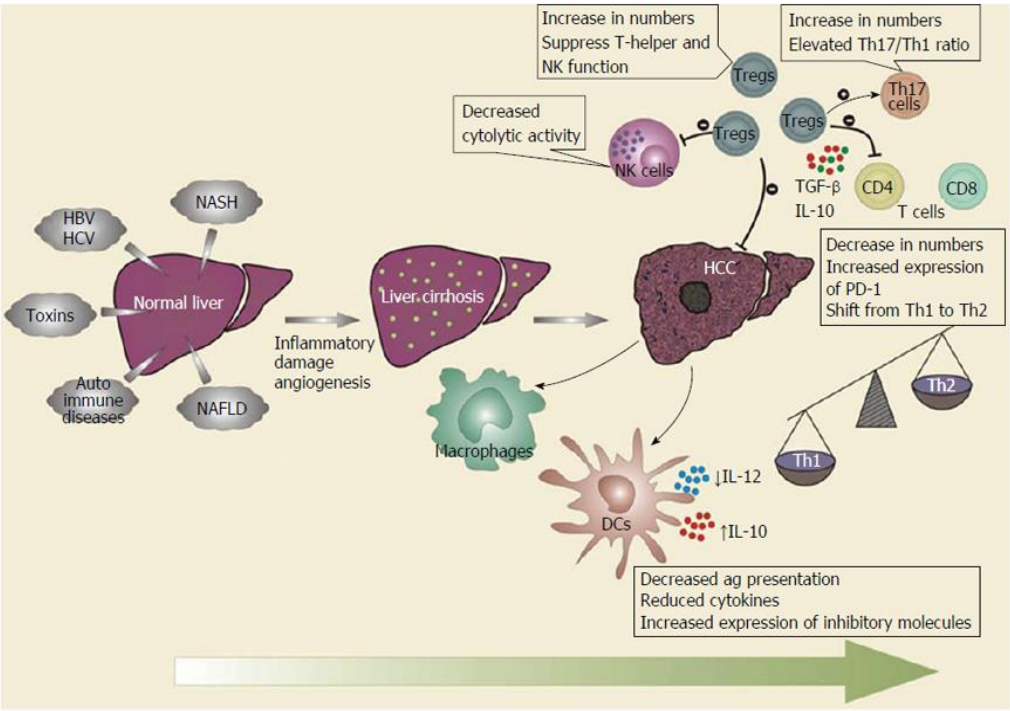


Figure 18: The functions of immune cells become dysregulated as the liver disease progresses from cirrhosis to hepatocellular Carcinoma. Dendritic cells (DCs) tend to lose their ability to process and present antigens with the reduced secretion of Th1 cytokines. Macrophages differentiate into an alternatively-activated phenotype that produces a Th2-type immune response which stimulates regulatory T cell (Tregs) recruitment and development. There is also a reduction in the cytolytic capabilities of Natural killer cells as well as decrease in number and function of $CD4^+$ and $CD8^+$ cells. Th17 cells increase in number and correlate with angiogenesis and poor-prognosis. Figure taken from (223).

HCC has a very poor prognosis and most patients usually die within one year of its detection. This could be attributed to lack of sensitive and specific diagnostic methods that would help in early detection of the cancer (239). HCC diagnostic procedures such as ultrasound have faired quite well. However, the efficacy of this test is highly operator dependent and small tumours cannot be detected (240). Early studies on serum proteins such as Alpha-fetoprotein (241), des-γ-carboxy prothrombin, glypican-3, TGFβ, insulin-like growth factor binding protein 2, Golgi protein-7 (**Figure 19**) have shown these to be efficient markers for HCC diagnosis but the sensitivity and specificity of their detection is not optimal (77), especially in patients with small tumours. Therefore, the use of these serum biomarkers is not recommended by most clinical practice. There

is an urgent need for the discovery of more sensitive and specific biomarkers that would supplement AFP in the diagnosis of early stage HCC. High-risk patients would be identified which would allow the opportunity to provide adjuvant therapy and increase survival (242).

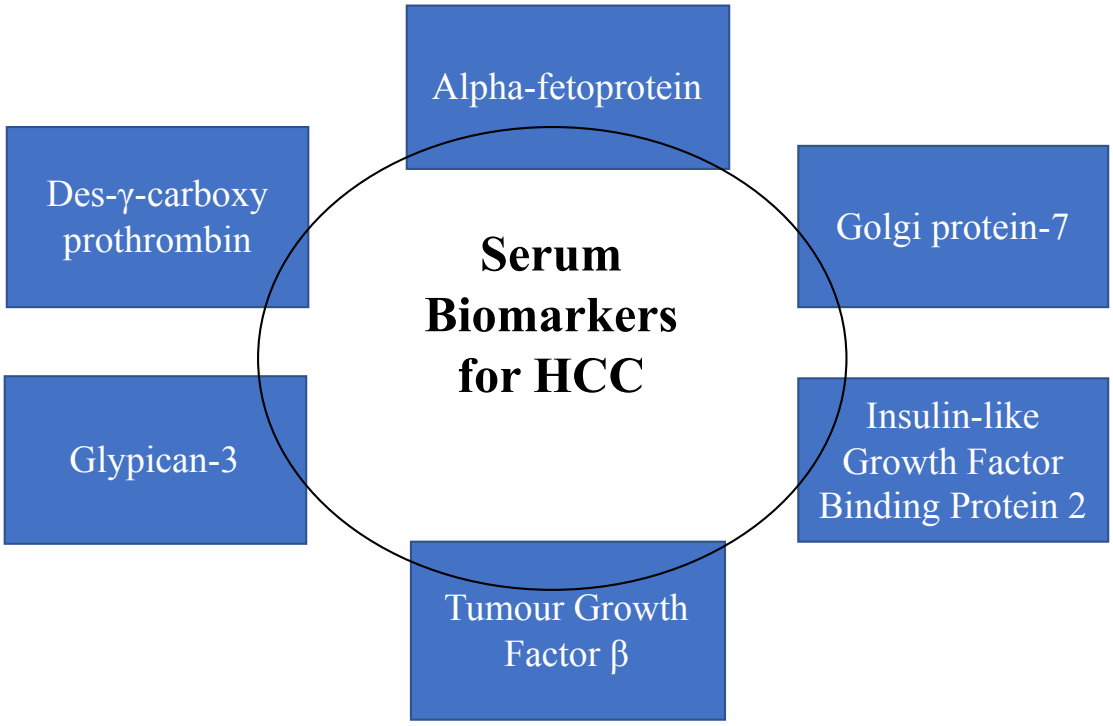


Figure 19: Proposed integration for biomarkers into HCC treatment. Proteins and metabolites released by the tumour into the circulation can provide a non-invasive method of early detection. However, these parameters cannot accurately predict optimal therapies for patients. Adapted from (243).

1.3.2.2 Autoantibodies as Immunological Reporters for Early HCC Diagnosis

Autoimmunity is seen as a humoral response manifested by the production of autoantibodies (244). Autoantibodies are antibodies produced by B cells and are directed against self-cellular proteins and nucleic acids. They have a broad reactivity for a wide range of antigens. The first study of autoimmunity was seen in Rheumatic

autoimmune disease and since then autoimmunity has become an important area of research in cancer (245). Autoantibody detection in patients' sera before clinical symptoms of the disease indicate that it can be used in some cases to predict the rate of progression towards the onset of the autoimmune disease (246). Their production precedes the clinical manifestation of the disease by several months to years (247). Hence, they provide a great potential value for the screening and early diagnosis of autoimmune diseases as well as several cancers. These antibodies provide a unique information that reflect the nature of the malignant process in the affected organ. This was demonstrated by Madrid *et al*, who compared sera from patients with autoimmune diseases with those from breast cancer. It was observed that sera from breast cancer patients had anti-mitochondria, multiple nuclear dots, centrosome and nucleolar antibodies after staining of cell sections by patients' sera. The production of autoantibodies in cancers is facilitated by the exposure to TAAs found on the surface of a cancer cell. Hence, the autoantibody signatures are considered as reporters of the immune system because they identify antigenic changes involved in the tumourigenesis. Autoantibody responses have also been implicated in cancers such as leukemias, (143), malignant melanomas (248), lung (249), or breast (250), pancreatic (251), colorectal (252), gastric (253), ovarian (254), prostate (255). This gives an insight into the relationship between malignancies and the immune response, which further gives rise to novel diagnostic and therapeutic ideas.

Autoantibodies most important for hepatological diseases include antinuclear autoantibodies, autoantibodies against smooth muscle actin, liver microsomal and anti-mitochondrial autoantibodies (256). Anti-TAA specific IgG autoantibodies in response to TAAs such as P53, P16, P62, Survivin, CENPF, Sui-1 and HNRNPL have been identified in the sera of patients with HCC (257, 258) and this provides an in vivo

amplification in patients sera of early carcinogenesis (241). Researchers have shown interest in the use of autoantibodies as serological markers for HCC diagnosis, mostly because of their absence or infrequently produced in normal individuals. A study conducted by Hong *et al*, showed that higher autoantibody responses to TAAs such as IMP2, HSP60 and CENPF are seen in HCC patients as compared to patients with chronic liver hepatitis and liver cirrhosis (259). Other reports have shown that these autoantibodies can be detected at the asymptomatic stage of the cancer and even five years prior to the clinical manifestation of the disease (260). Recently, detection of autoantibodies raised against TAAs has been proposed as an effective aid to early identification of HCC in patients. This is due to the fact that amplified signals of anti-TAA autoantibodies can be easier to detect compared to TAAs. The basis for this notion is that the changes in the autoantibody response during progression from the chronic liver disease to HCC could be linked to the aberrant cellular mechanisms inducing the immune responses. Hence, they could be used as probes to detect proteins involved in the malignancy (257). However, the detection of tumour shed proteins in serum may be very challenging due to the abundance of non-specific serum proteins such as albumin and the requirement of a larger tumour bulk to be able to detect the circulating shed protein (261). Autoantibodies are stable and persist in the serum of the patients for a long time (approximately 7 days), unlike the TAAs which are rapidly degraded or cleared (239, 262). Furthermore, autoantibodies are present in higher concentrations than respective TAAs. They are easily accessible to screening because they are found in the blood. Lastly, the variety of reagents and techniques available for antibody detection enhances the design of assays (263, 264). Research on TAAs and autoantibodies have provided an abundance of targets for therapy and uncovered

candidate biomarkers for early detection, prognostication and response to therapy (261).

Several studies have been conducted where autoantibodies were used to immuno-screen several TAAs in HCC and by so doing has helped in the diagnosis of the cancer. An earlier study conducted on HCC by Zhang *et al*, showed a high titre of autoantibodies against P62 and CENP-F (265). These autoantibodies were detected during the transitioning to the malignancy stage (265). Proteins such as Calreticulin, Cytokeratin 8, Nucleoside diphosphate kinase A, and F1-ATP synthase B subunit have also been identified using autoantibodies from HCC sera (148). The frequency of autoantibodies to P53, C-MYC, Survivin and IMP1 in HCC patients were recently studied where about 9% of HCC patients had one or more of the autoantibodies; in this circumstance, the AFP levels were normal, indicating that the autoantibodies could be useful in the serological diagnosis of HCC even in AFP negative cases (266). A similar outcome was obtained in a recent study where high titres of autoantibodies to CENPF, HSP60 and IMP2 were detected in HCC patients who were younger than 50 as compared to chronic liver disease patients and cirrhotic patients (259). Studies have shown that the sensitivity and specificity of autoantibodies to individual TAA is low for HCC diagnosis and hence using a multiple panel of TAAs would help achieve higher sensitivity and specificity (267). Thus, anti-TAA autoantibodies when analysed individually have little diagnostic value. Moreover, the test would be valid to patients whose tumours harbour the antigens. A panel of TAAs would enhance the ability to detect autoantibodies in HCC patients (267). Using protein microarray, humoral responses to a number of TAAs such as DEAD box polypeptide, apoptotic inducing factor (AIF), prostate binding protein (PBP) and eukaryotic translation elongation factor 2 (EIF2) were found in patients with HCC than chronic hepatitis or even normal

individuals. The sensitivity of any of these antigens in patients with stage 1 HCC ranged from 50% to 85% (239). As these four antigens were analysed the sensitivity increased to 90% (239). A similar study conducted by Dai *et al*, revealed that the sensitivity of individual anti-TAAs autoantibodies thus, anti-CAPERα, anti-p90, anti-Ral A, anti-NPM1, anti-MDM2, anti-14-3-3zeta autoantibodies was 6.6–21.1%, whereas the sensitivity and specificity of their combination were 69.7% and 83%, respectively (268).

The same pattern was seen in a study undertaken by Middleton *et al*, where it was noticed that the sensitivity of individual autoantibody for detection of HCC was only 0–10%, while the sensitivity and specificity of the combined autoantibodies were 45% and 92%, respectively (241). This clearly outlines the importance of panel detection of autoantibodies. This drawback could be overcome by using arrays of critically selected TAAs, and that different cancer types may require different TAA arrays to achieve the sensitivity and specificity required to make immuno-diagnosis a feasible adjunct to tumour diagnosis (239).

1.3.2.3 Generation of Anti-TAA Autoantibodies and Immunological Tolerance

Many clones of B lymphocytes are produced by the human body which circulate in the lymph and blood. These lymphocytes are produced in the fetal or adult bone marrow after which they undergo subsequent functional maturation in the secondary lymphoid organs such as the lymph nodes and spleen (269). B lymphocytes tend to express distinct surface receptors as they mature and these bind specific antigens which induce their activation, proliferation and maturation (269). The process of autoreactivity, thus B cells binding to self-antigens, is prevented by receptor editing, apoptosis and induction of anergy (negative selection) in B cells expressing an autoreactive B cell

receptor. In effect, there is an immunological tolerance to self where B cells which are matured tends to bind to only non-self-antigens (270). These B cells then become activated and move to the germinal centre in the lymph nodes where they undergo rapid clonal expansion, affinity maturation, class switching and differentiation into memory B cells or plasma cells (271). However, low affinity autoreactive cells still persist and as low affinity reactivity to self-antigens. This is essential for survival of B cells in the peripheral immune system (270, 272). It is no surprise as IgM and occasionally low titre IgG autoantibodies, such as rheumatoid factors, are still detected in healthy individuals (270).

Immune response in cancer is mostly initiated by alterations in the tumour which leads to increased immunogenicity to self-antigens. Thus, mutations in cancer cells lead to the generation of new or altered epitopes or exposure of TAAs that are overexpressed, mutated, misfolded or aberrantly degraded. During carcinogenesis, these TAAs are recognised by B cells (264). The B cell receptor found on the B cell surface binds to these tumour antigens which leads to crosslinking or clustering of B cell receptor which activates B cells and causes them to proliferate into plasma cells and then antibodies (264). However, antibody responses tend to be very weak and also a poor B cell memory is induced since cytokines or CD40 signal are not involved. This mechanism of B cell activation (direct activation) allows B cells to attract antigen specific T cell help (264).

T helper cells are required to help activate B cells to produce antibodies **(Figure 20)**. In this mechanism, tumour antigens are recognised by B cell receptors and are internalised, lysed and presented on the cell surface bound to MHC class II for the recognition by $CD4^+$ T helper cells which have earlier been primed by the same tumour antigen (264). The interaction leads to the expression of CD40L proteins on T helper

cells and this binds the CD40 protein on the surface of B cells. The interaction further results in the secretion of cytokines (IL-4, IL-5, IL-6) from T helper cells which stimulates B cells to proliferate and differentiate into thousands of identical antibody secreting plasma cells and memory B cells (264, 273). Antibodies produced by the plasma cells undergo class switching where changes occur in the constant region genes on chromosome 14 while the variable region remains the same and doesn't disrupt the specificity for the tumour antigen (264). Thus, IgM is switched to IgG isotype and this results in a more sustained and stronger immune response. This produces different antibody isotypes required to destroy specific tumour antigens. Studies have indicated that most of the anti-TAA autoantibodies detected in cancer patients' sera are IgG implying a strong secondary immune response (264).

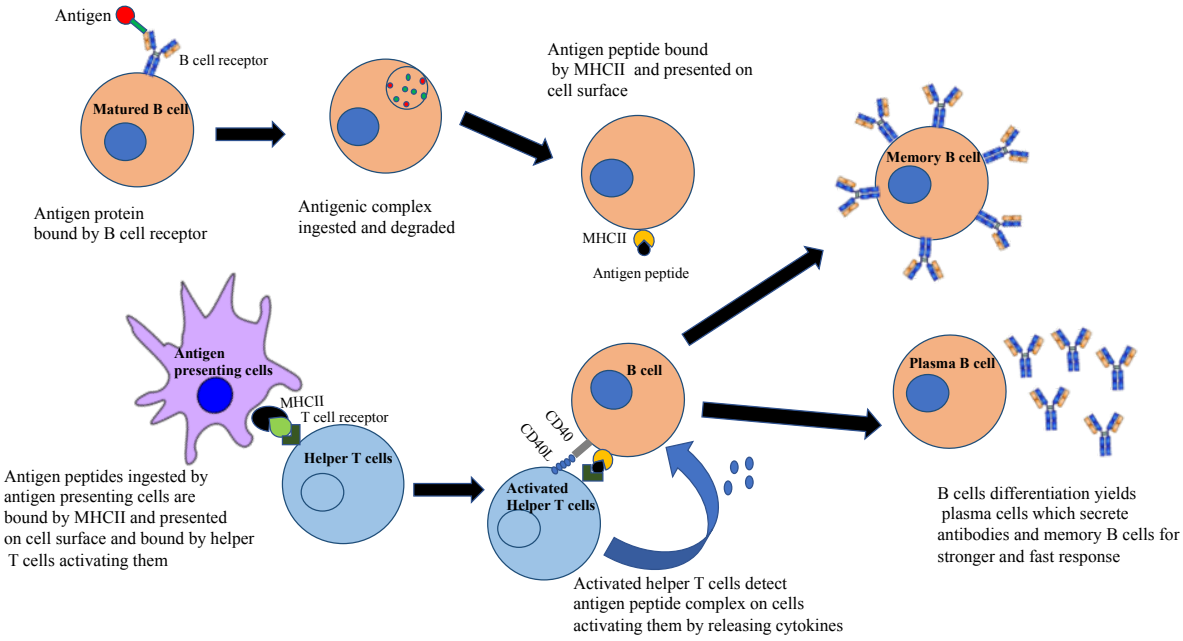


Figure 20: T cell dependent B cell activation. B cell receptors recognise and bind tumour antigens after which the antigens are internalised, lysed and presented on the cell surface bound to MHC class II. Antigen peptides bound by MHCII are recognised by activated $CD4^+$ T helper cells which have earlier been primed by the same tumour antigen presented by antigen presenting cells. The interaction leads to the expression of CD40L proteins on T helper cell which binds the CD40 protein on the surface of B cells. The interaction further results in the secretion of cytokines (IL-4, IL-5, IL-6) from activated $CD4^+$ T helper cells, which stimulates B cells to proliferate and differentiate into thousands of identical antibody secreting plasma cells and memory B cells. The plasma cells produce different immunoglobulin isotypes with distinct roles. Isotype class switching as well as hypermutation leads to a stronger and more sustained immune response. Adapted from (273).

Autoantibodies are immunoglobulins which exist in soluble forms and are secreted from the cell into the plasma or they are membrane bound which are attached to the B cell surface (B cell receptor). They are Y-shaped, and their molecular structure is divided into three parts upon digesting with papain (274). This includes two Fab regions which determines the specificity of the antibody. The third segment which is the Fc region helps determine the class of antibody as well as its biological function (275). Immunoglobulins are made up of four polypeptide chains; two heavy and two light chains **(Figure 21).** The heavy chain is made up of 440-550 amino acid residues whereas the light chain consists of 220 amino acid residues. Both light and heavy chains loci consist of sequence of V gene segments, D segment which is usually only for the heavy chain gene, J segment and c exons (275). Moreover, the heavy chains are made up from four segments (VH, D, JH and CH) while the light chains are made up of three segments (VL, JL, CL). There are two types of light chains. The Kappa chain is encoded by a Kappa (κ) locus on chromosome 2 and the Lamba chain is encoded by IgG lambda (λ) locus on chromosome 22 (275). Furthermore, there are five types of heavy chains which include γ, δ, α, μ, and ξ. Each light chain is composed of a constant (C_L) and a variable (V_L) while the heavy chain is composed of one variable (V_H) domain and three or four constant (C_{H1}, C_{H2}, C_{H3}, C_{H4}) domains, depending on the type of immunoglobulin. The variable domains of both light and heavy chains contain hypervariable regions which help to identify and bind specific antigens while the constant region of the heavy chain form the Fc domain. This is responsible for determining the effector functions of the immunoglobulin molecule through binding to Fc receptors (FcR) on the surface of cells of the immune system (274).

Immunoglobulins could be divided into five subtypes based on the type of heavy chain they contain. The subtypes differ depending on the sequence and number of constant

domains, hinge structure, as well as antigenic properties. These include IgM, IgG, IgA, IgE and IgD. IgG and IgA are further divided into sub-classes based on their differences in amino acid sequence in the heavy chains (275).

1.3.2.3.1 Immunoglobulin G (IgG)

IgG is the most abundant and extensively studied isotype found in the human body and it represents 80% of serum antibodies in humans **(Table 3)**. This type of immunoglobulin contains γ heavy chains of 50 kDa and two identical light chains of 25 kDa. This immunoglobulin has two antigen binding sites and is usually involved in secondary immune response (276). It is also involved in neutralisation of toxins and viruses. IgG interacts with macrophages, natural killer cells and neutrophils via the FcγR receptors in order to induce phagocytosis, antibody dependent cell cytotoxicity (ADCC). It also activates the complement pathway which helps to clear opsonized pathogens. There are four classes of IgG based on the structural antigenic and functional differences in the constant region of the heavy chain (C_{H1}, C_{H2}, C_{H3}) as well as the hinge region. This include IgG_1, IgG_2, IgG_3, IgG_4 (276).

IgG_1 is considered as the most abundant subclass, consisting of 60% of IgG. It has a molecular weight of 146 kDa and a half-life of 21 days **(Table 4)**. It is produced in response to protein antigens. Since it is flexible the Fab fragments are can rotate about their axes of symmetry (277). It binds to the all the classes of FcγR receptors on effector cells, such as macrophage, neutrophils and natural killer cells, and also efficiently binds C1q to activate the complement cascade. It is usually absent in a wide range of primary and secondary antibody deficiencies and result in hypogammaglobulinemia (277).

IgG_2 is the second abundant IgG subclass constituting 32%. It has a molecular weight of 146 kDa and a half of 21 Days **(Table 4).** Most IgG responses to bacterial

polysaccharide antigens are IgG_2. Hence, increased bacterial susceptibility to certain bacterial infections are associated with IgG_2. It binds only to FcγRII receptors and also does not effectively activate the complement cascade as compared to IgG_1 (277).

IgG_3 constitutes about 4% of IgG and has a molecular weight of 170 kDa and a half-life of 7-21 days. In IgG_3 **(Table 4)**, the Fab fragments are far away from the Fc fragment giving the molecule a greater flexibility. IgG_3 responses are produced in response to protein antigens (275). It binds to all the FcγR receptors of effector cells such as macrophage, neutrophils and natural killer cells and are effective in inducting effector functions such as phagocytosis and ADCC (276). IgG_3 further plays a potential role in limiting inflammatory responses and usually appear first during the course of viral infections. Moreover, this subclass effectively triggers the classical route of complement activation (276).

Lastly, IgG_4 constitutes 4% of IgG and has a molecular weight of 146 kDa with a half-life of 21 days **(Table 4)**. IgG_4 responses are usually produced in response to allergens. They are also formed after repeated or long-term exposures to an antigen in a non-infectious setting. IgG_4 only binds to the FcγRII and FcγRIII receptors on effector cells. Studies have shown that IgG_4 is usually associated with higher tumour recurrence in HCC (278).

1.3.2.3.2 Immunoglobulin M (IgM)

IgM is considered as the largest antibody and makes up 5%-10% of total serum antibodies. It is the first to be expressed during B cell development (expressed on the plasma membrane of B cells as a monomer) and also the first antibody to appear in response to initial exposure to an antigen **(Table 3)** (275). It forms a pentamer with a polypeptide chain called the J chain which contains 10 antigen-antibody binding sites.

IgM tends to be polyreactive allowing IgM bearing B cells to respond quickly to antigens (275). This antibody is mostly found in lymph fluid and blood and is efficient as a neutralising agent in early stage of a disease. IgM binds complement component C1 and activate the classical pathway, which further leads to the opsonisation of antigens. It is also termed as natural antibody as it can bind to specific antigens without prior immunisation (279).

1.3.2.3.3 Immunoglobulin A (IgA)

This immunoglobulin makes up about 10%-15% of total serum antibodies. IgA is highly expressed at mucosal surfaces and secretions, such as breast milk and saliva **(Table 3) (280)**. This antibody makes up 50% of the protein in colostrum. It occurs in a monomer in the serum while it exists as a dimer in the mucosa (281). IgA has two subclasses (IgA_1 and IgA_2) which differ particularly in their hinge regions. IgA_1 has a longer hinge region than $IgGA_2$, hence increasing the sensitivity of the former to bacterial pathogens and therefore IgA_2 exist mostly at the mucosal surfaces. IgA plays a vital role in protecting the internal body surfaces by preventing attachment of bacteria or viruses to mucous membranes (281).

1.3.2.3.4 Immunoglobulin D (IgD)

This antibody makes up 0.2% of the total serum antibodies and is also found on the surface of B cells along with IgM. IgD, together with monomeric IgM, are expressed during primary adaptive immune response, thus they are found on the surface of B cells as B cell receptors which are involved in the activation and regulation of B cells **(Table 3)** (282). In humans, some B cells class switch from IgM to IgD. IgD is usually found in serum, cerebrospinal fluids, nasal secretions in humans as well as amniotic fluids of pregnant women (282). Secreted IgD usually attack pathogens in the upper aero-digestive mucosa. Also, in IgA deficiency, IgD tends to provide protection to the

mucosa. IgD helps to promote immune defence by activating IgD interacting cells in tissues and production of activation factors which cause damage and inflammation of tissues (275).

1.3.2.3.5 Immunoglobulin E (IgE)

IgE exist as a monomer and makes up 0.002% of total serum antibodies. IgE binds strongly to FcεR1 on basophils, mast cells and eosinophils and therefore associated with allergic reactions and responses to parasitic worms and infections **(Table 3)** (275, 283). It provides protection to mucosal surfaces by promoting inflammation, which allow IgG, leucocytes and complement components to enter the tissue so as to cause the removal of microbial toxins (283).

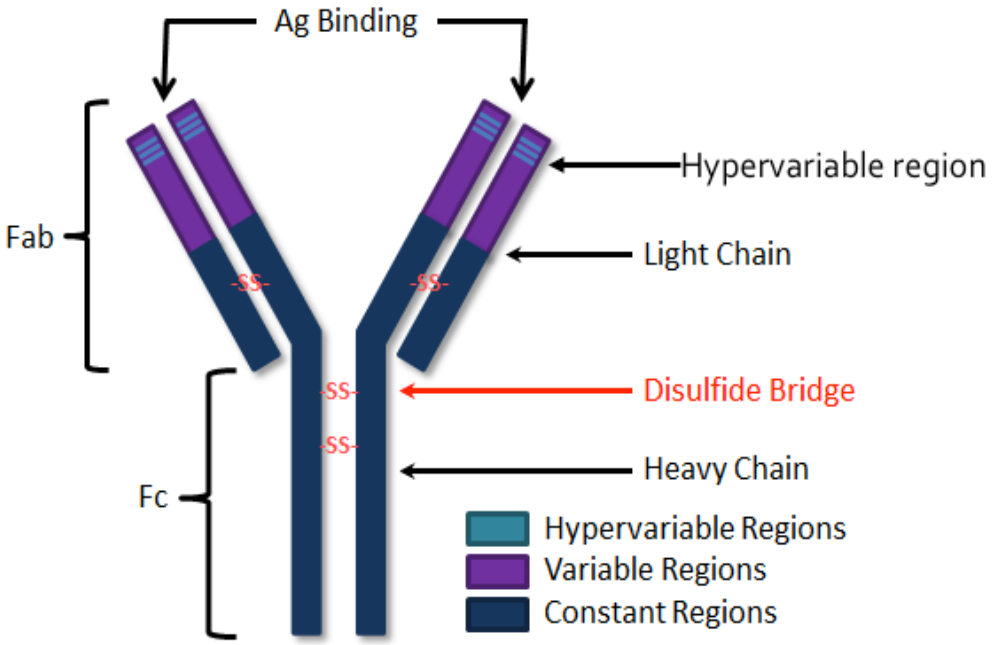


Figure 21: Structure of an Immunoglobulin (Antibody). An immunoglobulin or antibody is Y-shaped and consist of four polypeptide chains (two identical light and two identical chains) which are joined by disulphide bridges. The light chain consists of one constant region and variable region while the heavy chain consists of one variable region and three or four constant regions. The variable domain contains the hypervariable region which help to identify and bind specific antigens. The constant domain of the heavy chains helps to determine the effector functions of the molecule and also define the different immunoglobulin isotypes (IgG, IgM, IgA, IgE, IgD). The antibody upon digestion by papain is divided into the Fab and Fc regions. The Fab region contain the variable domain and hypervariable regions while the Fc region is responsible for Fc receptor mediated activities. Adapted from (275).

Table 3: Classes of immunoglobulins and their respective properties (275).

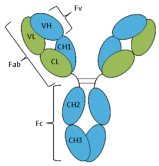
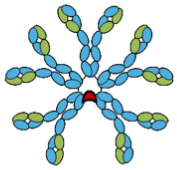
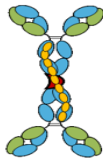
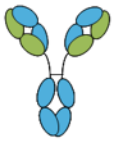
Characteristics	**IgG**	**IgM**	**IgA**	**IgD**	**IgE**
Structure	Monomer 	Pentamer 	Dimer 	Monomer 	Monomer 
% of total serum antibody	80%	5%-10%	10%-15%	0.2%	0.002%
location	Blood, lymph, intestine	Blood, lymph, B cell surface (monomer)	Blood, lymph, secretions (tears, saliva, mucus)	B cell, blood, lymph	Attached to mast cells, basophils
Molecular weight	150,000	970,000	405,000	175,000	190,000
Half-life	21	5	6	3	2
Complement fixation	Yes	Yes	No	No	No
Placental transfer	Yes	No	No	No	No
Functions	Enhances phagocytosis, neutralises viruses and toxins	First antibodies produced in response to initial infection, effective against microorganisms and agglutinating antigens	Localised protection on mucosal surfaces	Presence on B cells functions in initiation of immune response	Allergic reactions; lysis of parasitic worms

Table 4: Different subclasses of Immunoglobulin G (IgG) (276).

Property	IgG_1	IgG_2	IgG_3	IgG_4
Molecular weight	146	146	170	146
Amino acids in hinge region	15	12	62	12
Inter H chain disulphide bonds	2	4	11	2
Half life	21	21	7-21	21
Mean adult serum level (g/l)				
Relative abundance (%)	60	32	4	4

1.3.2.4 Effector Functions of Autoantibodies

The function of anti-TAA autoantibodies in HCC is undefined but it is likely to contribute to immune response to cancer in several ways, such as the typical antibody functions. One of the effector functions of a typical antibody includes neutralisation. This is where the antibody Fab domain interacts or binds specific antigen in order to prevent the activity of the antigen (284). Secondly, these antibodies attach to larger tumour antigens and further bind their Fc regions to the Fc receptors of mononuclear phagocytes (macrophages, monocytes, dendritic cells) and granulocytes (neutrophils) (285). This mechanism leads to the phagocytosis of the antigen-antibody complex by these effector cells using mechanisms such as secretion of antimicrobial peptides, release of metalloproteinases, secretion of cytokines, lipid mediators and reactive oxygen species, which cause either enzymatic digestion, membrane disruption and oxidative damage of antigens (284, 285). Moreover, antibodies are involved in complement mediated cytotoxicity. Pentameric IgM and glycosylated IgG antibodies bound to tumour antigens can form stable complexes with complement (proteins found

in blood and tissues of mammals) activating the cascade of complement proteins to form a membrane attack complex on tumours or pathogens (284). Hence, water and electrons are lost from the pathogen or tumour, disturbing the osmotic stability of the tumour cell. Furthermore, the complement pathway can help in opsonisation of antigens leading to phagocytosis by neutrophils and macrophages (284). Antibodies tend to have the ability to assist in the cytotoxic destruction of tumour cells and pathogens via antibody dependent cell cytotoxicity (ADCC) (285). ADCC occurs when the FcγIIIa receptors on natural killer cells crosslink with the Fc region of antibodies bound to the antigen of interest. This leads to the release of TNF, granzyme or perforin that drives the death of target tumour cells or pathogens (284). Lastly, antibodies interact with target antigens causing them to clump together so they can be eliminated by phagocytosis. This is termed agglutination (284).

1.3.2.5 Relevance of Autoantibodies in the Pathogenesis of Hepatitis C Virus Infection

HCV infection causes damage to the liver by inducing cirrhosis and HCC as mentioned earlier in this chapter. Studies have indicated that during persistent HCV infection, the virus may be involved in the loss of tolerance to self-antigens and may drive mechanism for the production of autoantibodies (286). HCV has an envelope protein E2 on its surface which can interact with CD81 receptors on B cells and further activates B lymphocytes to produce numerous autoantibodies (286). These autoantibodies have been indicated to play a role in the pathogenesis of autoimmune disorders in chronic HCV infection and the prevalence of these circulating autoantibodies is high among patients with chronic HCV infection (286). Particularly, autoantibodies such as non-organ specific autoantibodies, including smooth muscle autoantibodies (SMA), antinuclear autoantibodies (ANA) , anti-liver kidney microsomal-1 autoantibodies, as

well as organ specific autoantibodies, are mostly found in patients with chronic HCV infection (287). It has been shown that some autoantibodies in chronic HCV infection have histological, genetic and biochemical characteristics. Others may help predict the response to anti-viral treatments or prognosis in patients with HCV related chronic liver disease (287). The presence of non-organ specific autoantibodies in HCV infected patients have been shown to correlate with the gravity of fibrotic development, and necro-inflammation (288). Non-organ specific autoantibodies were initially described in autoimmune disorders but has now been found in chronic HCV carriers. Smooth muscle autoantibodies are prevalent in patients with chronic hepatitis C virus infection with its prevalence ranging from 4%-78%. On the other hand, anti-nuclear autoantibodies which serve as a marker for autoimmune liver diseases and other inflammatory conditions have been detected in 4%-54% of patients with chronic hepatitis C infection (287). Also, anti-liver kidney microsome autoantibodies are less abundant ranging from 0%-13% (287). There are no differences in the frequency of autoantibody response between men and women with chronic hepatitis C virus infection. However, this contradicts the higher prevalence of autoantibodies in females than males (289). The presence of anti-smooth muscle autoantibodies is associated with an increase in interface hepatitis score amongst men. Also, SMA or ANA carries an increased risk of fibrosis progression in chronic HCV patients (289). Severity of liver fibrosis of patients with HCV related chronic liver disease is associated with the presence of non-organ specific autoantibodies including ANAs and SMAs. However, the autoantibody titres of such autoantibodies are independent of the HCV genotype or HCV RNA load (290). Also, patients with higher autoantibodies non-organ specific autoantibodies are more likely to develop extrahepatic manifestations of the disease (291).

1.3.2.6 Immunological Approaches to Detection of Tumour Associated Antigens and Autoantibodies in HCC

In 1970, Old and his colleagues pursued the serological identification of human tumour antigens, which could be the origin of patients' autoantibodies (292). They developed autologous typing, an approach where autologous serum and culture cell lines from cancer patients were used to detect new antigens (292). Genomic, proteomic and high throughput approaches have accelerated interest in serum autoantibodies repertoire in human cancers (**Figure 22**) (293). A robust technique referred to as the serological analysis of recombination cDNA expression libraries method (SEREX) (209) has resulted in the identification of over 2000 immunogenic TAAs. In this approach, a cDNA library is constructed using the RNA from tumour specimens packaged into λ-phage vectors and expressed in *E. coli*. The recombinant proteins are then transferred into nitrocellulose membranes after which they are incubated with sera from cancer patients or control donors in order to isolate, characterise and identify autoantibodies involved in cancer. This technique was employed by Wang *et al*, where he separated 81 types of TAAs from the HepG2 cell line and further identified five differential autoantibodies in HCC patients (294). Another approach for detecting TAAs or autoantibodies in HCC is the cDNA or peptide phage display technology (**Figure 22**) (295). It is considered as a third-generation technology to identify autoantibodies. In this technique, the cDNA phage library is constructed from a tumour or a cancer cell line. The TAAs in the libraries are expressed and then displayed on a phage such as the T7 phage. The complex is further used as a bait to capture autoantibodies to TAAs using pools of patients' sera through immunoprecipitation and the corresponding antigens are sequenced for identification (295). The M13 phage display was used by Zhang where

he combined the screening results with AFP to diagnose patients with early HCC (296). The serological proteome analysis (SERPA) (**Figure 22**) also referred to as the Proteomex, is a proteome-based method where proteins in lysates are prepared from tumours or cancer cell lines and are separated by 2D gel electrophoresis based on isoelectric point (p*I*) and are further transferred unto membranes by electroblotting and incubated with the patients' sera (297). This technique was employed by Looi *et al*, in screening 20 HCC patients and 50 patients with chronic hepatitis and liver cirrhosis to HSP60 and HSP70 TAAs (298).

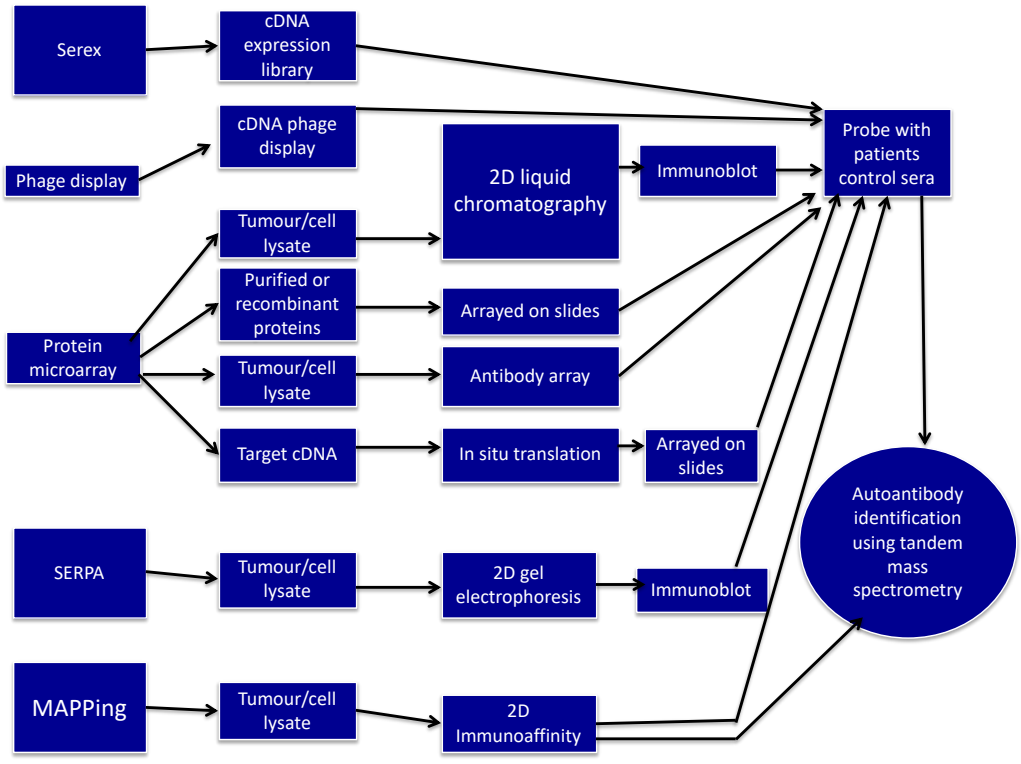


Figure 22: Technologies used for TAA and autoantibody identification in hepatocellular carcinoma Adapted from (262).

Protein microarray technology (**Figure 23**) appears to have the most promise in analysing the 'immune profile of a cancer. This technology has been developed for profiling serum autoantibodies in HCC patients' sera to hundreds of TAAs simultaneously (299). Robinson *et al*, used this technique where serial dilution of

eighteen autoantigens targeted in systemic autoimmune disease was used to determine the accuracy of autoantibody titre using small amounts of serum (300). The assay proved to be sensitive and showed minimal cross reactivity. The development of protein microarrays for autoantibody profiling in systemic autoimmune diseases has paved the way for the use of this technology in other diseases such as diabetes (301). Protein microarray was however, adapted as an alternative approach to already existing Enzyme Linked Immunosorbent Assay (ELISA) and western blot techniques and has since then been able to overcome many challenges of ELISA (300). This technique allows for a high throughput and scalable analysis. It requires a small amount of patient sample as well as reagents and therefore reduces time and cost to run the assay (300). It further provides a form of protein analysis at a scale beyond that which is achievable by a 2DE or ELISA. The potential application of protein microarrays include improved diagnosis, monitoring disease progression and response to therapy, development of individual therapies, identification of new autoantigens that could serve as disease biomarkers (301).

In this approach, a selected panel of purified or recombinant proteins, synthetic peptides or fractionated proteins obtained from a tumour or cancer cell lysates can be spotted robotically in replicates onto a microarray, which could either be glass slides, nitrocellulose or micro titre plates, and are then probed with patients sera suspected to contain the autoantibodies (302). A fluorescently conjugated anti-human IgG antibody is added after which the fluorescent intensity of the bound antibodies are identified (302). In cases of low concentrations, the signals can be amplified. This method allows the study of antigen-antibody interactions in a miniaturised and highly multiplexed manner (301). Current challenges in the use of this technology include optimal conditions to limit variation observed for autoantigen spotting and printing conditions,

minimize epitope alterations following attachment of antigens to a planar surface, which may result in efficient internal controls, validation of the arrays with well characterised serum samples before this technology is ready for use in clinical settings (301). Although this high throughput has been applied for autoimmune and other cancer diagnosis, it has not been reported in HCC. It is therefore necessary to utilise this immunologic high throughput approach in detecting autoantibody in HCC patients.

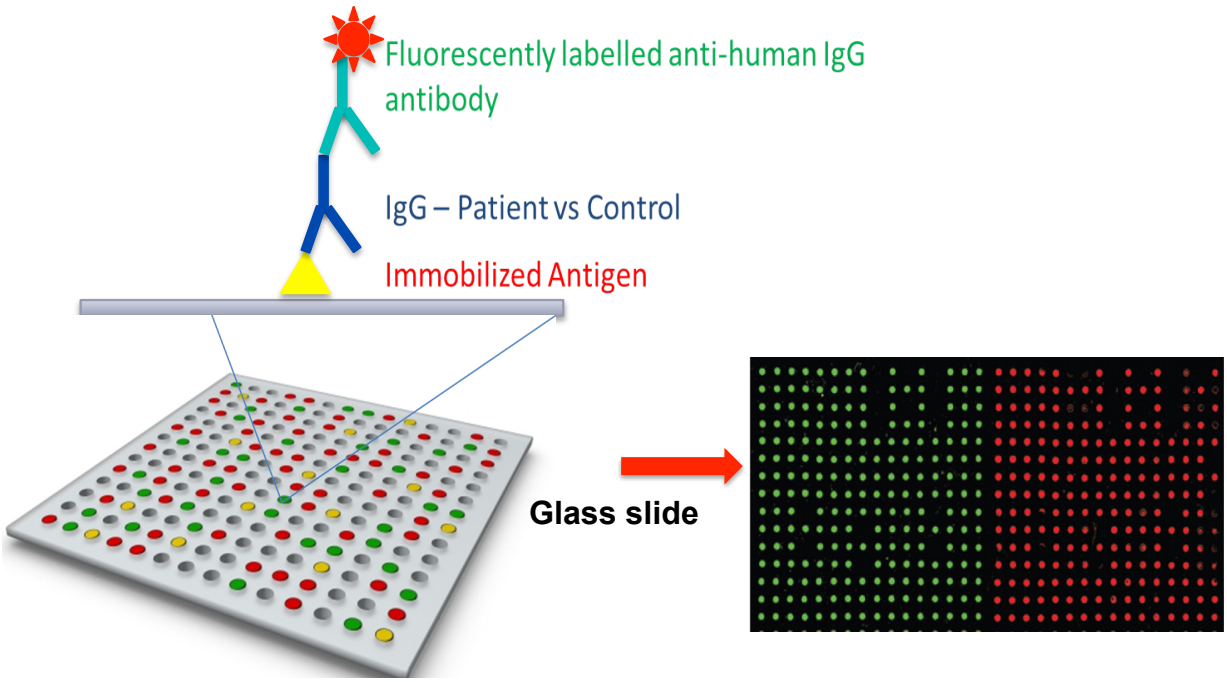


Figure 23: An example of Protein Microarray Technology. Proteins of interest can be detected using primary antibody or an antigen and further amplified by the use of secondary antibody tagged to biotin.

1.4 Diagnosis, Prevention and Management of Hepatocellular Carcinoma

1.4.1 Clinical Diagnosis of Hepatocellular Carcinoma

There are a variety of methods currently used to diagnose HCC. These include: clinical presentation, Alpha Feto-protein (AFP) levels detection, ultrasound, CT scan, MRI, angiography, radiographic imaging for extrahepatic spread and liver biopsy.

1.4.1.1 Clinical presentation:

The clinical presentations observed in HCC patients at the time of diagnosis mostly relate to the extent of hepatic reserve (303). Cirrhotic patients often present with non-specific signs and symptoms, such as jaundice, hepatic encephalopathy and anasarca. HCC can also malignantly invade the portal structures to present variceal bleeding and ascites (303). However, non-cirrhotic patients with HCC present a different clinical manifestation. Clinical symptoms like anorexia, malaise, wasting distension and right upper quadrant abdominal pain are mostly related to long-standing malignancy and tumour growth. When the tumour infiltrates adjacent extra-hepatic biliary structures, a painless obstructive jaundice is realised. HCC can rarely present a severe complication called tumour rupture (303). This occurs when the size of a vascular tumour becomes larger than its blood supply on the liver periphery. Patients with such conditions manifest peritoneal irritation, hypertension and suddenly severe abdominal pain, which could be confirmed by abdominal laparotomy (303). In advanced HCC, extra-hepatic manifestations may occur as a result of distant metastasis or paraneoplastic phenomena. In such cases, metastasis can occur through lymphatic or hematogenous routes to organs such as the bones, abdominal viscera and lungs (303).

1.4.1.2 Alpha-fetoprotein (AFP):

This is a protein that is encoded by the AFP gene in humans The AFP gene is located on the q arm of the chromosome 4 (4q25) (304). It is produced as a glycoprotein of 591 amino acids (pucci 91) and a carbohydrate moiety (305). Baig and colleagues (306) provided conclusive evidence that AFP is an important marker for HCC, and also an indicator of HCC risk, mostly in patient with cirrhosis and HCV/HBV infection. HCC patients in Thailand with AFP>400ng/ml have been shown to have greater tumour size, portal vein thrombosis and decreased survival. Thus, AFP levels correlated with tumour size and volume (307). Patients with high levels of AFP demonstrates poor differential tumours with reduced prognosis when AFP levels are >1000ng/ml (308). In situations where tumours were successfully removed by surgical operation, an immediate decrease in AFP levels to normal were achieved, however, incomplete resection resulted in persistent increased AFP levels (308).

1.4.1.3 Ultrasound:

It is a basic technique for imaging the liver structure. Although this technique is very fast and simple, limited resolution and specificity for small liver lesions are the greatest obstacles in its use. However, the use of contrast agents such as intra-arterial CO_2, and helium could help overcome these limitations (309, 310). Colour Doppler and Power Doppler imaging are two ultrasound principles useful in the assessment of hepatic vascular-flow. However, the Power Doppler imaging is more sensitive for registering flows in tumours (311). These techniques can differentiate blood thrombosis from tumour invasion in the portal vein. Contrast-enhanced ultrasound (CEUS) has the ability to show hypervascularity in HCC (312) and characterise HCC on cirrhosis for nodules >2cm in diameter (313). When two dynamic imaging modalities are coincident, nodules from 1 to 2 cm in diameter can be characterised (314). With the use of

ultrasound, portal hypertension complications such as ascites, splenomegaly and gastro-hepatic ligament varices can be visualised (315).

1.4.1.4 Computed Tomography of the liver (CT):

CT scanning is very useful and frequently used to evaluate liver masses and cirrhotic liver for HCC. Comparatively, CT scanning has the ability to assess the entire liver equally and produces a more systemic examination of extra-hepatic metastasis. In a multiphasic examination, the hepatic veins, liver parenchyma, the portal veins and the hepatic arteries could be systematically evaluated by CT (315). It can also be used to evaluate the vascularity of HCCs as well as local metastasis and invasion of the hepatic and portal veins. Intra-tumoural fibrous stranding (mosaic sign), fatty metamorphosis, necrosis or calcification can be revealed on CT in HCC (315).

1.4.1.3 Magnetic Resonance Imaging (MRI):

This technique plays a very significant role in the examination of hepatic lesions when HCC is suspected. Despite using similar concepts to CT imaging, MRI can produce extended imaging, evaluating numerous characteristics of tissues, organs and tumours. Thus, it produces efficient characterisation of tissues and tumours (316). MRI can produce T1 and T2 images, which represent different types of tissues characteristics (316). T2 weighted images typically appear hyper-intense than T1 weighted images; this inconsistency is caused by steatosis, focal haemorrhage, or copper and glycogen accumulation in tumour (317-319). When examining tumours <2cm in diameter, MRI has a very low sensitivity, however, the addition of some contrasting agents like super-paramagnetic iron oxide and gadolinium improve accuracy and characterization of HCC tumours (320). In most medical institutions, MRI has gained popularity as the preferred diagnostic imaging mode of HCC due to its high-resolution images.

1.4.1.4 Angiography:

Due to the hyper-vascularity nature of HCC, angiography serves as a useful diagnostic tool for HCC assessment because of its highly vascular nature. Although very useful, angiography is less sensitive when used to detect hepatic tumours of less than 2cm in diameter (320). Currently, the technique provides reliable results when used as guidance for transarterial chemoembolisation therapy.

1.4.1.5 Nuclear Mechanism:

This strategy has proven to be useful in HCC diagnosis. Nuclear medicine agents like ^{99m}Tcoctreotide (321), ^{18}F-Fluoro-deoxyglucose (^{18}F-FDG) (322, 323) and acetate (324) have been developed for HCC imaging. The high uptake of ^{18}F-FDG by the liver during positron emission tomography (PET) leads to obscuring of smaller hepatic lesions therefore showing very low sensitive or high false negative results (322, 323). The frequent use of the technique is also limited by its high cost.

1.4.1.6 Liver biopsy:

Cytologic and histologic samples from the liver represent a reliable and effective means to confirm HCC in patients with suspicious lesions. There is a high diagnostic accuracy when fine-needle aspiration (FNA) and core biopsy technique are used simultaneously giving a specificity of 95% and a sensitivity of 96% when compared with any other diagnostic test (325). In the microscopic examination of HCC, the following features are mostly seen: trabecular architecture, increased nuclear to cytoplasmic ratio, atypical naked nuclei and peripheral endothelial wrapping. In patients with small tumours, a liver biopsy is needed to pre-operatively confirm HCC in order to prevent high false positive diagnosis. Liver biopsy has a 95.6% accuracy when used to evaluate tumour lesions <2cm in diameter (325). The technique rarely has complications and also has

the following benefits: 0.006%-0.3% rate of mortality with a <1% risk of infection or serious haemorrhage (325).

1.4.2 Prevention

Prevention of HCC is necessary to reduce mortality rate associated with this malignancy. This is also important in order to lessen economic hardships resulting from high HCC incidences. There are three levels for the prevention of HCC: primary, secondary and tertiary preventions (326).

1.4.2.1 Primary Prevention:

This primary strategy is used to prevent an aetiological agent from initiating the carcinogenic process. This is particularly useful in the prevention of chemical, physical and viral causes of cancer. The immunisation against HBV infection is essential in HCC prevention. In 181 countries, HBV vaccine has been incorporated into the Expanded Programme of Immunisation (EPI) where about 80-90% of babies are now being immunised (327). This has resulted in a drastic reduction in the percentage of chronically infected babies born to highly infectious carrier mothers. A significant reduction in HCC has also been seen in highly endemic countries such as China, Singapore and Thailand as a result of the implementation of the vaccination program (328). Immunisation against HCV is another strategy that can immensely contribute to HCC prevention. Despite the considerable research directed towards HCV vaccine development, this goal is still some decades away because of the extreme variability of the genome, the numerous quasispecies in infected blood and the lack of evidence for an effective neutralising antibody against the virus (329). Notwithstanding, there are other important interventions that can contribute to the prevention of HBV/HCV. Such interventions are essential since the full beneficial effects of the HBV vaccines take years and that of HCV is yet to be developed. Effective screening of donated blood for

HCV and HBV viral inactivation in blood product manufacturing (330), practicing of safe injection (330), passive immunisation and the use of antiviral agents, such as interferon-alpha are useful strategies to primarily prevent against hepatitis viruses (331). Exposure to blue-green algae, microcystins, dietary iron overload and aflatoxin B1 contribute to the occurrence of HCC. Pragmatic interventions to prevent this exposure will minimise or prevent HCC occurrence (332). Studies have also shown that weight reduction (333) and treatment with Metformin (334) prevent the incidence of NAFLD and diabetes related HCC respectively.

1.4.2.2 Secondary Prevention:

Using natural or synthetic chemicals, which prevent the integration of carcinogens with tissue nucleophiles, can prevent HCC. Chlorophyllin, an anti-carcinogen (335) derived from natural chlorophylls has been shown to strongly complex with numerous carcinogens including AFB1, thereby reducing the bioavailability and carcinogenic potential (336). Chlorophyllin also been shown to possess antioxidant properties; thus, it prevents lipid peroxidation (337). Polyprenoic acid, a chemopreventive agent, has been shown to inhibit cell growth and promotes apoptosis and differentiation in human cancer cell lines. In a double blind, placebo-controlled trial in Japan, this agent was administered orally over 12 months (338, 339). An anti-schistosomal drug, oltipraz, which has a similar structure like dithiolethiones found in cruciferous vegetables has been revealed to possess anti-cancer properties (340, 341). Oltipraz increases and regulates the expression of detoxifying enzymes and anti-oxidative enzymes that ultimately contributes to the detoxification of AFB1 reactive metabolites (341), thus, preventing AFB1-induced HCC. The removal of accumulated iron from patients with hereditary hemochromatosis has been shown to secondarily prevent the development of cirrhosis and HCC formation. This has been shown to increase life expectancy,

improve prognosis and survival rate in cirrhotic patients (342). Chemoprevention of HCC is based on the consumption of leafy green vegetables, fruits and nuts. This is because their natural constituents contain Phytochemicals, such as isothiocyanates and glycosinolates, which possess anti-cancer properties and inhibit tumour formation in rats (343-345). These natural chemicals have a potential of decreasing the risk of HCC.

1.4.2.3 Tertiary Prevention:

This strategy prevents the progression of pre-cancerous lesion-like cirrhosis to cancer. HBV and HCV infection and alcohol abuse have been shown to be the major causes of cirrhosis and eventually HCC. Although few studies have been conducted on the use of IFN-α in preventing chronic HBV-induced HCC, most of the results generated have failed to demonstrate a conclusive evidence between IFN-α treatment and decreased risk of malignant transformation in cirrhotic patients (346). PEG-IFN has also been evaluated in the preventing of HCV-related HCC (347). Anti-viral therapy efficiently suppresses HBV infection and limits liver injury, which reduces HCC incidence (348). Glycyrrhizin has anti-cancer and anti-oxidative properties which reduces the risk of HCC by stimulating NK cells, increasing IFN-γ production, modulating the immune system and inhibiting hepatic inflammation (344).

1.4.3 Management and Treatment of Hepatocellular Carcinoma

Treatment of HCC depends on the location and degree of the cancer, as well as the general health of the liver. In addition, it is very important to know the various stages of the HCC (**Table 5**). However, patients with inherited liver disorders tend to have no specific treatment for HCC. HCC patients are staged based on the Barcelona Clinic Liver Cancer (BCLC) staging which was proposed in 1999 the Barcelona Clinic Liver

Cancer group (349). With this, HCC patients are divided into five stages namely, stages O, A, B, C and D (350). Stage O is defined as a single tumour <2cm in diameter while stage A is considered as single tumour >2cm. Patients in Stage B, C and D are regarded as those with multinodular asymptomatic tumours, extrahepatic spread and the poor performance stage respectively (350). These do not only give treatment allocation but also provide information on prognostic prediction such as the tumour size, number and vascular invasion.

Table 5: The Barcelona Clinic-Liver Cancer (BCLC) staging system of HCC (349).

HCC STAGE	DEFINITION
O	Single tumour <2cm
A	Single tumour >2cm
B	Multinodular asymptomatic tumours
C	Extrahepatic spread
D	End stage, poor performance

Resection is considered as the best treatment for HCC patients with small solitary nodules without underlying cirrhosis (351). The best candidate for this procedure is an HCC patient with stage O or A, usually with normal portal pressures and normal bilirubin (352). In this technique, the cancer as well as the surrounding normal tissue is removed. One major setback of this technique is the recurrence of the tumour and 5-

year rate of survival after hepatectomy is between 60% to 70% (351). Also, liver surgery in patients with chronic liver disease are likely to have hepatic failure. Studies have shown that recurrence of tumour after resection affects about 70% to 80% of cases after five years.

Liver transplantation is considered as the principle choice of treating patients with tumour <5cm or up to 3cm and have advanced liver dysfunction (353). Liver transplantation is often regarded as superior to resection since it has much lower rates of recurrence. Due to scarcity of living donors, most patients tend to die before receiving transplantation (353). The problem has slightly been resolved by the development of the adjuvant therapy system, which prevents progression of the tumour whilst waiting for transplantation.

The local ablation system of treatment is usually administered to patients at early stages of the cancer, i.e. patients with tumours <2cm (354). Patients with poorer liver function who are not candidates for liver transplantation (LT), with less than 3 nodules are usually indicated with ablated therapies (355). This technique uses several methods to destroy the tumour. First of all, the percutaneous ethanol injection (PEI) method subjects the lesion to ethanol (354). The thermal ablative therapy on the other hand subjects the tumour to heating between 60^{o}C to 100^{o}C. With the radio ablation, microwave and cryoablative therapy, the tumour is subjected to high frequency ultrasounds, microwave and freezing at -20^{o}C to -60^{o}C respectively (354). These therapies cause complete necrosis of the tumour as a result of protein denaturation and cellular dehydration (354). Survival of patients after local ablation therapy is usually 50%-70% at 5 years and this has challenged resection as the first line of treatment in patients with small solitary HCCs (314). Tumours larger than 5 cm usually have a

reduced response rate to the ablation. This technique is gradually becoming very popular as substitutes for the resection for patients waiting for liver transplantation (356).

The chemoembolisation therapy is the most popular treatment for people at the BCLC stage D, i.e. the advanced stage of the cancer (357). The rationale behind this technique is to induce cytotoxic and ischemic effect on the hepatic artery supplying the tumour and cellulose is usually the common material used (357). Chemoembolisation causes a delay in macrovascular invasion and tumour progression. A very common complication with this treatment is post embolisation syndrome occurring in more than 50% of patients where patients usually present with fever, nausea and abdominal pain. These symptoms are often self-limiting (358, 359). Knowledge in molecular mechanisms inducing HCC has helped with the development of treatment to abrogate the disrupted pathways. The mechanism of HCC involves a number of signalling pathways and therefore targeting them would be of great benefit. There was no first line of treatment for patients in the advanced stage of HCC until 2007. Different systemic agents including interferon, tamoxifen and conventional chemotherapy, such as doxorubicin and 5-fluorouracil, have been evaluated by several studies (355). None was able to exhibit survival benefits with any of these compounds. Sorafenib, a multikinase inhibitor, has been developed to treat advanced HCC (360). It is responsible for blocking the Raf, VEGF and C-kit pathways (360). Sorafenib has elevated the median survival in advanced HCC patients from 7.9 (placebo) to 10.7 months, with a hazard ratio (HR) of 0.69 (SHARP trial) (361). Recent studies have shown that sorafenib has serious side effects and therefore most patients are now placed on Bortezomib treatment (362). Unfortunately, patients tend to develop drug resistance to the Bortezomib therapy. This has led to the development of a new therapeutic opportunity, called

Ixazomib (MLN2238) (363), although is yet to be put on clinical phase trials. This drug has been shown to have great anti-tumour activity by reducing the cell viability and proliferation of HCC cells. It also induces apoptotic cell development in HCC cells and induces cell cycle arrest. Other systemic agents such as ertotinib, brivanib, everolimus and rapamycin, which are EGFR, FGFR/VEGFR and mTOR inhibitors respectively, are currently under late clinical developmental phases in first and second line for patients with advanced HCC (361). Other molecular therapies have been developed to target certain signalling pathways. Bevacizumab and cetuximab are monoclonal antibodies that have been developed to target the vascular endothelial, Endothelial growth factor and the MAP kinase signalling pathways respectively (364). By so doing, these therapies induce anti-proliferative and anti-angiogenic effects on the tumours, hence delaying their progression. Immune therapies have been developed to treat HCC. CTLA-4 is responsible for immune tolerance during HCC. Hence, the administration of CTLA-4 inhibitor augments anti-tumour immunity in HCC (365). This was observed in a study where patients with HCV-associated HCC who failed the traditional HCC therapy showed a partial response of 17.6% to CTLA-4 inhibitor.

1.5 Aims and Objectives

1.5.1 Aim

Hepatocellular carcinoma exerts a continuous devastating effect, claiming 600,000 lives every year. The extensive prevalence of this malignancy carries a significant economic burden on a country. HCC is mostly detected at the advanced stages and hence, patients tend to have a poor 5-year survival rate. The poor prognosis is attributed to lack of highly efficient diagnostic tools to detect the cancer early, which compromise successful treatment. HCC patients produce early detectable autoantibodies, which appear five years before the clinical manifestation of the disease. These recognise a wide range of TAAs during tumour development, making the autoantibody signature an effective approach for early diagnosis of the disease. It is therefore crucial to develop a high-throughput and robust screening system that would allow autoantibodies to be detected in HCC patients. In recent times, the antigen microarray is increasingly being used to profile autoantibodies in cancer patients, which has helped in the study of antigen-antibody interactions in a patients' sera in a multiplexed and high throughput manner. The main aim of this project is to develop the in-house microarray platform and to further utilise it to profile anti-TAA autoantibodies in HCC and underlying liver disease patients.

1.5.2 Specific Objectives

Below were the objectives for the entire work:

1. To identify a cohort of TAAs that have either been shown as immunogenic in HCC or any liver disease or are associated with HCC, but no autoantibody research has been undertaken on them.

2. To develop and assess the validity of the in-house antigen microarray technology in order to improve the accuracy and precision for this early biomarker detection in HCC patients.
3. To produce a panel of eight TAAs in HCC as recombinant proteins in eukaryotic expression system suitable for use on the microarray assay, which could assist in the detection of autoantibodies in high risk-patients.
4. To characterise serum autoantibody response in i) HCC patients, ii) high-risks (underlying liver disease) patients from different aetiologies and iii) healthy control groups, over a wide range of in-house and commercial TAAs produced both in eukaryotic and *E. coli* expression systems.
5. To identify immunogenic TAAs that could assist in the early detection of HCC in high-risk cohorts.

Chapter Two: Materials and Methods

2.1 Materials (Antigen Microarray Technology)

2.1.1 Chemicals and Reagents

All chemicals and reagents for the antigen microarray assay were purchased from Sigma-Aldrich (Poole, UK) unless otherwise stated.

2.1.1.1 Printing Buffers

To ensure that the natural characteristics and shape of proteins are preserved during immobilisation onto slide surfaces, three different printing buffers were tested to determine the optimal one. Thus, the ideal printing buffer should prevent protein denaturation and maintain protein stability during printing. These buffers are detailed in **table 6**.

Table 6: Composition of printing buffers tested for arraying proteins onto glass slides.

Printing buffer	Manufacturer	Composition
PBS-Trehalose-Betaine-Tween	Sigma, UK	1x PBS, 35mM Betaine, 50mM Trehalose, (0.01% v/v) Tween-20
PBS-Trehalose-Tween	Sigma, UK	1x PBS, 50mM Trehalose, (0.01% v/v) Tween-20
PBS-Trehalose	Sigma, UK	1x PBS 50mM Trehalose.

Abbreviations: i) Phosphate Buffered Saline (PBS), ii) PBS-Tre iii) PBS-Tre-Tw iv) PBS-Tre-Bet-Tw

2.1.1.2 Blocking Buffers

Before proteins immobilised onto slide surfaces were detected with antibodies, the remaining binding surfaces were blocked with a buffer. A suitable blocking buffer prevents non-specific binding of primary and secondary antibodies and reduces background noise, which interferes with positive signals. Tested blocking buffers are shown in the **Table 7**.

Table 7: Different blocking buffers tested.

Blocking buffers	Manufacturer	Composition
5% BSA Block	Sigma, UK	3.33ml 30% BSA in 16.67ml of 1X PBS-0.05% Tween-20
10% BSA Block	Sigma, UK	6.67ml 30% BSA in 13.33ml of 1X PBS-0.05% Tween-20
30% BSA Block	Sigma, UK	30% BSA kit
0.2% I block	R&D systems, MN, USA	0.05g I-block dissolved in 25ml PBS, 0.05% Tween-20
Super G Buffer	Grace Bio Labs, UK	Super G Blocking Kit
Avidin-Biotin Buffer	Invitrogen, UK	Avidin-Biotin blocking Kit

2.1.1.3 Wash Buffer

PBS-0.05% Tween 20 (pH 7.4) was used as a washing buffer. To prepare 10X PBS Tween, 10 PBS tablets were dissolved in 1 litre of deionised water (dH_20) and mixed with 0.5 ml Tween 20.

2.1.2 Substrate for array printing (Slide Surfaces)

Selecting the appropriate slide surface for protein immobilisation is essential for obtaining reproducible microarrays for diagnostic and research purposes. Several slide surface chemistries were tested to determine the optimal array surface to ensure that the antigenic epitopes of proteins are preserved during printing and processing **(Table 8)**.

Table 8: Different types of slide surfaces tested.

Slide surface	Manufacturer	Catalogue number
Aminosilane	Schott-Nexterion, UK	1064875
Poly-L-Lysine	Electron-Microscopy Sciences, UK	63478-AS
Nitrocellulose	Grace Bio-Labs, USA	305016
Epoxysilane	ThermoFisher, UK	12-550-55

2.1.3 Antibodies used for the Microarray Assay

A range of detection antibodies and quality controls were used for the development of the antigen microarray assay **(Table 9)**.

Table 9: Antibodies used for Antigen Microarray Assay.

Proteins and Reagents	Manufacturer	Catalogue number
Monoclonal mouse anti-DDK antibody	Sigma Aldrich, UK	F3165
Monoclonal mouse anti-Myc antibody	Insight Biotechnologies, UK	OAEA00011
Monoclonal mouse anti-His_6 antibody	Cell Signalling, UK	6AT18
Polyclonal Rabbit anti-His_6 antibody	Insight Biotechnology	35533
Biotinylated Goat anti-human IgG antibody	Vector Laboratories, UK	BA3080
Antibody diluent	DAKO, UK	S080983-2
Streptavidin Horseradish peroxidase	Bio-rad, USA	L9703206
Western-blot amplification module kit	Bio-rad, USA	1952737
Streptavidin-Cy5 conjugate	Molecular Probes, UK	SA1011
Streptavidin infrared	LI-COR Biosciences, UK	926-68031
Biotinylated goat anti-mouse Monoclonal (IgG) antibody	Insight Biotechnologies, UK	TA130072
Biotinylated goat anti-rabbit polyclonal (IgG) antibody	Insight Biotechnologies, UK	OASB01959

2.1.4 Commercial Tumour-Associated Antigens (TAAs)

Commercial hepatocellular carcinoma (HCC) recombinant tumour-associated antigens (TAAs) used in the study were either produced in *Escherichia coli* (*E. coli*) or eukaryotic systems. These were diluted in printing buffer and immobilised on activated glass slides **(Table 10)**.

Table 10: Commercial recombinant tumour-associated antigens arrayed onto glass slides.

TAA	Expression system	Tag	Concentration (μg/ml)	Company
AFP	*E. coli*	His	150	Oncimmune Ltd, UK
APCN	*E. coli*	His	224	Oncimmune Ltd, UK
GANKYRIN	*E. coli*	His	410	Oncimmune Ltd, UK
GRP78	*E. coli*	His	276	Oncimmune Ltd, UK
HDGF	*E. coli*	His	196	Oncimmune Ltd, UK
KRAS	*E. coli*	His	206	Oncimmune Ltd, UK
RALA	*E. coli*	His	149	Oncimmune Ltd, UK
IMP1	*E. coli*	His	229	Oncimmune Ltd, UK
HRAS	*E. coli*	His	391	Oncimmune Ltd, UK
P62	*E. coli*	His	431	Oncimmune Ltd, UK
KRAS	HEK 293 cells	Myc-DDK	1000	Oncimmune Ltd, UK
HRAS	HEK 293 cells	Myc-DDK	1000	Origene, USA
HDGF	HEK 293 cells	Myc-DDK	1000	Origene, USA

P16	HEK 293 cells	Myc-DDK	1000	Origene, USA
RALA	HEK 293 cells	Myc-DDK	1000	Origene, USA
P62	HEK 293 cells	Myc-DDK	1000	Origene, USA
P53	HEK 293 cells	Myc-DDK	1000	Origene, USA
Gankyrin	HEK 293 cells	Myc-DDK	1000	Origene, USA

2.1.5 In-house Recombinant Tumour-Associated Antigens

We opted for in-house HCC recombinant TAAs to be sure of the quality and purity of antigens produced. True human open reading frame (ORF) clones tagged with Myc/DDK (Flag) were purchased and transfected into HEK 293 cells. These proteins were diluted in printing buffer and immobilized onto glass slides **(Table 11)**.

Table 11: In-house recombinant tumour-associated antigens (TAAs) arrayed onto glass slides.

TAA	cDNA	Tag	Vector	Concentration(μg/ml)	Predicted Molecular weight	Company
KRAS	KRAS	Myc/DDK	pCMV6	1275	21.2	Origene, USA
HRAS	KRAS	Myc/DDK	pCMV6	518	44.2	Origene, USA
HDGF	HDGF	Myc/DDK	pCMV6	1751	26.6	Origene, USA
P16	CDKN2A	Myc/DDK	pCMV6	659	17.8	Origene, USA
RALA	RALA	Myc/DDK	pCMV6	733	23.4	Origene, USA
P62	KDRH1	Myc/DDK	pCMV6	708	44	Origene, USA

P53	TP53	Myc/DDK	pCMV6	855	44.1	Origene, USA
Gankyrin	PSMD10	Myc/DDK	pCMV6	1552	23.2	Origene, USA

2.1.6 Quality controls used for the Antigen Microarray Assay

Table 12: A selection of quality controls used in the antigen microarray assay.

Quality control	Manufacturer	Catalogue number
***Candida albicans* antigen**	Jena Biosciences, Jena, Germany	PR-BA117-S
***E. coli* antigen**	Cell Signalling, UK	12548
Tetanus toxoid	NIBSC, UK	02/232
Myc antibody control (Myc peptide)	Chromotek, UK	41107
Amino terminal Flag BAP^{TM} fusion protein)	Sigma Aldrich, UK	P7582
Cell lysate containing pCMV entry vector	Origene, USA	Sku LY5000001
Human purified IgG	Athens research and Technology	16-16-09707

2.1.7 Acquisition of Human Serum Specimens: Permission and Collection

Serum samples were obtained from 183 HCC patients with different aetiologies (hepatitis B virus (HBV), hepatitis C virus (HCV), non-alcoholic fatty liver disease (NAFLD), non-alcoholic steatohepatitis (NASH), alcoholic liver disease (ALD) and Type 1 diabetes (T1D), 46 healthy controls, 90 non-HCC cirrhotic and 133 non-HCC non-cirrhotic (chronic hepatitis) patients (**Table 13**). These samples were kindly provided by the Centre of Excellence for Autoimmunity in Cancer (CEAC), Prof. W. Irving, The Trent Cohort Study, Nottingham University Hospitals NHS Trust and HCV

Research Biobank, UK. Informed consent form was obtained from all participants. All serum samples were heat-inactivated at 56ºC for 30 minutes in the class II biosafety cabinet. They were further centrifuged at 3200 rpm for 10 minutes after which sera were stored as 200 µl aliquots at -80°C until use. This was done to prevent repeated freeze-thaw cycles. Ethical approval and informed consent were given for all samples prior to the study

Table 13: Information on clinical sample cohort.

Sample cohort	**Total number**	**Disease aetiology**						**Sex**		**Age**
		HBV	**HCV**	**NAFLD**	**ALD**	**NASH**	**T1D**	**M**	**F**	**Mean age**
HCC	183	6	152	1	16	4	4	141	42	63
Healthy controls	46	HEALTHY						10	36	61
Non-HCC non-Cirrhotic	133	HBV 1		HCV 126			Alcohol 6	101	32	58
Non-HCC Cirrhotic	90	HBV 0		HCV 90		Alcohol 0		68	22	59

2.2 Methods (Antigen microarray)

2.2.1 Plate Preparation and Storage of Plates

Ten His_6-tagged recombinant TAAs produced in an *E. coli* system (KRAS, HRAS, HDGF, RALA, P62, Gankyrin, AFP, APCN, GRP78, Imp1) and quality controls (*Candida albicans*, *E. coli*, Tetanus toxoid) were diluted in printing buffer (PBS-Trehalose-Betaine-Tween) to make a volume of 20 µl at concentrations ranging from 75 µg/ml-100 µg/ml. The protein dilutions were then transferred into a 384 microtiter well plate (Genetix, USA). In addition, a two-fold serial dilution of purified human IgG was prepared and placed on the same 384 well plate in 10 dilutions starting at a concentration of 0.05 mg/ml. The preparation was centrifuged (Universal 30 RF) at 1200 rpm for 5 minutes to remove bubbles and ensure all liquid was at the bottom of the microtiter well plate. Between print runs, plates were sealed and stored at -20^{o}C. To avoid contamination and evaporation during microarray preparation and storage, plates were handled carefully. Plates were thoroughly defrosted before placed in the arrayer.

2.2.2 Microarray Printing

Proteins were printed using the in-house microarrayer (BioRobotics MicroGrid II, USA) (**Figure 24**) situated at the Genomics facility at the Queens Medical Centre, University of Nottingham, United Kingdom. It employs the robotic contact spotting pin principle, which is termed split-pin, or quill-pin technology. The arrayer consists of a biobank with a plate holder that can carry up to 24 microtiter plates (source plates) and four slide trays, each of which can hold 27 slides. The pins are washed before the run starts and prior to visiting new source plate wells. Washing consists of visits to each of two recirculating baths which are supplied constantly with wash buffer (H_2O with

0.05% Tween) from two separate 2-liter reservoirs, for initial rinsing of pins between source plate visits. Pins are then washed at the third main wash station. It uses a flood and vacuum system to wash the pins in H_2O. This wash procedure is repeated 3 times before each new source plate visit. The silicon-arraying pin (Parallel Synthesis Technologies, USA) is a vital component of the arrayer because it is the only part of the instrument, which draws proteins diluted in printing buffer from the plate and further deposits them onto the slide surface. The pin is dipped into the wells of the microtiter plate to load 100 nl of liquid in its capillary channel and upon contact with a slide surface, deposits roughly 0.5-1 nl of fluid per spot. These form circular protein spots when it pulls away from the surface. Repeated deposition of such protein spots leads to the generation of a regular array on the slide surface. Each slide in a print run is printed with the same array.

The microarray printing (**Figure 25**) was undertaken using the TAS application software (Apogent, UK) with a customised array layout and print parameters. In order to produce high quality printed slides, which would determine the reproducibility, reliability and precision of the assay, a number of procedures were undertaken. To ensure that the operating parameters of the arrayer such as the humidifier, contact dwell time, sample volumes, spot location and target height of the pin were functioning effectively, test prints were made. This involved the printing of ink diluted in printing buffer on a slide to ensure the visibility of spots. The silicon pin was thoroughly cleaned by exposing to a blowtorch flame until glowing with red heat. This was undertaken three times after which it was washed in the circular bath. The pin wash cycle was performed automatically between pin loadings to ensure that no contamination occurred from one well to another. The relative humidity and printing temperature of the arrayer can affect the shape, and size, and thus printing density of spots as well as cause sample

evaporation or water condensation on the slide surface. Therefore, the printing process was performed in an air-conditioned room (18-22 °C) and the arrayer's humidifier was set to be between a minimum of 55% and a maximum humidity of 65%. After printing, arrayed slides were kept in a desiccator until use (longest storage period was one week). A lab coat and non-powdered gloves were always worn when handling and adjusting the arrayer. For reproducibility studies, the experiment was carried out on three consecutive days.



Figure 24: Photograph of the Biorobotics Microgrid II arrayer.

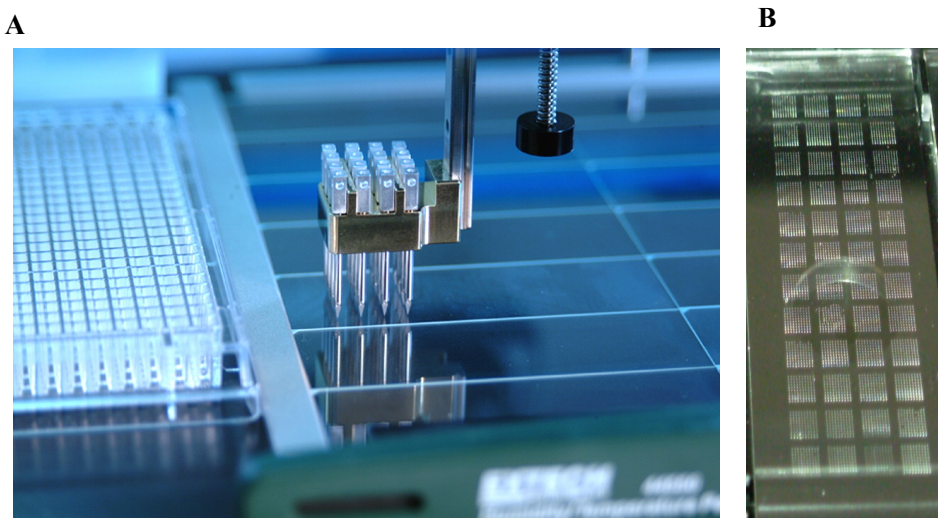


Figure 25: Illustrates A) microarray printing B) Proteins arrayed onto glass slides.

2.2.3 Initial Protocol for the Antigen Microarray Assay without Amplification

The Microgrid software was set to an optimal humidity (57%), a 16-pad slide layout (ie 16 arrays per slide as a 2x8 set or arrays) and an appropriate printing pattern to print *Candida albicans*, Tetanus toxoid and purified human IgG standards in ten replicates and quadruplicates respectively (**Figure 26**). Quality controls were diluted in printing buffer (PBS-Trehalose-Tween) to make a volume of 20 µl at a concentration of 100 µg/ml. In addition, a two-fold serial dilution of purified human IgG was prepared and placed on the same 384 well plate in 10 dilutions starting at a concentration of 0.05 mg/ml. All steps were performed at room temperature (20^{o}C). Printed slides (**Figure 27a**), containing multiple arrays were locked into 8 or 16 well plastic incubation gaskets (Grace BioLabs) (**Figure 27b**). This seals each array on the slide into a watertight well from its neighbour, so that each array can be individually probed with a different sample and process as required. One hundred µl of 5% BSA in PBST was added to each well then incubated for an hour with shaking at room temperature, ensuring slide gaskets were covered on top with a plastic sealing strip. Each well was then washed five times with 100 µl PBST for 3 minutes and emptied by inversion and tapping onto tissue paper. Two drops of Avidin blocking reagent (Life Technologies/Invitrogen, UK) were then added to each well and incubated at 10 minutes with shaking after which they were washed five times with PBST as before. The Avidin block was followed by a further 10-minute incubation with Biotin block solution and the washing step was repeated. Serum and purified IgG samples were diluted 1:500 in 5% BSA in PBST. 100 µl of each sample was added to separate wells (except the negative control wells). The wells were then sealed and incubated with gentle agitation for an hour at room temperature after which they were washed five times over 3 minutes to remove unbound antibodies.

100 µl of Biotinylated anti-human antibody (Vector Laboratories, UK), diluted 1:20,000 in antibody diluent (DAKO, UK) was added to each well. They were then covered and incubated with shaking for one hour at room temperature after which wells were washed 5 times with PBST as before. Streptavidin-conjugated cyanine 5 dye (Molecular Probes, UK) was diluted 1:5,000 in 5% BSA-PBST and 100µl was added to the wells and further incubated in the dark with shaking for 15 minutes. Wells were washed five times with PBST, then once with PBS only for 5 minutes. Slides were removed from the incubation gaskets, rinsed briefly with ultra-pure water and dried by centrifugation using a steel slide rack in a plate rotor (Universal 30 RF) at 1200 rpm for 5 minutes. Processed slides were scanned (**Figure 27d**) using a Genepix 4200AL scanner (Axon Genepix ®) at a wavelength of 635nm at 400 PMT and 100% laser power.

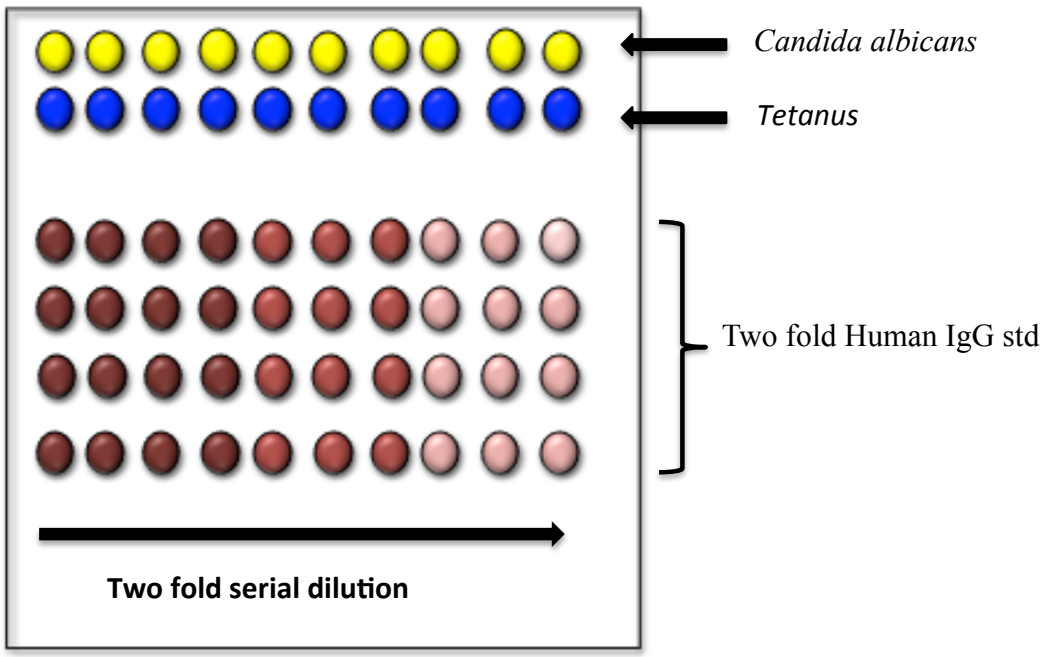


Figure 26: Schematic representation showing quality control antigens, *Candida albicans* and Tetanus (ten replicates) and a two-fold serial dilution of purified human IgG (quadruplicates) on a single (approximately 5x5mm) microarray grid.

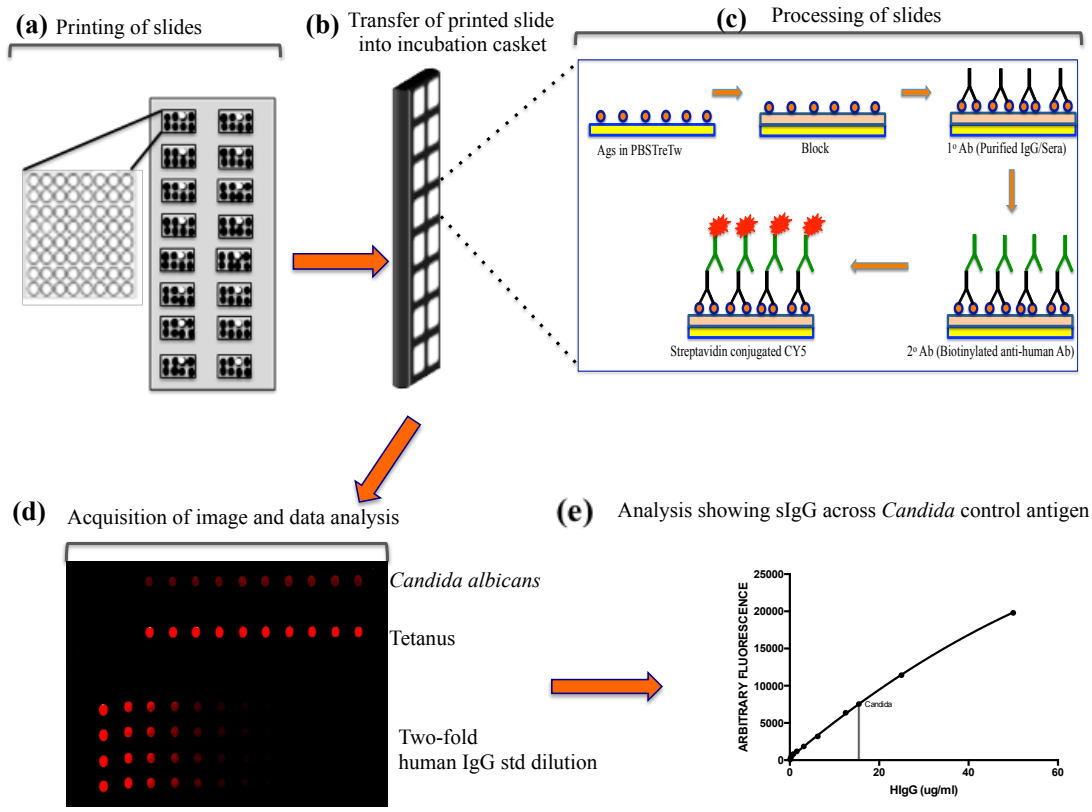


Figure 27: Schematic diagram showing the main processes in the initial antigen microarray assay. **(a)** Quality control antigens (*Candida albicans* and Tetanus) and a two-fold serial dilution of human IgG arrayed robotically onto a poly-L-lysine glass slide from a microtiter well plate. (**b**)Transfer of printed slide into an incubation casket **(c)** Slide probed with primary (sera/purified IgG) and secondary antibodies (biotinylated anti-human antibody) after which the interaction was detected with a Streptavidin conjugated Cy5 dye. **(d)** Fluorescent spots of control antigens and IgG standard in a scanned pad. **(e)** Analytical representation showing analysis of serum IgG across *Candida albicans* control antigen.

2.2.4 Antigen Microarray Assay with Amplification

The amplification step of the assay (**Figure 28)** was undertaken after detection step with secondary antibody was performed as stated above. Streptavidin-Horseradish Peroxidase (HRP) (Bio-rad, USA) was diluted 1:2,000 in antibody diluent and 100 µl was added to each well and incubated with shaking at room temperature in the dark for 15 minutes. Streptavidin binds strongly to biotin linked to the secondary antibodies. The slide was then washed 5 times with PBST as before. The amplification step, when required, was carried out avoiding excessive exposure to bright light. The amplification diluent, amplification reagent, (Bio-rad, USA) and ultra-pure water were mixed into a

ratio of 4:1:4 (800 µl: 200 µl: 800 µl). 100 µl of the mixture was added to each well for 10 minutes with shaking. After the amplification step, slides were washed three times with 20% Dimethyl Sulphoxide (DMSO)-PBST, then finally washed three times with PBST. Streptavidin-conjugated cyanine 5 (Molecular Probes, UK) was diluted 1:5,000 in 5% BSA-PBST and 100µl was added to each well after which the preparation was incubated in the dark with shaking for 15 minutes. Wells/arrays were washed five times with PBST then once with PBS only for 5 minutes and subsequently rinsed briefly with ultra-pure water. Slides were dried by spinning (Universal 30 RF) at 1200 rpm for 5 minutes. Slides were scanned as shown in the initial protocol.

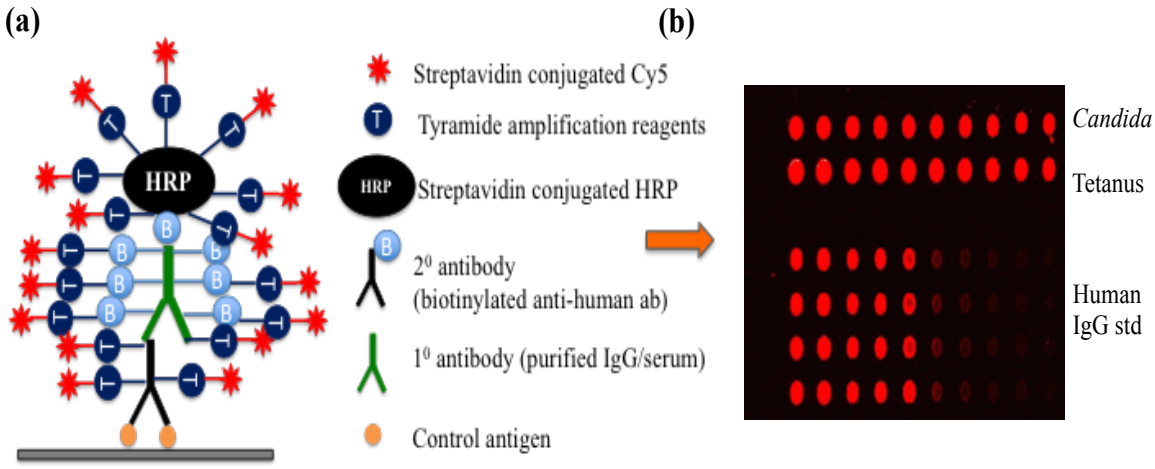


Figure 28: Schematic diagram showing Tyramide signal amplification in the antigen microarray assay. (a) Quality control antigens arrayed robotically onto a poly-L-lysine glass and subsequently probed with primary antibody (control sera) and secondary antibodies (biotinylated anti-human antibody). The interaction was amplified with Tyramide amplification reagents using after which the interaction was detected with a Streptavidin conjugated Cy5 dye.

2.2.5 Initial Protocol for Quantification of specific anti-TAA IgG levels in serum samples using HCC His-tagged Tumour-associated antigens

The Microgrid software was set to an optimal humidity (55%-65%), slide layout (16 pads) and printing pattern HCC His-tagged TAAs (AFP, Gankyrin and Mage) (**Figure 29**) diluted in printing buffer (PBS-Trehalose-Tween) to make a volume of 20 µl at a concentration of 100 µg/ml. In addition, a two-fold serial dilution of purified human IgG was prepared and placed on the same 384 well plate in 10 dilutions starting at a concentration of 0.05 mg/ml. All steps were performed at room temperature (20°C).

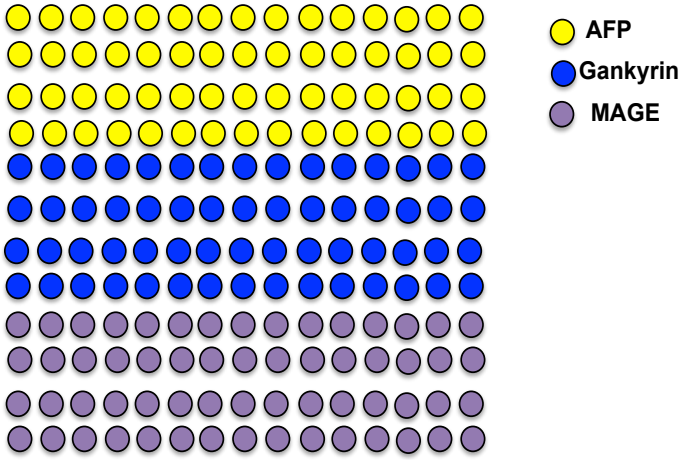


Figure 29: Annotated diagram showing the print pattern of His-tagged tumour-associated antigens on antigen microarray assay. AFP, Gankyrin and MAGE were printed in sixty replicates per array on a 16-pad slide.

His-tagged TAAs were detected with either 100 µl of polyclonal rabbit anti-His_6 antibody (Insight Biotechnology, UK), diluted 1:10,000 in 5% BSA or 100 µl of each serum sample, diluted 1:500 in 5% BSA in PBST, which were added to each well as required (except the negative control blocks). The wells were then sealed and incubated with gentle agitation for an hour at room temperature after which they were washed five times over 3 minutes to remove unbound antibodies. Biotinylated anti-human antibody (Vector Laboratories, UK), diluted 1:20,000 in antibody diluent (DAKO, UK)

was added, 100µl per well, to those wells previously incubated with serum samples. One Hundred µl of biotinylated anti-rabbit antibody (Insight Biotechnology, UK) diluted 1:30,000 in antibody diluent, was added to wells probed with anti-His_6 antibody, covered and incubated with shaking for one hour at room temperature. Wells were then washed three times as before. Streptavidin Horseradish Peroxidase (HRP) (Biorad, USA) was diluted 1:2000 in antibody diluent and 100 µl was added to each well and incubated with shaking at room temperature in the dark for 15 minutes. The amplification diluent, amplification reagent, (Bio-rad, USA) and ultra-pure water were mixed into a ratio of 4:1:4 (800 µl: 200 µl: 800 µl). 100 µl of the mixture was added to each well for 10 minutes with shaking. After the amplification step, wells were washed three times with 20% Dimethyl Sulphoxide PBST, then finally washed three times with PBST. The wells were then washed 5 times with PBST. Streptavidin-conjugated cyanine 5 (Molecular Probes, UK) was diluted 1:5,000 in 5% BSA-PBST and 100µl added to each well then incubated in the dark with shaking for 15 minutes. Wells were washed five times with PBST then once with PBS only for 5 minutes and subsequently rinsed briefly with ultra-pure water. Slides were dried by spinning (Universal 30 RF) at 1200 rpm for 5 minutes. Processed slides were scanned using Genepix 4200AL scanner (Axon Genepix ®) at a wavelength of 635nm at 400 PMT and 100% power.

2.2.6 Optimising the Antigen Microarray Assay Using Different Microtiter Volumes.

To test a combination of printing conditions that produce best spots and reduce spot variability, red (Cy5) and green (Cy3) Streptavidin conjugated Cy dyes were printed onto poly-L-Lysine glass slides from three different microtiter plate initial volumes (5 µl, 10 µl and 20 µl) (**Figure 30**). This was undertaken at a humidity of 65% instead of 57% as been used in previous experiments. Slides were then scanned for fluorescence.

This optimisation procedure was repeated using His-tagged TAAs (KRAS, HRAS, HDGF, AFP, RALA, GRP78, IMP1, Gankyrin, P62, APCN). Antigens were diluted in PBS-Trehalose-Tween and pipetted into 384 well microtiter plates as 5 µl, 10 µl and 20 µl volumes at 0.1mg/ml concentrations. Slides were further processed using the same protocol earlier described.

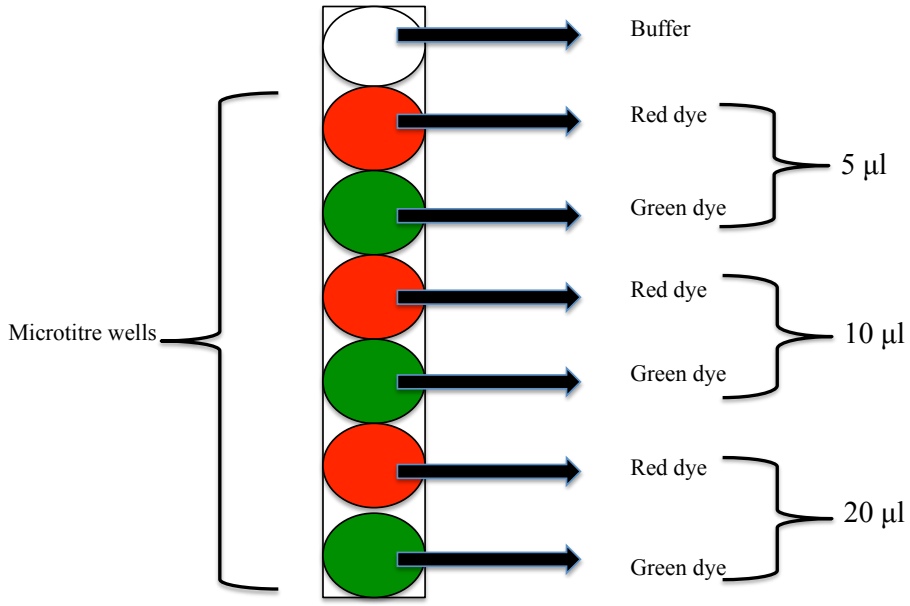


Figure 30: Green and red streptavidin conjugated cy5 dyes prepared in three different microtiter volumes (10 µl, 15 µl and 20 µl) in a 384 microtiter well plate.

2.2.7 Optimising the Antigen Microarray Assay using different Blocking Buffers.

A range of blocking buffers were tested to determine the optimal one that would prevent non-specific binding to reduce background noise. In this regard, four His-tagged TAAs (AFP, Gankyrin and 1MP1and APCN) were diluted in PBS-Tre-Tween-20 at a volume of 10 µl and were subsequently arrayed onto poly-L-Lysine glass slides at a concentration of 100 µg/ml. These arrays were then blocked with 5% BSA, 10% BSA, 30% BSA, I block or Super G buffers after slides were processed as stated earlier.

2.2.8 Optimising the Antigen Microarray Using Different Printing Buffers and Arrayers

Two His-tagged TAAs, AFP and Gankyrin, were printed to test the performance of different printing buffers. Each antigen was printed using contact and non-contact arrayers in PBS-Trehalose-Betaine-Tween, PBS-Trehalose-Tween and PBS-Trehalose. Antigens were printed as fifteen replicates each per array. The preparation of the antigens was the same for each buffer to assess its effect on spot variability. Slides were then processed as earlier described in the initial protocol.

2.2.9 Optimising the Antigen Microarray Using Different Slide surfaces

After different printing buffers were optimised, different modified slide surfaces were tested to determine the appropriate slide chemistry that could produce good morphological appearance of spots (circularity and evenness) and reduce spot variability. Two His-tagged TAAs, AFP and Gankyrin were diluted in PBS-Trehalose-Betaine-Tween to a volume of 10 µl at 0.1 mg/ml and printed as sixty replicates per array on four slide surfaces, Poly-L-lysine, Aminosilane, Epoxysilane and Nitrocellulose at a humidity of 65%. In this instance, the Nitrocellulose slide was blocked with Super G block buffer.

2.2.10 Optimising the Print Position of Antigens in the Microarray Assay

Three His-tagged antigens (AFP, Gankyrin and HCC1) were diluted in PBS-Tre-Betaine-Tween to a volume of 10 µl at 0.1 mg/ml and further printed in quadruplicates at the edges and middle positions in a 16-pad format on Aminosilane slide. The slide was then processed as earlier described in the initial protocol using an HCC serum

sample. This was undertaken to determine if the position of print on a glass slide affects the variability of individual spots**.**

2.2.11 Optimising Monoclonal mouse anti-His_6 antibody and Biotinylated anti-mouse antibody dilutions in Antigen microarray Assay

Monoclonal mouse anti-His_6 antibody and biotinylated anti-mouse antibodies were purchased to replace polyclonal rabbit anti-His_6 and biotinylated anti-rabbit antibodies, which were used in previous experiments. These new primary and secondary antibodies were assayed to determine the optimal concentrations for use on antigen arrays.

Four His-tagged TAAs (AFP, Gankyrin, GRP78 and Imp1) were diluted in PBS-Tre-Betaine-Tween to a volume of 10 µl at 0.1mg/ml. They were further printed in ten replicates in a 16-pad array format on Aminosilane slides. The antigens were probed with different concentrations of monoclonal anti-His_6 (1:2,000, 1:5,000, 1:7,000 and 1:10,000). The interaction was further detected using anti-mouse antibody at several concentrations (1:10,000, 1:20,000 and 1:30,000).

2.2.12 Finalised Antigen Microarray Assay Protocol for different categories of Tumour-Associated Antigens (Commercial and In-house)

2.2.12.1 Plate Preparation and Printing

Commercial His-tagged (KRAS, HRAS, HDGF, AFP, RALA, GRP78, IMP1, Gankyrin, P62, APCN) and Flag-tagged TAAs (KRAS, HRAS, HDGF, P16, RALA, P62, P53, Gankyrin) were diluted in printing buffer (PBS-Trehalose Betaine-Tween) to make a volume of 10 µl at a concentration of 100 µg/ml, while in-house Flag-tagged TAAs expressed in lysates (KRAS, HRAS, HDGF, P16, RALA, P62, P53, Gankyrin) were prepared in PBS-Trehalose Betaine. Quality control antigens and two-fold serial

dilution of purified human IgG were prepared in the same manner as shown in **section 2.2.3**. Antigens were printed at an optimal humidity of 65%.

2.2.12.2 Blocking of Slide

This was same in the initial protocol as stated in **section 2.2.5.**

2.2.12.3 Probing with primary antibody/serum samples

Probing of His-tagged antigens followed the same pattern as stated in section (**2.2.5**), however, poly-clonal rabbit anti-His_6 antibody was replaced with monoclonal mouse anti-His_6 antibody. Wells containing commercial Flag-tagged TAAs were probed with 100 µl of monoclonal mouse anti-Flag antibody (Insight biotechnology, UK), diluted 1:10,000 in 5% BSA whereas those containing in-house recombinant TAAs were probed with 100 µl of the same antibody diluted 1:1,000 in 5% BSA. All three sets of TAAs were probed with 100 µl serum samples diluted in 1:500 in 5% BSA.

2.2.12.4 Probing with secondary antibody

For wells probed with anti-His_6 and anti-Flag antibodies (applies to commercial His-tagged and Flag-tagged TAAs), 100 µl of biotinylated anti-mouse antibody (Vector Laboratories, UK) diluted 1:30,000 in antibody diluent, was added. However, this was different from other wells containing anti-Flag TAA (applies to in-house TAAs) as 100 µl of biotinylated anti-mouse antibody diluted 1:2,000 was added. One hundred µl of biotinylated anti-human antibody (Vector Laboratories, UK), diluted 1:20,000 in antibody diluent (DAKO, UK) was added to all wells probed with serum samples.

2.2.12.5 Amplification Step

Procedure for this step was the same as stated in earlier protocol (**section 2.2.4**). After this step, wells were washed with 20% DMSO-PBST and PBST in the same manner as stated in section **2.2.4**. One hundred µl of streptavidin-conjugated cyanine 5 (Molecular

Probes, UK), diluted 1:2,000 in 5% BSA-PBST, was added to each well and incubated in the dark with shaking for 15 minutes. Slides were washed five times with PBST then once with PBS only for 5 minutes and subsequently rinsed briefly with ultra-pure water. Slides were dried by centrifugation (Universal 30 RF) at 1200 rpm for 5 minutes. Processed slides were scanned using Genepix 4200AL scanner (Axon Genepix ®) at a wavelength of 635nm at 400 PMT and 100% power.

2.2.13 Scanning of Microarray Slides

Processed slides were immediately scanned using the Genepix 4200AL microarray scanner (Axon Genepix ®) (**Figure 31**) to measure the fluorescent dye Cy5. Prior to this, slides were inserted into a 36-position slide position carrier and loaded for automated slide handling, with the arrayed surface towards the first position and the bottom of the slide towards the left of the carrier. Fluorescent signals were excited at a wavelength of 635nm (laser standard red), Photomultiplier tube voltage of 400, pixel size 10µm, focus position of 20µm and 100% laser power (**Figure 32**). The above standards were set to prevent photo bleaching of the fluorescent Streptavidin-Cy5. Images were saved according to manufacturer's format (16-bit TIFF format file).



Figure 31: Photograph of the Genepix 4200AL Microarray Scanner.

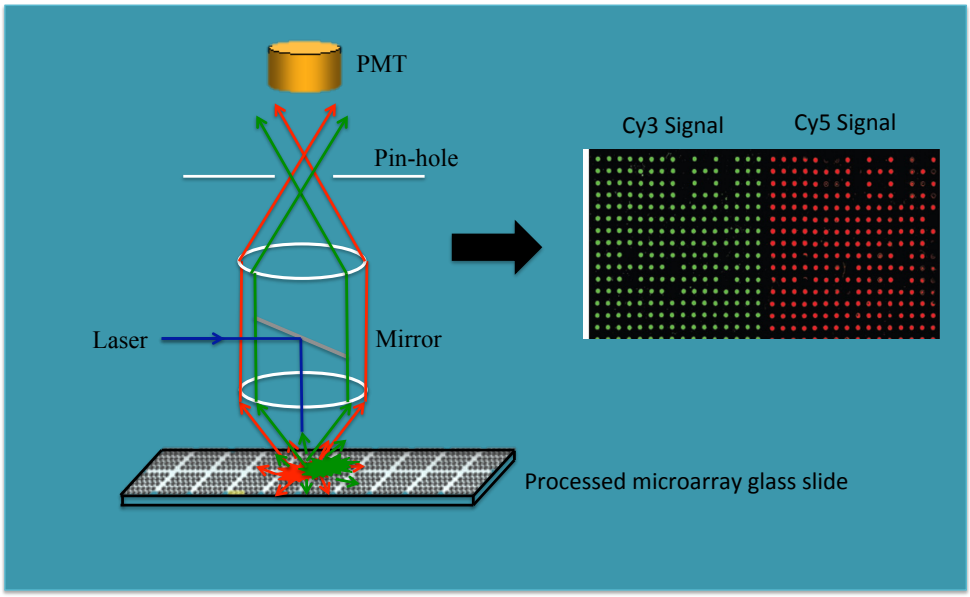


Figure 32: Principle Model of Microarray Scanning.

2.2.14 Generation of Genepix Array List Files (GAL) for Axon Genepix Pro Software

The Genepix Array List (GAL) File is a tab separated text file (identified with a. gal suffix), which contains specific information for the layout of each array (termed a block in a genepix file) such as the size and position of individual blocks, layout of feature indicators as well as the names and identifiers of arrayed proteins including the within array column and row identifier of all spots with their specific names and IDs. With the help of the GAL File, scanned images saved (saved in TIFF format) could be converted to numeric images. The GAL file is generated by the Microgrid II robot using the "clone tracking wizard" once an array pattern (a grid file) has been defined and a plate map giving the locations of each sample in the 384 well plate is input (**Figure 33**, left). This GAL file is loaded into the GenePix Pro 6.1 software and overlayed onto the TIFF images of scanned slides (**Figure 33**, right). The theoretical array grid depicted in the GAL file was semi-automatically aligned with the actual array image spots, in order

to identify the diameter and shape of the spot, its actual location, and define an area of local background around each spot. Once done, the image was analysed to quantify the fluorescence of each spot. The resultant file was an industry standard Genepix results file (GPR file) containing all the quantitative values of the data for each fluorescent spot such as the signal intensity, circularity, background noise, diameter, etc.

plate	row	column	name	ID	dilution	Conc (ug/ml)
1	A	1	KRAS-A	1A1	1	100
1	B	1	HRAS-A	1B1	1	100
1	C	1	HDGF-A	1C1	1	100
1	D	1	P16-A	1D1	1	100
1	E	1	RAL A-A	1.00E+01	1	100
1	F	1	p62-A	1F1	1	100
1	G	1	p53-A	1G1	1	100
1	H	1	GANK-A	1H1	1	100
1	I	1	KRAS-B	1I1	1	100
1	J	1	HRAS-B	1J1	1	100
1	K	1	HGDF-B	1K1	1	100
1	L	1	RALA-B	1L1	1	100
1	M	1	GANK-B	1M1	1	100
1	N	1	AFP-B	1N1	1	100
1	O	1	P62-B	1O1	1	100
1	P	1	APCN-B	1P1	1	100
1	A	2	GRP78-B	1A2	1	100
1	B	2	IMP1-B	1B2	1	100
1	C	2	KRAS-C	1C2	1	200
1	D	2	HRAS-C	1D2	1	200
1	E	2	HDGF-C	1.00E+02	1	200
1	F	2	P16-C	1F2	1	200
1	G	2	RALA-C	1G2	1	200
1	H	2	P62-C	1H2	1	200
1	I	2	P53-C	1I2	1	200
1	J	2	GANK-C	1J2	1	200

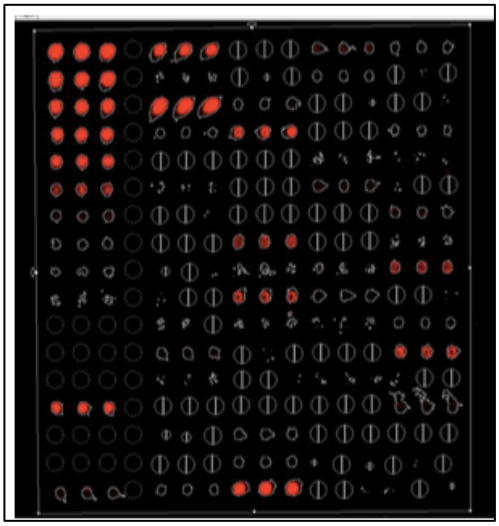


Figure 33: An example of a plate map (Left) and the alignment of a resultant Genepix Array List (GAL) file grid onto corresponding spots on a TIFF image (right) to obtain the median fluorescence per each spot. Circles with lines through are deemed by the Genepix software as being below local background or absent from the array (with a corresponding data flag in the Genepix results (GPR) files), but numerical values are reported for all spots.

2.2.15 Statistical Analysis

The fluorescent signal of each spot was extracted from the Genepix results (GPR) files (median foreground (spot) fluorescence minus local background, for each arrayed protein) (**Figure 34**). Poor quality features were flagged for removal by the Genepix software based upon mathematical and statistical data with regards to spot morphology (circularity and size), signal uniformity, local background and signal to noise ratio. After the data were filtered, regular spots were analysed using R statistical package (RPPAnalyser version 3.1.2, 2014) to generate mean signal levels (**Figure 34**). This

statistical software employs two tab-delimited files namely: (***slidedescription.txt)*** and ***(sampledescription.txt***) which are usually connected to the equivalent gpr files. The Slide description file defines the location and number of arrays on a slide (called pads by the R module), the sample used to probe each array and the number of slides to be examined. The sample description file lists the antigens in each well of the source 384 well microtiter plate as well as the dilutions if any of the samples and replicate identifiers.

Graph Pad prism 7 (Graph Pad 7, USA) software (**Figure 34**) was used to generate graphs as well as interpolate IgG standard curves). Signal arithmetic mean of fluorescent signals, median, standard deviation, range and percentiles for all antigens were generated during the statistical analysis. Cut-off values for identifying seropositive (anti-TAA autoantibodies in serum) were 95^{th} percentile of the healthy group. Samples which were estimated to be positive for an autoantibody response to a specific TAA if the mean signal intensity was above the chosen cut-off. Further statistical analysis was performed using Microsoft excel and IBM SPSS Statistics 23 (**Figure 34**).

2.2.17 Microarray Validation

2.2.17.1 Intra and Inter Assay Precision

To determine the precision of the antigen microarray, which is the coefficient of variation (CV%) of multiple measurements or repeats, intra-assay and inter-assay tests were conducted. Intra-assays were performed repeatedly over the same slide on the same day and inter-assays performed over a period of two to three consecutive days. The precision was calculated by dividing the standard deviation of multiple repeats by

its mean. The accepted level of precision was set at ≤15% and ≤20% for intra and inter-assay respectively.

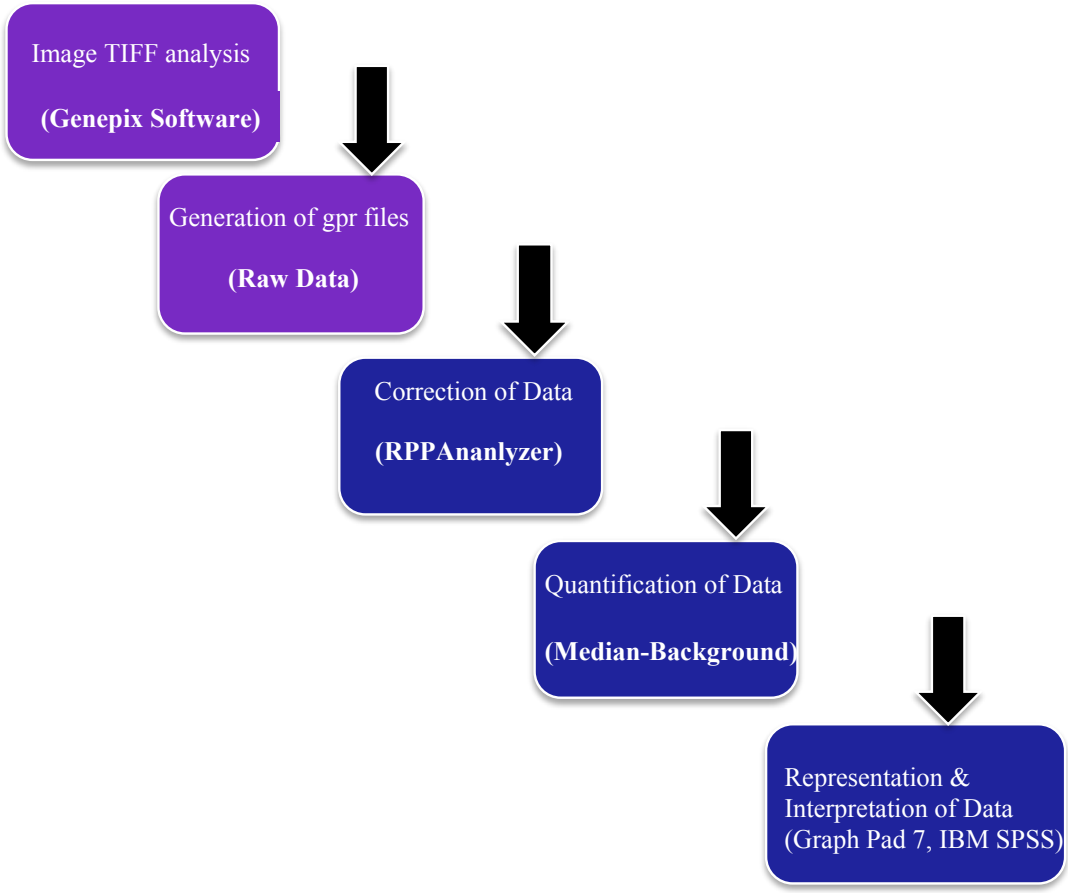


Figure 34: Statistical softwares and workflow used in the analysis and interpretation of Microarray data.

2.3 Materials (Production of In-House HCC TAAs)

2.3.1 Media, reagents, solutions

All chemicals and reagents to produce HCC recombinant TAAs were purchased from ThermoFisher Scientific, UK and Sigma-Aldrich (Poole, UK) unless otherwise stated. All solutions used were sterilised by filtration through a 0.2 µm Minisart® high-flow

syringe filter (Sartorius). All human cell work was performed in a class II tissue culture hood.

2.3.2 Plasmids

Eight C-Terminal Myc-DDK (Flag) tagged human TrueORF cDNA clones with pCMV6 entry vectors were purchased from Origene, UK. These lyophilised clones (10 µg) were dissolved in 100 µl of nuclease free water (Ambion, UK) and stored at -20°C until use (**Table 14**).

Table 14: List of C-Terminal Myc-DDK (Flag) tagged human TrueORF cDNA clones used in the study.

Human cDNA clone	Catalogue #	Predicted MW (kDa)	mRNA Accession #	ORF size	Antibiotic resistance
KRAS	RC201958	21.2	NM_004985	567bp	Geneticin
HRAS	RC216409	44.2	NM_005343	513bp	Geneticin
HDGF	RC204148	26.6	NM_004494	732bp	Geneticin
RALA	RC208076	23.4	NM_005402	621bp	Geneticin
P62	RC200263	44	NM_006559	1332bp	Geneticin
P53	RC200003	44.1	NM_000546	1182bp	Geneticin
Gankyrin	RC202025	23.2	NM_002814	681bp	Geneticin
CDKN2A	RC211784	17.8	NM_058195	522bp	Geneticin

2.3.3 Expression Systems

Baculovirus, *E. coli* and mammalian systems are some of the most common prokaryotic and eukaryotic expression systems mostly used in the laboratory. For recombinant protein expression, eukaryotic expression system, was selected over *E.coli* due to number of reasons. Eukaryotic systems are more likely to produce properly folded and authentically glycosylated human proteins as well as introduce appropriate post-translational modifications, unlike bacterial systems. Human Embryonic Kidney 293 cells (HEK 293t ATCC 15E058, Public Health England) stably transfected with the SV40 large T-antigen was used in this study. This cell line binds to the SV40 origin of replication that is often engineered into expression vectors, thus increasing protein expression. HEK 293 is an excellent cell line to use in transfection experiments and recombinant protein production because of its biochemical machinery. Thus, it is capable of undertaking most posttranslational folding and processing required to generate mature and functional proteins.

2.3.4 Culture media, Reagent and buffers

Culture media and buffers (**Table 15**) were stored at 2-8^{o}C. Aliquots of 1x trypsin Ethylenediaminetetracetic acid (EDTA) were kept at -20^{o}C. Dulbecco's Modified Eagle's Media (DMEM) (ThermoFisher Scientific, UK) is a modification of Basal Medium Eagle (BME), which has a higher concentration of vitamins (Folic acid, Riboflavin, B_{12}) and amino acids as well as supplementary constituents such as salts (Calcium Chloride, Sodium Chloride, Potassium Chloride and Magnesium Sulphate) and glucose, which are involved in the cell's metabolic processes.

Table 15: List of growth media, reagents and buffers used in cell culture.

Incomplete media	500ml DMEM (Low glucose), 5ml Penicillin/streptomycin, 5ml L-Glutamine (200mM), 5ml Hepes buffer (1M).
Complete Media	For 50ml, 45ml of incomplete media, 5ml Fetal bovine serum (Sigma Aldrich, UK).
10% FBS/DPBS	45ml Dulbecco's Phosphate buffered saline (ThermoFisher Scientific, UK), 5ml FBS
1XTrypsin/EDTA	5ml x10 Trypsin/EDTA (ThermoFisher Scientific, UK), 45ml DPBS.

2.3.5 Transfection reagent

An appropriate transfection reagent is required to ensure an efficient insertion of genetic material (DNA) into eukaryotic cells. The optimal transfection reagent used for transfecting human TrueORF cDNA clones into HEK 293 cells was Amaxa® cell line nucleofector® Kit V (Lonza, UK), which consist of a nucleofector® solution, supplement and pmaxGFP vector and gives a cell viability variation between 75%-85%. Nucleofection reagents were stored at 4^{o}C except for pmaxGFP vector, which was stored at -20^{o}C.

2.3.6 Antibiotics

To prevent bacterial contamination of cell cultures, the cell culture media is supplemented with Penicillin and Streptomycin antibiotics (**Table 16**) due to their effective combined action against gram-positive and gram-negative bacteria. Penicillin usually acts by activating the release of enzymes that alter the cell wall and interferes

with the turnover of the bacterial cell while Streptomycin binds to the 30S subunit of the bacterial ribosome, resulting in inhibition of protein synthesis and death in susceptible bacteria. Secondly, Geneticin (G418) is added to the cell culture media in order to select cells successfully transfected with human cDNA clone containing the drug resistant gene in its construct.

Table 16: List of antibiotics used. Antibiotics were stored at -20ºC.

Antibiotic	Stock concentration	Solvent	Working concentration (μg/ml)	Source
Penicillin and Streptomycin	100 μ/ml 10 mg/ml	DPBS	1 μ/ml 0.1 mg/ml	Sigma Aldrich, UK
Geneticin (G418)	50 mg/ml	Nuclease free water	1mg/ml	Gibco, UK

2.3.7 Growth Conditions and Storage

HEK 293 cells were passaged in sterile, 25 cm^2 tissue culture-treated flasks with flat, orange, vented caps (Corning Inc.), in DMEM– with 10% sterile heat-inactivated fetal bovine serum (FBS; Sigma Aldrich, UK). Unless stated otherwise, this preparation of DMEM was used in all situations. Growing cell stocks were passaged, at a cell density of 2-5x10,000 cells/cm^2, using 1x trypsin/EDTA (ThermoFisher scientific, UK) every 72 – 96 hrs, when 70-80% confluence was reached and incubated at 37ºC/5%CO_2 (Grant JB series Incubator, Grant UK).

2.4 Methods (Production of In-House HCC TAAs)

2.4.1 Transfection of cDNA clones into HEK 293 cells

HEK 293 cells were passaged 2-3 days until 70%-80% confluence prior to the transfection procedure. Cells at 50% confluence were harvested by trypsinizing with 5 ml 1x trypsin/EDTA after which 5 ml 10% FBS/DPBS was added for 5 minutes to neutralise the effect of the trypsin. The cell suspension ($1x10^6$ cells per sample) was centrifuged (Rotina 46, UK) at 300 *g* for 10 minutes at room temperature after which the supernatant was discarded. The cell pellet ($1x10^6$ cells per sample) was carefully re-suspended in 100 µl of nucleofector solution V (Lonza, UK). 100 µl of each cell suspension was combined with 2 µg of human cDNA ORF clone (KRAS, HRAS, CDKN2A (P16), HDGF, RALA, P62, P53, Gankyrin and pmaxGFP) (Origene, UK) (**Figure 35**). The cell/cDNA clone suspension was then transferred into certified cuvettes after which cells were transfected with the nucleofector program A-023 using the nucleofector device (Lonza, UK). Contents of the cuvette were then transferred into a sterile 6 well culture plate containing 1.5 ml pre-warmed complete medium (**Figure 35**). Cells were incubated in humidified incubator at 37ºC/5%CO_2 (Grant JB series, UK) for 48 hours until further analysis. The percentage of GFP positive cells was determined (transfection efficiency) using a Beckman Coulter FC500 at the flow cytometry unit.

2.4.2 Generation of Stable Cell line (Selective Pressure)

Forty-eight hours after transfection, old cell culture media was replaced with fresh complete media containing 1 mg/ml Geneticin (G418) (Gibco, UK). Stable selection and growth of resistant clones was allowed up to 1 or 2 weeks until selected cells reached 80% confluence. Selective media was replaced every 3 days to ensure adequate

selection of resistant clones (transfected cells containing plasmid with resistant constructs).

2.4.3 Preparation of Cell Lysate

Old medium was removed from the adherent cells and washed once with 1000 µl cold DPBS (Sigma Aldrich, UK) for 30 minutes. 1000 µl of cold RIPA buffer (Thermo Fischer Scientific, UK), 10 µl of Protease/Phosphatase inhibitor cocktail and 5 µl of 1unit/µl Benzonase (Sigma Aldrich, UK) were added to the cover the culture. The preparation was incubated on ice with shaking for 30 minutes after which samples were transferred into 1.5 ml microcentrifuge tubes. Samples were then centrifuged (IEC Micromax RF, UK) at 16,000 *g* for 15 minutes at 4°C. The clarified lysate was removed and stored at -20°C until further use (**Figure 35**).

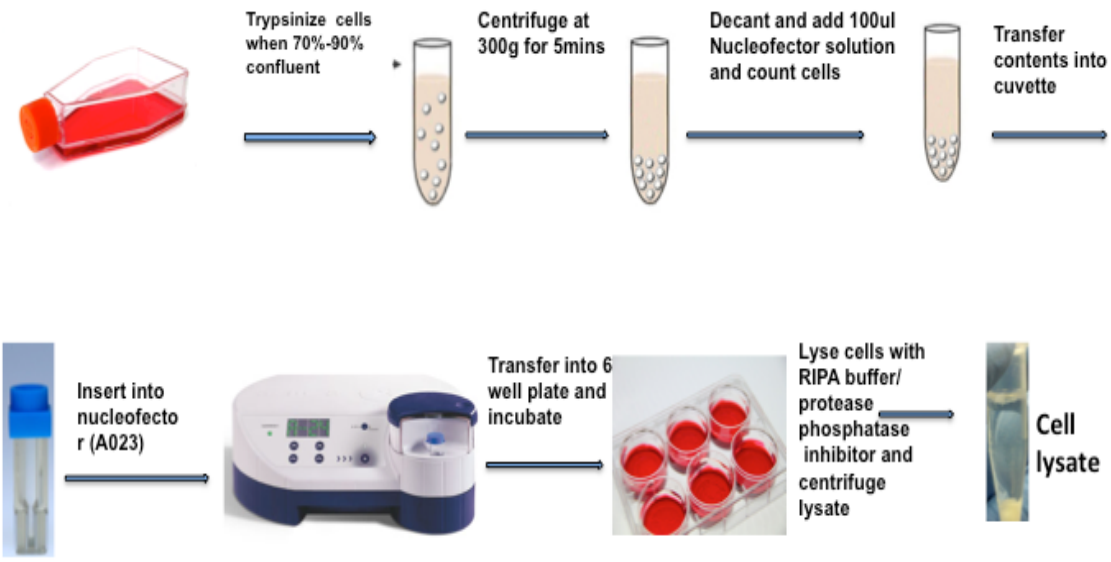


Figure 35: Schematic diagram outlining the main procedures involved in generating Hepatocellular carcinoma (HCC) recombinant tumour associated antigens using HEK 293 cells. The processes above show the transfection of HEK 293 cells with KRAS, HRAS, HDGF, P16, RALA, P62, P53 and Gankyrin human cDNA ORF clones, using the Amaxa nucleofection solution kit V. Resistant cells were selected with G418 and allowed for a 1-2 weeks selection. Resistant cells were then lysed, and proteins were further characterized by western blot.

2.4.4 Protein Buffer Exchange, Concentration and Quantification

2.4.4.1 Protein Concentration by Ultrafiltration

Proteins were concentrated using Amicon® Ultra 2 ml and 15 ml 10K MWCO centrifugal filter units (Merck Millipore, USA) according to manufacturer's instructions (**Figure 36**).

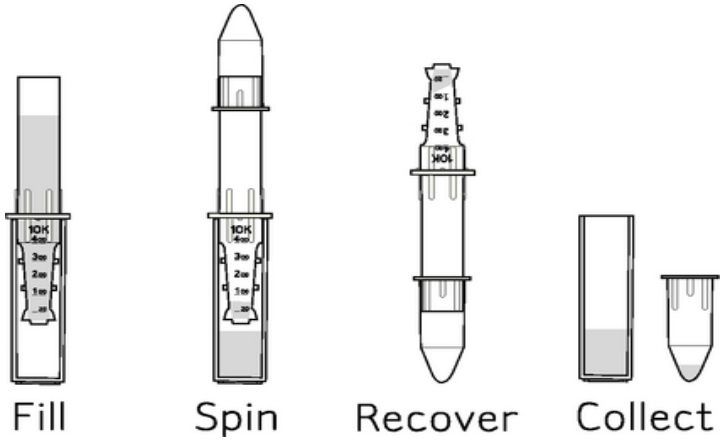


Figure 36: Schematic diagram showing the processes involved in Ultracentrifugation.

2.4.4.2 Protein Quantification by BCA Assay

The PierceTM BCA Protein Assay Kit (Thermo Scientific, UK) was used according to manufacturer's instructions; using nine bovine serum albumin (BSA) size standards (2000, 1500, 1000, 750, 500, 250, 125, 25, 0 µg/ml; Thermo Scientific, UK). Samples and standards were added to working reagent in 1 in 20 dilutions (**Figure 37**). Absorbance was measured at 562 nm using the FLUOStar Omega plate reader and analysed using Graph Pad Prism 7 software.

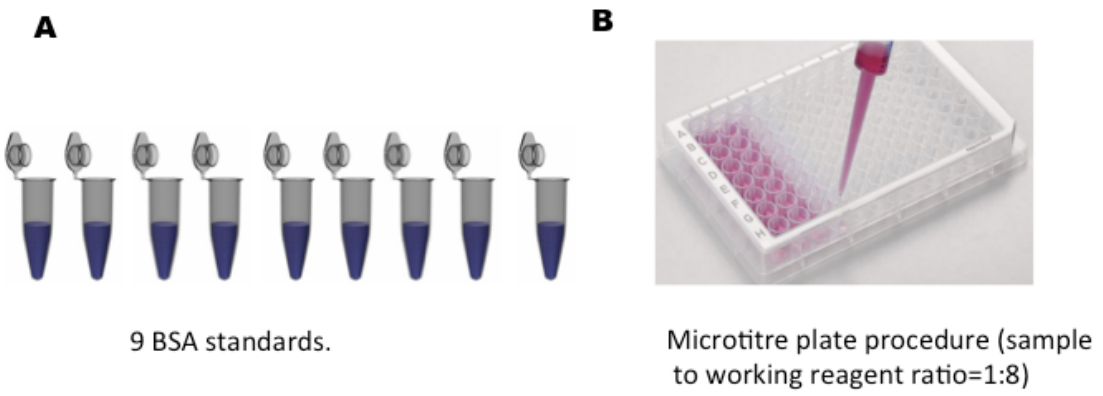


Figure 37: The diagram above shows the processes involved in protein quantification using the BCA assay kit. (A) Nine serial dilutions of BSA standards. **(B)** Samples (in duplicates) diluted in working reagent (1:8) and further transferred into a 384-microtitre well plate. Samples were incubated at 37ºC/5% for 30 minutes after which the absorbance was read at 562nm.

2.4.4.3 Protein Detection

Proteins were stored at 4°C or -20°C for long-term storage before protein analysis was carried out. The various analysis methods are outlined below;

2.4.4.3.1 Sodium Dodecyl Sulphate Polyacrylamide Gel Electrophoresis (SDS-PAGE)

Equal volumes of samples and 1 × Sodium Dodecyl Sulphate (SDS) loading buffer (620mM Tris-HCl [pH 6.8], 5% SDS, 25% Glycerol, 12.5% β-mercaptoethanol, 0.002% Bromophenol blue and make up to 25 ml with deionized water, Novex, Invitrogen, UK) were mixed (10 µl:10 µl). Samples were denatured by heating them at 95ºC for 10 minutes on PCR block (Omnigene, UK), before loading alongside with either Spectra Multicolour Broad range protein ladder (10-260 kDa) (ThermoFisher Scientific, UK), Pre-stained Protein marker (11-250 kDa) (Cell signalling), Magic Mark™ XP (20-220 kDa) (ThermoFisher Scientific) to facilitate an estimation of protein size. Precast 15-well Mini-Tris Glycine gels (4%-20% and 10%-20%) (Invitrogen, UK) were used, running 15 µl protein sample at 130 V for 1.5 hrs at 35 mA and 1x running buffer (Tris-Glycine-SDS) (ThermoFisher Scientific, UK) were used.

Gel staining was performed using TM Silver Stain Kit (ThermoFisher Scientific, UK) or Protein gel stain (Invitrogen, UK).

2.4.4.3.2 Staining Proteins in Polyacrylamide Gels

2.4.4.3.2.1 Silver Staining of Gels

All steps in this procedure were performed in a clean staining tray (plastic or glass) with constant gentle shaking. The Pierce Silver Stain Kit (Thermo Scientific, UK) was used. Gels were washed immediately in two changes of ultrapure water for 5 minutes after which they were fixed in water, ethanol and acetic acid solution at ratio of 6:3:1 for 15 minutes. This procedure was repeated for another 15 minutes. After the fixing, gels were further washed in two changes of 10% ethanol solution and two changes of ultra-pure water 5 minutes each. Gels were incubated for 30 minutes in a sensitizer working solution for 1 minute and subsequently washed in two changes of ultra-pure water for 1 minute each. Gels were then incubated in a stain working solution for 30 minutes and washed in two changes of ultra-pure water for 20 seconds each. They were incubated in a developer working solution for 2-3 minutes until protein bands appeared. When the desired band intensity was reached, the developer working solution was replaced with two changes of 5% acetic acid for 10 minutes each in order to stop the reaction, after which they were scanned.

2.4.4.3.2.2 Imperial Staining of Gels

Precast gels were placed in a clean tray and washed three times for 5 minutes with 100 ml of ultrapure water. 25 ml of Pierce Imperial^{TM} Protein stain (Thermo Scientific, UK) was added to cover gels completely after which the tray was placed on a shaker. To achieve the desired level of sensitivity, the gel was kept in the stain for 2 hours. The

staining reagent was discarded and replaced with 20 ml of ultrapure water to reduce the background. In order to increase the band intensity, the washing was extended. Stained pre-cast gels were scanned afterwards.

2.4.4.3.3 Western Blot

2.4.4.3.3.1 Transfer of blots

An SDS-PAGE gel was transfer-assembled with 1x transfer buffer (10x Tris-Glycine diluted 1 in 10 in deionized water, 10% methanol) (ThermoFisher Scientific, UK) in a clean plastic tray next to a 0.2 µm HybondTM-ECLTM nitrocellulose membrane (ThermoFisher Scientific, UK) or 0.2 µm PVDF membrane (ThermoFisher Scientific, UK). The complex was sandwiched between two pre-wet filter papers and placed on Transblot SD wet transfer cell (Invitrogen, UK). This was encased by 3 pieces of filter paper. All components were soaked in 1x transfer buffer. The membrane was placed closest to the positive electrode after which transfer was run at 30 V at 100 mA for 1.5 hrs.

2.4.4.3.3.2 Membrane Blocking and antibody incubation

The membrane was blocked using 25 ml 1x Tris Buffered Saline (TBS), 0.1% Tween 20 (100%) with 5% w/v skimmed dry milk (Tesco, UK) at RT for 1 hr at 10 rpm. This was followed by 3 washes 5 minutes each with 1x TBS, 0.1%Tween 20 (100%) (ThermoFisher Scientific, UK). Primary antibody incubation was undertaken based on the type of antibody used and as per manufacturer's instructions. Nitrocellulose membrane was incubated in 5 ml mouse anti-DDK (Sigma Aldrich, UK), (diluted 1:1000 in 5% milk) overnight at 4^{o}C. Anti-Myc as well as antigen specific antibodies such as anti-KRAS, anti-P16, anti-P62 and anti-P53 were diluted (1:500, 1:300, 1:300,

1:50) in 5% milk respectively. The membrane was washed three times for 5 minutes each in 15 ml TBST at 30 rpm. For chemiluminescence detection, the membrane was probed with polyclonal goat anti-mouse HRP (DAKO, UK), (diluted 1:2000, 1:1000, 1:500, 1:500, 1:500, 1:50 in 5% milk for DDK, Myc tagged proteins and non-tagged (KRAS, P16, P62 and P53) proteins respectively), for 1 hour at room temperature with rocking, followed by three washes. The membrane was immersed in Amersham™ enhanced chemiluminescent (ECL™) western blotting detection reagents (GE Healthcare) for a minute and developed using Amersham Hyperfilm ECL™ high performance chemiluminescence film (GE Healthcare), Carestream® Kodak® autoradiography GBX developer/replenisher and fixer/replenisher (Sigma). In the case of fluorescence immunoblots, the membrane was incubated in Licor Odyssey anti-mouse antibody-IR680LT (680nm) conjugate, diluted 1:5,000 in TBST, after which the membrane was washed and scanned using the Licor Odyssey scanner.

2.4.4.3.4 Dot Blot

Grids were drawn on 0.2 μm nitrocellulose membranes using a pencil to indicate the regions where samples would be put. Two μl of samples were spotted onto the membrane and allowed to dry for an hour. The probing and film development procedure was the same as seen with western blot stated above.

2.4.4.3.5 Protein Purification

2.4.4.3.5.1 FLAG-Tag Affinity Chromatography

Prior to the purification process, glycerol in the Anti-Flag® M2 affinity gel (Cat. A2220 Sigma Aldrich, UK) was separated from the resin. The affinity column was washed with 0.5 ml x1 wash buffer (10x wash buffer (0.5M Tris-HCL, 1.5M NaCl) diluted 1:9 in deionized water) (Sigma Aldrich, UK) after which the column was packed with resin.

Subsequently, resin was washed once with 1x wash buffer to allow equilibration. The column was then loaded with three and five column volumes of elution buffer (0.1M Glycine) and 1x wash buffer respectively (**Figure 38**). Briefly, buffered lysates containing FLAG-fusion protein and BAP fusion protein (50 ng/µl) were passed through 1 ml Anti-Flag® M2 affinity gel by gravity flow. After washing with 10 column volumes of 1x wash buffer, FLAG-fusion proteins were eluted in six 1 ml fractions by acid elution (0.1M glycine-HCl) (pH 3.5) (**Figure 38**) after which the elution fractions were neutralised with Tris Buffered Saline (50mM Tris-HC, 150mM NaCl (pH 10.0)).

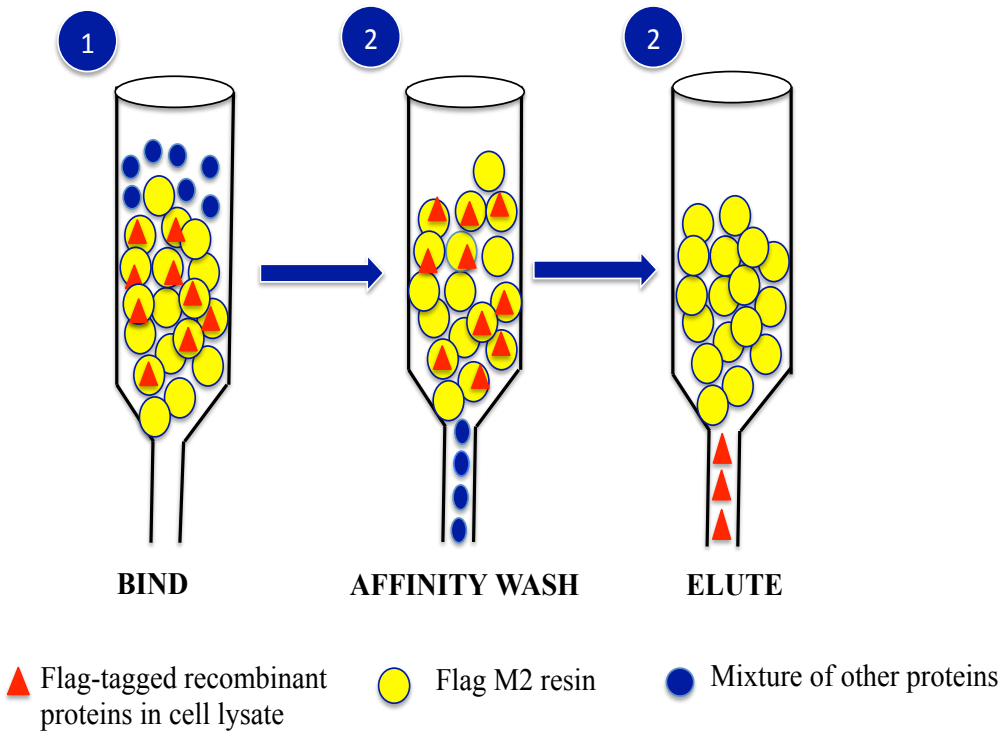


Figure 38: Diagram showing the processes involved in Flag-tag affinity chromatography. 1. Anti-Flag® M2 affinity gel mixed with cell lysate to allow flag-tagged recombinant proteins to bind the resin **2**. Resin is washed with TBS (50mM Tris-HCL, 15mM NaCl, pH 7.4) to remove unbound proteins from resin. **3.** Bound target (Flag-tagged tagged proteins) eluted from resin using 0.1M Glycine HCL (pH 3.5) and further neutralised with Tris-Buffered Saline (50mM Tris-HC, 150mM NaCl (pH 10.0).

2.4.4.3.5.2 Anti-Flag® M2 Magnetic Bead Chromatography

Anti-Flag® M2 magnetic beads (Cat. M8823, Sigma Aldrich, UK) were gently re-suspended by inversion after which 50 µl was transferred into Eppendorf tubes. Tubes were then securely held in a magnetic separator rack to collect beads after which the storage buffer was discarded. Beads were washed with 10 packed bead volumes of Tris buffered saline buffer (TBS) (50mM Tris-HCl, 150mM NaCl, PH 7.4) after which the buffer was discarded. 500 µl of cell lysate, BAP fusion protein (50 ng/µl, diluted 1:25 in TBS) (positive control) and 1 ml TBS (negative control) were added to the beads. Samples were further incubated overnight at 4^{o}C. Beads were collected, and supernatant was removed (**Figure 39**). The magnetic beads were washed with TBS. FLAG-fusion and BAP recombinant proteins were eluted under acidic conditions with five packed bead volumes of 0.1M Glycine-HCl (pH 3.0) (**Figure 39**) after which elution fractions were neutralised with Tris Buffered Saline (50mM Tris-HC, 150mM NaCl (pH 10.0)). Aside acid elution bound recombinant proteins were also eluted with 2x SDS-PAGE sample buffer (125mM Tris HCL, pH 6.8, 4% SDS, 20% (V/V) glycerol and 0.004% bromophenol blue) without DTT or 2-mercaptoethanol after which samples were boiled for three minutes. Fractions containing the expressed protein were pooled, desalted, and concentrated against phosphate buffered saline (PBS). Desalted recombinant proteins were quantified using the Pierce BCA assay kit (Thermo Scientific) following manufacturer's instructions. The purity and identity of the recombinant protein were assessed using SDS-PAGE and immunoblot.

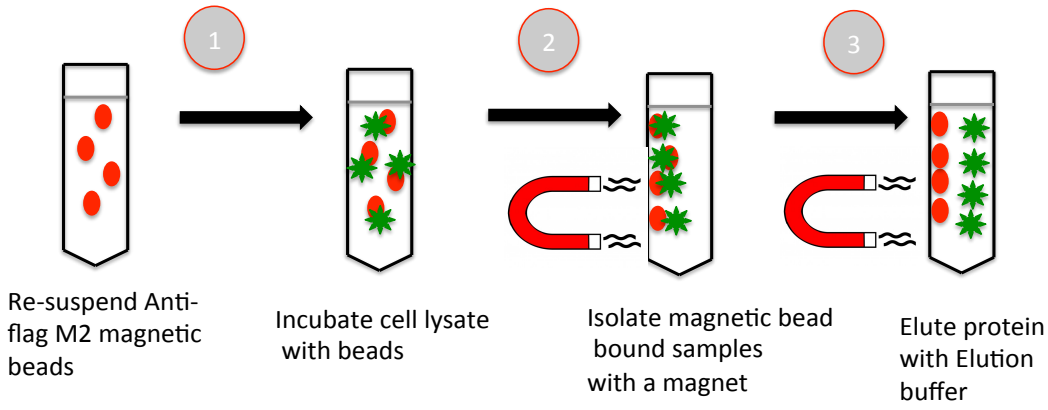


Figure 39: Diagram showing the processes involved in anti-Flag® M2 Magnetic bead protein chromatography. Anti-Flag® M2 magnetic beads mixed with cell lysate to allow desired target to bind to beads **2**. Beads washed with TBS (50mM Tris-HCL, 15mM NaCl, pH 7.4) to remove unbound proteins from beads. **3.** Bound target (Myc-DDK tagged proteins) eluted from beads using 0.1M Glycine HCL (pH 3.0) after which the elution fractions were neutralised with Tris Buffered Saline (50mM Tris-HC, 150mM NaCl (pH 10.0)).

2.4.4.3.5.3 Immunoprecipitation of Proteins using Myc Trap® Magnetic Beads

Immunoprecipitation of Myc-tagged proteins using the Myc Trap® magnetic beads (Cat. YTA-10, Chromotek, UK) employed a similar principle as the Anti-Flag® M2 magnetic bead immunoprecipitation procedure. Myc Trap® magnetic beads were thoroughly vortexed and 25 µl bead slurry was pipetted into 500 µl ice-cold dilution buffer (150mM NaCl, 0.5 mM EDTA, 0.0018% sodium azide). The mixture was centrifuged at 2500 x *g* for 2 minutes at 4°C and supernatant was discarded. Beads were then washed twice with ice-cold dilution wash buffer. Cell lysate suspected to contain Myc tagged proteins was added to equilibrated magnetic beads and incubated for 1 hour at 4^0C, after which the mixture was centrifuged at 2500 x *g* for 2 minutes at 4^0C. Myc-Trap® beads were further re-suspended in 500 µl ice-cold wash buffer and subsequently centrifuged at the same speed after which the supernatant was discarded. This stage was carried out twice. For elution of Myc-tagged proteins in cell lysates, two approaches were undertaken. Firstly, 2x Myc peptide (Chromotek, UK) reconstituted in PBS to a final concentration of 1 mg/ml was used. Reconstituted Myc peptide was diluted to 100

µg/ml in dilution buffer and 100 µl was added to Myc Trap® beads. The preparation was incubated for 15 minutes at room temperature and further centrifuged at 2500 x g for 2 minutes. Supernatants were carefully transferred into a new tube and this step was repeated to increase the elution efficiency. The Myc peptide procedure was undertaken to displace Myc-tagged proteins from the Myc Trap® beads. Alternatively, Myc Trap beads were re-suspended in 100µl 2x SDS sample buffer after which re-suspended beads were heated for 10 minutes at 95ºC to dissociate immunocomplexes from beads. Beads were then centrifuged, and supernatants were collected.

Chapter Three: Development of the Antigen Microarray Technology for Autoantibody detection in Hepatocellular Carcinoma Patients

3.1 Introduction

Microarray technology is a multiplex lab-on-a-chip assay which allows large quantities of biological samples to be arrayed onto a solid substrate (either on a glass slide or silicon thin film) using high-throughput, miniaturised, parallel processing and detection methods (366, 367). Producing an immunoassay in a 'microspot' fashion was instigated in the 1960s, where depositing spots of antigen solution was utilised in the detection of serum autoantibodies against thyroglobulin in autoimmune hepatitis. However, the concept of microspot took shape with the development of DNA microarray technology. It is considered as one of the most recent advances being used for cancer research and aids in pharmacological approaches to treat diseases. There are different types of microarray technology; DNA microarray measures the expression of a large number of genes simultaneously and helps to identify single-nucleotide polymorphisms (SNPs) and mutations, target genes of tumour suppressors, cancer biomarkers, genes associated with chemo-resistance and drug discovery (366). Antibody microarrays usually consist of capture antibodies immobilised onto a solid surface, such as glass, in order to detect antigens. This type of microarray is often used to detect expression of proteins in cell lysates in general research and biomarkers for diagnostic purposes (366, 368).

Antigen microarray has emerged as one of the most robust and promising tools for the screening of a wide range of conditions, including the identification of protein-protein interactions and examination of humoral immune responses in diseases (300). With

early screening techniques, such as Enzyme Linked Immunosorbent Assay (ELISA), autoantibodies to a variety of tumour-associated antigens (TAAs) are analysed individually in single-analyte experiments (300). However, with the introduction of microarray technology, the reactivities of autoantibodies to a panel of antigens can now be examined in a high-throughput and multiplexed manner by spotting them robotically onto planar surfaces (299). Antigen microarrays offer an incomparable tool to examine the immune response in autoimmune disorders, with important possible applications for disease management. These include determining individuals who are at risk of developing a specific autoimmune disease, monitoring progression of the disease and response to therapy and early diagnosis of individuals developing autoimmune disorders before symptoms appear (369).

Spotting antigens directly onto an array surface generates a microarray. When these microarrays are incubated with patient samples, the spotted antigens function to capture autoantibodies whose reactivity can be determined by either utilising a secondary antibody detector or the use of a direct label such as fluorescent-labelled autoantibodies directly from a serum specimen (370). Reproducible printing of antigen spots on a solid surface with a positioning precision is a requirement of this technology. The technology is undertaken in a temperature and humidity controlled environment in order to preserve the structure and function of the materials printed (370). The development of high throughput methods for analysis of antibody reactivity was initiated by the construction of a multiplex ELISA using 96 well (370). Antigen microarrays are more sensitive compared to ELISA as the signal is typically fluorescent rather than colorimetric (**Figure 40**). Additionally, this technology is able to quantify hundreds of antigen-antibody interactions using very small volumes of samples (300, 371).

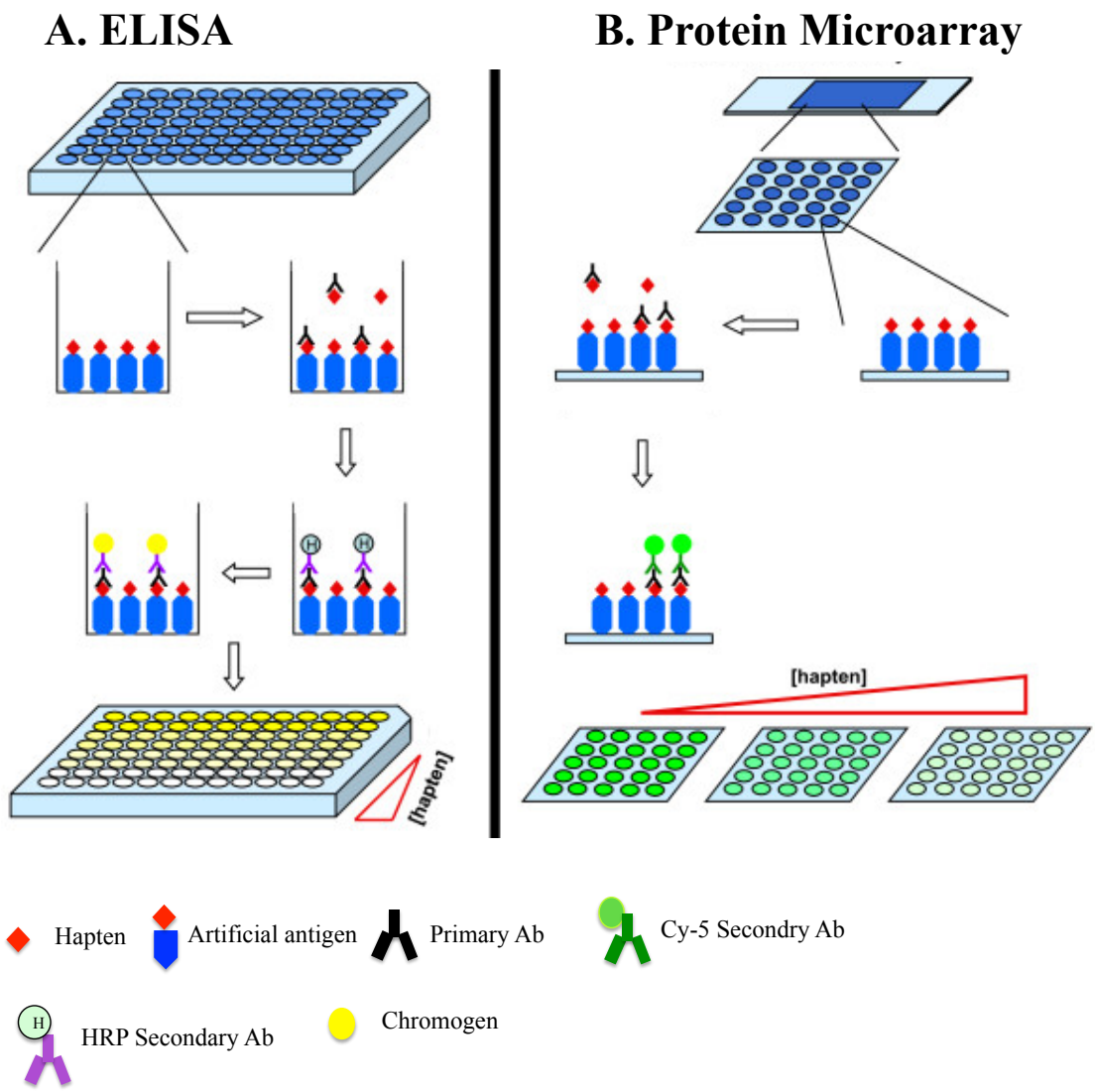


Figure 40: Enzyme Linked Immunosorbent Assay (ELISA) vs Protein microarray. Adapted from (368).

The antigen microarray technology has some limitations with respect to analysing antibody responses. For example, the structure of antigens can be affected by drying of microarrays or during adsorption to the solid surface. This variations in antigen structure can interfere with the conformational epitopes of clinical relevance and can also show epitopes that are not accessible to antibodies (369). Thus, a critical feature of the microarray technology is the provision of optimal binding without conformational change (372). Initially, polyvinylidene fluoride (PVDF) membranes were the main choice of solid support for protein microarrays (373). The subsequent

application of glass as solid support for the microarray resulted in high binding capacity with low non-specific background. The change from DNA to protein microarrays also compelled a more challenging task, thus the provision of a surface that houses proteins of different structure and composition in a manner such that their three-dimensional structure, binding sites and functionality are preserved (372). Several surfaces have been recommended in order to meet the requirement of protein microarray and this can be broadly divided into three major groups. The first consists of two-dimensional (2D) plain glass slides (**Figure 41**), which are activated with different kinds of coupling chemistries such as aldehyde, epoxy or carboxylic esters. These surfaces bind proteins and antibodies either by formation of covalent bonds, or electrostatic interactions (372). A number of surface chemistries have been assessed for the immobilisation of capture agents on protein microarrays. Surfaces such as poly-lysine coated glass slides, which are hydrophilic and positively charged, allow for non-covalent protein adsorption, but this usually gives problems, such as protein desorption, which can lead to signal loss (374). Covalent binding via amines or amino acid side chains on chemically coated surfaces, such as aldehyde, is considered as an alternative method for protein attachment to surfaces. The benefit of covalent binding is its stability, and the capture agents are immobilised at very high densities. This leads to a highly sensitive detection (375). However, one drawback is protein denaturation. On the other hand, there are three-dimensional (3D) gels or membrane-coated surfaces (**Figure 41**), such as polyacrylamide (376), agarose (377), and nitrocellulose (378). These bind proteins primarily by physical adsorption and have the benefit of preserving the native conformation of proteins. Nitrocellulose coated slides or gel pads permit passive adsorption leading to non-specific and non-covalent attachment of proteins, whereas surfaces such as epoxy-activated surfaces allow for a covalent attachment of proteins

through their accessible amine, hydroxy or thiol groups. Unlike epoxy-activated or nitrocellulose-coated surfaces, which allow for a random orientation of the proteins, affinity tag coated surfaces permit a uniform orientation of the proteins (13). However, large variations in signal intensity are a drawback of these surfaces. An optimal solid surface chemistry for protein microarrays should be able to preserve the functionality of the capture agent after immobilisation, have a high binding capacity, have high reproducibility, give high signal-to-noise ratio, and should be reasonably easy to manipulate (379, 380). There is no common specific slide surface chemistry which is ideal for all microarray applications. Usually, a considerable amount of time has to be channelled into developing an optimal surface chemistry, in addition to fine tuning the assay protocols appropriately before utilising the full value of planar affinity arrays. Numerous aspects need to be considered, such as whether the arrayed proteins can retain their structure, conformation and functional ability without denaturing them. A comparable effort has to be spent for detecting the optimal buffer to block arrays before sample application. As such there are many challenges linked with the antigen microarray technology as compared to DNA microarrays (379).

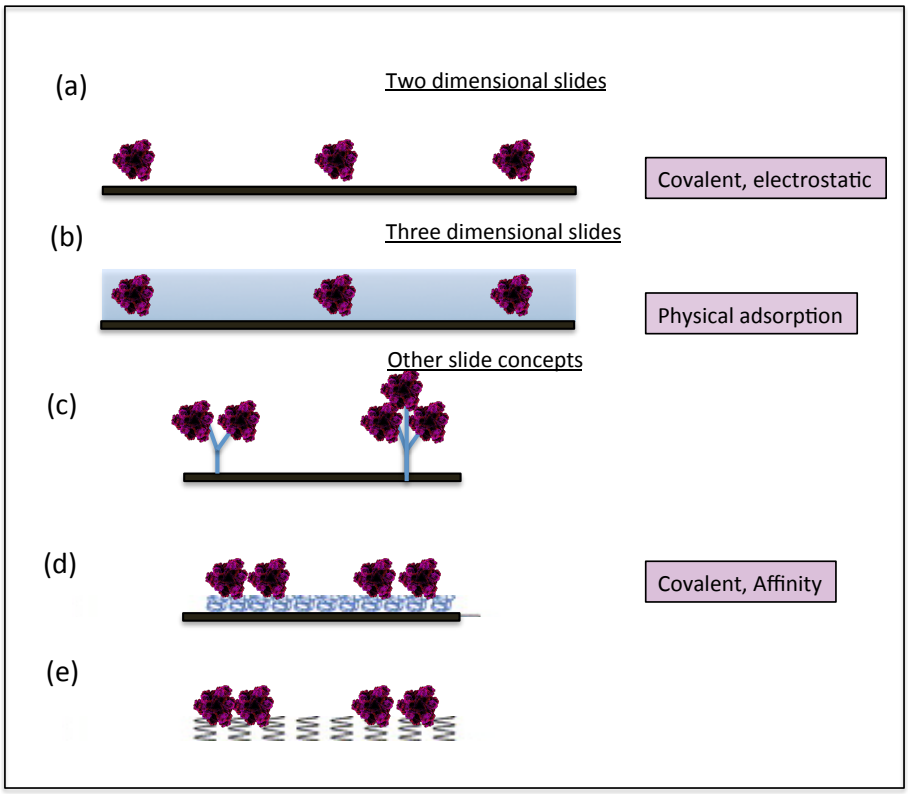


Figure 41: Slide surface chemistries for protein microarrays. The figure above shows the various classes of slide surface chemistries and further highlights their main binding approaches. **(a)** Shows the direct binding of proteins by two-dimensional slide surfaces, on the other hand, **b)** three-dimensional slide surfaces by means of physical adsorption retain proteins within the gel structure. Other slide surface concepts include surface coatings such as **(c)** dendrimer slides, **(d)** avidin or dendrimer slides and **(e)** polyethylene glycol-epoxy slides.

With the advances in microarray technology, there has also been an increase in the development of sensitive and reliable detection methods. As such, protein detection methods have gradually undergone a significant transition from labelled based to sensitive label free technologies, which are very useful for the study of interactions and functions of large amounts of proteins (381). In addition, protein microarrays allow for increase in simultaneous measurement of analyte, hence having an increased throughput potential over other current technologies.

As already mentioned above, during microarray preparation it is essential that the capture agent stays in the functional state once it has been arrayed onto the solid surface (382). Buffers with similar properties to the physiological fluid are mainly used for the

preparation of capture agents in order to maintain their functional integrity and this is done prior to spotting. The addition of stabilisers such as glycerol can help preserve the native properties of proteins (375). The production of the microarray itself presents as one of the principal technical challenges of microarray measurements. Printing technologies presently exist in two forms; contact and non-contact arrayers. Contact printing is based on a direct contact between a metal pin head and the solid surface (**Figure 42A**). This type of printing usually comes in three formats, solid pin, quill, as well as pin and ring. A solid pin printing assembly comprises of a solid pin with a flat end. The pin submerged into the liquid transfers a sub-nanolitre volume of sample to the tip of the pin. Direct contact of the pin with the surface dispenses the fluid to the surface of the solid support (381). On the other hand, the quill printing assembly (**Figure 42B**) is made up of a flat pin head with a distinct hollow bore where the sample wicks into the hollow space and gets deposited on the solid surface. The volume of liquid dispensed during the contact printing procedure varies from 0.3-2 nl per drop (381). One of the main challenges with contact printing is that proteins might remain attached to the pinhead following washing and this may result in the cross-contamination of samples. Also, proteins might be denatured during the printing procedure as the pin touches the solid surface (381). Moreover, assay variability occurs during contact printing as a result of less homogenous protein spotting. Non-contact printers employ a sensor, which is either piezoelectric crystal or solenoid and it deposits printing solutions above the solid surface (381). This type of printing is assumed to produce the lowest spot to spot variability in the amount of sample deposited. The capillary does not touch the surface hence; less harm is caused to the protein structure. However, during droplet delivery, the shear forces produced may have a negative effect on protein structure (381).

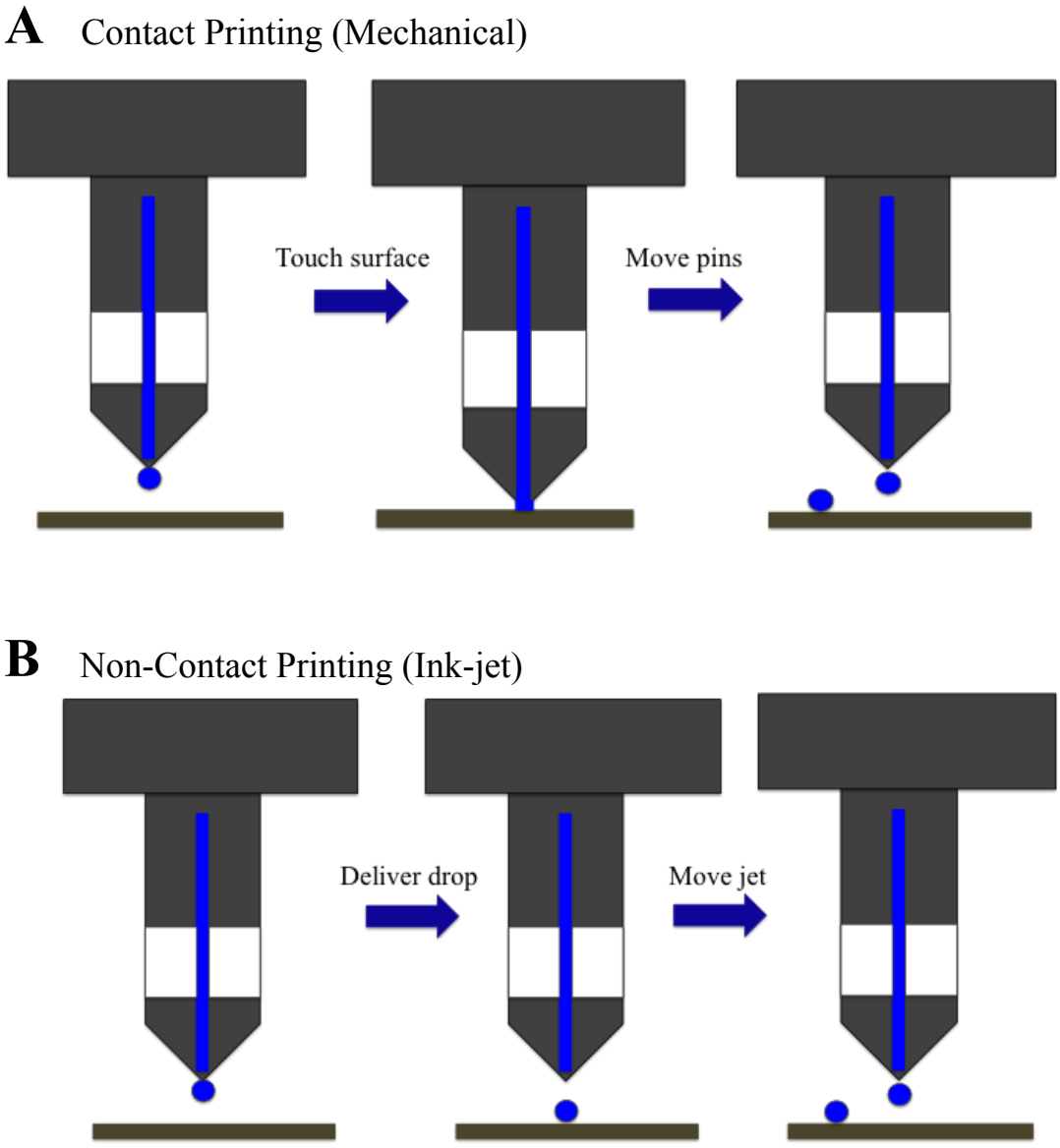


Figure 42: Microarray printing. The figure above shows (**A)** contact printing, where the solid pin makes direct contact with the surface to dispense proteins while (**B)** in non-contact microarray, the solid pin does not contact the slide surface as it drops proteins unto the slide surface by the ink-jet method.

The heterogeneous nature of the proteins and peptides used in antigen microarrays, as compared to nucleic acids used in transcript profiling, has plagued antigen microarray technology. For example, this antigen heterogeneity has produced substantial variability in the binding of antigens to array surfaces, and therefore can limit autoantibody detection (300, 383). Variation within and between antigen microarrays

may also be as a result of the heterogeneity of buffers and macromolecules required to solubilise them. This variance negatively affects the ability to accurately detect subtle and very important differences between patients or within a patient over time (300). Despite modern advances, the need for development in antigen microarrays is still tremendous due to a number of distinctive technical challenges facing the technology. These include technical issues pertaining to printing, probing and normalisation strategies (383). One of the principal aims of this work was to use the in-house antigen microarray platform to profile autoantibodies in sera of hepatocellular carcinoma patients. The performance of the in-house antigen microarray was investigated by firstly undertaking validation studies, since one of the main obstacles of the technology in general is the difficulty in reproducing microarray assays. Subsequently, a thorough optimisation of the technology was undertaken by investigating multiple parameters concurrently, including the printing and blocking buffers, edge effect, antigen concentrations, slide surfaces, detection antibodies, fluorescent dyes, target humidity, etc. in order to improve assay conditions to build a successful and robust microarray platform. This newly developed diagnostic technology would generate sensitive, consistent, reliable and reproducible assays for the detection of specific IgG anti-TAA autoantibodies in HCC patients' sera.

Validation of an assay is the process used to approve that the analytical method utilised for a specific test is accurate and reproducible for its intended application. The outcome of an assay validation can be used to review the quality, reliability and consistency of results, which is a vital part of any good analytical practice. The validation process is usually undertaken following guidelines provided by regulatory agencies such as the Food and Drug Administration (FDA) to determine the assay functions and limitations for the intended purposes. Specific guidelines for method validation have been

published by the FDA. This involves thorough experimental steps that would evaluate and document the performance of an assay including the following: accuracy, precision, specificity, reproducibility and reliability, limits of detection and quantitation (**Figure 43**). The above validation points will serve as a robust test into the nature of the antigen microarray technique and should enable the researcher to decide whether it is a reliable method to quantitate autoantibody responses in HCC patients.

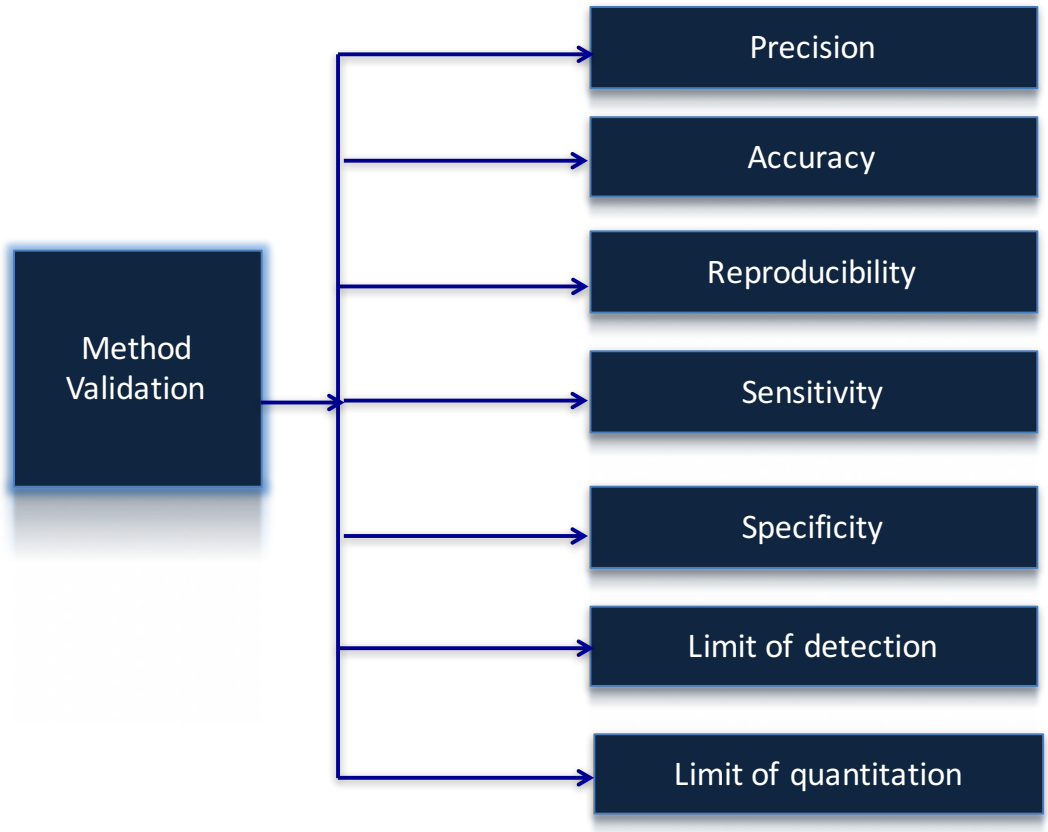


Figure 43: Schematic diagram showing the various steps involved in the Method Validation Assay.

Reproducibility is the degree of agreement between the results of experiments conducted at different times. Thus, the ability to obtain consistent results when repeated. The precision of a procedure shows the closeness of agreement between series of measurements obtained from multiple sampling of the homogeneous sample under

the same prescribed conditions. The precision can be calculated by dividing the standard deviation of multiple repeats by mean of the same repeats multiplied by 100. Precision of an assay is divided into two categories namely: intra- and inter-assay precisions. Intra-assay variability in the context of the protein microarray is defined as the coefficient of variation of signal intensities between replicates of analytes either on or different pads of a processed slide (**Figure 44**). Calculating and comparing the coefficient of variations of corresponding replicates of antigens on the same slide determine the intra assay precision of a microarray experiment. On the other hand, Inter-assay precision is the coefficient of variation of signal intensities between corresponding spot replicates of antigens processed on different days (**Figure 45**). These are usually done to determine if the assay yields similar outcomes when replicates of antigens are printed and processed on the same slide or on different days under same experimental conditions. This parameter serves as a good pointer of how internal experimental (e.g. buffers, dilutions) and external environmental (e.g. temperature, light) factors might affect the precision of the assay when it is tested on multiple days. The limits of precision, which is largely accepted and agreed between developers of immunoassays and prescribed by FDA guidelines range between 20-30%. However, this level varies depending on to the nature of biological samples and technique used. Therefore, three CV% values were established for the specific IgG microarray platform in lines with the limits prescribed by many microarray system developers: Intra assay variability (CV%) < 15% and Inter assay variability (CV%) < 20%. Consequently, the calculated CV% values that fall within the established CV% limits of microarray platform will be considered precise and reproducible.

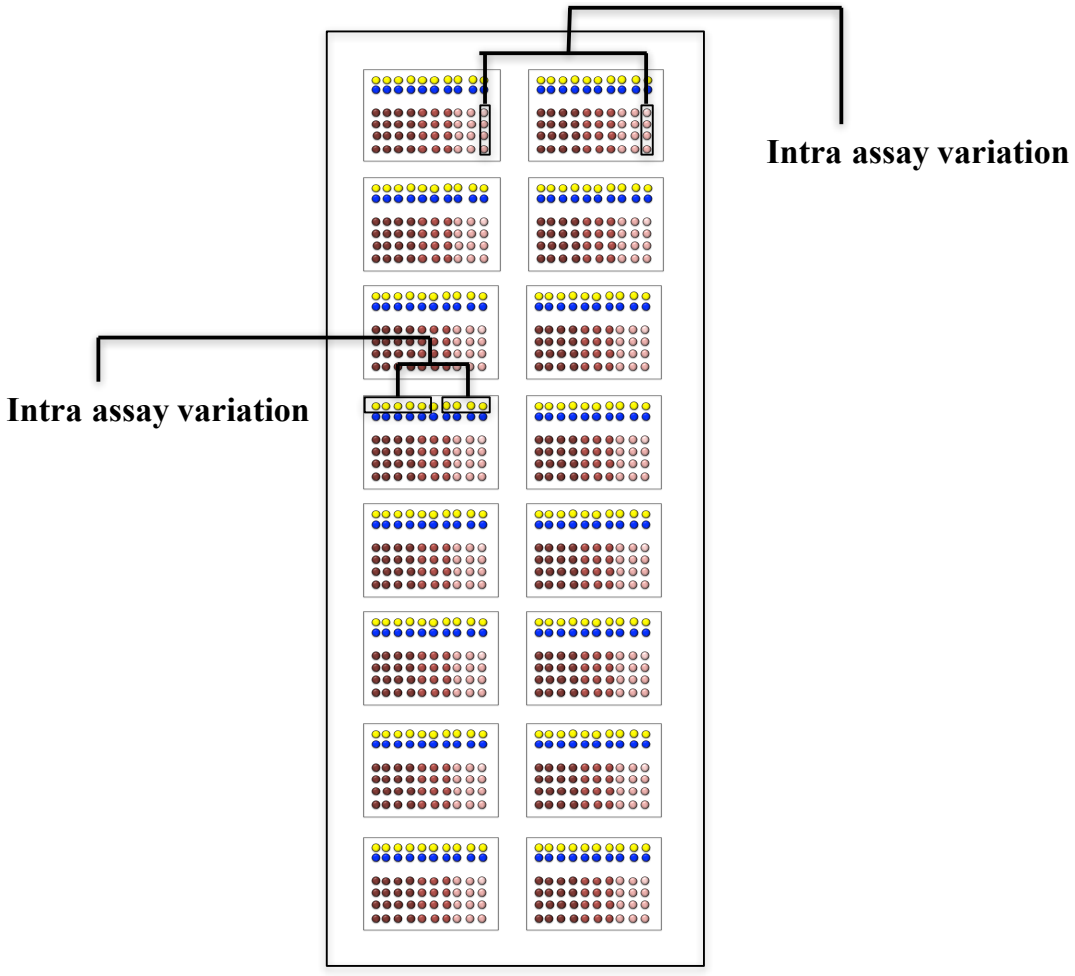


Figure 44: Diagram elucidating the intra-assay variability (CV%) for ten and four spot replicates of *Candida* antigen and human IgG serial dilution standard respectively.

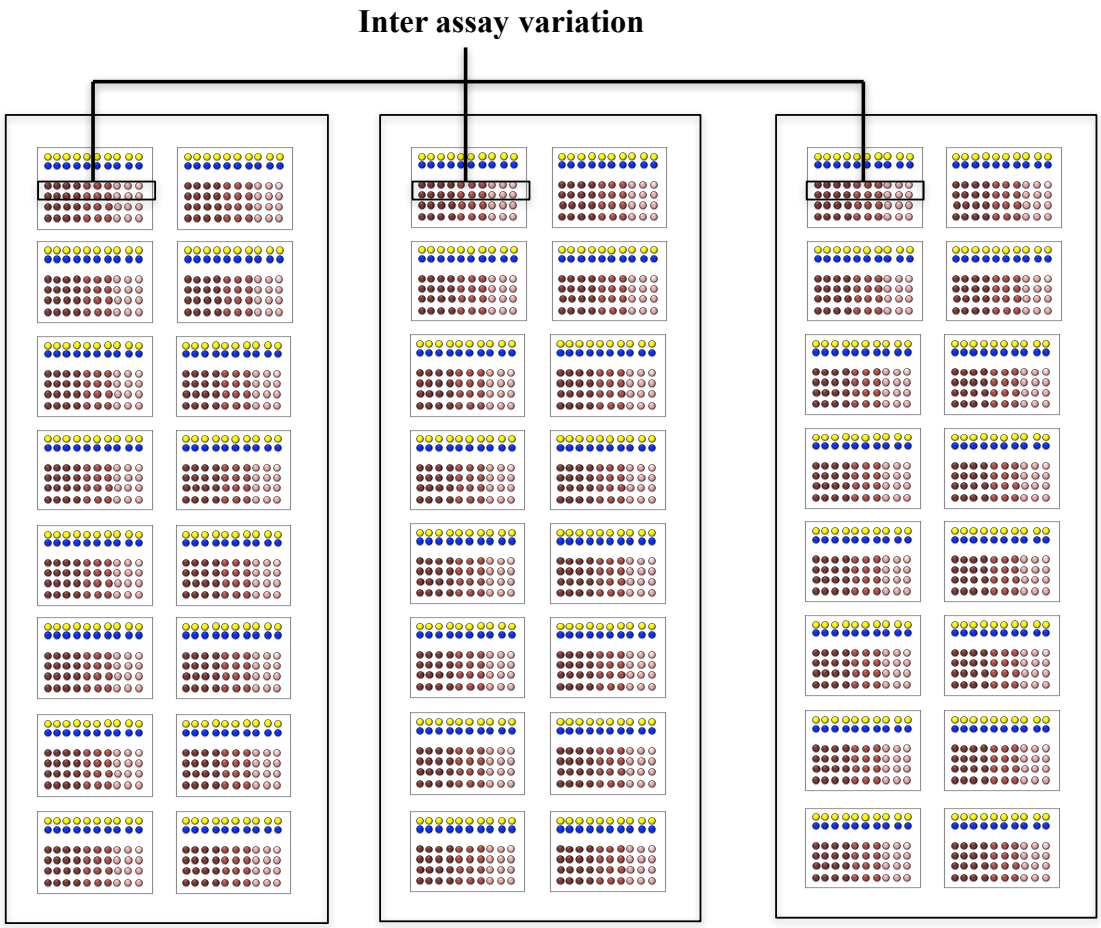


Figure 45: Diagram showing the inter assay variability (CV%) for ten 10 spot replicates of human IgG serial dilution standard respectively.

The aim of this chapter is thus to optimise and validate the microarray-based technology that will be used for measuring autoantibody responses to tumour-associated antigens in hepatocellular carcinoma. These optimisation and validation steps are summarised in **Figure 46.**

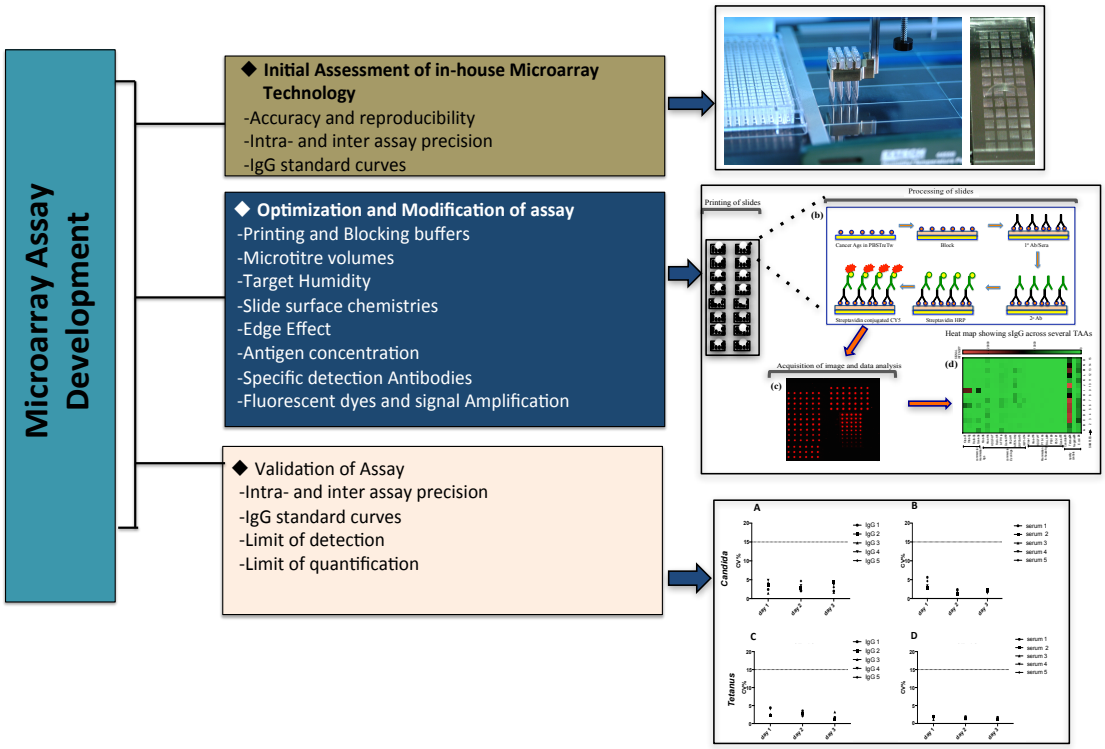


Figure 46: Schematic diagram outlining the various processes involved in the development of the Antigen Microarray Technology, for the detection of autoantibodies in HCC patients.

3.2 Materials and Methods

Validation assays were undetaken on the antigen microarray prior to carrying out optimisation studies in order to determine whether it gave reproducible and consistent outcomes, before being used as a diagnostic platform to profile HCC patients sera. His_6-tagged recombinant TAAs produced in an *E. coli* system (KRAS, HRAS, HDGF, RALA, P62, Gankyrin, AFP, APCN, GRP78, Imp1, HCC1, MAGE), as well as two antigen quality controls, namely *Candida albicans* and Tetanus toxoid, were diluted in different printing buffers (PBS-Tween, PBS-Trehalose-Tween, PBS-Trehalose-Betaine-Tween) to make a volume of either 5 µl, 10 µl or 20 µl at concentrations ranging from 75µg/ml-100µg/ml. Protein dilutions were then transferred into a 384 microtiter well plate (Genetix, USA). In addition, a two-fold serial dilution of purified human immunoglobulin IgG was prepared and placed on the same 384 well plate in 10 dilutions starting at a concentration of 50 µg/ml. His-tagged antigens were prepared in quadruplicates or ten replicates, while IgG dilutions were made in quadruplicates. These were subsequently printed onto a range of slide surface chemistries (Poly-L-lysine, Aminosilane, epoxysilane, Nitrocellulose) at a humidity of 57%-65% and further secured in either 8 or 16 pad incubation gaskets. Antigens were either printed at the edges or the centre of slides. Wells containing antigens were blocked with either 100 µl of 5% BSA, 10% BSA, 30% BSA, I-block or Super G (for nitrocellulose slides) in PBS-$Tween_{20}$ (PBST), sealed with a plastic strip, and then incubated for an hour with shaking at room temperature. Each well was washed five times with 100 µl PBST for 3 minutes. Two drops of Avidin blocking reagent (Life Technologies/Invitrogen) were then added to each well and incubated at 10 minutes with shaking after which they were washed five times with PBST. The Avidin block was followed by a further 10-minute incubation with Biotin block solution and the washing step was repeated. Blocked wells

were probed with either 100 µl of control samples (purified IgG and serum, diluted 1:500 and 1:1000 in 5% BSA in PBST respectively), 100 µl of monoclonal or polyclonal mouse or rabbit anti-His_6 antibody (Cell Signalling), diluted 1:10,000 in 5% BSA with the exception of negative control blocks). Wells were then incubated with gentle agitation for an hour at room temperature after which they were washed five times over 3 minutes to remove unbound antibodies. 100 µl of Biotinylated anti-human antibody (Vector Laboratories), diluted 1:20,000 in antibody diluent (DAKO) was added to wells probed with purified IgG or serum samples. Alternatively, 100 µl of anti-mouse antibody (Vector Laboratories) diluted 1:10,000, 1:20,000, 1:30,000 in antibody diluent, was added to wells probed with anti-His_6 antibody. Slides were covered and incubated with shaking for one hour at room temperature after which arrays were then washed three times. Streptavidin Horseradish Peroxidase (HRP) (BIORAD, USA) was diluted 1:2,000 in antibody diluent and 100 µl was added to each block and incubated with shaking at room temperature in the dark for 15 minutes.

Tyramide amplification process (TA) was carried out to increase the sensitivity of microarray assay by increasing signal intensity and minimizing background noise to the lowest levels. To undertake this procedure, the amplification diluent, amplification reagent, (Bio-rad, USA)) and ultrapure water were mixed in a ratio of 4:1:4 (800 µl: 200 µl: 800 µl). 100 µl of the mixture was added to each block for 10 minutes with shaking. After the amplification step, slides were washed three times with 20% Dimethyl Sulphoxide PBST, then finally washed five times with PBST. 100 µl of Streptavidin-conjugated Cyanine 5 (Molecular Probes, UK) was diluted 1:5,000 in 5% BSA-PBST after which the preparation was incubated in the dark with shaking for 15 minutes. Slides were washed five times with PBST then once with PBS only for 5 minutes and subsequently rinsed briefly with ultrapure water. Slides were dried by

centrifugation (Universal 30 RF) at 1200 rpm for 5 minutes. Processed slides were scanned using Genepix 4200AL scanner (Axon Genepix ®) at a wavelength of 635nm (laser standard red) at 400 PMT and 100% power. The Axon Genepix Pro 6.1 software was used to measure the fluorescent signal of each spot and the GPR files (median fluorescence minus background for each arrayed protein) were generated. Poor quality features were flagged for removal by the Genepix software based upon mathematical and statistical data with regards to spot morphology (circularity and size) (**Figure 47**), signal uniformity, local background and signal to noise ratio. After the data were filtered, they were analyzed using R statistical package (RPPAnalyzer version 3.1.2, 2014) to general mean signal levels. Graph Pad prism 7 (Graph Pad 7, USA) software was used to generate Graphs as well as interpolate IgG standard curves. Signal arithmetic mean of fluorescent signals, median, standard deviation, range and percentiles for all antigens were generated during the statistical analysis. Determining the reproducibility of arbitrary fluorescence required that the precision, which is the coefficient of variation (CV%) of multiple measurements or repeats is calculated. Intra-assays were performed repeatedly over the same slide on the same day and inter-assays performed over a period of two to three consecutive days. The precision was calculated by dividing the standard deviation of multiple repeats by its mean. The accepted level of precision was set at <15% and <20% for intra and inter-assay respectively.

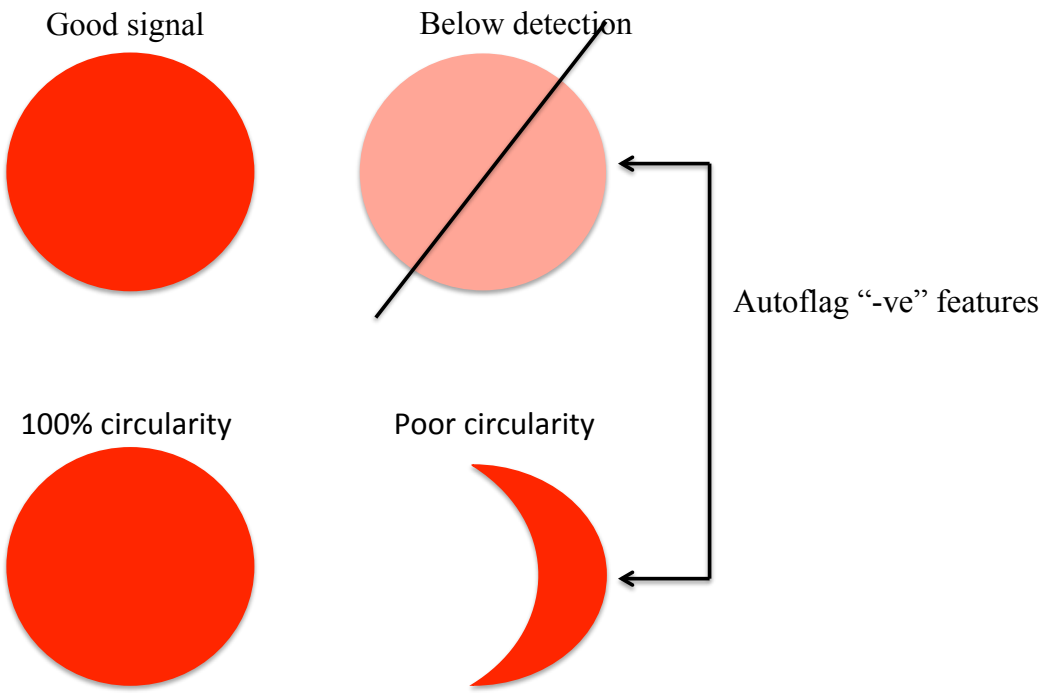


Figure 47: The figure above shows the acceptable level of signal uniformity and regularity of spots required for statistical analysis of microarray data.

3.3 Results

3.3.1 Validation Assessment of the In-House Antigen Microarray Assay

Reproducibility tests were first carried out on the in-house microarray platform using two quality control antigens, namely *Candida albicans* and *Tetanus* toxoid. These were selected as most human serum contain antibodies to them. Control antigens, as well as a two-fold human IgG serial dilutions, were printed onto Poly-L-lysine slides and further probed with control samples (serum and purified IgG from serum, diluted 1:500 and 1:1,000 in 5% BSA in PBST respectively). This was followed by the addition of a secondary biotinylated anti-human antibody. The antigen-antibody complex was then detected with a Streptavidin conjugated Cy5 dye, after which the slides were scanned. This procedure was undertaken over a period of three consecutive days under the same experimental conditions. Scanned images of the three processed slides across different days showed morphological differences in the diameter, sizes, shape, as well as signal intensity of spots (**Figure 48**). Unexpectedly, large spots of increased signal intensity were observed on day 3 (**Figure 48**). Moreover, antibody responses to *Tetanus* were high as compared to *Candida* (**Figure 49**) peaking 18,000 AFU and 23,000 AFU for purified IgG and sera respectively.

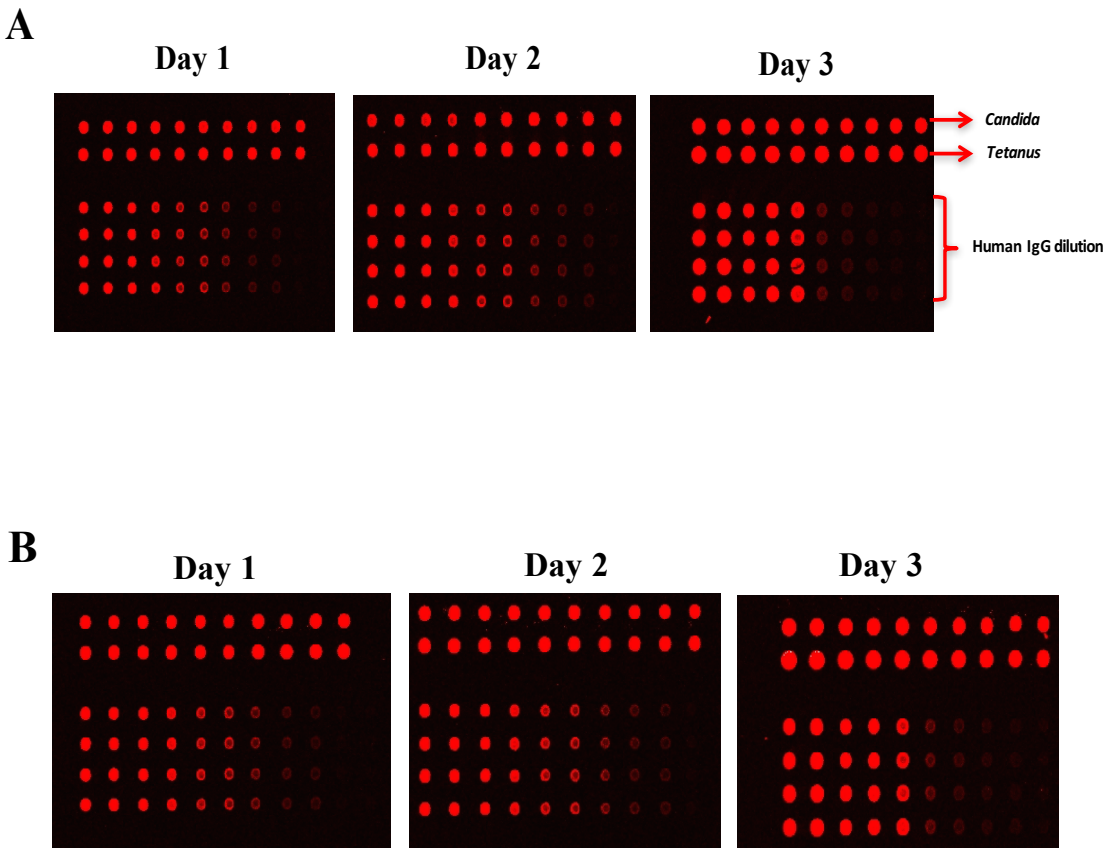


Figure 48: Morphological differences in spots of control antigens. Quality control antigens, *Candida* and Tetanus as well as a two-fold human IgG dilution were printed onto Poly-L-lysine slides in ten replicates and quadruplicates respectively, after which they were probed with control samples (sera and purified IgG from same sera). The antigen-antibody complex was further detected with a Streptavidin conjugated CY5 dye and scanned at 635 wavelength at 400 PMT using Axon Genepix 4200AL scanner. **(A)** and **(B)** represent the morphology of spots when slides were incubated with purified IgG and sera respectively on three consecutive days.

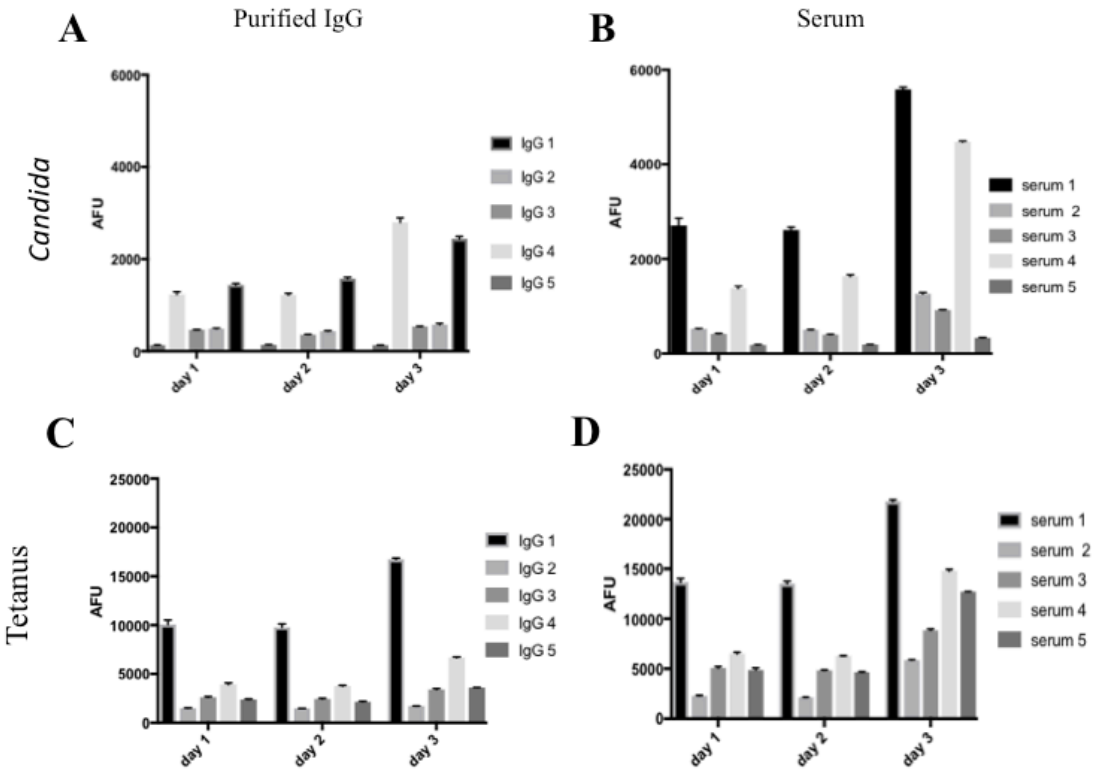


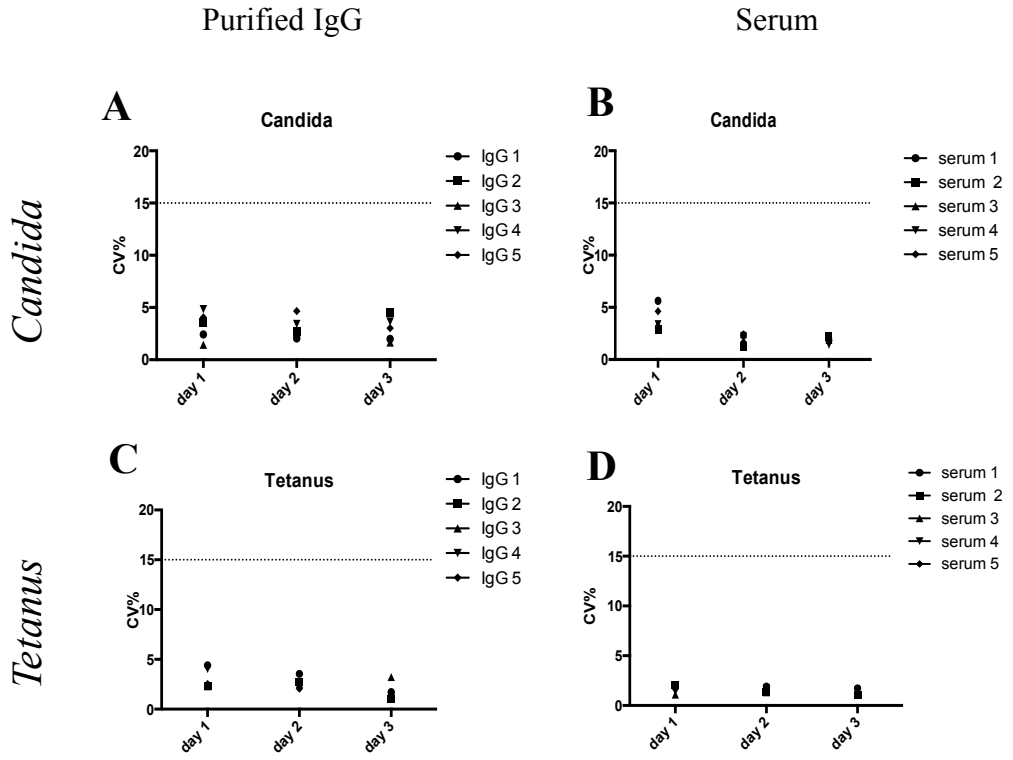
Figure 49: Differences in arbitrary fluorescence in response to quality control antigens across different days. Quality control antigens, *Candida* and Tetanus were probed with five different purified IgG and sera after which slides were subsequently incubated with biotinylated anti-human secondary antibody. The interaction was then detected with a Streptavidin conjugated CY5 dye and further scanned at 635 wavelength at 400 PMT using Axon Genepix 4200AL. The assay was carried out on three consecutive days under same experimental conditions. **(A)** and (**B)** represent the mean fluorescence (minus local background) of antibody responses to *Candida* while (**C**) and (**D)** show the mean fluorescence of antibody responses to Tetanus when incubated with purified IgG and sera respectively. Data were analysed using Graph pad prism 6 and a column statistics multiple comparison test ($P< 0.05$) was used to calculate significance, indicating 95% confidence interval.

Reproducibility of the assay was then determined by calculating the intra- and inter-assay precision. This was undertaken before and after signal intensities were normalised with the human IgG standard curve, with the expectation that normalising to a standard curve would produce lower CVs. The intra assay precision was within the acceptable limits (CV ≤15%) when examined before normalisation (**Figure 50A-D**), but inter assay precision had many points above the acceptable limit of 20% CV (**Figure 50 E-F**).

Human IgG standard curves (probed with both purified IgG and serum) showed similar signal intensities on days 1 and 2, but as seen in the images shown above, there were significantly higher signals on day 3 (**Figure 51**). Thus, it was expected that normalising to the standard curve on the day of the assay would improve the poor inter assay CVs observed before interpolation.

The intra assay precision of the normalised or interpolated values were within the acceptable limit (≤15%), as was seen with the uninterpolated values above (**Figure 52A-D**). A reduction in inter assay precision was seen with interpolated values as compared to before interpolation, although not all CV% of samples attained acceptable limits of precision (CV≤ 20%) (**Figure 52E-F**).

I. Intra assay variations before normalisation with Human IgG standard curve



II. Inter assay variations before normalisation with Human IgG standard curve

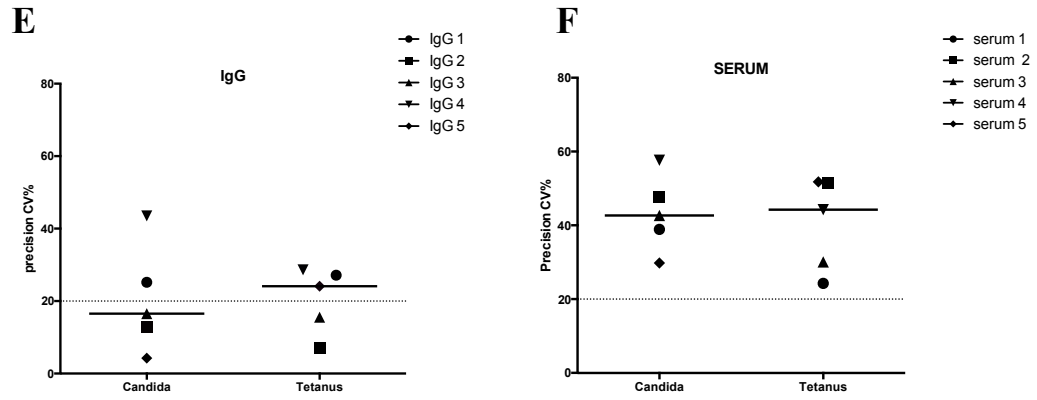


Figure 50: Intra- and inter- assay precision of arbitrary fluorescence. The precision (coefficient of variation of multiple repeats) of signals in response to *Candida* and Tetanus were calculated. **(A)** and (**B)** represent the intra-assay precision (within a day) of signal intensities in response to *Candida.* (**C**) and (**D)** represent the intra-assay precision (%) of signal intensities in response to Tetanus. (**E)** and **(F)** represent the inter-assay precision (across different days) of signal intensities in response to *Candida* and Tetanus when incubated with purified IgG and sera. Dashed lines represent the acceptable limits of precision while solid lines represent the median of each group.

III. Human IgG standard curve

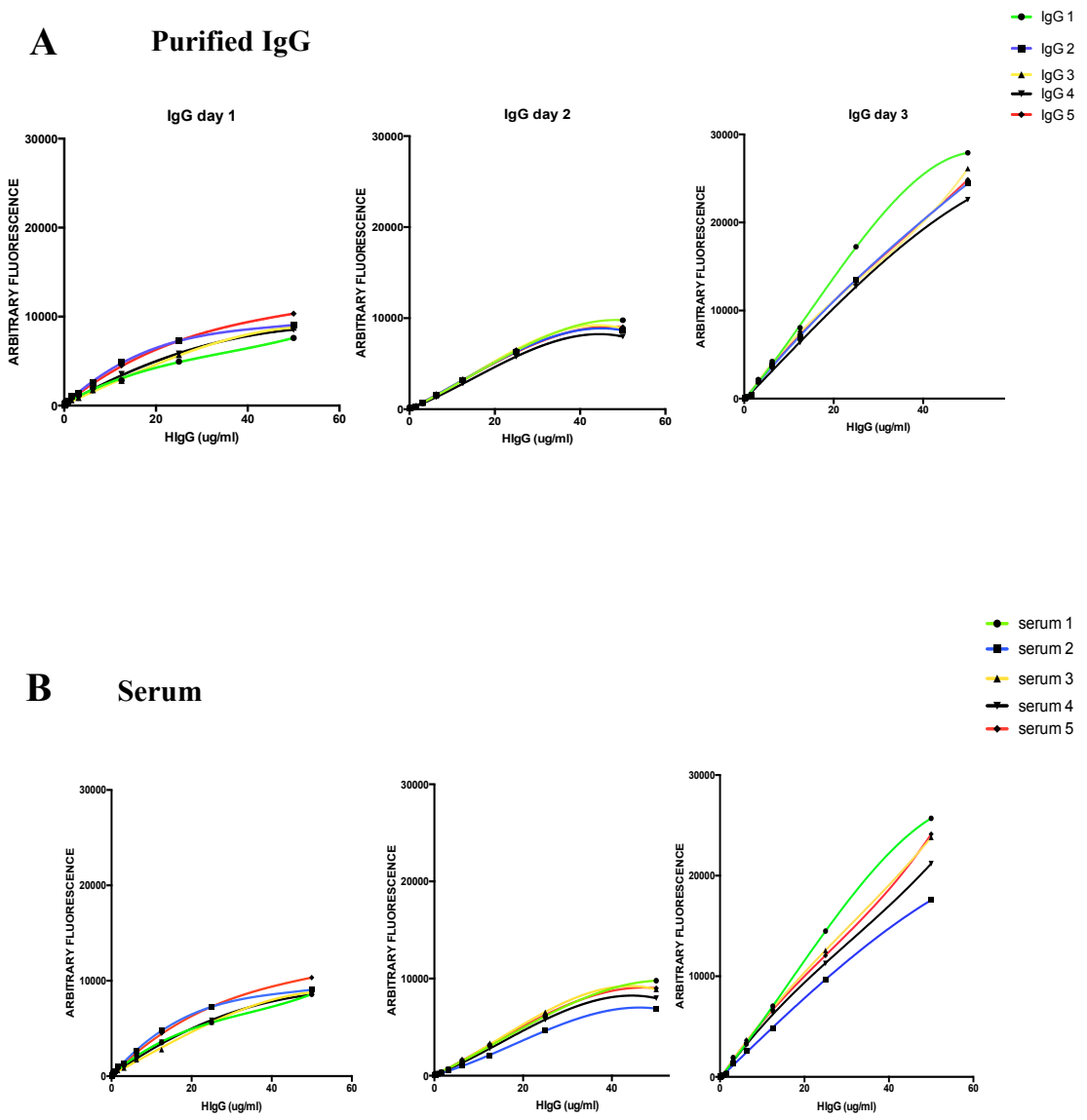
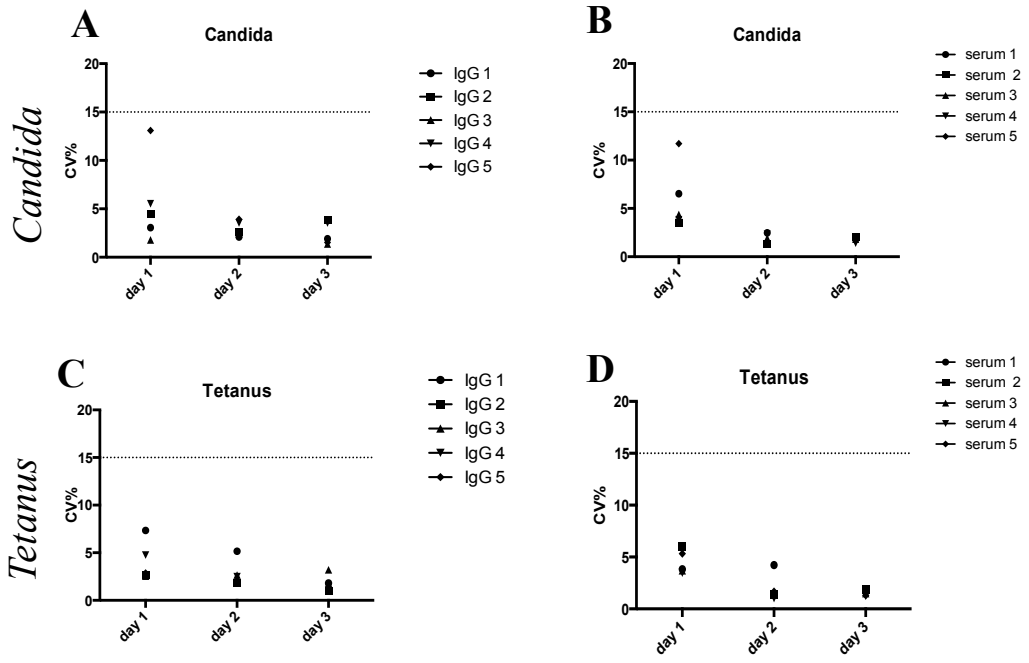


Figure 51: Human IgG standard curves across three consecutive days. A two-fold serial dilution of purified human immunoglobulin (IgG) was prepared and placed on the same 384 well plate in 10 dilutions starting at a concentration of 0.05 mg/ml and further printed onto Poly-L-Lysine slides. These were probed with either purified IgG or sera after which they were subsequently incubated with biotinylated anti-human antibody. The interaction was then detected with a Streptavidin conjugated CY5 dye and further scanned at 635 wavelength at 400 PMT using Axon Genepix 4200AL. The dilution curves of human IgG were plotted as a mean of signal intensities. These were used to normalise signals to total immunoglobulin concentrations in control samples. **(A)** and **(B)** show the signal intensities of human IgG dilutions when incubated with purified IgG and serum respectively on three consecutive days.

IV. Intra assay variations after normalisation with Human IgG standard curve



V. Inter assay variations after interpolation

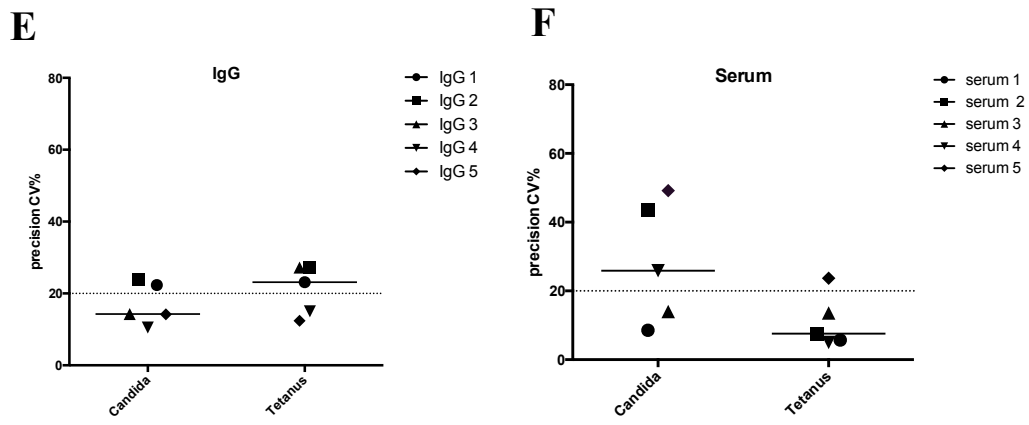


Figure 52: Intra- and inter- assay precision after normalisation with human IgG standard curve. Signal intensities of antibody responses to *Candida* and Tetanus were normalised using human IgG standard to total immunoglobulin concentrations. The precision (coefficient of variation of multiple repeats) of normalised mean values were calculated. **(A)** and (**B)** represent the intra-assay precision (within a day) of normalised values with regards to *Candida*. (**C**) and (**D)** represent the intra-assay precision (%) of normalised values with regards to Tetanus. (**E)** and **(F)** represent the inter-assay precision (across different days) of normalised values when incubated with purified IgG and sera. Dashed lines represent the acceptable limits of precision while solid lines represent the median of each group.

3.3.2 Assessing the reproducibility of signal intensities using HCC tumour-associated antigens

His-tagged HCC TAAs, which would be used for profiling autoantibodies in HCC sera, were then used to determine the validity of the assay. Three His-tagged HCC antigens: AFP, Gankyrin and MAGE4 were printed onto two Poly-L-lysine slides in sixty replicates. Each slide was probed with either a control HCC serum or rabbit anti-His_6 antibody (diluted 1:500 and 1:5,000 respectively in 5% BSA in PBST). Slides were further incubated with biotinylated anti-human antibody or anti-rabbit antibody (diluted 1:20,000 and 1:5,000 respectively in 5% BSA PBST) after which the interaction was detected with a Streptavidin conjugated Cy5 dye. This experimental procedure was undertaken for two consecutive days under same working conditions. Spot morphology in terms of the circularity, shape and diameter for all TAAs were consistent over the two days (**Figure 53**). There were no significant differences in signal intensities of antigen replicates ($p>0.05$) between days when anti-His_6 antibody (**Figure 54A**) and serum sample were tested (**Figure 54B**). High intra-slide variation was detected with slides probed with anti-His_6 antibody on days one and two. However, lowest CVs of signal intensities were seen with slides probed with serum on both days (**Table 17**).

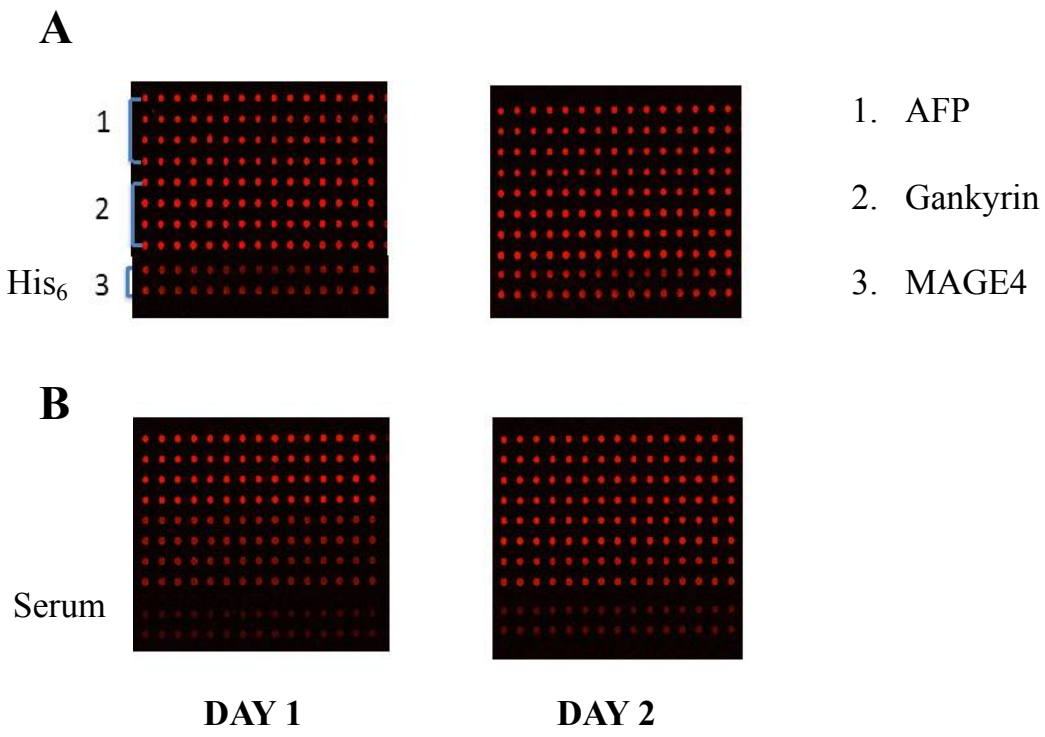
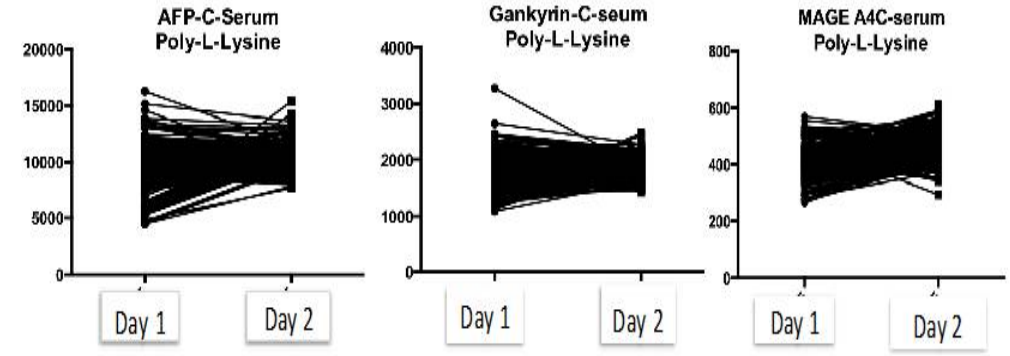


Figure 53: Morphological appearance of HCC His-tagged tumour-associated antigen spots on Poly-L-lysine slides. Three HCC His-tagged antigens; AFP, Gankyrin and MAGE4 were printed as sixty replicates onto Poly-L-lysine slides after which they were probed with anti-His_6 antibody or control serum. The complex was further incubated with biotinylated anti-human antibody or anti-rabbit antibody after which the interaction was detected with a Streptavidin conjugated Cy5 dye. Slides were then scanned at 635 wavelength at 400 PMT using Axon Genepix 4200AL. **(A)** and **(B)** represent the morphology of antigen spots on slides when incubated with control serum and rabbit anti-His_6 antibody respectively for two consecutive days.

A. Anti-His_6 antibody



B. Serum

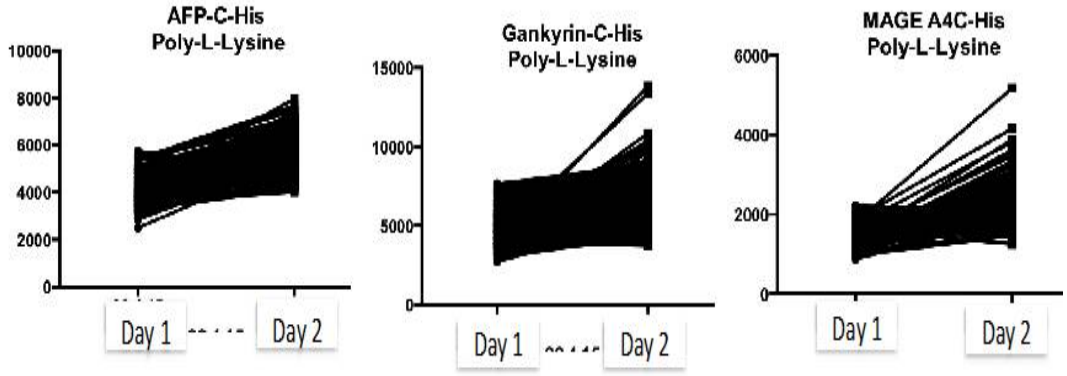


Figure 54: Difference in signal intensities to HCC tumour-associated antigens between two days. Three HCC His-tagged tumour associated antigens; AFP, Gankyrin and MAGE4 were probed with anti-His_6 antibody or control serum and then incubated with anti-human antibody or anti rabbit antibody. The interaction was further detected with a Streptavidin conjugated CY5 dye. The figures above represent graphs of signal intensities of replicates of AFP, Gankyrin and MAGE when incubated with **(A)** anti-His antibody and **(B)** serum for two consecutive days. Data were analysed using Graph pad prism 6 and a Two Way Anova multiple comparison test was used to calculate significance, indicating 95% confidence interval.

Table 17: Intra slide variation of AFP, Gankyrin and MAGE spot signals within and across eight blocks on the Poly-L-lysine slides when probed with (A) anti-His6 antibody and (B) control serum on two consecutive days.

A. Anti-His_6 antibody

DAY 1

Antigens	B1	B2	B3	B4	B5	B6	B7	B8	Average CV%
AFP	8.64%	14.25%	16.46%	14.40%	12.17%	13.11%	12.93%	20.35%	16.03%
Gankyrin	8.55%	23.95%	25.49%	22.14%	17.45%	14.24%	16.55%	29.53%	21.47%
MAGE	12.77%	8.71%	11.49%	12.15%	16.64%	20.34%	16.93%	17.42%	15.81%

DAY 2

Antigens	B1	B2	B3	B4	B5	B6	B7	B8	Average CV%
AFP	5.89%	7.74%	6.92%	9.66%	7.61%	10.86%	13.33%	8.37%	13.58%
Gankyrin	10.24%	21.24%	16.57%	15.40%	12.57%	20.59%	17.76%	12.22%	23.78%
MAGE	5.83%	10.15%	10.30%	13.17%	10.75%	12.74%	23.90%	14.52%	23.34%

B. Serum

DAY 1

HCC Antigens	B1	B2	B3	B4	B5	B6	B7	B8	Inter block CV%
AFP	15.72%	9.36%	11.45%	6.83%	10.36%	8.93%	9.23%	10.65%	21.73%
Gankyrin	6.98%	7.30%	19.52%	13.14%	12.20%	14.91%	7.50%	9.64%	19.08%
MAGE	5.13%	6.63%	5.35%	6.16%	14.86%	6.31%	5.45%	8.37%	13.95%

DAY 2

HCC Antigens	B1	B2	B3	B4	B5	B6	B7	B8	Inter block CV%
AFP	14.65%	9.16%	10.64%	11.52%	12.06%	7.53%	10.71%	14.33%	11.99%
Gankyrin	8.35%	8.49%	8.19%	9.62%	9.64%	8.20%	7.94%	6.20%	11.06%
MAGE	7.88%	13.28%	9.89%	8.70%	9.70%	8.59%	11.52%	14.77%	12.21%

3.3.3 Optimisation of the Antigen Microarray Technology

The protein microarrayer is a robotic equipment, which is fashioned to reduce technical errors made by humans and increase productivity using small volumes of reagents and samples. Studies have shown that one of the main obstacles in this technology is the difficulty in reproducing consistent results and a highly controlled assay that is relevant

and appropriate for all proteins due to their structural complexity and natural tendency to unfold when immobilised. Preliminary validation experiments conducted with quality control antigens *Candida* and *Tetanus,* as well as HCC TAAs, showed variations in morphological appearance of antigen spots across different days, giving rise to increased inter assay variations. There are multiple factors that can contribute to the generation of high quality microarrays. These factors were tested simultaneously in order to select the optimum parameters based on the experimental requirements. These factors include humidity, temperature, microtiter volumes, slide surface chemistries, printing and blocking buffers, print position, detection antibodies, etc. Results obtained from optimisation tests were examined for parameters like signal intensity, spot morphology and intra-assay precision.

3.3.4 Determining the Optimal Relative Humidity and Microtiter Volumes for Printing

Earlier experiments showed continuous morphological differences and disparities in the appearance of antigen spots as well as signal intensities, which gave rise to high intra- and inter- assay CVs. Optimum humidity in the spotting chamber is very important during antigen printing as it prevents spots from evaporating or drying immediately after being dispensed. Drying causes a drop in intra spot uniformity and is regarded as the main cause of printing variation during consecutive deposition (**Figure 55**). Additionally, the volume of sample in the microtiter well plate during printing is very critical. This is because it can lead to extra samples being collected around the contact pin for printing or less samples being taken up by the pin (**Figure 56**). Hence, resulting in either more or less volumes of samples deposited on the slide surface. This can introduce lots of intra and inter spot variations.

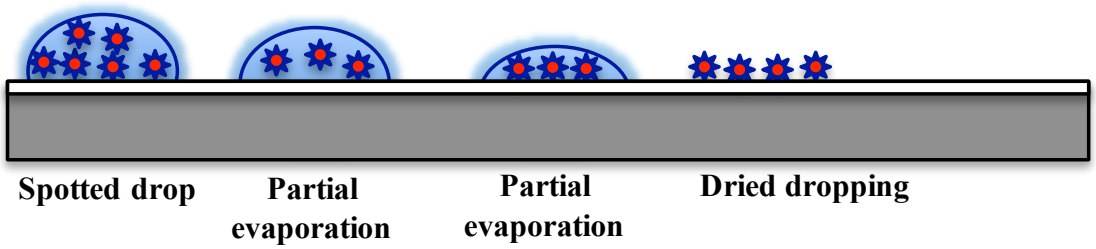


Figure 55: Schematic diagram showing the effect of inadequate relative humidity on appearance of antigen spots. The figure above shows the assumed drying of spots on glass slides when the optimum relative humidity is not utilised during the arraying process.

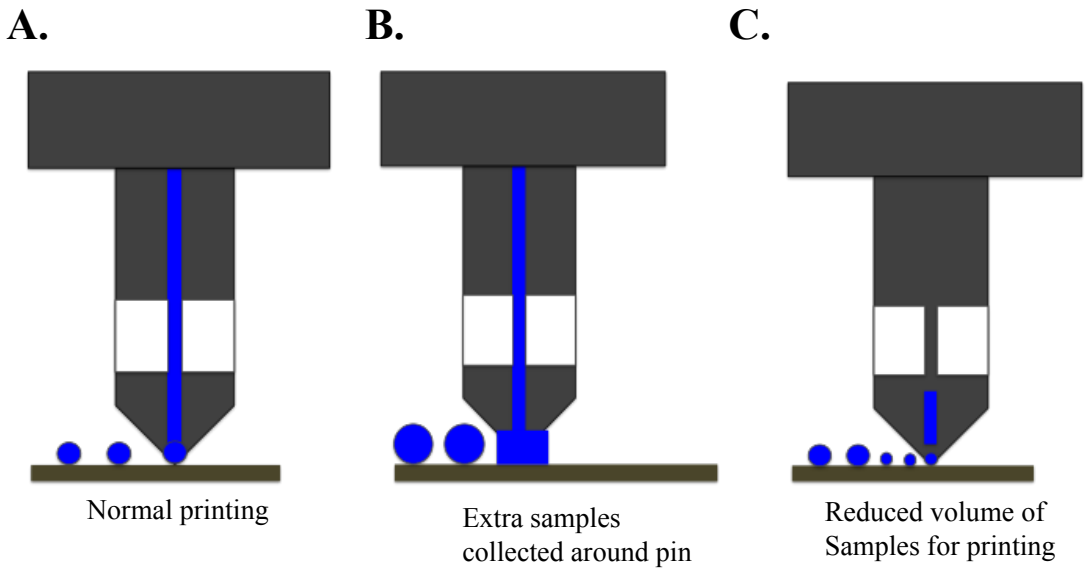


Figure 56: Deposition of samples unto glass slides. The contact pin of the microarrayer sucks liquid containing proteins by capillary action from microtiter well plates and transfers them unto glass slides. **(A)** shows the consistency in shape of spots when the required microtiter volume of sample is used, **(B)** shows larger spots at the initial stage of print when the microtitre volume of sample is used due to extra samples collected around the pin. **(C)** shows consistent spots at the initial stage of print but dwindles with time as the microtitre volume is not sufficient for the entire print.

Experiments were conducted using Streptavidin conjugated fluorecent dyes; Cyanine 3 (cy3-Green) and Cyanine 5 (cy5-Red) in order to investigate the impact of microtiter volume on the precision of the microarray assay. Cy3 and Cy5 dyes were prepared in printing buffer (PBS-trehalose-Tween) in three different volumes 5 µl, 10 µl and 20 µl in a 384 microtitre well plate (**Figure 57**). Cy3 and Cy5 dyes were each arrayed on a Poly-L-lysine slide in a hundred and fifty replicates in a three pad format at 57% relative

humidity after which spots on the slide were visualised at 532 and 635 nm respectively at 100% power using the Axon Genepix 4200AL scanner.

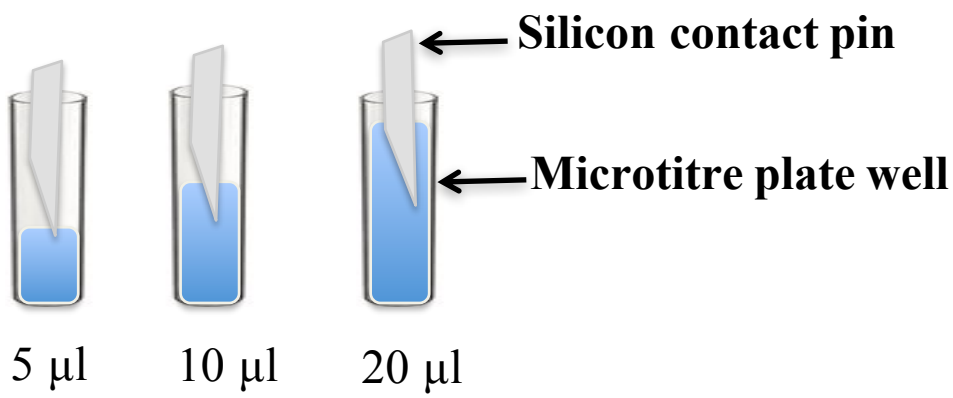
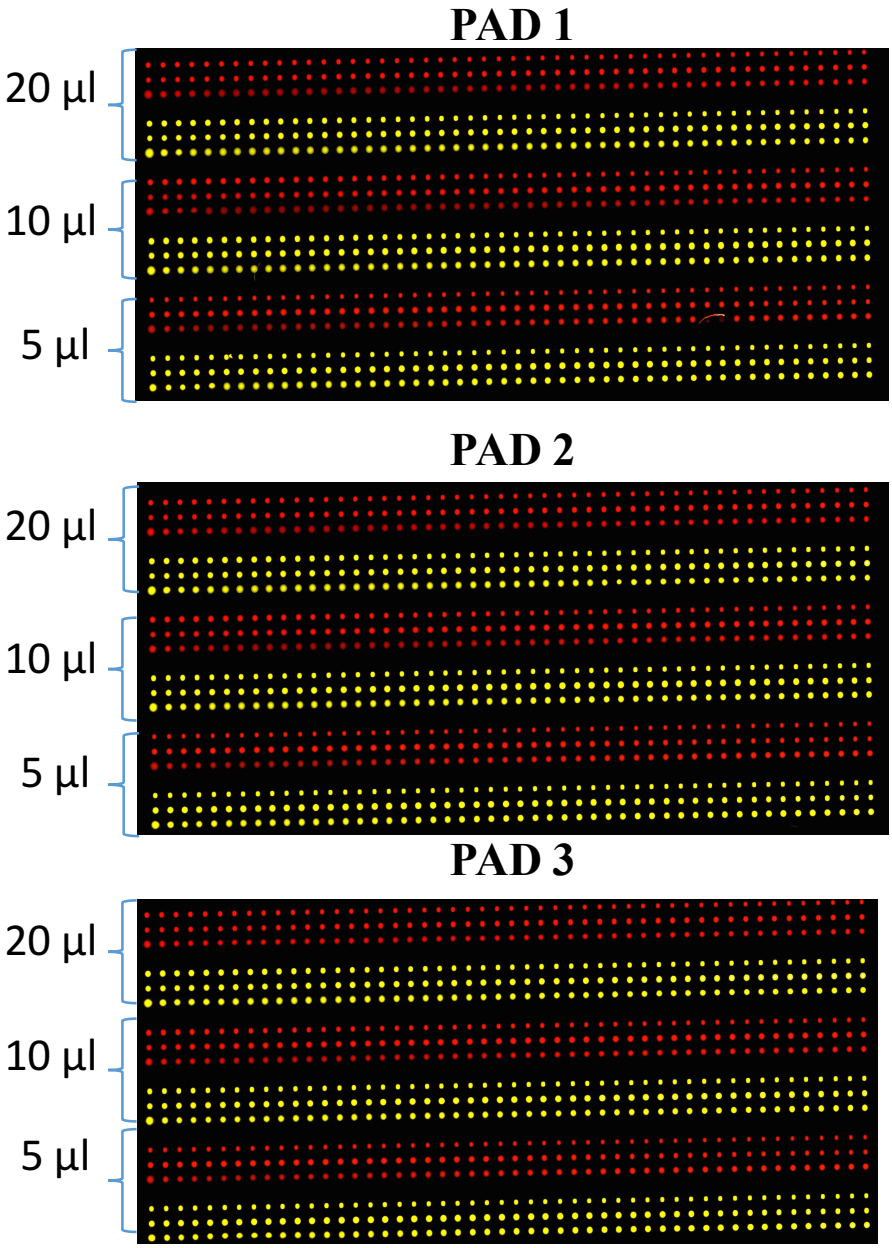


Figure 57: Testing different microtiter volumes for microarray printing. Different microtiter volumes were tested to see their effect on printing conditions as well as the precision of an assay.

Visual examination of scanned slide shows the morphological appearance of Cy3 and Cy5 spots printed from the different microtitre volumes in three pad layout (**Figure 58A**). Closer examination of all the different layouts of the first fifty replicates irrespective of the microtitre volume from which it was printed showed bigger spots at the start of print (**Figure 58B**). This clearly indicates the importance of pre-spotting during the arraying process so as to eliminate irregularities in spotting during the early printing stages. Cy3 and Cy5 dyes printed from 5 µl and 20 µl had inconsistencies in spotting throughout the print. More cases of larger spots were seen at the early stages of print with regards to 20 µl but reduced in the course of the arraying procedure. Spots printed from 5 µl was not sufficient and hence spots began to diminish at as printing continued. However, spots printed from 10 µl were mostly consistent throughout.

The mean signal intensities and diameter of spots were then calculated (**Table 18 A, B, C**). The precision of the assay was determining by evaluating the intra assay variability of signals and diameter of spots. Generally, the variation of spots with regards to the signal intensities were higher as compared to the diameter (**Table 18 A**). The variability of signals and diameter of Cy3 and Cy5 spots printed from the 5 µl and 20 µl were mostly above of the acceptable limit of precision (CV≤15%) unlike those from 10 µl where variability of signals and diameter were within the acceptable limit (**Table 18 A**). The same trend was seen when the variation of the second (**Table 18 B**) and third (**Table 18 C)** fifty sets of spots were investigated. However, in comparing the three batches of replicates the second batch (**Table 18 B)** had the least variation of spots. This implies that using 10 µl for the printing process would improve the precision of the assay but this was not concluded as further investigations with HCC antigens and a thorough probing procedure would give an accurate representation.

A.



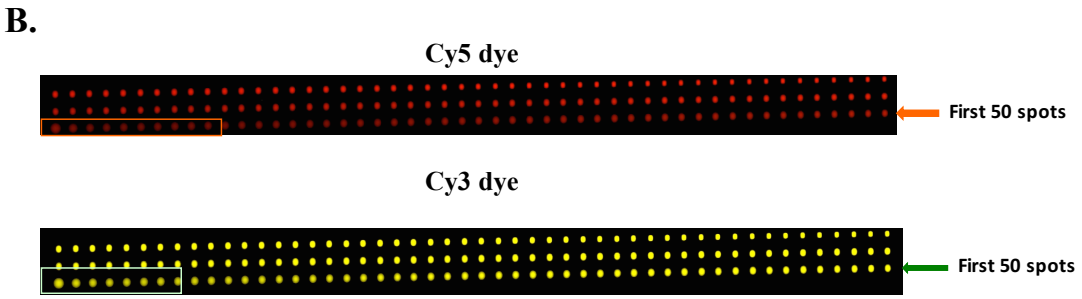


Figure 58: Spot morphology of Cy3 and Cy5 Streptavidin dyes on a Poly-L-lysine slide printed from three different microtiter volumes. Fluorescent dyes Cy3 (green) and Cy5 (red) were prepared in PBS-Tre-Tween-20 and arrayed in a hundred and fifty replicates each unto a Poly-L-Lysine slide from three different microtiter volumes; 5 µl, 10 µl and 20 µl in a three pad layout. Green and red spots were visualised using a Genepix Axon 4200AL scanner at 532nm and 635nm at 100% power.

The tables below represent the intra slide variability (CV%) of a hundred and fifty Cy3 and Cy5 spots printed from three different microtiter volumes; 5 µl, 10 µl and 20 µl in a three-pad format on a Poly-L-lysine slide. **(A), (B) and (C)** show the coefficient of variation of the diameter and signal intensities of spots across the first, second and third fifty batch of replicates.

Table 18: Intra-slide variability (CV%) of the signals and diameter of **(A)** first fifty **(B)** second fifty and **(C)** third fifty Cyanine (Red and Green) spots from three microtiter volumes.

A.

	Microtitre volume	Dye	Pad 1	Pad 2	Pad 3	Average
Signals	5 µl	RED	17.36	18.19	18.91	18.15
		GREEN	15.97	19.47	16.30	17.24
	10 µl	RED	13.80	12.24	11.56	12.53
		GREEN	10.42	9.31	9.39	9.70
	20 µl	RED	19.33	20.39	22.78	20.83
		GREEN	20.81	19.50	21.70	20.67
Diameter	5 µl	RED	9.42	11.50	10.48	10.47
		GREEN	9.21	11.57	10.52	10.43
	10 µl	RED	7.63	6.52	8.16	7.44
		GREEN	5.94	6.03	6.54	6.17
	20 µl	RED	13.59	13.61	16.28	14.49
		GREEN	14.64	13.35	12.17	13.38

B.

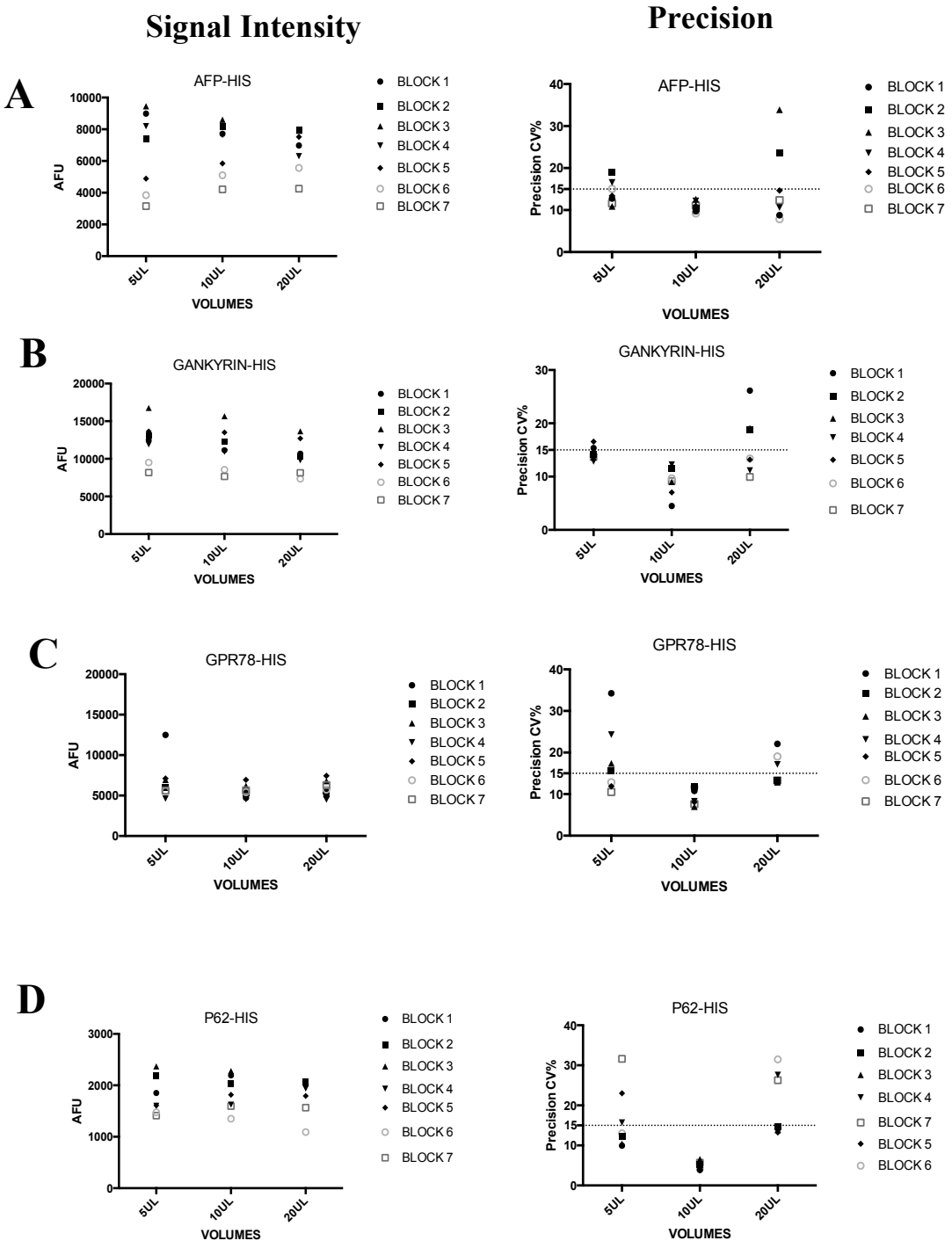
	Microtitre volume	Dye	Pad 1	Pad 2	Pad 3	Average
Signal	5 µl	RED	15.36	16.19	17.91	16.48
		GREEN	15.97	18.47	16.30	16.91
	10 µl	RED	12.80	10.24	11.56	11.53
		GREEN	9.42	9.31	7.39	8.70
	20 µl	RED	18.33	19.39	21.78	19.83
		GREEN	19.81	19.50	18.70	19.33
Diameter	5 µl	RED	7.42	9.50	9.48	8.8
		GREEN	7.21	9.57	8.52	8.4
	10 µl	RED	5.63	4.52	4.16	4.77
		GREEN	3.94	4.03	4.54	4.17
	20 µl	RED	9.59	12.61	15.28	12.49
		GREEN	12.64	10.35	13.17	12.05

C.

	Microtitre volume	Dye	Pad 1	Pad 2	Pad 3	Average.
Signals	5 µl	RED	16.36	17.19	16.91	16.82
		GREEN	14.97	14.47	14.30	14.58
	10 µl	RED	13.80	11.24	12.56	12.53
		GREEN	10.42	10.31	8.39	9.71
	20 µl	RED	19.33	20.39	22.78	20.83
		GREEN	20.81	21.50	20.70	21
Diameter	5 µl	RED	10.42	9.50	10.48	10.1
		GREEN	8.21	9.57	9.52	9.1
	10 µl	RED	6.63	7.52	6.16	6.1
		GREEN	5.94	5.03	6.54	5.83
	20 µl	RED	13.59	15.61	15.28	14.82
		GREEN	14.64	13.35	12.17	13.45

Subsequently this optimisation procedure was repeated with TAAs. Five His-tagged TAAs: AFP, Gankyrin, GRP78, P62 and APCN were prepared in printing buffer (PBS-Trehalose-Tween-20) at three different volumes as stated in earlier experiment. Prior to printing, the relative humidity of the microgrid arrayer was set to 65% target. Antigens were printed onto Poly-L-Lysine slides in a seven-pad format and further probed with rabbit anti-His_6 antibody and biotinylated anti-rabbit secondary antibody after which the binding was detected with a Streptavidin conjugated Cy5 dye.

10 µl gave consistent spot circularity as well as less intra spot variation (CV≤15%) for all five antigens as compared to 5 µl and 20 µl, which produced high intra spot variations (**Figure 59 A-E**). Irrespective of the microtiter volume used, there was low intra spot variation when assessing diameter (**Figure 60 F-J**). This could be explained that the antigens prepared in 20 µl volumes filled up the microtiter wells as earlier described and therefore contributed to extra liquid been collected around the contact pin as it dipped into the sample during the printing procedure. Hence, bigger spots at initial start of print were seen but dwindled during later stages. 5 µl gave consistent spots at the start of print but was not sufficient for the entire printing. These limitations were however absent with 10 µl where consistent spot morphologies of antigens were observed with intra spot variations below 15%. Hence 10 µl was as the optimal microtiter volume for printing analytes onto slides surfaces.


Signal Intensity
Precision
A
AFP-HIS
AFU
VOLUMES
Precision CV%
BLOCK 1
BLOCK 2
BLOCK 3
BLOCK 4
BLOCK 5
BLOCK 6
BLOCK 7
5UL
10UL
20UL
B
GANKYRIN-HIS
C
GPR78-HIS
D
P62-HIS

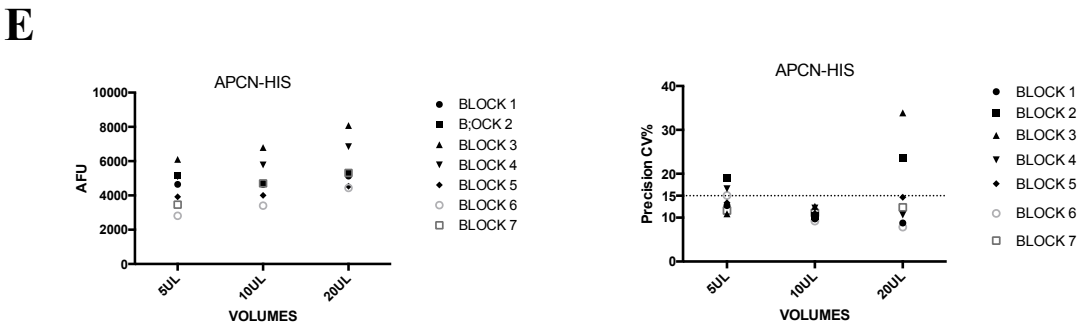
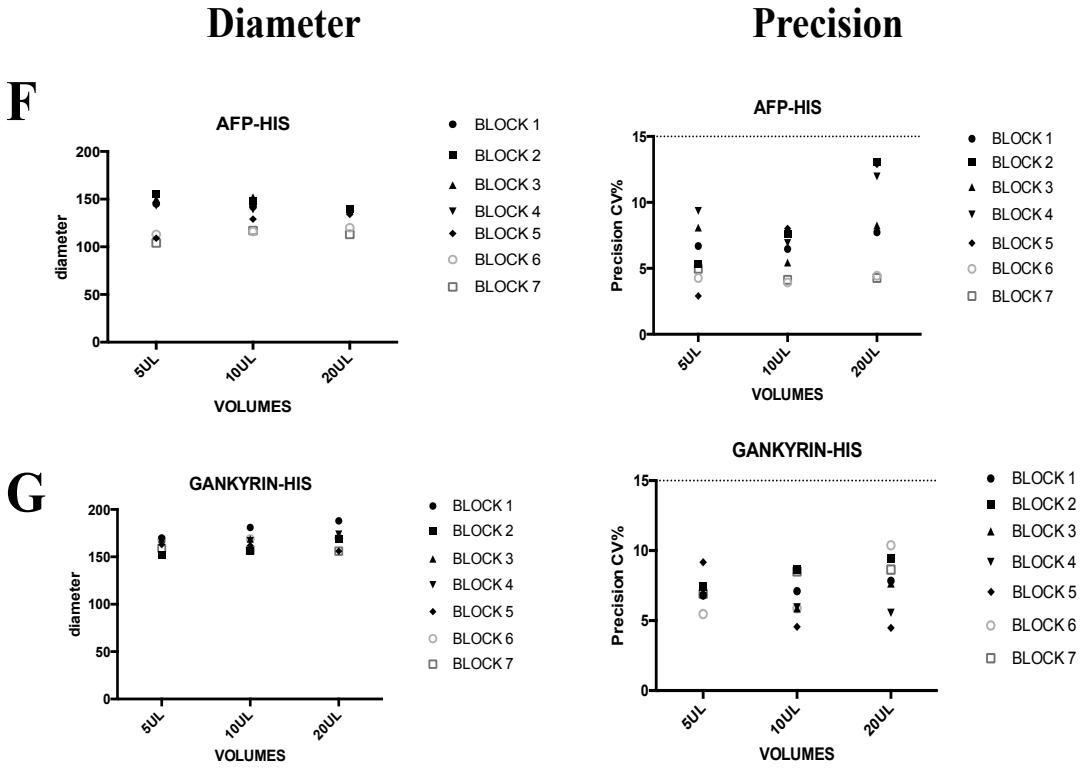


Figure 59: Effect of different microtiter volumes on intra spot variation. Five HCC His-tagged tumour-associated antigens printed onto a Poly-L-lysine slide in a seven-pad format were probed with rabbit anti-His_6 antibody and further incubated with anti-rabbit antibody. The complex was then detected with a Streptavidin conjugated Cy5 dye after which the slide was scanned at 635 wavelength and 400PMT using Axon Genepix 4200AL scanner. The graphs above represent the signal intensities (mean) and coefficient of variation of signal intensities of **(A)** AFP, **(B)** Gankyrin, **(C)** GRP78, **(D)** P62, **(E)** APCN at 65% humidity at three different microtiter volumes: 5 µl, 10 µl and 20 µl. Dashed lines represent the acceptable limits of precision. Data were analysed using Graph pad prism 6 software.



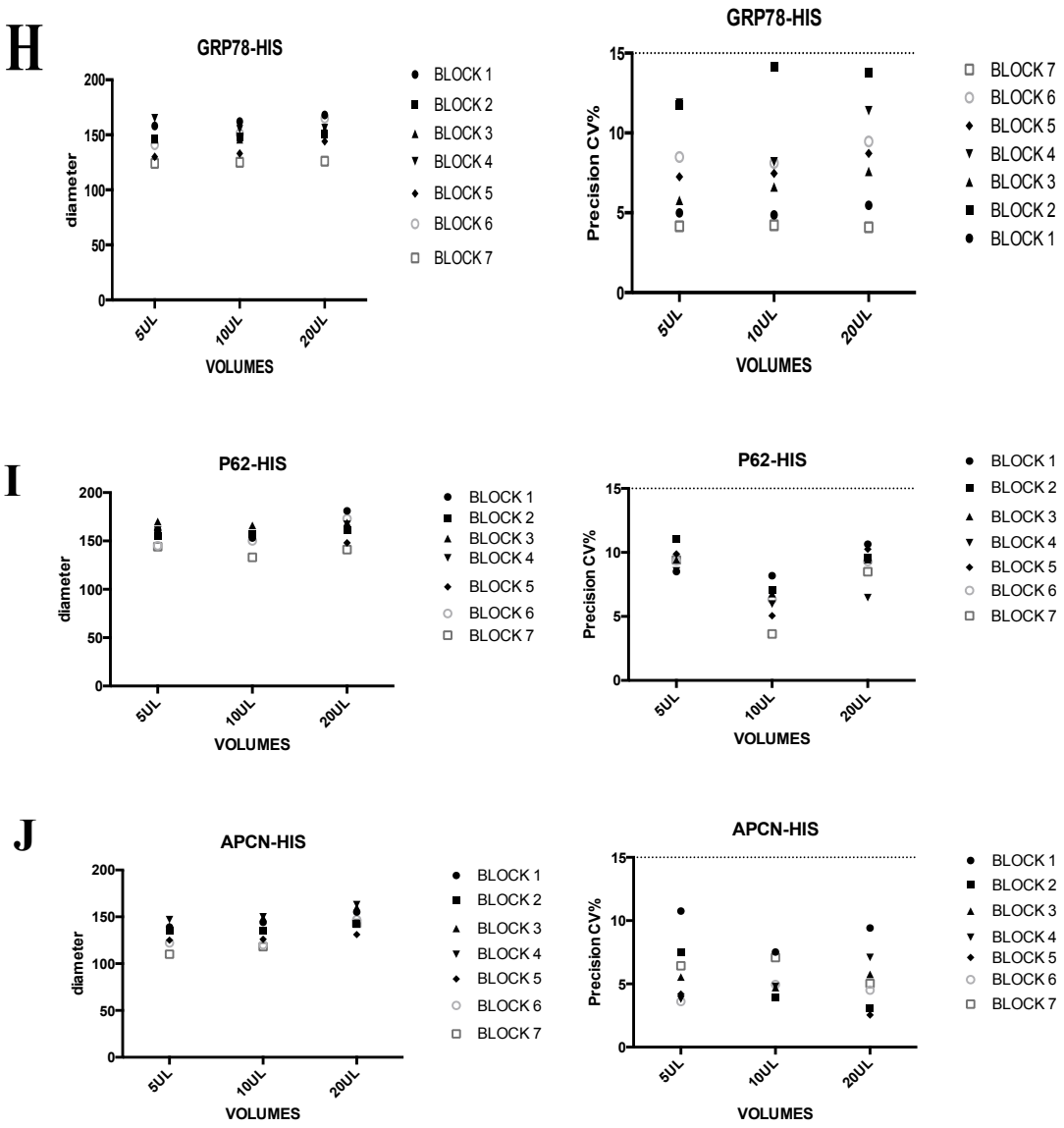


Figure 60: Effect of different microtiter volumes on diameter of spots. The graphs above represent the diameter (mean) and coefficient of variation of diameter of five HCC-His-tagged antigens: **(F)** AFP, **(G)** Gankyrin, **(H)** GRP78, **(I)** P62, **(J)** APCN printed unto Poly-L-lysine slide from three different microtiter volumes 5 µl, 10 µl and 20 µl and at 65% humidity. Dashed lines represent the acceptable limits of precision. Data were analysed using Graph pad prism 6 software.

3.3.5 Optimisation of Printing Buffers

Proteins should be prepared in an optimal printing buffer at the required concentration as it can have a significant effect on the printing conditions as well as assay reproducibility. A suitable print buffer performs a wide range of tasks, such as printing even, small and round spots on slide surfaces, it distributes samples evenly in spots,

enhances the binding of samples onto a slide surface, prevents evaporation within microtiter well plates, stabilises printed samples, as well as prolonging the storage of samples (beginners guide to microarray). In order to determine the suitable buffer that would enable effective immobilisation of proteins onto slides, AFP and Gankyrin were prepared in three print buffers (PBS-Trehalose, PBS-Trehalose-Tween, PBS-Trehalose-Betaine-Tween) and arrayed in thirty replicates using the contact and non-contact microgrid arrayers. Slides were incubated with rabbit anti-His_6 antibody and anti-rabbit antibody after which the interaction was detected with a Streptavidin conjugated Cy5 dye and scanned with Genepix 4200AL scanner. The spot morphology was considered, and the median signal intensities of spots were calculated. The intra and inter slide variation of signal intensities generated from spots were also determined.

Different buffers had effects on the morphological appearance of spots. Larger and more uniform spots of the AFP antigen were observed with PBS-Trehalose-Betaine-Tween as compared to the other PBS-Trehalose-Tween and PBS-Trehalose (**Figure 61**). Higher signal intensities to AFP and Gankyrin was seen with PBS-Trehalose-Betaine-Tween as compared to the remaining two (**Figure 62**). Interestingly, a different outcome was observed with Gankyrin, where consistent spots was seen with PBS-Trehalose-Betaine-Tween and this clearly reflected on the precision as intra and inter slide variation were very low. Moreover, though signals were very low, the non-contact arrayer generally gave low intra slide variations with both AFP and Gankyrin as compared with the contact arrayer since the pin does not contact the slide surface. Hence, there was more consistent protein spotting. Looking at all the three print buffers, it is possible to say that PBS-Tre-Betaine-Tween is the most suitable buffer and would be used in subsequent experiments since it produced the highest intensities, good morphology of spots, as well as low intra assay variability.

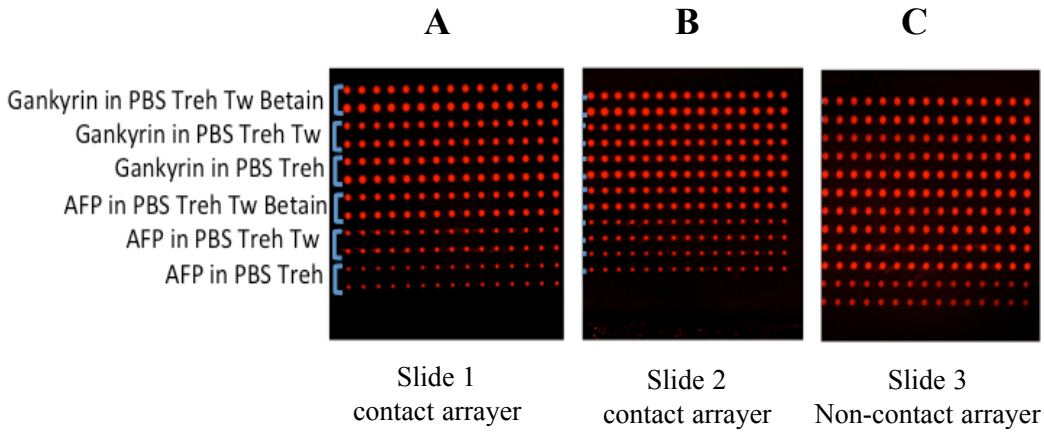
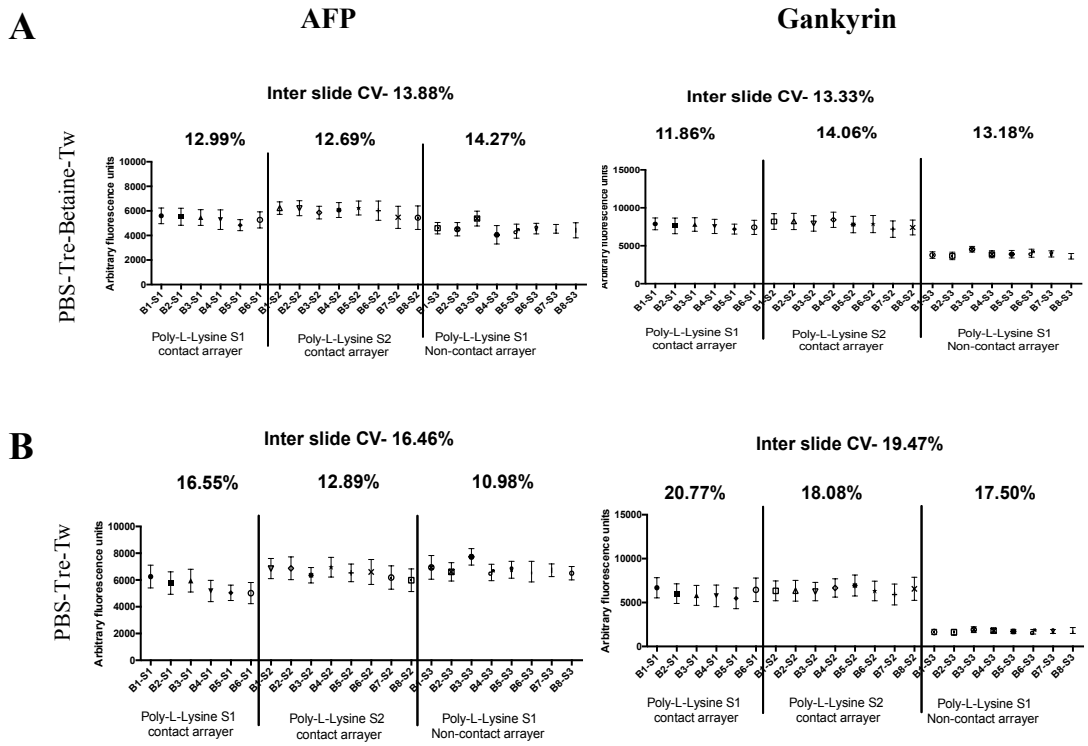


Figure 61: Spot morphology of HCC antigens when tested with different printing buffers and arrayers. AFP and Gankyrin were prepared in three buffers; PBS-Trehalose-Betaine-Tween, PBS-Trehalose-Tween and PBS-Trehalose and further printed in thirty replicates onto three Poly-L-lysine slides. Slides were then incubated with rabbit anti-His_6 antibody and ant-rabbit antibody and detected with a Streptavidin conjugated Cy5 dye after which they were scanned at 635 wavelength and 400 PMT using Axon Genepix 4200AL scanner. **(A)**, **(B)** and **(C)** show the morphology of spots when antigens were printed using the contact and non-contact arrayers.



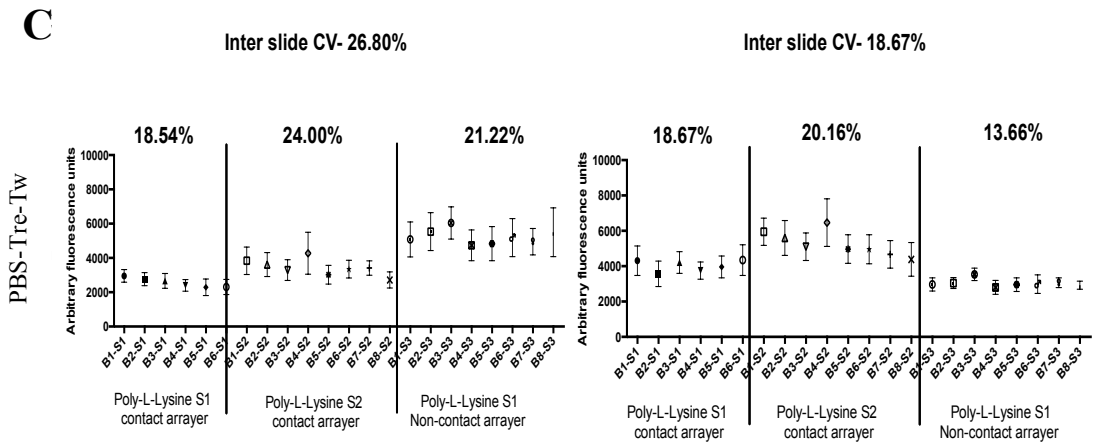


Figure 62: Testing the effect of printing buffers and arrayers on assay variability. Different HCC antigens: AFP and Gankyrin were prepared in three different printing buffers and printed unto three Poly-L-lysine slides using two different arrayers. Slides were further incubated with rabbit- anti-His_6 antibody and anti-rabbit antibody and the interaction was detected by Streptavidin conjugated Cy5 dye. The graphs above represent the mean signals of AFP and Gankyrin replicates and the coefficient of variation of signals within blocks on a slide and across different slides when printed with **(A)** PBS-Trehalose-Betaine-Tween, **(B)** PBS-Trehalose-Tween and **(C)** PBS-Trehalose buffers using contact and non-contact arrayers.

3.3.6 Assessing the Position of Print on a Slide

Printing at different parts of the slides was tested in order to see if it had an effect on the diameter and signals of spots. AFP, Gankyrin and HCC1 were arrayed at the edges and middle positions in a sixteen-pad format on a Poly-L-lysine slide (**Figure 63**). The slide was then probed with a positive control serum sample and further incubated with biotinylated anti-human antibody after which the antigen-antibody interaction was detected with a Streptavidin conjugated Cy5 dye. The morphological appearance of antigen spots was consistent with respect to the diameter. All the antigens bound appropriately to the slide surface with the exception of HCC1 which bound poorly to the slide and therefore contributing to its faint-like appearance (**Figure 63**). Low variation in signals and diameter of AFP and Gankyrin was observed within and across 16 blocks when printed at the edge and centre of the slide (**Table 19**). Though the variation of signals was lower with spots at the centre compared to the edges, they were

all within the acceptable limits of precision (CV≤15%). It therefore implicates that there is no difference between spots printed onto the middle and edge positions of a slide.

A

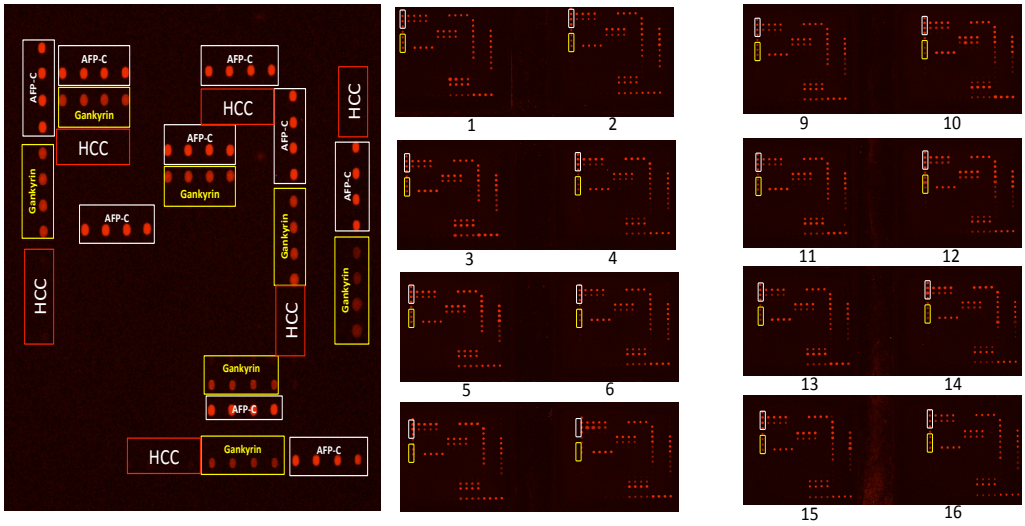


Figure 63: Image to show the print positions of HCC antigens on a slide. The scanned image above **(A)** shows the pattern of three different HCC antigens: AFP, Gankyrin and HCC1 printed at the edges and the middle positions on a Poly-L-lysine slide in a sixteen-pad format. Slides were probed with a positive control serum and anti-human secondary antibody after which a Streptavidin conjugated CY5 dye was used to detect the binding. Slides were scanned using the Genepix 4200AL scanner at 635 wavelength and 400PMT.

Table 19: Effect of print positions of antigens on the precision of an assay. The tables below show the coefficient of variation of signal intensities and diameter of **(A)** AFP and **(B)** Gankyrin spots within and across blocks when printed at the edge and centre positions on a Poly-L-lysine slide in a 16-pad format.

A **AFP**

		B1	B2	B3	B4	B5	B6	B7	B8	B9	B10	B11	B12	B13	B14	B15	B16	Inter block CV
Edge	Signal Intensity (CV %)	11.21%	9.72%	9.03%	12.81%	10.50%	4.45%	10.56%	3.42%	3.04%	7.66%	7.79%	11.41%	9.77%	9.07%	10.50%	1.96%	12.7%
	Diameter (CV%)	8.91%	7.51%	4.62%	6.42%	5.83%	4.08%	5.63%	4.62%	4.44%	3.51%	4.62%	5.83%	3.92%	3.39%	3.64%	8.51%	5.63%
Centre	Signal Intensity (CV%)	5.63%	3.91%	4.17%	1.36%	4.95%	2.09%	0.89%	2.81%	2.21%	4.12%	2.79%	5.49%	3.86%	4.60%	2.79%	2.67%	3.39%
	Diameter (CV%)	0.00%	3.77%	0.00%	5.02%	3.72%	0.00%	3.92%	0.00%	4.08%	0.00%	3.64%	0.00%	0.00%	0.00%	0.00%	4.26%	2.48%

B **Gankyrin**

		B1	B2	B3	B4	B5	B6	B7	B8	B9	B10	B11	B12	B13	B14	B15	B16	Inter block CV
Edge	Signal Intensity (CV%)	2.79%	3.71%	2.45%	1.09%	2.51%	6.01%	2.80%	5.03%	1.38%	17.56%	3.41%	12.96%	9.83%	13.13%	3.32%	1.77%	14.19%
	Diameter (CV%)	4.08%	4.65%	3.92%	5.50%	0.00%	5.50%	4.62%	0.00%	3.92%	4.22%	4.26%	4.72%	5.50%	3.51%	4.65%	0.00%	4.03%
Centre	Signal Intensity (CV%)	3.55%	3.40%	2.63%	3.77%	1.97%	3.84%	4.75%	3.23%	6.53%	21.58%	3.72%	1.65%	1.55%	11.25%	2.77%	1.69%	12.89%
	Diameter (CV%)	3.92%	4.88%	0.00%	4.88%	0.00%	0.00%	4.08%	0.00%	4.08%	29.99%	6.80%	3.39%	5.50%	0.00%	4.65%	4.62%	3.58%

3.3.7 Testing different Slide Surface Chemistries

Slide surface plays a pivotal role in the microarray assay as it has a direct effect on the printing performance, processing, detection and the precision of the assay. To investigate the influence of the solid support on the assay precision, different slide surfaces were tested to determine the most suitable surface chemistry for printing antigens. AFP and Gankyrin were printed (sixty replicates of each) onto Poly-L-lysine, Aminosilane, Epoxysilane and Nitrocellulose coated slides. They were then probed with anti-His_6 antibody diluted 1:10,000 in 5% BSA and further incubated with

biotinylated anti-rabbit antibody diluted 1:30,000 in antibody diluent. The interactions on Aminosilane, Epoxysilane and Poly-L-lysine were further detected with Streptavidin conjugated Cy5 dye, whereas Streptavidin conjugated infrared dye was used for Nitrocellulose slide.

Scanned image of the slides showed the morphology of spots with low background intensity on all slides (**Figure 64 A-D**). However, spots were more intense on Aminosilane slide for both AFP and Gankyrin compared to the remaining slides (**Figure 64 B**). Data analysis of images showed slightly elevated levels of signals with regards to AFP and Gankyrin on Aminosilane slide with the lowest signals observed with Nitrocellulose (**Figure 65-66**). Epoxysilane slide showed large diameter of antigen spots compared to other slide surfaces (**Figure 65-66**). There was a high level of variability of AFP signals within each array when printed onto Poly-L-lysine, Aminosilane and Epoxysilane and Nitrocellulose (**Table 20 A**). The same trend was observed with Gankyrin as the least variation of signals was seen with Epoxysilane and Aminosilane unlike Poly-L-lysine and Nitrocellulose slides (**Table 20 B**). The CV% of diameter of spots of both antigens was very low irrespective of the type of slide used, although the lowest variability was attained with Aminosilane slide (**Table 20 A&B**). Aminosilane slides often offer a high concentration of positively amine groups at the surface forming multiple ionic interactions that bind covalently with the negatively charge immobilised proteins. Thus, it allows adequate protein loading to produce high signal intensities and low background noise as seen above. It also produces consistent spot morphology and interacts well with PBS-Tre-Betaine-Tween. Epoxysilane slides are very successful in multiplex PCR and DNA microarrays. This type of slide provides a high level of intensity when processed immediately. However, its surface loses reactivity and gives low signal intensities when exposed to moisture in the air. Poly-L-

lysine slides give moderate to high levels of signal intensities and consistent spot morphology although it gives a high degree of auto-fluorescence that could be misread as false-positive results. Nitrocellulose provide a thin nitrocellulose coating that permits for a non-covalent yet irreversible surface for the adhesion of molecules of interest. This adhesion property of Nitrocellulose is thought to have contributed to the consistent spot morphologies. However, a drawback was seen in that it gave very low signals, making it unsuitable for printing tumour antigens. In conclusion, Aminosilane slide is the optimal solid surface for the microarray assay since it offered the highest level of consistency with respect to the signals and spot morphology. Also, it offered an increase in intensity of signals making it appropriate for forthcoming antigen microarray work.

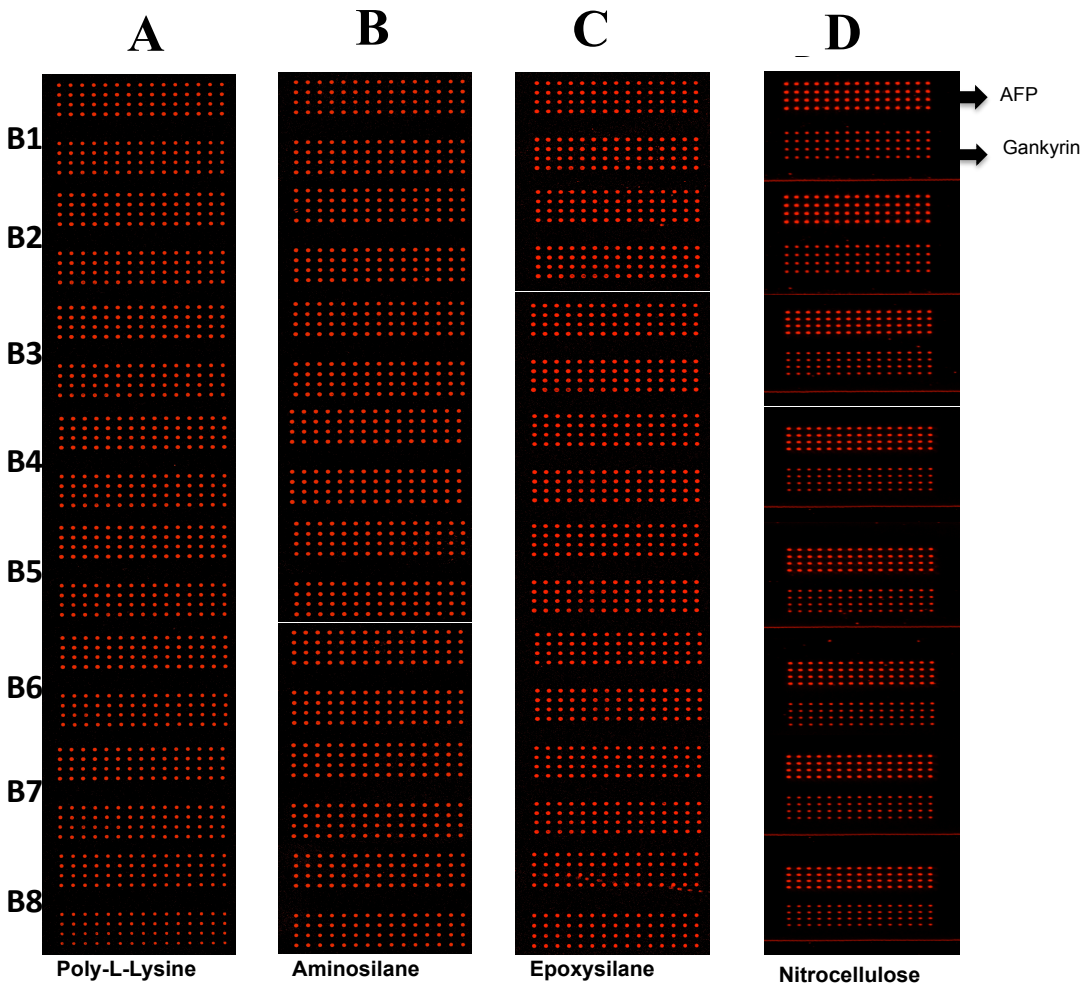
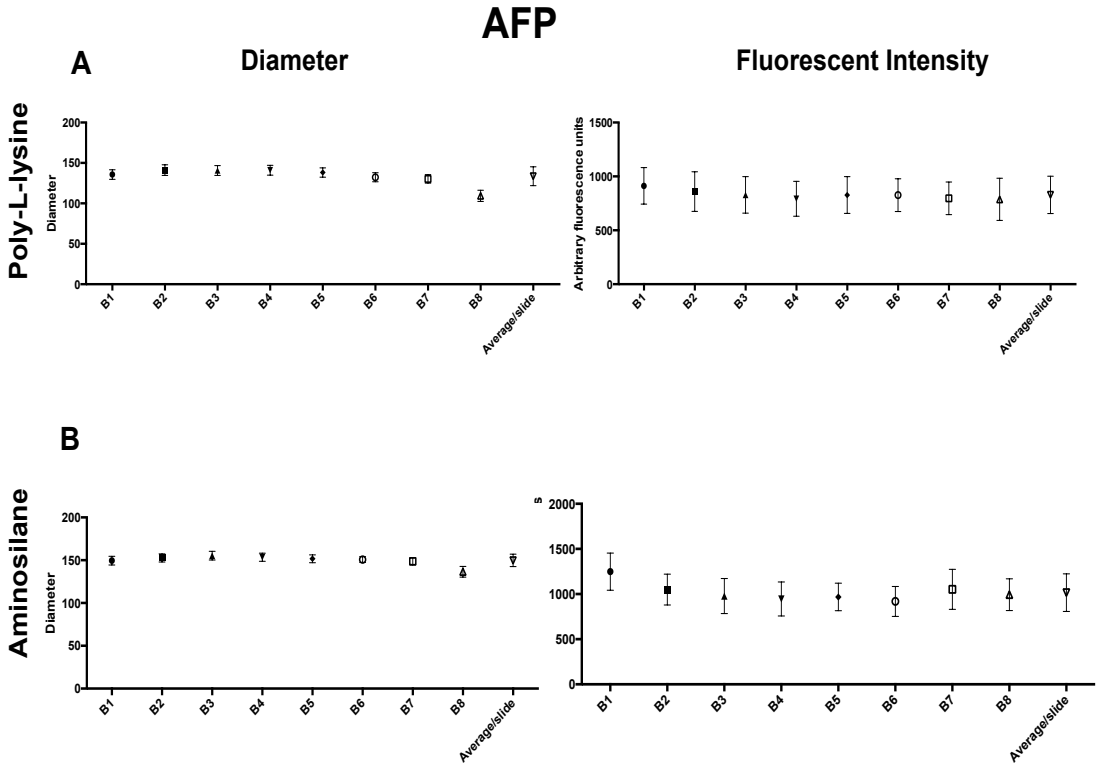


Figure 64: Morphology of spots on different slide surfaces. The image above shows two HCC antigens (AFP and Gankyrin) printed as sixty replicates each in eight arrays on four different slide surfaces; **(A)** Poly-L-lysine, **(B)** Aminosilane, **(C)** Epoxysilane and **(D)** Nitrocellulose. Slides were incubated with anti-His_6 and anti-mouse antibodies after which the binding was detected with either a Streptavidin conjugated Cy5 except Nitrocellulose, where Streptavidin conjugated infrared dye was used. Slides were scanned at 635 wavelength and 400 PMT using the Axon Genepix 4200AL scanner with the exception of Nitrocellulose which was scanned with the Licor Odyssey scanner.



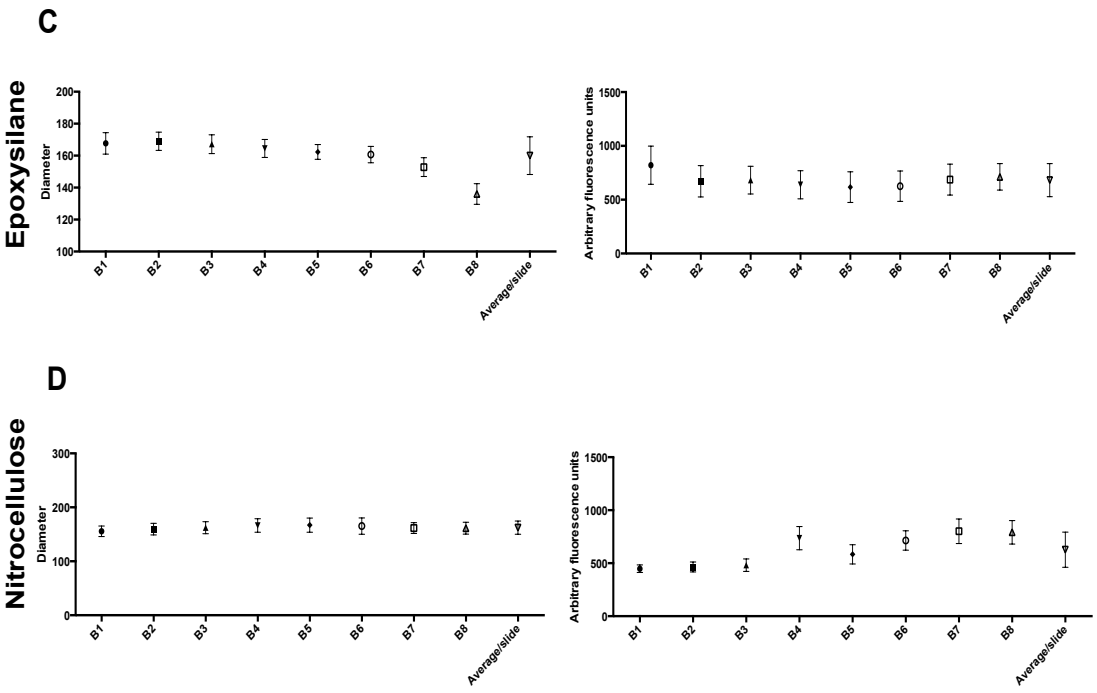
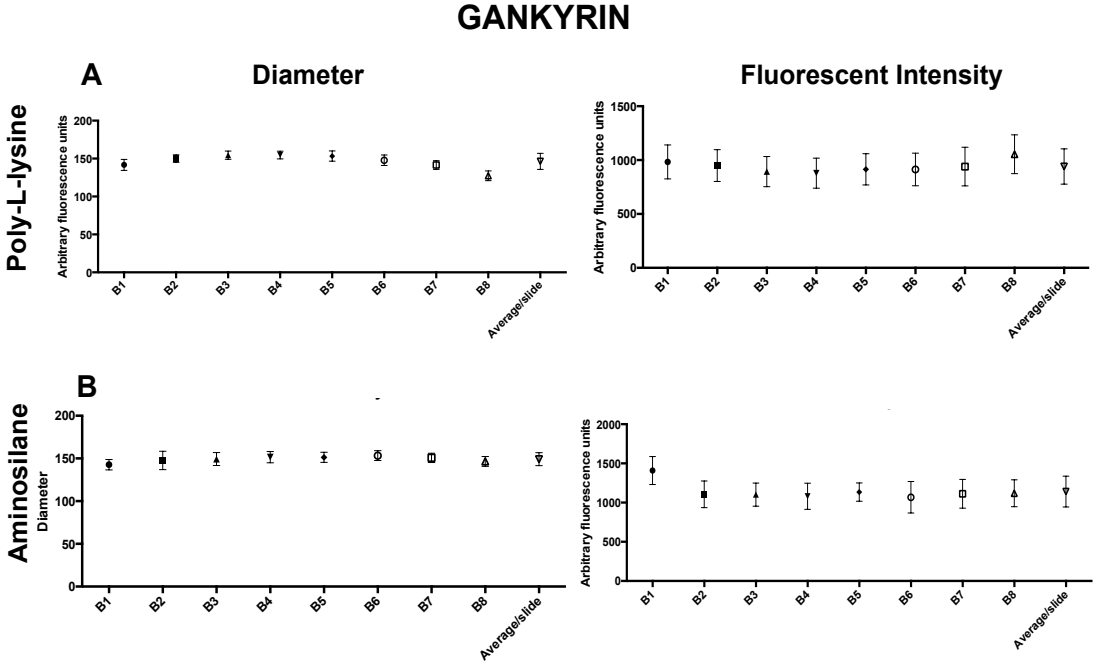


Figure 65: Analysis of diameter and signal intensities of AFP on different slide surfaces. AFP was printed onto four different slide surfaces and probed with anti-His_6 and anti-mouse antibodies after which the binding was detected with either a Streptavidin conjugated CY5 or Streptavidin conjugated infrared dye depending on the slide used. Slides were either scanned at 635 wavelength and 400PMT using the Axon Genepix 4200AL or the Licor Odyssey scanner. The graphs above represent the diameter and signal intensities (mean) of antigen-antibody interactions on **A)** Poly-L-lysine, **(B)** Aminosilane, **(C)** Epoxysilane and **(D)** Nitrocellulose slide surfaces.



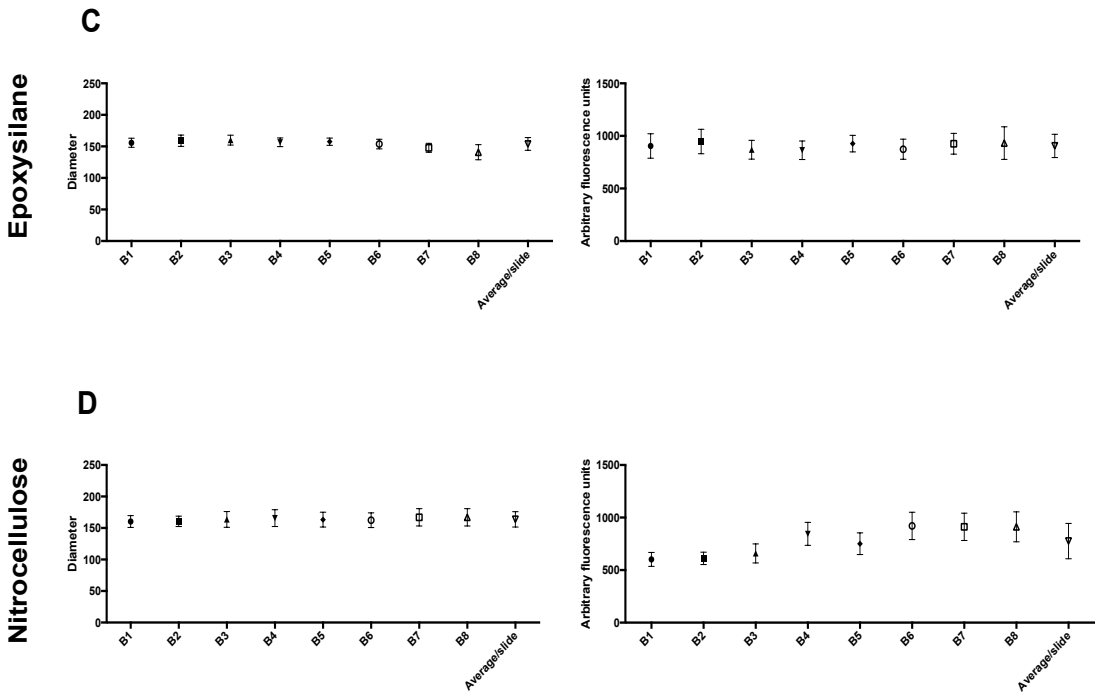


Figure 66: Analysis of diameter and signal intensities of Gankyrin on different slide surfaces. Gankyrin was printed onto four different slide surfaces and probed with anti-His_6 and anti-mouse antibodies after which the binding was detected with either a Streptavidin conjugated CY5 or Streptavidin conjugated infrared dye depending on the slide used. Slides were either scanned at 635 wavelength and 400PMT using the Axon Genepix 4200AL or the Licor Odyssey scanner. The graphs above represent the diameter and signal intensities (mean) of antigen-antibody interactions on (A) Poly-L-lysine, (B) Aminosilane, (C) Epoxysilane and (D) Nitrocellulose slide surfaces.

Table 20: Effect of different Slide Surfaces on Assay Precision. The tables below show the variation of signal intensities and diameter of AFP and Gankyrin spots within and across blocks when printed on Poly-L-lysine, Aminosilane, Epoxysilane and Nitrocellulose slide surfaces.

A

AFP		B1	B2	B3	B4	B5	B6	B7	B8	Inter block (CV%)
Poly-L-Lysine	Signals (CV%)	18.53%	21.40%	20.45%	20.41%	20.65%	18.37%	18.96%	24.90%	20.87%
	Diameter (CV%)	4.37%	4.72%	4.31%	4.27%	4.11%	4.26%	3.99%	6.27%	8.68%
Aminosilane	Signals (CV%)	16.47%	16.27%	19.92%	19.88%	15.69%	17.99%	21.03%	17.69%	20.50%
	Diameter (CV%)	3.36%	3.16%	3.24%	3.13%	3.01%	2.21%	2.90%	4.64%	4.64%
Epoxysilane	Signals (CV%)	21.58%	21.66%	18.91%	20.40%	23.11%	22.54%	20.91%	17.26%	22.56%
	Diameter (CV%)	4.01%	3.39%	3.50%	3.44%	2.86%	3.21%	3.83%	4.73%	7.35%
Nitrocellulose	Signals (CV%)	7.95%	10.20%	12.22%	14.92%	15.57%	12.76%	14.38%	13.96%	26.39%
	Diameter (CV%)	6.30%	6.72%	6.84%	7.50%	7.90%	9.15%	6.15%	6.80%	7.53%

B

Gankyrin		B1	B2	B3	B4	B5	B6	B7	B8	Inter block cv%
Poly-L-Lysine	CV%	16.03%	15.56%	15.68%	15.84%	15.87%	16.51%	19.11%	17.04%	17.37%
	Dia.	5.06%	3.25%	3.46%	3.25%	4.44%	4.68%	4.08%	4.98%	7.25%
Aminosilane	CV%	12.67%	15.35%	13.42%	15.36%	10.30%	18.80%	16.45%	15.38%	17.22%
	Dia.	4.25%	7.31%	5.06%	4.35%	3.94%	3.73%	3.64%	3.94%	5.09%
Epoxysilane	CV%	12.89%	12.29%	10.26%	10.26%	8.46%	10.99%	10.63%	16.60%	12.23%
	Dia.	4.62%	5.64%	4.88%	4.37%	3.63%	4.95%	4.84%	8.50%	6.55%
Nitrocellulose	CV%	11.06%	9.65%	13.76%	12.98%	13.65%	14.11%	14.26%	15.59%	21.63%
	Dia.	5.85%	5.11%	7.63%	8.04%	7.19%	7.21%	8.20%	8.20%	7.39%

3.3.8 Testing different blocking Buffers

The surface of a microarray slide is not covered entirely with the target protein and therefore can lead to the unbound regions binding non-specifically to the detection antibody during subsequent steps. This can often lead to high backgrounds limiting the detection of the target protein. A low background is crucial when detecting low abundant proteins in samples. An optimal blocking buffer will bind to all available sites of the slide surface thereby preventing non-specific binding of detection antibody and thus improving the sensitivity of the assay. It should have minimal effects on specific antibody-antigen interactions. Hence, adequate blocking is necessary for obtaining the best signal to noise ratio for any microarray experiment. The signal to noise ratio is referred to as the signal obtained with a sample containing the target protein, as compared to that obtained with a sample without the target protein. Blocking buffers usually range from highly purified proteins to milk, Bovine serum albumin or normal serum. However, changes in these blocking conditions can influence antibody binding. In developing the microarray assay, it is important that several blocker buffers are tested and examined for the highest signal to noise ratio. An Aminosilane slide immobilized with thirty replicates of AFP, Gankyrin and APCN antigens were treated with five blocking buffers; 5% BSA, 10% BSA, 30% BSA, I-Block and Super G. These buffers had diverse effects on the intensity of the background. Scanned results for an Aminosilane slide and five blocker buffers are shown in **Figure 67**. The morphology of antigen spots varied amongst different blocker buffers. The first pad of the slide was efficiently blocked by 5% BSA and spots were consistent and had the typical round doughnut shape. 10% BSA and 30% BSA also satisfactorily blocked the slide but fairly inconsistent morphology was noted for antigen spots as some spots showed comet-like structures as the concentration of BSA was increased. This shows the importance of

using an adequate amount of blocker in an assay as it has a significant effect on the appearance of spots. Very low background was observed with areas blocked with 5% BSA as compared to the remaining blocking buffers. Areas probed with I-Block and Super G were poorly blocked as very high signal to noise ratio was seen due to high background which masked the clarity of spots and in some cases smearing of slides was seen. This may due to the fact that Super-G may be more suitable for 3D surfaces (such as Nitrocellulose) as compared to a 2-D surface (such as Aminosilane, Epoxysilane and Poly-Lysine). I-Block, which is a purified form of casein, is suitable for antibody microarrays. Out of the five blockers, 5% BSA effectively blocked the slide and was selected as the optimal solution to be used for subsequent microarray experiments.

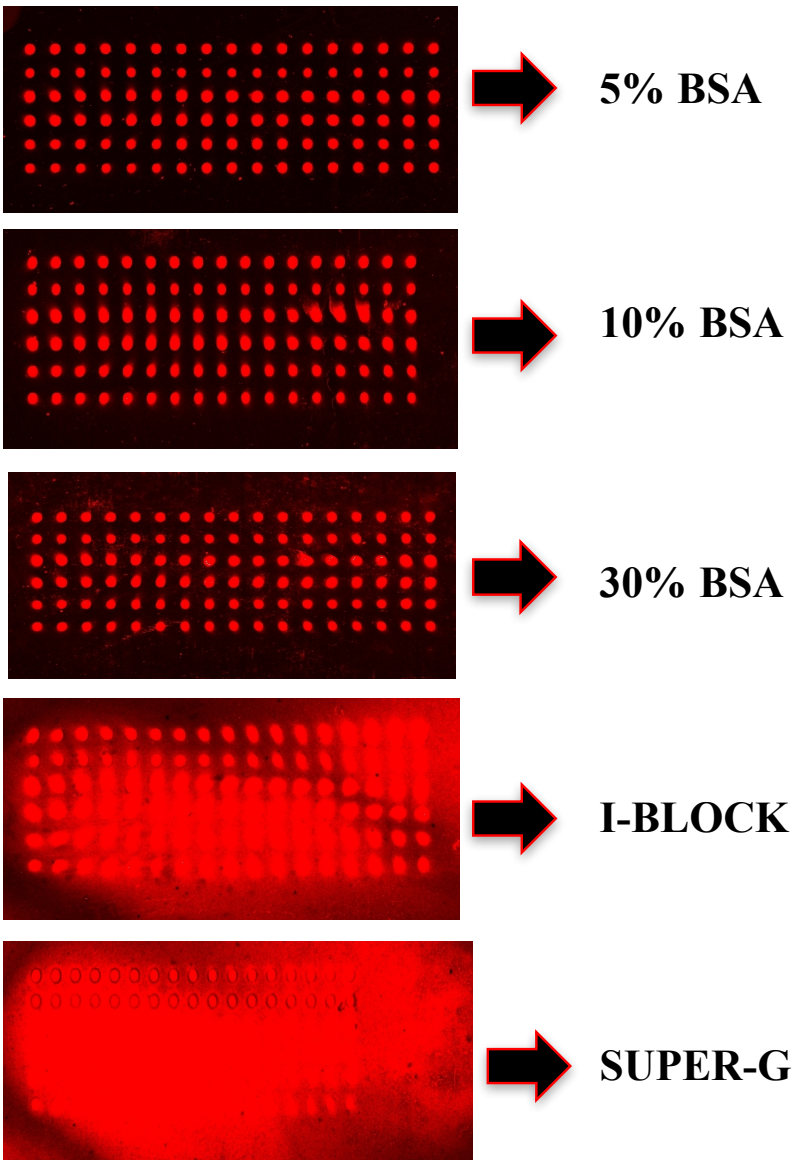


Figure 67: Evaluation of different blocking buffers for antigen microarrays. An Aminosilane slide immobilized with thirty replicates each of AFP, Gankyrin and APCN antigens were tested with five different solutions; 5% BSA, 10% BSA, 30% BSA, I-Block and Super G to determine the optimal blocking buffer suitable for improving the sensitivity of the microarray assay as well as reducing the background noise. Slides were scanned using Axon Genepix scanner 4200AL at 100% power and 632nm wavelength.

3.2.9 Optimisation of Monoclonal Primary and Secondary Antibodies

A primary antibody specifically recognises and binds the target protein immobilised onto the solid surface during a microarray. A secondary antibody binds to a primary antibody to assist in detection of target antigens. These are usually developed as polyclonal or monoclonal antibodies using mouse, rat, rabbit, goat, and other animal species as hosts. Polyclonal antibodies were used in earlier experiments, but new batches of monoclonal antibodies were purchased so as to reduce the possibility of cross reactivity and to provide highly specific and reproducible assay outcomes. In an attempt to enhance the reproducibility of the microarray platform, newly purchased monoclonal antibodies were tested to determine the optimal dilution which would give high signal intensity as well as low intra assay variability. HCC antigens, namely AFP, Gankyrin, GRP78 and IMP1, were arrayed onto an Aminosilane slide in a 16-pad layout. Different layouts of the slide were incubated with varying dilutions of monoclonal mouse anti-His_6 antibody (1:2,000, 1:5,000, 1:7,000, 1:10,000 dilutions made in 5% BSA) for an hour. These were subsequently probed with biotinylated anti-mouse antibody diluted 1:10,000, 1:20,000, 1:30,000 in antibody diluent. This reaction was amplified and further detected using a Streptavidin conjugated Cy5 dye after which the slide was scanned. Scanned slide shows the morphology of the various antigen spots after treatment with different dilutions of primary and secondary antibodies (**Figure 68**). Graphical evaluation of the scanned slide showed consistency in the morphology of all antigen spots with low background intensity (**Figure 68**). The mean signal intensity and standard deviation of spots were calculated after which the intra slide variability was determined based on the mean signal intensities obtained. Highest signal intensities obtained were dependent on the antigen. Highest signal intensities of AFP, Gankyrin, GRP78 and Imp1 were respectively obtained at the following primary and secondary

Ab dilutions; 1:5,000/1:30,000, 1:2,000/1:30,000, 1:5,000/1:20,000, 1:7,000/1:30,000 (**Figure 69**). Highest signal intensities of most antigens were attained at 1:5,000/ 1:30,000 although after assessment of intra slide variabilities 1:10,000/1:30,000 dilutions, gave the lowest level of intra assay precision (ranging from 5%-7%) with fairly good signal intensities (**Figure 70**). Overall, 1:10,000/1:30,000 were selected as the optimal antibody dilution at which the monoclonal anti-His_6 and anti-mouse antibodies were prepared for future microarray assays.

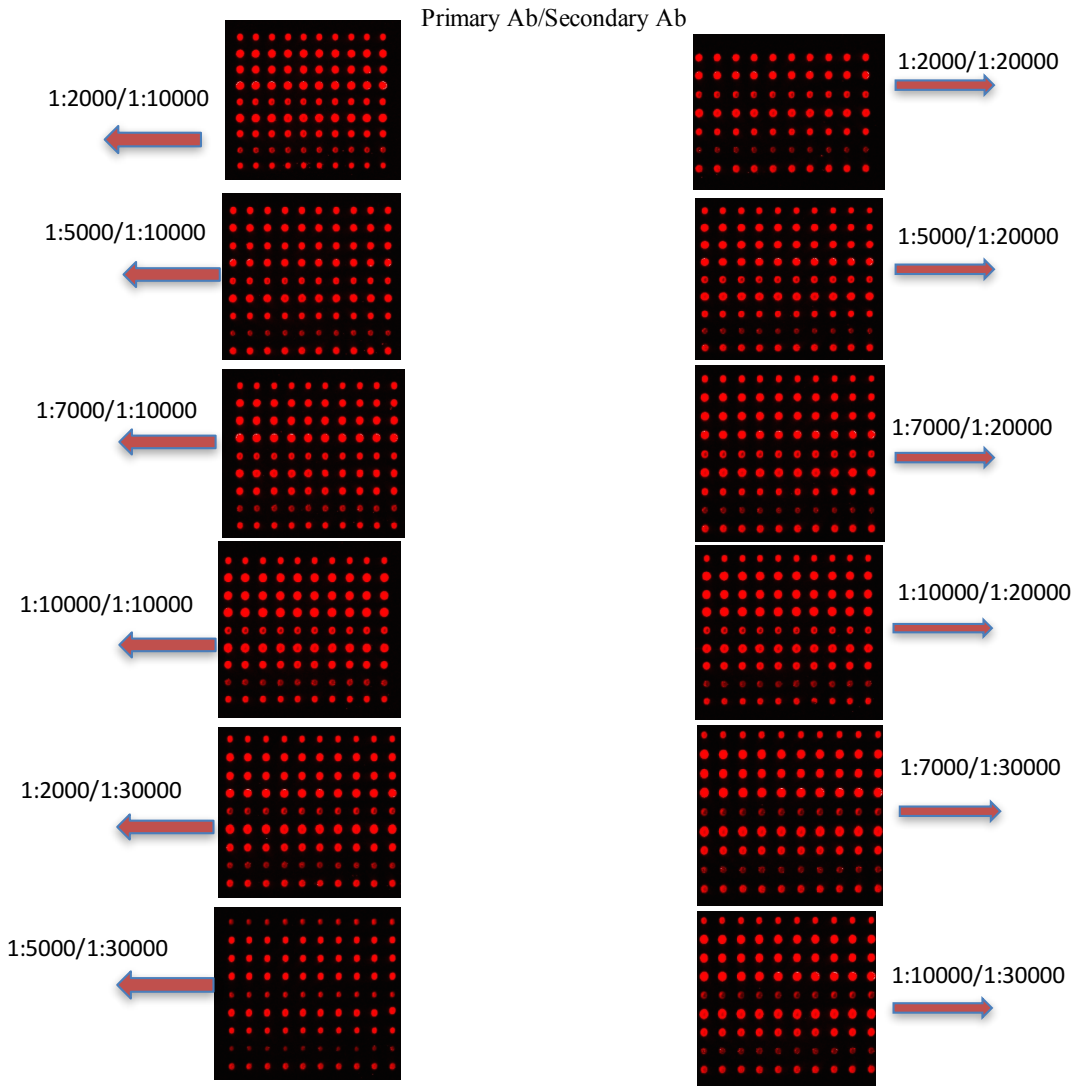


Figure 68: Scanned morphology of TAAs tested with different dilutions of monoclonal mouse anti-His_6 and anti-mouse antibodies. Four HCC TAAs (AFP, Gankyrin, GRP78, IMP1) were arrayed onto an Aminosilane slide in a 16-pad format after which the different pads were probed with various dilutions (1:2,000, 1:5,000, 1:7,000, 1:10,000) of monoclonal anti-His_6 antibody in 5% BSA. Pads were further incubated with anti-mouse antibody at 1:10,000, 1:20,000, 1:30,000 in antibody diluent. The reaction was further amplified with a Tyramide kit and subsequently detected with a cy5 dye. The slide was scanned with an Axon Genepix scanner at a wavelength of 632nm, 100% power and 400 PMT.

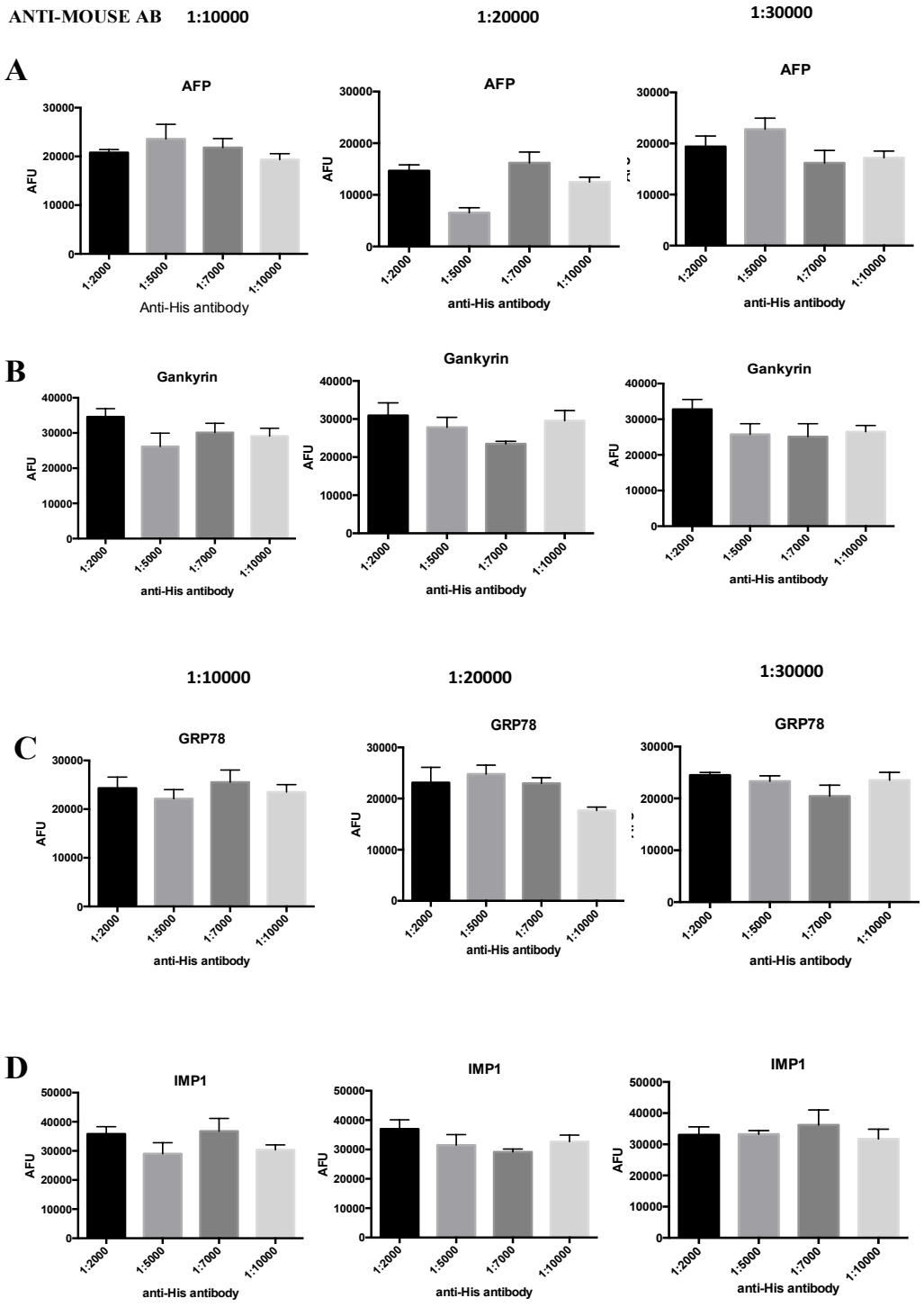


Figure 69: Arbitrary fluorescence of HCC TAAs tested with monoclonal mouse anti-His_6 and anti-mouse antibodies. Immobilised HCC TAAs **(**AFP, Gankyrin, GRP78, IMP1) on an Aminosilane slide were probed with different dilutions (1:2,000, 1:5,000, 1:7,000, 1:10,000) of monoclonal anti-His_6 antibody after which they were subsequently incubated with biotinylated anti-mouse antibody at 1:10,000, 1:20,000, 1:30,000 prepared in antibody diluent. The amplified reaction (Tyramide) was then detected with a Streptavidin conjugated Cy5 dye and further scanned at 635 wavelength at 400 PMT using Axon Genepix 4200AL. **(A)**, **(B)**, **(C)**, **(D)** show the mean fluorescence of (minus local background) of antibody responses to AFP, Gankyrin, GRP78 and IMP1 respectively when treated with various dilutions of primary and secondary antibodies. Data were analysed using Graph pad prism 6 and column statistics were represented by column statistics.

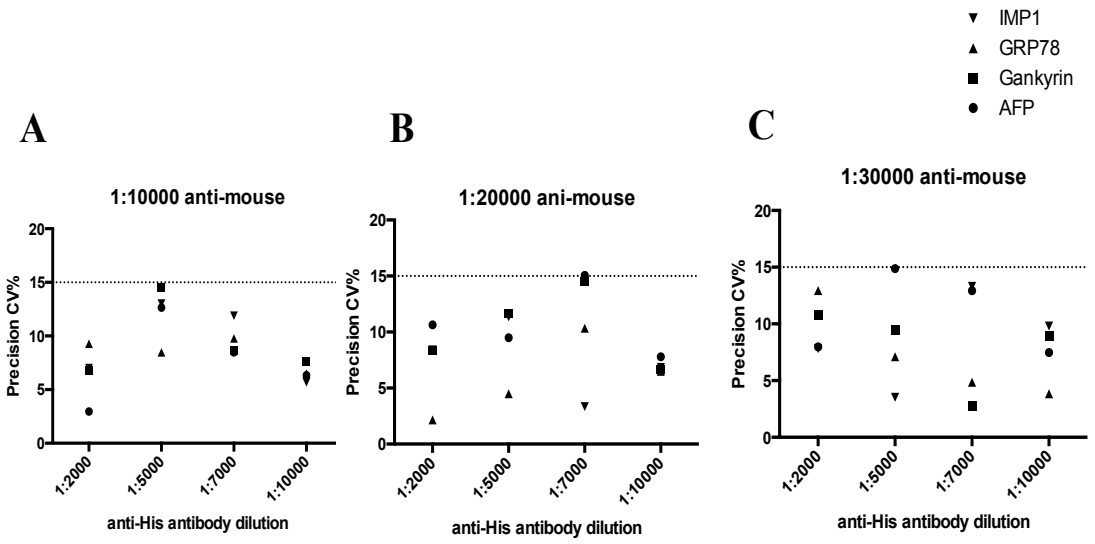


Figure 70: Investigating the precision of arbitrary fluorescence across different dilutions of anti-His_6 and anti-mouse antibodies used on the microarray. The precision (coefficient of variation) of signal intensities obtained in response to AFP, Gankyrin, GRP78 and IMP1 were calculated. **(A)**, **(B)** and **(C)** represent the CV% of signal intensities of the four HCC TAAs when incubated with several dilutions of monoclonal mouse anti-His_6 (1:2,000, 1:5,000, 1:7,000, 1:10,000) and biotinylated anti-mouse (1:10,000, 1:20,000, 1:30,000) antibodies respectively. Dashed lines represent the acceptable limits of precision (≥15%).

3.3.10 Re-validation of the Antigen Microarray Technology

Subsequent validation studies were undertaken on the antigen microarray technology after it had been subjected to series of optimisations (namely printing buffers, relative humidity, microtiter volume, slide surface chemistry, blocking buffer, edge effect, primary and secondary antibody dilutions).

Specifically, ten His-tagged TAAs: AFP, Gankyrin, APCN, GRP78, HDGF, KRAS, RALA, P62 and HRAS were printed in twelve replicates onto three Aminosilane slides and each slide was probed with monoclonal mouse anti-His_6 antibody (diluted 1:10,000 in 5% BSA in PBST). Slides were further incubated with monoclonal anti-mouse antibody (diluted 1:30,000 in antibody diluent) after which the interaction was amplified with tyramide kit. The complex was subsequently detected with a

Streptavidin conjugated Cy5 dye and slides were scanned. This experimental procedure was undertaken over a period of three consecutive days. Graphical assessment of scanned slides showed consistency in the morphological appearance of all spots with respect to their shape and size (**Figure 71**). The fluorescence of Gankyrin spot was the highest with low fluorescence observed with Ral A (**Figure 71A**). There was uniformity in the arbitrary fluorescence of all antigen spots across the different days (**Figure 71B**).

The mean signal intensities of antibody responses to all antigens across the different days ranged from 8,000 AFU to 35,000 AFU (**Figure 72**). There was consistency in signal intensities across the three days, with slightly elevated levels observed on the second day. Intra-assay variability of the mean signal intensities calculated across each day were within the acceptable limits of precision (CV ≤15%) (**Figure 73 A-C**), as were the inter assay variabilities (CV ≤ 20%) (**Figure 73D**).

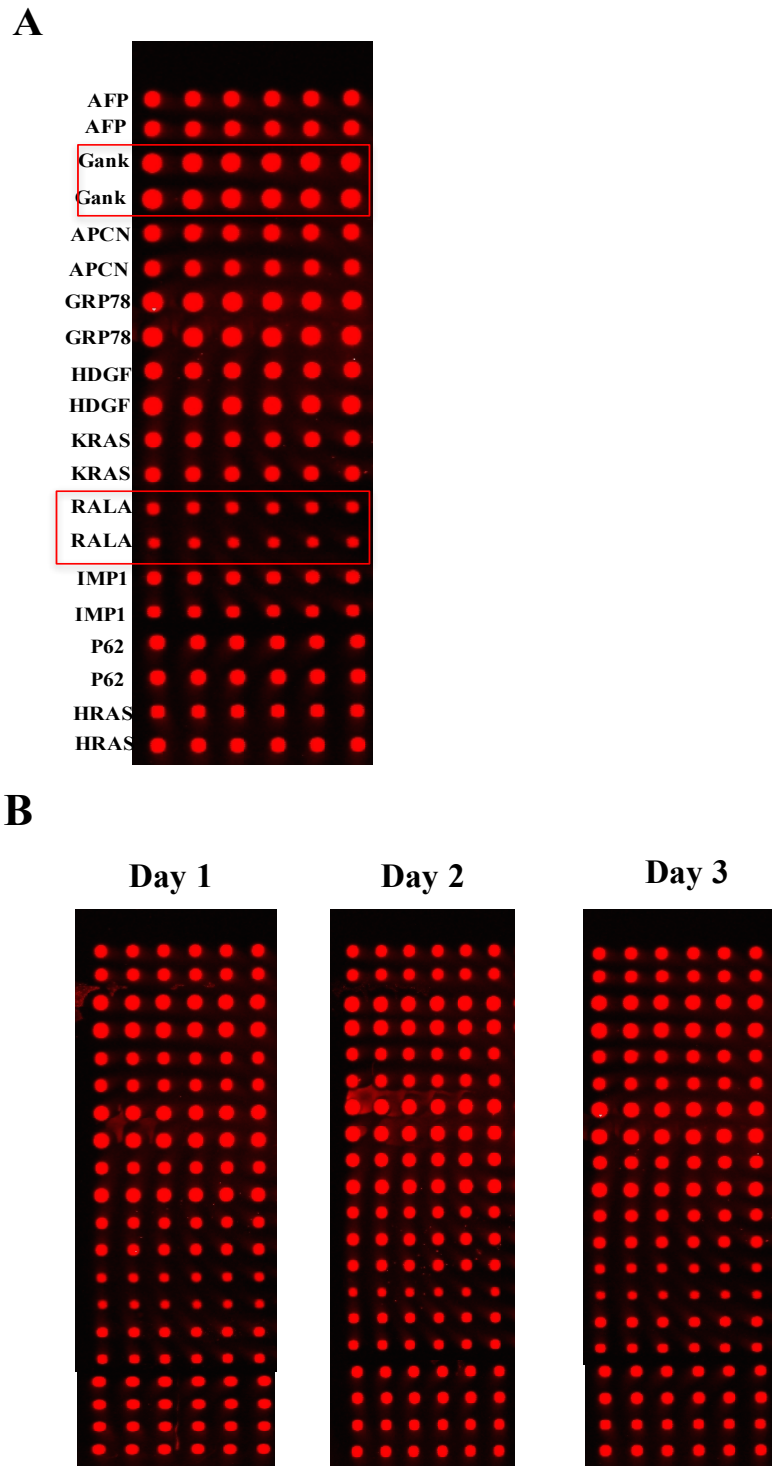


Figure 71: Morphological appearance of HCC antigen spots across different days. HCC His-tagged antigens; AFP, Gankyrin, APCN, GRP78, HDGF, KRAS, RALA, IMP1, HRAS and P62 were printed as twelve replicates onto Aminosilane slides after which they were probed with monoclonal mouse anti-His_6 antibody. The complex was further incubated with monoclonal anti-mouse antibody and further detected using Streptavidin conjugated Cy5 dye respectively. Slides were subsequently scanned at 635 wavelength at 400 PMT using Axon Genepix 4200AL scanner. **(A)** Represent the outline of ten His-tagged HCC antigens printed onto Aminosilane slides. **(B)** Morphology of antigen spots on slides when incubated with monoclonal mouse anti-His_6 antibody for three consecutive days.

I. SIGNAL INTENSITIES

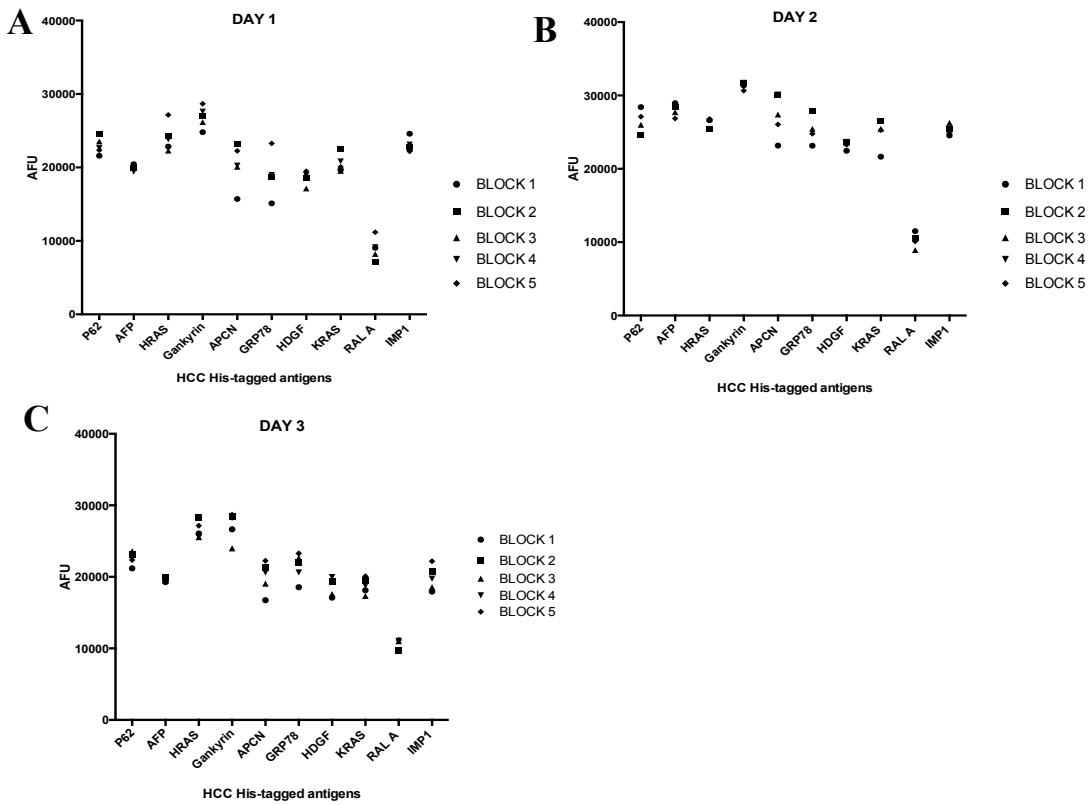
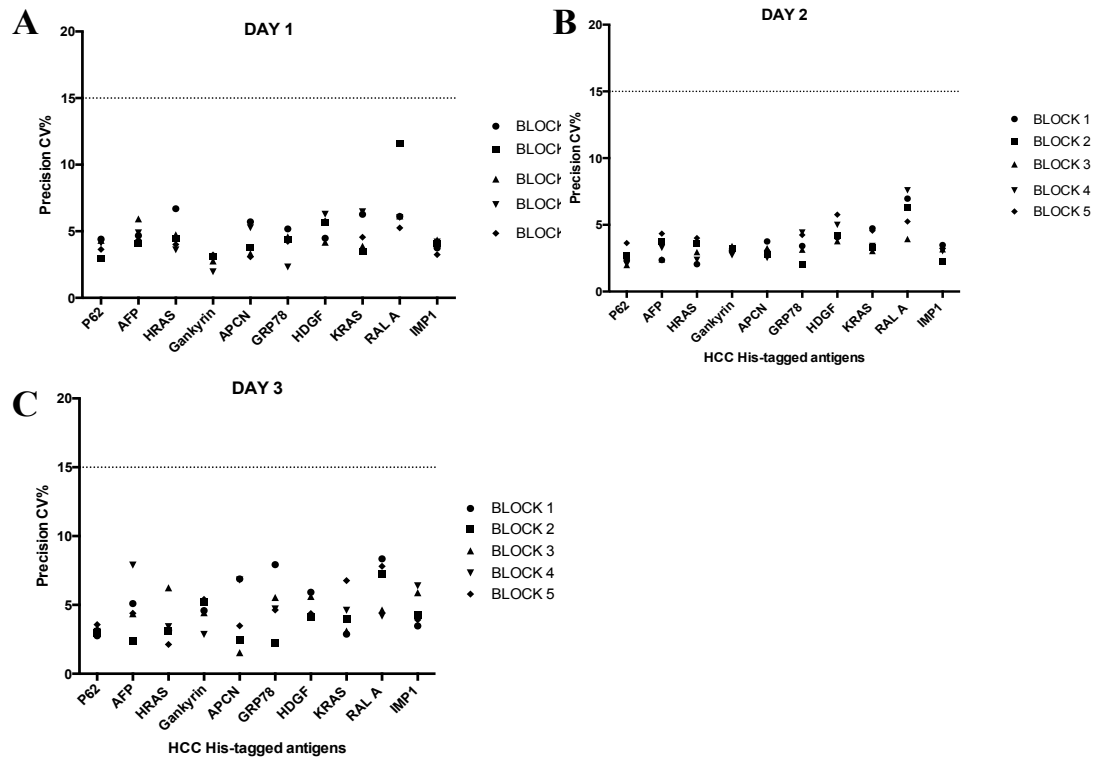


Figure 72: Signal intensities in response to HCC antigens. Ten HCC His-tagged antigens; AFP, Gankyrin, APCN, GRP78, HDGF, KRAS, RALA, IMP1, HRAS and P62 were printed as twelve replicates onto Aminosilane slides after which they were probed with monoclonal mouse anti-His_6 antibody. The complex was further incubated with monoclonal anti-mouse antibody after which the interaction was amplified with Tyramide and Streptavidin conjugated CY5 dye. Slides were then scanned at 635 wavelength at 400 PMT using Axon Genepix 4200AL scanner. Signal intensities of HCC antigen replicates were analysed. **(A)(B) and (C)** Represent the mean fluorescence (minus local background) of Anti-His_6 antibody responses the different HCC antigens over a period of three consecutive. Data were analysed using Graph Pad Prism 6 Software.

II. INTRA ASSAY CV



III. INTER-ASSAY CV

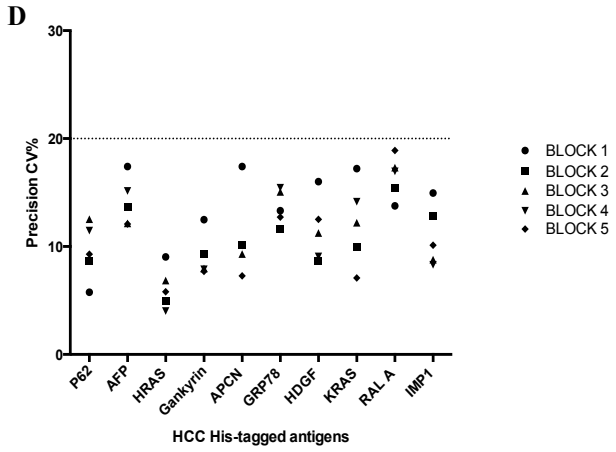


Figure 73: Intra and Inter-assay precision of Anti-His6 antibody responses to HCC antigens. Ten HCC His-tagged antigens; AFP, Gankyrin, APCN, GRP78, HDGF, KRAS, RALA, IMP1, HRAS and P62 were printed as twelve replicates onto Aminosilane slides after which they were probed with monoclonal mouse anti-His_6 antibody. The complex was further incubated with monoclonal anti-mouse antibody after which the interaction was amplified with tyramide and Streptavidin conjugated Cy5 dye. Slides were then scanned at 635 wavelength at 400 PMT using Axon Genepix 4200AL scanner. Signal intensities of HCC antigen replicates were analysed to determine the intra assay precision. **(A) (B) and (C)** Represent intra assay cv% of signal intensities in response to HCC antigens within a day. **(D)** Represent the inter-assay coefficient of variation (CV%) of signal intensities in response to all antigens across the three consecutive days. Data were analysed using Graph Pad Prism 6 software. Dashed lines represent the acceptable limits of precision (intra-assay ≤15%, inter-assay ≤20%)

3.2.11 Testing the Validity of the Microarray platform with HCC patients sera

Further reproducibility studies were undertaken using clinical samples. AFP, Gankyrin, APCN, GRP78, HDGF, KRAS, Ral A, P62 and HRAS, as well as a two fold human IgG dilutions, were printed onto Aminosilane slides in nine and four replicates respectively after which slides were probed with HCC sera (diluted 1:500 in 5% BSA in PBST). Slides were then incubated with biotinylated anti-human antibody (diluted 1:20,000 in antibody diluent) after which the interaction was amplified. The complex was subsequently detected with a Streptavidin conjugated Cy5 dye and further scanned . This experimental procedure was carried over a period of three consecutive days. Intra and inter assay CV% of signal intensities of antibody responses to antigens, as well as interpolated values after normalisation with human IgG dilution curve, were calculated. Spot morphology for all HCC antigens and IgG dilutions, as well as arbitrary fluoresecence of antibody responses, were consistent with low background observed on all slides across different days (**Figure 74**). Intense spots were seen with Gankyrin and GRP78 (**Figure 74**). Serum samples five and six repeatedly showed higher antibody responses to Gankyrin, GRP78, APCN, IMP1 and HRAS (**Figure 75**) while the other sera showed decreased responses (**Figure 75**). Acceptable level of intra assay precision was achieved even before normalisation with human IgG (CV% ≤15%) (**Figure 76**). The intra assay variation after normalisation with human IgG were also within acceptable limits (**Figure 77**). The inter assay variation without normalisation were mainly within 20%, whereas the interpolated values had even fewer samples above 20% CV (**Figure 78**). Those samples that gave highest CVs occured in the samples with very low abundant antibodies in HCC sera.

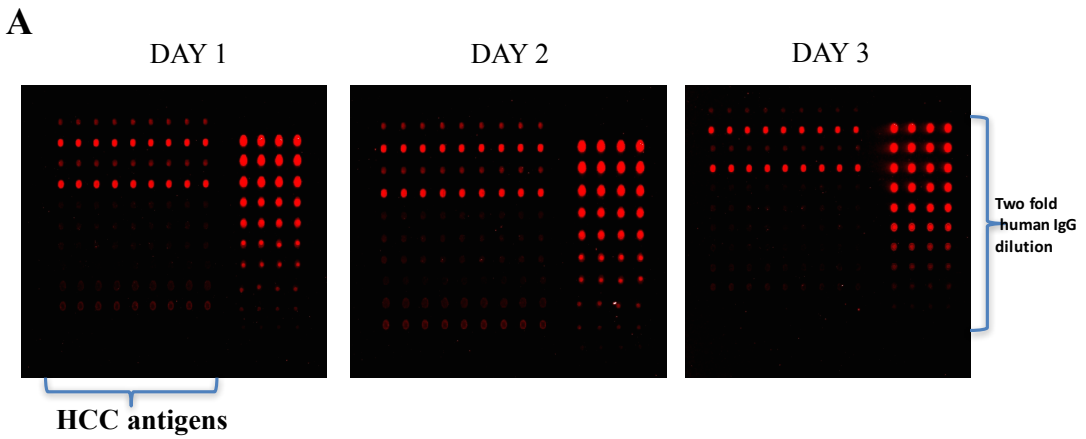
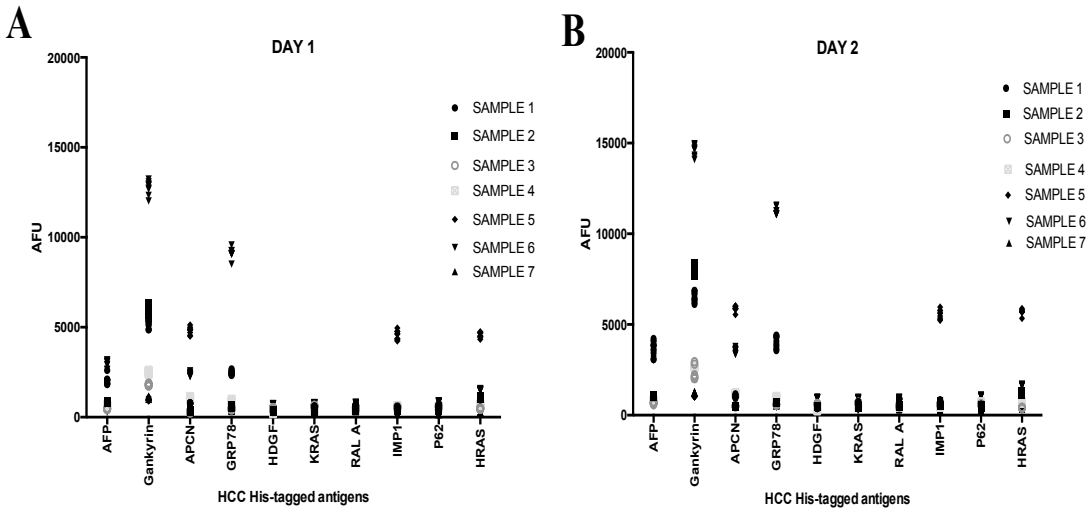


Figure 74: Spot morphology of HCC antigen probed with control sera. Ten HCC His-tagged antigens; AFP, Gankyrin, APCN, GRP78, HDGF, KRAS, RALA, IMP1, HRAS and P62 were printed as ten replicates onto Aminosilane slides after which they were probed with different control sera. The complex was further incubated with biotinylated anti-human antibody after which the interaction amplified with Tyramide and Streptavidin conjugated Cy5 dye. Slides were then scanned at 635 wavelength at 400 PMT using Axon Genepix 4200AL. **(A)** Represent the appearance of antigen spots on slides when incubated with control sera for three consecutive days.

I. ARBITRARY FLUORESCENCE



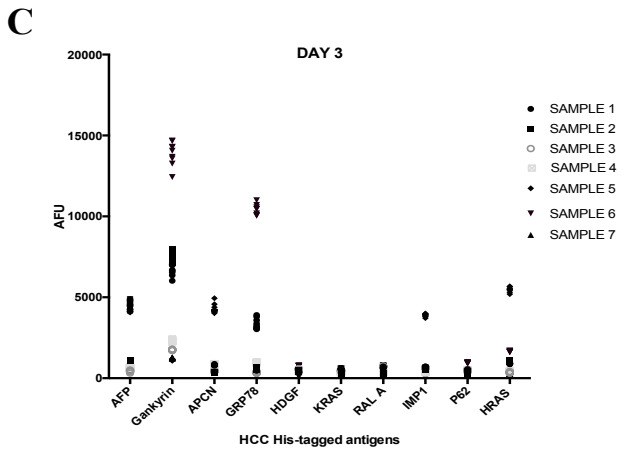
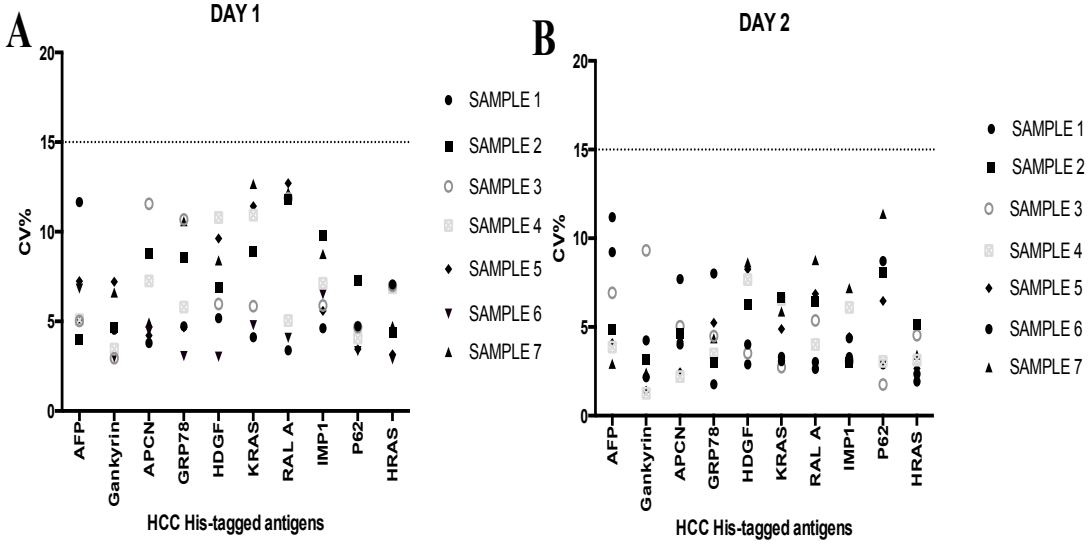


Figure 75: Arbitrary fluorescence of antibody responses to HCC antigens. Ten HCC His-tagged antigens; AFP, Gankyrin, APCN, GRP78, HDGF, KRAS, RALA, IMP1, P62 and HRAS were printed as ten replicates onto Aminosilane slides after which they were probed with different control sera. The complex was further incubated with biotinylated anti-human antibody after which the interaction amplified with tyramide and Streptavidin conjugated Cy5 dye. Slides were then scanned at 635 wavelength at 400 PMT using Axon Genepix 4200AL. **(A)**, (**B) and (C)** represent the mean fluorescence (minus local background) of antibodies in response to ten HCC antigens using seven control sera. Data were analysed using Graph Pad Prism 6 Software.

II. INTRA ASSAY CV (BEFORE INTERPOLATION)



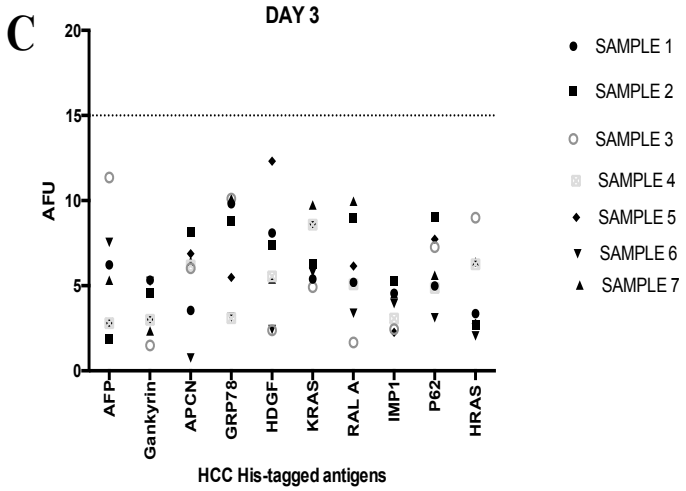
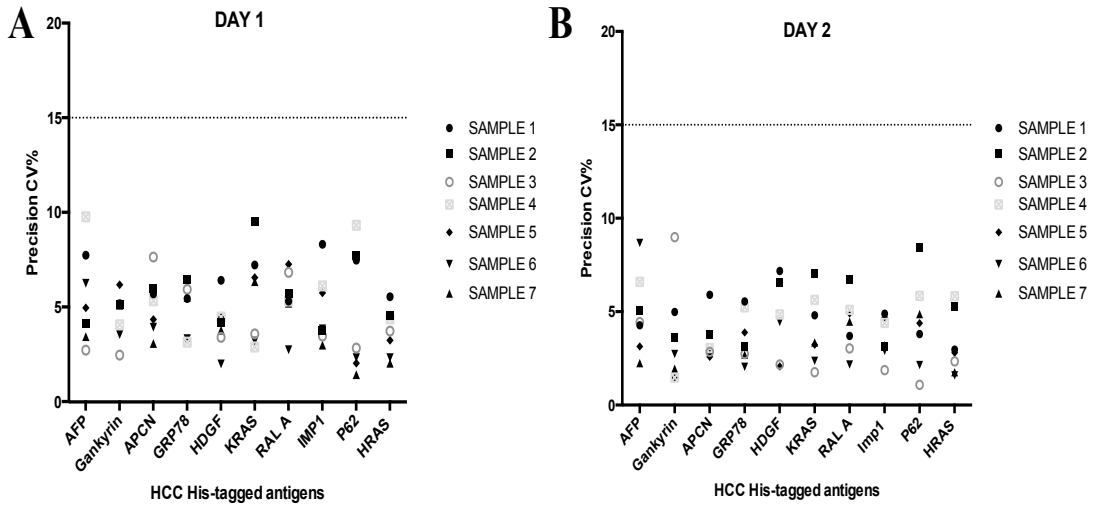


Figure 76: Intra-assay precision of arbitrary fluorescence. The arbitrary fluorescence of ten HCC His-tagged antigens; AFP, Gankyrin, APCN, GRP78, HDGF, KRAS, RALA, IMP1, HRAS and P62 were analysed to determine the coefficient of variation within and across three consecutive days. **(A)**, (**B) and (C**) Represent the intra-assay coefficient of variation (CV%) of signal intensities in response to all HCC antigens before normalisation with human with human IgG. Dashed lines represent the acceptable limits of precision (≤15%).

III. INTRA ASSAY CV (AFTER INTERPOLATION)



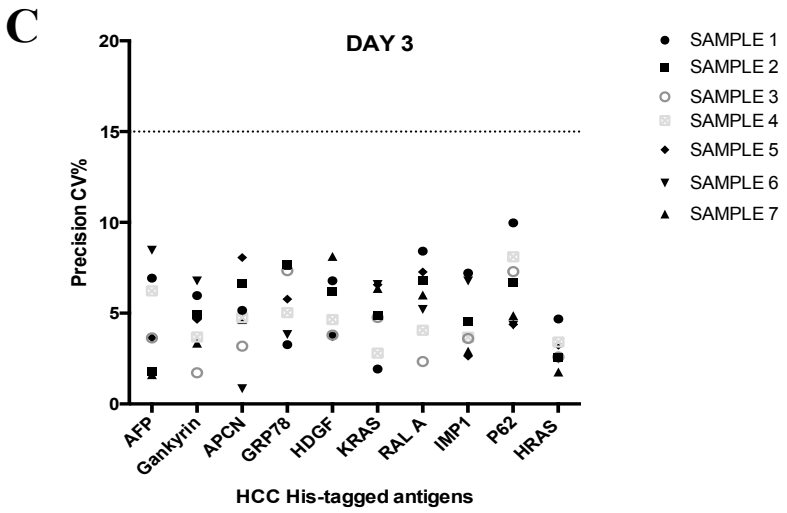


Figure 77: Intra-assay precision after normalising with human IgG. Interpolated values of arbitrary fluorescence in response to AFP, Gankyrin, APCN, GRP78, HDGF, KRAS, RALA, IMP1, HRAS and P62 antigens were analysed to determine the coefficient of variation within the different days. **(A)**, **(B)** and **(C)** represent the intra-assay CV% of normalised signals in response to all the HCC antigens within each experimental day. Dashed lines represent the acceptable limits of precision (≤15%).

IV. INTER ASSAY CV BEFORE AND AFTER INTERPOLATION

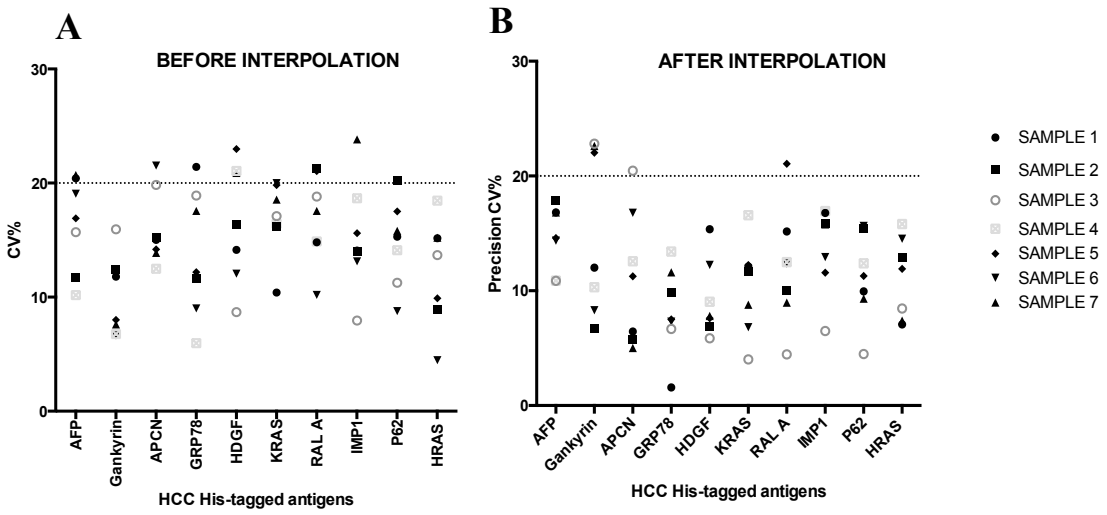


Figure 78: Inter-assay precision before and after normalising with human IgG. Responses to AFP, Gankyrin, APCN, GRP78, HDGF, KRAS, RALA, IMP1, HRAS and P62 antigens before and after been extrapolated from the human IgG dilution curve were analysed to determine the coefficient of variation across the days. **(A)** and **(B)** represent the inter-assay CV% of mean arbitrary fluorescence and interpolated values across the three consecutive days in response to HCC antigens when incubated with control sera. Dashed lines represent the acceptable limits of precision (≤20%).

3.3 Discussion

In this chapter, several experimental and analytical factors that affect the performance of an antigen microarray platform were optimised. These involved testing a wide range of slide surface chemistries, printing and blocking buffers, microtiter print volumes and edge effect. These were tested in order to find the most suitable combination that would allow detection of low concentrations of serum IgG autoantibodies in HCC patients. In addition, the validity of the in-house antigen microarray was investigated in order to determine its variability. Modification to the printing conditions and processing methodology have the potential to improve the reliability of data.

Firstly, a validation experiment was conducted using quality control antigens, *Candida* and *Tetanus* over three consecutive days. There was an increase in variation of spot morphology of antigens across days, leading to an increase in the inter assay variability. A number of factors are thought to have contributed to the high variability of assay. Optimum humidity in the spotting chamber is very important during antigen printing as it prevents spots from drying immediately after being dispensed (384). Although the humidity was set to a run rate of 57%, it fluctuated over different printing days. As such, decreased humidity during printing was thought to have contributed to spot to spot variation as samples could have evaporated from the microtiter plate during the arraying process. Also, condensation of moisture on the slide surface, which potentially affects the concentration of samples dispensed, may be a contributing factor to increased variations. Although not fully understood, temperature has been suggested to play a critical role in the performance of microarray as it affects array-printing quality (383). In this study, different temperature gradients were recorded on the different printing days which is believed to have affected binding capacity within the sample

during the printing and probing process, thus contributing to a higher variation accross days. Additionally, different sample volumes in the microtiter well during printing could have contributed to an increased signal variability over the days. Microtiter wells with higher volumes of sample have been shown to produce relatively bigger spots at initial print stages. This can be attributed to the collection of extra samples at the tip of the silicon pin as it dips into the well. Higher signals in response to *Tetanus* were observed compared to *Candida,* which could be explained that most patients used had been immunised against the *Tetanus*. There was a considerable increase in signal intensities observed with serum compared to purified IgG. This could be attributed to the loss of IgG during the purification process where as in serum all IgG were present. A human IgG standard curve was used for normalising signals in order to eliminate variation between assays. However, normalisation using human IgG standard can have some minor challenges (383). For example, at lower concentrations of the standard dilution curves there are very low signals and this can have had an effect when measuring low abundant proteins, giving rise to higher inter-assay variations.

When HCC His-tagged TAAs were used in the validation process, a similar pattern was seen as there were differences in signal intensities within and across days. Slides probed with anti-His_6 antibody gave higher signals compared to serum. This is believed to be as a result of high affinity binding between the anti-His_6 antibody and the corresponing His-tagged epitopes. Within the same sample, high intra-slide variation of signals could be attributed to the heterogenous nature of TAAs and printing buffer solubilising them which could affect the binding of proteins to the array surface thereby contributing to the increased variability.

Due to low level of precision mentioned above, several parameters were explored to determine their impact on signal intensity, spot morphology and reproducibility.

Printing buffers play a vital role in the efficient immobilisation of analytes onto a solid support in order to achieve good spot quality for fabrication of antigen microarrays. From this study, it can be deduced that PBS-Trehalose-Betaine-Tween is the optimal printing buffer since it produced high signal intensities and uniform profile of spots and this resulted in high reproducibility. Trehalose is a naturally-linked alpha disaccharide that forms a gel-like surface on the slide. It stabilises proteins during printing, preventing antigens from drying out (385). It also maintains the 3-D structure of proteins as well as their functionality. Betaine on the other hand, is essential for maintenance of spots sizes while Tween-20 provides additional stability. Furthermore, this printing buffer allows antigen to maintain its reactivity when it binds to the detection antibodies during processing of slides (386). A reduced spot to spot variation was observed with the non-contact arrayer compared to the contact arrayer although at lower signal intensities. This could be that in the non-contact arrayers the pins do not touch the slides, so spots sizes become consistent, whereas in contact arrayers the impact between the pin and the slide could cause aberrations which can eventually disrupt spot sizes. Also, in contact arrayers, constant humidity level is difficult to control, hence, spots may dry out during printing at low humidities, unlike non-contact arrayers where the presence of capillaries prevent the evaporation of fluids during the dispensing process (386). Likewise, in contact arrayers, the vertical movement of the dispensing head during printing may possibly add mechanical variations during printing (386), which is absent in the non-contact arrayer.

In assessing different microtiter volumes of antigens, 10 µl gave the most consistent spot morphology with reduced intra-slide variation as compared to 20 µl and 5 µl. This could be explained that the 20 µl volume filled up the microtiter well so extra samples might have collected around the contact pin which contributed to bigger spots seen at

the initial printing stage but dwindled during later stages. 5 µl gave consistent spots at the start of print but was not sufficient for the entire printing. These limitations were however absent with 10µl where consistent spots were observed with an intra slide variation below 15%.

Different slide surfaces such as Poly-L-Lysine, Aminosilane, Epoxysilane and Nitrocellulose were evaluated for spot morphology, signal intensity and spot to spot variation. This was carried out because preliminary experiments, which utilised Poly-L-lysine slides, although worked for some antigens, gave high spot to spot variation. Intra slide CVs of spot signals for AFP and Gankyrin ranged from 20.50 % to 26.39% respectively where low variations were seen with Aminosilane and Epoxysilane respectively. However, Aminosilane demonstrated excellent results with very low CVs of diameter of spots with regards to the different antigens used. Aminosilane was the most suitable array surface for this assay as it offers a high concentration of positive amine groups at the surface forming multiple ionic interactions that bind covalently with the negatively charge immobilised proteins. Thus, it allows adequate protein loading to produce high signal intensities and low background noise, as seen in this study. It also produces consistent spot morphology and interacts well with PBS-Tre-Betaine-Tween. This is in agreement with a study conducted by Servoss *et a*l, which showed that Aminosilane surfaces are preferable for antigen microarrays (387). Epoxysilane slides are very successful in multiplex PCR and DNA microarrays. This type of slide provides a high level of intensity when processed immediately. However, its surface loses reactivity and give low signal intensities when exposed to moisture in the air (388). Poly-L-lysine slides give moderate to high levels of signal intensities and consistent spot morphology although it gives a high degree of auto-fluorescence that could be misread as false-positive results (388). Nitrocellulose slides provide a thin

nitrocellulose coating that permits for a non-covalent yet irreversible surface for the adhesion of molecules of interest. This adhesion property of Nitrocellulose is thought to have contributed to the consistent spot morphologies. However, a drawback was seen in that it gave very low signals, making it unsuitable for printing tumour-associated antigens.

The performance of different blocking buffers was also assessed and 5% BSA was the optimal blocking buffer suitable for our antigen microarray as it gave a very low background and good spot morphology. This because BSA increases the possibility of antibodies binding only to the antigen of interest and also improves the sensitivity of the assay. Super G and I-block gave very high background intensity and poor morphology of spots. This may be due to the fact that Super-G may be more suitable for 3D surfaces such as Nitrocellulose as compared to a 2-D surface such as Aminosilane, Epoxysilane and Poly-Lysine (389). I-Block, which is a purified form of casein, is mostly suitable for antibody microarrays (388).

Having undertaken all the required optimisations, the newly developed assay was used to undertake a preliminary validation experiment using ten His_6-tagged HCC antigens. Antigens were probed with monoclonal anti-His_6 antibody to detect the presence of tagged antigens. The morphology of antigen spots was consistent within and across the different days and this subsequently yielded a very high intra and inter assay precision. Pre-spotting during printing helped to reduced variation in spot sizes at the initial stage. A subsequent validation assay was carried out by probing ten His-tagged HCC antigens with HCC sera and this showed a similar pattern as spot morphology and signal intenisities of antibody responses were consistent across the different days. More intense spots and higher signals were detected in response to Gankyrin and GRP78 as

compared to other antigens. This can be explained as both are overexpressed proteins and they are highly immunogenic. Human IgG was used for normalising signals to the total immunoglobulin present in the control samples in order to eliminate variation between assays (383). This could explain why the intra and inter assay precision of normalised signals were lower compared to non-normalised signals. Also, at lower concentrations of the standard dilution curves, there were minimal signals and this could have had an effect when measuring low abundant antibody responses to antigens giving rise to higher inter-assay variations.

In summary, the antigen microarray assay for future use has been optimised. We have shown that 10 µl sample volume was the optimal microtiter volume for printing as it produced the least variability in spot sizes and signal intensities. Also, our findings demonstrated that PBS-Trehalose-Betaine-Tween was the optimal amongst several printing buffers in terms of spot morphology and spot-to-spot variance. Though the non-contact arrayer produced low intra-spots variability, signals were consistently low; thus, ineffective for autoantibody screening. Aminosilane presented as the ideal slide surface for printing antigens. This indicate that considerable variations in antigen properties, humidity control, temperature, printing behaviour, blocking agents, slide surface, and adequate normalisation strategies, require fine-tuning to ensure an improvement in the reliability of the antigen microarray performance. In conclusion, we have optimised a diagnostic platform that it is highly reproducible for detecting anti-TAA IgG autoantibodies for the serodiagnosis of hepatocellular carcinoma.

Chapter Four: Production and Purification of a Panel of Recombinant Tumour-Associated Antigens in Hepatocellular Carcinoma

4.1 Introduction

4.1.1 Tumour Antigens

Tumour antigens (TAs) are proteins, peptides, nucleic acids, glycoproteins, carbohydrates and glycolipids that are expressed mostly by tumour cells and they act as targets for the immune system. Those expressed only on tumour cells are referred to as tumour specific antigens (TSA) while those found on both tumour or normal cells are referred to as tumour-associated antigens (TAAs) (390). TAAs could either be aberrantly expressed (AFP, P62) (391), mutated (HRAS, KRAS, P16 and P53) (294), over-expressed (Gankyrin, HDGF, GRP78 and RALA) (392, 393) or altered (NYESO-1) (394). The identification of specific TAAs can help in the detection of tumours. There have been reports of an increase in the number of TAAs in hepatocellular carcinoma (HCC) patients and the different kinds of TAAs identified in HCC are shown in **Table 21** (260). These are mostly presented by MHC class I molecules on the surface of tumour cells. They are then recognised by cytotoxic T cells which may destroy the cells before they proliferate and spread to other parts of the body (395). These can therefore act as potential targets for cancer immunotherapy. Studies have also shown that autoantibodies against these TAAs can be produced as part of the immune response during the development of HCC (260).

This study was focused on using TAAs relating to hepatocellular carcinoma to profile

autoantibodies in patients' sera. In this regard, TAAs were selected to be included in the panel for the early discovery of HCC. This is because a panel of multiple TAAs would increase autoantibody detection in patients (396). Through a thorough literature search, the panel of TAAs were selected based on its association with any liver disease or HCC, or a proof of previously documented autoantibody response in HCC or other solid tumours. The selected TAAs include the following: KRAS, HRAS, HDGF, P16 (CDK2NA), Gankyrin, P62, P53 and RALA. We chose to make in-house recombinant TAAs in order to produce enough protein for the entire period of study and to be sure of the quality and purity of antigens used.

Table 21: Different tumour-associated antigens discovered in patients with hepatocellular carcinoma patients since 1993.

TAAs reported	**Reference**
hnRNPL	Yau *et al* (258)
HSP70, SOD2, PRDX6	Akada *et al* (367)
Glucose-regulated protein 78	Shao *et al* (167)
Ku86	Nomura *et al* (397)
CENPF, DDX3, HSPA4, HSPA5, VIM, LMNB1, and p53	Liu *et al* (398)
CRT	Pekarikova *et al* (147)
Sui1, RalA	Chen *et al* (399)
KRT23, AHSG and FTL	Wang *et al* (294)
RalA	Wang *et al* (393)
HSP60, HSP70	Looi *et al* (400)
DDX3, eEF2, AIF, hnRNP A2, PBP, and TIM	Li *et al* (401)
EIF3SI, LDHA, RFC2, and MCART1	Chen *et al* (402)
IMP1, IMP2, IMP3, p53, c-myc, cycin B1, survivin, p16	Zhang *et al* (267)

p53	Akere *et al* (403)
HCC-22-5	Zhou *et al* (404)
HSP70, GAPDH, PRX, Mn-SOD	Takashima *et al* (405)
p16	Looi *et al* (406)
Survivin	Yagihashi *et al* (407)
IMP2	Su *et al* (408)
IMPs	Himoto *et al* (409)
IMPs, p53, c-myc, and survivin	Himoto *et al* (266)
c-myc, cyclin B1, IMP1, Koc, p53, IMP2, and surviving	Zhang *et al* (265)
p53, IMP2, Koc, CENP-F, p90	Soo Hoo *et al* (208)
CRT, CK8, NDK-A, and ATP5B	Le Naour *et al* (148)
IMP2, CENPF	Zhang *et al* (265) Zhang *et al* (245)
IMP2	Zhang *et al* (169)
p53	Raedle *et al* (410)
Cyclin B1	Covini *et al* (411)
HCC1	Imai *et al* (248)

4.1.2 Recombinant Protein Expression Systems

Approaches for the expression of recombinant proteins involve transfecting/ transforming cells with a cDNA vector that contains the gene of interest, after which the cells are cultured in order to transcribe and translate the protein of interest (412). A number of these systems are widely used and mostly classified as prokaryotic or eukaryotic (412). They both have unique advantages and challenges and hence selecting the right system is crucial for successful recombinant protein expression. The selection criteria are highly dependent on the type, toxicity and yield of protein, how to purify

the protein of interest, production costs, facilities and expertise available (413). Examples of these systems include mammalian, bacterial, insect, yeast and cell-free systems (**Figure 79**) (413).

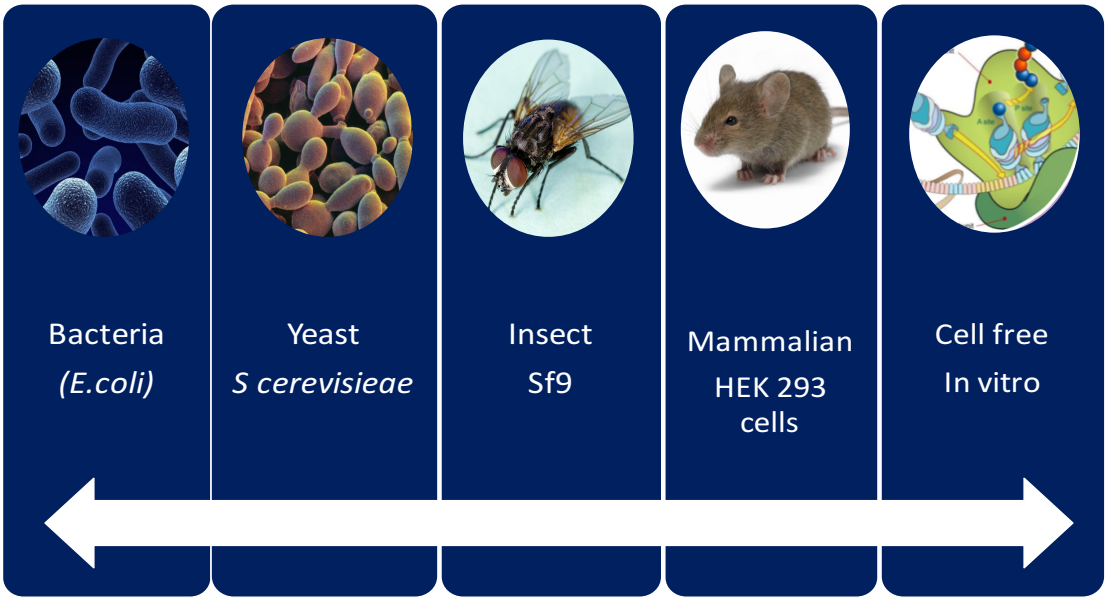


Figure 79: Protein expression systems. Different systems have been developed to express recombinant proteins. This include: bacteria (*E.coli*), yeast (S.cerevisieae), insect (sf9), mammalian (HEK 293 cells) and cell free systems. Adapted from (412).

One of the most popular expression systems for human proteins is the mammalian protein system (413, 414). This provides an ex vivo condition similar to the native proteins, especially in terms of post-translational modification which varies from mammalian to bacterial systems. Two major expression systems in this category are the Human Embryonic Kidney cells (HEK) and Chinese Hamster ovary (CHO) cells. These are usually used for either stable or transient expression of human proteins (414). The mammalian system results in increased levels of post-translational modification as well as proper folding and authentic glycosylation of proteins. (413, 415). Proteins obtained through these systems always remain biologically active and are much closer to naturally occuring human proteins in terms of nature and functions. Moreover, the

functionality of expressed proteins is higher, bacteria show very low immunogenicity to humans, are compatible to humans and are safer to use (414). Though CHO cells have been the mainstay for the production of recombinant proteins (416), the HEK 293 cell line has become relevantly prominent and suitable because proteins produced in them are a closer match to naturally occurring human proteins in terms of their function and post-translational modification (417). Challenges associated with this type of expression are low yield of proteins, slow growth rate of cells and excessive cost of complex media (418, 419). The most popular expression system is bacteria (*Escherichia coli*) and there are a number of *E. coli* strains used. These include *E. coli* C43 (DE3) and C41 (DE3) and *E. coli* BL21 (420). However, *E. coli* BL21 is frequently exploited because they have rapid growth, easy to culture, inexpensive costs, time-saving, produce increased yields of protein and they are easily manipulated genetically (420). Middleton *et al*, used *E.coli BL21* to express a panel of 22 HCC TAAs (AFP-C-BirA, RALA-C-BirA, HRAS-C-BirA, Gankyrin-C-BirA, HCC1-C-BirA, etc), which were further used for serum autoantibody measurement in HCC patients (241). Colorectal cancer TAAs (MAGE A4, HuD, HCC1, MUC1, CEA, Annexin A1, rhUteroglobulin) generated in *E. coli BL21* were also employed by Ola *et al*, in screeening autoantibodies in colorectal cancer patients (252). However, human proteins expressed in bacteria are not functional because they are redundant in their capacity to post-translationally modify and fold proteins, they could potentially introduce endotoxins which could induce antibody responses which could potentially cross-react with autoantibodies in patients' sera. Also, these proteins are difficult to purify due to the presence of inclusion bodies (420).

Another option is baculovirus infected insect cells. They are also used for high level protein expression and protein modifications are similar to that of mammalian systems.

These are usually used for large scale production of proteins, are easy to infect and offer as easy purification of expressed proteins due to the lysis of cells by the virus (421). The challenges involved with this protein expression system include the following: virus infection may lead to lysis of cells and degradation of expressed proteins, glycosylation may be different to mammalian cells as well the culture media used are expensive (421). This system was employed by Bin Li, to express HCA587, which is a tumour-associated antigen in HCC (422). However, the antigenicity of the protein was quite low as compared to the naturally occurring ones.

Cell free expression is quite different from the rest as it requires an in-vitro synthesis of proteins, using translation compatible extracts of the cells (418). This expression system allows labelling of proteins with modified amino acids and fast production of recombinant proteins. It is also easier and there is a simultaneous expression of different proteins (423). This expression system is very expensive and there is limited post-translational modification of proteins (423).

Lastly, yeast systems include: *Kluyveromyces*, *Hansenula* and *Yarrowia*, *Saccharomyces*, *Pichia* (424). They have a rapid growth, easily manipulated genetically, post-translationally modify proteins and are less costly. Nevertheless, they are very expensive and the glycosylation is different from human proteins (424).

Most studies have focused on utilising HCC TAAs expressed in the *E. coli* system to screen cancer patients' sera with no study undertaken using TAAs expressed in HEK 293 systems. It will therefore be novel to use the mammalian expression system, specifically HEK 293 cells, to produce TAAs. Also having highlighted the advantages of the mammalian system, we deemed it as our preferred choice for the production of our in-house TAAs. This is because these antigens are human proteins and would

primarily be used for high throughput screening of autoantibodies in human sera. Using bacteria, yeast and virus insect cells could easily contaminate expressed proteins which would in turn stimulate antibodies which might cross-react with autoantibodies in the sera of patients, giving rise to false positive outcomes.

4.1.3 Mammalian Cell Transfection Platforms

The introduction of foreign or exogenous nucleic acid into a mammalian cell line in order to obtain genetically modified cells is referred to as transfection. This technique is a great tool for studying the functionality of gene and gene products, gene regulation and the production of recombinant proteins (425, 426). Transfecting mammalian cells can be undertaken in several ways depending on the characteristeristic of the cell line as well as the nature of the genetic material (427). Mammalian cell lines could either be transiently or stably transfected. In stable transfection, the introduced genetic material usually have a marker gene for selection and this is referred to as the transgene (**Figure 80**). The genetic material integrates into the genome of the host and sustains transgene expression even after host cells replicate (428). In transient transfection, genetic materials are not integrated into the host genome and are expressed only within a limited time (427). However, these genetic materials could easily be lost through cell division and other environmental factors. Certain parameters should be considered before a transfection procedure is undertaken. The cell health affects transfection and in order to increase the transfection efficiency, cells must be grown in a fresh and appropriate medium, incubated at the correct temperature (37^0C) and relative humidity (100%). The confluence and growth of many cells are vital, in that cells should be transfected at 40% to 80% confluency in order to avoid contact inhibition causing cells to be resistant to DNA uptake. Lastly, the quality and quantity of DNA should be carefully considered. It should be free of proteins, RNA and chemicals (425). Many

transfection methods have been developed and these utilise different approaches. A suitable method should have a very high transfection efficiency, low cell toxicity level, be easy to use and must be reproducible.

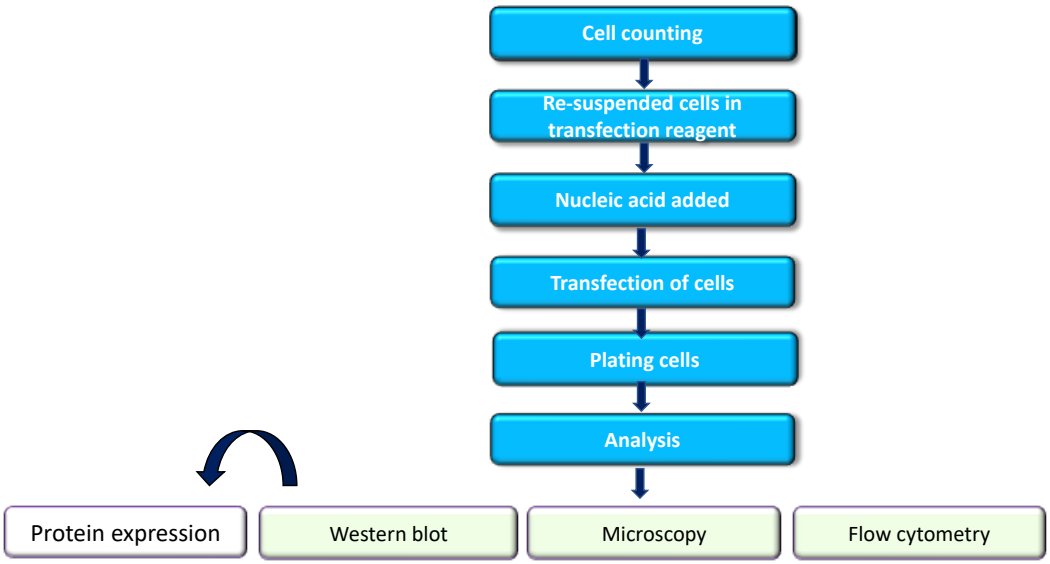
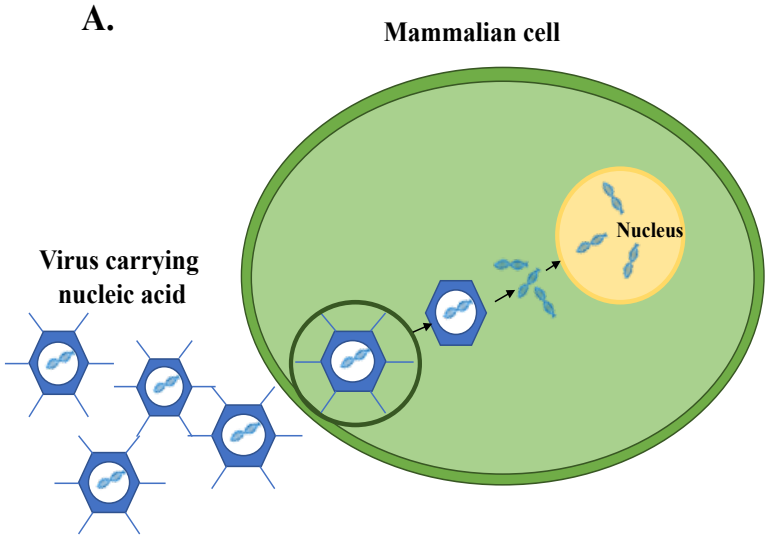


Figure 80: Workflow of transfection in mammalian cells.

These different approaches are put into three categories namely; biological, chemical and physical mediated methods (425). The virus mediated transfection (**Figure 81A)** is a common biological method mostly used in clinical research. It is very efficient and easy to attain a suitable transgene expression because virus integrates naturally into host genomes. This method has huge set backs such as inducing cytotoxicity and immunogenicity (429). As a result, other non-viral methods of transfection such as chemical and physical ones have been developed. The chemical transfection methods (**Figure 81B**) was the first to be utilised to introduce exogenous genetic material into mammalian cells and it requires calcium phosphate, cationic lipid or cationic amino acid. The positively charged calcium phosphate forms a complex with the negatively charged nucleic acids so they could easily permeate the negatively charged membranes of cells after which they are taken further into the cell by endocytosis. Cationic lipid

performs the lipid mediated transfection (lipofection) where the nucleic acid is transferred into the cells via liposomes which merges with the cell membrane (430). Though low cytotoxicity and mutagenesis are encountered, low transfection is usually encountered due to factors such as pH of solution, cell membrane conditions and nucleic acid/chemical ratio (425).

The most recent methods of transfection are the physical approaches which use a wide range of tools to deliver genetic materials into mammalian cells. This involves electroporation (**Figure 81C**) (425), ultrasound (431), magnetofection (432) and laser-based transfection (433), biolistic particle delivery (434) and direct micro injection (435). These methods employ either a high electrical pulse, ultrasound or magnetic field, laser and high velocity to induce pores into the cell membrane so the nucleic acid could immediately be transferred into the cell. The microinjection requires a direct injection of a naked DNA into a cell. These physical methods are mostly very reliable and straight forward but are labour intensive, expensive and may cause physical damage to samples (425). However, our choice of transfection for this study was electroporation as it is easy, rapid, large number of cells can be transfected in a short time, has high efficiency and can be applied to all cell types.



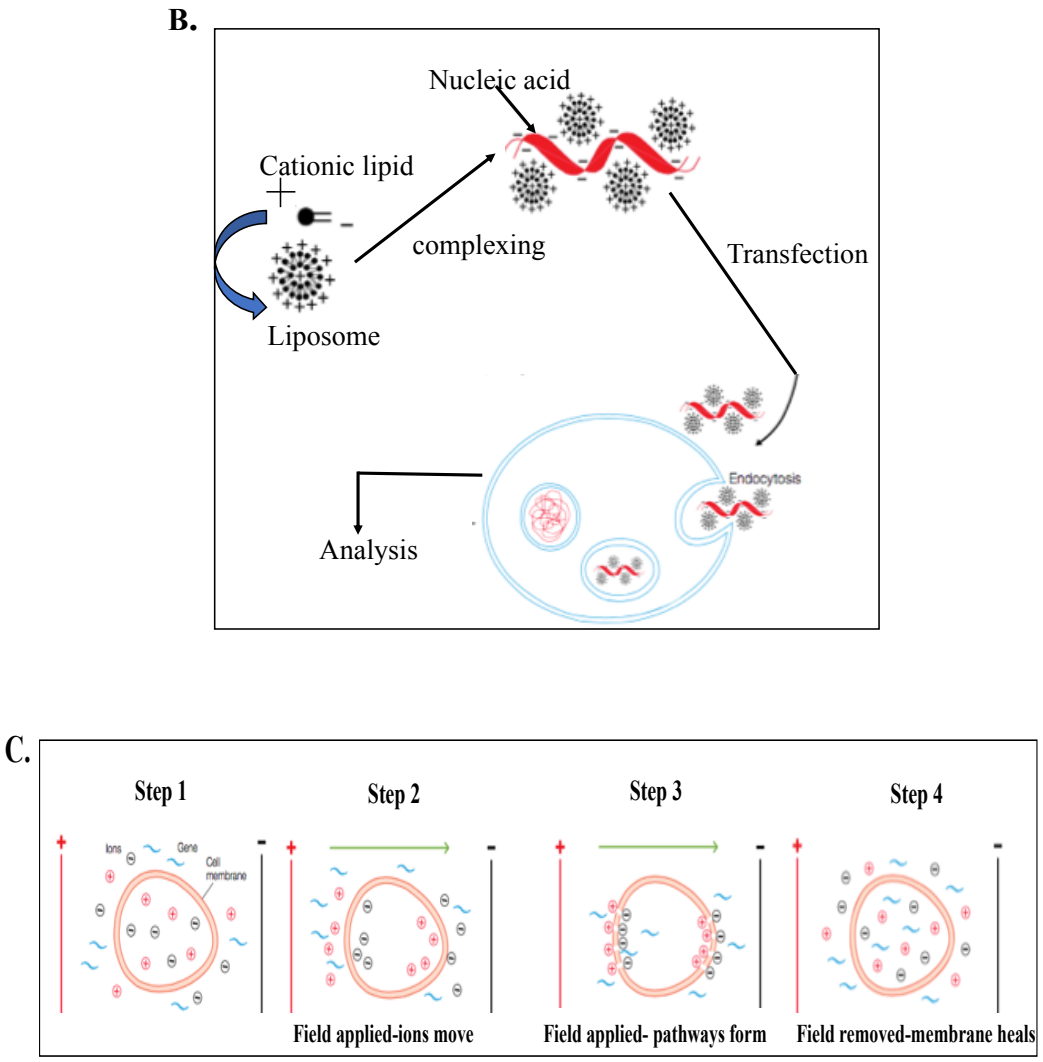


Figure 81: Common methods of transfecting mammalian cells. There are diverse ways of introducing exogenous plasmid DNA into cells. These are categorised into the biological (virus), chemical (cationic lipids) and physical (electroporation) approaches. **(A)** Virus transfers nucleic acid into a cell by integrating into the host genome, **(B)** cationic lipid (liposome) forms a complex with the nucleic acid and enters the cell via endocytosis, **(C)** shows the transfer of nucleic acid into a mammalian cell using high electric pulse which create pores on the cell membrane.

4.1.4 Purification systems for expressed recombinant proteins

Recombinant proteins are required in industrial and academic settings for a wide range of applications such as high-throughput screening, biopharmaceutical production, exploratory research and drug discovery (436). It is essential that proteins expressed in

mammalian cells and other systems are purified to attain accurate characterisation of the structure, function and interactions of the protein of interest. This comprises several processes to isolate the desired protein from a complex mixture of other proteins in a cell lysate (436). Purification of proteins utilises the differences in protein size, binding affinity, physio-chemical properties and biological activity (437). Developing an economical and effective strategy for purifying proteins is a major challenge encountered by industrial and academic laboratories. Several traditional and recently developed approaches are employed in purifying proteins. Purification platforms include the affinity column, ion exchange, size exclusion and hydrophobic interaction chromatography (437). However, the affinity-based method is widely used in purifying proteins and it is undertaken in several ways; of which Protein A Chromatography is the most commonly used, especially in the purification of antibodies (438, 439). The use of fusion tags (**Table 22),** i.e. amino acid sequences attached to recombinant proteins, is another approach of affinity-based purification. Fusion tags have selective and high affinities for a ligand which is immobilized on a chromatography column therefore enabling the purification of recombinant proteins (436, 440). Moreover, the properties of a tag facilitate the identification of the protein of interest as well as provide a one-step purification procedure by passing the cell lysates or supernatants through columns of an appropriate matrix such as affinity chromatography (440, 441). Many different affinity tags are used to purify proteins expressed in mammalian cells **(Table 22).** Tagged proteins are convenient and simple to work with. Also, a single purification step, using a commercially available chromatography column, is sufficient for many applications. This type of purification can be used for different recombinant proteins. In this study, the Flag-tag® and Myc-tag® affinity chromatography were employed in the purification of recombinant proteins expressed in HEK 293 cells. The Flag affinity

tag referred to as FLAG™, is extensively used for highly specific and rapid one step purification (442). The tag consists of eight amino acids comprising an enterokinase-cleavage site, which is specifically designed for immunoaffinity chromatography (443). It allows highly specific pull-downs that contain low nonspecific background (444). These tags have not only been successfully used to pull down recombinant proteins made in mammalian cells but also in baculovirus system, *Saccharomyces cerevisiae and Schizosaccharomyces pombe* systems (444).

Table 22: Affinity tags used in purification of recombinant proteins expressed in mammalian cells (440).

Tag	Size (amino acid)	Ligand/separation method	reference
Polyhistidine	5-15aa	IMAC	(445)
FLAG	8aa	mAb based	(446)
Strep tag I	8aa	Streptavidin	(396)
Strep tag II	9aa	Streptacin	(258)
Soft tag 1	13aa	mAb based	(367)
Soft tag 3	8aa	mAb based	(167)
T7-tag	11-16	mAb based	(397)
c-myc	10aa	mAb based	(398)
S-peptide	15aa	S-protein	(147)
Polyaspartic acid	5-16aa	Ion-exchange	(399)
VSV tag	11aa	mAb based	(298)
Calmodulin binding peptide	26aa	Calmodulin	(401)

Glutathion-s-transferase	26kDa	Glutathione	(402)
Maltose binding domain	40kDa	Maltose, Amylose	(267)
Pin-point (Promega)	13kDa	Streptavidin/avidin	(403)
Cellulose binding domain	27-189aa	Cellulose	(398)
Xylanase 10A	163aa	Cellulose	(404)
HA tag	9aa	mAb based	(260)

4.2 Materials and Methods

4.2.1 Materials and reagents

C-Terminal Myc-DDK (Flag-tagged) human TrueORF cDNA clones; KRAS, HRAS, HDGF, CDKN2A, RALA, P62, P53 and Gankyrin which had pCMV6 entry vectors were purchased from Origene, UK while Human Embryonic Kidney 293 cells (HEK 293 ATCC 15E058), stably transfected with SV40 large T-antigen was obtained from Public Health England.

4.2.2 Transfection and Flow Cytometry

HEK 293 cells were passaged 2-3 days at a confluency 50%-80% before transfection. Cells were carefully pelleted aseptically by centrifugation at 300g for 10 minutes at room temperature after which the supernatant was discarded. The cell pellet ($1x10^6$ cells per sample) was carefully re-suspended in 100 µl of nucleofector solution V and the suspension was combined with either 1 or 2 µg of a cDNA ORF clone. HEK 293 cells were then transfected with clones using the nucleofecter device, program A-023

(Lonza, UK). The mixture was then transferred into a 6-well culture plate containing 1.5 ml pre-warmed complete culture media (DMEM/10% FBS) and further incubated at 37°C/5%CO_2 (Grant JB series, UK). The Beckman Coulter FC500 at the flow cytometry unit was used to determine the transfection efficiency of reagents at 48 hours of post-transfection. Viable HEK 293 cells transfected with GFP plasmid at a density of $1x10^6$ cells/mL were removed from the culture, centrifuged and re-suspended in 500 µL of 10% FBS/DPBS prior to loading unto the flow cytometer. Flow cytometry data was further analyzed using Weasel analysis software (**Figure 82**).

4.2.3 Selection of Resistant Cells

Old culture media was replaced with fresh complete media containing 1 mg/ml Geneticin (G418) (Gibco, UK), 48 hours after transfection. Stable selection and growth of resistant clones (transfected cells containing plasmid with resistant constructs) was allowed to grow for to 1- 2 weeks for cells to reach 80% confluency. The selective media was replaced every 3 days to ensure adequate selection of resistant clones.

4.2.4 Cell lysate preparation and BCA assay

To lyse cells with resistant constructs, old selective medium was removed from the adherent cells and washed once with 1000 µl cold DPBS (Sigma Aldrich, UK) for 30 minutes. 1000 µl of cold RIPA buffer (ThermoFisher Scientific, UK), 10 µl of Protease/Phosphatase inhibitor cocktail and 5 µl of Benzonase (Sigma Aldrich, UK), which served as the lysis buffer were added to cover the entire culture. The preparation was incubated on ice with shaking for 30 minutes after which samples were transferred into microcentrifuge tubes and then centrifuged (IEC Micromax RF, UK) at 16000*g* for 15 minutes at 4°C. The clarified lysate was removed and stored at -20°C until further use. Proteins present in cell lysates were concentrated in Amicon® Ultra 2 ml and 15

ml 10K MWCO centrifugal filter units (Merck Millipore, USA) according to manufacturer's instructions. The concentration of proteins in a lysate were determined using the PierceTM BCA Protein Assay Kit (Thermo Scientific, UK), which consisted of 9 bovine serum albumin (BSA) size standards (2000, 1500, 1000, 750, 500, 250, 125, 25, 0 µg/ml; Thermo Scientific, UK). Samples and standards were added to working reagent in 1 in 20 dilutions after which the absorbance was measured at 562 nm using the FLUOStar Omega plate reader and analysed using Graph Pad Prism 6 software.

4.2.5 SDS-PAGE and Immunoblot

In-house recombinant TAAs expressed in cell lysates as well as commercial TAAs were detected using several approaches (**Figure 82**). Firstly, lysates were run on SDS polyacrylamide gels before carrying out detection methods like western blot, silver and imperial staining. Equal volumes of proteins (cell lysates or commercial TAAs) and x1 loading buffer were mixed in an Eppendorf tube after which they were denatured by heating for 10 minutes at 95^{o}C on PCR block. 15 µl of each sample was run along with either Spectra Multicolour Broad range protein ladder (10-260 kDa) (ThermoFisher Scientific, UK), Pre-stained Protein marker (11-250 kDa) (Cell signalling) or Magic Mark™ XP (20-220 kDa) (ThermoFisher Scientific) at 130 V for 1.5 hrs at 35 mA using a 15 well precast Mini-Tris Glycine gel (4%-20% and 10%-20%) (Invitrogen, UK). Staining of gels undertaken with TM Silver Stain Kit (ThermoFisher Scientific, UK) or Protein gel stain (Invitrogen, UK) after which gels were scanned. These were carried out on commercial recombinant TAAs or purified in-house TAAs to validate the molecular weight of bands. Western blot was carried out immediately after SDS-PAGE. Gels and 0.2 µm HybondTM-ECLTM nitrocellulose membrane (ThermoFisher

Scientific, UK) or 0.2 μm PVDF membrane (ThermoFisher Scientific, UK) equilibrated in transfer buffer after which the gel was layered on the membrane. The complex was sandwiched between two pre-wet filter papers and placed on Transblot SD wet transfer cell (Invitrogen, UK). All components were soaked in 1x transfer buffer. The membrane was placed closest to the positive electrode after which transfer was run at 30 V at 100 mA for 1.5 hrs. The membrane was blocked using 25 ml 1X Tris Buffered Saline TBS, 0.1%Tween 20 (100%) with 5% w/v skimmed dry milk (Tesco, UK) at room temperature (RT) for 1 h at 10 rpm. The membrane was washed three times at 5 minutes intervals with 1x TBS, 0.1%Tween 20 (100%) (ThermoFisher Scientific, UK) after which primary antibody incubation was undertaken as per the manufacturer's instructions. Nitrocellulose membrane (0.2 μm) or 0.2 μm PVDF membrane was incubated in 5 ml mouse anti-DDK (Sigma Aldrich, UK), (diluted 1:1000 in 5% milk) overnight at 4^{o}C. Anti-Myc, as well as antigen specific antibodies such as anti-KRAS, anti-P16, anti-p62 and anti-P53, were diluted (1:500, 1:300, 1:300, 1:300:1:50) in 5% milk respectively. The membrane was washed three times at 5 minutes intervals in 15 ml TBST at 30 rpm. For chemiluminescence detection, the membrane was tagged with polyclonal goat anti-mouse HRP (DAKO, UK), (diluted 1:2000, 1:1000, 1:500, 1:500, 1:500, 1:50 in 5% milk for DDK, Myc tagged proteins, non-tagged KRAS, P16, P62 and P53 proteins respectively), for 1 hour at RT with rocking, followed by 3 washes. The membrane was immersed in AmershamTM enhanced chemiluminescent (ECLTM) western blotting detection reagents (GE Healthcare) for a minute and developed using Amersham HyperfilmTM ECLTM high performance chemiluminescence film (GE Healthcare), Carestream® Kodak® autoradiography GBX developer/replenisher and fixer/replenisher (Sigma, UK). In the case of fluorescence immunoblot, the membrane was incubated in Licor Odyssey anti-mouse antibody (680nm), diluted 1:5,000 in TBST

after which it was scanned using the Licor Odyssey scanner. A dot blot procedure, which is similar to the western blot was used to confirm the presence of the tagged proteins before determining the size.

Recombinant proteins (Flag-tagged) present in cell lysates were purified using anti-Flag® M2 affinity gel, anti-Flag® M2 magnetic and Myc Trap® magnetic bead chromatography (**Figure 82**). The flag-tag affinity column was thoroughly washed with 0.5 ml x1 wash buffer (x10 wash buffer (0.5M Tris-HCL, 1.5M Nacl) diluted 1:9 in deionized water) (Sigma Aldrich, UK) after which the column was packed with resin. The column was washed again with x1 wash buffer to allow equilibration and further loaded with three and five column volumes of elution buffer (0.1M Glycine) and x1 wash buffer respectively. Cell lysate containing flag-tagged proteins was passed through 1 ml anti-Flag® M2 affinity gel by gravity flow. This was repeated for BAP fusion protein (50 ng/µl), which served as the positive control for the procedure. The column was washed with 10 column volumes of x1 wash buffer after which the Flag-tagged proteins were eluted in six 1 ml fractions by acid elution (0.1M glycine-HCl) (pH 3.5) and further neutralised with Tris Buffered Saline (50mM Tris-HC, 150mM NaCl (pH 10.0)). Unsuccessful purification of proteins with the Flag-tagged affinity chromatography required the utilisation of the anti-Flag® M2 magnetic resin beads. The magnetic beads were gently re-suspended by inversion after which 50 µl was transferred into Eppendorf tubes. The tubes were securely held in a magnetic separator rack to collect the beads after which the storage buffer was discarded. Beads were washed with 10 packed gel volumes of Tris buffered saline buffer (TBS) after which the buffer was discarded. 500 µl of cell lysate, BAP fusion protein (50 ng/µl, diluted 1:25 in TBS) (positive control) and 1 ml TBS (negative control) were added to the beads. Samples were further incubated overnight at 4°C. The supernatant was removed, beads were

collected and were further washed with 20 packed gel volumes of TBS. FLAG-fusion and BAP recombinant proteins were eluted under acidic conditions with five packed gel volumes of 0.1M Glycine-HCl (pH 3.0). Aside acid elution bound recombinant proteins were also eluted with 2x SDS-PAGE sample buffer without DTT or 2-mercaptoethanol. After which samples were boiled for three minutes. Fractions containing expressed proteins were pooled, desalted, and concentrated against phosphate buffered saline (PBS). Myc Trap® magnetic beads (Chromotek, UK), which has the same immunoprecipitation procedure as the anti-Flag M2 magnetic bead, was employed to immunoprecipitate flag-tagged proteins in cell lysates. The beads were thoroughly vortexed and 25 µl of bead slurry was pipetted into 500 µl ice-cold dilution buffer. The mixture was centrifuged at 2500*g* for 2 minutes at 4^0C and supernatant was discarded. Beads were then washed twice with ice-cold dilution wash buffer. Cell lysate was added to the equilibrated magnetic beads and incubated for 1 hour at 4^0C after which the mixture was centrifuged at 2500 x *g* for 2 minutes at 4^0C. The supernatant was then discarded, and beads were washed twice in 500 µl ice-cold wash buffer. 100 µl of reconstituted Myc peptide (diluted to 100 µg/ml in dilution buffer) was added to magnetic beads in order to elute Myc-tagged proteins were eluted. The preparation was incubated for 15 minutes at room temperature and further centrifuged at 2500g for 2 minutes. Supernatants were carefully transferred into a new tube and this step was repeated to increase the elution efficiency. Alternatively, Myc Trap® magnetic beads were re-suspended in 100µl 2x SDS sample buffer after which re-suspended beads were heated for 10 minutes at 95°C to dissociate immunocomplexes from beads. Beads were then centrifuged, and supernatants were collected.

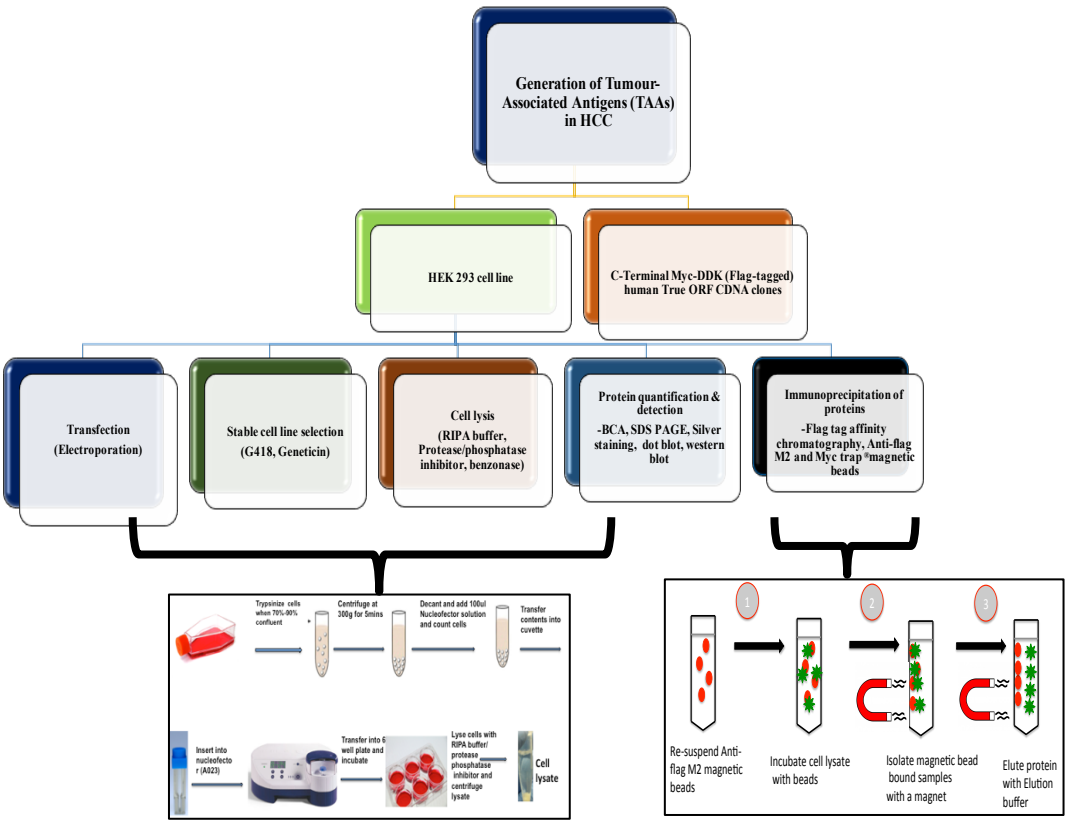


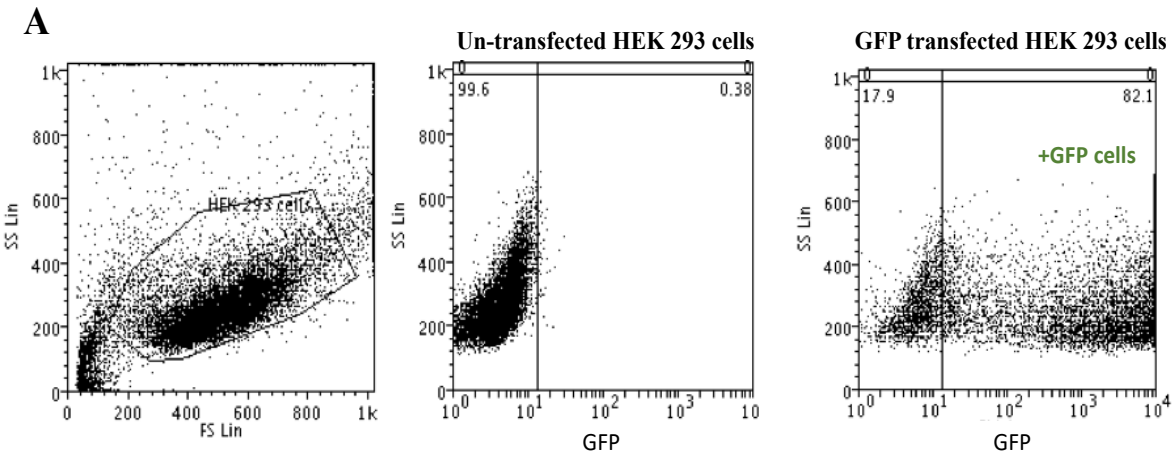
Figure 82: Outline of the procedures involved in the expression, detection and purification of Myc-DDK(Flag-tagged) recombinant tumour-associated antigens in HCC.

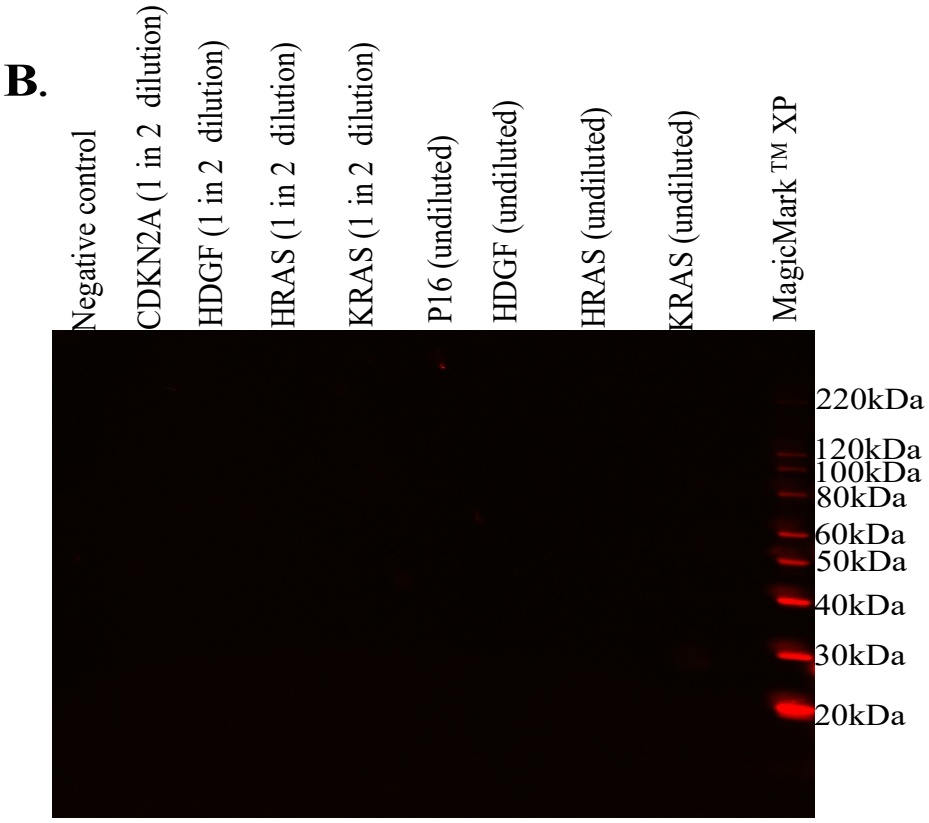
4.3 Results

4.3.1. Preliminary Expression of Recombinant Flag-tagged proteins in HEK 293 cells

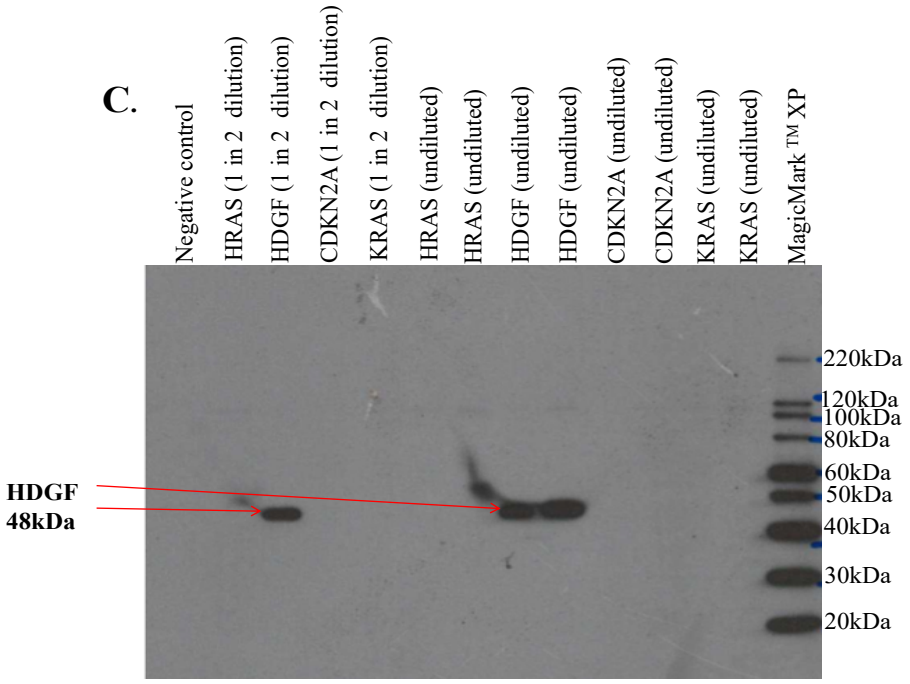
To produce a panel of recombinant proteins suitable for use on the antigen microarray system, an existing batch of HEK 293 cells in the laboratory, seeded at 1.0 x 10^6 cells per sample were each transfected with 2 μg of the Myc-DDK human cDNA ORF clones; KRAS, HRAS, HDGF, CDKN2A as well as a GFP plasmid as a positive control. A negative control omitting a plasmid or clone was also prepared. The transfection efficiency determined for GFP positive cells was 82.1% (**Figure 83A**). BCA assay carried out on cell lysates determined protein concentrations of 706 μg/ml, 930 μg/ml, 1160 μg/ml, 686 μg/ml and 101.307 μg/ml, for KRAS, HRAS, HDGF, CDKN2A and the negative control respectively at a wavelength of 562 nm. Cell lysates were further resolved by SDS-PAGE and the identity of Flag-tagged recombinant proteins was confirmed by western blot analysis using an anti-Flag antibody (**Figure 83 B-D**). Proteins expressed in the existing batch of HEK 293 cells yielded no immuno-reactive bands for all cell lysates (**Figure 83B**). Preliminary expression of Flag-tagged recombinant proteins confirmed that human ORF clones were not successfully transfected in the HEK 293 cells, hence proteins of interest were not detected. Consequently, a new batch of HEK 293 cell line was used for the in vitro expression of the Myc-DDK human TrueORF clones using the same procedure. Chemiluminiscence western blot analysis carried out on recombinant proteins expressed in these new batch of cells produced strong immuno-reactive bands of 48 kDa for the different dilution of HDGF protein (**Figure 83C**). However, no bands were seen for the KRAS, HRAS and CDKN2A. A similar pattern of band strength of 48 kDa was observed for HDGF using

a fluorescent western blot and as such no bands were seen for KRAS, HRAS and CDKN2A (**Figure 83D**).





C.


Negative control
HRAS (1 in 2 dilution)
HDGF (1 in 2 dilution)
CDKN2A (1 in 2 dilution)
KRAS (1 in 2 dilution)
HRAS (undiluted)
HRAS (undiluted)
HDGF (undiluted)
HDGF (undiluted)
CDKN2A (undiluted)
CDKN2A (undiluted)
KRAS (undiluted)
KRAS (undiluted)
MagicMark ™ XP
220kDa
120kDa
100kDa
80kDa
60kDa
50kDa
40kDa
30kDa
20kDa
HDGF
48kDa

D.

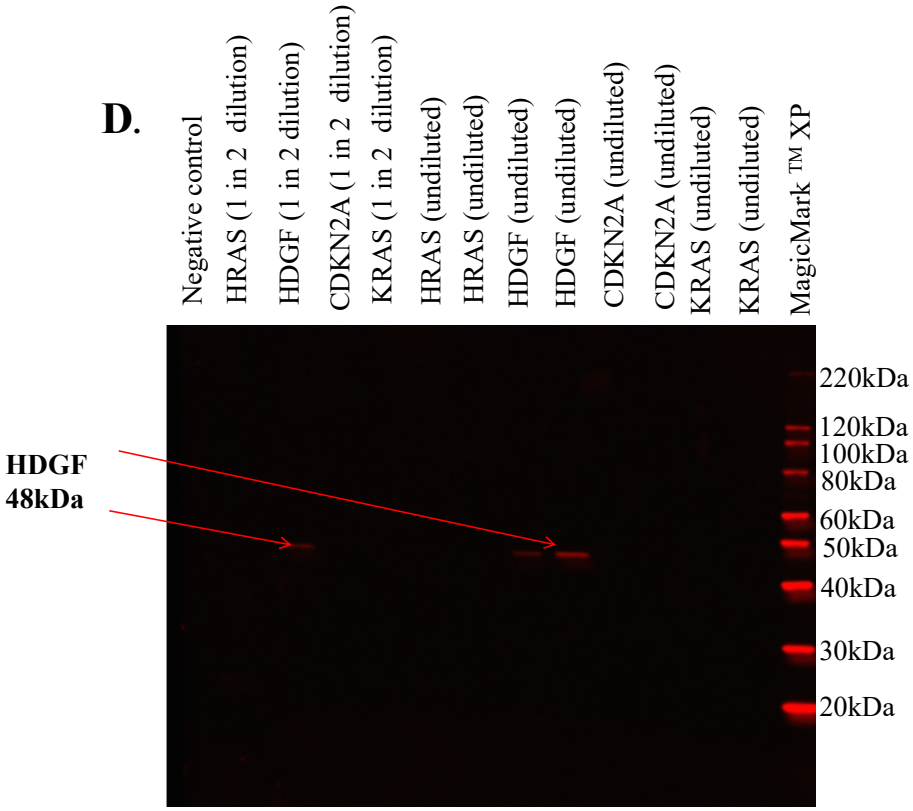

Negative control
HRAS (1 in 2 dilution)
HDGF (1 in 2 dilution)
CDKN2A (1 in 2 dilution)
KRAS (1 in 2 dilution)
HRAS (undiluted)
HRAS (undiluted)
HDGF (undiluted)
HDGF (undiluted)
CDKN2A (undiluted)
CDKN2A (undiluted)
KRAS (undiluted)
KRAS (undiluted)
MagicMark ™ XP
220kDa
120kDa
100kDa
80kDa
60kDa
50kDa
40kDa
30kDa
20kDa
HDGF
48kDa

Figure 83: Preliminary expression of Flag-tagged recombinant proteins in HEK 293 cells. Old and new batch of HEK 293 cells seeded at a density of $1.0x10^6$ cells/ml were transfected with 2 μg of four Myc-DDK human ORF cDNA clones (KRAS, HRAS, HDGF, CDKN2A) and a GFP plasmid using nucleofector solution kit V. **(A)** shows the transfection efficiency of GFP positive cells using the FC500, 48 hours post-transfection. Resistant cells (cells successfully transfected with cDNA clones) were allowed to be stably selected over a period of 7 days with G418. Cells were then lysed using RIPA buffer and recombinant proteins present in lysates were further detected by western blot using an anti-Flag antibody. **(B)** Shows a Fluorescent Western Blot analysis on cell lysates prepared from the batch of HEK 293 cells, **(C)** and **(D)** represent the chemiluminiscence and fluorescent immunoblot of cell lysates prepared from the new batch HEK 293 cells revealing strong immunoreactive bands of HDGF protein. An arrow indicates the location of the HDGF protein at different dilutions. Molecular mass standards (M) are given in kilodaltons. MagicMark™ XP (ThermoFisher Scientific, Cat no LC5602, 20-220kDa) was used as a molecular weight marker to help indicate molecular size of protein bands.

4.3.2 In Vitro expression of KRAS, HRAS and CDKN2A proteins in HEK 293 Cell Extracts

Previous experiments showed unsuccessful expression of KRAS, HRAS and CDKN2A recombinant proteins despite the utilisation of a new batch of HEK 293 cell line. Some studies had indicated that proteins with predicted low molecular weight such as KRAS, HRAS and CDKN2A require up to 5-7 days of expression in their expression system before stable selection with G418 instead of 48 hours which was done previously. The transfection procedure was repeated, and expression of recombinant proteins were left up to a week before selecting resistant cells with the required antibiotic. Proteins in lysates were resolved and detected with SDS-PAGE and western blot. Low molecular weight run through membranes with pores 0.45 μm during the protein transfer process and hence nitrocellulose membrane (0.2 μm) was selected for the immunoblot of proteins instead of 0.45 μm used initially. Immunoblot analysis of cell lysates probed with anti-flag antibody repeatedly yielded no immunoreactive bands for KRAS, HRAS and CDKN2A, while strong 48 kDa bands were detected again for HDGF (**Figure 84**).

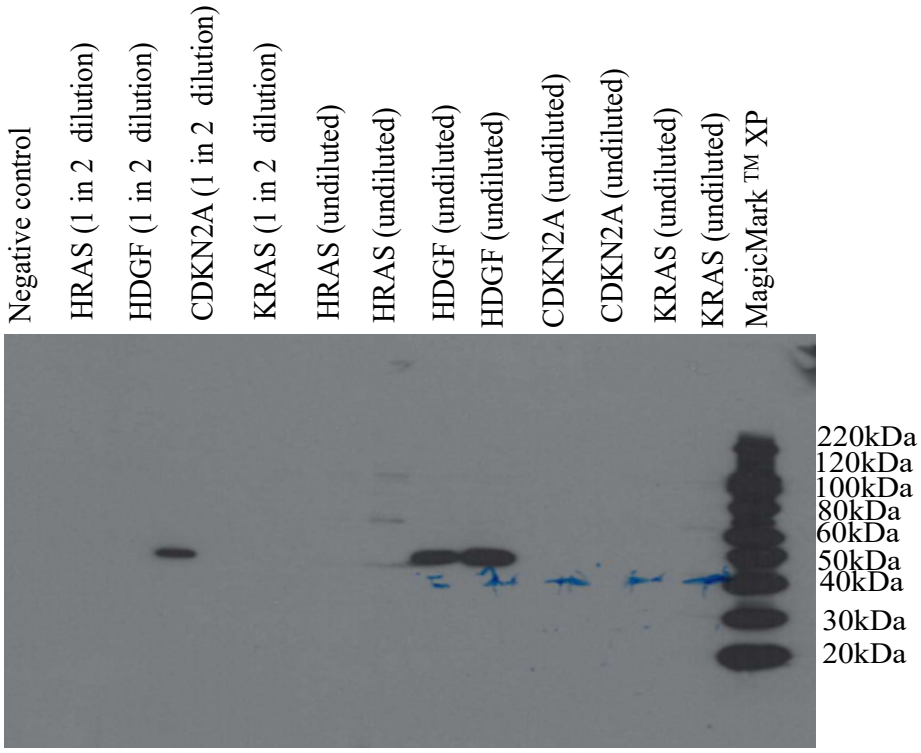


Figure 84: Analysis of recombinant HDGF over-expression with anti-Flag antibody. HEK 293 cell lysates resulting from transfection with 2 µg of four Myc-DDK human ORF cDNA clones (KRAS, HRAS, HDGF, CDKN2A) and further selection of resistant cells with G418, fractionated cells resolved on 4-20% SDS-PAGE and analysed by western blotting using anti-Flag antibody only detected HDGF. MagicMark™ XP (ThermoFisher Scientific, Cat no LC5602, 20-220kDa) was used as a molecular weight marker to help indicate molecular size of protein bands.

4.3.3. Recombinant Flag-tagged Protein Detection by Dot Blot Analysis.

Despite using a new HEK 293 cell line, allowing longer expression of proteins and using a nitrocellulose membrane of pore size 0.2 µm, immunoreactive bands for the three proteins (KRAS, HRAS and CDKN2A) were not detected. As such, the transfection procedure was repeated using a higher concentration of cDNA clone. HEK 293 cells seeded at 1.0 x 10^6 cells were transfected with 3 µg of four Myc-DDK human

cDNA ORF clones (KRAS, HRAS, HDGF and CDKN2A) per sample. Proteins were left for expression for 7 days after which resistant cells for each clone were selected with 1mg/ml Geneticin (G418) over a period of 14 days. Cells were lysed, after which 2 µl of each cell lysate, positive control BAP fusion protein and a negative control (HEK 293 transfected with empty vector) were spotted unto nitrocellulose membrane and allowed to dry for an hour at room temperature. Flag-tagged proteins were confirmed by incubating membrane with anti-Flag antibody overnight at 4°C and anti-mouse goat HRP for an hour at room temperature. Immunoblot analysis produced strong immuno-reactive spots for KRAS, HRAS, HDGF, CDKN2A and positive control (BAP fusion protein). (**Figure 85**).

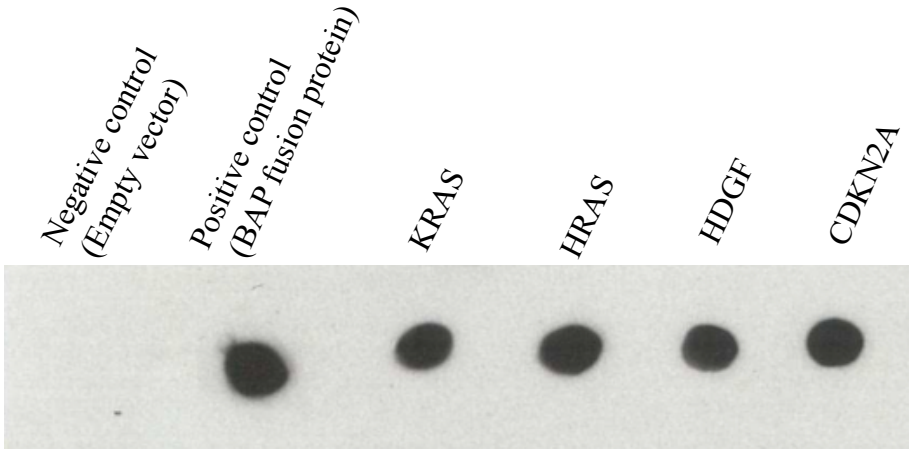


Figure 85: Dot blot analysis of KRAS, HRAS, HDGF and CDKN2A overexpressed in HEK 293 cells. HEK 293 cells seeded at a density of $1.0x10^6$ cells/ml were transfected with 3 µg of four Myc-DDK human ORF cDNA clones (KRAS, HRAS, HDGF, CDKN2A) and a GFP plasmid using nucleofector solution kit V. A negative control excluding the plasmid was included. Protein expression was allowed up to a period of one week until resistant cells were stably selected over 14 days with G418. Lysates were then prepared from stably selected cells. 2 µl of each of the four cell lysates, positive control (BAP fusion protein), a negative control (HEK 293 transfected with empty vector), were spotted unto 0.2 µm nitrocellulose membrane and allowed to dry for an hour at room temperature. Flag-tagged proteins were confirmed by incubating nitrocellulose membrane with anti-Flag antibody overnight at 4°C and polyclonal goat anti-mouse HRP for an hour and developed using Amersham HyperfilmTM ECLTM high performance chemiluminescence film in the dark. Bands were observed on the positive control spots as well as the four-experimental Flag tagged TAAs with the exception of the negative control.

4.3.4 Affinity Pull-Down of Flag-tagged Recombinant Proteins Using Anti-FLAG® M2 Affinity Gel.

Due to unsuccessful detection of Flag-tagged recombinant proteins with western blot analysis, an immunoprecipitation of these proteins (KRAS, HRAS, HDGF, CDKN2A) was carried out from the filtered cell lysate under native conditions using anti-Flag M2 affinity gel. This was conducted as a preliminary experiment to test the efficacy of the purification kit (Sigma Aldrich, UK). The flow through, wash and elution fractions were pooled, filtered, and concentrated to 50 µl. Samples were blotted unto nitrocellulose membrane and incubated with anti-Flag antibody. Dot blot of the elution fractions as well as the positive control BAP fusion protein revealed no immunoreactive spot for proteins. However, strong immunoreactive spots of Flag-tagged proteins were detected in the flow through and wash fractions. This indicates that the Flag-tagged proteins were loosely bound to the agarose beads (**Figure 86**).

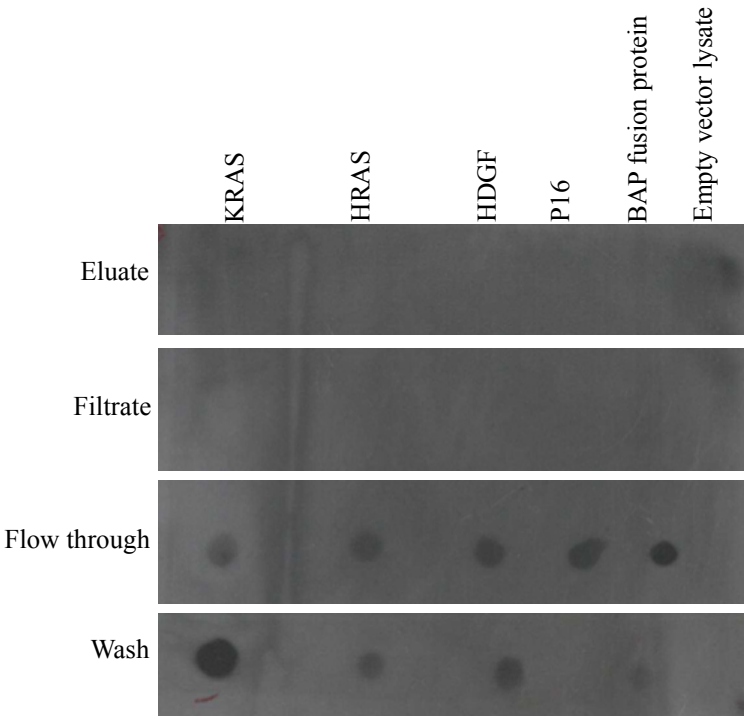


Figure 86: Dot blot analysis of the elution, filtrate, flow through and wash fractions of Flag-tagged recombinant proteins after purification with Anti-Flag® M2 affinity gel.

4.3.5 Purification of Flag-Tagged Recombinant Proteins using Anti-Flag® M2 Magnetic Beads

Native elution of recombinant proteins from anti-Flag® M2 magnetic beads allow the identification of proteins as well as functional analysis using biochemical activity assays. The purification of flag-tagged proteins (KRAS, HRAS, HDGF, CDKN2A) was carried out on filtered cell lysates under native conditions using these magnetic beads. The flow through, wash and elution fractions were pooled, filtered, and concentrated to 50µl by ultracentrifugation after which samples were blotted unto nitrocellulose membrane and further incubated with an anti-Flag antibody. A dot blot analysis revealed strong immunoreactive spots for flow through portions, with weak immunoreactive spots detected with the elution fractions for all recombinant proteins (**Figure 87A**). Due to major technical difficulties encountered with the magnetic beads, the procedure was optimised to ensure successful purification of proteins from cell lysates. Thus, the pH of wash and elution buffers, volume of packed beads and cell lysates were optimised. The optimal pH for wash and elution buffer was 7.4 and 3.0 respectively while the packed gel volume of beads was increased from 50 µl to 200 µl to increase the binding of proteins to magnetic beads. Consequently, another purification procedure on cell lysates was undertaken after which a BCA assay determined protein concentrations of 118 µg/ml, 96 µg/ml, 101 µg/ml, 103 µg/ml, 80 µg/ml for positive control (BAP fusion protein), KRAS, HRAS, HDGF and CDKN2A respectively. An immunoblot analysis conducted on elution fractions showed strong immunoreactive spots for the respective elution fractions for positive control BAP fusion protein, KRAS, HRAS, HDGF and CDKN2A (**Figure 87B**).

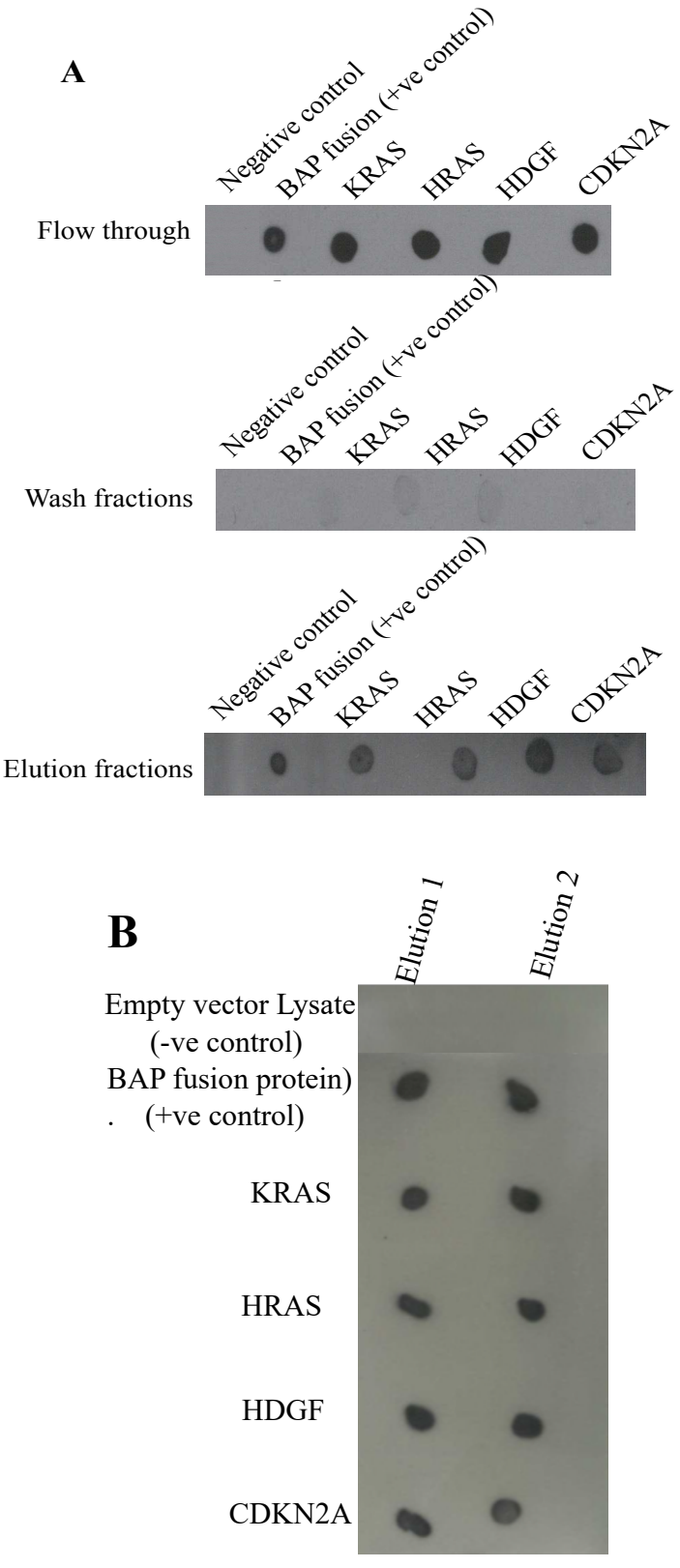
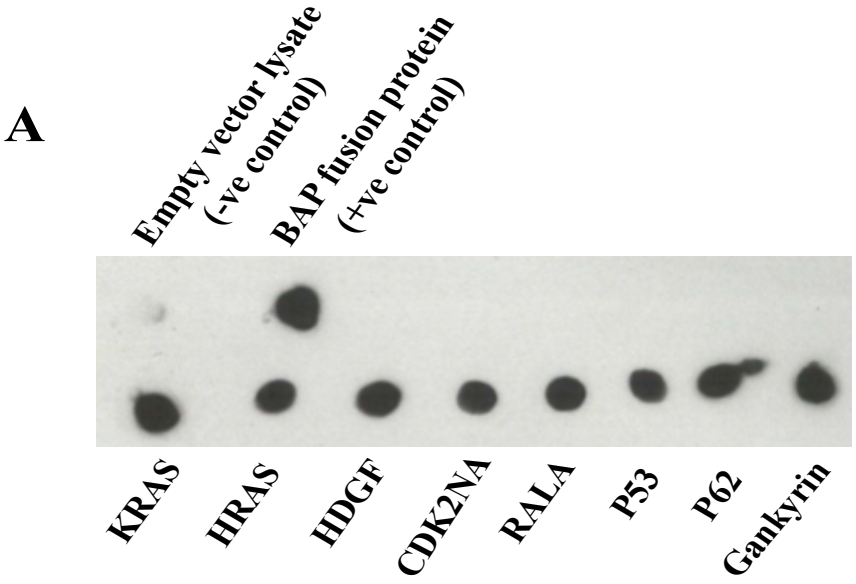
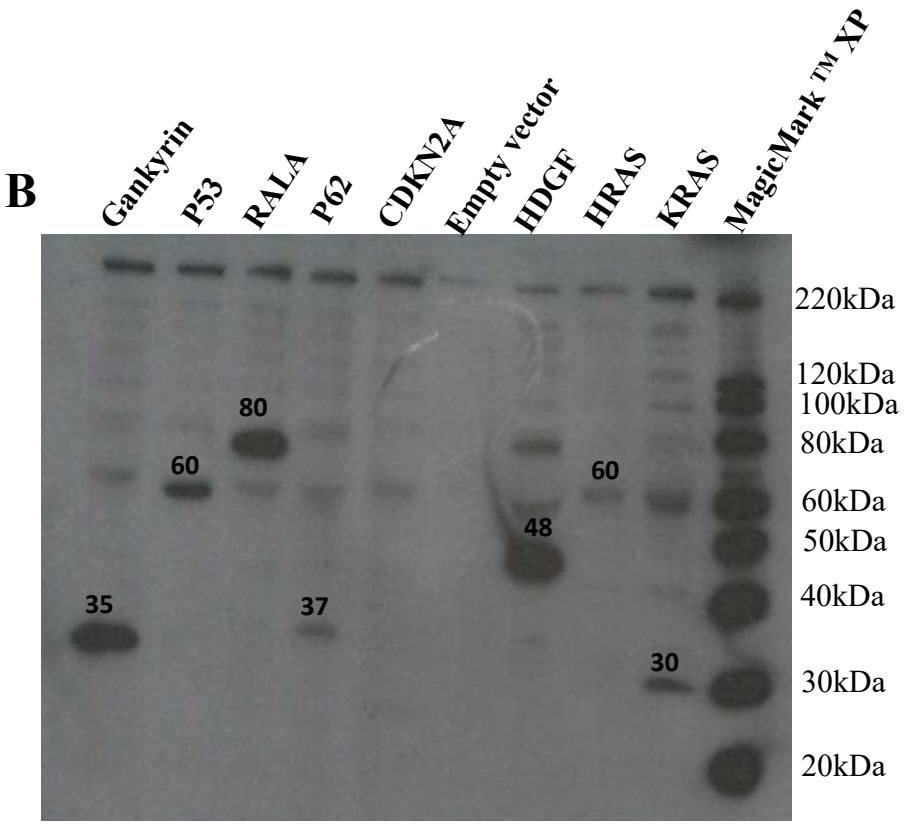


Figure 87: Anti-Flag® M2 magnetic bead purification of flag-tagged proteins from HEK 293 cell lysates. Flag-tagged recombinant proteins were purified from filtered cell lysates under native conditions. **(A)** shows the dot blot analysis of flag-tagged proteins in flow through and the elution fractions after purification **(B)** represents the dot blot of all elution fractions after optimisation of the purification procedure.

4.3.6 Analysis of the expression of eight Recombinant Flag-tagged proteins with an Anti-Flag antibody.

HEK 293 cells were transfected with four newly purchased Myc-DDK tagged CDNA clones (RALA, P53, P62 and Gankyrin) together with KRAS, HRAS, HDGF, CDKN2A and GFP cDNA clones. BCA assay carried out on cell lysates determined protein concentrations of 1275µg/ml, 518 µg/ml, 1751 µg/ml, 659 µg/ml, 733 µg/ml, 708 µg/ml, 855 µg/ml, 1552 µg/ml and 102 µg/ml for KRAS, HRAS, HDGF, CDKN2A, RAL A, P53, P62, Gankyrin and the negative control respectively at wavelength of 562 nm. Dot blot analysis was carried out on cell lysates as a preliminary experiment to determine the presence of Flag-tagged proteins (**Figure 88A**). A western blot analysis showed highly induced immunoreactive bands of 30kDa, 35kDa, 80kDa, 48kDa, 60kDa, 60kDa, and 37kDa for KRAS, Gankyrin, RALA, HDGF, P53, HRAS, and P62 respectively (**Figure 88B**). These corresponded to the expected band size for each recombinant protein and band strengths correlated with protein concentrations of each sample. However, a very faint band was seen with respect to the CDKN2A protein and the negative sample produced no bands. CDKN2A has a very low molecular weight (25kDa) and could not be detected appropriately since a lower Tris Glycine SDS precast gel (4%-20%) was used. Consequently, samples were run on a higher Tris Glycine SDS precast gel percentage (10%-20%). In this regard, a strong band of 25kDa was detected for P16 (**Figure 88C**). Molecular sizes of the recombinant Flag-tagged recombinant proteins were compared with that of the manufacturers sheet (**Figure 88D**).


A
Empty vector lysate (-ve control)
BAP fusion protein (+ve control)
KRAS
HRAS
HDGF
CDK2NA
RALA
P53
P62
Gankyrin


B
Gankyrin
P53
RALA
P62
CDKN2A
Empty vector
HDGF
HRAS
KRAS
MagicMark ™ XP
220kDa
120kDa
100kDa
80kDa
60kDa
50kDa
40kDa
30kDa
20kDa
80
60
60
48
35
37
30

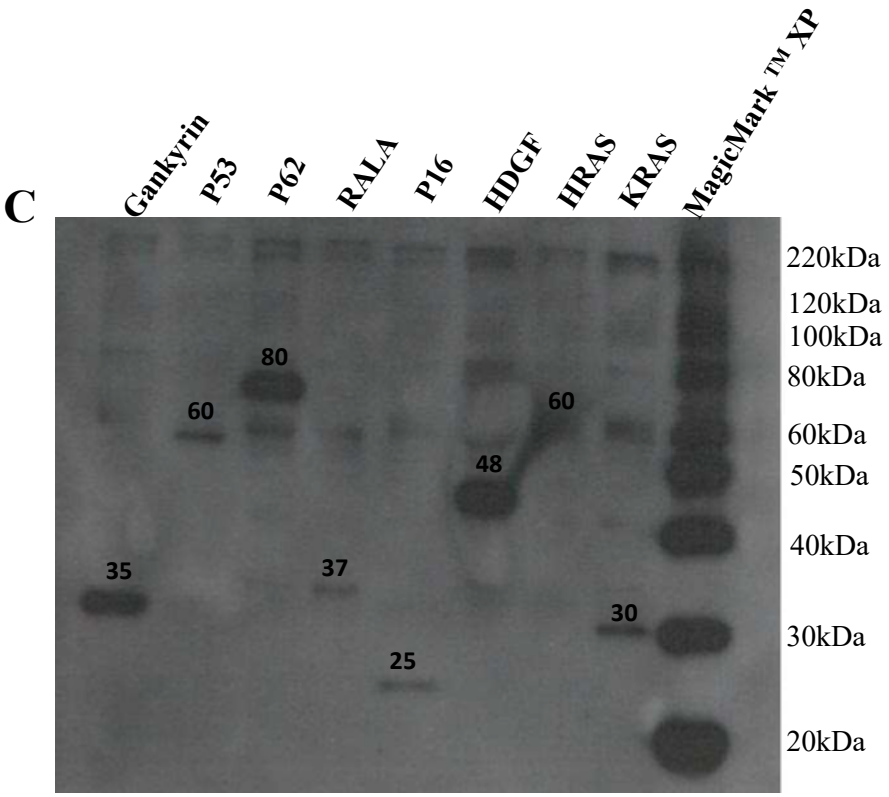
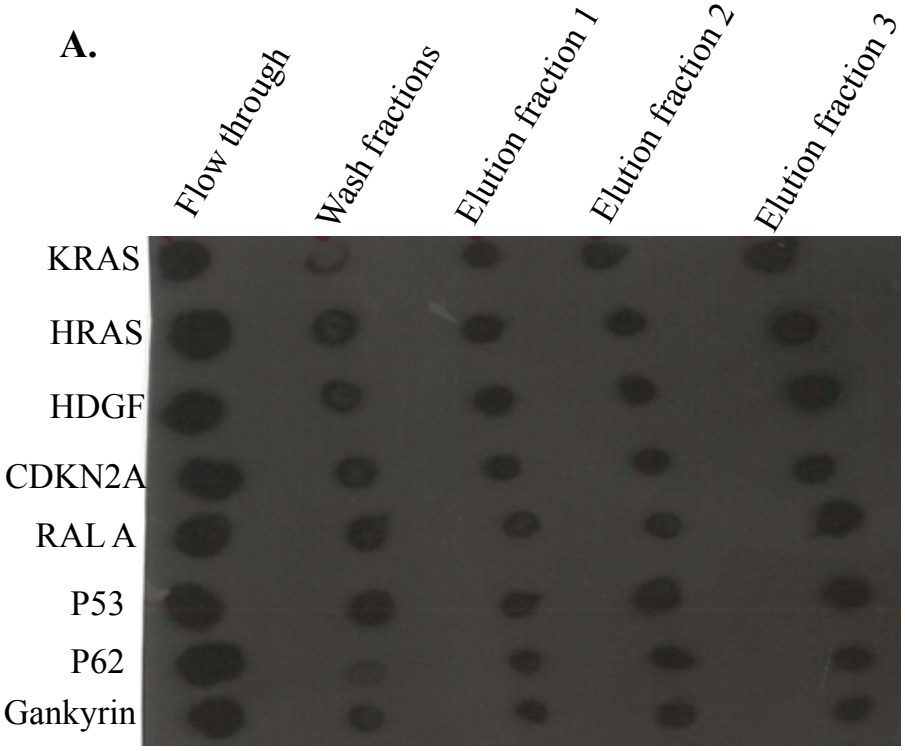


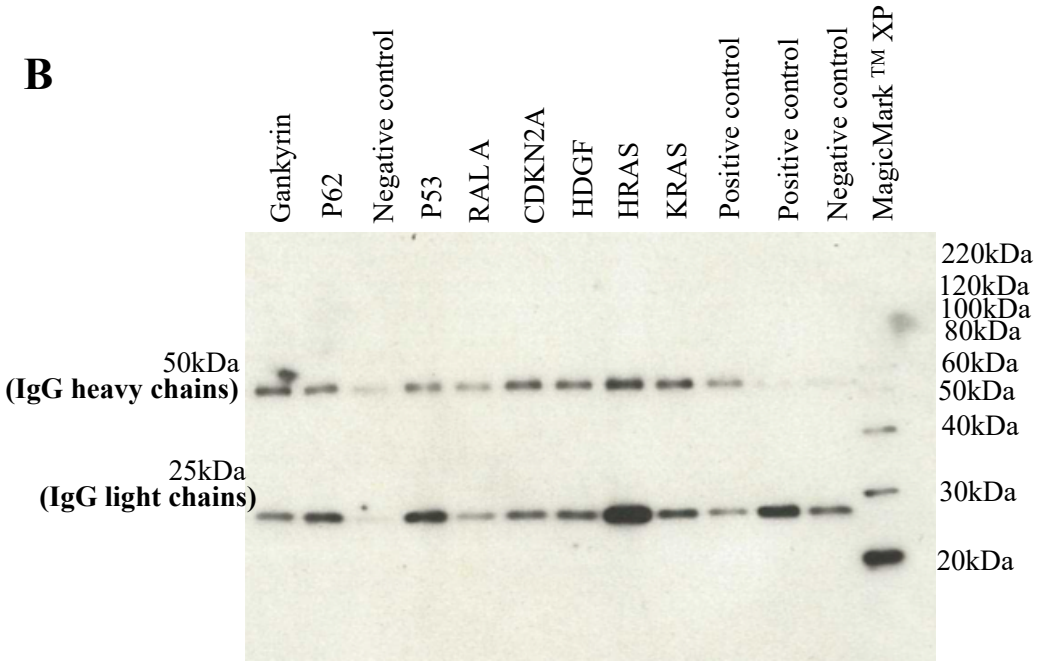
Figure 88: Analysis of the expression of eight recombinant Flag-tagged proteins with anti-Flag antibody. HEK 293 cell lysates expressing eight recombinant flag-tagged proteins were fractionated by 4-20% SDS-PAGE, **(A)** Dot blot analysis of recombinant flag-tagged proteins in cell lysates. **(B)** Western blot analysis of cell lysates showing strong immunoreactive bands for seven recombinant proteins KRAS, HRAS, HDGF, RALA, P62, P53 and Gankyrin with the exception of CDKN2A at their expected band sizes, when 4%-20% Tris glycine gel was used for resolving proteins **(C)** Shows strong immunoreactive bands for all proteins using 10%-20% Tris glycine gel. MagicMark™ XP (ThermoFisher Scientific, Cat no LC5602, 20-220kDa) was used as a molecular weight marker to help indicate molecular size of protein bands.

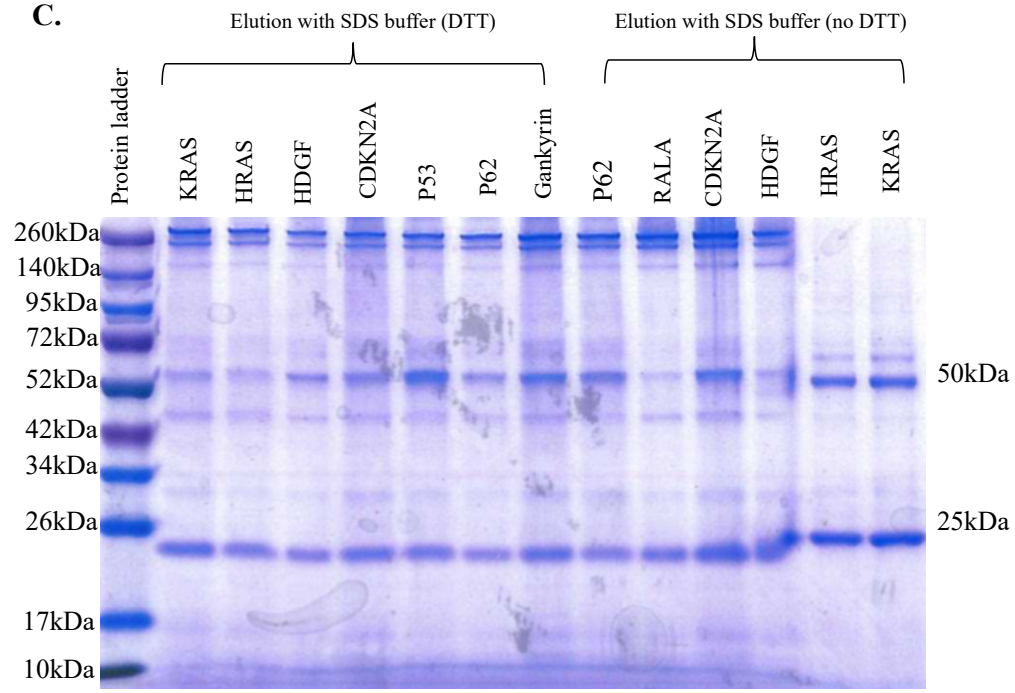
4.3.7 Purification of Flag-tagged Recombinant proteins from HEK 293 cells transfected with Eight Myc-DDK cDNA clones

On successful detection of eight recombinant proteins expressed in HEK 293 cells, a one-step purification of eight Flag-tagged recombinant proteins, KRAS, HRAS, HDGF, CDK2NA, RALA, P62, P53 and Gankyrin proteins was carried out using a newly purchased anti-Flag® M2 Magnetic bead kit under native conditions as described in the Materials and Methods section. A dot blot analysis was subsequently undertaken on the flow, wash and elution fractions to determine the presence of Flag-tagged proteins eluted from the beads. **Figure 89A** illustrates some degree of purification, as strong immunoreactive spots were detected in the flow through as compared to different elution fractions **(Figure 89A)**. Evidently, Flag-tagged proteins were lost through the wash procedure **(Figure 89A)**. A western blot analysis was done on pooled elution fractions to determine the identity of proteins of interest in purified samples. Surprisingly, none of the proteins of interest in any of the purified samples produced a band, as western blot produced a low background with bands of antibody heavy (50kDa) and light chains (25kDa) detected (**Figure 89B**). To effectively obtain clean and specific western blot signals of target proteins to circumvent this problem, a variety of strategies were devised. The purification procedure was repeated with reduced volume of cell lysates (300 µl), increased volume of magnetic beads (200 µl) and a reduced volume of wash buffer (50 µl) per wash. Moreover, other methods of elution provided by the manufacturer were tested; addition of SDS sample buffer (with and without a reducing agent) to beads incubated with cell lysates, after which immunoprecipitated IP beads were heated, supernatant collected and further resolved by SDS-PAGE. (**Figure 89C**) and western blot analysis (**Figure 89D**) still revealed contaminating signals from the heavy or light chain immunoglobulins. Hence, cell

lysates containing KRAS, HRAS, HDGF, CDKN2A and RAL A were denatured with SDS buffer and heated before the purification process was initiated. A western blot analysis revealed bands of the respective Flag-tagged proteins as well as the heavy and light chains of Flag-tagged antibody bound to the magnetic beads in the flow through fractions (**Figure 89E**). On the other hand, proteins of interest were undetected in either the wash or elution fractions.




B
Gankyrin
P62
Negative control
P53
RALA
CDKN2A
HDGF
HRAS
KRAS
Positive control
Positive control
Negative control
MagicMark ™ XP
220kDa
120kDa
100kDa
80kDa
60kDa
50kDa
40kDa
30kDa
20kDa
50kDa
(IgG heavy chains)
25kDa
(IgG light chains)


C.
Elution with SDS buffer (DTT)
Elution with SDS buffer (no DTT)
Protein ladder
KRAS
HRAS
HDGF
CDKN2A
P53
P62
Gankyrin
P62
RALA
CDKN2A
HDGF
HRAS
KRAS
260kDa
140kDa
95kDa
72kDa
52kDa
42kDa
34kDa
26kDa
17kDa
10kDa
50kDa
25kDa

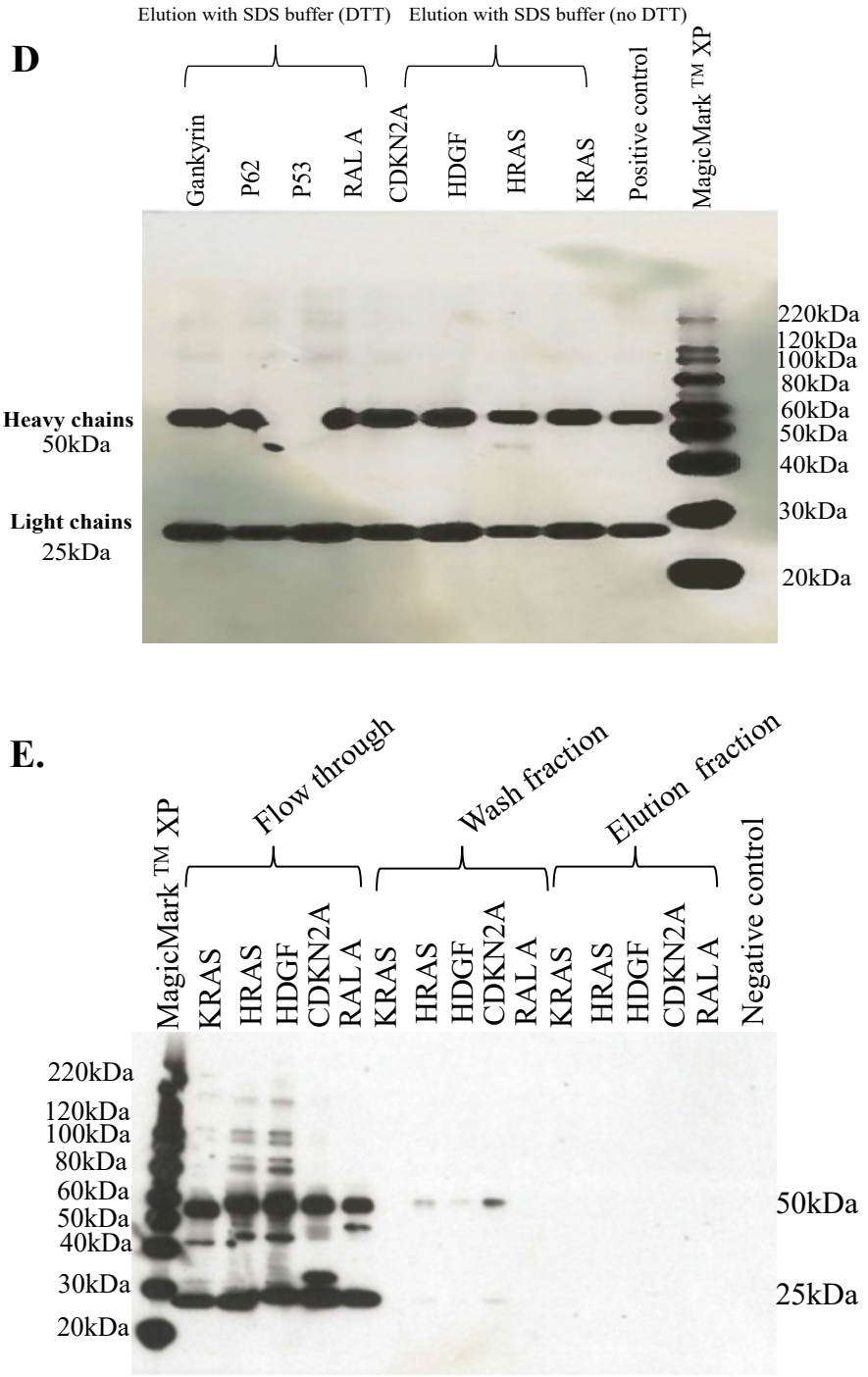


Figure 89: Affinity Purification of Flag-tagged Recombinant proteins from HEK 293 cell lysates on anti-FLAG M2 magnetic bead chromatography. Following immunoprecipitation of HEK 293 cell lysates, the presence of Flag-tagged proteins in purification products (flow through, wash and elution fractions) were identified with an anti-Flag antibody by either **(A)** dotting them directly onto nitrocellulose membranes, which shows strong immunoreactive spots of all Flag-tagged proteins in the flow through as compared to the wash and elution fractions, (**B**) western blot to detect purified products after magnetic bead immunoprecipitation (**C) and (D)** protein stained gel and western blot to detect purified proteins eluted with SDS sample with or without a reducing agent **(C)** or probed with an anti-Flag antibody **(D)** while **(E)** shows the western blot affinity purification of denatured proteins in cell lysates. MagicMark™ XP (ThermoFisher Scientific, Cat no LC5602, 20-220kDa) was used as a molecular weight marker to help indicate molecular size of protein bands in figures B, D and E, while Spectra Multicolour Broad range protein ladder (ThermoFisher Scientific, Cat no 26634, 10-260 kDa) was used for figure C.

4.3.8 Detection of HCC recombinant TAAs in Cell Lysates using Anti-Myc and Antigen specific antibodies (anti-KRAS and anti-P53)

The validity of anti-Flag antibody utilised in previous experiments were determined using an anti-Myc antibody and other antigen specific antibodies; anti-KRAS and anti-P53. An immunoblot analysis was undertaken on lysate over-expressing HDGF protein using an anti-Myc antibody at a dilution of 1:500 and 1:1000 goat anti-mouse HRP in 5% TBST milk respectively. A strong immunoreactive band of HDGF at the expected size (48kDa) was detected with anti-Myc antibody (**Figure 90A**). P53 protein expressed in lysate at the expected size (60kDa) was best detected with an anti-P53 antibody and goat anti-mouse HRP at a dilution of 1:50 and 1:500 in 5% milk TBST respectively, after several optimisations were undertaken to determine the optimal dilution of primary and secondary antibodies (**Figure 90B**). Many attempts were made to detect KRAS in lysates with anti-KRAS antibody. However, the optimal anti-KRAS and goat anti-mouse HRP antibodies to effectively identify KRAS at the right band size was 1:300 and 1:500 in 5% milk TBST respectively (**Figure 90C-D**).

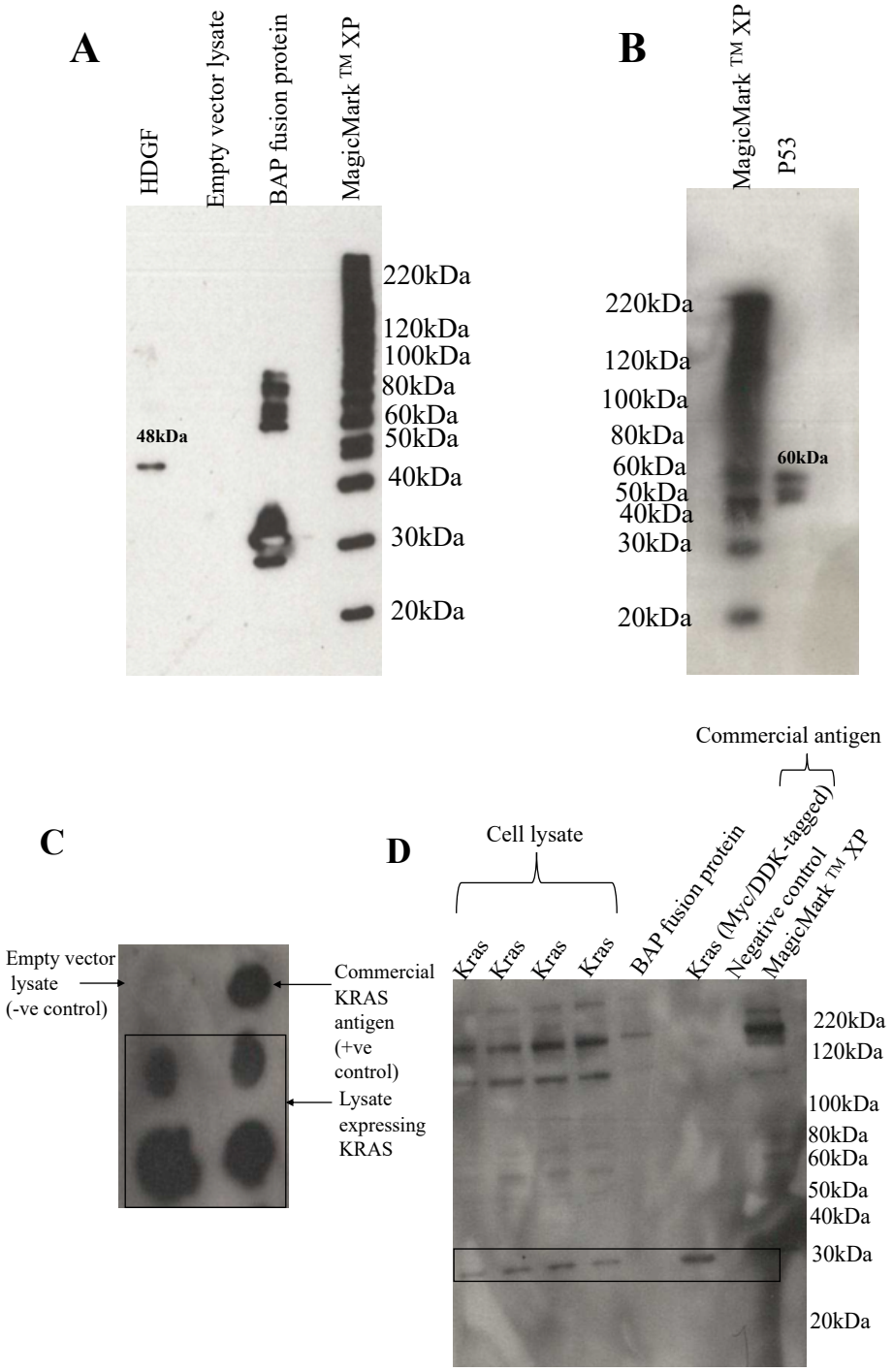


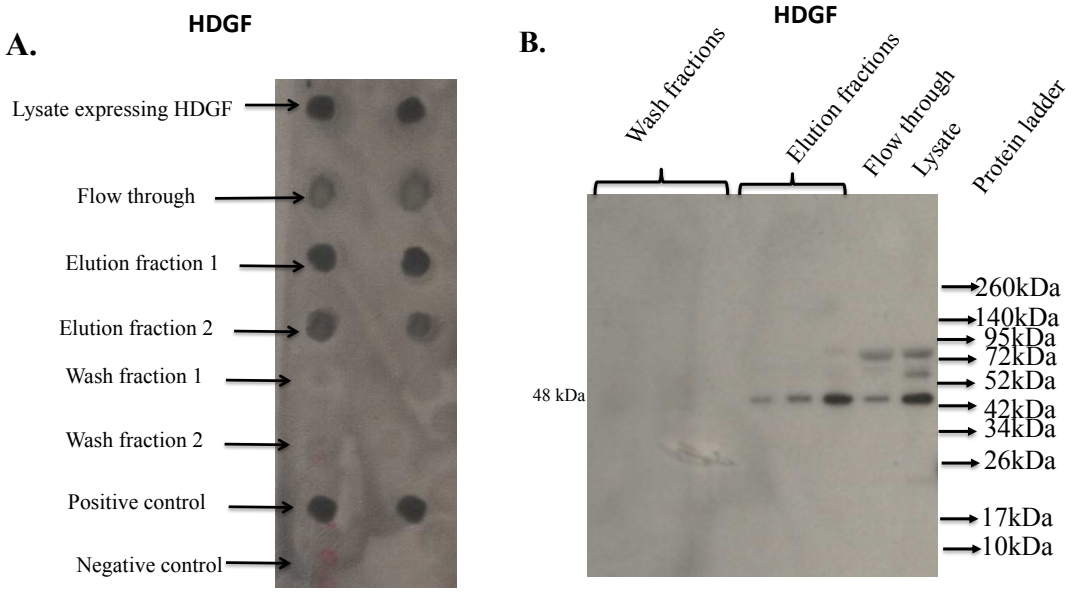
Figure 90: Recombinant HCC TAAs in lysates detected by anti-Myc, anti-P53 and anti-KRAS antibodies. Cell lysates expressing HDGF, P53 and KRAS were detected at their expected band sizes (48kDa, 60kDa and 30kDa respectively) using **(A)** anti-Myc antibody at an optimal dilution of 1:500 in 5% milk TBST **(B)** anti-P53 antibody at an optimal dilution of 1:50 in 5% milk TBST, **(C)(D)** anti-KRAS antibody at an optimal dilution of 1:300 in 5% milk TBST. Lysates prepared from HEK cells transfected with an empty vector were used as a negative control in all blots while BAP fusion protein and commercial Myc/DDK tagged KRAS antigen were used as positive controls in **(A), (C) or (D)**.

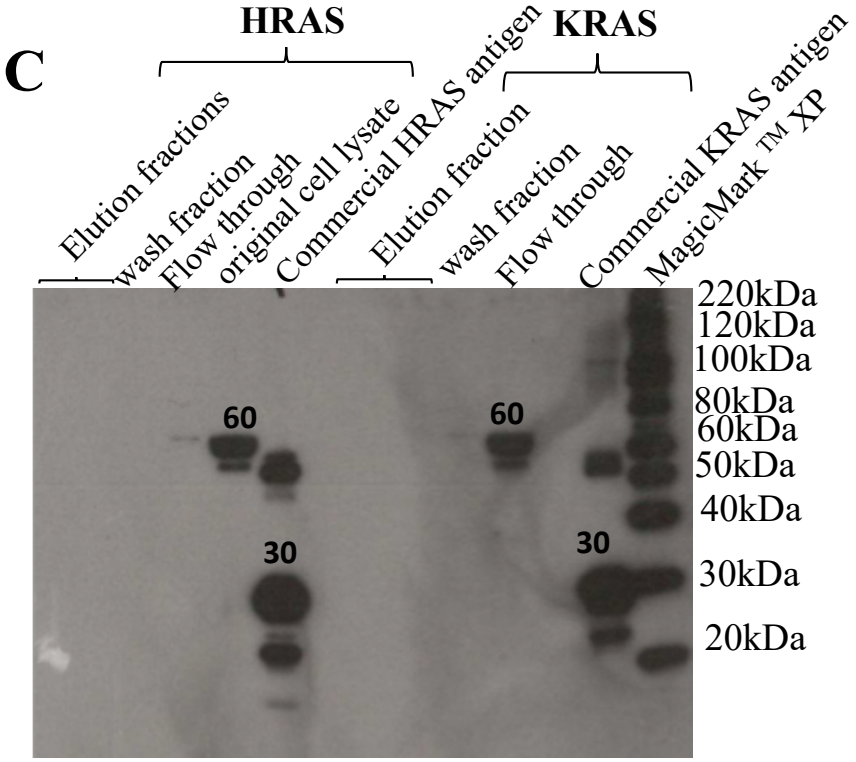
MagicMark™ XP (ThermoFisher Scientific, Cat no LC5602, 20-220kDa) was used as a molecular weight marker to help indicate molecular size of protein bands.

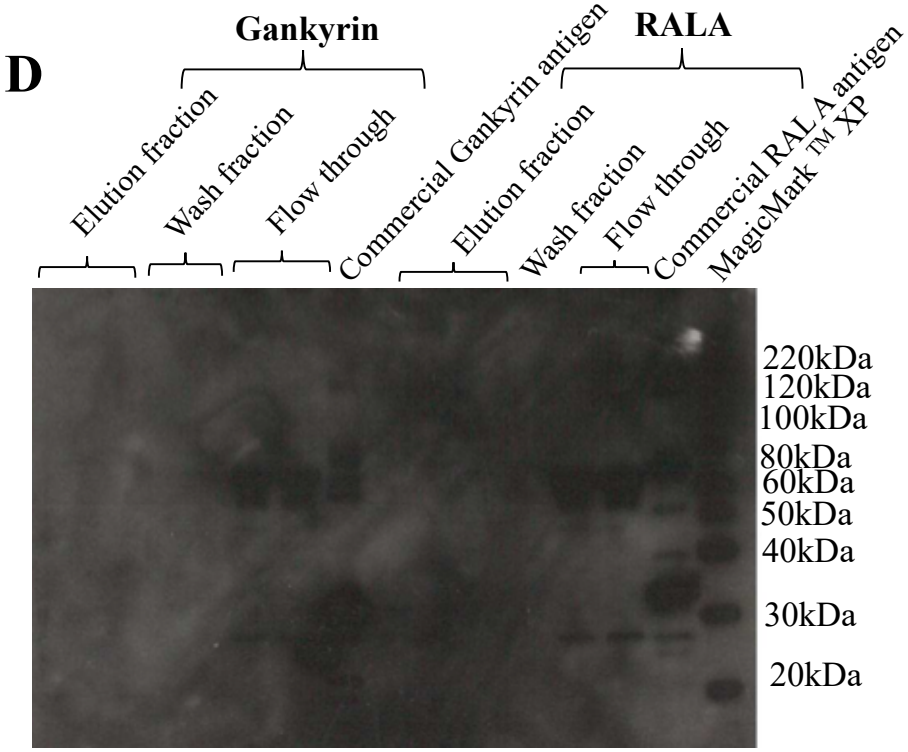
4.3.9 Purification of Myc-DDK tagged proteins using Myc®Trap MA Magnetic Beads

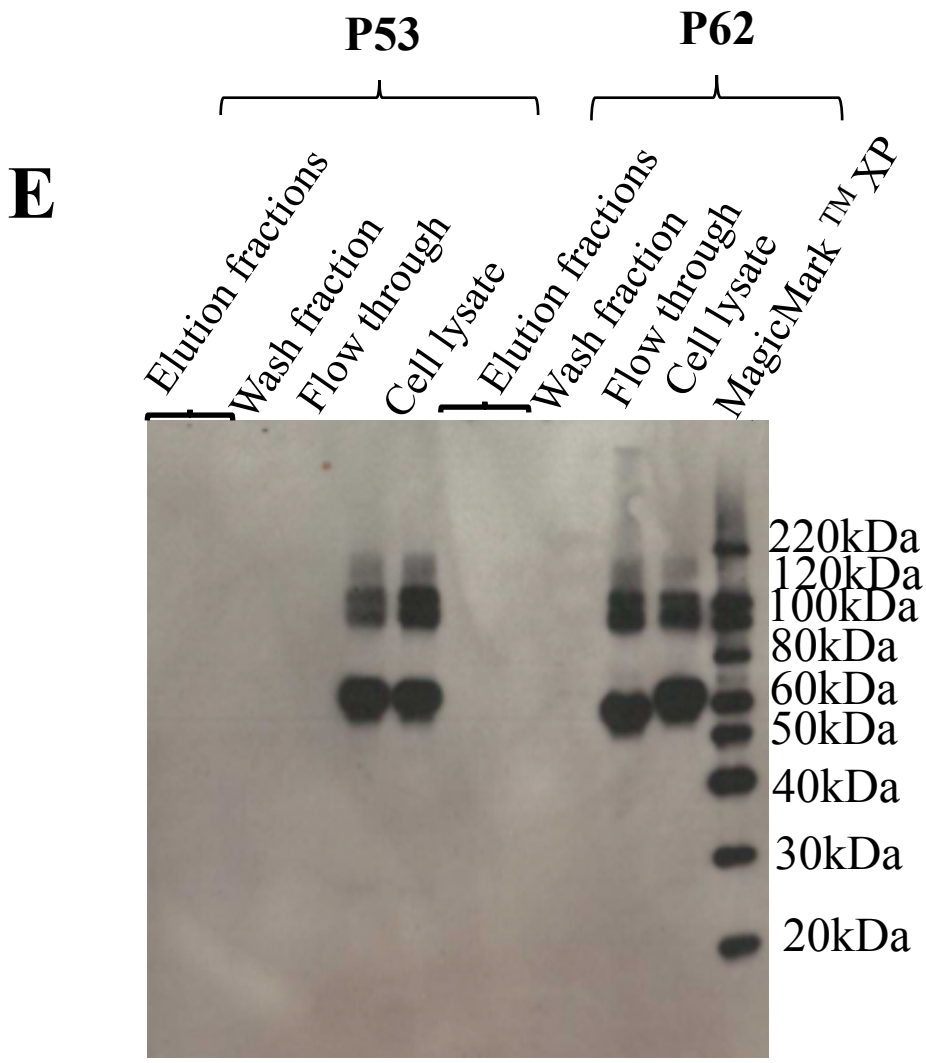
After several efforts channelled to purifying recombinant proteins from cell lysates proved futile, the Myc®Trap MA kit was employed as an alternative to obtaining recombinant proteins in purified forms since proteins were Myc-DDK tagged. A preliminary purification was undertaken using lysates expressing HDGF where 200 µl of cell lysate was incubated with 50 µl of thoroughly washed Myc Trap bead slurry for an hour at 4°C. Beads were washed with 500 µl of ice-cold wash buffer after which recombinant proteins bound to the Myc Trap beads were efficiently pulled using a Myc peptide. Dot blot analysis carried on the original cell lysate, flow through, wash and elution fractions showed strong immunoreactivity of HDGF in elution fractions with weak and no immunoreactive blots of the protein seen in the flow through and wash fractions respectively (**Figure 91A**). This shows that the purification of HDGF was successful using this immunoprecipitation procedure. This was subsequently followed by conducting western blot on the elution fractions and the expected band size of HDGF was achieved (**Figure 91B**). This attainment led to the immunoprecipitation of consequent lysates containing recombinant proteins (KRAS, HRAS, RALA and Gankyrin, P53, P62) using the Myc Trap MA kit. With regards to purification of HRAS and KRAS from lysates, proteins of interest were present in the flow through which existed as dimers and elution fractions did not show immunoreactive bands for both proteins (**Figure 91C**). This same outcome was achieved in during the purification of RALA and Gankyrin (**Figure 91D**) as well as P53 and P62 (**Figure 91E**). This shows that the Myc Trap kit was ineffective for immunoprecipitation of recombinant proteins

except for HDGF. It was realised that most of the proteins of interest were usually detected in the flow through fraction as dimers and it was anticipated that the dilution/wash buffer (10mM Tris/CL pH 7.5; 150Mm NaCl; 0.5Mm EDTA) with which the immunoprecipitation procedure was undertaken contributed to this occurrence. Therefore, the immunoprecipitation procedure was repeated with lysate expressing P62 using four dilution buffers at different pH; 6.0, 7.4, 9.0 as well as RIPA Lysis buffer (10mM Tris/CL pH 7.5; 150Mm NaCl; 0.5Mm EDTA, 0.1% SDS; 1% Triton x-100, 1% Sodium Deoxycholate), after which a western blot analysis was conducted on various purification fractions. A chromogenic development of the blot revealed the existence of KRAS dimers in the flow through fraction, despite testing different buffers (**Figure 91F**). Due to dimerisation of proteins, they were unable to expose their Myc tags to bind the Myc Trap beads so as to attain thorough purification of recombinant proteins.




C
HRAS
KRAS
Elution fractions
wash fraction
Flow through
original cell lysate
Commercial HRAS antigen
Elution fraction
wash fraction
Flow through
Commercial KRAS antigen
MagicMark ™ XP
220kDa
120kDa
100kDa
80kDa
60kDa
50kDa
40kDa
30kDa
20kDa
60
60
30
30


D
Gankyrin
RALA
Elution fraction
Wash fraction
Flow through
Commercial Gankyrin antigen
Elution fraction
Wash fraction
Flow through
Commercial RALA antigen
MagicMark ™ XP
220kDa
120kDa
100kDa
80kDa
60kDa
50kDa
40kDa
30kDa
20kDa


E
P53
P62
Elution fractions
Wash fraction
Flow through
Cell lysate
Elution fractions
Wash fraction
Flow through
Cell lysate
MagicMark ™ XP
220kDa
120kDa
100kDa
80kDa
60kDa
50kDa
40kDa
30kDa
20kDa

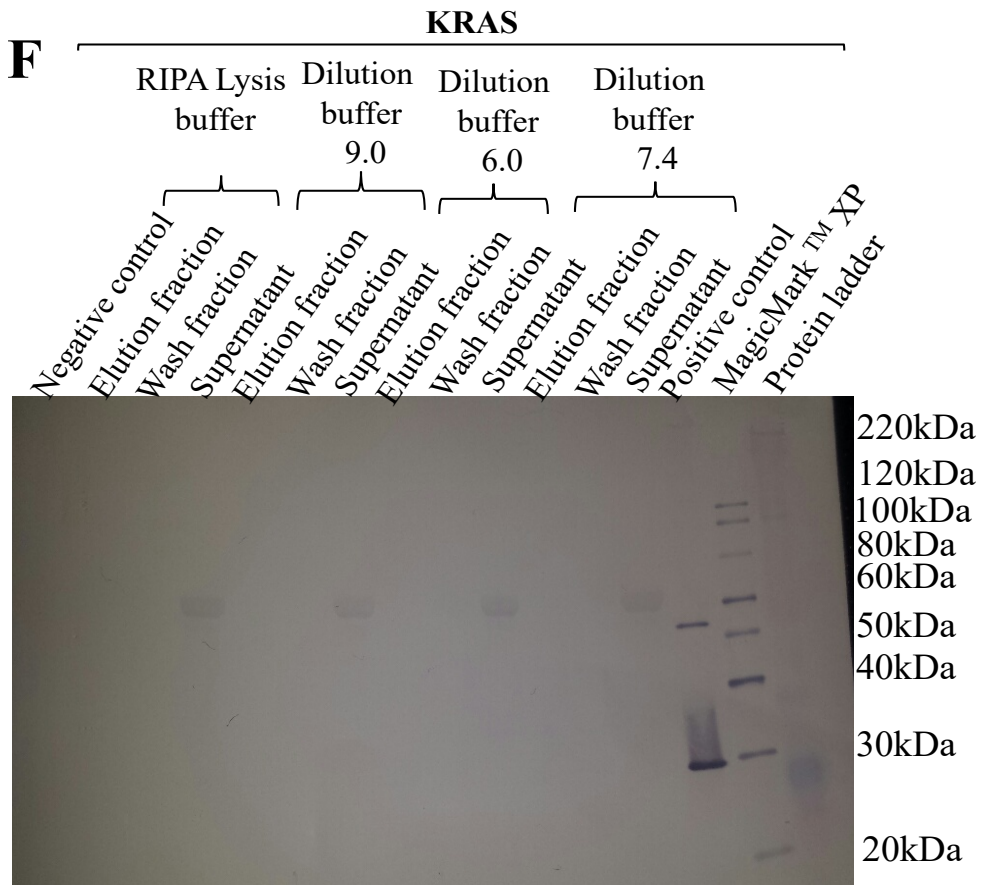
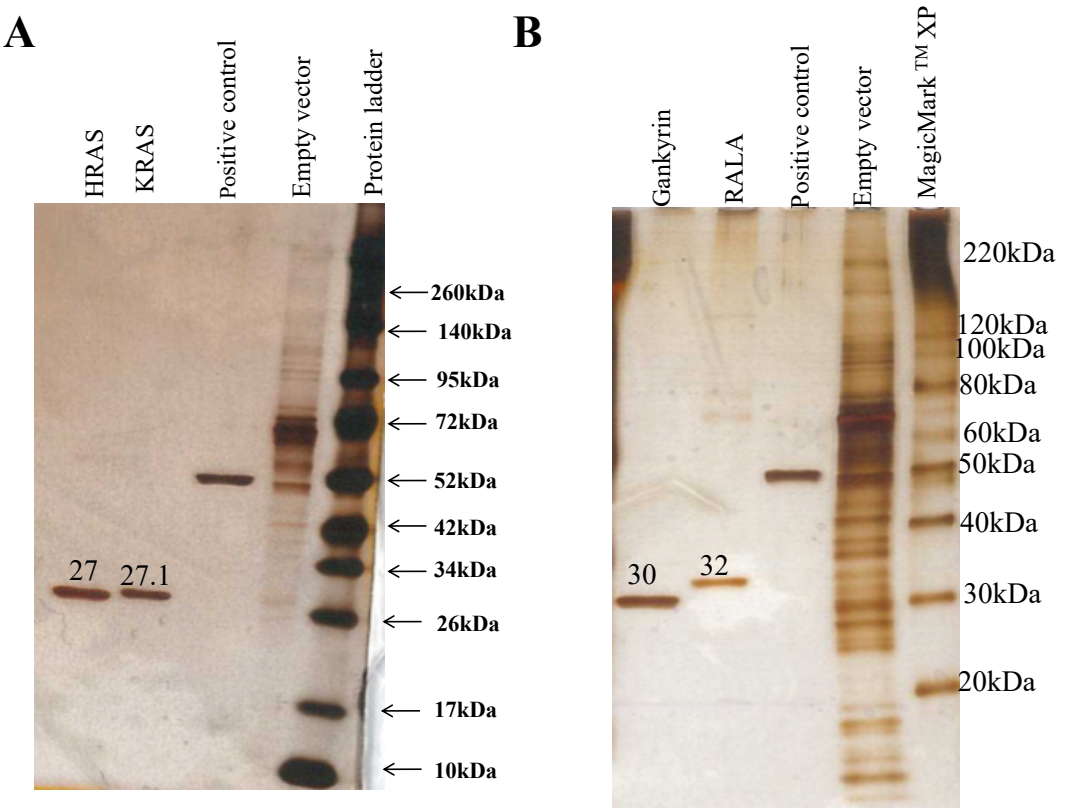


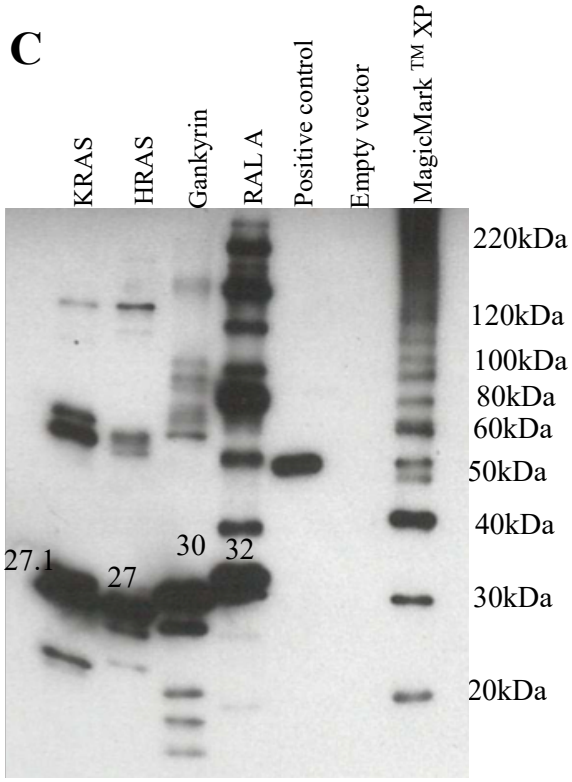
Figure 91: Recombinant Myc-DDK tagged protein purification using Myc Trap MA Magnetic Beads. Lysates expressing HDGF, KRAS, HRAS, RALA, Gankyrin, p53 and p62 were immunoprecipitated using the Myc-Trap MA kit under native conditions. 200 µl of lysate was incubated with 50 µl of washed bead slurry at 4°C for an hour. Beads were washed twice with ice-cold dilution buffer after which recombinant proteins bound to magnetic beads were eluted using the displacement with Myc peptide. **(A)** and **(B)** show a dot blot and western blot analysis on purification products of HDGF, where elution fraction expressed the expected band size HDGF (48kDa). Dimerization of **(C)** KRAS and HRAS in original cell lysate and flow through. Commercial KRAS and HRAS Myc tagged antigens were used as positive controls while P CMV empty vector lysates were used as a negative control. **(D)** shows dimerization of RALA and Gankyrin in flow through and original cell lysate. Commercial Gankyrin and RALA Myc-tagged antigens were used as positive controls while empty vector lysates were used as negative control. **(E)** P53 and P62 was seen in cell lysates and the flow through fractions respectively after immunoprecipitation. **(F)** Reveals the existence and dimerization of KRAS in the flow through fraction despite the use of various dilution/wash buffers at different pH. All blots were probed with anti-Myc antibody. MagicMark™ XP (ThermoFisher Scientific, Cat no LC5602, 20-220kDa) used as a molecular weight marker to help indicate molecular size of protein bands in figures C, D, E and F, while Spectra Multicolour Broad range protein ladder (ThermoFisher Scientific, Cat no 26634, 10-260 kDa) was used for figure B.

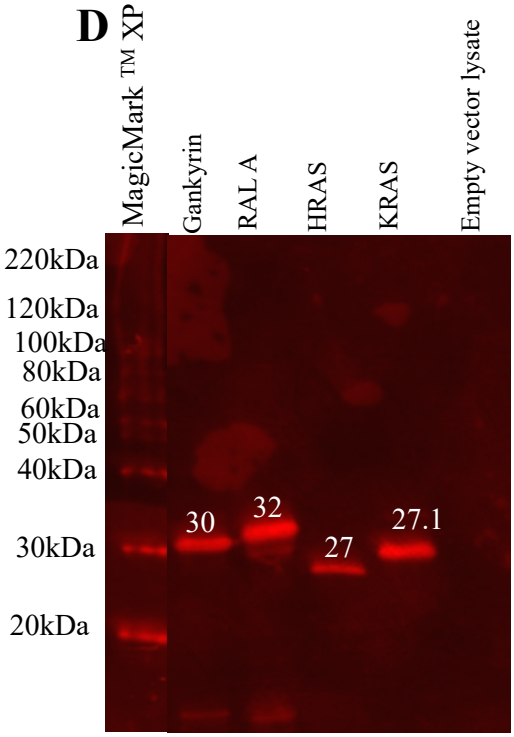
4.3.10 Quality Assessment of Commercial HCC Tumour-associated Antigen Panel

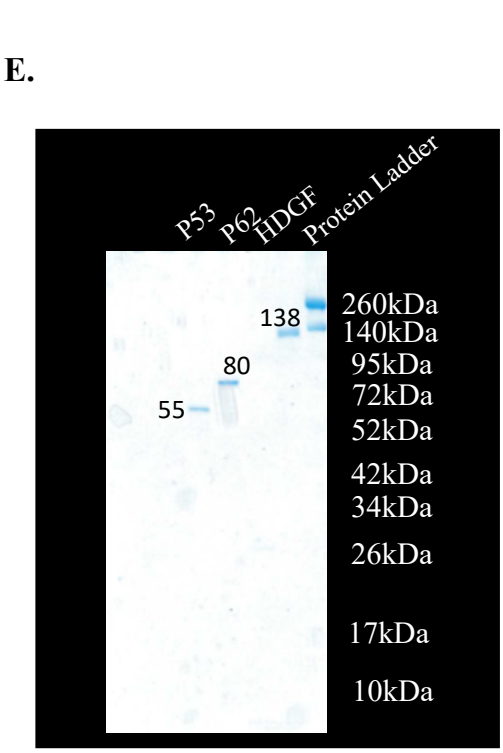
Purification of the in-house HCC recombinant proteins from cell lysates was challenging as several approaches to attaining a refined panel of recombinant proteins was unsuccessful. Hence, a panel of the same HCC TAAs produced in HEK 293 cells were purchased in addition to the ones expressed in cell lysates. Though there has been a remarkable growth in the business of research antigens and antibodies, there is still a universal lack of trust in commercial proteins. Hence, there was the urgent need to conduct a validation to avoid jeopardizing proposed experiments. Validation would help to determine if there is satisfactory proof for the potential clinical utility of these commercial biomarkers utilising them for subsequent diagnostic tests. Validating the expression of commercial TAAs mostly rely on the available antibody that detects them. Commercial Flag-tagged recombinant TAAs; KRAS, HRAS, HDGF, CDK2NA, RAL A, P62, P53 and Gankyrin were verified for antigen concentration and analysed upon delivery in order to determine their purity and integrity. 1 µg of each commercial TAA was run on 10-20% precast polyacrylamide gels together with lysates of HEK 293 cells transfected as well as PCMV empty vector (negative control) and a BAP fusion protein (positive controls). KRAS, HRAS, RALA and Gankyrin were either silver stained (**Figure 92A-B**) or probed with an anti-Flag antibody using chemiluminiscence (**Figure 92C**) and fluorescent western blot (**Figure 92D**). HDGF, P62 and P53 were imperial stained or detected using fluorescent western blot with an anti-Flag antibody (**Figure 92E-F**). Lastly, CDKN2A was silver stained **(Figure 92H)** to determine its purity. A panel of ten HCC His-tagged recombinant TAAs produced in an *E. coli* expression system were also validated with a silver stain procedure (**Figure 92G**) since they would be utilised together with eukaryotic generated TAAs to compare

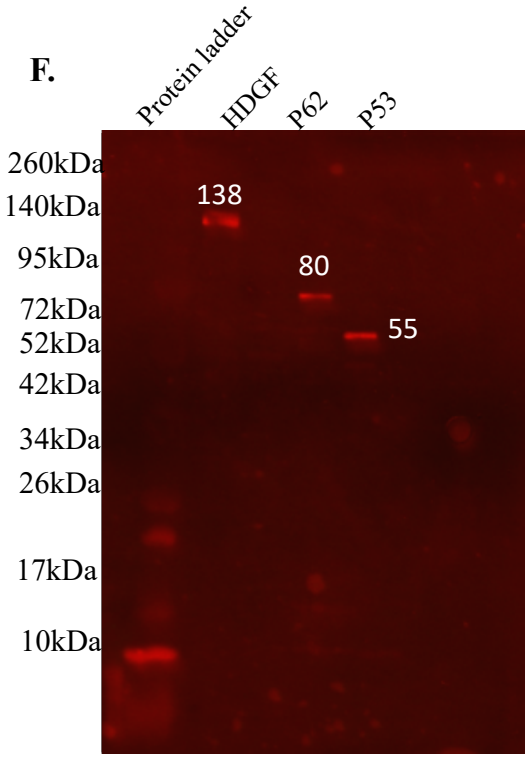
autoantibody profiles in HCC patients. The expected and observed molecular weight of the examined commercial Flag-tagged TAAs; KRAS, HRAS, HDGF, CDKN2A, RAL A, P62, P53 and Gankyrin were 27.1, 27, 138, 25, 32, 80, 55, and 30 kDa respectively (**Figure 92 A, B, C, D, E, F, H**). On the other hand, commercial *E. coli* generated TAAs KRAS, HRAS, HDGF, RALA, AFP, P62, GRP78, Gankyrin, APCN, IMP1 had expected and observed molecular weights of 21, 15, 32, 23, 55, 52, 11, 22, none, 52kDa respectively (**Figure 92G**). No band was detected for APCN after three repetitive experiments.




C
KRAS
HRAS
Gankyrin
RAL A
Positive control
Empty vector
MagicMark ™ XP
220kDa
120kDa
100kDa
80kDa
60kDa
50kDa
40kDa
30kDa
20kDa
27.1
27
30
32


D
MagicMark ™ XP
Gankyrin
RAL A
HRAS
KRAS
Empty vector lysate
220kDa
120kDa
100kDa
80kDa
60kDa
50kDa
40kDa
30kDa
20kDa
30
32
27
27.1


E.
P53
P62
HDGF
Protein Ladder
260kDa
140kDa
95kDa
72kDa
52kDa
42kDa
34kDa
26kDa
17kDa
10kDa
138
80
55


F.
Protein ladder
HDGF
P62
P53
260kDa
140kDa
95kDa
72kDa
52kDa
42kDa
34kDa
26kDa
17kDa
10kDa
138
80
55

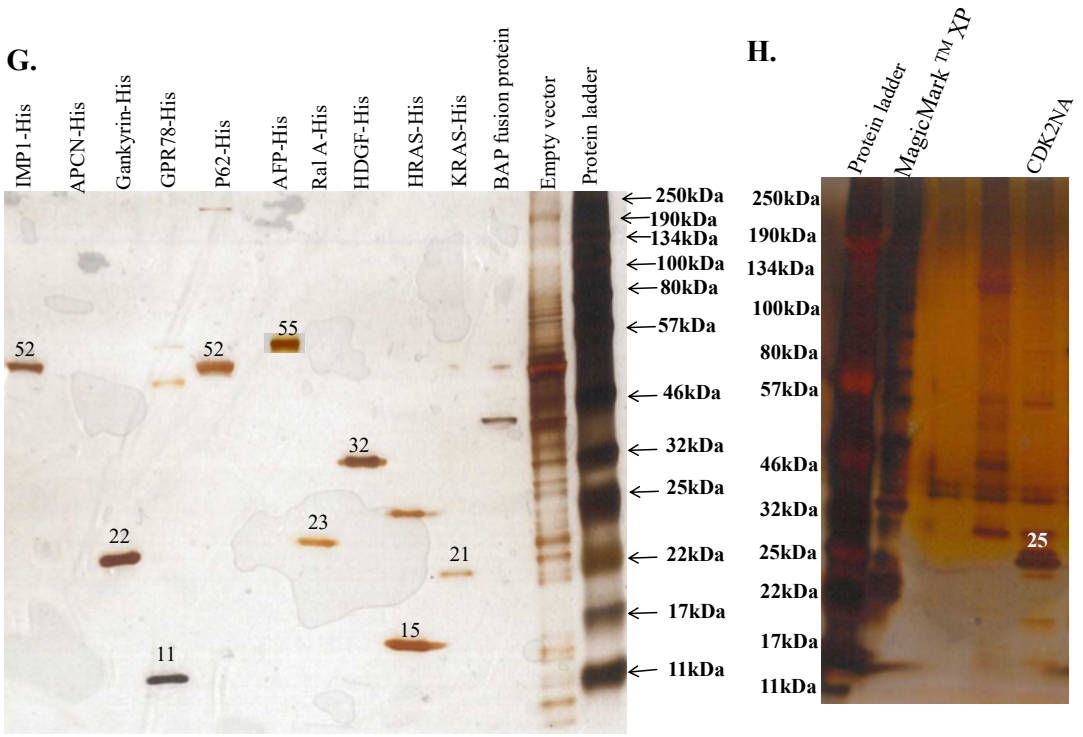


Figure 92: Representative analysis of a panel of eukaryotic and *E. coli* generated HCC TAAs. One µg of each commercial TAA was run on a 4-20% precast polyacrylamide gel with a broad range of protein markers and controls. **(A)(B)(C)(D)** shows a silver stained gel, fluorescent and chemiluminescent western blot revealing immunoreactive bands of commercial HEK 293 expressed proteins; HRAS, KRAS, Gankyrin and RALA (27, 27.1, 30, 32kDa respectively), **(E) and (F)** Shows a fluorescent western blot and an imperial protein stained gel analysis showing bands for HEK 293 expressed proteins ; HDGF, P62 and P53 (138, 80, 55 kDa), (**G**) is a silver stain gel analysis revealing ten commercial E. coli generated recombinant proteins (KRAS, HRAS, HDGF, RALA, AFP, P62, GRP78, Gankyrin, APCN, IMP1) at expected molecular weight of 21, 15, 32, 23, 55, 52, 11, 22, none, 52kDa respectively. **(H)** shows a silver stain gel analysis of CDKN2A at expected molecular weight of 25 kDa. MagicMark™ XP (ThermoFisher Scientific, Cat no LC5602, 20-220kDa) used as a molecular weight marker to help indicate molecular size of protein bands in figures B, C, and D, while Spectra Multicolour Broad range protein ladder (ThermoFisher Scientific, Cat no 26634, 10-260 kDa) was used for figures A, E and F. Lastly, Prestain Protein Marker (Cell Signalling, Cat no. 77205, MW 11-250KDa) was used for figure G and H.

4.4 Discussion

Tumour-associated antigens (TAAs) play an important role in the disease development process as their release from tumour cells elicit the production of corresponding autoantibodies in patients, which can act as reporters for the early diagnosis of HCC (257). The aim of this chapter was to produce a panel of HCC recombinant tumour-associated antigens in a cost effective and scalable manner in order to profile autoantibodies in HCC patients sera using the developed in-house microarray technology. A thorough literature search was conducted to select TAAs that are described to be related with HCC or liver disease and could elicit measurable autoantibody response in HCC patients. These antigens included AFP, KRAS, HRAS, HDGF, P16 (CDKN2A), RALA, P53, P62 and Gankyrin. Gankyrin, HDGF and RALA are regarded as overexpressed antigens, AFP and P62 as aberrantly expressed (391) while HRAS, KRAS, P16 and P53 belong to the mutated antigen category (294).

In the production of recombinant proteins for research, the profound questions which are usually asked include: which type of expression system should be used? Should the proteins be tagged, and which kind of tag is mostly effective? What is the most suitable purification strategy? Although several expression systems for recombinant proteins have markedly improved yields and lowered costs, the mammalian system, specifically the HEK 293 cell line, was selected over *E.coli* for the expression of HCC TAAs due to a number of reasons. Mammalian cells have the benefit of being able to accurately and authentically glycosylate and properly fold proteins and do not cause immune responses due to post-translational modifications as they are similar to naturally occurring human proteins (413). However, this method of expression is time consuming, slightly expensive and gives a low yield of proteins as compared to the

others and this could present as a barrier in some instances (412). The introduction of Myc-DDK tagged cDNA clones in HEK 293 cells for expression was achieved by electroporation which applies electric impulses to create pores in the cell membrane of cells by exploiting the weak interactions between phospholipid bilayers that stabilise the integrity of cell membranes. This was chosen over other methods of transfection due to its efficiency, low requirements of DNA, as well as it's less cumbersome and fast procedure (425). Myc-DDK tagged cDNA clones were stably transfected because it has been shown to be a beneficial technique for the quick production of recombinant proteins due to its ability to produce milligram quantities within few weeks following cloning of their corresponding cDNA, as well as reduced variation as compared to transient transfection method (421).

Preliminary expression of HCC recombinant proteins in HEK 293 cells was conducted using four Myc-DDK tagged (FLAG) cDNA clones; (KRAS, HRAS, HDGF and P16, which proved unsuccessful upon numerous attempts. An explanation for this could be that since the HEK 293 cell line had undergone more than 100 passages, the cells might have suffered undue stress. Cell stress leads to improper protein response (incorrect folding of proteins), which results in the production of inactive proteins (447). Cell stress could also be caused by heat shock and nutrient depletion (448). Secondly, there might have been the loss of a gene from the host cell due to structural changes in the recombinant gene such as mutation (447). Moreover, there could be plasmid loss arising from unequal distribution upon cell division (plasmid segregational instability) (449). This is actually one of the main causes of reduced recombinant protein productivity (448). In accordance with previous results, transfection of cDNA clones was carried out in a new HEK 293 cell line and only HDGF was over-expressed at the expected molecular size of 48 kDa. KRAS, HRAS and P16 failed to be expressed. Other studies

have shown that, low molecular size proteins usually take a longer time for expression before selective pressure with antibiotics (450). In the experimental procedure, expression of all proteins was allowed for up to 48 hours. This could explain lack of protein production as selection with G418 might have interrupted adequate expression of KRAS, HRAS and P16 by increasing the metabolic burden on cells. Furthermore, 0.45 μm nitrocellulose membrane was used during transfer of proteins and hence it was anticipated that, lower molecular size proteins might have run through the membranes during the process due to its large pores.

With these in consideration, a subsequent transfection was undertaken allowing a longer timeframe for protein expression. Consequently, western blot analysis was carried out using nitrocellulose membrane with 0.2 μm pore size. However, this approach was also unsuccessful as HDGF was the only protein still detected. We anticipated that the recurrent negative outcome could be have been due to a number of reasons. For example, the concentration of DNA could be low and therefore resulted in low protein expression or the cDNA was not properly integrated into the host genome (451). Also, the transfected DNA could be lost by dilution in host cell replicate (451). Lastly, the selection of cells with G418 could have resulted in clones that were highly resistant to drug yet produced no protein at all (452). Consequently, we conducted a transfection using a higher plasmid concentration (3 μg) and the number of cells per concentration of antibiotic (data not shown) was optimised to ensure adequate selection thus, $5x10^6$ of transfected cells to 1 mg/ml of G418. An immunoblot carried out on four different cell lysates showed strong immuno-reactivity for KRAS, HRAS, HDGF, P16 and positive control (BAP fusion protein) indicating the presence of successfully expressed Myc-DDK (FLAG) tagged recombinant proteins in cell lysates.

The production of recombinant proteins requires an efficient purification system. However, proteins produced without natural affinities are less easily purified. This shows how recombinant protein purification hugely rely on affinity chromatography, most importantly, the usage of engineered affinity tags for principal recovery, improved expression and solubility of proteins. A large range of affinity tags are used but the FLAG (Myc-DDK tag) was employed since it is still one of the most common and efficient for affinity tag purification. Anti-Flag® M2 agarose resin beads, Anti-Flag M2® magnetic beads and Myc Trap® MA magnetic beads were employed in the study.

Purification of Flag-tagged recombinant proteins (KRAS, HRAS, HDGF, P16) from the filtered cell lysate was undertaken under native conditions using anti-Flag M2 affinity gel to test the efficacy of the purification kit. Dot blot analysis revealed strong immunoreactive blots of the four proteins in the flow through and wash fractions with none detected in the elution fractions. This suggest that the purification kit was out of date because it had lost its sensitivity, thus, poor affinity, tags were embedded, and the pH content of buffer was too high. This informed the decision to purchase anti-Flag® M2 magnetic beads for the immunoprecipitation of Flag-tagged recombinant proteins from HEK 293 cell lysates. Though elution fractions were seen to have contained Flag-tagged recombinant proteins through dot blot analysis, the flow through still contained some of the proteins of interest. This could be attributed to the high volume of cell lysate used against a reduced volume of packed beads. Therefore, beads the were saturated and could not bind all recombinant proteins. Prior to a subsequent purification procedure, optimisations were undertaken which highlighted several factors that affect efficient protein purification such as the pH of buffers, volume of cell lysate and volume of packed magnetic beads. Consequently, a dot blot analysis of the elution fractions

revealed strong immunoreactive bands for KRAS, HRAS, HDGF and P16, demonstrating efficient binding of proteins to magnetic beads.

Transfections undertaken on a new set of cDNA clones: RAL A, P53, P62, Gankyrin as well as KRAS, HRAS, HDGF and P16 yielded successful outcomes as dot and western blot on cell lysates showed strong reactivity of flag-tagged proteins to anti-Flag antibody at the expected molecular size of 30kDa, 35kDa, 80kDa, 48kDa, 60kDa, 60kDa, 35kDa, 25kDa for KRAS, Gankyrin, RAL A, HDGF, P53, HRAS, P62 and P16 respectively. Band intensity correlated with the protein concentrations of each sample, which indicates an increased expression of proteins in the HEK 293 cells.

Eight successfully expressed recombinant proteins in HEK 293 cells were immunoprecipitated using anti-Flag® M2 magnetic beads and a dot bot analysis on purified products showed strong immunoreactivities with anti-Flag antibody. However, this was not a true representation of correctly purified Flag-tagged proteins, as results were obscured. This was because a western blot analysis of elution fractions showed a concomitant recovery of huge amounts of immunoglobulin (light and heavy chains IgG), which masked the Flag-tagged recombinant proteins of interest. Intrusion from antibody bands during gel analysis is usually an encountered problem in various immunoprecipitation approaches. Elution with Glycine-HCL at about a pH of 2.8 which was undertaken and clearly spelt out in the manufacturers data sheet, does not always maintain antibody integrity (453). The potential drawback of this elution method is that the elution efficacy of the target protein may not be as efficient (453) and this was evident in our work as flag-tagged recombinant proteins were not appropriately eluted from beads. Several approaches were employed to circumvent antibody contamination and to effectively release bound proteins from magnetic beads. According to (453), the harsh elution of target proteins from beads using SDS buffer is quite common as it

completely strips bead off bound proteins although beads do not become reusable. Hence, an alternate method of obtaining absolute proteins with elution with SDS sample buffer was opted for. This method is termed as soft elution and considered to be very effective in obtaining target proteins and preventing the elution of large amounts of immunoglobulin (454). Using reducing agents such as DTT or heating beads incubated with lysates was done because they enable recombinant proteins to be efficiently dissociated from magnetic beads (453). Nevertheless, the performance of the 'soft elution' was not superior to the Glycine-HCL elution in our work as target proteins were never recovered in the elution fraction. Since proteins were in their native conformation state, we anticipated that their epitopes of interest were buried and therefore antibody bound to magnetic beads could not recognise them. Therefore, denaturation proteins would adequately reveal their epitopes for detection. This enables effective binding proteins to immunoprecipitated beads which yield good purification outcomes. Consequently, proteins in lysates were denatured with 0.2% SDS before the immunoprecipitation procedure, but this was also unsuccessful. Amid the constant contamination with immunoglobulins, the Myc Trap® MA kit was employed since it has had the reputation of avoiding this problem and it further recognizes the internal site of flag-tagged recombinant proteins and not just the N- and C- terminus of the Myc tag sequence. Moreover, it utilises nanobodies, which are covalently coupled to the surface of magnetic beads and binds very tiny amounts of target proteins. By this, the immunoprecipitation of HDGF from HEK 293 cell lysate was successful. However, it was speculated that since the other flag-tagged recombinant proteins had undergone dimerization, immunoprecipitation could not be attained for these recombinant proteins expressed in cell lysates. One of the aims of the study is to compare autoantibody responses in HCC patients' sera to TAAs produced from different expression systems.

Therefore, commercial TAAs (expressed in *E. coli*) donated by the Centre of Excellence for Autoimmunity in Cancer (CEAC) were validated with silver stain to verify their purity and band size. Proteins were pure as there was no contamination observed. Also, the band size was no different from that observed on the manufacturer's datasheet indicating they were acceptable to be added to the panel of TAAs. Due to the inconsistencies in the in-house purification of HCC Flag-tagged recombinant proteins from HEK 293 cell extracts, we decided to buy in commercial HCC tumour-associated antigens produced in a mammalian expression system, which have been proven to work efficiently.

In spite of the challenges associated with the expression and purification of in-house TAAs, we successfully optimised methods to over express our TAAs of interest. Although we faced drawbacks in streamlining methods for purification, we still managed to purify reasonable amount of HDGF which would be included in downstream assays along with commercially acquired TAAs.

Having fully validated the in-house and commercially acquired TAAs generated from eukaryotic cells as well as *E. coli*, future work will involve:

1. Testing the suitability of the in-house TAAs expressed in cell lysates as well as commercially acquired TAAs expressed in both *E. coli* and eukaryotic systems on the antigen microarray technology.
2. Re-validating the microarray assay with these different cohort of TAAs.
3. Utilising the panel of TAAs to characterise autoantibody responses in the sera of (i) HCC patients, (ii) High risk patients and (iii) healthy individuals.

Chapter Five:
Testing In-house and Commercial TAAs on Microarray platform

5.1 Introduction

Hepatocellular carcinoma patients display an immune response to tumour-associated antigens through the release of autoantibodies against the antigenic elements of the patient's own tissues (260). The presence of these autoantibodies can be used as an aid for the early detection of HCC which would help to improve diagnosis, monitor disease progression as well as the patients' response to therapy (455). This is because they appear up to five years prior to the clinical manifestation of the disease and additionally, they show up even when the serum AFP is in the normal range. With the development of screening technologies, the diagnostic value of autoantibodies could be further explored and validated, which would provide more reliable evidence for the diagnosis and prognosis of HCC. Interestingly, protein microarray technology has recently emerged as a robust tool for the examination of humoral immune responses in the sera of patients with cancer, autoimmune disorders as well as allergies (456).

In the case of HCC, protein microarrays can be used to directly detect autoantibodies that correlate with cancer in a patient's serum. This technology offers a useful platform for characterisation of hundreds or even thousands of proteins in a multiplexed and high-throughput way (369). Three types of protein microarray have been identified namely; analytical, functional and reverse phase microarrays. In the analytical microarray set-up, proteins are detected after antibody capture using direct protein labeling (457). In functional microarray, individually purified proteins are used to study

the biochemical properties of proteins such as their binding activities (457). Lastly, the reverse phase microarray enables the investigation of many samples obtained at different conditions by directly immobilising tissue, cell lysates or even fractionated cell lysates on a glass slide (458). Antigen microarray which is the most common type of functional microarray, allows the study of interactions between an antigen and antibody in a miniaturized fashion. Thus, antigens of interest are printed on a solid surface as spots. The high throughput is as a result of small spot-size on the microarray (~150–200 μm) and hence, a large number of spots are seen per microarray. The slide can carry a variety of self-antigens, such as cell membrane proteins, cytoplasmic proteins, cell nuclear components, phospholipid proteins, cell matrix proteins, secreted proteins, and other tissue-specific proteins which are used to detect the specificities of thousands of autoantibodies in a quantitative manner (459). Moreover, antigen microarray assays are highly sensitive and require very small volume of serum (1-5 μl) for probing antigens and this saves patients having to provide large volumes of blood. Compared to the micro titre plate format used in ELISA, a typical spot is more than 25 times smaller (460). The benefit acquired by miniaturization, high sensitivity, and high throughput makes antigen microarrays a potentially powerful technology for the discovery of biomarkers (456). These advantages are especially important for clinical research that uses precious samples, such as human serum samples. In addition, the high sensitivity and specificity of protein microarrays provides a powerful tool in quantifying and profiling proteins, such as autoantibodies. It has been shown that data generated by autoantigen arrays correlate very well with the data generated by ELISA, but with a higher sensitivity (458). This technology is currently being used in the detection of autoantibodies in breast and lung cancer patients and allows the measurement of several proteins concurrently in complex biological samples for

quantitative studies. Autoantigens are printed on slides and are reacted with cancer patients' sera after which the bound antibodies are identified by fluorescently labeled secondary reagents. The proteomic technology method foretells a promising future for implementation of sensitive and specific tests for the detection of cancers.

Therefore, the antigen microarray technology was employed for profiling autoantibodies in hepatocellular carcinoma patients against a wide range of HCC tumour-associated antigens. The antigen microarray was developed and validated (**detailed in Chapter 3**) for the quantification of serum TAA-specific IgG in patients' sera. Over some years, studies on TAAs have targeted the identification of a panel of biomarkers instead of single markers because the latter do not exhibit adequate sensitivity and specificity to construct a reliable assay for early detection. Upon literature mining and existing knowledge such as association with hepatocellular carcinoma and liver disease, we selected a panel of TAAs to for the study and consequently, our reason for generating eight TAAs (**in Chapter 4**). It is challenging for many research laboratories to purify large quantities of recombinant TAAs and this was not shocking as our in-house TAAs were still expressed in HEK 293 lysates **(Chapter 4)**. In obtaining resultant reproducible and reliable antigen microarrays, the quality of TAAs is a crucial feature to be considered. It was imperative that the performance of our in-house TAAs expressed in lysates was assessed on the microarray before using them for further study as previous developmental microarray assays had utilized only purified commercial purified *E. coli* produced TAAs. Typically, cell lysates are highly utilized in the reverse phase protein microarray technology by arraying them on nitrocellulose slides. Protein lysates, unlike commercial TAAs, contain a wide range of proteins apart from the expressed recombinant TAAs. Hence, there was the need to optimize the antigen microarray to fully suit the in-house TAAs.

This required visual inspection of the quality of each array in order to determine the optimal print buffer for lysates, concentration of lysates as well as their binding capacities on Aminosilane slide surface.

This chapter presents the development and application of protein lysate microarray technology for verification and quantification of in-house recombinant TAAs (KRAS, HRAS, HDGF, CDKN2A, RALA, P62, P53, Gankyrin). Experiments using the aforementioned TAAs, together with commercial eukaryotic and *E. coli* generated recombinant proteins (KRAS, HRAS, HDGF, CDKN2A, RALA, P62, P53, Gankyrin, GRP78, AFP, APCN, IMP1), were replicated to reveal precision of the assay.

5.2 Materials and Methods

Eight in-house Myc-DDK tagged recombinant TAAs expressed in HEK 293 lysates (KRAS, HRAS, HDGF, CDKN2A, RALA, P62, P53, Gankyrin), commercial purified *E. coli* produced (KRAS, HRAS, HDGF, RALA, P62, IMP1, APCN, AFP, Gankyrin), as well as eukaryotic generated TAAs (KRAS, HRAS, HDGF, CDKN2A, RALA, P62, P53, Gankyrin) were diluted in different printing buffers (PBS-Tween, PBS-Trehalose-Betaine, PBS-Trehalose-Betaine-Tween) to make a volume of 10 µl at a concentration of either 100 µg/ml or 200 µg/ml (**Figure 93**). Cell lysate concentration used were based on the total protein concentration shown in **Chapter 4**. Additionally, a two-fold dilution of purified human Immunoglobulin IgG as prepared at a starting concentration of 0.05 mg/ml. TAAs, together with ten dilutions of the purified IgG, were placed in a 384 well plate. These were subsequently printed onto an Aminosilane slide at a humidity of 65% after which they were secured in either eight or sixteen pad incubation holders. Antigens were arrayed onto slides in either quadriplicates, five, six or ten replicates (**Figure 93**). Antigens were blocked with 100 µl of 5% BSA in PBST and then incubated for an hour with shaking at room temperature. Each well was washed five times with 100 µl PBST for three minutes. Two drops of avidin blocking reagent were then added to each block and incubated at ten minutes with shaking after which they were washed five times with PBST after each step. The avidin block was followed by a further ten-minute incubation with biotin block solution and the washing step was repeated. Slides printed with in-house TAAs were probed with either 100 µl of samples (sera, diluted 1:500 in 5% BSA in PBST respectively) or 100 µl of monoclonal mouse anti-DDK, diluted 1:1,000 in 5% respectively. Slides printed with commercial *E. coli* generated TAAs were probed with anti-His_6 antibody diluted 1:10,000 in 5% BSA. Conversely, slides printed with commercial eukaryotic TAAs were probed with anti-

DDK antibody diluted either 1:5,000, 1:7,000 and 1:10,000 in 5% BSA (with the exception of negative control blocks). Slides were then incubated with gentle agitation for an hour at room temperature after which they were washed five times over 3 minutes to remove unbound antibodies. One hundred µl of biotinylated anti-human antibody diluted 1:20,000 in antibody diluent (DAKO) was added to the wells probed with serum samples while 100 µl of anti-mouse diluted 1:2,000, 1:10,000, 1:20,000, 1:30,000 in antibody diluent, was added to the wells probed with either mouse anti-His_6 or anti-DDK antibody. Slides were covered and incubated with shaking for one hour at room temperature after which arrays were washed three times. Streptavidin Horseradish Peroxidase (HRP) (BIORAD, USA) was diluted 1:2,000 in antibody diluent and 100 µl was added to each block and incubated with shaking at room temperature in the dark for fifteen minutes. This was followed by the amplification procedure where 100 µl of the amplification diluent, amplification reagent and ultrapure water (4:1:4) was added to each block for ten minutes with shaking. After the amplification step, slides were washed three times with 20% dimethyl sulphoxide in PBST, then finally washed three times with x1PBST. The slide was then washed 5 times with PBST. 100 µl of streptavidin-conjugated Cyanine 5 (Molecular Probes, UK) was diluted 1:2,000 in 5% BSA-PBST after which the preparation was incubated in the dark with shaking for fifteen minutes. Slides were washed five times with PBST then once with PBS only for five minutes and subsequently rinsed shortly with ultra-pure water. Slides were dried by centrifugation at 1200 rpm for five minutes (**Figure 93**). Processed slides were scanned using Genepix 4200AL scanner at a wavelength of 635nm (laser standard red) at 400 PMT and 100% power. Fluorescent signal intensity of each spot was measured using the Axon Genepix Pro 6.1 software after which GPR files were generated (median fluorescence minus background for each arrayed protein) were generated (**Figure 93**).

Based upon mathematical and statistical software poor quality features were flagged for removal by the Genepix software with regards to spot morphology (circularity and size), signal uniformity, local background and signal to noise ratio. After the data was filtered, high quality spots were analysed using R statistical package (RPPAnalyzer version 3.1.2, 2014) to Graph Pad prism 7 (Graph Pad 7, USA) software was used to generate graphs as well as interpolate IgG standard curves.

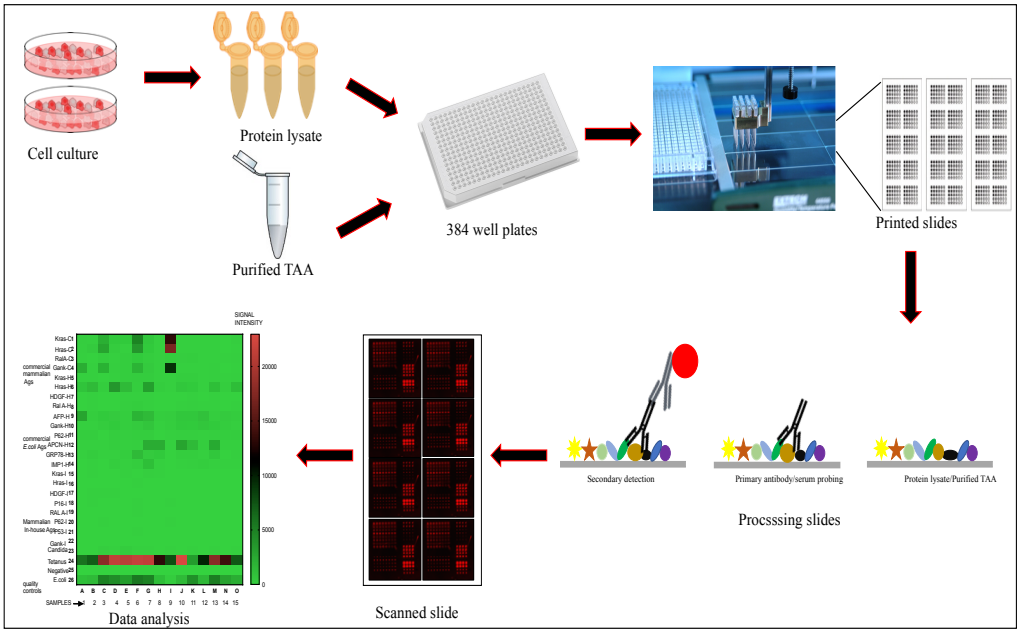


Figure 93: Schematic diagram outlining the processes involved in the Antigen Microarray Assay (lysates). Native HCC TAAs expressed in HEK 293 lysate or purified TAAs were prepared in printing buffer and loaded onto a 384 well plate. Each TAA was immobilised in either an 8x8 or 16x16 array format onto aminosilane-coated glass slides using a Biorobotics Microgrid II arrayer (Microgrid) and a silicon contact pin after which they were detected by a specific monoclonal antibody. Also, using immobilized TAAs as bait, autoantibodies from patients' sera allowed to react with the immobiliSed antigen. The complex was then detected with a secondary antibody after which the reaction was amplified with a tyramide amplification kit and a steptavidin Cy5 dye was used to help visualize the reaction. Slides were scanned at 635nm and the data analyzed using the GenePix Pro Software (Axon GenePix1). The mean local background was subtracted from the median fluorescence of each spot and the corrected fluorescence was used to calculate the average fluorescence signal as well as the standard deviation.

5.3 Results

5.3.1 Establishment of Optimal Conditions for Printing In-house Recombinant TAAs

Different strategies were explored to obtain purified forms of in-house TAAs expressed in HEK 293 lysates. We sought to use lysates on the microarray platform, even though the antigen microarray assay was initially developed with purified antigens (**Chapter 3**). Nonetheless, both in-house and commercial TAAs would have to be arrayed simultaneously on the same slide for subsequent screening of patients' samples. Hence, the first step was to determine the binding of in-house lysate TAAs onto Aminosilane slide surface. To evaluate in-house TAAs, lysates were prepared in a PBS-Trehalose-Betaine-Tween buffer were at a concentration of 200 μg/ml in twelve replicates together with a two-fold human IgG dilution arrayed in four replicates on each pad on an Aminosilane slide surface. In previous optimisation assays, the optimal dilution utilised for human sera and secondary antibodies were 1:500 and 1:20,000 in 5% BSA and antibody diluent respectively (**see Chapter 3**). With this, slides were probed with control sera (1:500 in 5% BSA) and subsequently incubated with biotinylated anti-human antibody (1:20,000 in antibody diluent). After the amplification, Streptavidin Cy5 dye (1:2,000 in 5% BSA) was used to visualise the complex. Scanned images were assessed, and the data was not analysed as there was an extensive smearing as well as poor visibility of spots on all pads of the slide with the exception of the purified human IgG standard (**Figure 94**). Consequently, this led to high backgrounds on all regions of the slide.

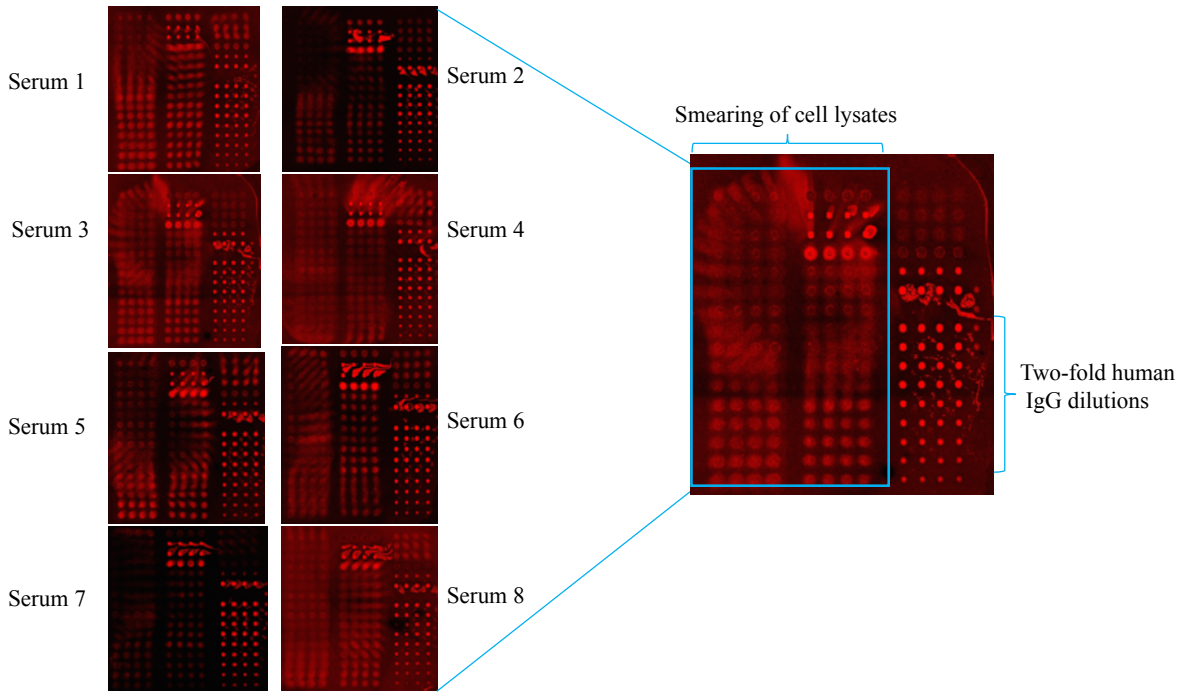
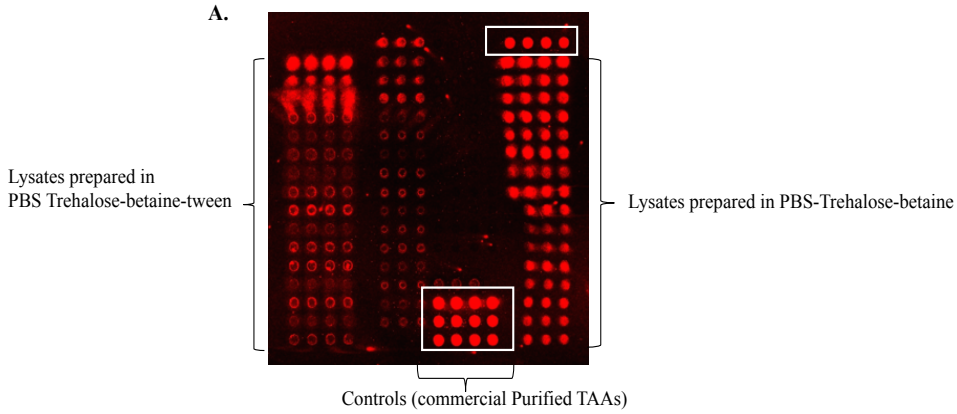


Figure 94: Reveals spot morphology of in-house TAAs probed with different sera. In-house TAAs were printed at a concentration of 200 µg/ml in an eight-pad format unto an Aminosilane slide surface. TAAs were immobilised in twelve replicates together with a two-fold human IgG dilution standard arrayed in four replicates. The slide was probed with control sera (1:500 in 5% BSA) and the interaction was subsequently detected with a biotinylated anti-human antibody (1:20,000 in antibody diluent). After the amplification step, streptavidin cy5 dye, 1:2,000 in 5% BSA was used to aid the visualisation of the interaction. Visually, all TAAs with the exception of the human IgG standard produced a non-homogenous spot morphology with comet-tail characteristics and extensive smearing.

5.3.2 Optimising Printing Buffers for In-house Recombinant Tumour-Associated Antigens

Earlier experiments had indicated poor features of spots due to indequate binding of in-house TAAs expressed in lysates on Aaminosilane surface. Though PBS-Trehalose-Betaine-Tween was determined as the optimum print buffer for the entire assay in **Chapter 3**, it was anticipated that it could be the contributing factor to the extensive smearing and comet-tail effect of the lysate spots since the tween may have increased the viscosity of the lysates. Printing buffers play a critical role in the fabrication of microarrays and it is essential to modify the print buffer in order to efficiently immobilize lysates onto the slide to produce high quality spots. Hence, the effect of

different print buffers on protein immobilisation was investigated for improving the quality and stability of spots on Aminosilane slides. In this work, the different TAAs expressed in lysates were prepared in PBS-Trehalose-Betaine-Tween and PBS-Trehalose-Betaine. Additionally, four Myc-DDK tagged purified TAAs borrowed from CEAC (HDGF, SDCCAG8, UTP14A, TRAG3) were printed at a concentration of 100 µg/ml in four replicates. A two-fold dilution of each TAA was made starting at a concentration of 200 µg/ml. Each dilution was printed in quadruplicates on an Aminosilane slide after which the slide was processed (**as shown in section 5.2**). Results indicated that lysate TAAs prepared in PBS-Trehalose-Betaine-Tween produced poor quality spots as they were severely smeared across all pads (**Figure 95B**). On the other hand, PBS-Trehalose betaine buffer produced uniform spots, although due to the extensive smearing effect of lysate TAAs prepared in PBS-Trehalose-Betaine-Tween, it was not possible to properly examine the morphology of spots printed (**Figure 95B**). The outcome provides an optimum buffer (PBS-Trehalose-Betaine) for printing high-performance lysate microarrays.



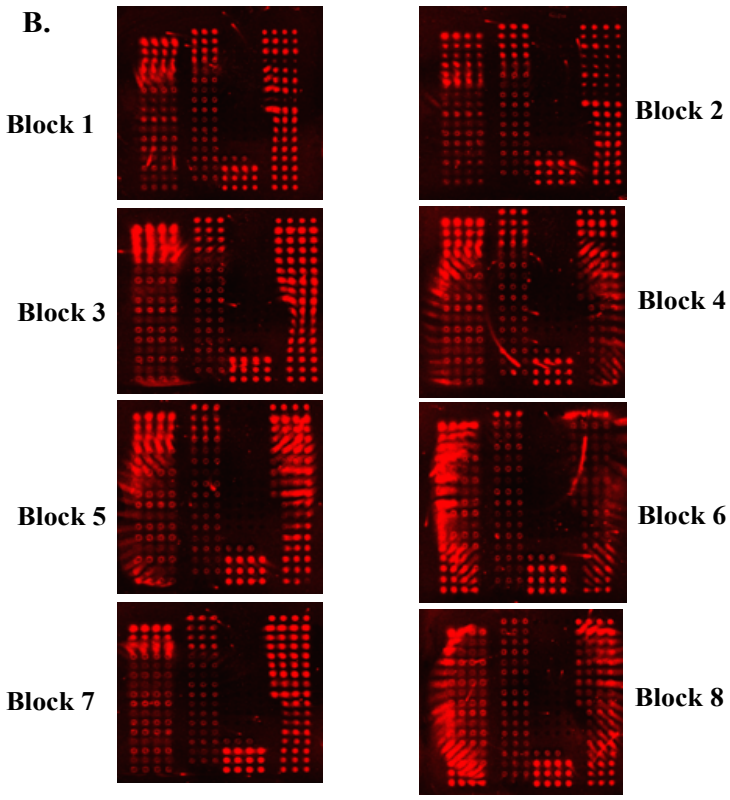
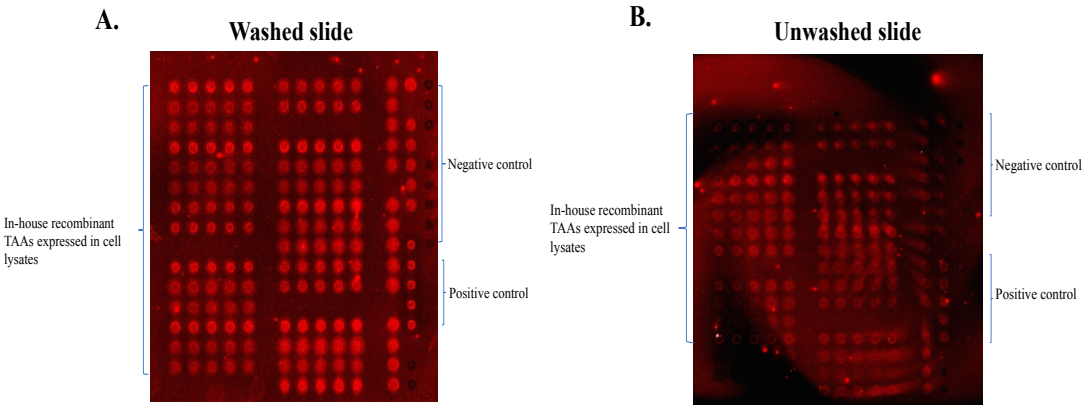


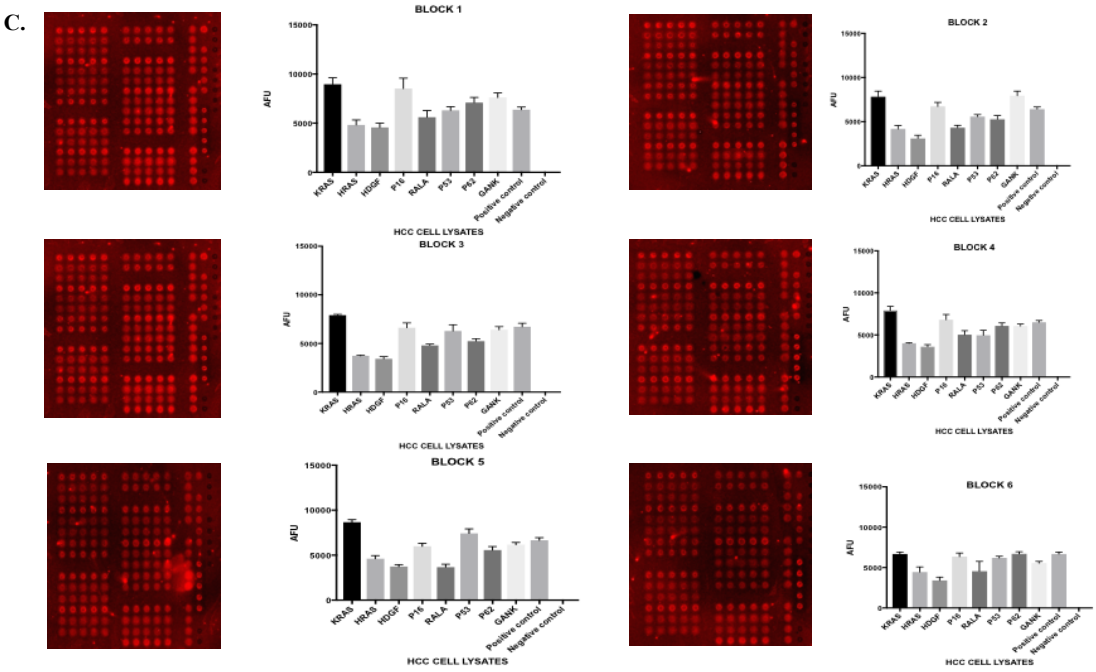
Figure 95: Determining the optimal print buffer for in-house TAAs. In-house TAAs expressed in lysates were prepared in different buffers (PBS-Trehalose-Betaine-Tween and PBS-Trehalose-Betaine) to determine the optimal print buffer for immobilising them unto the array. A two-fold dilution of each lysate was made starting a concentration of 200 µg/ml. Additional purified TAAs (HDGF, SDCCAG8, UTP14A, TRAG3) were also immobilised unto the solid support. Each dilution of TAA was printed in quadruplicates on the Aminosilane slide after which slides were processed. **(A)** Appearance of TAAs on a scanned slide, **(B)** eight-pad scan revealing poor quality of spots as well as smearing of TAAs prepared in PBS-Trehalose-Betaine-Tween, while PBS-Trehalose-Betaine produced uniform and more intense spots.

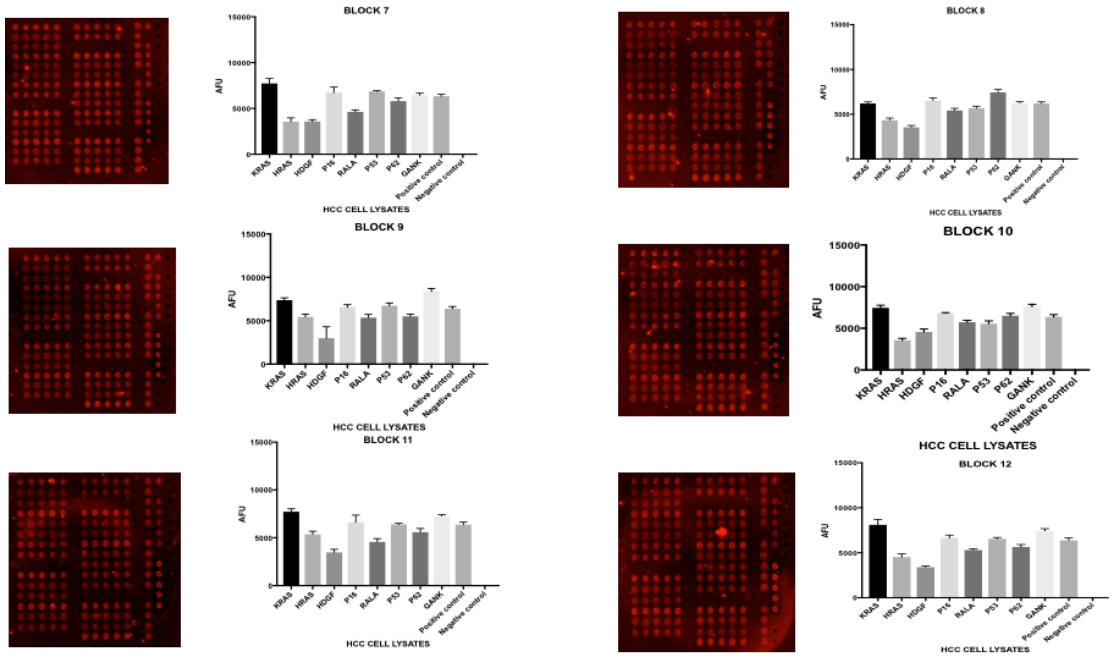
5.3.3 Effect of Stringent Washing condition Prior to Slide Processing

Earlier experiments demonstrated the suitability of PBS-Trehalose-Betaine for immobilising in-house TAAs on Aminosilane slides. However, not all of the contents of the lysate had bound to the slide during the arraying procedure leading to increased local backgrounds following slide processing. The antigen microarray involves many steps: plate preparation, slide printing, blocking, washing, probing, amplification, fluorescent detection, scanning, and data acquisition and any issues in the process may negatively affect the experiment. Among these, the washing step is a vital step for a successful microarray as it removes unbound protein from the slide and thus reduces

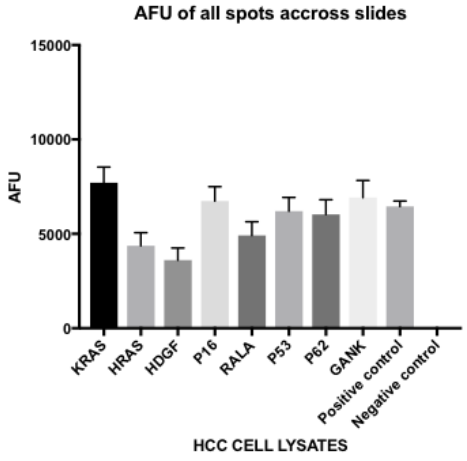
the local background noise. However, up until this time the step had always been employed after blocking the printed slide. However, we compared the effect of washing lysate printed slides before and after the blocking step to see if local background could be reduced. Subsequently, slides were incubated with anti-DDK (1:1,000 in % BSA) and anti-mouse antibodies (1:2,000 in antibody diluent). Lysate microarrays were constructed by printing spots of lysates containing eight expressed TAAs (KRAS, HRAS, HDGF, CDKN2A, RALA, P62, P53, Gankyrin) onto two Aminosilane slides. Microarrays contained five spots of each antigen, in four batches on each slide pad. One slide (**Figure 96A**) was washed rigorously with 1x PBST while the other slide (**Figure 96B**) was blocked immediately. Both slides were further processed and scanned. Results showed uniform morphology, no smearing or comet-tail characteristic of spots on the slide with more stringent washing condition prior to the blocking step (**Figure 96C**). A low background was also seen on all pads of the rigorously washed slide (**Figure 96C**). Data read from the washed slide showed a similar pattern of signal intensities across all pads. Signal intensities ranged from 3,000 AFU to approximately 10,000 AFU with KRAS and Gankyrin giving highest signal intensities (**Figure 96D**). The coefficient of variation across six TAAs was within the acceptable limit of precision (≤15%) with the exception of HRAS and HDGF, which fell were slightly below the limit (16% and 18% respectively). This was primarily due to their low signals. On the other hand, the slide directly processed without washing demonstrated a rosy smearing pattern (**Figure 96F**), obscuring morphological feature of spots. This made it difficult to analyse data generated form this slide. The results from the washing conditions prior to slide processing improved the quality of spots as well as the reproducibility of the assay.


A.
Washed slide
In-house recombinant TAAs expressed in cell lysates
Negative control
Positive control
B.
Unwashed slide
In-house recombinant TAAs expressed in cell lysates
Negative control
Positive control

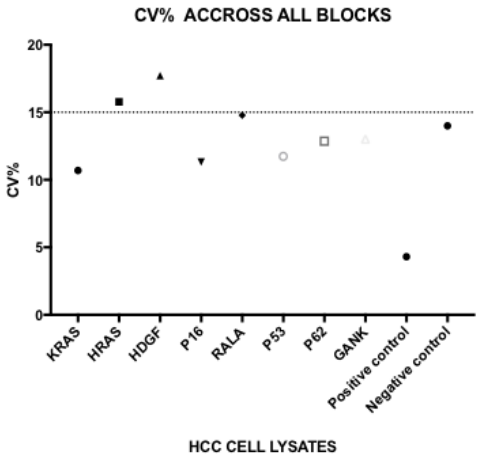

C.
BLOCK 1
BLOCK 2
BLOCK 3
BLOCK 4
BLOCK 5
BLOCK 6
AFU
HCC CELL LYSATES
KRAS
HRAS
HDGF
P16
RALA
P53
P62
GANK
Positive control
Negative control


BLOCK 7
BLOCK 8
BLOCK 9
BLOCK 10
BLOCK 11
BLOCK 12
AFU
KRAS
HRAS
HDGF
P16
RALA
P53
P62
GANK
Positive control
Negative control
HCC CELL LYSATES

D.


AFU of all spots accross slides
AFU
15000
10000
5000
0
KRAS
HRAS
HDGF
P16
RALA
P53
P62
GANK
Positive control
Negative control
HCC CELL LYSATES

E.


CV% ACCROSS ALL BLOCKS
CV%
20
15
10
5
0
KRAS
HRAS
HDGF
P16
RALA
P53
P62
GANK
Positive control
Negative control
HCC CELL LYSATES

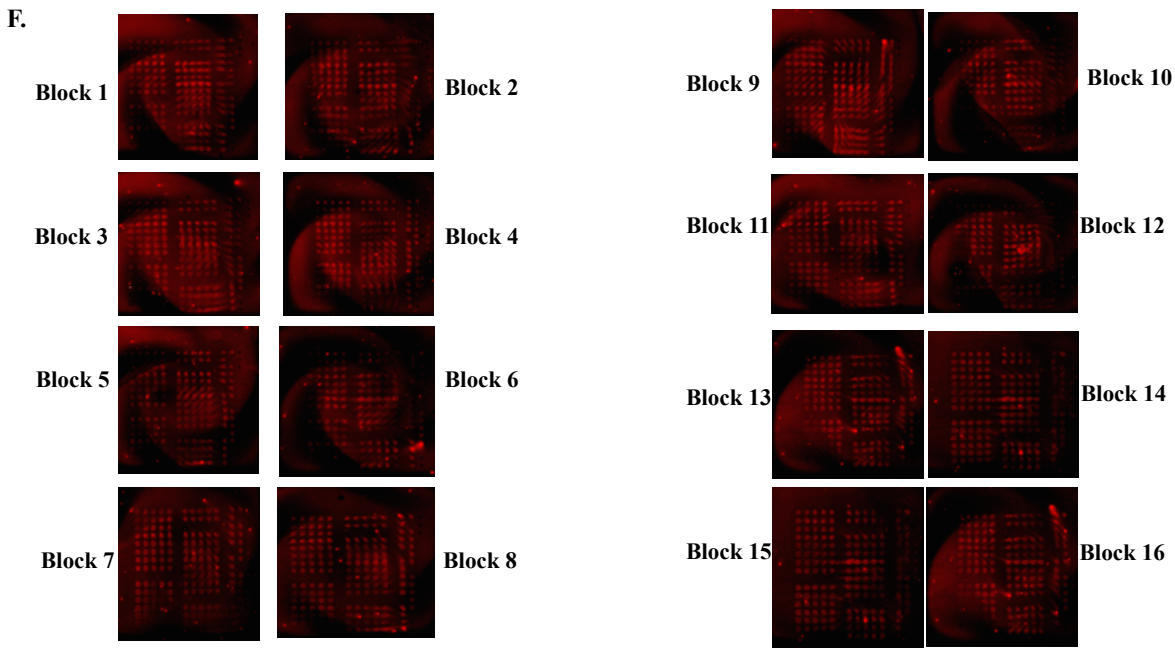


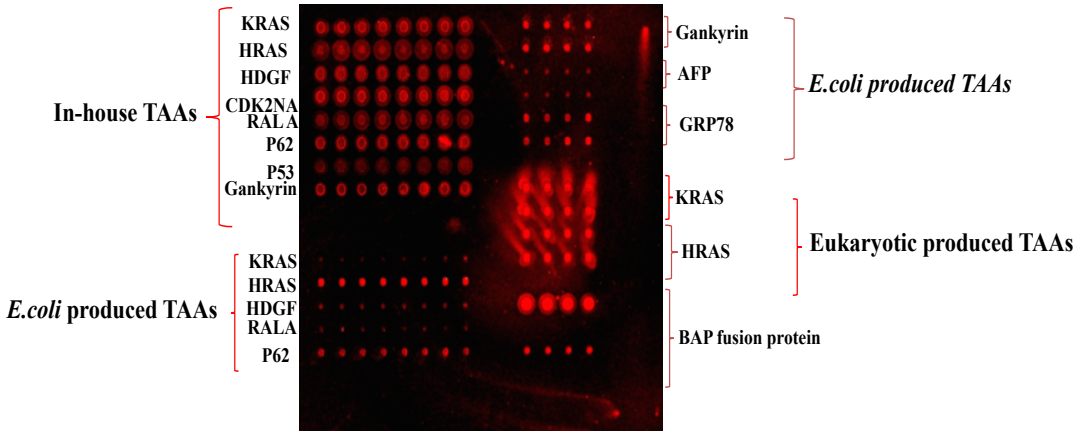
Figure 96: Comparing spot morphology when the slide was rigorously washed prior to and after processing. Lysates expressing the different TAAs (KRAS, HRAS, HDGF, CDK2NA, RALA, P62, P53, Gankyrin) were immobilised onto two Aminosilane slides at a concentration of 200 µg/ml. One printed slide **(A)** was washed stringently with x1 PBST before processing while the other; **(B)** was processed without washing. **(C)** shows the uniform morphology and signal intensities of spots on the slide with more stringent washing condition prior to processing. **(D)** Mean signal intensities of all TAAs (ranging from 3000AFU to 8000AFU) across the different pads of stringently washed slide. **(E)** The coefficient of variation of signal intensities of all TAAs across the different pads of washed slide **(F)** The slide directly processed without washing showing a rosy smearing pattern of spots.

5.3.4 Simultaneous Print of In-house and Commercial HCC Tumour - Associated Antigens on the Microarray Platform.

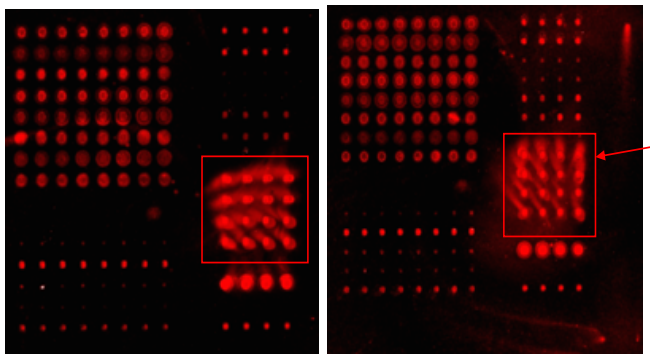
Eukaryotic generated Myc-DDK tagged TAAs (KRAS and HRAS) were purchased in addition to the cohort of in-house and commercial *E. coli* produced TAAs. This was undertaken in order to compare autoantibody responses in patients sera to the different categories of TAAs. The microarray had earlier been developed for both commercial *E.coli* generated TAAs and in-house TAAs. Here, we decided to examine commercial eukaryotic TAAs on the antigen microarray assay concurrently with these TAAs. Commercial *E. coli* produced (KRAS, HRAS, HDGF, RALA, P62, Gankyrin, AFP, GRP78) and eukaryotic produced (KRAS, HRAS) were each prepared in PBS-trehalose-Betaine-Tween at a concentration of 100 µg/ml, while in-house TAAs

(KRAS, HRAS, HDGF, CDKN2A, RALA, P62, P53, Gankyrin) were prepared in PBS-Trehalose-Betaine at a concentration 200 µg/ml. Proteins were arrayed in eight replicates on a slide and allowed to air dry overnight. The slide was stringently washed with x1 PBST after which it was processed, scanned and analysed (**as shown in section 5.2**). The scanned image shows the morphological appearance of all antigen spots in a pad (**Figure 97A**). However, spots of the newly purchased TAAs (KRAS and HRAS) exhibited comet-tail features and high background as compared to other TAAs which had excellent uniformity and spot morphology (**Figure 97B**). The intensity and comet-tail feature of commercial eukaryotic TAA (KRAS, HRAS) spots could be a result of probing with the anti-DDK and anti-mouse concentrations optimised for in-house TAAs. We repeated the experiment with focus placed on these two commercial eukaryotic TAAs (KRAS, HRAS) by testing them with three different dilutions of anti-DDK and anti-mouse antibodies (1:5,000 &1:15,000, 1:7,000 & 1:20,000, 1: 10,000 & 1:30,000). From **Figure 97C**, block 3 probed with 1:10,000 anti-DDK and 1:30000 anti-mouse antibodies gave an improved spot morphology of the two TAAs as well as low background noise. It was therefore deduced that the aforementioned antibody dilutions are optimal for commercial eukaryotic TAAs.

A.



B.

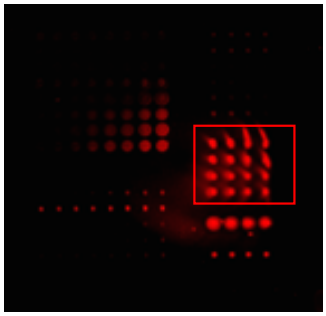


- High background
- Smearing of eukaryotic TAAs

- anti-DDK ab (1:1000 in 5% BSA)
- anti-mouse ab (1: 2000 in antibody diluent)

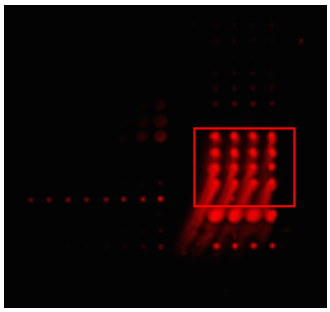
C.

Block 1



anti-DDK ab (1:5000 in 5% BSA)
anti-mouse ab (1: 15000 in antibody diluent)

Block 2



anti-DDK ab (1:7000 in 5% BSA)
anti-mouse ab (1: 20000 in antibody diluent)

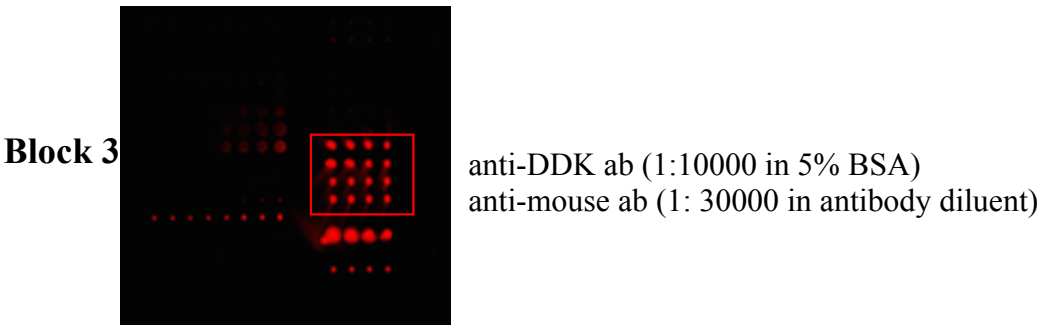


Figure 97: Immobilisation of in-house and commercial HCC TAAs simultaneously onto an Aminosilane slide surface. (A) Scanned pad displaying the outline of arrayed TAAs; **(B)** shows non-uniform spot morphology of two commercial eukaryotic TAAs (KRAS, HRAS) with very high background. **(C)** reveals the optimisation of anti-DDK and anti-mouse antibodies for commercial eukaryotic TAAs on three pads of an arrayed slide. Blocks 1, 2 and 3 were probed with anti-DDK and anti-mouse at the following dilutions respectively (1:5,000 in 5% BSA, 1:15,000 in antibody diluent), (1:7,000 in 5% BSA, 1:20,000 in antibody diluent) and (1:10,000 in 5% BSA, 1:30,000 in antibody diluent). Generated spots of KRAS and HRAS from Block 3 uniform with lower background indicating anti-DDK and anti-mouse antibodies at (1:10,000 in 5% BSA, 1:30000 in antibody diluent) were optimal for detecting commercial eukaryotic TAAs.

The experiment was repeated using six random sera (run blindly) to test the performance of different batches of TAAs. The different sets of TAAs as well as two-fold human IgG dilutions were each printed in eight replicates and in quadruplicates respectively in a six-pad format on an Aminosilane slide (**Figure 98A**). Each pad was probed with a serum sample (diluted 1:500 in 5% BSA) and further incubated with biotinylated anti-human antibody (diluted 1:20,000 in antibody diluent). Slides were processed as discussed above. The scanned image revealed the expected morphological appearance of spots indicating autoantibody responses to TAAs and the human IgG dilution standard. There was uniformity in all spots - those of the commercial TAAs were of even higher in quality since they existed in purified forms. Interestingly, although the sera were used blindly, autoantibody responses to some TAAs were detected via visual assessment of scanned image (**Figure 98B**). Responses to some commercial *E. coli* TAAs were detected in almost all the sera.

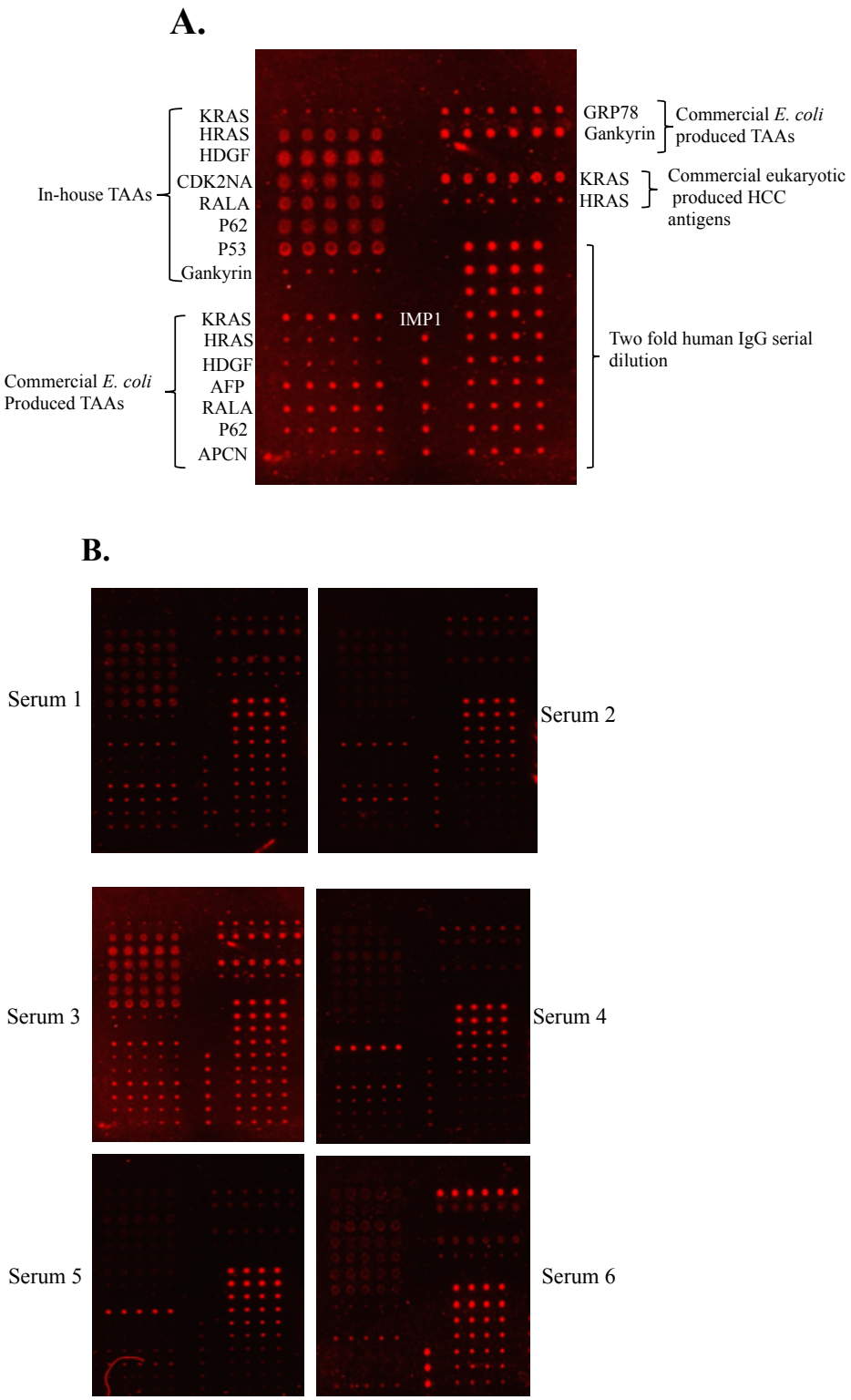


Figure 98: Testing the performance of different sets of TAAs on the microarray with serum samples. Twenty TAAs including in-house (KRAS, HRAS, HRAS, HDGF, CDK2NA, RALA, P62, P53, Gankyrin), commercial eukaryotic (KRAS, HRAS), commercial E. coli (KRAS, HRAS, HDGF, RALA, P62, AFP, APCN, GRP78, Gankyrin, IMP1) and a two-fold human IgG standard were printed in either four, five or six replicates unto an aminosilane slide. **(A)** Scanned image showing the arrangement of arrayed TAAs on a pad; **(B)** show the spot morphology of TAAs on six different pads of an Aminosilane slide incubated with six serum samples. Visually, circular and more consistent spot morphology was seen after assay conditions had been optimized for the different TAA category.

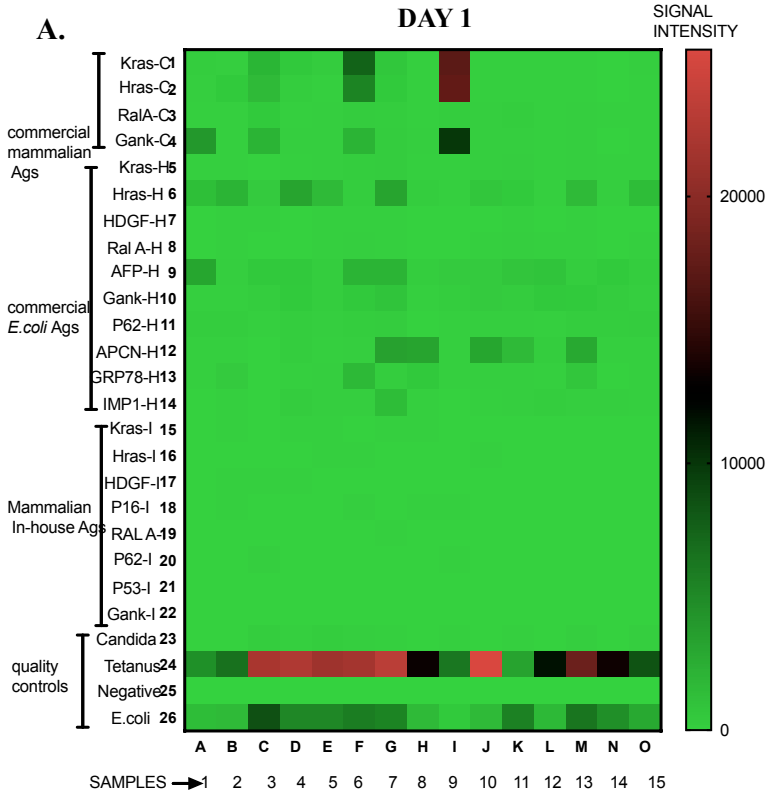
5.3.5 Validation of Twenty-Two In-house and Commercial Recombinant Tumour-associated antigens using random serum samples

One of the fundamental metrics to consider when choosing a diagnostic tool for examining autoantibody responses in cancer patients is its ability to present reproducible and reliable outcomes. This would help to ensure accurate measurements of TAA specific IgG in HCC patients' sera. In **Chapter 3**, the antigen microarray was validated after major optimisation of the parameters of the assay was carried out. However, this was done using *E. coli* produced TAAs. Additional sets of TAAs had been added to the existing array of antigens and the assay had been modified to suit each TAA category.

This section re-evaluates the validity of the amended antigen microarray assay for the quantification of TAA specific IgG before commencement of major screening with patients' sera.

Reproducibility of autoantibody responses to 22 TAAs, namely in-house (KRAS, HRAS, HDGF, CDKN2A, RALA, P62, P53, Gankyrin), commercial *E. coli* produced (KRAS, HRAS, HDGF, RALA, AFP, Gankyrin, P62, APCN, GRP78, IMP1), and commercial eukaryotic produced (KRAS, HRAS, RALA, Gankyrin) TAAs were examined in this study within a day and across three different days. The above TAAs, controls (*Candida,* Tetanus toxoid, *E. coli* antigen, cell lysate expressing empty vector) were each printed in quadruplicates on a pad of the six Aminosilane slides on three consecutive days. Also, a two-fold purified human IgG standard was added to each corresponding pad of the various slides. The two printed slides were processed on three different days. It was also ensured that assay conditions for all slides across the different days were the same. Serum TAA-specific IgG levels were quantified in fifteen serum

samples (run blindly). Data analysis was performed, and the median signal intensities were calculated for each serum sample over the different TAAs. As seen from the **Figure 99A**, increased IgG levels (AFU) were mostly seen in response to commercial eukaryotic TAAs (KRAS, HRAS, Gankyrin) and *E. coli* TAAs (HRAS, AFP, APCN, GRP78 and IMP1). The highest anti-TAA IgG autoantibody measurement in response to commercial eukaryotic KRAS (22,000AFU) and HRAS (21,000AFU), were seen in serum 9 (**Figure 99A**). High IgG responses to *Tetanus* and *E. coli* were observed in all sera. The outcomes obtained on day 1 (**Figure 99A**) were no different from day 2 (**Figure 99B)** or day 3 (**Figure 99C**) with the exception of serum sample 6 exhibiting high IgG levels to *Candida* on day 2 (**Figure 99B**).



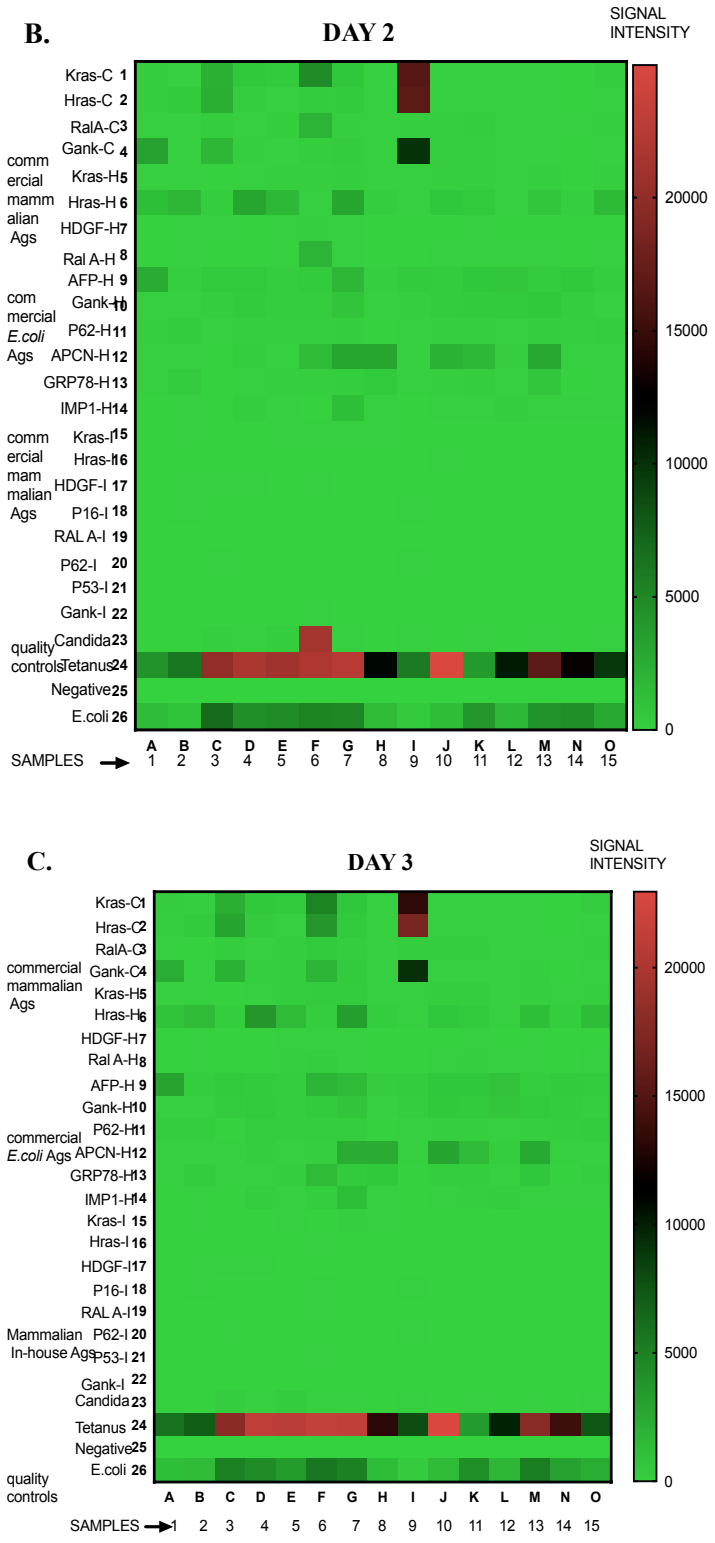
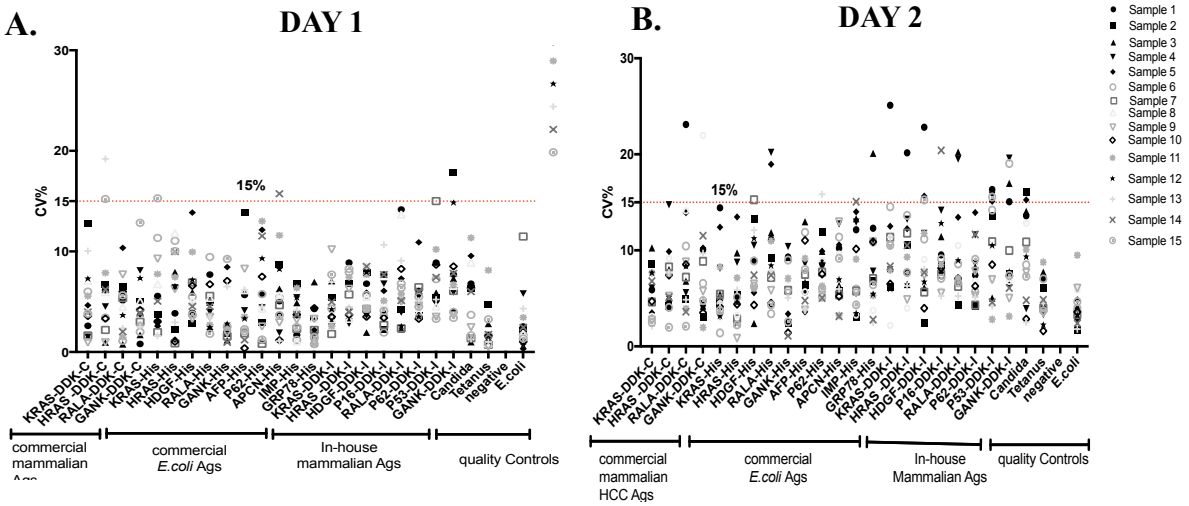
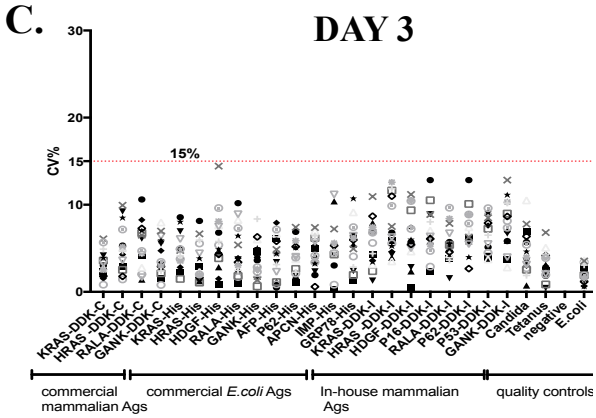


Figure 99: Heat Map showing signal intensities of total IgG levels in 15 serum samples. Fifteen random serum samples (run blindly) were measured for serum TAA-specific IgG with the antigen microarray platform using 22 TAAs across **(A)** day 1; **(B)** day 2; and **(C)** day 3. *Candida*, Tetanus, *E. coli* and empty vector were used as quality controls. The 22 TAAs were outlined on the vertical axis to the left and the serum samples on the horizontal axis. The relative degree of reactivity of specific antibodies in the sera is indicated by bright red for high, dark-green for medium, and light green for low signals or negative reactivity. The colour scale is presented to the right of the plot.

The precision of the antigen microarray was calculated to investigate variations between corresponding signal intensities of TAA spots on six slides that were processed on the three different days. Intra-assay CV% was determined by measuring the CV values of signal intensities among four replicate spots of each TAA on the same pad within an assay. The mean and standard deviation for the four spots were measured and the CV% values were calculated. Variability analysis revealed that intra-assay CV% of all TAA replicates in day 1 were mostly within the acceptable criteria of precision (≤15%) with the exception of one *E. coli* produced TAA (APCN) and in-house TAA (Gankyrin) which gave CV values of 17% and 19% respectively (**Figure 100A**). On Day 2, high variation was observed across replicates of some in-house TAAs ranging from 16% to 25%. Elevated CV values were seen in in-house produced TAA (KRAS-24%) and commercial eukaryotic produced (RALA-23%) (**Figure 100B**). On the third day, CV% of all replicates were within the acceptable limit of precision (≤15%) (**Figure 100C**). In the case of inter-assay variation, CV% was calculated for signal intensities of twelve replicate spots of each TAA across the three days. Most of the CV values were outside the acceptable limits for all TAAs whereas some were within the criteria (ranging from 21% to 38%) (**Figure 100D**).

(I). Intra-assay variation before normalisation





(II). Inter-assay variation before normalisation

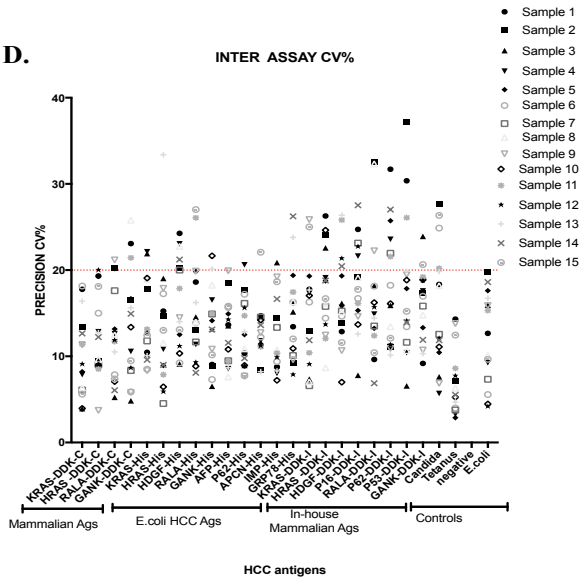
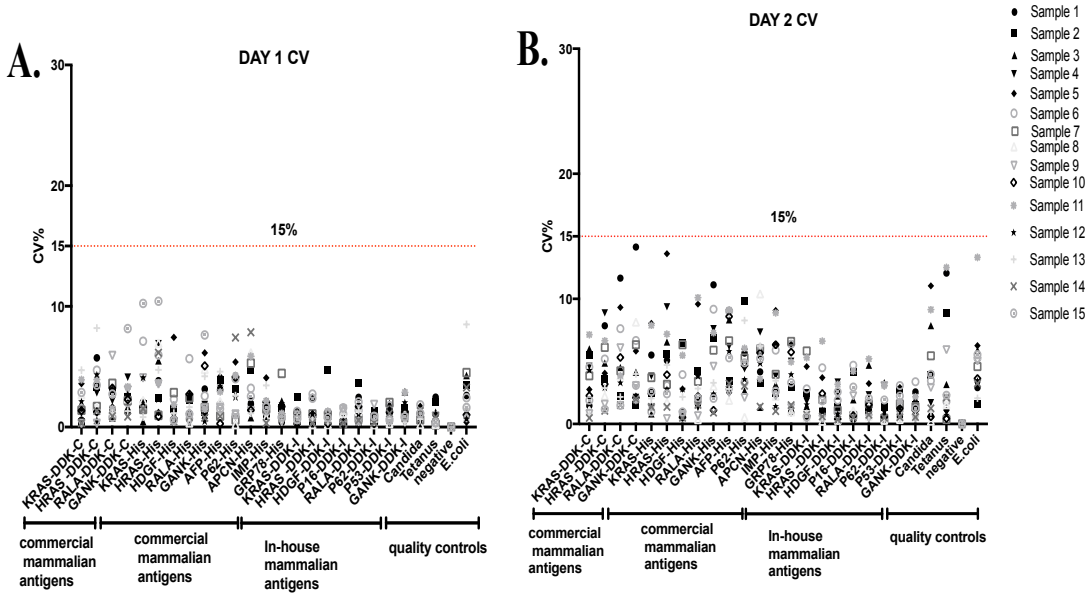


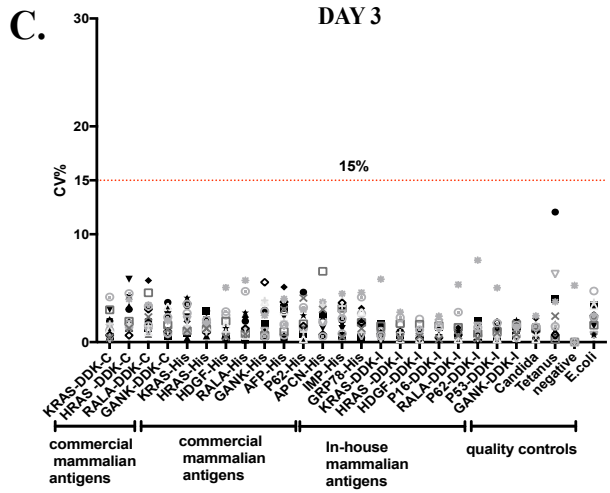
Figure 100: Precision of signal intensities before normalisation. Twenty-two TAAs were printed onto six Aminosilane slides and processed with fifteen random serum samples over a period of three consecutive days. Signal intensities generated for each of the TAAs was calculated after which the coefficient of variation for each TAA within a day (intra-assay variability) and over different days (inter-assay variability) were generated**. (A-C)** indicate the intra-assay CV values on days 1, 2 and 3 respectively while **(D)** represent the inter-assay CV values over the three days. Dashed lines represent the acceptable criteria of precision for intra-assay (≤15%) and inter-assay variation (≤20%).

In a microarray experiment, many undesirable variations may be observed. Normalisation plays an important role in microarray data analysis as it removes some sources of variation which affect measured signal intensities. In this assay, purified human IgG standard curve was used as the normalisation tool to correct differences in the fluorescent signal intensity measurements reported in **Figure 100**. A reduction in intra-assay variations of signal intensities for all TAAs in days 1, 2 and 3 were observed after normalisation with IgG standard curve. CV% ranged from 2% to 14% across the different days and these indicate that data obtained from individual assays were reproducible (**Figure 101A-C,**). Analysis of the inter-assay variability after normalisation showed a drastic drop, with over 95% of CV values falling within the

acceptable criteria (≤20%) (**Figure 101D**). All these indicate how precise the assay is when carried out multiple times under the same working conditions and normalising using a standard IgG curve.

(III). Intra assay variations after normalisation





(IV). Inter assay variations after normalisation

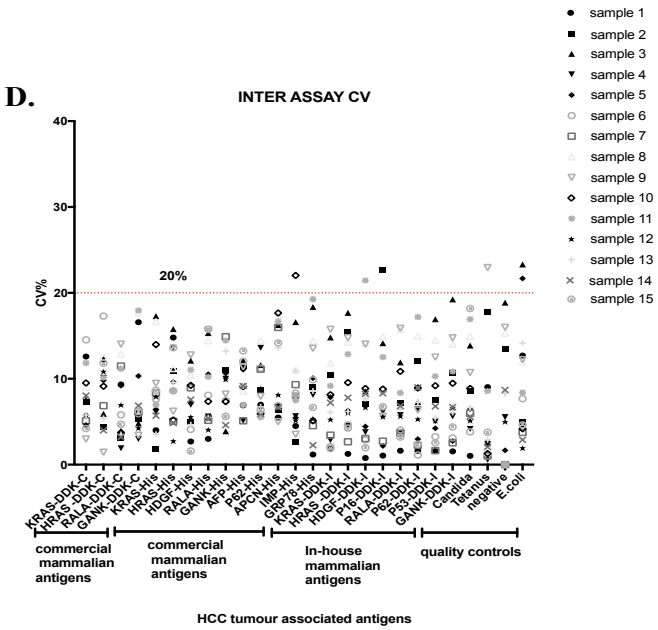


Figure 101: Precision after normalisation of signal intensities. Twenty-two TAAs were printed onto six Aminosilane slides and processed with 15 random serum samples over a period of three consecutive days. Signal intensities generated for each of the TAAs were normalised with a two-fold IgG standard curve after which the coefficient of variation of interpolated values from the standard were calculated for precision of an assay run in one day (intra-assay variability) and across different days (inter-assay variability). **(A-C)** indicate the intra-assay CV for interpolated values on days 1, 2 and 3 respectively while **(D)** represent the inter-assay CV of interpolated values over the three days. Dashed lines represent the acceptable criteria of precision for intra-assay (≤15%) and inter-assay variation (≤20%).

5.4 Discussion

One of the objectives of this chapter was to test the performance of in-house and commercial TAAs concurrently on the microarray. Testing the binding of in-house TAAs expressed in lysates on the Aminosilane surface in this chapter was essential as the major optimisation experiments (**Chapter 3**) were conducted with purified proteins. It is of huge importance to efficiently immobilise antigens onto a substrate with good spot quality for fabrication of protein microarrays. Print buffers are important in the fabrication process for the microarrays. From this chapter, some challenges were encountered in ensuring TAAs expressed in lysates were effectively printed and stabilised onto slide during processing. In this work, lysates expressing different TAAs were prepared in PBS-Trehalose-Betaine-Tween, as it was the optimal buffer determined during the optimisation of the assay (**in Chapter 3**). In assessing the quality of spots, it was noticed that there was an extensive smearing of spots as well as comet-tail features on the glass slide. It was anticipated that the addition of tween, which is supposed to help prevent evaporation of spots, did not support the nature of lysates and contributed to the non-homogenous appearance of spots. On the other hand, lysates were prepared in a different print buffer, PBS-Trehalose-Betaine and tested on the microarray. Interestingly, this composition of buffer effectively eliminated non-homogeneous morphology of the spots and significantly improved the signal intensities. This indicated that the PBS-Trehalose-Betaine was optimal for arraying lysates. Stringent wash of printed slides helped to enhance the in-house TAAs by improving the quality of spots and minimising extensive smearing, which obscured the visualisation of commercial TAAs. This could be explained by the fact that not all lysate printed on the slide effectively and hence washing removed these unbound proteins.

The second objective of this chapter was to validate the modified antigen microarray technology. Validation was based on a number of parameters from the FDA guidelines such as reproducibility (intra- and inter-assay variability) (461). Reproducibility (precision) is critical for an antigen microarray as it helps to determine the functioning and limitation of antigen microarray platform for quantification of serum IgG autoantibodies in HCC patients. Precision can be defined as the reproducibility of a technique with regard to how close the measured replicates are to one another (461). The reproducibility (precision) of antigen microarray was examined on signal intensities generated from the interaction of a different TAAs with 15 serum samples on three consecutive days under same assay conditions. The majority of the intra-assay CV values fell within the acceptable limits on the different days although some CV values on day 2 fell out of the acceptable criteria due to low abundant IgG giving rise to low signal intensities. The inter-assay variation was also outside the acceptable limit for some of the autoantibody responses measured. It was thus important to print the human IgG standard on each array to normalize the subtle differences in how features are printed, such as variation in antigen concentration due to evaporation during the progression of a print run or technical errors (460). A drastic reduction in variation was seen in both intra- and inter-assay assays after normalisation to this IgG standard curve. Thus, the developed antigen microarray platform has now demonstrated suitability, reproducibility and reliability for quantification of serum IgG autoantibodies in HCC patients.

The next chapter will use this optimised and validated microarray to run a large cohort of clinical samples to determine the effectiveness of our TAA panel for profiling autoantibody responses in HCC.

Chapter Six: Clinical Utility of the Microarray Platform for the Detection of Autoantibodies in Hepatocellular Carcinoma Patients

6.1 Introduction

Hepatocellular carcinoma is a primary liver cancer and is considered as the third most common cause of cancer deaths worldwide (462). The extensive prevalence of this cancer carries a significant economic burden on a country. Hepatitis B, hepatitis C, non-alcoholic fatty liver and excessive alcohol intake are considered as prominent risk factors associated with the malignancy (29). Physical symptoms, such as pain or a lump in the upper belly, yellowish skin and eyes, pale chalky bowel movement and weight loss have been implicated in the diagnosis of HCC (463).

HCC is usually detected at the advanced stages and this is attributed to the lack of sensitive and specific methods to detect the tumour early. Current imaging technologies, such as Computed Topography (CT) scan and Magnetic Resonance Imaging (MRI), do not detect the early spread of tumour cells, hence, effective curative treatment is compromised. The addition of serum Alpha Fetoprotein (AFP) measurement to the screening tools is also not ideal, as its sensitivity is suboptimal (464). Once diagnosed, HCC patients tend to have a poor 5-year survival rate of 0%-10% (314). This clearly indicates that a test for early detection of HCC is required, since it would help in efficient monitoring and successful treatment of patients and this could increase survival rates to over 70% (465), according to the German S3 guidelines for HCC. It is well known that cirrhotic, chronic liver and non-alcoholic fatty liver disease

patients, irrespective of their etiologies, are at high risk of developing hepatocellular carcinoma (HCC). It is therefore not surprising that it is highly recommended to undertake regular screening tests in patients with liver cirrhosis as they would benefit from an early tumour diagnosis (314). This is because HCC occurs at the background of cirrhosis.

The evidence of circulating autoantibodies in cancer patients' sera has recently generated opportunities for immune system exploitation as source of cancer biomarkers. These biomarkers are elicited by the release of tumour-associated antigens (TAAs) from the tumour. In recent years, extensive research has been channelled into the potential use of autoantibodies in detection of different cancers such as lung (249), pancreatic (251), oesophageal (466), gastric (247), breast (467), HCC (241). Autoantibodies are preferable because they are secreted and easily accessible, they persist and are stable in the serum for a long time. They are also present in the sera before the TAAs can be identified. Moreover, many reagents and techniques are available for their detection, shortening assay development. These autoantibody signatures make screening possible for patients who are likely to develop the cancer by monitoring their autoantibody profiles before clinical manifestation of symptoms (396).

The main aim of this chapter is to utilise the newly developed microarray assay on a defined set of serum samples derived from HCC patients with different etiologies (HBV, HCV, Non-alcoholic fatty liver disease (NALFD), Non-alcoholic steatohepatitis (Nash), Alcoholic liver disease (ALD), Type 1 diabetes (T1D)), cirrhotic (liver cirrhosis) and non-cirrhotic (chronic liver hepatitis) patients, as well as healthy individuals. The newly developed diagnostic platform would be used for

immunoprofiling anti-TAA specific autoantibodies against twenty-six TAAs produced in different expression systems in a single step with small volumes of samples.

6.2 Materials

6.2.1 Tumour-associated antigens (TAAs)

Twenty-six TAAs were utilised for the screening of autoantibodies in patients' sera, of which eight were produced in-house (**Chapter 4**).

6.2.2 Patients samples

Three independent patient sample sets were used (**Table 23**). The first set (n = 84) consisted of HCC and healthy serum samples which were kindly given by Prof. W. Irving, The Trent Cohort Study, Nottingham University Hospitals NHS Trust. Samples from this source was labelled as 'Cohort 1'. The Centre of Excellence for Autoimmunity in Cancer (CEAC) donated 88 samples, of which 45 were HCC and 43 were non-HCC non-cirrhotic samples (chronic hepatitis patients). These were named 'Cohort 2'. The third group of patients' samples (n=280) were collected from the HCV Biobank, UK of which 100, 90 and 90 were HCC, non-HCC cirrhotic and non-HCC non-cirrhotic respectively. These were also named 'Cohort 3'. All HCC patients had cirrhosis while 'non-HCC cirrhotics' were patients who had just liver cirrhosis and neither HCC or chronic liver hepatitis. On the other hand, 'non-HCC non-cirrhotics' were patients who had just chronic liver hepatitis. Healthy controls were individuals who had no obvious symptoms of viral hepatitis or any form of liver disease. Ethical approval and informed consent were given for all samples prior to the study.

6.3 Methodology

6.3.1 Detection of autoantibody reactivity using Antigen Microarray

Aliquots of sera (50 µl) were incubated in a PCR block for 30 minutes at temperatures at 56°C after which sera were allowed to cool before testing with antigen microarray. In-house (KRAS, HRAS, HDGF, CDKN2A, RALA, P62, P53, Gankyrin), commercial *E. coli* produced (KRAS, HRAS, HDGF, RALA, P62, APCN, AFP, IMP1, GRP78, Gankyrin), commercial eukaryotic (KRAS, HRAS, HDGF, CDKN2A, RALA, P62, P53, Gankyrin), quality controls (*Candida*, Tetanus, *E. coli*, empty vector) were prepared in either PBS-Trehalose-Betaine or PBS-Trehalose-Betaine-Tween at concentrations of 200µg/ml or 100µg/ml. Purified human IgG standard was prepared in PBS-Trehalose-Betaine-Tween at a starting concentration of 50 µg/ml. Samples were transferred into a 384 microtiter well plate. The plate was further sealed with aluminium tape (Corning Costar, USA) and centrifuged at 1200 rpm for 5 minutes. The microtiter plate was loaded onto the arrayer, which was set to the optimal relative humidity 65%, slide layouts (sixteen-pads) and printing pattern (four-replicates). Aminosilane slides were fixed onto the arrayer's tray and samples were printed in each slide pad and printed slides were left overnight in a desiccator or array to dry. Slides on the day of processing were taken from the vacuum chamber and washed with 1x PBST after which they were blocked for an hour with 5% BSA in PBST for 1 hour. After incubation, slides were washed thrice with wash buffer (1x PBST). Serum samples (HCC, non-HCC cirrhotic, non-HCC non-cirrhotic, healthy control) were each diluted (1:500 in 5% BSA) and 100 µl of each was added to a corresponding well and incubated for an hour. Slides were subsequently washed and further incubated with 100 µl of biotinylated anti-human antibody diluted (1:20,000 in antibody diluent) for another hour. Slides were washed

and 100 µl of 1:2,000 diluted streptavidin-HRP (Bio- RAD, USA) was added per pad and incubated for 15 minutes in the dark. Slides were washed and 100µl of Bio-Rad Tyramide Amplification Reagent (amplification reagent dilution ratio 4:1:4) was added for 10 mins in the dark. Subsequently, slides were washed three times with 20% DMSO-PBST and further washed three times with x1PBST. After the washing step, 100 µl of 1:2000 diluted streptavidin- conjugated cy5 (E-Biosciences, UK) was added to each pad and incubated at room temperature for 15 mins in the dark. Slides were thoroughly washed 3 times and rinsed thoroughly in ultrapure water after which they were centrifuged dry (1200rpm for 3 minutes). Finally, slides were scanned with the 4200 AL microarray scanner at 635nm (Axon GenePix®) and fluorescence was quantified using the GenePix Pro Software (Axon GenePix®).

6.3.2 Statistical Data Analysis

The median fluorescence of each spot was measured (minus background) and the corrected fluorescence was used to calculate the average fluorescence signal across the standard detectable ranges after which generated data was sorted using R statistical package. Cut-off values for identifying seropositive samples (positive anti-TAA autoantibodies) were 95^{th} percentile of the healthy group. Statistical analysis was performed on raw and seropositive data using Microsoft excel, Graph Pad Prism 7 and IBM SPSS Statistics 21:

- Shapiro Wilk tests and descriptive statistics normal Q-Q was used to test the normality of distributions.
- Since the data was a non-parametric, the Kruskal-Wallis test was used to evaluate differences between two or three separate distributions while the Wilcoxon and Friedman tests were used to determine paired differences

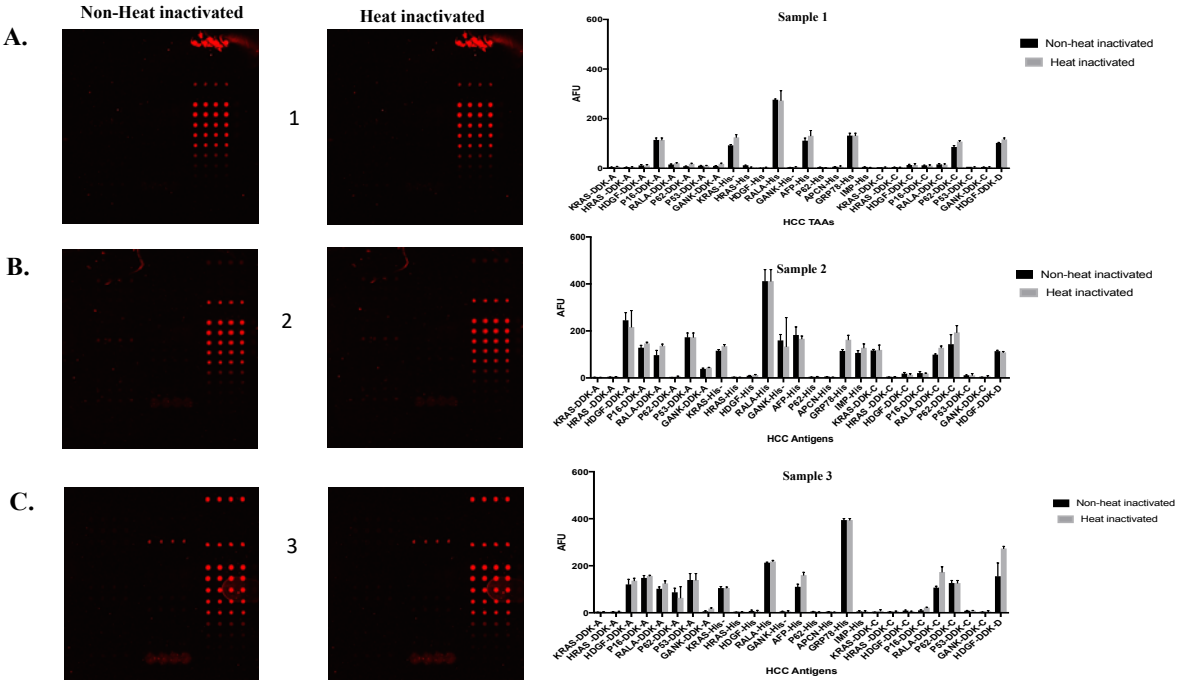
between two separate distributions (the proportion of samples containing anti-TAA antibodies).

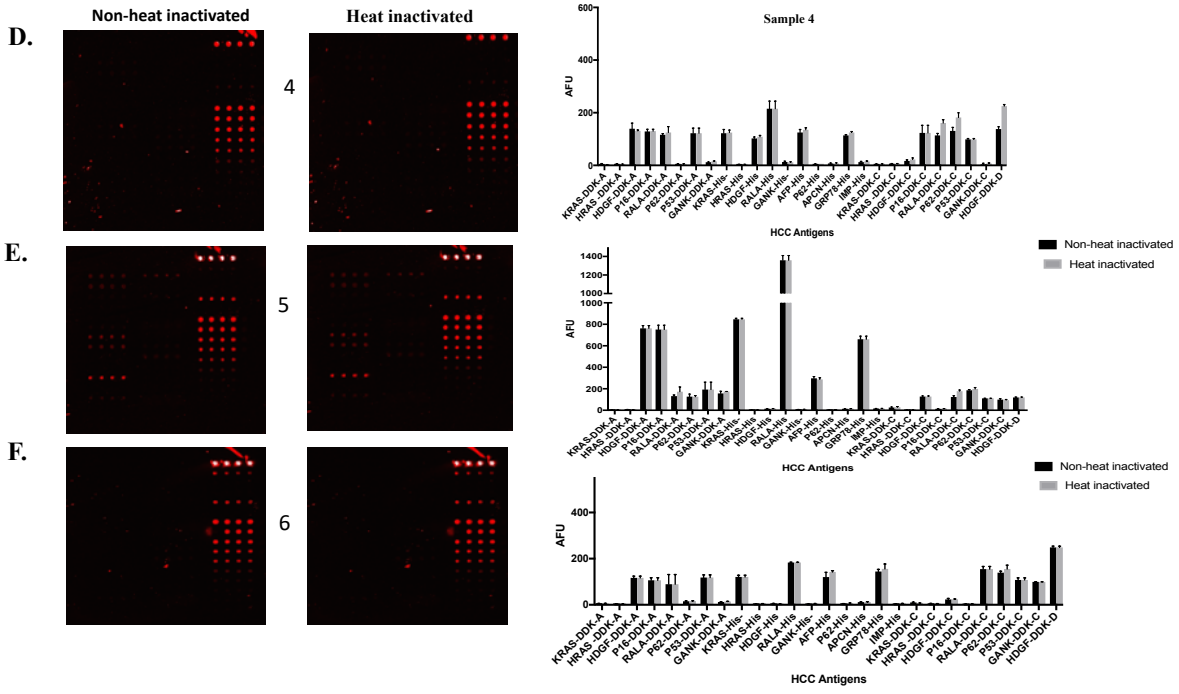
- Bonferroni corrections were performed for multiple comparisons, and $p<0.05$ was considered statistically significant.
- Quantities of seropositives were calculated as: number of positive samples/number of samples tested.
- The Spearman's bivariate correlation was used to measure the direction of association that exist between two variables.

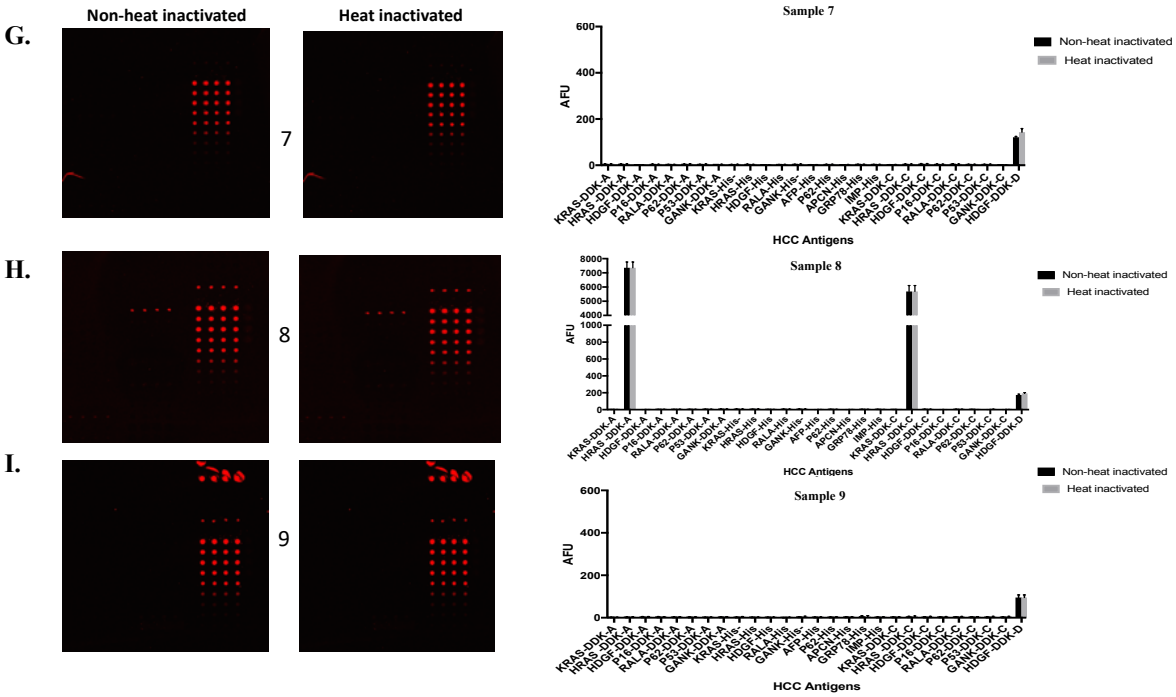
6.4 Results

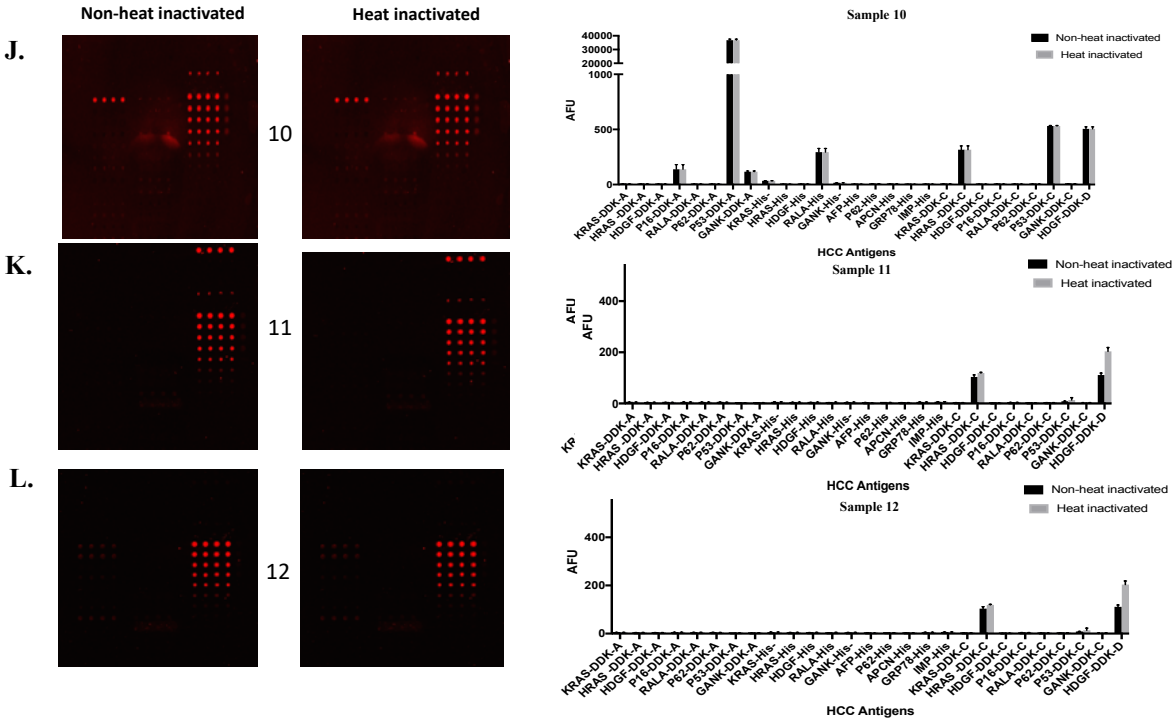
6.4.1 Effect of Heat Treatment of Human Serum on Autoantibody Measurement in HCC patients

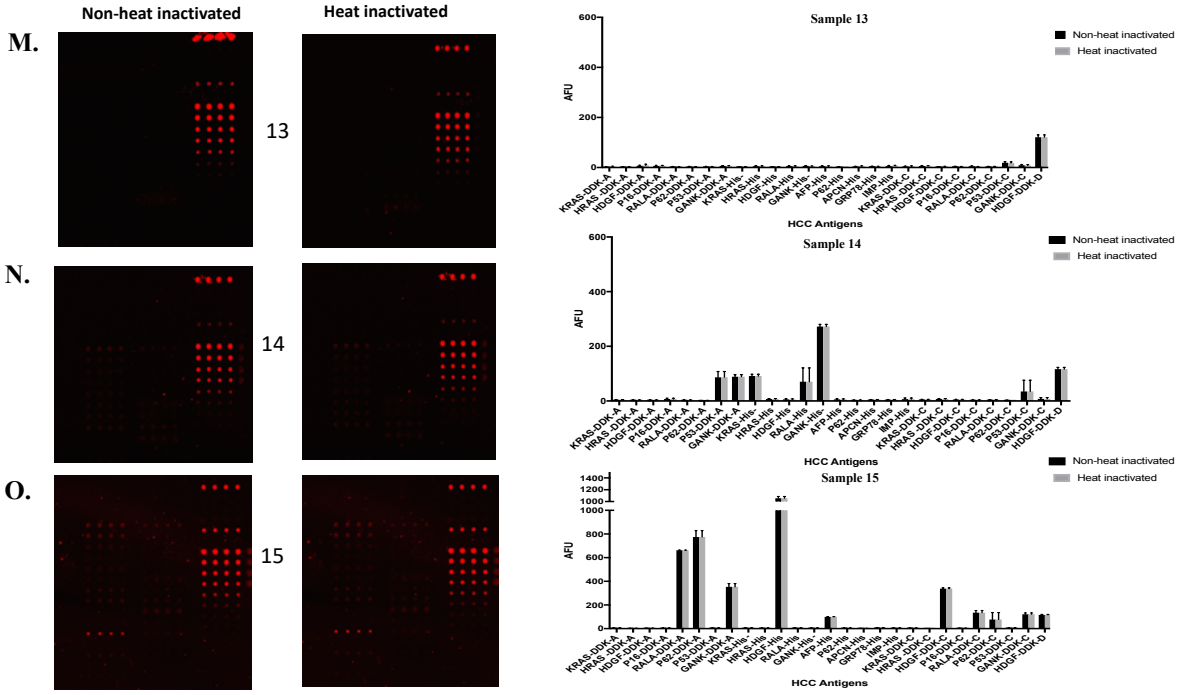
HCC is associated with different aetiologies and Hepatitis B and Hepatitis C viruses are regarded as the major risk factors for this type of malignancy. It was therefore not surprising that about 82% of patients' clinical samples were viral-associated. Prior to major screening of patients' sera against TAAs, it was essential to investigate the effect of heat treatment (used to inactivate the virus) on autoantibody responses to TAAs, so as to be informed whether or not virally infected sera could be safely screened for autoantibodies using the newly developed microarray technology. Twenty-six (26) HCC and non-HCC sera (all known to be virus free) were divided into two equal aliquots of which one was heated to 56°C for 30 minutes and the other left at room temperature. These were screened against twenty-six (26) TAAs; in-house (KRAS, HRAS, HDGF, CDKN2A (P16), RALA, P62, P53, Gankyrin) and commercially acquired TAAs either expressed in eukaryotic (KRAS, HRAS, HDGF, CDKN2A (P16), RALA, P62, P53, Gankyrin) and *E. coli* system (KRAS, HRAS, HDGF, RALA, P62, APCN, AFP, IMP1, GRP78, Gankyrin), to test the impact of heat treatment on anti-TAA autoantibody levels. It was noticed that heat treatment of the 26 sera did not cause a significant change (**Figure 102**) in anti-TAA specific autoantibody levels (p value >0.05) in sera irrespective of the presence or the absence of HCC. In other words, all the sera had levels of anti-TAA autoantibodies which were unaltered by heat treatment. Hence, heat inactivation had no effect on the detectability of autoantibodies to the various sets of TAAs.

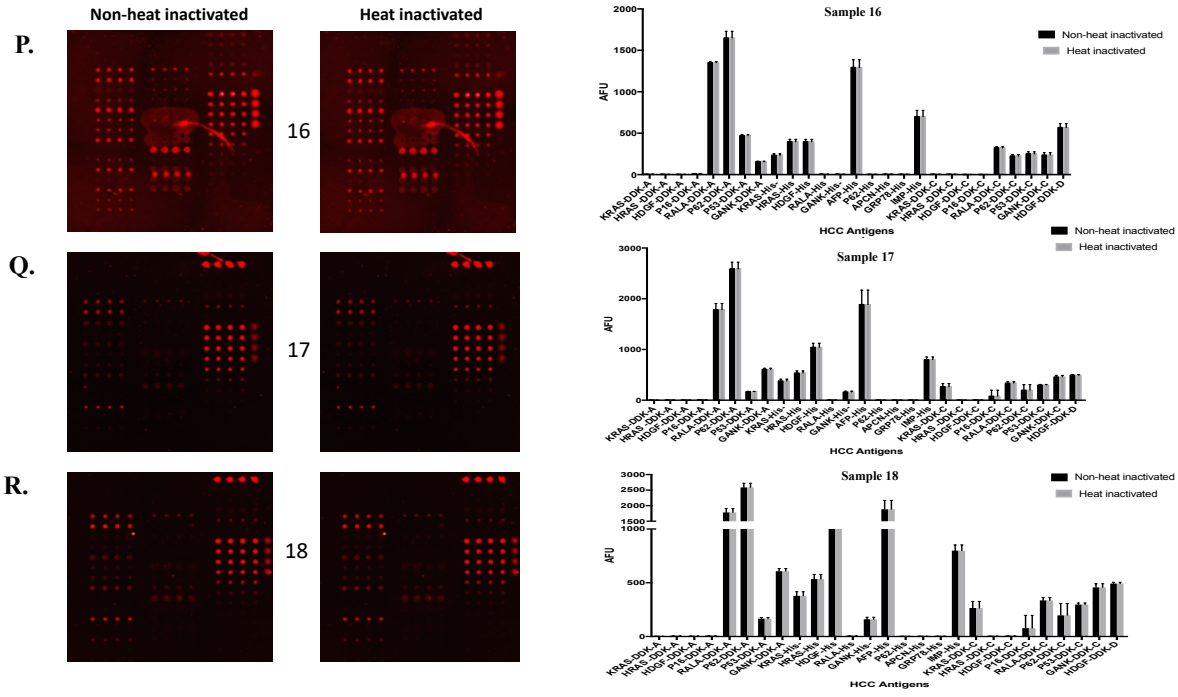

A.
Non-Heat inactivated
Heat inactivated
1
Sample 1
Non-heat inactivated
Heat inactivated
AFU
HCC TAAs
B.
2
Sample 2
HCC Antigens
C.
3
Sample 3
HCC Antigens

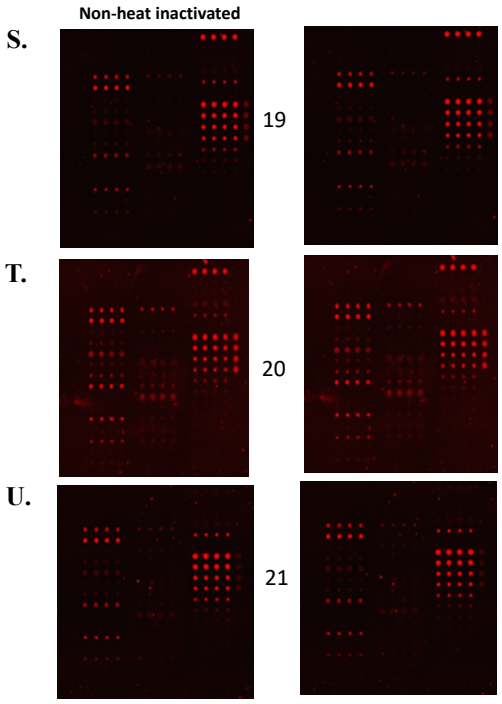

D.
Non-heat inactivated
Heat inactivated
4
Sample 4
HCC Antigens
E.
5
F.
6
Non-heat inactivated
Heat inactivated
AFU
HCC Antigens

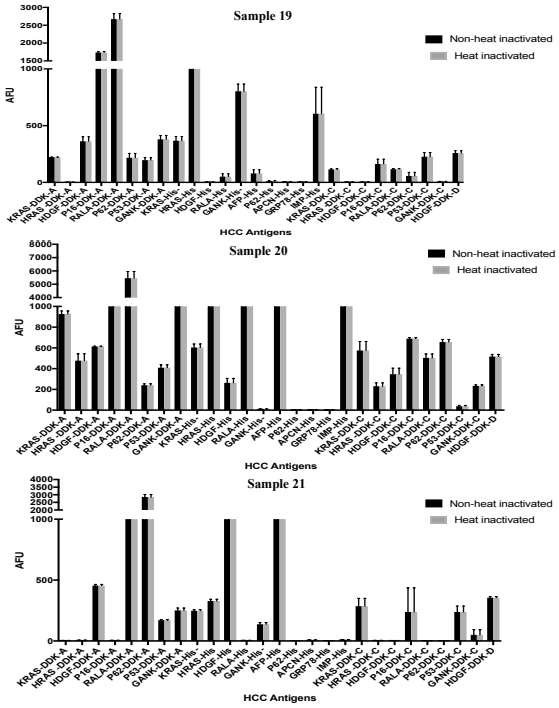

G.
Non-heat inactivated
Heat inactivated
7
Sample 7
AFU
Non-heat inactivated
Heat inactivated
HCC Antigens
H.
8
Sample 8
I.
9
Sample 9

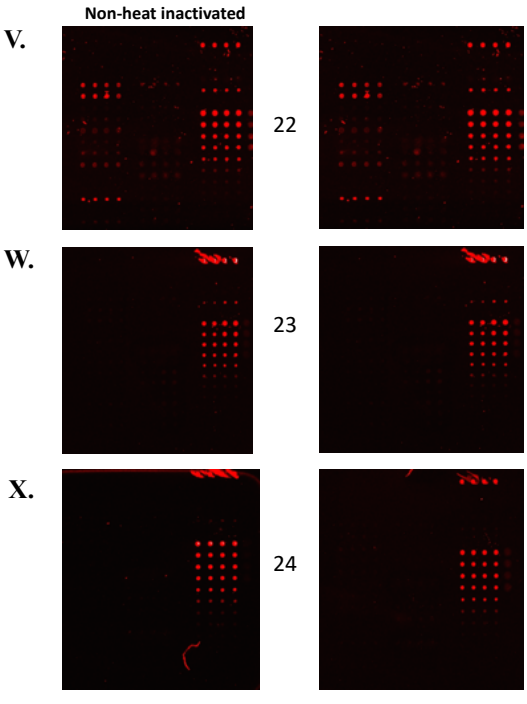

J.
Non-heat inactivated
Heat inactivated
10
Sample 10
AFU
HCC Antigens
K.
11
Sample 11
L.
12
Sample 12

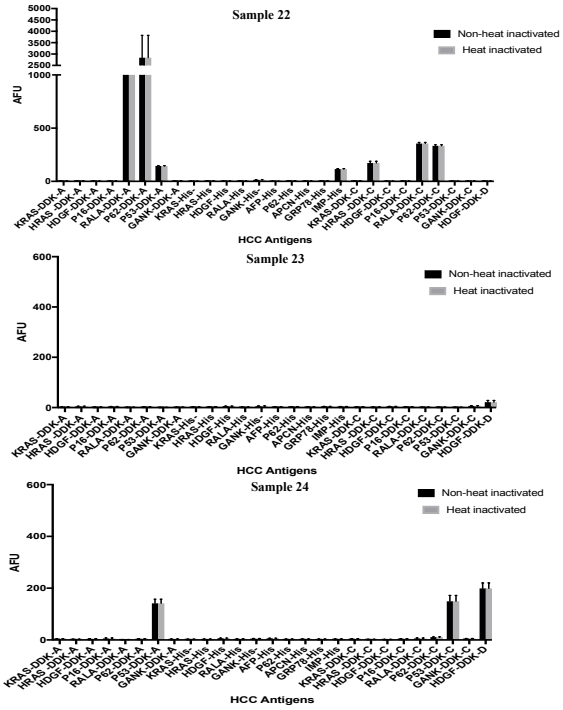

Non-heat inactivated
Heat inactivated
M.
13
N.
14
O.
15
Sample 13
Sample 14
Sample 15
Non-heat inactivated
Heat inactivated
AFU
HCC Antigens


Non-heat inactivated
Heat inactivated
P.
16
Q.
17
R.
18
Sample 16
Sample 17
Sample 18
Non-heat inactivated
Heat inactivated
AFU
HCC Antigens


Non-heat inactivated
S.
19
T.
20
U.
21


Sample 19
Sample 20
Sample 21
Non-heat inactivated
Heat inactivated
AFU
HCC Antigens


Non-heat inactivated
V.
22
W.
23
X.
24


Sample 22
Sample 23
Sample 24
Non-heat inactivated
Heat inactivated
AFU
HCC Antigens

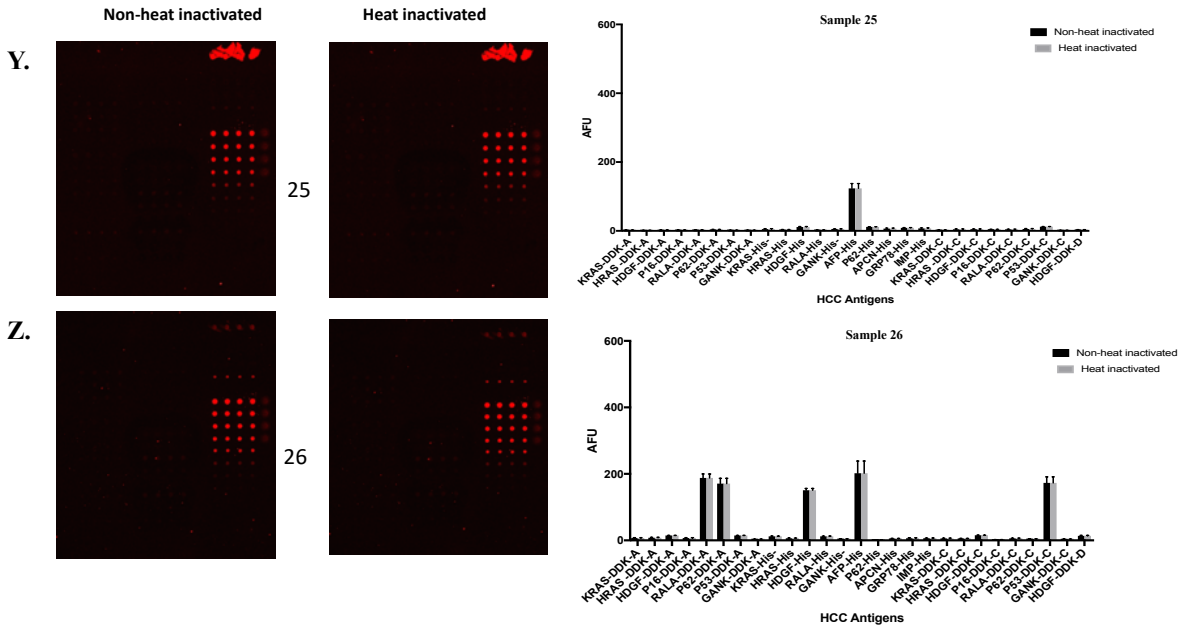


Figure 102: Effect of heat treatment on autoantibody measurement in HCC and non-HCC subjects. Twenty-six HCC and non-HCC sera divided into two aliquots, were either heated at 56ºC for 30 minutes or left at room temperature. Binding of specific anti-TAA autoantibodies in these two classes of sera to twenty-six TAAs; in-house antigens (KRAS, HRAS, HDGF, CDKN2A, RALA, P62, P53, Gankyrin), commercially acquired antigens expressed in eukaryotic (KRAS, HRAS, HDGF, CDKN2A, RALA, P62, P53, Gankyrin) and E. coli systems (KRAS, HRAS, HDGF, RALA, P62, APCN, AFP, IMP1, GRP78, Gankyrin), were tested on the antigen microarray assay. This was undertaken to determine whether heat inactivation affects autoantibody responses in patients' sera. (p value>0.05).

6.4.2 Characterisation of Research Subjects in the Study

A total of 452 clinical samples were used in the study and these were provided from three different locations. The three sample datasets were named Cohort 1, Cohort 2 and Cohort 3 (**Table 23**). Cohort 3 comprised the largest group of samples (280), followed by Cohort 2 (88) and Cohort 1 (84), where the mean age was 59.45±7.4, 65±5.8 and 59.45±7.4 respectively (**Table 23**). Of the three sets, there was an uneven distribution of gender as the majority of subjects were male (320) rather than female (132). The majority of samples were HCV positive across the three different cohorts. However, samples from Cohort 1 had a wide array of aetiologies, ranging from HCV, HBV, ALD, Nash, NAFLD and diabetes, unlike the other datasets which were limited to HBV, HCV and ALD. Clinical samples from the Cohorts 1 and 2 were collected within similar time

intervals (2011-2013) while those from Cohort 3 were more recent (2012-2015). Clinical samples were thus grouped into four cohorts namely: HCC, non-HCC cirrhotics (liver cirrhosis), non-HCC non-cirrhotics (chronic liver hepatitis) and healthy controls (**Table 24**).

Table 23: Clinical Characterisation of Research Subjects from three datasets.

	(Cohort 1)	**(Cohort 2)**	**(Cohort 3)**
Age			
Mean +SD	59.17±14.25	65±5.8	59.45±7.4
Age range	37-93	55-81	41-79
Gender			
Male (%)	43 (51.2)	62 (70.5)	215 (76.8)
Female (%)	41 (48.8)	26 (29.5)	65 (23.3)
Aetiology			
HCV (%)	7 (8.3)	45 (51.1)	280 (100)
HBV (%)	2 (2.4)	4 (4.5)	0
ALD (%)	14 (16.7)	8 (9.1)	0
Nash (%)	4 (4.8)	0	0
NAFLD (%)	1 (1.2)	0	0
Diabetes (%)	1 (1.2)	0	0
Others (%)	11 (13)	0	0
Cohort			
HCC only (%)	38 (45.2)	45 (51.1)	100 (35.7)
Non-HCC cirrhotic (%)	0	0	90 (32.1)
Non-HCC non-cirrhotic (%)	0	43(4.89)	90 (32.1)
Healthy (%)	46 (54.8)	0	0
Sample collection	11/05/2011-02/07/2013	22/03/2011-13/02/2013	01/08/2012-03/11/2015

Table 24: Information on clinical samples and related aetiologies.

Subjects	Total number of cases	HCV	HBV	ALD	Nash	NAFLD	Diabetes
HCC	183	152	6	16	4	1	4
Non-HCC cirrhotics	90	-	-	-	-	-	-
Non-HCC non-cirrhotics (chronic liver disease)	133	126	1	6	-	-	-
Healthy controls	46	-	-	-	-	-	-

6.4.3 Measurement and Comparison of Autoantibody Responses against TAAs across Different Cohorts

Antigen Microarray assays were used to determine levels of anti-TAA specific autoantibody responses in the sera of the four sets of subjects (183 HCC, 90 non-HCC cirrhotics, 133 non-HCC non-cirrhotics and 46 healthy subjects) to twenty-six TAAs. Specific anti-TAA autoantibody responses to individual TAAs were grouped into three sets. This was based on the system in which the TAAs were expressed. Anti-TAA autoantibody responses to commercial TAAs produced in HEK 293 cells were categorised as **set A** (anti-KRAS, anti-HRAS, anti-HDGF, anti-P16, anti-RALA, anti-P62, anti-P53, anti-Gankyrin), while autoantibody responses to commercial *E. coli* produced TAAs were defined as **set B** (anti-KRAS, anti-HRAS, anti-HDGF, anti-RALA, anti-P62, anti-Gankyrin, anti-AFP, anti-APCN, anti-AFP, anti-GRP78). Lastly, autoantibody responses to in-house TAAs expressed in HEK 293 cells were named as **set C** (anti-KRAS, anti-HRAS, anti-HDGF, anti-P16, anti-RALA, anti-P62, anti-P53, anti-Gankyrin).

95th percentiles of anti-TAA autoantibody responses in the healthy subjects were used as cut-offs of all specific anti-TAA autoantibody responses (**Table 25**). Shapiro-Wilk tests and descriptive statistics in SPSS were employed to test the distribution of anti-

TAA autoantibody responses across the different subjects in order to determine the normality of distribution. However, since anti-TAA responses were not normally distributed, the Kruskal-Wallis test which is a non-parametric test (compares two or more groups) was employed to compare the distribution of specific anti-TAA autoantibody responses across the four patients sets. This was done to determine if there was a significant difference in anti-TAA responses across the different study subjects. Adjustments were made to P values from pairwise comparisons using Bonferroni correction in SPSS since several independent statistics were undertaken simultaneously. There were significant differences in the distribution of anti-TAA specific responses across the four set of study subjects with the exception of anti-P16-A, anti-RALA-B and anti-Gankyrin-B autoantibody responses (**table 26**), which indicated that responses in the four cohorts were the same.

A pairwise comparison test was further undertaken to compare the distribution of specific anti-TAA responses between two subjects (HCC vs Non-HCC cirrhotics, HCC vs Non-HCC non-cirrhotics, HCC vs Healthy). Autoantibody responses to most TAAs (**Figure 103 A-Z**) in the HCC group were higher than that of the other subjects. However, anti-P53-A (26,181 AFU) (**Figure 103R**) and anti-P16-C (35,229 AFU) (**Figure 103K**) were the highest mean autoantibody responses across HCC patients. Interestingly, autoantibody responses in non-HCC non-cirrhotic patients were close to that observed in HCC patients and slightly higher than those in non-HCC cirrhotics. Interestingly, the distribution of anti-TAA responses between the HCC and healthy groups were the same with the exception of anti-KRAS-A (**Figure 103A**), anti-HRAS-A (**Figure 103D**), anti-HRAS-B (**Figure 103E**), and anti-APCN-B (**Figure 103Z**). Moreover, there were significant differences in responses between HCC and non-HCC cirrhotics with the exception of anti-Gankyrin B (**Figure 103U**), anti-RALA-A (**Figure**

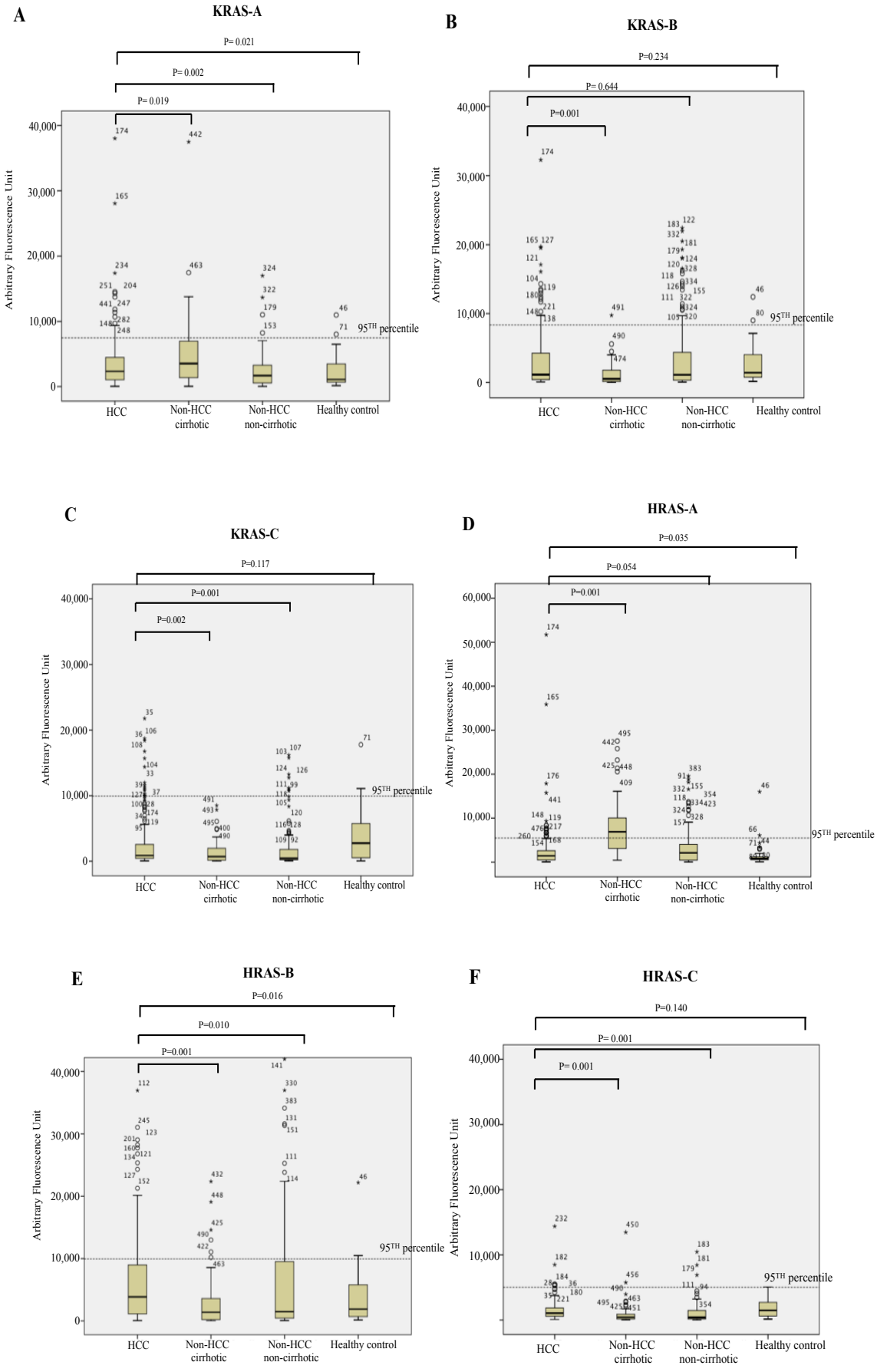
103L), anti-RALA-B (**Figure 103M**), anti-P16-A (**Figure 103J**) and anti-AFP-B (**Figure 103X**), which indicated distribution of responses were same. Lastly, autoantibody responses to most TAAs between HCC and non-HCC non-cirrhotics were significantly different with the exception of anti-KRAS-B (**Figure 103B**), anti-HRAS-A (**Figure 103 D**), anti-HDGF-A (**Figure 103G**), anti-P16A (**Figure 103J**), anti-RAL A-B (**Figure 103M**), anti-Gankyrin-B (**Figure 103U**), anti- and anti-AFP-B (**Figure 103X**).

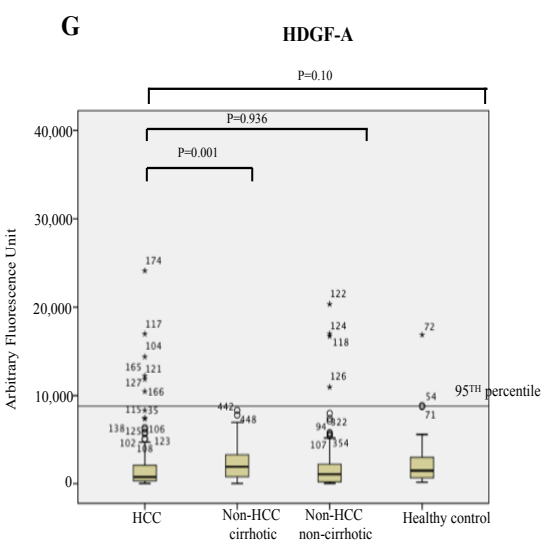
Table 25: 95th percentile of specific anti-TAA autoantibody responses in healthy controls.

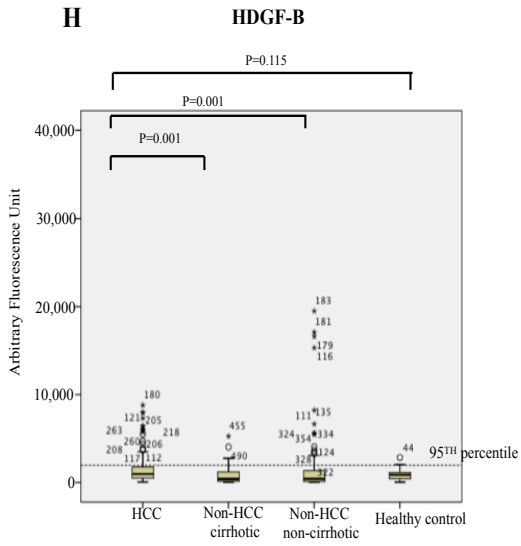
Anti-TAAs (set A)	Cut-off (AFU)	Anti-TAAs (set B)	Cut-off (AFU)	Anti-TAAs (set C)	Cut-off (AFU)
KRAS	7485	KRAS	8326	KRAS	9952
HRAS	5489	HRAS	10334	HRAS	7801
HDGF	8814	HDGF	1950	HDGF	5018
P16	5835	RALA	3246	P16	29479
RALA	6642	P62	14661	RALA	4087
P62	5920	Gankyrin	7655	P62	6966
P53	12928	APCN	4035	P53	3095
Gankyrin	7333	GRP78	4369	Gankyrin	4476
-	-	AFP	4324	-	-
-	-	IMP1	4369	-	-

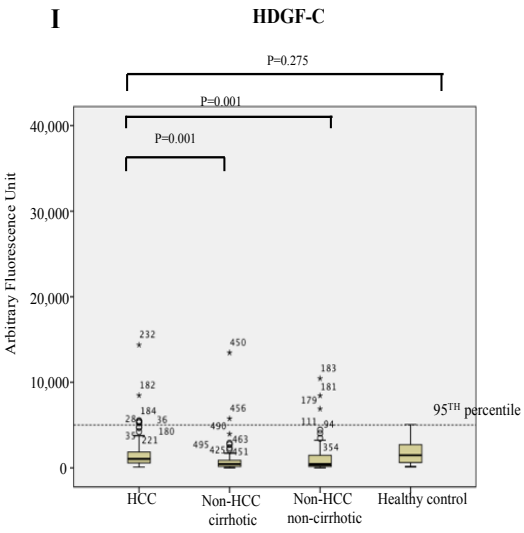
Table 26: Kruskal-Wallis statistical tests of the distribution of anti-TAA autoantibody responses across the four sample cohorts (HCC, non-HCC cirrhotic, non-HCC, non-cirrhotic and Healthy controls).

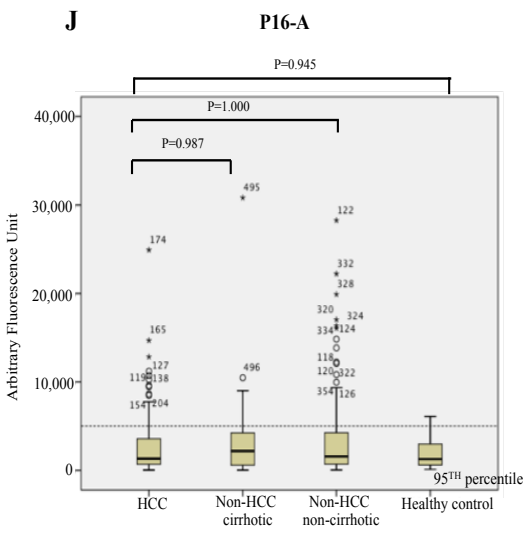
Anti-TAAs	Kruskal-Wallis P value
KRAS-A	0.001
HRAS-A	0.001
HDGF-A	0.001
P16-A	0.495
RALA-A	0.001
P62-A	0.016
P53-A	0.001
Gankyrin-A	0.007
KRAS-B	0.001
HRAS-B	0.001
HDGF-B	0.001
RALA-B	0.183
P62-B	0.001
Gankyrin-B	0.241
AFP-B	0.041
APCN-B	0.001
IMP-B	0.001
GRP78-B	0.005
KRAS-C	0.001
HRAS-C	0.001
HDGF-C	0.001
P16-C	0.001
RALA-C	0.001
P62-C	0.001
P53-C	0.001
Gankyrin-C	0.001

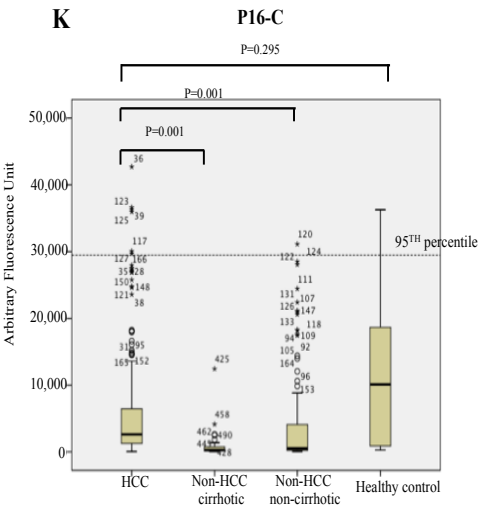

A
KRAS-A
P= 0.021
P= 0.002
P= 0.019
Arbitrary Fluorescence Unit
95TH percentile
HCC
Non-HCC cirrhotic
Non-HCC non-cirrhotic
Healthy control
B
KRAS-B
P=0.234
P= 0.644
P=0.001
Arbitrary Fluorescence Unit
95TH percentile
HCC
Non-HCC cirrhotic
Non-HCC non-cirrhotic
Healthy control
C
KRAS-C
P=0.117
P=0.001
P=0.002
Arbitrary Fluorescence Unit
95TH percentile
HCC
Non-HCC cirrhotic
Non-HCC non-cirrhotic
Healthy control
D
HRAS-A
P=0.035
P=0.054
P=0.001
Arbitrary Fluorescence Unit
95TH percentile
HCC
Non-HCC cirrhotic
Non-HCC non-cirrhotic
Healthy control
E
HRAS-B
P=0.016
P=0.010
P=0.001
Arbitrary Fluorescence Unit
95TH percentile
HCC
Non-HCC cirrhotic
Non-HCC non-cirrhotic
Healthy control
F
HRAS-C
P=0.140
P= 0.001
P= 0.001
Arbitrary Fluorescence Unit
95TH percentile
HCC
Non-HCC cirrhotic
Non-HCC non-cirrhotic
Healthy control

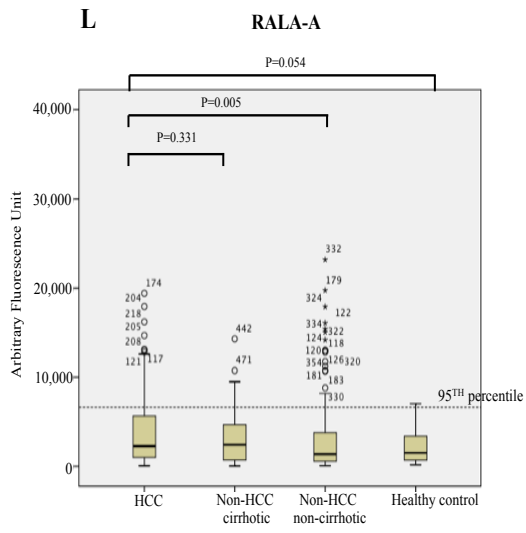

G
HDGF-A
P=0.10
P=0.936
P=0.001
Arbitrary Fluorescence Unit
95TH percentile
HCC
Non-HCC cirrhotic
Non-HCC non-cirrhotic
Healthy control

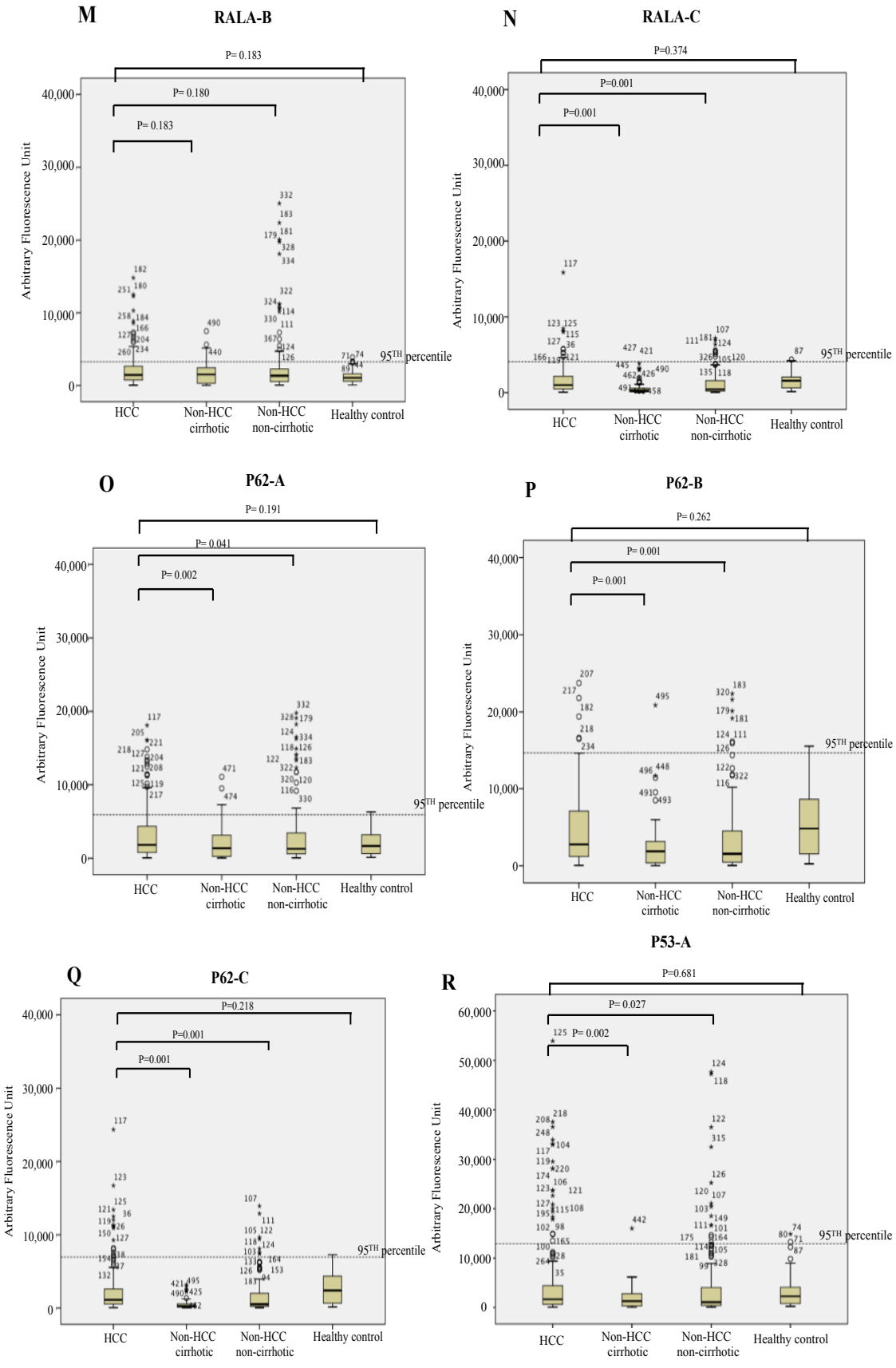

H
HDGF-B
P=0.115
P=0.001
P=0.001
Arbitrary Fluorescence Unit
95TH percentile
HCC
Non-HCC cirrhotic
Non-HCC non-cirrhotic
Healthy control

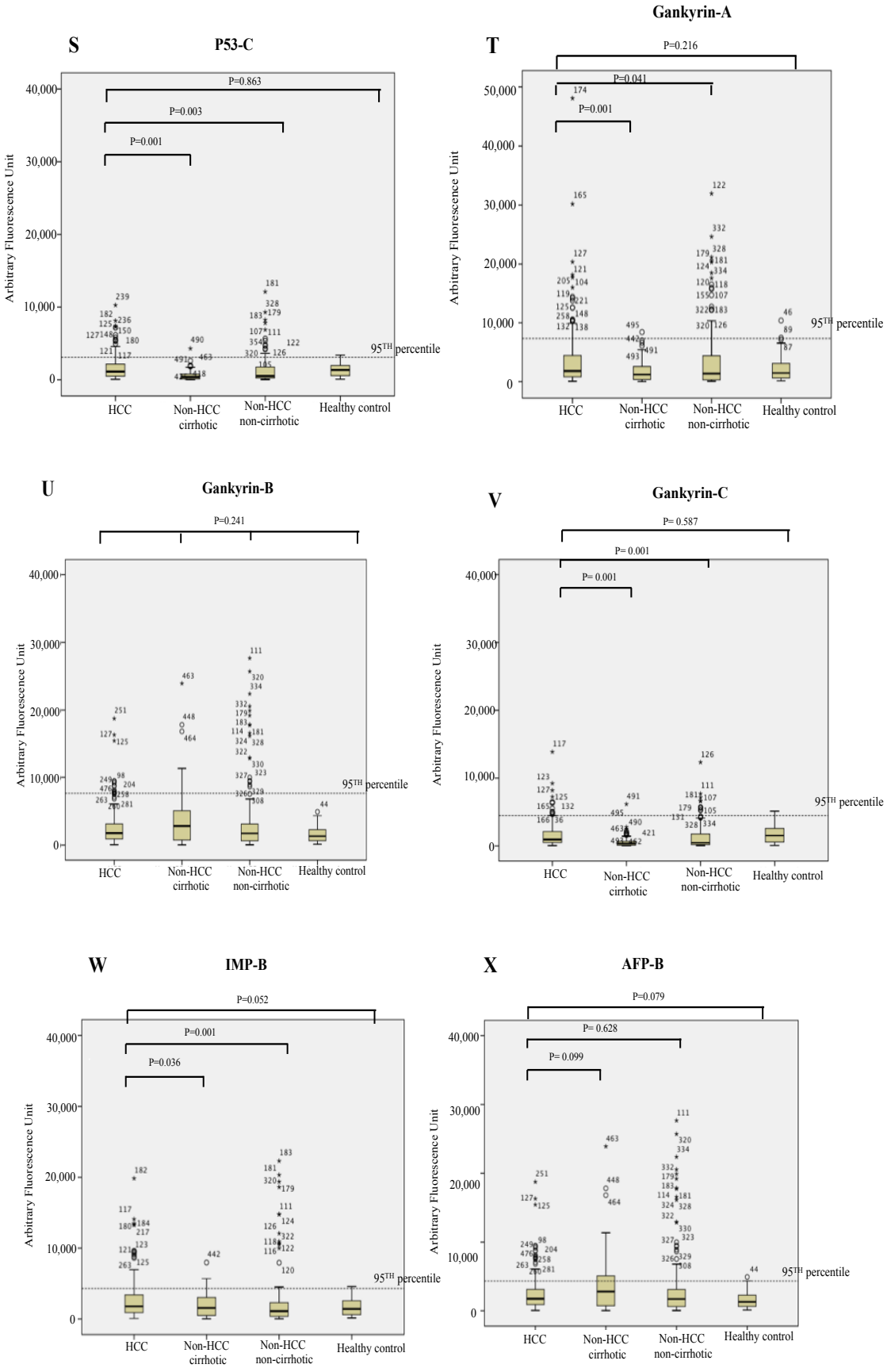

I
HDGF-C
P=0.275
P=0.001
P=0.001
Arbitrary Fluorescence Unit
95TH percentile
HCC
Non-HCC cirrhotic
Non-HCC non-cirrhotic
Healthy control


J
P16-A
P=0.945
P=1.000
P=0.987
Arbitrary Fluorescence Unit
95TH percentile
HCC
Non-HCC cirrhotic
Non-HCC non-cirrhotic
Healthy control


K
P16-C
P=0.295
P=0.001
P=0.001
Arbitrary Fluorescence Unit
95TH percentile
HCC
Non-HCC cirrhotic
Non-HCC non-cirrhotic
Healthy control


L
RALA-A
P=0.054
P=0.005
P=0.331
Arbitrary Fluorescence Unit
95TH percentile
HCC
Non-HCC cirrhotic
Non-HCC non-cirrhotic
Healthy control


M
RALA-B
P= 0.183
P= 0.180
P= 0.183
Arbitrary Fluorescence Unit
40,000
30,000
20,000
10,000
0
95TH percentile
HCC
Non-HCC cirrhotic
Non-HCC non-cirrhotic
Healthy control
N
RALA-C
P=0.374
P=0.001
P=0.001
Arbitrary Fluorescence Unit
95TH percentile
HCC
Non-HCC cirrhotic
Non-HCC non-cirrhotic
Healthy control
O
P62-A
P= 0.191
P= 0.041
P= 0.002
Arbitrary Fluorescence Unit
95TH percentile
HCC
Non-HCC cirrhotic
Non-HCC non-cirrhotic
Healthy control
P
P62-B
P= 0.262
P= 0.001
P= 0.001
Arbitrary Fluorescence Unit
95TH percentile
HCC
Non-HCC cirrhotic
Non-HCC non-cirrhotic
Healthy control
Q
P62-C
P=0.218
P=0.001
P=0.001
Arbitrary Fluorescence Unit
95TH percentile
HCC
Non-HCC cirrhotic
Non-HCC non-cirrhotic
Healthy control
P53-A
R
P=0.681
P= 0.027
P= 0.002
Arbitrary Fluorescence Unit
60,000
50,000
40,000
30,000
20,000
10,000
0
95TH percentile
HCC
Non-HCC cirrhotic
Non-HCC non-cirrhotic
Healthy control


S
P53-C
P=0.863
P=0.003
P=0.001
Arbitrary Fluorescence Unit
95TH percentile
HCC
Non-HCC cirrhotic
Non-HCC non-cirrhotic
Healthy control
T
Gankyrin-A
P=0.216
P=0.041
P=0.001
U
Gankyrin-B
P=0.241
V
Gankyrin-C
P= 0.587
P= 0.001
W
IMP-B
P=0.052
P=0.036
X
AFP-B
P=0.079
P= 0.628
P= 0.099

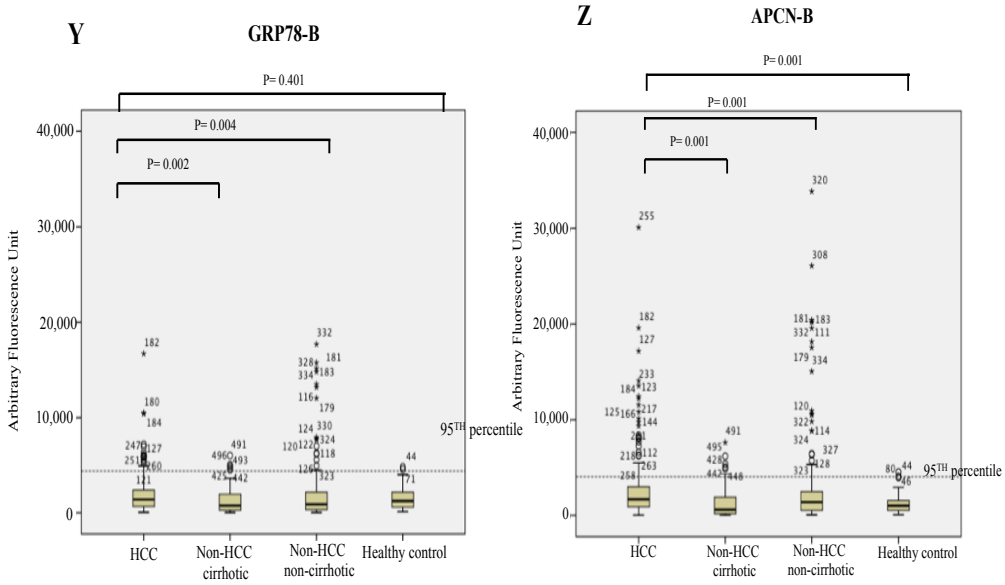
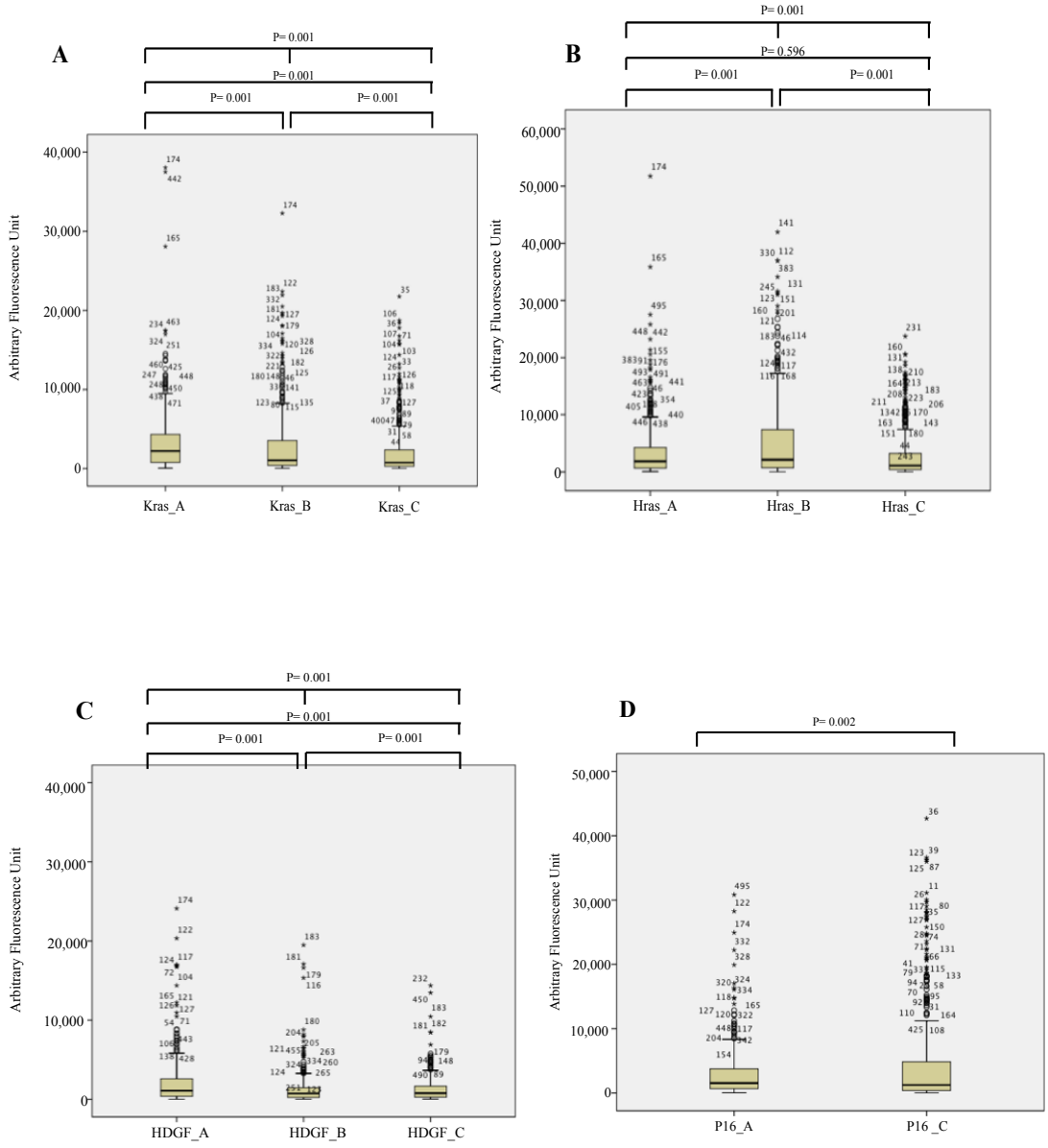


Figure 103: Differences in anti-TAA responses in subjects with HCC, non-HCC cirrhosis (liver cirrhosis only), non-HCC non-cirrhosis (chronic liver hepatitis) and healthy groups: Kras-A, Kras-B, Kras-C, Hras-A, Hras-B, Hras-C, HDGF-A, HDGF-B, HDGF-C, P16-A, P16-C, RALA-A, RALA-B, RALA-C, P62-A, P62-B, P62-C, P53-A, P53-C, Gankyrin-A, Gankyrin-B, Gankyrin-C, IMP-B, AFP-B, GRP78-B, APCN-B(A-Z, respectively). The difference in anti-TAA responses; **(A)** anti-Kras-A, **(B)** anti-Kras-B, **(C)** anti-Kras-C **(D)** anti-Hras-A, **(E)** anti-Hras-B, **(F)** anti-Hras-C, **(G)** anti-HDGF-A, **(H)** anti-HDGF-B**, (I)** anti-HDGF-C, **(J)** anti-P16-A, **(K)** anti-P16-C, **(L)** anti-RALA-A, **(M)** anti-RALA-B, **(N)** anti-RALA-C, **(O)** anti-P62-A, **(P)** anti-P62-B, **(Q)** anti-P62-C, **(R)** anti-P53-A, **(S)** anti-P53-C, **(T)** anti-Gankyrin-A, **(U)** anti-Gankyrin-B, **(V)** anti-Gankyrin-C, **(W)** anti-IMP-B, **(X)** anti-AFP-B, **(Y)** anti-GRP78-B, (**Z**) anti-APCN-B were examined in subjects with HCC, non-HCC cirrhosis, non-HCC non-cirrhosis and healthy groups. Pair-wise tests were performed to compare each two groups. There were significant differences between HCC and healthy subjects for anti-Kras-A, anti-Hras-A, anti-Hras-B, anti-APCN-B except anti-Kras-B, anti-Kras-C, anti-Hras-C, anti-HDGF-A, anti-HDGF-B, anti-HDGF-C, anti-P16-A, anti-P16-C, anti-RALA-A anti-RALA-B, anti-RALA-C, anti-P62-A, anti-P62-B, anti-P62-C, anti-P53-A, anti-P53-C, anti-Gankyrin-A anti-Gankyrin-B, anti-Gankyrin-C, anti-IMP1-B and anti-AFP-B anti-GRP78-B. Subsequently pairwise comparisons tests were undertaken between HCC and non-HCC cirrhotics which showed significant differences for anti-Kras-A, anti-Kras-B, anti-Kras-C, anti-Hras-A, anti-Hras-B, anti-Hras-C, anti-HDGF-A anti-HDGF-B, anti-HDGF-C, anti-P16-C, anti-RALA-C, anti-P62-A, anti-P62-B, anti-P53-A, anti-P53-C, anti-Gankyrin-A, anti-Gankyrin-C, anti-IMP-B, anti-GRP78-B, anti-APCN-B except anti-P16-A, anti-RALA-A, anti-RALA-B, anti-P62-C, anti-Gankyrin-B and anti-AFP-B responses. Lastly, a significant difference was seen between HCC and non-HCC non-cirrhotics for anti-Kras-A, anti-Kras-C, anti-Hras-B, anti-Hras-C, anti-HDGF-B**,** anti-HDGF-C, anti-P16-C, anti-RALA-A, anti-RALA-C, anti-P62-A, anti-P62-B, anti-P62-C, anti-P53-A, anti-P53-C, anti-Gankyrin-A, anti-Gankyrin-C, anti-IMP-B, anti-GRP78-B, anti-APCN-B except anti-Kras-B anti-Hras-A, anti-HDGF-A, anti-P16-A, anti-RALA-B, , anti-Gankyrin-B and anti-AFP-B responses.

6.4.4 Autoantibody Responses between Commercial and In-house Tumour-Associated Antigens in All Cohorts

The three categories of TAAs (Sets A, B and C) all contained two or more of the following antigens; KRAS, HRAS, HDGF, P16, RALA, P62, P53 and Gankyrin. Although the aforementioned antigens in each category are the same, they differed in the type of expression system in which they were produced as well as the forms in which they exist (purified or whole cell lysate). As such, we wished to examine if the autoantibody responses to the antigens produced in the different expression systems were the same. Comparative analysis using Friedman two-way analysis test was performed to determine the distribution of autoantibody responses to the three sets of TAAs. The Wilcoxon test was employed when two distributions were compared. As seen from **Figure 104A**, there was a significant difference in autoantibody responses to KRAS-A, KRAS-B, KRAS-C, indicating that anti-TAA responses across the three were not the same. Differently, anti-HRAS-A and anti-HRAS-C responses were not significantly different, but these were both significantly different to HRAS-B (as seen in **Figure 104B)**. When anti-HDGF-A, anti-HDGF-B and anti-HDGF-C were compared, significant differences were seen with highest anti-HDGF-A responses obtained in cohorts (**Figure 104C**). On the other hand, the distribution of anti-P16-A and anti-P16-C were significantly different with higher anti-P16-C responses as compared to anti-P16-A (**Figure 104D**). A significant difference in the distribution of anti-RALA-A, anti-RALA-B, anti-RALA-C was noticed with highest autoantibody responses to RALA-A (**Figure 104E**). Highest autoantibody responses to P62-B was seen as compared to P62-A and P62-C with significant difference observed in their distribution (**Figure 104F**). Distribution of autoantibody responses to the two sets of P53 (A, B) as well as Gankyrin (A, B, C) were significantly different with highest

responses seen in anti-P53-A (**Figure 104G**) and anti-Gankyrin A (**Figure 104H**) respectively. High autoantibody responses were produced to commercial TAAs expressed in HEK 293 cells followed by commercial TAAs produced in *E. coli* with least responses seen in TAAs made in-house.



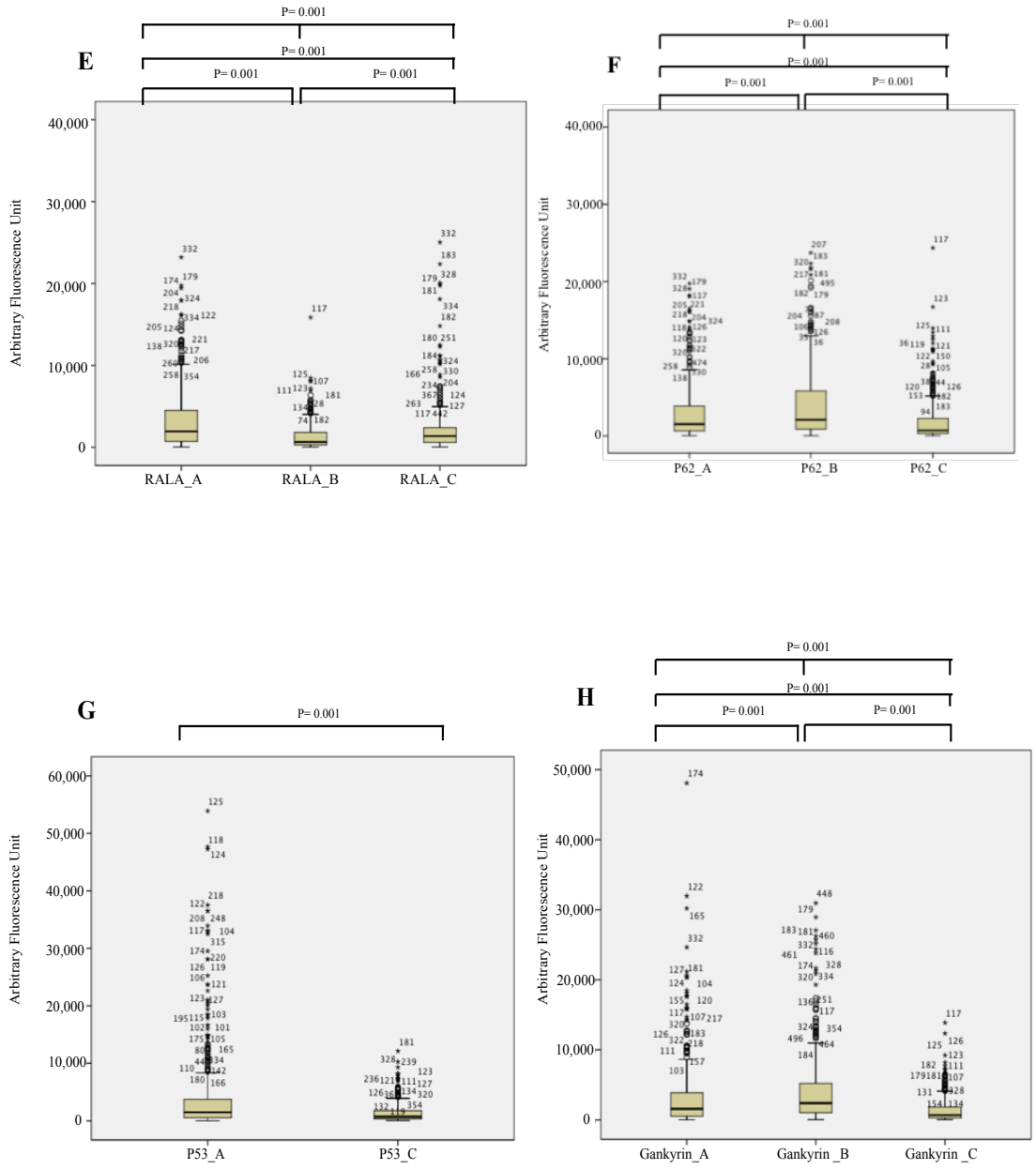


Figure 104: Box plots showing autoantibody responses amongst the three categories of TAAs (A, B, C) in HCC, non-HCC cirrhotic, non-HCC non-cirrhotic and healthy subjects. Autoantibody responses to **(A)** KRAS **(B)** HRAS, **(C)** HDGF, **(D)** P16, **(E)** RALA, **(F)** P62, **(G)** P53 and **(H)** Gankyrin were investigated in subjects with HCC, non-HCC cirrhotic, non-HCC non-cirrhotic and healthy controls. Friedman two-way and Wilcoxon tests were employed to compare the distribution of anti-TAA response amongst the three sets of TAAs. A pairwise comparison was made to determine whether there was a significant difference in autoantibody responses between two TAA categories.

6.4.5 Prevalence of Autoantibody Positivity to Individual TAAs across different Cohorts

The frequency of autoantibodies in clinical samples to individual TAAs was analysed. Sera containing higher levels than the cut-off (the 95th percentiles) of the healthy cohort was regarded as seropositive. Frequency of positive autoantibody responses to TAAs in sets A, B and C were examined.

In regard to set A TAAs (commercial TAAs), higher frequency of autoantibodies in HCC patients was found in response to P62 (18%) followed by RALA (17.4%), Gankyrin (14%), P53 (10.9%), KRAS (10%), P16 (9.3%), HRAS (9.3%) and HDGF (3.2%) (**Table 27**). In non-HCC cirrhotic patients, autoantibody frequency to individual TAAs ranged from 0 to 22%, with very higher autoantibody frequency to HRAS (22%). When the sera from patients with non-HCC non-cirrhosis were tested against the panel of the set A TAAs, autoantibody frequencies ranged from 3% to 19.5% with highest frequency again to HRAS (19.5%). The response in the HCC positive patients to HRAS was only 9.3%, suggesting autoantibodies to this TAA may be down-regulated in cancer. The reactivity of healthy sera was low, ranging from 0 to 4.3% to any individual TAA. Prevalence of positive autoantibody responses to set A TAAs was significantly higher ($p<0.05$) in HCC patients than healthy controls and non-HCC cirrhotic patients **Table 27**. On the contrary, there was no significant difference ($p<0.05$) in positive autoantibody frequency between HCC and non-HCC non-cirrhotic patients with the exception of anti-Kras (**Table 27)**.

Table 27: Frequency of positive autoantibody responses to set A tumour-associated antigens.

Sera	No. tested	KRAS N (%)	HRAS N (%)	HDGF N (%)	P16 N (%)	RALA N (%)	P62 N (%)	P53 N (%)	Gankyrin N (%)
HCC	2	19(10)	17(9.3)	6(3.2)	17(9.3)	32(17.4)	33(18)	20(10.9)	26(14)
NHC	90	13(14)[b]	20(22)[b]	0(0)	16(17)	11(12)[b]	9(10)[b]	0(0)[b]	5(5.5)[b]
NHNC	133	4 (3)[c]	26(19.5)	4 (3)	22(16.5)	8(6)	20(15)	13(9.7)	25(18.7)
H	46	1(2.7)[a]	2 (4.3)[a]	1(2.7)[a]	1(2.7)[a]	1(2.7)[a]	1(2.7)[a]	0(0)[a]	0(0)[a]

NHC-(Non-HCC cirrhosis), **NHNC**-(Non-HCC non-cirrhosis), **H-**Healthy, Cut—off value for each anti-TAA is the 95th percentile of the healthy group. P value analysed by Kruskal-Wallis test to compare differences in frequencies of positive anti-TAA responses. **a**-significance in autoantibody positivity between HCC and H, b-significance in autoantibody positivity between HCC and NHC, **c**- significance in autoantibody positivity between HCC and NHNC. p value<0.05.

In determining autoantibody positivity to individual TAAs in set B (*E. coli* derived TAAs), the highest frequencies in HCC patients were against HDGF (21%) followed by HRAS (20%), IMP1 (19%) and APCN (18%), AFP (15%), Gankyrin (13%), GRP78 (9%), KRAS (9%) and P62 (3%) (**Table 28)**. Frequency of positive responses to individual TAAs in non-HCC cirrhotic patients ranged from 0%-33% with highest frequencies to AFP (33%) while that in non-HCC cirrhotic patients ranged from 4% to 25% with highest frequency to HRAS (23%) (**Table 28)**. Autoantibody titre in healthy controls were the least ranging from 0%-4%. The prevalence of autoantibody positivity to set B TAAs was significantly higher ($p<0.05$) in HCC patients than healthy controls. There was no significant difference ($p<0.05$) in autoantibody positive responses between HCC, non-HCC cirrhotic and non-HCC non-cirrhotic patients with the exception of anti-KRAS, anti-HRAS, and anti-IMP1(**Table 28)**.

Table 28: Frequency of positive autoantibody responses to set B tumour-associated antigens.

Sera	No. tested	Kras	Hras N(%)	HDGF N(%)	RalA N(%)	P62 N(%)	Gank N(%)	Apcn N(%)	IMP1 N(%)	Grp78 N(%)	AFP N(%)
HCC	183	17(9)	36(20)	38(21)	32(18	5(3)	24(13	32(18	35(19)	17(9)	27(15)
NHC	90	1(1) [b]	1(1) [b]	16(18)	18(20	1(1) [b]	17(19	10(19	9(10)	8(9)	30(33)
NHNC	133	20(15	33(25)	19(14)	20(15	6(5)	5(4)	22(17	13(10) [c]	16(12	25(19)
H	46	2(4) [a]	2(4) [a]	2(4) [a]	1(2) [a]	1(2) [a]	0(0) [a]	1(2) [a]	0(0) [a]	0(0) [a]	0(0) [a]

NHC-(Non-HCC cirrhosis), **NHNC**-(Non-HCC non-cirrhosis), **H-**Healthy, Cut—off value for each anti-TAA is the 95th percentile of the healthy group. P value analysed by Kruskal-Wallis test to compare differences in frequencies of positive anti-TAA responses. **a**-significance in autoantibody positivity between HCC and H, b-significance in autoantibody positivity between HCC and NHC, **c**- significance in autoantibody positivity between HCC and NHNC. p value<0.05.

In examining the prevalence of positive responses to TAAs in set C (in-house eukaryotic TAAs), highest frequencies in HCC patients were against HRAS (23%), P53 (14%), RALA (8.7%) and Gankyrin (7.1%), followed by KRAS (7%), P16 (3.2%), HDGF (3.2%) (**Table 29)**. The autoantibody frequency to individual TAAs in non-HCC cirrhotic patients ranged from 0%-10% with highest frequencies to P53 (10%) while those in non-HCC cirrhotic patients ranged from 0.8% to 10.5% with highest frequency also to P53 (10.5%) (**Table 29)**. Autoantibody titre in healthy controls were the least ranging from 0%-2.1%. A similar trend was seen with set C antigens as the prevalence of autoantibody positivity to TAAs was significantly higher ($p<0.05$) in HCC patients than healthy controls and non-HCC cirrhotic patients. However, there was no significant difference in autoantibody positive responses between HCC and non-HCC non-cirrhotic patients with the exception of HRAS (**Table 29)**.

Table 29: Frequency of positive autoantibody responses to set C tumour-associated antigens.

Sera	No. tested	KRAS N(%)	HRAS N(%)	HDGF N(%)	P16 N(%)	RALA N(%)	P62 N(%)	P53 N(%)	Gankyrin N(%)
HCC	183	13 (7)	43 (23)	6 (3.2)	6(3.2)	16(8.7)	15(8.2)	26(14)	13(7.1)
NHC	90	0(0) [b]	1(1.1) [b]	6(6.7)	0(0)	2(2.2) [b]	0(0) [b]	9(10)	5(5.5)
NHNC	133	8 (6.0)	13(9.7) [c]	3(2.3)	1(0.8)	8(6.0)	7(5.3)	14(10.5)	10(7.5)
H	46	1(2.1) [a]	1(2.1) [a]	0(2.1) [a]	1(2.1) [a]	1(2.1) [a]	0(2.1) [a]	1(2.1) [a]	0(0) [a]

NHC-(Non-HCC cirrhosis), **NHNC**-(Non-HCC non-cirrhosis), **H-**Healthy, Cut—off value for each anti-TAA is the 95th percentile of the healthy group. P value analysed by Kruskal-Wallis test to compare differences in frequencies of positive anti-TAA responses. **a**-significance in autoantibody positivity between HCC and H, b-significance in autoantibody positivity between HCC and NHC, **c**- significance in autoantibody positivity between HCC and NHNC. p value<0.05.

Interestingly, prevalence of seropositives to *E. coli* generated TAAs were higher as compared to commercial and in-house TAAs generated in HEK 293 cells. The finding of high titre autoantibodies in non-HCC non-cirrhotic patients is of interest because titres of autoantibodies are higher in HCC patients than subjects who don't have the cancer. This may be due to the expression system being used leading to measurement of antibody responses to *E. coli* proteins in the preparations.

6.4.6 Correlation in Autoantibody Measurement between Commercial and In-house generated TAAs.

Two sets of eukaryotic generated TAAs (KRAS, HRAS, HDGF, P16, RALA, P62, P53 Gankyrin) were either purchased or made in-house. Commercial TAAs existed in purified forms while the latter were in lysates. A comparative analysis using the Bivariate Spearman's rank correlation was conducted to assess if there was a relationship between autoantibody levels detected against the two sets of TAAs. From **Table 30**, there were significant but weak degrees of correlation in autoantibody responses with respect to anti-KRAS (r=0.488, p value=0.001), anti-HRAS (r=0.292, p value=0.001), anti-HDGF (r=0.597, p value=0.001), anti-P16 (r=0.567, p value=0.001) autoantibody responses. Likewise, there were strong and significant degrees of correlation in autoantibody responses with respect to anti-RAL A (r=0.709, p value=0.001), anti-P62 (r=0.724, p value=0.001), anti-P53 (r=0.792, p value=0.001) and anti-Gankyrin (r=0.821, p value=0.001) to as seen in **Table 30**. This indicates that there is a relationship in autoantibody responses between the two sets of eukaryotic generated TAAs although they existed in different forms.

Table 30: Correlation between autoantibody responses to commercial and in-house TAAs produced in HEK 293 cells.

Commercial	In-house	Spearman's correlation	p-value
KRAS	KRAS	0.488	0.001
HRAS	HRAS	0.292	0.001
HDGF	HDGF	0.597	0.001
P16	P16	0.567	0.001
RALA	RALA	0.709	0.001
P62	P62	0.724	0.001
P53	P53	0.792	0.001
Gankyrin	Gankyrin	0.821	0.001

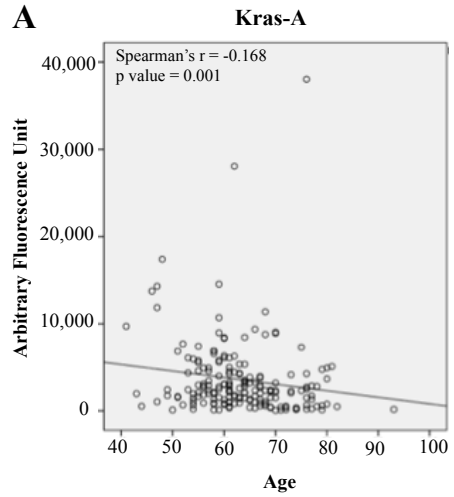
Secondly, the association between autoantibodies produced to commercial eukaryotic and *E. coli* generated TAAs were examined. This was no different from the previous correlation as there was a weak but significant link in autoantibody responses with regards to anti-KRAS, anti-HRAS, anti-HDGF as shown in **Table 31.** A strong and significant correlation in anti-TAA responses were seen with anti-RALA, anti-P62 and anti-Gankyrin **(Table 31).**

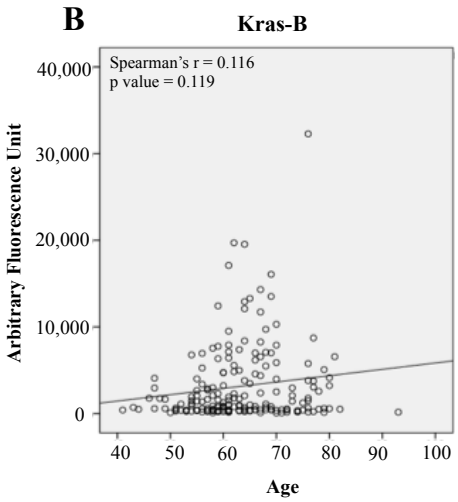
Table 31: Correlation between autoantibody responses to commercial TAAs produced in HEK 293 cells and *E. coli.*

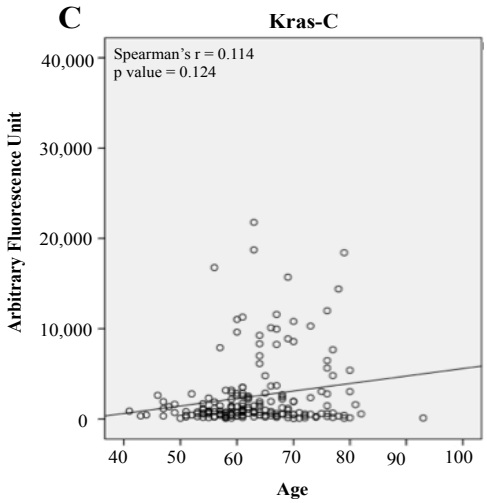
Eukaryotic	***E. coli***	**Spearman's correlation**	**p-value**
KRAS	KRAS	0.480	0.001
HRAS	HRAS	0.394	0.001
HDGF	HDGF	0.596	0.001
RALA	RALA	0.861	0.001
P62	P62	0.795	0.001
Gankyrin	Gankyrin	0.847	0.001

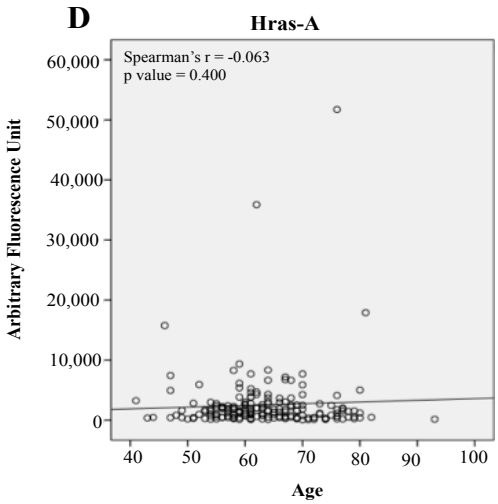
6.4.7 Effect of Age on Autoantibody Response in Hepatocellular Carcinoma

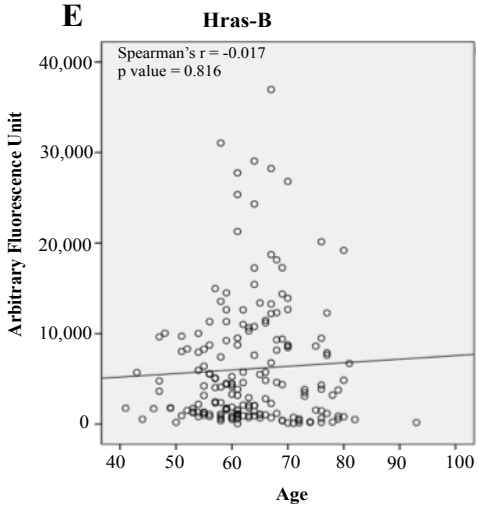
As ages of HCC patients ranged from 40 up to 93 years we wanted to exclude age as a confounding factor for the results (**Figure 105 A-Z**). This revealed that only autoantibodies to HDGF-A showed a trend towards a positive and significant correlation with age (r=0.154, p value=0.038) (**Figure 105G**). In addition, negative but significant correlations were seen between age and autoantibody responses to KRAS-A (r=-0.168, p value=0.001) (**Figure 105A**), HRAS-C (r=-0.178, p value=0.016) (**Figure 105F**) and APCN-B (r=-0.174, p value=0.019) (**Figure 105Z**), However, autoantibody responses to remaining twenty-one TAAs showed no significant correlations with age (**Figure 105 B,C,D,E,H-Y**). Taken together this suggests there was no strong correlation of autoantibodies responses with age in HCC patients.

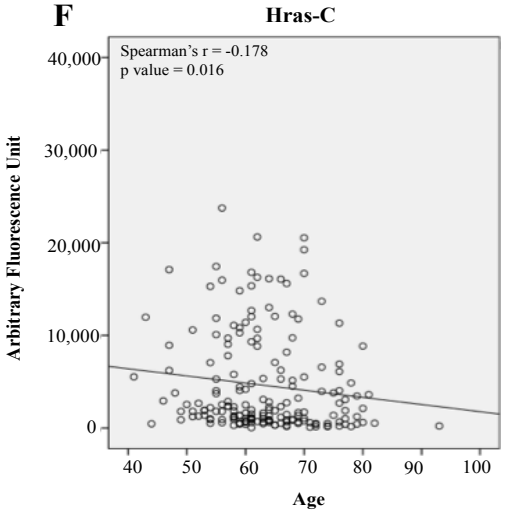

A
Kras-A
Spearman's r = -0.168
p value = 0.001
Arbitrary Fluorescence Unit
40,000
30,000
20,000
10,000
0
40
50
60
70
80
90
100
Age

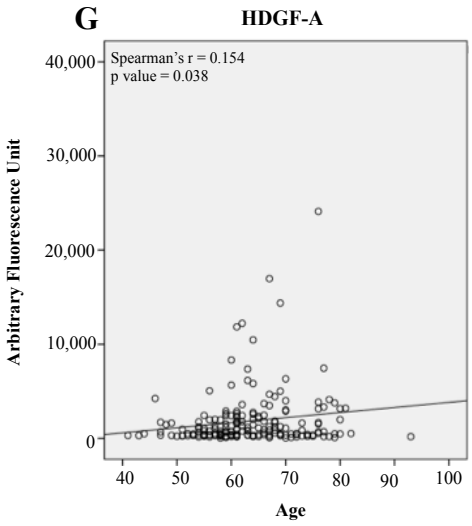

B
Kras-B
Spearman's r = 0.116
p value = 0.119
Arbitrary Fluorescence Unit
40,000
30,000
20,000
10,000
0
40
50
60
70
80
90
100
Age

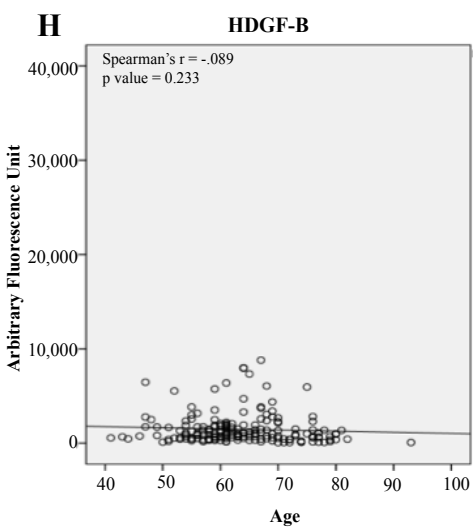

C
Kras-C
Spearman's r = 0.114
p value = 0.124
Arbitrary Fluorescence Unit
40,000
30,000
20,000
10,000
0
40
50
60
70
80
90
100
Age

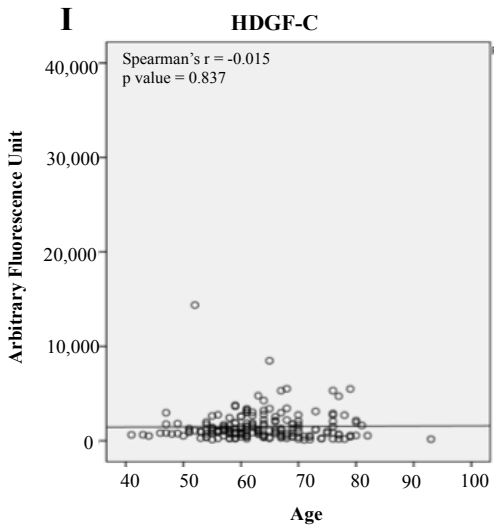

D
Hras-A
Spearman's r = -0.063
p value = 0.400
Arbitrary Fluorescence Unit
60,000
50,000
40,000
30,000
20,000
10,000
0
40
50
60
70
80
90
100
Age

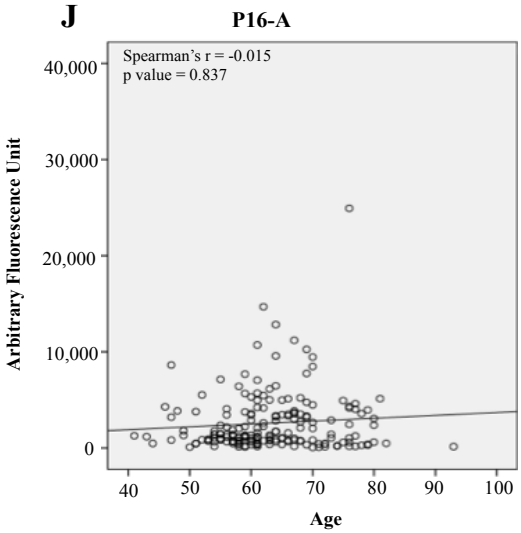

E
Hras-B
Spearman's r = -0.017
p value = 0.816
Arbitrary Fluorescence Unit
40,000
30,000
20,000
10,000
0
40
50
60
70
80
90
100
Age

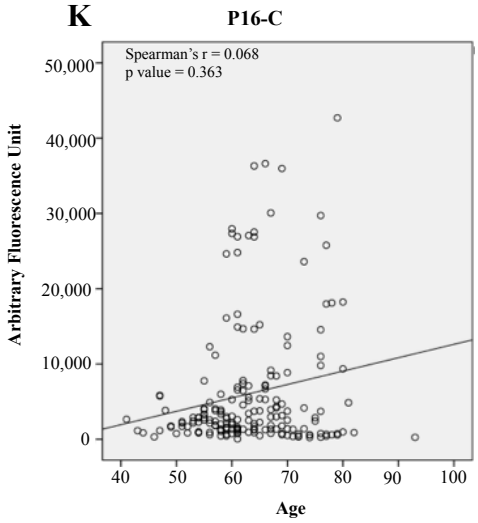

F
Hras-C
Spearman's r = -0.178
p value = 0.016
Arbitrary Fluorescence Unit
40,000
30,000
20,000
10,000
0
40
50
60
70
80
90
100
Age

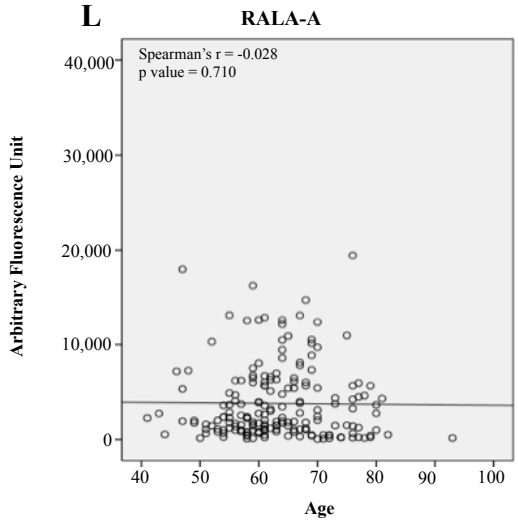

G
HDGF-A
Spearman's r = 0.154
p value = 0.038
Arbitrary Fluorescence Unit
40,000
30,000
20,000
10,000
0
40
50
60
70
80
90
100
Age

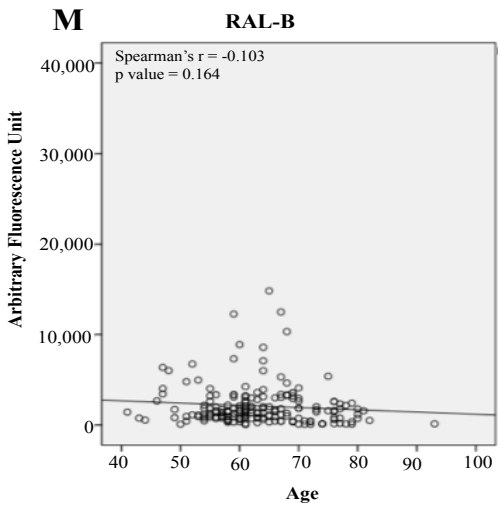

H
HDGF-B
Spearman's r = -.089
p value = 0.233
Arbitrary Fluorescence Unit
40,000
30,000
20,000
10,000
0
40
50
60
70
80
90
100
Age

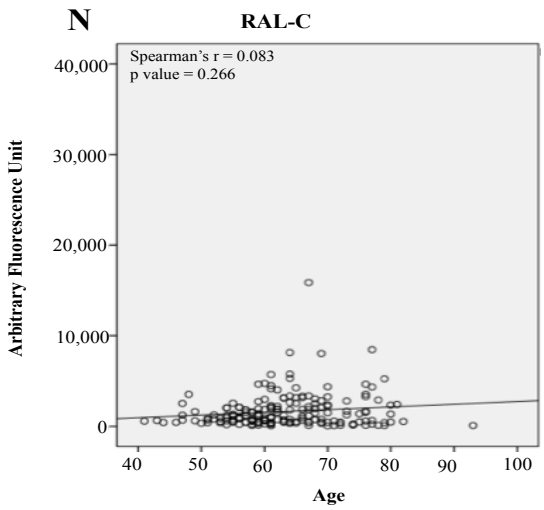

I
HDGF-C
Spearman's r = -0.015
p value = 0.837
Arbitrary Fluorescence Unit
40,000
30,000
20,000
10,000
0
40
50
60
70
80
90
100
Age

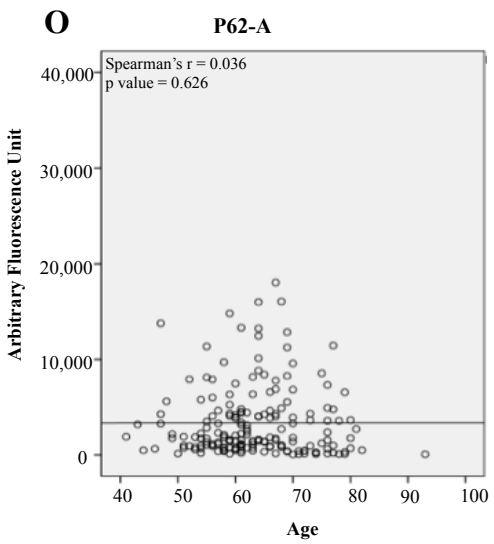

J
P16-A
Spearman's r = -0.015
p value = 0.837
Arbitrary Fluorescence Unit
40,000
30,000
20,000
10,000
0
40
50
60
70
80
90
100
Age

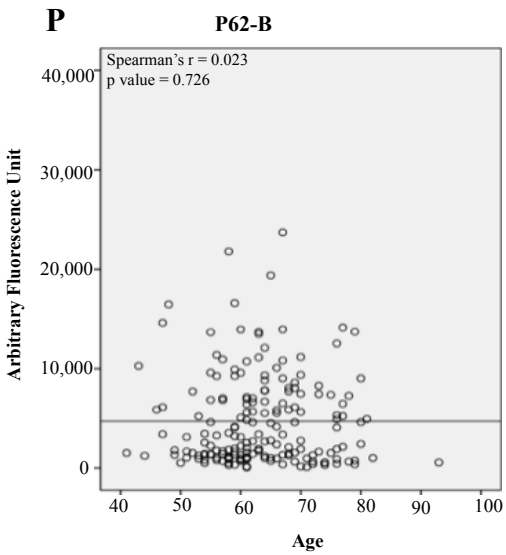

K
P16-C
Spearman's r = 0.068
p value = 0.363
Arbitrary Fluorescence Unit
50,000
40,000
30,000
20,000
10,000
0
40
50
60
70
80
90
100
Age

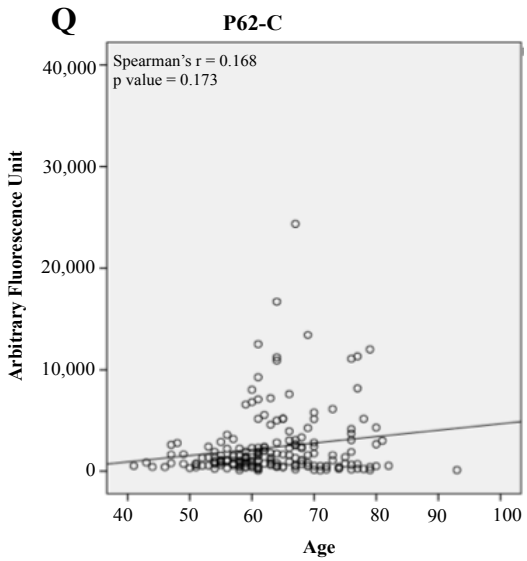

L
RALA-A
Spearman's r = -0.028
p value = 0.710
Arbitrary Fluorescence Unit
40,000
30,000
20,000
10,000
0
40
50
60
70
80
90
100
Age

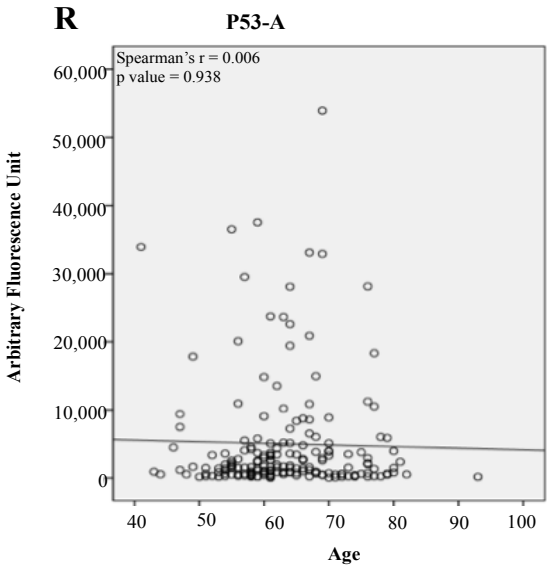

M
RAL-B
Spearman's r = -0.103
p value = 0.164
Arbitrary Fluorescence Unit
40,000
30,000
20,000
10,000
0
40
50
60
70
80
90
100
Age

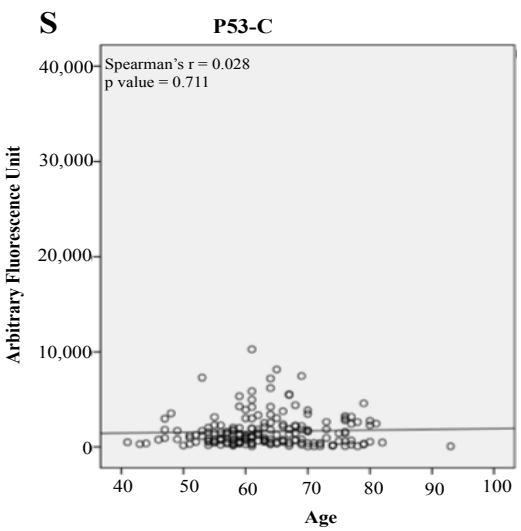

N
RAL-C
Spearman's r = 0.083
p value = 0.266
Arbitrary Fluorescence Unit
40,000
30,000
20,000
10,000
0
40
50
60
70
80
90
100
Age

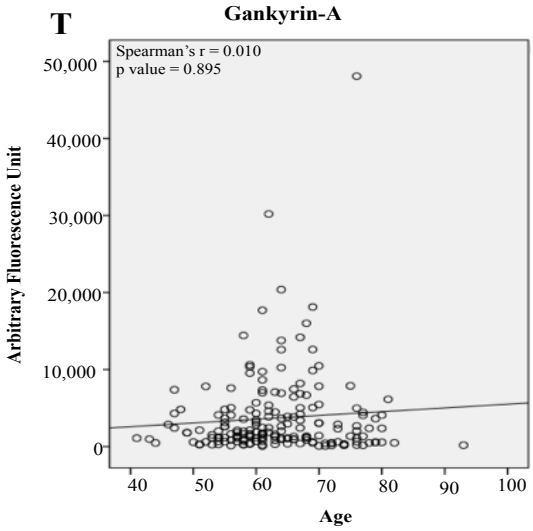

O
P62-A
Spearman's r = 0.036
p value = 0.626
Arbitrary Fluorescence Unit
40,000
30,000
20,000
10,000
0
40
50
60
70
80
90
100
Age

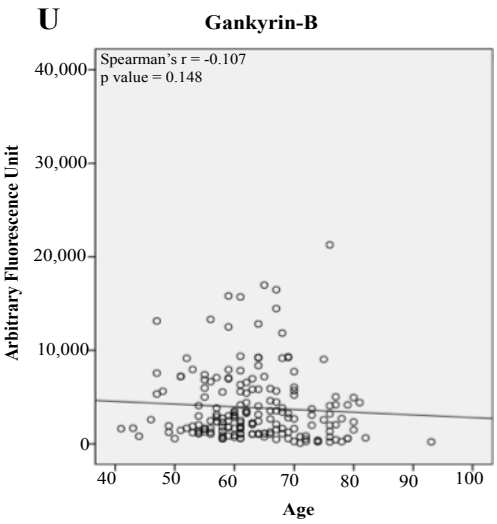

P
P62-B
Spearman's r = 0.023
p value = 0.726
Arbitrary Fluorescence Unit
40,000
30,000
20,000
10,000
0
40
50
60
70
80
90
100
Age

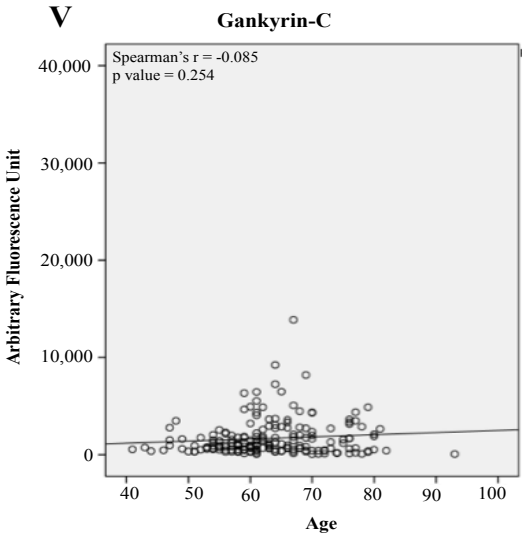

Q
P62-C
Spearman's r = 0.168
p value = 0.173
Arbitrary Fluorescence Unit
40,000
30,000
20,000
10,000
0
40
50
60
70
80
90
100
Age

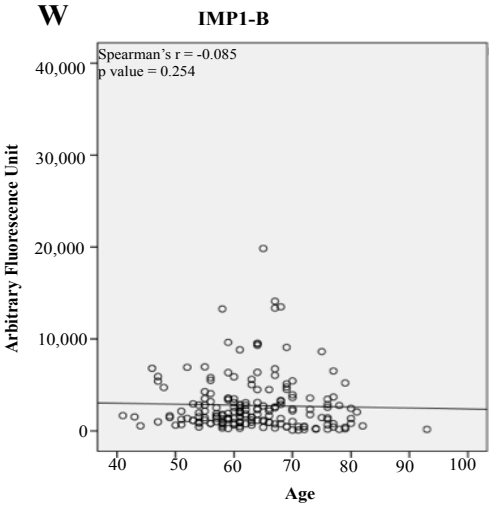

R
P53-A
Spearman's r = 0.006
p value = 0.938
Arbitrary Fluorescence Unit
60,000
50,000
40,000
30,000
20,000
10,000
0
40
50
60
70
80
90
100
Age

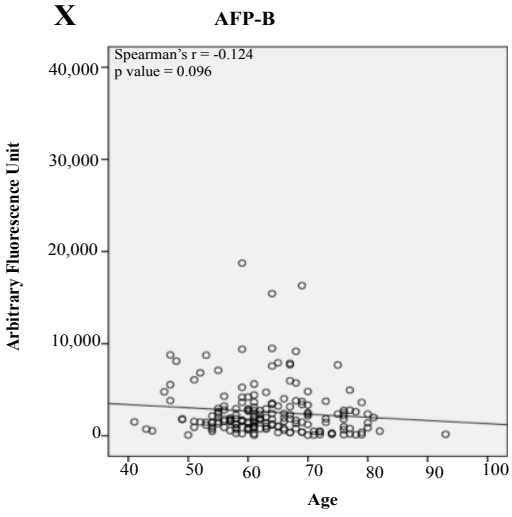

S
P53-C
Spearman's r = 0.028
p value = 0.711
Arbitrary Fluorescence Unit
40,000
30,000
20,000
10,000
0
40
50
60
70
80
90
100
Age


T
Gankyrin-A
Spearman's r = 0.010
p value = 0.895
Arbitrary Fluorescence Unit
50,000
40,000
30,000
20,000
10,000
0
40
50
60
70
80
90
100
Age


U
Gankyrin-B
Spearman's r = -0.107
p value = 0.148
Arbitrary Fluorescence Unit
40,000
30,000
20,000
10,000
0
40
50
60
70
80
90
100
Age


V
Gankyrin-C
Spearman's r = -0.085
p value = 0.254
Arbitrary Fluorescence Unit
40,000
30,000
20,000
10,000
0
40
50
60
70
80
90
100
Age


W
IMP1-B
Spearman's r = -0.085
p value = 0.254
Arbitrary Fluorescence Unit
40,000
30,000
20,000
10,000
0
40
50
60
70
80
90
100
Age


X
AFP-B
Spearman's r = -0.124
p value = 0.096
Arbitrary Fluorescence Unit
40,000
30,000
20,000
10,000
0
40
50
60
70
80
90
100
Age

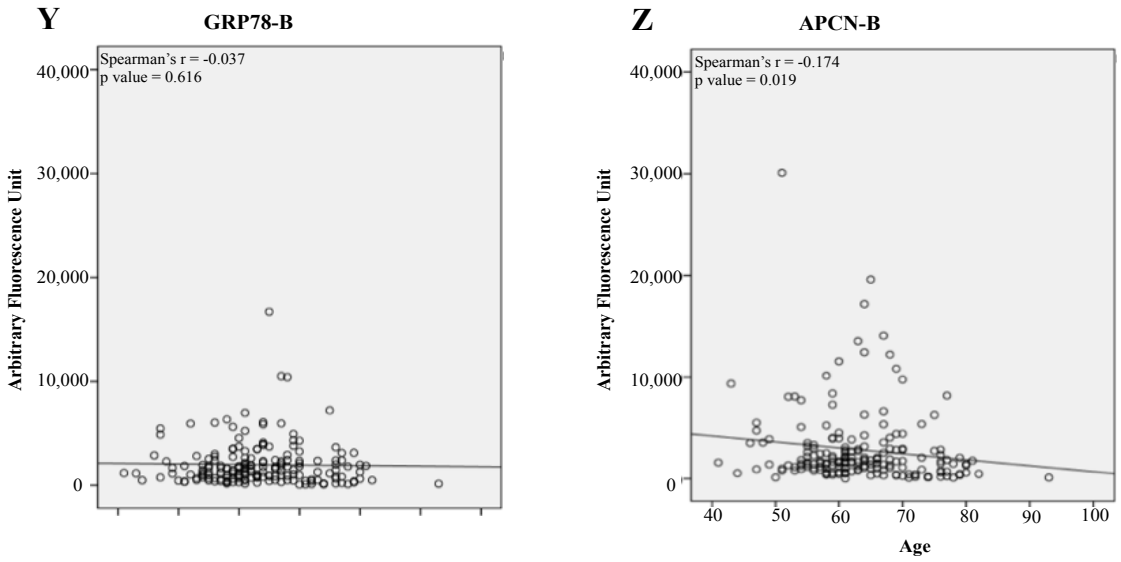


Figure 105: Correlation between "age" and autoantibody responses to KRAS-A, KRAS-B, KRAS-C, HRAS-A, HRAS-B, HRAS-C, HDGF-A, HDGF-B, HDGF-C, P16-A, P16-C, RALA-A, RALA-B, RALA-C, P62A, P62B, P62C, P53A, P53-C, Gankyrin-A, Gankyrin-B, Gankyrin-C, IMP-B, AFP-B, GRP78. Spearman's Rank correlation tests were performed to compare the relationship between "age" and the measurement of autoantibody responses to twenty TAAs. **(G)** Anti-HDGF-A showed a weak but positive correlation with age in HCC patients' responses while **(A)** Anti-KRAS-A, (**F**) anti-HRAS-C, (**Z)** anti-APCN-B responses showed a negative but significant correlation with age in HCC patients. Lastly, **(B)** Anti-KRAS-B, **(D)** anti-HRAS-A (**H)** anti-HDGF-B, **(I)** anti-HDGF-C and **(J)** anti-P16-A **(A)** Anti- KRAS-C, **(C)** anti-HRAS-B **(K)** Anti-P16-C, **(L)** anti-RALA-A, **(M)** anti-RALA-B, and **(N)** anti-RALA-C**(O)** Anti-P62A, **(P)** anti-P62B, anti-**(Q)** P62C **(R)** anti-P53A **(S)** Anti-P53-C, **(T)** anti-Gankyrin-A, **(U)** anti-Gankyrin-B, and **(V)** anti-Gankyrin-C **(W)** anti-IMP-B, **(X)** anti-AFP-B and **(Y)** anti-GRP78, responses showed no significant correlation with age in HCC patients.

6.4.8 Effect of Gender on the development of Hepatocellular Carcinoma

In addition, Bivariate Spearman's rank correlation test was conducted to determine if gender had an impact on autoantibody responses in HCC patients (**table 32**). Results showed a weak but significant correlation between gender and anti-HRAS-C (r=, 0.171, p value= 0.021), anti-HDGF-C (r=0.149, p value=0.044), anti-RALA-C (r=0.153, p value=0.039), anti-P62-C (r=0.153, p value=0.039), anti-P53-C (r=0.155, p value=0.036) and anti-Gankyrin-C (r=0.162, p value=0.028) responses. However the correlation between gender and autoantibody responses to the remaining twenty TAAs (KRAS-A, HRAS-A, HDGF-A, P16-A, RALA-A, P62-A, P53-A, Gankyrin-A, KRAS-B, HRAS-B, HDGF-B, RALA-B, P62-B, Gankyrin-B, IMP1-B, AFP-B, APCN-B,

GRP78-B, KRAS-C, P16-C) were all weak and non-significant indicating that gender does not have an influence on HCC progression in the study.

Table 32: Correlation between Gender and Autoantibody responses in HCC.

TAAs	Spearman's correlation (r)	P value
KRAS-A	0.093	0.209
KRAS-B	0.143	0.053
KRAS-C	0.070	0.347
HRAS-A	0.102	0.171
HRAS-B	0.078	0.296
HRAS-C	0.171	0.021
HDGF-A	0.127	0.087
HDGF-B	0.112	0.131
HDGF-C	0.149	0.044
P16-A	0.111	0.134
P16-C	0.117	0.116
RALA-A	0.091	0.222
RALA-B	0.094	0.203
RALA-C	0.153	0.039
P62-A	0.089	0.229
P62-B	0.027	0.721
P62-C	0.153	0.039
P53-A	0.004	0.953
P53-C	0.155	0.036
Gankyrin-A	0.116	0.117
Gankyrin-B	0.124	0.094
Gankyrin-C	0.162	0.028
IMP1-B	0.038	0.611
AFP-B	0.088	0.235
GRP78-B	0.073	0.324
APCN-B	0.040	0.592

6.5 Discussion

Many studies have shown that HCC patients' sera contain autoantibodies that react with a wide range of autologous cellular antigens and these serve as good serological biomarkers to aid in early identification of the cancer as compared to imaging tests currently used in health care settings (257). Determination of specific anti-TAA autoantibody levels in HCC and high-risk patients permits therapeutic interventions to be introduced which could help improve survival rates. In recent studies, autoantibody measurement to TAAs in HCC patients' sera have been undertaken mostly with traditional techniques such as ELISA (468, 469), Western (239) blot or SERPA (260), but these studies used very small samples sizes.

The fundamental objective of this chapter was to test the developed antigen microarray platform using a panel of commercial and in-house TAAs on large number of serum samples to see its applicability as a tool to detect anti-TAA autoantibody responses. In this work, the presence of anti-TAA specific autoantibody responses in the sera of patients with HCC, cirrhosis, chronic hepatitis disease and healthy volunteers were determined by screening autoantibody responses to twenty-six TAAs. Most previous studies utilised TAAs produced in *E. coli* and it was hypothesised that using such TAAs may trigger false positive responses as patients may produce antibodies to the *E. coli* antigen. Hence, this work was novel as TAAs produced in eukaryotic and *E. coli* expression systems were tested. TAAs, which might be valuable for the early detection of autoantibodies in HCC were categorised into three sets (commercial and in-house TAAs produced in a HEK 293 cells as well as commercial antigens produced in *E. coli*) so as to determine whether there would be significant differences or correlations in autoantibody responses to them. The panel of TAAs in screening

included KRAS, HRAS, HDGF, P16, RALA, P62, P53, Gankyrin, APCN, IMP1, AFP and GRP78.

Screening virally infected sera is not safe and therefore inactivating viruses is essential. With this in mind, a preliminary study was conducted to determine if heat treatment had detrimental effects on autoantibody levels in patients' sera. Previous studies had shown that heat treatment either significantly elevated anti-SOX2 autoantibody responses in HCC patients (241) or reduced anti-Toxoplasma IgM antibody levels in patients' sera (470). Our findings contradicted the above as heat treatment of sera neither enhanced or reduced anti-TAA autoantibody levels in HCC patients.

In assessing autoantibody responses to individual TAAs, varying responses were seen across HCC, non-HCC cirrhotic, non-HCC non-cirrhotics, as well as healthy groups. Hence, we needed to set a 95th percentile cut-off to eradicate the noise of pre-existing autoantibodies in healthy individuals and further examine only elevated levels of autoantibodies. Some autoantibodies may be detectable at elevated levels before the signs and symptoms of the cancer and thus, might act as early warning systems of malignant conversions in high-risk patients. It was no surprise that non-HCC cirrhotic (liver cirrhosis) and non-HCC non-cirrhotic (chronic hepatitis) patients had elevated autoantibody responses to individual TAAs in our study. This demonstrates that malignant transition to HCC is also associated with increased autoantibody responses to certain TAAs and might have a role in cancer development. The outcome confirms a study undertaken by Koziol *et al*, where autoantibodies to a panel of twelve TAAs indicated the presence of HCC prior to diagnosis in HBV/HCV chronic liver disease patients (396). Autoantibody responses

in chronic hepatitis patients were nearly as high as those in HCC patients which was unexpected as no study had shown such increased autoantibody response in such patients. It is worth noting that responses to two *E. coli* generated TAAs (RALA-B, Gankyrin-B) showed the same responses across the different cohorts. This could be anticipated that the patients' antibodies reacted to the *E. coli* proteins and most people have been exposed to *E. coli* at some points in their lives. A comparison of raw signal intensities between HCC and healthy groups revealed no significant difference in the distribution of autoantibody responses especially to some individual TAAs. This reveals the importance of looking at the TAAs as a panel instead of individually.

Our study further confirmed the previously reported potential of antigens such as P53-A (471) and P16-C (472) as important TAAs in HCC, since highest autoantibody responses were produced against them in HCC patients. P53 is responsible for apoptosis and cell cycle regulation after DNA damage and it is found in most cancers, including HCC. Their expression is further elevated after patients are exposed to radiation (473). High expression of P53 in in some HCC patients could stem from the fact that they had been exposed to imaging tools such as CT scans, MRI and ultrasound. The elevated expression is further indicative of poor prognosis in HCC patients used in our study (474). P16 is a tumour suppressor gene actively engaged in cell cycle regulation and its high levels could also be suggestive of poor survival of HCC patients in our study (472).

Eight TAAs (KRAS, HRAS, HDGF, P16, RAL-A, P62, P53 and Gankyrin) were grouped into three categories based on their expression system and forms in which they existed. Autoantibody responses to commercial TAAs produced in eukaryotic systems were significantly higher than those detected against *E. coli* and in-house

TAAs. Lower detection of autoantibodies measured to the in-house antigens could be attributed to the fact that they existed in impurified forms and the concentration of TAAs of interest in the midst of other proteins was insufficient to sensitively measure autoantibody responses. As this work was the first of a kind to compare anti-TAA responses to different forms of the same TAA, it was difficult to compare the outcome as no publication has examined the differences between such antigens. Interestingly, we see a strong correlation in anti-TAA responses to commercial and in-house TAAs produced in HEK 293 cells (RAL-A, P62, P53, Gankyrin). This indicates that although the aforementioned antigens existed in cell lysates, they were still able to detect some level of autoantibodies in serum similarly to the purified TAAs.

Previous studies had indicated that the risk of HCC increases with age (475). In our work, we investigated the effect of age in relation to the levels of autoantibody responses in HCC patients. No correlation between age and all anti-TAA autoantibody responses was observed, with the exception of autoantibodies to HDGF-A which showed a weak but significant correlation with increase in age. Although a different TAA was used, Ying *et al*, showed no significant correlation between anti-Osteopontin response and age (476) while Hong *et al* in contrary, revealed an increase in anti-CENPF and anti-HSP60 in patients less than 50 years (260). Moreover, Xueyou *et al*, showed an increase in anti-P16 responses in patients over 50 years (472). Although our study showed that age is not a good indicator of autoantibody responses in patients, overall, correlation between age and autoantibody response is highly dependent on the panel of TAA used.

Over several years, there have been a rise in the number of men developing HCC compared to women. There seems to be inadequate knowledge on the relationship

between serological biomarkers and gender of HCC patients. In this study, we investigated the association between autoimmune responses to all TAAs and gender. No significant correlation was observed in autoantibody response to TAAs and the gender of patients, however it must be acknowledged that we did have a higher number of males than females in this study. Our findings confirm Ying's study where there were no correlation between anti-GRP78 autoantibody responses and the gender of research subjects (455). In our study, anti-P62, anti-HRAS and anti-HDGF responses had the highest prevalence of autoantibody positivity in HCC patients with regards to both eukaryotic and *E. coli* expressed TAAs.

The high frequency of anti-P62 autoantibodies in HCC patients detected in our work confirms a previous study by Weihong *et al*, where anti-P62 autoantibodies were expressed in high abundance in the sera of HCC patients in China (477). Also, Zhang and his colleagues showed a high prevalence of autoantibodies to P62 (25%) in HCC patients (239). According to Dai *et al*, autoantibodies to P62 was present in 21% of patients with HCC but not in the precursor conditions of chronic hepatitis and liver cirrhosis (144). P62 is an IGF-2 mRNA binding protein which is absent in adult tissues, mediates in oxidative stress signaling in carcinogenesis (478) and has been shown to one of the most established TAAs in HCC. It is therefore not surprising that high autoantibody frequency to P62 was shown in our study.

High autoantibody levels to HDGF in HCC samples was also detected. This protein is responsible for inducing cell growth activity, acts as an anti-apoptotic factor and therefore helps accentuate cancer development. Its expression is usually increased at the early stages of HCC and patients with higher expression tends to have poor survival and earlier recurrence (479). Studies have shown that reducing the expression of HDGF minimises the growth of tumour (479) and hence, it could be a potential target for anti-

HCC therapy. High frequency of anti-HRAS autoantibodies in HCC clearly confirms the increased expression of HRAS in HCC liver tissues indicating that it plays an important role in the pathogenesis of cancer (480). HRAS inhibits the activation of nuclease which stimulates apoptosis and its associated with higher HCC recurrence in patients (480).

Highest frequencies of positive autoantibody responses in non-HCC cirrhotics and non-HCC non-cirrhotics who are regarded as high-risk patients were anti-HRAS, anti-AFP and anti-P53 autoantibodies irrespective of the category of TAA. This imply that anti-TAA autoantibodies may exist in conditions that pre-date malignancy, thus, autoantibodies to these TAAs are up-regulated before the development of the tumour. This is confirmed in a work conducted by Himoto, where elevated levels of anti-P53 was seen in chronic liver disease patients associated with diabetes mellitus (481). The prospective for autoantibodies to be early serological markers for HCC have been shown by their presence in patients who have a higher risk of developing HCC such as individuals with chronic liver disease (263). It is crucial to note that high prevalence of the above autoantibodies in cirrhosis and chronic hepatitis patients suggest their potential value in HCC detection. However, further characterisation of these autoimmune responses in pre-malignant conditions needs to be investigated. Our study has shown that anti-HRAS autoantibodies are produced in both the pre-malignant condition and in HCC. It has further been shown that the frequency of anti-TAA autoantibodies in HCC serum samples is significantly higher than values in cirrhotics and healthy controls, while there is not much difference in anti-TAA autoantibody frequencies between HCC and chronic hepatitis group. Overall, the study has shown high frequency of anti-TAA autoantibody responses in both HCC and underlying liver disease patients to our panel of HCC TAAs using the developed in-house high-

throughput platform. Hence, this could aid in the efficient diagnosis of HCC. Our study has a potential to offer an assistance to clinicians in assessing individuals at increased risk of the disease.

Chapter Seven: General Discussion

7.1. Epidemics and Fatality of Hepatocellular Carcinoma

Hepatocellular carcinoma (HCC) is a prevalent primary malignancy of the liver. It is recognised as one of the most common cancers worldwide, where over 0.8 million people are affected yearly (29) and the number of new cases of HCC increases every year. Alarmingly, a million people die on a yearly basis to the cancer and therefore it is not surprising that it is the third most common cause of cancer related mortalities worldwide. These increasing incidences and high mortality rates are seen in many populous regions of the world, especially China and Sub-Saharan Africa and in recent years, gradually growing in developed countries, such the USA (482). The increasing incidence of HCC has been attributed primarily to the growing presence of risk factors, such as chronic hepatitis B and C virus infections. Moreover, the incidence of long standing abuse of alcohol, nonalcoholic fatty liver disease (NAFLD) and consumption of aflatoxins are well known causes of increased chronic liver disease and ultimately HCC progression (482). HCC has poor prognosis, with most patients having a short survival time of up to just twelve months. This poor outlook is associated with late detection of advanced tumours by current diagnostic platforms. Present-day diagnosis is based on imaging studies such as computed tomography, magnetic resonance imaging, ultrasound, as well as serological laboratory tests such as serum Alpha Fetoprotein measurements (AFP) (30). Although serum AFP measurement has been recommended as an assistive tool to go with the imaging tests (483), its sensitivity is still sub-optimal in that there are about 40% of cases of HCC patients who have normal AFP levels. With this in mind, the urgent need to identify biomarkers for the early diagnosis of HCC is clearly unmet. Interestingly, some candidate biomarkers have

emerged to aid in early HCC diagnosis and these include mediators of the tumour microenvironment, as well as host immune response such as cytokines (Interleukin-8, Tumour Necrosis Factor-β), enzymes (proteasomes) (484) and tumour-associated antigens (TAAs). These are, however, not as effective as autoantibodies found in the serum of patients which react with cellular antigens produced by the tumour. In view of the knowledge that autoantibodies have greater advantages as early diagnostic markers, such as (i) appearing several months to years before clinical diagnosis of the tumour, (ii) their magnified signals of early carcinogenesis are easier to detect than TAAs themselves and (iii) they are measured in the blood (non-invasive), our research aimed to profile autoantibody responses to a wide range of TAAs in a Hepatocellular carcinoma background.

7.2 Development of the New Antigen Microarray Platform

The ultimate goal of this thesis was to design a reliable, high-throughput, diagnostic platform that would primarily be used to quantify and characterise anti-TAA specific IgG autoantibodies in HCC patients. In **Chapter 3** we examined the reproducibility of the in-house antigen microarray assay. Specifically, optimisation, redesigning assay protocols, and determining the validity of the established platform were studied to ensure the antigen microarray assay was reliable for this early biomarker detection. The first step taken was to assess the reproducibility (precision) of the existing antigen microarray protocol using quality control antigens such as *Candida albicans* and Tetanus toxoid because the available HCC TAAs, as well as HCC serum, were precious, and we did not want to use them all up for optimisation. Intra- and inter-assay values of IgG measurements and spot morphology of control antigens probed with purified IgG and control sera were determined. In the study, the acceptable limits of precision of CV values in a day (intra-assay) and across different days (inter-assay)

were ≤15% and ≤20% respectively and these were adapted in accordance with pharmacokinetic guidelines provided by the Food and Drugs Administration. Inter-assay CV values of IgG responses falling outside the accepted precision criteria was problematic. However, the introduction of human IgG standard curve helped to standardize the values as inter-assay values, after interpolation on the standard curve, mostly fell within the acceptable limits of precision. Hence, going forward, the human IgG standard curve would be used when measuring IgG responses in patient samples. The morphological appearance of antigen spots on the slide is very crucial with respect to obtaining reproducible outcomes (388, 485, 486). We decided to assess spot morphology of antigens, as well as variation in signals without incorporating human IgG standards. We did this because our intention was to minimise variations as much as possible before utilising normalisation strategies. In this regard, we tested some HCC TAAs with its corresponding antibody or control sera over two days, after which we compared the signal intensities generated and the morphology of spots on the slide. We noticed some slight differences in signals and spot sizes across two days in terms of the inter-assay precision, but this was minimal as compared to previous experiments. This enlightened us to redesign the antigen microarray assay to suit our study, since the existing protocol was developed for a different purpose. **Chapter 3** gave an in-depth explanation of the progressive steps taken to investigating and optimising the assay. Investigations were undertaken on parameters such as relative humidity, microtitre volumes, edge effect, slide surface chemistries, printing and blocking buffers, antibody dilutions, antigen concentrations as these are very vital in obtaining optimal conditions for the assay (384, 486-488).

We carefully assessed different printing buffers prepared in-house to determine the one which would be suitable for arraying TAAs. PBS-Trehalose-Betaine-tween produced

uniform morphology of spots, high signal intensity and low background noise, making them ideal for our antigen microarray platform. Interestingly, in a study by Selvarajah *et al*, PBS-Trehalose-Tween gave consistent spot morphologies, but this was printing capture antibodies, not antigens. This shows that the choice of printing buffer is affected by the type of protein printed. Different slide surface chemistries were tested with the optimal printing buffer to determine the suitable array surface for immobilising antigens as this has an effect on microarray precision (488). Aminosilane slide surface together with PBS Trehalose-Betaine-tween gave a reduction in spot to spot variation as well as high signal intensities. Other studies have shown that Poly-L-lysine (388) and Nitrocellulose (489) give higher signal intensities and low background noise. However, these studies arrayed antibodies and lysates respectively and so it was no surprise that we had a contradictory outcome. This further reveal that the choice of array surface is influenced by the nature of antigen or protein arrayed. In addition, elements such as 10 µl microtiter volume, 65% relative arrayer humidity, 5% BSA blocking reagent, increasing the wash steps, dilution of reagents/antibodies all aided to enhance the performance of the antigen microarray and this was in accordance with published studies (486). Having built the assay to suit our TAAs, patient samples and reagents, we moved to validating the technology by testing some analytical parameters such as the reproducibility (precision) and reliability. This time around, we utilised commercial TAAs expressed in *E. coli*, along with patients' sera. CV values were within the acceptable limits of precision (≤15% and ≤20% respectively) and these were in accordance with validation studies undertaken by Wood (490) and Lucas (491). Hence, the in-house microarray assay was now established for profiling autoantibody responses in HCC patients.

Quite a number of challenges were encountered while developing and validating the microarray and these needed to be addressed. However, faults associated with the arrayer affects the aforementioned parameters and this significantly affected the outcome of print (383, 384). Faulty settings and mechanical breakdown impeded the optimisation phase. Efforts were channelled into adjusting the settings of the machine and fixing mechanical breakdown other than focusing on developing the assay from the printing and probing stages. With this, the arrayer had to be closely monitored regularly during prints of slides to ensure there was no error with the contact pin, circulating water bath and humidity. Another challenge faced was that, factors such as temperature easily affected the performance of the assay. In that, signal intensities and background noise improved in winter, where there was a drop-in temperature compared to the summer. With this, regular maintenance of the equipment would help to eliminate such issues.

7.3 Generation of Recombinant TAAs for the Microarray Assay

As already stated, TAAs found on the tumour surface can induce the release of autoantibodies in cancer patients. We conducted a thorough literature search in order to identify TAAs that would elicit a measurable immune response in HCC patients. Thus, our identification was based on the criteria that TAAs showed strong immunogenicity in HCC or any solid tumour and were associated with liver disease. Researchers had highlighted that using a single TAA or marker lacks sensitivity and specificity for accurate cancer detection (257). However, increasing the panel of markers may offer an improvement in diagnostic performance. With this, 30 TAAs expressed in a mammalian system were identified for the study. However, the cost of these 30 TAAs was prohibitive so we opted to generate a panel of eight in-house TAAs expressed in HEK 293 cells and this which was addressed in **Chapter four**. One benefit of doing

this over purchasing commercial TAAs was also to be sure of the purity of TAAs and also have enough protein for the study. Eight TAAs; KRAS (492, 493), HRAS (241, 494), HDGF (479, 495), P16 (CDKN2A) (239, 496), RALA (241, 497), P62 (498), P53(499) and Gankyrin (500, 501) were selected for recombinant production in HEK 293 cells. Although studies on measuring autoantibody responses in HCC (468) or other cancers (273) mainly used bacterial (*E. coli*) expressed TAAs, we selected the mammalian system (HEK 293 cell line) because recombinant proteins are biologically active, post-translationally modified and they are similar to naturally occurring human proteins (413). So, our work was novel in term of using mammalian expressed TAAs to measure autoantibody responses in HCC. Initially four Myc-DDK tagged human cDNA clones (KRAS, HRAS, HDGF, P16) were purchased from Origene, USA and transfected into HEK 293 cells by electroporation after which resistant cells were selected with Geneticin G418. KRAS, HRAS and P16 were eventually successfully expressed after a new batch of cell line was used and the transfection procedure was carefully optimised by increasing the following: plasmid concentration, time of protein expression and the length of stable cell line selection with G418. Using old cell lines for transfection can result in cell stress, improper protein folding and inactive proteins (447), low cDNA concentration can lead to low protein expression (451) and low molecular weight proteins often take a long time for protein expression (450). Hence, it is not surprising that a combination of the new batch of cell line and the optimised transfection protocol enabled us to express the proteins in cell lysates.

Now we had expression, the next task was to purify the proteins from the cell lysates. Many challenges were encountered in trying to purify the recombinant proteins from lysates irrespective of the type of purification kit used. Three Flag (Myc-DDK) purification kits were tested; anti-Flag® M2 affinity gel (Sigma Aldrich, UK), anti-

Flag® M2 magnetic beads (Sigma Aldrich, UK) and Myc Trap® MA magnetic beads (Chromotek, UK). Firstly, purification of expressed proteins in lysates (KRAS, HRAS, HDGF, P16) was undertaken with anti-Flag M2 affinity gel. This purification system is suggested to effectively pull-down Flag-tag proteins using its M2-conjugated agarose resin (502). Unfortunately, it was unsuccessful because the resin had lost its sensitivity (unfortunately it was out of date) and therefore had poor affinity for proteins expressed in lysates. Anti-Flag® M2 magnetic beads was the alternative kit tested. It consists of an anti-Flag® M2 monoclonal antibody attached to magnetic beads, which recognises and binds the Flag peptide sequence of either the N-, Met-N and C terminus of recombinant proteins in mammalian extracts. It was therefore expected that this kit could immunoprecipitate all recombinant proteins (KRAS, HRAS, HDGF, P16, RALA. P62, P53, Gankyrin) expressed in lysates. Unexpectedly, purified products were heavily contaminated with IgG heavy and light chains from the magnetic beads, which masked the Flag-tagged recombinant proteins. This was encountered despite trying different elution methods (Glycine-HCL pH 2.8, SDS with or without DTT) as well as altering the volumes of magnetic beads and lysates. This was no surprise as earlier studies had shown that elution with glycine-HCL doesn't always maintain antibody integrity (453). We were limited with respect to further optimisation procedures because the anti-Flag M2 magnetic beads are generally used for small scale purification and therefore there wasn't sufficient for our work. Finally, we tested Myc-Trap® MA magnetic beads as the purification tool. Unlike previous immunoprecipitation beads which were 50 μm, Myc Trap are nanobodies (40 μm) that have high affinity binding. These beads are coupled to small antibody fragments instead whole antibody and therefore there should be no heavy or light chain contamination in downstream applications. With this methodology, just a single polypeptide chain is needed to capture an antigen of interest

(503). Lastly, they have the advantage of not only binding the N and C terminals of fusion proteins but also the internal site (503). Encouragingly, the Myc Trap successfully purified one recombinant protein (HDGF) from HEK 293 cell extract. An unexpected dimerisation of the remaining recombinant proteins (KRAS, HRAS, P16, RALA, P62, P53, Gankyrin) occurred and therefore immunoprecipitation with Myc Trap was also unsuccessful. The process of generating in-house TAAs took a substantial amount of time, approximately nine months and was far more expensive than anticipated. This informed our decision to obtain commercial purified TAAs expressed in HEK 293 cells in addition to the in-house tumour antigens expressed in lysates. Other commercial TAAs produced in *E. coli* were kindly donated by the Centre of Excellence for Autoimmunity in Cancer (CEAC).

7.4 Development of the Antigen Microarray Technology for TAAs expressed in Lysates

The fourth aim of the thesis was to test the performance of in-house TAAs expressed in lysates as well as commercial TAAs produced in HEK 293 cells on the developed microarray platform (**Chapter 5)**. This was required because the antigen microarray was initially developed using commercial TAAs produced in a bacterial expression system, *E. coli*. It was imperative to optimise the antigen microarray to fully suit this group of TAAs so as obtain good spot quality. This required pictorial inspection of the feature of each array in order to determine the optimal array buffer for printing TAAs, concentration, wash regimes, required dilution of primary and secondary antibodies for probing printed slides, as well as the optimal Cy5 dye for visualising the antigen-antibody interaction. In reverse phase protein microarray, which allows a large number of biological samples to be measured concurrently, lysates containing human tissues are prepared in 2% SDS especially because they are immobilised onto Nitrocellulose

slides (504). In our study, PBS-Trehalose-Betaine was deemed as the most suitable for arraying TAAs expressed in cell lysates as it did not contain Tween and minimised extensive smearing across slide pads which improved signal intensities of spots. On the other hand, PBS-Trehalose-Betaine-Tween was optimal for arraying commercial TAAs expressed in HEK 293 cells. It was very vital to check the most suitable array buffer for each set of TAA and not assume one buffer would be suitable for all TAAs (505). Analysis showed that the developed antigen microarray platform was highly precise as values of signal intensities fell within the acceptable criteria recommended by the FDA when performed multiple times within a day or across different days. This makes the technology reliable to quantify TAA specific IgG autoantibodies in patients' sera.

7.5 Application of the developed Antigen Microarray Platform for Autoantibody Detection

The last aim of the thesis was to use the developed in-house microarray to run a large set of clinical samples to test the effectiveness of our TAA panel for profiling autoantibody responses in HCC and examine how successful the platform is as a diagnostic tool. Firstly, the platform was used to screen TAA specific IgG autoantibodies in four different patient cohorts (183 HCC, 90 non-HCC cirrhotic, 133 non-HCC non-cirrhotic and 46 matched healthy) using 26 TAAs as described in **Chapter 6**. Eight of the TAAs screened were produced in-house as described in **Chapter 4** of the thesis. Ten of the TAAs were donated by CEAC for use while the remaining eight were obtained commercially.

Before samples could be run of the microarray platform, we needed to test the effect of heat treatment on detection of antibody levels. This was key as many samples were from Hepatitis B and C positive individuals and these could not be handled on the microarray without first inactivating viruses by heat treatment. From our study, heat

treatment of cancer sera did not have an effect on the detectability of autoantibody responses in HCC and non-HCC patients' sera. Interesting, previous studies had shown an increase in levels of anti-SOX2 responses in HCC sera following heat treatment (241), but we observed no differences in responses to our TAAs. Therefore, virally-infected serum samples were inactivated so they could be safely used for immunological screening.

Anti-P16 and anti-P53 had the highest autoantibody responses observed in HCC patients. This signifies that P16 and P53 antigens, which are tumour suppressor genes, were highly expressed in most HCC patients and therefore highlights their role in the development of the cancer (496). The elevated anti-TAA responses observed in HCC patients as compared to patients with liver cirrhosis and the healthy group in our study clearly demonstrates that autoantibody responses are strongly associated with the cancer development, as also shown by the study by Wang *et al* (506). Unexpectedly, values of autoantibody responses in non-HCC non-cirrhotics (chronic hepatitis) were close to that obtained in HCC patients, which is different to previous studies that showed that responses in chronic hepatitis patients usually express the least anti-TAAs responses (267). This could indicate that the transition to the cancerous stage is linked with autoantibody responses to certain cellular antigens that might have a role in cancer development (257). The observed similar distribution of autoantibody responses to some *E. coli* generated TAAs across the different cohorts could be linked to the fact that most people have been exposed to *E. coli* at some points in their lives and thus the assay may actually be measuring anti-*E. coli* responses. This highlights the importance of using mammalian expression systems to produce TAAs (447).

Our study was the first to compare autoantibody responses amongst the different categories of TAAs; a strong correlation between autoimmune responses to commercial and in-house eukaryotic TAAs (RAL-A, P62, P53, Gankyrin) shows that TAAs, irrespective of the form in which exist, can identify adequate autoantibody levels in patients' sera.

Our study revealed no relationship between autoantibody responses and age or gender of HCC patient, although increase in age poses as a risk factor for HCC (475). This contrasted previous studies where age significantly increased autoantibody responses in HCC patients, although different TAAs were used (476). Hence, our work suggest that age does not have an effect on autoantibody responses to our panel of TAAs.

The highest autoantibody level was observed for anti-P62, anti-HRAS and anti-HDGF in HCC patients. This may indicate that they were highly expressed in HCC tumours and therefore elevated expression is indicative of poor survival of patients (479). This implies that P62, HRAS and HDGF are very important TAAs in HCC development and therefore stand as potential targets for immunotherapy. Our data also emphasise the importance of anti-HRAS, anti-AFP and anti-P53 autoantibodies in the high-risk cohort (cirrhosis and chronic hepatitis patients) as they could hold a prospective value in the malignant transformation of HCC. This further informs that patients at the chronic liver disease and liver cirrhosis stages should be carefully monitored before tumour development. As such, a comprehensive analysis of these the aforementioned anti-TAA responses in pre-malignant conditions should be conducted in order to validate their contribution to HCC diagnosis.

There were a few limitations with this study that warrant mention. Firstly, there were limitations in the serodiagnosis aspect of the study. Amongst the three datasets, only one provided clinical information of patients pertaining to tumour size, while the remaining provided general information about the diagnosis of each sample. Amazingly, no information on patients' serum AFP were provided for any of the samples, which is the current serological biomarker for HCC surveillance. Since AFP has been demonstrated to yield unsatisfactory results in the early diagnosis of HCC, it would have been ideal to compare these levels with the outcomes of our work. Consequently, this affected our ability to conduct correlation analysis between the prevalence of anti-TAA responses and clinicopathological characteristics of patients. Another limitation was that majority of sera were from patients with HCV-related HCC, liver cirrhosis or chronic hepatitis. It would have been ideal to have an equal distribution of other aetiologies such as HBV, NAFLD, alcohol, diabetes, etc. Additionally, majority of the clinical samples were from males and therefore made it difficult to compare anti-TAA responses between the two genders. Moreover, it would have been beneficial to add the HCV antigen to our panel in order to confirm patients' responses to them. Autoantibody responses to TAAs could not be verified with another immunological technique such as ELISA due to limited time frame and sample volume Lastly, a longitudinal study of "at risk" patients/ needs to be conducted to show if the developed microarray could provide a platform for early diagnosis.

In conclusion, we have shown that autoantibodies to our selected panel of TAAs gives a good aid for HCC detection. Our work proposes that using our microarray of TAAs (KRAS, HRAS, HDGF, P16, RALA, P62, P53, Gankyrin) could be used as a non-invasive approach to help detect HCC in pre-malignant conditions such as liver cirrhosis and chronic hepatitis.

7.6 Conclusions

This thesis documents work undertaken to detect and characterise autoantibodies to tumour-associated antigens (TAAs) in hepatocellular carcinoma (HCC) patients using a high-throughput screening tool. Given the devastating effects of HCC and the problems associated with early detection of this cancer, the in-house antigen microarray platform was firstly developed by exploring multiple parameters. The platform was further optimised and validated to aid in the detection of specific anti-TAA autoantibody responses in HCC patients. Eight recombinant TAAs of interest were successfully expressed in HEK 293 cell lysates, despite the drawbacks faced in streamlining methods of purification. These TAAs were used, in combination with commercial eukaryotic and *E. coli* expressed TAAs, as targets for profiling autoantibodies in the sera of HCC and high-risk patients. We used the developed platform to run a large set of clinical samples to determine the effectiveness of our TAA panel for profiling autoantibody responses in HCC, cirrhosis and chronic hepatitis patients. Our study has thus developed a blood test which is highly efficient and has the potential to offer a competitive benefit over present HCC diagnostic tools as it is easy to use, portable, non-invasive and inexpensive. It could be applicable as an annual check in GP surgery to provide reports of greater relevance that could be used for effective treatment strategies. This would undeniably enhance the future of HCC diagnosis and help lower mortality rates associated with this malignancy.

7.8 Future Directions

An extensive amount of work had been conducted to develop the antigen microarray platform for the diagnosis of hepatocellular carcinoma. However, there are a number of areas of work that could be undertaken in the future.

- Processing printed slides often takes up to 8 hours excluding printing and statistical analysis because these are done manually. It would be necessary to reduce the time if it is incorporated as an annual check-up in general practice (GP) surgery. Hence, developing an efficient robotic system that could undertake the probing of serum samples would be essential. This would also eliminate human errors, especially with pipetting tiny volumes of samples and reagents. Also, developing an appropriate analytical software to analyse data faster would allow a broader clinical audience to profit from this technique. Eight or sixteen pad slides were used for quantification of autoantibody levels in sera. Developing and using 64 pads would allow more clinical samples to be tested at once. Additionally, it would be enlightening if generated signals during scanning could indicate whether someone has HCC or not.
- The antigen microarray platform has demonstrated good performance for the detection of specific anti-TAA IgG autoantibodies in HCC and pre-cancerous conditions. Nevertheless, it would be appropriate to have a direct comparison between the in-house microarray platform and other diagnostic methods such as ELISA to further evaluate the functioning and limitation of the technique.
- Having a widespread data set on the clinical history of patients is utmost for meaningful interpretation of results. Therefore, subsequent studies should focus on ensuring that sample sets obtained from different sources all have a thorough

set of clinical information about the patients, such as ethnicity, underlying liver aetiology, geographical region, tumour size, staging of the cancer according to the BCLC stage, current imaging diagnosis, serum AFP titre levels and full patient treatment. This would generate more comprehensive results and show the correlation between anti-TAA autoantibody responses and the clinicopathological conditions of patients.

- Also, equal number of samples in each cohort (HCC, cirrhotic, chronic hepatitis and healthy controls) would be desirable. Additionally, twenty-six TAAs from different expression systems were used on the antigen microarray. However, this microarray platform is not just limited to these sets of TAAs. Testing other TAAs that are highly associated with HCC and produced in a eukaryotic system can be exploited. Several challenges were encountered during the production of recombinant TAAs. Therefore, subsequent studies in an attempt to produce in-house TAAs should ensure the laboratory is equipped with the facilities in undertaking work of such nature. Moreover, purification of Flag-tagged TAAs in lysates proved futile and so purchasing clones with a different tag could be explored in future studies.
- It would be ideal to obtain sequential pre-diagnosis samples so as to determine how long (lead time) the autoantibodies are detectable before the tumour appears. Additionally, it would be interesting to determine whether the same autoantibodies are present from start of the tumour development by the immune system.
- Investigating the differences in expression patterns of IgG isotypes profiles and whether these change over time, will also give novel insights into autoantibody responses in HCC. Studies on HCC are mostly focused on the detection of IgG

autoantibodies as biomarkers for early diagnosis of HCC. It would be interesting to explore IgM autoantibodies to TAAs in HCC patients and whether there are differences between the two immunoglobulin groups.

- Furthermore, examining the binding of autoantibodies to either the surface or intracellular components of HCC cells would help to inform whether these early biomarkers have significant effects on HCC cells, such as signalling pathways, growth of the tumour and whether they enhance effector functions such as complement activation, antibody dependent cell cytotoxicity (ADCC). These would help outline their distinct functions in HCC.
- The antigen microarray technology platform can be implicated in both research and management of HCC patients in that it could be used by clinicians to monitor drug treatment plan of patients in health care settings in the future.

References

1. Ferlay, J., H. R. Shin, F. Bray, D. Forman, C. Mathers, and D. M. Parkin. 2010. Estimates of worldwide burden of cancer in 2008: GLOBOCAN 2008. *International Journal of Cancer. Journal International Du Cancer* 127 (12): 2893-2917.
2. Siegel, R. L., K. D. Miller, and A. Jemal. 2017. Cancer Statistics, 2017. *CA Cancer J Clin* 67 (1): 7-30.
3. Parkin, D. M., F. Bray, J. Ferlay, and P. Pisani. 2005. Global cancer statistics, 2002. *CA: A Cancer Journal for Clinicians* 55 (2): 74-108.
4. Ferlay, J., I. Soerjomataram, R. Dikshit, S. Eser, C. Mathers, M. Rebelo, D. M. Parkin, D. Forman, and F. Bray. 2014. Cancer incidence and mortality worldwide: Sources, methods and major patterns in GLOBOCAN 2012. *International Journal of Cancer* 136 (5): E359-E386.
5. Cancer Research United Kingdom. 2015. Cancer Statistics for the UK.
6. Jemal, A., F. Bray, M. M. Center, J. Ferlay, E. Ward, and D. Forman. 2011. Global cancer statistics. *CA: A Cancer Journal for Clinicians* 61 (2): 69-90.
7. Ferlay J, S. I., Ervik M, Dikshit R, Eser S, Mathers C, *et al*. 2012. GLOBOCAN 2012. Cancer Incidence and Mortality Worldwide. *IARC Cancerbase* No. 11.
8. Danaei, G., S. Vander Hoorn, A. D. Lopez, C. J. Murray, and M. Ezzati. 2005. Causes of cancer in the world: comparative risk assessment of nine behavioural and environmental risk factors. *Lancet (London, England)* 366 (9499): 1784-1793.
9. Vogelstein, B., and K. W. Kinzler. 1993. The multistep nature of cancer. *Trends in Genetics* 9 (4): 138-141.
10. Floor, S. L., J. E. Dumont, C. Maenhaut, and E. Raspe. 2012. Hallmarks of cancer: of all cancer cells, all the time? *Trends in Molecular Medicine* 18 (9): 509-515.
11. Hanahan, D., and R. A. Weinberg. 2011. Hallmarks of cancer: the next generation. *Cell* 144 (5): 646-674.
12. Knudson, A. G. 2001. Two genetic hits (more or less) to cancer. *Nature Reviews. Cancer* 1 (2): 157-162.
13. Cheng, N., A. Chytil, Y. Shyr, A. Joly, and H. L. Moses. 2008. Transforming growth factor-beta signaling-deficient fibroblasts enhance hepatocyte growth factor signaling in mammary carcinoma cells to promote scattering and invasion. *Molecular Cancer Research* 6 (10): 1521-1533.
14. Davies, M. A., and Y. Samuels. 2010. Analysis of the genome to personalize therapy for melanoma. *Oncogene* 29 (41): 5545-5555.
15. Collado, M., and M. Serrano. 2010. Senescence in tumours: evidence from mice and humans. *Nature Reviews. Cancer* 10 (1): 51-57.
16. Mooi, W. J., and D. S. Peeper. 2006. Oncogene-induced cell senescence--halting on the road to cancer. *N Engl J Med* 355 (10): 1037-1046.
17. Lee, E. Y., and W. J. Muller. 2010. Oncogenes and Tumor Suppressor Genes. In *Cold Spring Harb Perspect Biol* 2 (10): a003236.
18. Brierley, J. 2006. The evolving TNM cancer staging system: an essential component of cancer care. In *CMAJ 174 (2):* 155-156.
19. Brown, K. F., H. Rumgay, C. Dunlop, M. Ryan, F. Quartly, A. Cox, A. Deas, L. Elliss-Brookes, A. Gavin, L. Hounsome, D. Huws, N. Ormiston-Smith, J.

Shelton, C. White, and D. M. Parkin. 2018. The fraction of cancer attributable to modifiable risk factors in England, Wales, Scotland, Northern Ireland, and the United Kingdom in 2015. *British Journal of Cancer* 118 (8): 1130-1141.

20. Rowlands, M. A., D. Gunnell, R. Harris, L. J. Vatten, J. M. Holly, and R. M. Martin. 2009. Circulating insulin-like growth factor peptides and prostate cancer risk: a systematic review and meta-analysis. *International Journal of cancer. Journal International Du Cancer* 124 (10): 2416-2429.
21. Roukos, D. H. 2009. Genome-wide association studies: how predictable is a person's cancer risk? *Expert Review of Anticancer Therapy* 9 (4): 389-392.
22. Meropol, N. J., and K. A. Schulman. 2016. Cost of Cancer Care: Issues and Implications. http://dx.doi.org/10.1200/JCO.2006.09.6081.
23. Laudicella, M., B. Walsh, E. Burns, and P. C. Smith. 2016. Cost of care for cancer patients in England: evidence from population-based patient-level data. In *Br J Cancer* 114 (11): 1286-1292.
24. Sachdeva, M., Y. K. Chawla, and S. K. Arora. 2015. Immunology of hepatocellular carcinoma. *World J Hepatol* 7 (17): 2080-2090.
25. Abdel-Misih, S. R. Z., and M. Bloomston. 2010. Liver Anatomy. *Surg Clin North Am* 90 (1): 643-653.
26. Frevert, U., S. Engelmann, S. Zougbede, J. Stange, B. Ng, K. Matuschewski, L. Liebes, and H. Yee. 2005. Intravital observation of Plasmodium berghei sporozoite infection of the liver. *PLoS biology* 3 (6): e192.
27. Ramadori, G., F. Moriconi, I. Malik, and J. Dudas. 2008. Physiology and pathophysiology of liver inflammation, damage and repair. *J Physiol Pharmacol* 59 (Suppl 1): 107-117.
28. Kmiec, Z. 2001. Cooperation of liver cells in health and disease. *Adv Anat Embryol Cell Biol* 161: III-XIII, 1-151.
29. Ghouri, Y. A., I. Mian, and J. H. Rowe. 2017. Review of hepatocellular carcinoma: Epidemiology, etiology, and carcinogenesis. In *J Carcinog* 16: 1.
30. Balogh, J., D. Victor, E. H. Asham, S. G. Burroughs, M. Boktour, A. Saharia, X. Li, R. M. Ghobrial, and H. P. Monsour. 2016. Hepatocellular carcinoma: a review. In *J Hepatocell Carcinoma* 3: 41-53.
31. Wu, J. 2017. The changing epidemiology of hepatocellular carcinoma in Asia versus United States and Europe. *Advances in Modern Oncology research 3* (1): 182.
32. Kumar, N., and E. Mayo. 2017. The Global Incidence And Prevalence Of Hepatocellular Carcinoma. *Journal of Cancer Research & Therapeutics* 13 (1): pS49-S50.
33. Song, P. 2013. Standardizing management of hepatocellular carcinoma in China: devising evidence-based clinical practice guidelines. *Bioscience Trends* 7 (5): 250-252.
34. Ascione, A., L. Fontanella, M. Imparato, L. Rinaldi, and M. De Luca. 2017. Mortality from cirrhosis and hepatocellular carcinoma in Western Europe over the last 40 years. *Liver Int* 37 (8): 1193-1201.
35. Seeff, L. B., and J. H. Hoofnagle. 2006. Epidemiology of hepatocellular carcinoma in areas of low hepatitis B and hepatitis C endemicity. In *Oncogene*, England. 25 (27): 3771-3777.
36. Cancer Research United Kingdom. 2015. Liver cancer incidence statistics. *Cancer Research UK*.
37. Clark, T., S. Maximin, J. Meier, S. Pokharel, and P. Bhargava. 2015. Hepatocellular Carcinoma: Review of Epidemiology, Screening, Imaging

Diagnosis, Response Assessment, and Treatment. *Curr Probl Diagn Radiol* 44 (6): 479-486.

38. Okuda, K., Y. Nakanuma, and M. Miyazaki. 2002. Cholangiocarcinoma: recent progress. Part 2: molecular pathology and treatment. *Journal of Gastroenterology and Hepatology* 17 (10): 1056-1063.
39. Shariff, M. I., I. J. Cox, A. I. Gomaa, S. A. Khan, W. Gedroyc, and S. D. Taylor-Robinson. 2009. Hepatocellular carcinoma: current trends in worldwide epidemiology, risk factors, diagnosis and therapeutics. *Expert Rev Gastroenterol Hepatol* 3 (4): 353-367.
40. Scherzed, A., S. Hackenberg, K. Froelich, M. Kessler, C. Koehler, R. Hagen, A. Radeloff, G. Friehs, and N. Kleinsasser. 2011. BMSC enhance the survival of paclitaxel treated squamous cell carcinoma cells in vitro. *Cancer biology & therapy* 11(3): 349-357.
41. Yu, M. C., and J. M. Yuan. 2004. Environmental factors and risk for hepatocellular carcinoma. In *Gastroenterology*, United States. 127 (5): S72-78.
42. Rudolph, H. B. E. K. L. 2007. Hepatocellular Carcinoma: Epidemiology and Molecular Carcinogenesis 132 (7): 2557–2576.
43. Yeh, S. H., and P. J. Chen. 2010. Gender disparity of hepatocellular carcinoma: the roles of sex hormones. *Oncology* 78 (1): 172-179.
44. Ma, W. L., C. L. Hsu, C. C. Yeh, M. H. Wu, C. K. Huang, L. B. Jeng, Y. C. Hung, T. Y. Lin, S. Yeh, and C. Chang. 2012. Hepatic androgen receptor suppresses hepatocellular carcinoma metastasis through modulation of cell migration and anoikis. *Hepatology (Baltimore, Md.)* 56 (1): 176-185.
45. Hashem B. El-Serag, K. L. R. 2007. Hepatocellular Carcinoma: Epidemiology and Molecular Carcinogenesis. 132 (7): 2557–2576.
46. Ahmet, G., Ayma, P., Koteish, Z., Esteban M. 2015. Hepatocellular Carcinoma (LiverCancer):Introduction.https://www.halstedsurgery.org/GDL_Disease.aspx?CurrentUDV=31&GDL_Disease_ID=A349F0EC-5C87-4A52-9F2E-69AFDB80C3D1&GDL_DC_ID=9AA60584-3607-4D15-A459-BD3F67A3A4A7
47. El-Serag, H. B., and K. L. Rudolph. 2007. Hepatocellular carcinoma: epidemiology and molecular carcinogenesis. In *Gastroenterology* 132 (7): 2557-2576.
48. Mindie H Nguyen, A. W., Ruel T Gracia, sarra. 2004. Role of ethnicity in risk for hepatocellular carcinoma in patients with chronic hepatitis C and cirrhosis. *Gateroenterology* 2 (9): 820–824.
49. Wong, V. W., J. Yu, A. S. Cheng, G. L. Wong, H. Y. Chan, E. S. Chu, E. K. Ng, F. K. Chan, J. J. Sung, and H. L. Chan. 2009. High serum interleukin-6 level predicts future hepatocellular carcinoma development in patients with chronic hepatitis B. *International journal of cancer. Journal International Du Cancer* 124 (12): 2766-2770.
50. Haworth, E. A., V. Soni Raleigh, and R. Balarajan. 1999. Cirrhosis and primary liver cancer amongst first generation migrants in England and Wales. *Ethnicity & Health* 4 (1): 93-99.
51. Artinyan, A., B. Mailey, N. Sanchez-Luege, J. Khalili, C. L. Sun, S. Bhatia, L. D. Wagman, N. Nissen, S. D. Colquhoun, and J. Kim. 2010. Race, ethnicity, and socioeconomic status influence the survival of patients with hepatocellular carcinoma in the United States. *Cancer* 116 (5): 1367-1377.

52. Chen, Y., Q. Yi, and Y. Mao. 2008. Cluster of liver cancer and immigration: a geographic analysis of incidence data for Ontario 1998-2002. *International Journal of Health Geographics* 7: 28.
53. Kulkarni, K., E. Barcak, H. El-Serag, and R. Goodgame. 2004. The impact of immigration on the increasing incidence of hepatocellular carcinoma in the United States. *Alimentary Pharmacology & Therapeutics* 20 (4): 445-450.
54. Aravalli, R. N. 2013. Role of innate immunity in the development of hepatocellular carcinoma. *World Journal of Gastroenterology* 19 (43): 7500-7514.
55. Uhl, P., G. Fricker, U. Haberkorn, and W. Mier. 2014. Current Status in the Therapy of Liver Diseases. *International Journal of Molecular Sciences* 15 (5): 7500-7512.
56. Farazi, P. A., and R. A. DePinho. 2006. Hepatocellular carcinoma pathogenesis: from genes to environment. In *Nature Reviews. Cancer*, England 6(9): 674-687.
57. McMahon, B. J., S. R. Alberts, R. B. Wainwright, L. Bulkow, and A. P. Lanier. 1990. Hepatitis B-related sequelae. Prospective study in 1400 hepatitis B surface antigen-positive Alaska native carriers. *Archives of Internal Medicine* 150 (5): 1051-1054.
58. Lee, H. W., and S. H. Ahn. 2016. Prediction models of hepatocellular carcinoma development in chronic hepatitis B patients. *World J Gastroenterol* 22 (37): 8314-8321.
59. Kane, M. A. 2003. Global control of primary hepatocellular carcinoma with hepatitis B vaccine: the contributions of research in Taiwan. *Cancer epidemiology, biomarkers & prevention : A Publication of the American Association for Cancer Research, cosponsored by the American Society of Preventive Oncology* 12: 2-3.
60. Goldstein, S. T., F. Zhou, S. C. Hadler, B. P. Bell, E. E. Mast, and H. S. Margolis. 2005. A mathematical model to estimate global hepatitis B disease burden and vaccination impact. *International Journal of Epidemiology* 34 (6): 1329-1339.
61. Tokino, T., H. Tamura, N. Hori, and K. Matsubara. 1991. Chromosome deletions associated with hepatitis B virus integration. In *Virology*, United States. 185 (2): 879-882.
62. Szabo, E., C. Paska, P. Kaposi Novak, Z. Schaff, and A. Kiss. 2004. Similarities and differences in hepatitis B and C virus induced hepatocarcinogenesis. *Pathol Oncol Res* 10 (1): 5-11.
63. Liu, C. J., and J. H. Kao. 2007. Hepatitis B virus-related hepatocellular carcinoma: epidemiology and pathogenic role of viral factors. In *J Chin Med Assoc*, China Republic 70 (4):141-145.
64. Feitelson, M. A., B. Sun, N. L. Satiroglu Tufan, J. Liu, J. Pan, and Z. Lian. 2002. Genetic mechanisms of hepatocarcinogenesis. *Oncogene* 21 (16): 2593-2604.
65. Hiraoka, A., S. Hidaka, Y. Shimizu, H. Utsunomiya, Y. Imai, H. Tatsukawa, N. Tazuya, H. Yamago, N. Yorimitsu, T. Tanihira, A. Hasebe, Y. Miyamoto, T. Ninomiya, H. Kawasaki, M. Hirooka, M. Abe, Y. Hiasa, B. Matsuura, M. Onji, and K. Michitaka. 2012. Recent trends of Japanese hepatocellular carcinoma due to HCV in aging society. *Hepatogastroenterology* 59 (118): 1893-1895.
66. World Health Organization. 2017. Global hepatitis report 2017. http://www.who.int/iris/handle/10665/255016.
67. Shire, N. J., and K. E. Sherman. 2015. Epidemiology of Hepatitis C Virus: A Battle on New Frontiers. *Gastroenterol Clin North Am* 44 (4): 699-716.

68. Bowen, D. G., and C. M. Walker. 2005. Adaptive immune responses in acute and chronic hepatitis C virus infection. In *Nature*, England. 436 (7053): 946-952.
69. Donato, F., A. Tagger, U. Gelatti, G. Parrinello, P. Boffetta, A. Albertini, A. Decarli, P. Trevisi, M. L. Ribero, C. Martelli, S. Porru, and G. Nardi. 2002. Alcohol and hepatocellular carcinoma: the effect of lifetime intake and hepatitis virus infections in men and women. *American Journal of Epidemiology* 155 (4): 323-331.
70. El-Serag, H. B. 2002. Hepatocellular carcinoma and hepatitis C in the United States. In *Hepatology (Baltimore, Md.)*, United States. 36 (5): S74-83.
71. Shepard, C. W., L. Finelli, and M. J. Alter. 2005. Global epidemiology of hepatitis C virus infection. In *Lancet Infect Dis*, United States. 5 (9): 558-567.
72. El-Zayadi, A. R., H. M. Badran, E. M. Barakat, D. Attia Mel, S. Shawky, M. K. Mohamed, O. Selim, and A. Saeid. 2005. Hepatocellular carcinoma in Egypt: a single center study over a decade. *World Journal of Gastroenterology* 11 (33): 5193-5198.
73. Suruki, R. Y., N. Mueller, K. Hayashi, D. Harn, V. DeGruttola, C. A. Raker, H. Tsubouchi, and S. O. Stuver. 2006. Host immune status and incidence of hepatocellular carcinoma among subjects infected with hepatitis C virus: a nested case-control study in Japan. In *Cancer Epidemiology, Biomarkers & Prevention : a Publication of the American Association for Cancer Research, Cosponsored by the American Society of Preventive Oncology*, United States. 15 9 (12): 2521-2525.
74. Hino, O., K. Kajino, T. Umeda, and Y. Arakawa. 2002. Understanding the hypercarcinogenic state in chronic hepatitis: a clue to the prevention of human hepatocellular carcinoma. *J Gastroenterol* 37 (11): 883-887.
75. Majumder, M., A. K. Ghosh, R. Steele, R. Ray, and R. B. Ray. 2001. Hepatitis C virus NS5A physically associates with p53 and regulates p21/waf1 gene expression in a p53-dependent manner. *Journal of Virology* 75 (3): 1401-1407.
76. Macdonald, A., K. Crowder, A. Street, C. McCormick, K. Saksela, and M. Harris. 2003. The hepatitis C virus non-structural NS5A protein inhibits activating protein-1 function by perturbing ras-ERK pathway signaling. In *The Journal of Biological Chemistry*, United States. 278 (20): 17775-17784.
77. Liang, T. J., and T. Heller. 2004. Pathogenesis of hepatitis C-associated hepatocellular carcinoma. In *Gastroenterology*, United States. 127 (5): S62-71.
78. Fattovich, G. 2004. Hepatocellular carcinoma in cirrhosis: Incidence and risk factors. 127 (5): S35–S50.
79. McClain, C. J., D. B. Hill, Z. Song, I. Deaciuc, and S. Barve. 2002. Monocyte activation in alcoholic liver disease. In *Alcohol*, United States. 27 (1): 53-61.
80. Campbell, J. S., S. D. Hughes, D. G. Gilbertson, T. E. Palmer, M. S. Holdren, A. C. Haran, M. M. Odell, R. L. Bauer, H.-P. Ren, H. S. Haugen, M. M. Yeh, and N. Fausto. 2005. Platelet-derived growth factor C induces liver fibrosis, steatosis, and hepatocellular carcinoma. *Proc Natl Acad Sci* United States. 102 (9): 3389-3394.
81. Singal, A. K., A. Singh, S. Jaganmohan, P. Guturu, R. Mummadi, Y. F. Kuo, and G. K. Sood. 2010. Antiviral therapy reduces risk of hepatocellular carcinoma in patients with hepatitis C virus-related cirrhosis. In *Clin Gastroenterol Hepatol*. 2010 AGA Institute. Published by Elsevier Inc, United States. 8 (2): 192-199.

82. Corrao, G., and S. Arico. 1998. Independent and combined action of hepatitis C virus infection and alcohol consumption on the risk of symptomatic liver cirrhosis. *Hepatology (Baltimore, Md.)* 27 (4): 914-919.
83. Yamanaka, T., K. Shiraki, S. Nakazaawa, H. Okano, T. Ito, M. Deguchi, K. Takase, and T. Nakano. 2001. Impact of hepatitis B and C virus infection on the clinical prognosis of alcoholic liver cirrhosis. *Anticancer Res* 21 (4B): 2937-2940.
84. World Health Organization, International Agency for Research on Cancer. 1987.Overall evaluations of carcinogenicity: an updating of IARC Monographs volumes 1 to 42. *IARC Monographs on the Evaluation of Carcinogenic Risks to Humans.* Supplement / 7 (suppl 7): 1-440.
85. Aguilar, F., C. C. Harris, T. Sun, M. Hollstein, and P. Cerutti. 1994. Geographic variation of p53 mutational profile in nonmalignant human liver. *Science (New York, N.Y.)* 264 (5163): 1317-1319.
86. Turner, P. C., A. Sylla, M. S. Diallo, J. J. Castegnaro, A. J. Hall, and C. P. Wild. 2002. The role of aflatoxins and hepatitis viruses in the etiopathogenesis of hepatocellular carcinoma: A basis for primary prevention in Guinea-Conakry, West Africa. *Journal of Gastroenterology and Hepatology* 17 Suppl: S441-448.
87. Garner, R. C., E. C. Miller, and J. A. Miller. 1972. Liver microsomal metabolism of aflatoxin B 1 to a reactive derivative toxic to *Salmonella typhimurium* TA 1530. *Cancer Research* 32 (10): 2058-2066.
88. Bedogni, G., L. Miglioli, F. Masutti, C. Tiribelli, G. Marchesini, and S. Bellentani. 2005. Prevalence of and risk factors for nonalcoholic fatty liver disease: the Dionysos nutrition and liver study. *Hepatology (Baltimore, Md.)* 42 (1): 44-52.
89. Falck-Ytter, Y., Z. M. Younossi, G. Marchesini, and A. J. McCullough. 2001. Clinical features and natural history of nonalcoholic steatosis syndromes. *Semin Liver Dis* 21 (1): 17-26.
90. Bugianesi, E., E. Vanni, and G. Marchesini. 2007. NASH and the risk of cirrhosis and hepatocellular carcinoma in type 2 diabetes. *Current Diabetes Reports* 7 (3): 175-180.
91. Adams, L. A., P. Angulo, and K. D. Lindor. 2005. Nonalcoholic fatty liver disease. In *CMAJ*. 172 (2): 899-905.
92. Vogel, N., Schweitzer, A. 2013. Liver Tumors - Epidemiology, Diagnosis, Prevention and Treatment. *http://dx.doi.org/10.5772/55908*
93. Ertle, J., A. Dechene, J. P. Sowa, V. Penndorf, K. Herzer, G. Kaiser, J. F. Schlaak, G. Gerken, W. K. Syn, and A. Canbay. 2011. Non-alcoholic fatty liver disease progresses to hepatocellular carcinoma in the absence of apparent cirrhosis. *International Journal of Cancer. Journal international du cancer* 128 (10): 2436-2443.
94. Sanyal, A. J., C. Campbell-Sargent, F. Mirshahi, W. B. Rizzo, M. J. Contos, R. K. Sterling, V. A. Luketic, M. L. Shiffman, and J. N. Clore. 2001. Nonalcoholic steatohepatitis: association of insulin resistance and mitochondrial abnormalities. *Gastroenterology* 120 (5): 1183-1192.
95. Fromenty, B., M. A. Robin, A. Igoudjil, A. Mansouri, and D. Pessayre. 2004. The ins and outs of mitochondrial dysfunction in NASH. *Diabetes & Metabolism* 30 (2): 121-138.
96. Neuschwander-Tetri, B. A., and S. H. Caldwell. 2003. Nonalcoholic steatohepatitis: summary of an AASLD Single Topic Conference. In *Hepatology (Baltimore, Md.)*, United States. 37 (5): 1202-1219.

97. Stickel, F., and C. Hellerbrand. 2010. Non-alcoholic fatty liver disease as a risk factor for hepatocellular carcinoma: mechanisms and implications. In *Gut*, England. 59 (10): 1303-1307.
98. Aleffi, S., I. Petrai, C. Bertolani, M. Parola, S. Colombatto, E. Novo, F. Vizzutti, F. A. Anania, S. Milani, K. Rombouts, G. Laffi, M. Pinzani, and F. Marra. 2005. Upregulation of proinflammatory and proangiogenic cytokines by leptin in human hepatic stellate cells. *Hepatology (Baltimore, Md.)* 42 (6): 1339-1348.
99. Calle, E. E., C. Rodriguez, K. Walker-Thurmond, and M. J. Thun. 2003. Overweight, Obesity, and Mortality from Cancer in a Prospectively Studied Cohort of U.S. Adults. *New England J Med* 348 (17): 1625-1638.
100. Motola-Kuba, D., D. Zamora-Valdes, M. Uribe, and N. Mendez-Sanchez. 2006. Hepatocellular carcinoma. An overview. *Annals of Hepatology* 5 (1): 16-24.
101. Wyles, D. L., M. S. Sulkowski, and D. Dieterich. 2016. Management of Hepatitis C/HIV Coinfection in the Era of Highly Effective Hepatitis C Virus Direct-Acting Antiviral Therapy. In *Clin Infect Dis*. 63 (suppl 1): S3-S11.
102. Regimbeau, J. M., M. Colombat, P. Mognol, F. Durand, E. Abdalla, C. Degott, F. Degos, O. Farges, and J. Belghiti. 2004. Obesity and diabetes as a risk factor for hepatocellular carcinoma. *Liver transplantation : official publication of the American Association for the Study of Liver Diseases and the International Liver Transplantation Society* 10 (2): S69-73.
103. Maheshwari, S., A. Sarraj, J. Kramer, and H. B. El-Serag. 2007. Oral contraception and the risk of hepatocellular carcinoma. *Journal of Hepatology* 47 (4): 506-513.
104. Boffetta, P., L. Matisane, K. A. Mundt, and L. D. Dell. 2003. Meta-analysis of studies of occupational exposure to vinyl chloride in relation to cancer mortality. *Scandinavian Journal of work, environment & Health* 29 (3): 220-229.
105. De Benedetti, V. M., J. A. Welsh, M. C. Yu, and W. P. Bennett. 1996. p53 mutations in hepatocellular carcinoma related to oral contraceptive use. *Carcinogenesis* 17 (1): 145-149.
106. Korula, J., A. Yellin, G. Kanel, G. Campofiori, and P. Nichols. 1991. Hepatocellular carcinoma coexisting with hepatic adenoma. Incidental discovery after long-term oral contraceptive use. *West J Med* 155 (4): 416-418.
107. El-Serag, H. B., T. Tran, and J. E. Everhart. 2004. Diabetes increases the risk of chronic liver disease and hepatocellular carcinoma. In *Gastroenterology*, United States. 126 (2): 460-468.
108. Yu, M. W., H. H. Hsieh, W. H. Pan, C. S. Yang, and C. H. CJ. 1995. Vegetable consumption, serum retinol level, and risk of hepatocellular carcinoma. *Cancer research* 55 (6): 1301-1305.
109. Yu, M. W., I. S. Horng, K. H. Hsu, Y. C. Chiang, Y. F. Liaw, and C. J. Chen. 1999. Plasma selenium levels and risk of hepatocellular carcinoma among men with chronic hepatitis virus infection. *American Journal of Epidemiology* 150 (4): 367-374.
110. Bosch, F. X., J. Ribes, R. Cleries, and M. Diaz. 2005. Epidemiology of hepatocellular carcinoma. *Clinics in Liver Disease* 9 (2): 191-211.
111. Delhaye, M., H. Louis, C. Degraef, O. Le Moine, J. Deviere, B. Gulbis, D. Jacobovitz, M. Adler, and P. Galand. 1996. Relationship between hepatocyte proliferative activity and liver functional reserve in human cirrhosis. *Hepatology (Baltimore, Md.)* 23 (5): 1003-1011.

112. Wege, H., and T. H. Brummendorf. 2007. Telomerase activation in liver regeneration and hepatocarcinogenesis: Dr. Jekyll or Mr. Hyde? *Curr Stem Cell Res Ther* 2 (1): 31-38.
113. Wege, H., M. S. Chui, H. T. Le, S. C. Strom, and M. A. Zern. 2003. In vitro expansion of human hepatocytes is restricted by telomere-dependent replicative aging. *Cell Transplantation* 12 (8): 897-906.
114. Wright, W. E., and J. W. Shay. 1992. The two-stage mechanism controlling cellular senescence and immortalization. *Experimental Gerontology* 27 (4): 383-389.
115. Artandi, S. E., S. Chang, S. L. Lee, S. Alson, G. J. Gottlieb, L. Chin, and R. A. DePinho. 2000. Telomere dysfunction promotes non-reciprocal translocations and epithelial cancers in mice. *Nature* 406 (6796): 641-645.
116. Farazi, P. A., J. Glickman, S. Jiang, A. Yu, K. L. Rudolph, and R. A. DePinho. 2003. Differential impact of telomere dysfunction on initiation and progression of hepatocellular carcinoma. *Cancer research* 63 (16): 5021-5027.
117. Van Gijssel, H. E., C. B. Maassen, G. J. Mulder, and J. H. Meerman. 1997. p53 protein expression by hepatocarcinogens in the rat liver and its potential role in mitoinhibition of normal hepatocytes as a mechanism of hepatic tumour promotion. *Carcinogenesis* 18 (5): 1027-1033.
118. Bataller, R., and D. A. Brenner. 2005. Liver fibrosis. *J Clin Invest* 115 (2): 209-218.
119. Giannelli, G., C. Bergamini, E. Fransvea, C. Sgarra, and S. Antonaci. 2005. Laminin-5 with transforming growth factor-beta1 induces epithelial to mesenchymal transition in hepatocellular carcinoma. *Gastroenterology* 129 (5): 1375-1383.
120. Pikarsky, E., R. M. Porat, I. Stein, R. Abramovitch, S. Amit, S. Kasem, E. Gutkovich-Pyest, S. Urieli-Shoval, E. Galun, and Y. Ben-Neriah. 2004. NF-kappaB functions as a tumour promoter in inflammation-associated cancer. *Nature* 431 (7007): 461-466.
121. Ogata, H., T. Kobayashi, T. Chinen, H. Takaki, T. Sanada, Y. Minoda, K. Koga, G. Takaesu, Y. Maehara, M. Iida, and A. Yoshimura. 2006. Deletion of the SOCS3 gene in liver parenchymal cells promotes hepatitis-induced hepatocarcinogenesis. In *Gastroenterology*, United States. 131 (1): 179-193.
122. Wiemann, S. U., A. Satyanarayana, M. Tsahuridu, H. L. Tillmann, L. Zender, J. Klempnauer, P. Flemming, S. Franco, M. A. Blasco, M. P. Manns, and K. L. Rudolph. 2002. Hepatocyte telomere shortening and senescence are general markers of human liver cirrhosis. *FASEB Journal : Official Publication of the Federation of American Societies for Experimental Biology* 16 (9): 935-942.
123. Ito, Y., N. Matsuura, M. Sakon, E. Miyoshi, K. Noda, T. Takeda, K. Umeshita, H. Nagano, S. Nakamori, K. Dono, M. Tsujimoto, M. Nakahara, K. Nakao, N. Taniguchi, and M. Monden. 1999. Expression and prognostic roles of the G1-S modulators in hepatocellular carcinoma: p27 independently predicts the recurrence. *Hepatology (Baltimore, Md.)* 30 (1): 90-99.
124. Plentz, R. R., Y. N. Park, A. Lechel, H. Kim, F. Nellessen, B. H. Langkopf, L. Wilkens, A. Destro, B. Fiamengo, M. P. Manns, M. Roncalli, and K. L. Rudolph. 2007. Telomere shortening and inactivation of cell cycle checkpoints characterize human hepatocarcinogenesis. *Hepatology (Baltimore, Md.)* 45 (4): 968-976.
125. Yamada, T., A. T. De Souza, S. Finkelstein, and R. L. Jirtle. 1997. Loss of the gene encoding mannose 6-phosphate/insulin-like growth factor II receptor is an

early event in liver carcinogenesis. *Proceedings of the National Academy of Sciences of the United States of America* 94 (19): 10351-10355.

126. Dennis, P. A., and D. B. Rifkin. 1991. Cellular activation of latent transforming growth factor beta requires binding to the cation-independent mannose 6-phosphate/insulin-like growth factor type II receptor. *Proceedings of the National Academy of Sciences of the United States of America* 88 (2): 580-584.
127. Iakova, P., S. S. Awad, and N. A. Timchenko. 2003. Aging reduces proliferative capacities of liver by switching pathways of C/EBPalpha growth arrest. *Cell* 113 (4): 495-506.
128. Micsenyi, A., X. Tan, T. Sneddon, J. H. Luo, G. K. Michalopoulos, and S. P. Monga. 2004. Beta-catenin is temporally regulated during normal liver development. *Gastroenterology* 126 (4): 1134-1146.
129. de La Coste, A., B. Romagnolo, P. Billuart, C. A. Renard, M. A. Buendia, O. Soubrane, M. Fabre, J. Chelly, C. Beldjord, A. Kahn, and C. Perret. 1998. Somatic mutations of the beta-catenin gene are frequent in mouse and human hepatocellular carcinomas. *Proceedings of the National Academy of Sciences of the United States of America* 95 (15): 8847-8851.
130. Wong, C. H., and C. Y. Cheng. 2005. Mitogen-activated protein kinases, adherens junction dynamics, and spermatogenesis: a review of recent data. *Developmental Biology* 286 (1): 1-15.
131. Hoshida, Y., B. C. Fuchs, N. Bardeesy, T. F. Baumert, and R. T. Chung. 2014. Pathogenesis and prevention of hepatitis C virus-induced hepatocellular carcinoma. *J Hepatol* 61 (1): S79-90.
132. Baba, M., R. Yamamoto, H. Iishi, and M. Tatsuta. 1997. Ha-ras mutations in N-nitrosomorpholine-induced lesions and inhibition of hepatocarcinogenesis by antisense sequences in rat liver. *International journal of cancer. Journal international du cancer* 72 (5): 815-820.
133. Calvisi, D. F., S. Ladu, A. Gorden, M. Farina, E. A. Conner, J. S. Lee, V. M. Factor, and S. S. Thorgeirsson. 2006. Ubiquitous activation of Ras and Jak/Stat pathways in human HCC. *Gastroenterology* 130 (4): 1117-1128.
134. Hu, T. H., C. C. Huang, P. R. Lin, H. W. Chang, L. P. Ger, Y. W. Lin, C. S. Changchien, C. M. Lee, and M. H. Tai. 2003. Expression and prognostic role of tumor suppressor gene PTEN/MMAC1/TEP1 in hepatocellular carcinoma. *Cancer* 97 (8): 1929-1940.
135. Yoshiji, H., R. Noguchi, S. Kuriyama, J. Yoshii, Y. Ikenaka, K. Yanase, T. Namisaki, M. Kitade, M. Yamazaki, M. Uemura, and H. Fukui. 2005. Different cascades in the signaling pathway of two vascular endothelial growth factor (VEGF) receptors for the VEGF-mediated murine hepatocellular carcinoma development. *Oncology Reports* 13 (5): 853-857.
136. Karin, M. 2006. Nuclear factor-kappaB in cancer development and progression. *Nature* 441 (7092): 431-436.
137. Stanger, B. Z., A. J. Tanaka, and D. A. Melton. 2007. Organ size is limited by the number of embryonic progenitor cells in the pancreas but not the liver. In *Nature*, England. 445 (7130): 886-891.
138. Marra, M., I. M. Sordelli, A. Lombardi, M. Lamberti, L. Tarantino, A. Giudice, P. Stiuso, A. Abbruzzese, R. Sperlongano, M. Accardo, M. Agresti, M. Caraglia, and P. Sperlongano. 2011. Molecular targets and oxidative stress biomarkers in hepatocellular carcinoma: an overview. *J Transl Med* 9: 171.

139. Warrington, R., W. Watson, H. L. Kim, and F. R. Antonetti. 2011. An introduction to immunology and immunopathology. *Allergy, Asthma & Clinical Immunology* 7 (1): S1.
140. Chaplin, D. D. 2010. Overview of the Immune Response. *J Allergy Clin Immunol* 125 (2): S3-23.
141. Adam, J. K., B. Odhav, and K. D. Bhoola. 2003. Immune responses in cancer. In *Pharmacol Ther*, England. 99 (1): 113-132.
142. Schreiber, R. D., L. J. Old, and M. J. Smyth. 2011. Cancer immunoediting: integrating immunity's roles in cancer suppression and promotion. *Science (New York, N.Y.)* 331 (6024): 1565-1570.
143. Old, L. J., and Y. T. Chen. 1998. New paths in human cancer serology. *The Journal of experimental medicine* 187 (8): 1163-1167.
144. Dai, L., N. Lei, M. Liu, and J. Y. Zhang. 2013. Autoantibodies to tumor-associated antigens as biomarkers in human hepatocellular carcinoma (HCC). *Experimental hematology & oncology* 2 (1): 15.
145. Michalak, M., E. F. Corbett, N. Mesaeli, K. Nakamura, and M. Opas. 1999. Calreticulin: one protein, one gene, many functions. *Biochem J* 344 (2): 281-292.
146. Chignard, N., S. Shang, H. Wang, J. Marrero, C. Brechot, S. Hanash, and L. Beretta. 2006. Cleavage of endoplasmic reticulum proteins in hepatocellular carcinoma: Detection of generated fragments in patient sera. *Gastroenterology* 130(7): 2010-2022.
147. Pekáriková, A., D. Sánchez, L. Palová-Jelínková, M. Šimšová, Z. Beneš, I. Hoffmanová, P. Drastich, I. Janatková, T. Mothes, H. Tlaskalová-Hogenová, and L. Tučková. 2010. Calreticulin is a B cell molecular target in some gastrointestinal malignancies. *Clinical and Experimental Immunology* 160 (2): 215-222.
148. Le Naour, F., F. Brichory, D. E. Misek, C. Brechot, S. M. Hanash, and L. Beretta. 2002. A distinct repertoire of autoantibodies in hepatocellular carcinoma identified by proteomic analysis. *Mol Cell Proteomics* 1 (3): 197-203.
149. Manjasetty, B. A., 2017. X-ray structure of human gankyrin, the product of a gene linked to hepatocellular carcinoma. *Proteins: Structure, Function, and Bioinformatics* 55 (1): 214-217.
150. Fu, X. Y., H. Y. Wang, L. Tan, S. Q. Liu, H. F. Cao, and M. C. Wu. 2002. Overexpression of p28/gankyrin in human hepatocellular carcinoma and its clinical significance. *World Journal of Gastroenterology : WJG* 8 (4): 638-643.
151. Higashitsuji, H., K. Itoh, T. Sakurai, T. Nagao, Y. Sumitomo, T. Masuda, S. Dawson, Y. Shimada, R. J. Mayer, and J. Fujita. 2005. The oncoprotein gankyrin binds to MDM2/HDM2, enhancing ubiquitylation and degradation of p53. *Cancer Cell* 8 (1): 75-87.
152. Feig, L. A. 2003. Ral-GTPases: approaching their 15 minutes of fame. *Trends Cell Biol* 13 (8): 419-425.
153. Smith, S. C., G. Oxford, A. S. Baras, C. Owens, D. Havaleshko, D. L. Brautigan, M. K. Safo, and D. Theodorescu. 2007. Expression of ral GTPases, their effectors, and activators in human bladder cancer. *Clinical Cancer Research : an Official Journal of the American Association for Cancer Research* 13 (13): 3803-3813.
154. Lim, K. H., A. T. Baines, J. J. Fiordalisi, M. Shipitsin, L. A. Feig, A. D. Cox, C. J. Der, and C. M. Counter. 2005. Activation of RalA is critical for Ras-

induced tumorigenesis of human cells. In *Cancer Cell*, United States. 7 (6): 533-545.

155. Nakamura, H., H. Kambe, T. Egawa, Y. Kimura, H. Ito, E. Hayashi, H. Yamamoto, J. Sato, and S. Kishimoto. 1989. Partial purification and characterization of human hepatoma-derived growth factor. *Clinica Chimica acta; International Journal of Clinical Chemistry* 183 (3): 273-284.
156. Enomoto, H., K. Yoshida, Y. Kishima, T. Kinoshita, M. Yamamoto, A. D. Everett, A. Miyajima, and H. Nakamura. 2002. Hepatoma-derived growth factor is highly expressed in developing liver and promotes fetal hepatocyte proliferation. *Hepatology (Baltimore, Md.)* 36 (6): 1519-1527.
157. Ren, H., X. Tang, J. J. Lee, L. Feng, A. D. Everett, W. K. Hong, F. R. Khuri, and L. Mao. 2004. Expression of hepatoma-derived growth factor is a strong prognostic predictor for patients with early-stage non-small-cell lung cancer. *Journal of Clinical Oncology : Official journal of the American Society of Clinical Oncology* 22 (16): 3230-3237.
158. Bernard, K., E. Litman, J. L. Fitzpatrick, Y. G. Shellman, G. Argast, K. Polvinen, A. D. Everett, K. Fukasawa, D. A. Norris, N. G. Ahn, and K. A. Resing. 2003. Functional proteomic analysis of melanoma progression. *Cancer Research* 63 (20): 6716-6725.
159. Little, E., M. Ramakrishnan, B. Roy, G. Gazit, and A. S. Lee. 1994. The glucose-regulated proteins (GRP78 and GRP94): functions, gene regulation, and applications. *Critical Reviews in Eukaryotic Gene Expression* 4 (1): 1-18.
160. Dudek, J., J. Benedix, S. Cappel, M. Greiner, C. Jalal, L. Muller, and R. Zimmermann. 2009. Functions and pathologies of BiP and its interaction partners. *Cellular and Molecular Life Sciences : CMLS* 66 (9): 1556-1569.
161. Gonzalez-Gronow, M., M. A. Selim, J. Papalas, and S. V. Pizzo. 2009. GRP78: a multifunctional receptor on the cell surface. *Antioxidants & Redox Signaling* 11 (9): 2299-2306.
162. Luk, J. M., C. T. Lam, A. F. Siu, B. Y. Lam, I. O. Ng, M. Y. Hu, C. M. Che, and S. T. Fan. 2006. Proteomic profiling of hepatocellular carcinoma in Chinese cohort reveals heat-shock proteins (Hsp27, Hsp70, GRP78) up-regulation and their associated prognostic values. *Proteomics* 6 (3): 1049-1057.
163. Arnaudeau, S., P. Arboit, P. Bischof, M. K. Shin-ya, O. Irion, M. M. Cohen, M. 2017. Glucose-regulated protein 78: A new partner of p53 in trophoblast. *Proteomics* 9 (23): 5316-5327.
164. Taylor, D. D., C. Gercel-Taylor, and L. P. Parker. 2009. Patient-derived tumor-reactive antibodies as diagnostic markers for ovarian cancer. *Gynecologic Oncology* 115 (1): 112-120.
165. Al-Hashimi, A. A., J. Caldwell, M. Gonzalez-Gronow, S. V. Pizzo, D. Aboumrad, L. Pozza, H. Al-Bayati, J. I. Weitz, A. Stafford, H. Chan, A. Kapoor, D. W. Jacobsen, J. G. Dickhout, and R. C. Austin. 2010. Binding of Anti-GRP78 Autoantibodies to Cell Surface GRP78 Increases Tissue Factor Procoagulant Activity via the Release of Calcium from Endoplasmic Reticulum Stores. In *The Journal of Biological Chemistry*. 285 (37): 28912-28923.
166. Tsunemi, S., T. Nakanishi, Y. Fujita, G. Bouras, Y. Miyamoto, A. Miyamoto, E. Nomura, T. Takubo, and N. Tanigawa. 2010. Proteomics-based identification of a tumor-associated antigen and its corresponding autoantibody in gastric cancer. *Oncology Reports* 23 (4): 949-956.
167. Shao, Q., P. Ren, Y. Li, B. Peng, L. Dai, N. Lei, W. Yao, G. Zhao, L. Li, and J. Zhang. 2012. Autoantibodies against glucose-regulated protein 78 as

serological diagnostic biomarkers in hepatocellular carcinoma. In *Int J Oncol*. 41 (3): 1061-1067.
168. Hoffman, B., and D. A. Liebermann. 2008. Apoptotic signaling by c-MYC. *Oncogene* 27 (50): 6462-6472.
169. Zhang, J. Y., E. K. Chan, X. X. Peng, and E. M. Tan. 1999. A novel cytoplasmic protein with RNA-binding motifs is an autoantigen in human hepatocellular carcinoma. *The Journal of Experimental Medicine* 189 (7): 1101-1110.
170. Sideras, K., S. J. Bots, K. Biermann, D. Sprengers, W. G. Polak, I. J. JNM, R. A. de Man, Q. Pan, S. Sleijfer, M. J. Bruno, and J. Kwekkeboom. 2015. Tumour antigen expression in hepatocellular carcinoma in a low-endemic western area. In *Br J Cancer*. 112 (12): 1911-1920.
171. Zeng, J.-Z., Y. Liu, F. Huang, Z.-H. He, H. Sun, Y.-D. Lu, J.-H. Lei, and R.-C. Luo. 2017. Glypican-3-specific cytotoxic T lymphocytes induced by human leucocyte antigen-A*0201-restricted peptide effectively kill hepatocellular carcinoma cells in vitro. *Asian Pacific Journal of Tropical Medicine* 10 (11): 1084-1089.
172. Chevaleyre, C., N. Benhamouda, E. Favry, E. Fabre, A. Mhoumadi, H. Nozach, E. Marcon, G. Cosler, E. Vinatier, S. Oudard, S. Hans, F. Le Pimpec-Barthes, A. S. Bats, F. A. Castelli, E. Tartour, and B. Maillere. 2015. The Tumor Antigen Cyclin B1 Hosts Multiple CD4 T Cell Epitopes Differently Recognized by Pre-Existing Naive and Memory Cells in Both Healthy and Cancer Donors. *J Immunol* 195 (4): 1891-1901.
173. Choi, W. T., and S. Kakar. 2017. Immunohistochemistry in the Diagnosis of Hepatocellular Carcinoma. *Gastroenterol Clin North Am* 46 (2): 311-325.
174. Kim, K. M., S.-H. Park, J. S. Bae, S. J. Noh, G.-Z. Tao, J. R. Kim, K. S. Kwon, H. S. Park, B.-H. Park, H. Lee, M. J. Chung, W. S. Moon, K. G. Sylvester, and K. Y. Jang. 2017. FAM83H is involved in the progression of hepatocellular carcinoma and is regulated by MYC. *Scientific Reports* 7 (1): 3274.
175. Ahsani, Z., S. Mohammadi-Yeganeh, V. Kia, H. Karimkhanloo, N. Zarghami, and M. Paryan. 2017. WNT1 Gene from WNT Signaling Pathway Is a Direct Target of miR-122 in Hepatocellular Carcinoma. *Appl Biochem Biotechnol* 181 (3): 884-897.
176. Sun, C., L. Sun, Y. Li, X. Kang, S. Zhang, and Y. Liu. 2013. Sox2 expression predicts poor survival of hepatocellular carcinoma patients and it promotes liver cancer cell invasion by activating Slug. *Med Oncol* 30 (2): 503.
177. Lane, D. P. 1992. P53, guardian of the genome. *Nature* 358 (6381): 15-16.
178. Gadducci, A., M. Ferdeghini, F. Buttitta, S. Cosio, A. Fanucchi, C. Annicchiarico, O. Gagetti, G. Bevilacqua, and A. R. Genazzani. 1999. Assessment of the prognostic relevance of serum anti-p53 antibodies in epithelial ovarian cancer. *Gynecologic Oncology* 72 (1): 76-81.
179. Jongeneel, V. 2001. Towards a cancer immunome database. In *Cancer Immun*, United States. 3:1.
180. Benchimol, S., D. Pim, and L. Crawford. 1982. Radioimmunoassay of the cellular protein p53 in mouse and human cell lines. *The EMBO Journal* 1 (9): 1055-1062.
181. Abendstein, B., C. Marth, E. Muller-Holzner, M. Widschwendter, G. Daxenbichler, and A. G. Zeimet. 2000. Clinical significance of serum and ascitic p53 autoantibodies in epithelial ovarian carcinoma. *Cancer* 88 (6): 1432-1437.

182. Soussi, T. 2000. p53 Antibodies in the sera of patients with various types of cancer: a review. *Cancer Research* 60 (7): 1777-1788.
183. Houbiers, J. G., S. H. van der Burg, L. M. van de Watering, R. A. Tollenaar, A. Brand, C. J. van de Velde, and C. J. Melief. 1995. Antibodies against p53 are associated with poor prognosis of colorectal cancer. *British Journal of Cancer* 72 (3): 637-641.
184. Sui, G., X. Ma, S. Liu, H. Niu, and Q. Dong. 2012. Study of the correlation between H-ras mutation and primary hepatocellular carcinoma. *Oncology letters* 4 (4): 779-782.
185. Bos, J. L. 1989. ras oncogenes in human cancer: a review. *Cancer Research* 49 (17): 4682-4689.
186. Campbell, S. L., R. Khosravi-Far, K. L. Rossman, G. J. Clark, and C. J. Der. 1998. Increasing complexity of Ras signaling. *Oncogene* 17 (1): 1395-1413.
187. Singh, A., and J. Settleman. 2009. Oncogenic K-ras "addiction" and synthetic lethality. In *Cell cycle (Georgetown, Tex.)*, United States. 8 (17): 2676-2677.
188. Schubbert, S., K. Shannon, and G. Bollag. 2007. Hyperactive Ras in developmental disorders and cancer. *Nature Reviews. Cancer* 7 (4): 295-308.
189. Serrano, M. 1997. The tumor suppressor protein p16INK4a. *Experimental Cell Research* 237 (1): 7-13.
190. Sherr, C. J. 2001. The INK4a/ARF network in tumour suppression. *Nature Reviews. Molecular Cell Biology* 2 (10): 731-737.
191. Tsuchiya, T., L. Wang, A. Yafune, M. Kimura, T. Ohishi, K. Suzuki, K. Mitsumori, and M. Shibutani. 2012. Disruptive cell cycle regulation involving epigenetic downregulation of Cdkn2a (p16(Ink4a)) in early-stage liver tumor-promotion facilitating liver cell regeneration in rats. *Toxicology* 299 (2-3): 146-154.
192. Fischer, C. A., M. Kampmann, I. Zlobec, E. Green, L. Tornillo, A. Lugli, M. Wolfensberger, and L. M. Terracciano. 2010. p16 expression in oropharyngeal cancer: its impact on staging and prognosis compared with the conventional clinical staging parameters. *Annals of Oncology : Official Journal of the European Society for Medical Oncology* 21 (10): 1961-1966.
193. Dominguez, G., J. Silva, J. M. Garcia, J. M. Silva, R. Rodriguez, C. Munoz, I. Chacon, R. Sanchez, J. Carballido, A. Colas, P. Espana, and F. Bonilla. 2003. Prevalence of aberrant methylation of p14ARF over p16INK4a in some human primary tumors. *Mutation Research* 530 (1-2): 9-17.
194. Ikuerowo, S. O., M. A. Kuczyk, R. von Wasielewski, O. B. Shittu, U. Jonas, S. Machtens, and J. Serth. 2007. p16INK4a expression and clinicopathologic parameters in renal cell carcinoma. *European Urology* 51 (3): 732-737.
195. Valenzuela, M. T., R. Galisteo, A. Zuluaga, M. Villalobos, M. I. Nunez, F. J. Oliver, and J. M. Ruiz de Almodovar. 2002. Assessing the use of p16(INK4a) promoter gene methylation in serum for detection of bladder cancer. *European Urology* 42 (2002): 622-628.
196. Lambert, A. P., F. Anschau, and V. M. Schmitt. 2006. p16INK4A expression in cervical premalignant and malignant lesions. *Experimental and Molecular Pathology* 80 (2): 192-196.
197. Suh, S. I., H. Y. Pyun, J. W. Cho, W. K. Baek, J. B. Park, T. Kwon, J. W. Park, M. H. Suh, and D. A. Carson. 2000. 5-Aza-2'-deoxycytidine leads to down-regulation of aberrant p16INK4A RNA transcripts and restores the functional retinoblastoma protein pathway in hepatocellular carcinoma cell lines. *Cancer Letters* 160 (1): 81-88.

198. Tien, L. T., M. Ito, M. Nakao, D. Niino, M. Serik, M. Nakashima, C. Y. Wen, H. Yatsuhashi, and H. Ishibashi. 2005. Expression of beta-catenin in hepatocellular carcinoma. *World Journal of Gastroenterology* 11 (16): 2398-2401.
199. Wang, X., X. Meng, X. Sun, M. Liu, S. Gao, J. Zhao, F. Pei, and H. Yu. 2009. Wnt/beta-catenin signaling pathway may regulate cell cycle and expression of cyclin A and cyclin E protein in hepatocellular carcinoma cells. *Cell cycle (Georgetown, Tex.)* 8 (10): 1567-1570.
200. Ambrosini, G., C. Adida, and D. C. Altieri. 1997. A novel anti-apoptosis gene, survivin, expressed in cancer and lymphoma. *Nature Medicine* 3 (8): 917-921.
201. Islam, A., H. Kageyama, N. Takada, T. Kawamoto, H. Takayasu, E. Isogai, M. Ohira, K. Hashizume, H. Kobayashi, Y. Kaneko, and A. Nakagawara. 2000. High expression of Survivin, mapped to 17q25, is significantly associated with poor prognostic factors and promotes cell survival in human neuroblastoma. *Oncogene* 19 (5): 617-623.
202. Stockert, E., E. Jäger, Y. T. Chen, M. J. Scanlan, I. Gout, J. Karbach, M. Arand, A. Knuth, and L. J. Old. 1998. A Survey of the Humoral Immune Response of Cancer Patients to a Panel of Human Tumor Antigens. *The Journal of Experimental Medicine* 187 (8): 1349-1354.
203. Bird, T. G., P. Dimitropoulou, R. M. Turner, S. J. Jenks, P. Cusack, S. Hey, A. Blunsum, S. Kelly, C. Sturgeon, P. C. Hayes, and S. M. Bird. 2016. Alpha-Fetoprotein Detection of Hepatocellular Carcinoma Leads to a Standardized Analysis of Dynamic AFP to Improve Screening Based Detection. *PLoS One* 11 (6): e0156801.
204. Huang, G., Z. Zhou, H. Wang, and E. S. Kleinerman. 2012. CAPER-alpha alternative splicing regulates the expression of vascular endothelial growth factor(1)(6)(5) in Ewing sarcoma cells. *Cancer* 118 (8): 2106-2116.
205. Dutta, J., G. Fan, and C. Gelinas. 2008. CAPERalpha is a novel Rel-TAD-interacting factor that inhibits lymphocyte transformation by the potent Rel/NF-kappaB oncoprotein v-Rel. *Journal of Virology* 82 (21): 10792-10802.
206. Kondo, F., K. Wada, Y. Nagato, T. Nakajima, Y. Kondo, N. Hirooka, M. Ebara, M. Ohto, and K. Okuda. 1989. Biopsy diagnosis of well-differentiated hepatocellular carcinoma based on new morphologic criteria. In *Hepatology (Baltimore, Md.)*, United States. 9 (15): 751-755.
207. Doyle, G. A., N. A. Betz, P. F. Leeds, A. J. Fleisig, R. D. Prokipcak, and J. Ross. 1998. The c-myc coding region determinant-binding protein: a member of a family of KH domain RNA-binding proteins. In *Nucleic Acids Res*, England. 26 (22): 5036-5044.
208. Soo Hoo, L., J. Y. Zhang, and E. K. Chan. 2002. Cloning and characterization of a novel 90 kDa 'companion' auto-antigen of p62 overexpressed in cancer. *Oncogene* 21 (32): 5006-5015.
209. Shi, Y. Y., H. C. Wang, Y. H. Yin, W. S. Sun, Y. Li, C. Q. Zhang, Y. Wang, S. Wang, and W. F. Chen. 2005. Identification and analysis of tumour-associated antigens in hepatocellular carcinoma. *British Journal of Cancer* 92 (5): 929-934.
210. Negahdary, M., A. Eftekhari, S. Mirzaei, M. Basirizadeh, and S. Ghobadzadeh. 2015. Tumor Markers and Hepatocellular Carcinoma. *Lexis Publishing Corporation* 4 (2): 124-131.
211. Kudo, M. 2018. Immuno-Oncology in Hepatocellular Carcinoma: 2017 Update. *Oncology* 93 (1): 147-159.

212. Nishida, N., and M. Kudo. 2017. Immunological Microenvironment of Hepatocellular Carcinoma and Its Clinical Implication. *Oncology* 92 (Suppl)1: 40-49.
213. Thompson, E. D., H. L. Enriquez, Y. X. Fu, and V. H. Engelhard. 2010. Tumor masses support naive T cell infiltration, activation, and differentiation into effectors. *The Journal of Experimental Medicine* 207 (8): 1791-1804.
214. Zanetti, M. 2015. Tapping CD4 T cells for cancer immunotherapy: the choice of personalized genomics. *J Immunol* 194 (5): 2049-2056.
215. Ninomiya, T., S. M. Akbar, T. Masumoto, N. Horiike, and M. Onji. 1999. Dendritic cells with immature phenotype and defective function in the peripheral blood from patients with hepatocellular carcinoma. *Journal of Hepatology* 31 (2): 323-331.
216. Matsui, M., S. Machida, T. Itani-Yohda, and T. Akatsuka. 2002. Downregulation of the proteasome subunits, transporter, and antigen presentation in hepatocellular carcinoma, and their restoration by interferon-gamma. *Journal of Gastroenterology and Hepatology* 17 (18): 897-907.
217. Han, Y., Z. Chen, Y. Yang, Z. Jiang, Y. Gu, Y. Liu, C. Lin, Z. Pan, Y. Yu, M. Jiang, W. Zhou, and X. Cao. 2014. Human CD14+ CTLA-4+ regulatory dendritic cells suppress T-cell response by cytotoxic T-lymphocyte antigen-4-dependent IL-10 and indoleamine-2,3-dioxygenase production in hepatocellular carcinoma. *Hepatology (Baltimore, Md.)* 59 (2): 567-579.
218. Kuang, D. M., Q. Zhao, Y. Wu, C. Peng, J. Wang, Z. Xu, X. Y. Yin, and L. Zheng. 2011. Peritumoral neutrophils link inflammatory response to disease progression by fostering angiogenesis in hepatocellular carcinoma. *Journal of Hepatology* 54 (5): 948-955.
219. Subleski, J. J., R. H. Wiltrout, and J. M. Weiss. 2009. Application of tissue-specific NK and NKT cell activity for tumor immunotherapy. *Journal of Autoimmunity* 33 (3-4): 275-281.
220. Tian, Z., Y. Chen, and B. Gao. 2013. Natural Killer Cells in Liver Disease. *Hepatology (Baltimore, Md.)* 57 (4): 1654-1662.
221. Gao, B., S. Radaeva, and O. Park. 2009. Liver natural killer and natural killer T cells: immunobiology and emerging roles in liver diseases. *Journal of Leukocyte Biology* 86 (3): 513-528.
222. Berzofsky, J. A., and M. Terabe. 2009. The contrasting roles of NKT cells in tumor immunity. *Current Molecular Medicine* 9 (6): 667-672.
223. Ormandy, L. A., T. Hillemann, H. Wedemeyer, M. P. Manns, T. F. Greten, and F. Korangy. 2005. Increased populations of regulatory T cells in peripheral blood of patients with hepatocellular carcinoma. *Cancer Res* 65 (6): 2457-2464.
224. Ghiringhelli, F., C. Menard, F. Martin, and L. Zitvogel. 2006. The role of regulatory T cells in the control of natural killer cells: relevance during tumor progression. *Immunological Reviews* 214: 229-238.
225. Zhang, J. Y., K. S. Looi, and E. M. Tan. 2009. Identification of tumor-associated antigens as diagnostic and predictive biomarkers in cancer. *Methods in Molecular Biology (Clifton, N.J.)* 520: 1-10.
226. Ikeguchi, M., and Y. Hirooka. 2005. Interleukin-2 gene expression is a new biological prognostic marker in hepatocellular carcinomas. *Onkologie* 28 (5): 255-259.
227. Akiba, J., H. Yano, S. Ogasawara, K. Higaki, and M. Kojiro. 2001. Expression and function of interleukin-8 in human hepatocellular carcinoma. *Int J Oncol* 18 (2): 257-264.

228. Wolk, K., E. Witte, K. Witte, K. Warszawska, and R. Sabat. 2010. Biology of interleukin-22. *Seminars in Immunopathology* 32 (1): 17-31.
229. Wong, R., and D. A. Corley. 2008. Racial and ethnic variations in hepatocellular carcinoma incidence within the United States. *The American Journal of Medicine* 121 (6): 525-531.
230. Tsou, P., H. Katayama, E. J. Ostrin, and S. M. Hanash. 2016. The Emerging Role of B Cells in Tumor Immunity. *Cancer Res* 76 (19): 5597-5601.
231. Yuen, G. J., E. Demissie, and S. Pillai. 2016. B lymphocytes and cancer: a love-hate relationship. *Trends Cancer* 2 (12): 747-757.
232. Tsou, P., H. Katayama, E. J. Ostrin, and S. M. Hanash. 2016. The Emerging Role of B Cells in Tumor Immunity.*Cancer Res* 76 (19): 5596-5601.
233. Garnelo, M., A. Tan, Z. Her, J. Yeong, C. J. Lim, J. Chen, K. H. Lim, A. Weber, P. Chow, A. Chung, L. L. P. Ooi, H. C. Toh, M. Heikenwalder, I. O. L. Ng, A. Nardin, Q. Chen, J. P. Abastado, and V. Chew. 2017. Interaction between tumour-infiltrating B cells and T cells controls the progression of hepatocellular carcinoma. In *Gut*. 66 (2): 342-351.
234. Korangy, F., B. Hochst, M. P. Manns, and T. F. Greten. 2010. Immune responses in hepatocellular carcinoma. 2010 S. Karger AG, Basel., Switzerland. In *Dig Dis*. 28 (1): 150-154.
235. Schmidt, N., C. Neumann-Haefelin, and R. Thimme. 2015. Cellular Immune Responses to Hepatocellular Carcinoma: Lessons for Immunotherapy. *Digestive Diseases* 30 (5): 483-491.
236. Tatsumi, T., T. Takehara, K. Katayama, K. Mochizuki, M. Yamamoto, T. Kanto, Y. Sasaki, A. Kasahara, and N. Hayashi. 1997. Expression of costimulatory molecules B7-1 (CD80) and B7-2 (CD86) on human hepatocellular carcinoma. In *Hepatology (Baltimore, Md.)*, United States. 25 (5): 1108-1114.
237. Shi, F., M. Shi, Z. Zeng, R. Z. Qi, Z. W. Liu, J. Y. Zhang, Y. P. Yang, P. Tien, and F. S. Wang. 2011. PD-1 and PD-L1 upregulation promotes CD8(+) T-cell apoptosis and postoperative recurrence in hepatocellular carcinoma patients. *International Journal of Cancer. Journal International Du Cancer* 128 (4): 887-896.
238. Chen, S., L. F. Lee, T. S. Fisher, B. Jessen, M. Elliott, W. Evering, K. Logronio, G. H. Tu, K. Tsaparikos, X. Li, H. Wang, C. Ying, M. Xiong, T. VanArsdale, and J. C. Lin. 2015. Combination of 4-1BB agonist and PD-1 antagonist promotes antitumor effector/memory CD8 T cells in a poorly immunogenic tumor model. In *Cancer Immunol Res*. United States. 3 (2): 149-160.
239. Zhang, J. Y., and E. M. Tan. 2010. Autoantibodies to tumor-associated antigens as diagnostic biomarkers in hepatocellular carcinoma and other solid tumors. *Expert Rev Mol Diagn* 10 (3): 321-328.
240. Jeong Min Lee, J.-H. Y., Kyung Won Kim. 2012. Diagnosis of Hepatocellular Carcinoma: *Newer Radiological Tools.* 39 (4): 399–409.
241. Middleton, C. H., W. Irving, J. F. Robertson, A. Murray, C. B. Parsy-Kowalska, I. K. Macdonald, J. McElveen, J. Allen, G. F. Healey, B. J. Thomson, S. J. Ryder, S. Holdenrieder, and C. J. Chapman. 2014. Serum autoantibody measurement for the detection of hepatocellular carcinoma. *PloS one* 9 (8): e103867.
242. Casiano, C. A., M. Mediavilla-Varela, and E. M. Tan. 2006. Tumor-associated Antigen Arrays for the Serological Diagnosis of Cancer*. *Mol Cell Proteomics* 5 (10): 1745-1759.

243. Faltermeier, C., R. Busuttil, and A. Zarrinpar. 2015. A Surgical Perspective on Targeted Therapy of Hepatocellular Carcinoma. *Diseases* 3 (4): 221-252.
244. Blumberg, B. S. 1997. Hepatitis B virus, the vaccine, and the control of primary cancer of the liver. *Proc Natl Acad Sci USA* 94 (14): 7121-7125.
245. Zhang, J. Y., W. Zhu, H. Imai, K. Kiyosawa, E. K. Chan, and E. M. Tan. 2001. De-novo humoral immune responses to cancer-associated autoantigens during transition from chronic liver disease to hepatocellular carcinoma. *Clinical and Experimental Immunology* 125 (1): 3-9.
246. Qian, Y., C. Liu, J. Hartupee, C. Z. Altuntas, M. F. Gulen, D. Jane-Wit, J. Xiao, Y. Lu, N. Giltiay, J. Liu, T. Kordula, Q. W. Zhang, B. Vallance, S. Swaidani, M. Aronica, V. K. Tuohy, T. Hamilton, and X. Li. 2007. The adaptor Act1 is required for interleukin 17-dependent signaling associated with autoimmune and inflammatory disease. *Nature Immunology* 8 (3): 247-256.
247. Werner, S., H. Chen, S. Tao, and H. Brenner. 2015. Systematic review: serum autoantibodies in the early detection of gastric cancer. *Int J Cancer* 136 (10): 2243-2252.
248. Imai, H., E. K. Chan, K. Kiyosawa, X. D. Fu, and E. M. Tan. 1993. Novel nuclear autoantigen with splicing factor motifs identified with antibody from hepatocellular carcinoma. *J Clin Invest* 92 (5): 2419-2426.
249. Dai, L., J.-C. J. Tsay, J. Li, T.-A. Yie, J. S. Munger, H. Pass, W. N. Rom, Y. Zhang, E. M. Tan, and J.-Y. Zhang. 2016. Autoantibodies against tumor-associated antigens in the early detection of lung cancer. *Lung Cancer* 99: 172-179.
250. Bassaro, L., S. J. Russell, E. Pastwa, S. A. Somiari, and R. I. Somiari. 2017. Screening for Multiple Autoantibodies in Plasma of Patients with Breast Cancer. *Cancer Genomics Proteomics* 14 (6): 427-435.
251. Dumstrei, K., H. Chen, and H. Brenner. 2016. A systematic review of serum autoantibodies as biomarkers for pancreatic cancer detection. In *Oncotarget* 7 (10): 11151-11164.
252. Negm, O. H., M. R. Hamed, R. E. Schoen, R. L. Whelan, R. J. Steele, J. Scholefield, E. M. Dilnot, H. M. Shantha Kumara, J. F. Robertson, and H. F. Sewell. 2016. Human Blood Autoantibodies in the Detection of Colorectal Cancer. *PLoS One* 11 (7): e0156971.
253. Zayakin, P., G. Ancans, K. Silina, I. Meistere, Z. Kalnina, D. Andrejeva, E. Endzelins, L. Ivanova, A. Pismennaja, A. Ruskule, S. Donina, T. Wex, P. Malfertheiner, M. Leja, and A. Line. 2013. Tumor-associated autoantibody signature for the early detection of gastric cancer. *Int J Cancer* 132 (1): 137-147.
254. Anderson, K. S., D. W. Cramer, S. Sibani, G. Wallstrom, J. Wong, J. Park, J. Qiu, A. Vitonis, and J. LaBaer. 2015. Autoantibody signature for the serologic detection of ovarian cancer. *J Proteome Res* 14 (1): 578-586.
255. Schlick, B., P. Massoner, A. Lueking, P. Charoentong, M. Blattner, G. Schaefer, K. Marquart, C. Theek, P. Amersdorfer, D. Zielinski, M. Kirchner, Z. Trajanoski, M. A. Rubin, S. Müllner, P. Schulz-Knappe, and H. Klocker. 2016. Serum Autoantibodies in Chronic Prostate Inflammation in Prostate Cancer Patients. In *PLoS One* 11 (2): e0117739.
256. Tan, E. M., and J. Zhang. 2008. Autoantibodies to tumor-associated antigens: reporters from the immune system. In *Immunological Reviews*, Denmark 222: 328-340.

257. Pan, X., Y. Gao, J. Liu, C. Liu, and Y. Xia. 2016. Progress in studies on autoantibodies against tumor-associatd antigens in hepatocellular carcinoma. *Transl Cancer* 5 (6): 845-859.
258. Yau, W. Y., H. C. Shih, M. H. Tsai, J. C. Sheu, C. H. Chen, and L. P. Chow. 2013. Autoantibody recognition of an N-terminal epitope of hnRNP L marks the risk for developing HBV-related hepatocellular carcinoma. *J Proteomics* 94: 346-358.
259. Hong, Y., J. Long, H. Li, S. Chen, Q. Liu, B. Zhang, X. He, Y. Wang, Y. Li, T. Zhang, C. Lu, H. Yan, M. Zhang, Q. Li, B. Cao, Z. Bai, J. Wang, Z. Zhang, S. Zhu, J. Zheng, X. Ou, H. Ma, J. Jia, H. You, S. Wang, and J. Huang. 2015. An Analysis of Immunoreactive Signatures in Early Stage hepatocellular Carcinoma. *EBioMedicine* 2 (5): 438-446.
260. Hong, Y., and J. Huang. 2015. Autoantibodies against tumor-associated antigens for detection of hepatocellular carcinoma. *World J Hepatol* 7 (11): 1581-1585.
261. Lu, H., V. Goodell, and M. L. Disis. 2008. Humoral immunity directed against tumor-associated antigens as potential biomarkers for the early diagnosis of cancer. *J Proteome Res* 7 (4): 1388-1394.
262. Zaenker, P., and M. R. Ziman. 2013. Serologic autoantibodies as diagnostic cancer biomarkers--a review. *Cancer Epidemiol Biomarkers Prev* 22 (12): 2161-2181.
263. Tan, H. T., J. Low, S. G. Lim, and M. C. Chung. 2009. Serum autoantibodies as biomarkers for early cancer detection. In *FEBS J*, England. 276 (23): 6880-6904.
264. Zaenker, P., E. S. Gray, and M. R. Ziman. 2016. Autoantibody Production in Cancer--The Humoral Immune Response toward Autologous Antigens in Cancer Patients. *Autoimmun Rev* 15 (5): 477-483.
265. Zhang, J. Y., C. A. Casiano, X. X. Peng, J. A. Koziol, E. K. Chan, and E. M. Tan. 2003. Enhancement of antibody detection in cancer using panel of recombinant tumor-associated antigens. *Cancer Epidemiology, Biomarkers & Prevention : A publication of the American Association for Cancer Research, cosponsored by the American Society of Preventive Oncology* 12 (2): 136-143.
266. Himoto, T., S. Kuriyama, J. Y. Zhang, E. K. Chan, Y. Kimura, T. Masaki, N. Uchida, M. Nishioka, and E. M. Tan. 2005. Analyses of autoantibodies against tumor-associated antigens in patients with hepatocellular carcinoma. *Int J Oncol* 27 (4): 1079-1085.
267. Zhang, J. Y., R. Megliorino, X. X. Peng, E. M. Tan, Y. Chen, and E. K. Chan. 2007. Antibody detection using tumor-associated antigen mini-array in immunodiagnosing human hepatocellular carcinoma. *J Hepatol* 46 (1): 107-114.
268. Dai, L., P. Ren, M. Liu, H. Imai, E. M. Tan, and J. Y. Zhang. 2014. Using immunomic approach to enhance tumor-associated autoantibody detection in diagnosis of hepatocellular carcinoma. *Clin Immunol* 152 (1-2): 127-139.
269. Janeway CA Jr, Travers P, Walport M. 2001. Immunobiology: The Immune System in Health and Disease. 5th edition. New York: Garland Science; 2001. B-cell activation by armed helper T cells. https://www.ncbi.nlm.nih.gov/books/NBK27142.
270. Hoffman, W., F. G. Lakkis, and G. Chalasani. 2016. B Cells, Antibodies, and More. In *Clin J Am Soc Nephrol*. 11 (1): 137-154.

271. Suurmond, J., and B. Diamond. 2015. Autoantibodies in systemic autoimmune diseases: specificity and pathogenicity. In *J Clin Invest*. 125 (6): 2194-2202.
272. Elkon, K., and P. Casali. 2008. Nature and functions of autoantibodies. *Nat Clin Pract Rheumatol* 4 (9): 491-498.
273. Macdonald, I. K., C. B. Parsy-Kowalska, and C. J. Chapman. 2017. Autoantibodies: Opportunities for Early Cancer Detection. *Trends Cancer* 3 (3): 198-213.
274. Berlot, G., P. Rossini, and F. Turchet. 2015. Biology of Immunoglobulins. In *Transl Med UniSa*. 11: 24-27.
275. Schroeder, H. W., and L. Cavacini. 2010. Structure and Function of Immunoglobulins. *J Allergy Clin Immunol* 125 (2): S41-52.
276. Vidarsson, G., G. Dekkers, and T. Rispens. 2014. IgG Subclasses and Allotypes: From Structure to Effector Functions. *Front Immunol* 5: 520.
277. Irani, V., A. J. Guy, D. Andrew, J. G. Beeson, P. A. Ramsland, and J. S. Richards. 2015. Molecular properties of human IgG subclasses and their implications for designing therapeutic monoclonal antibodies against infectious diseases. *Molecular Immunology* 67 (2 part A): 171-182.
278. Wu, J., X. L. Ma, L. Tian, C. Y. Zhang, B. L. Wang, Y. Y. Hu, X. H. Gao, Y. Zhou, M. N. Shen, Y. F. Peng, B. S. Pan, J. Zhou, J. Fan, X. R. Yang, and W. Guo. 2017. Serum IgG4:IgG Ratio Predicts Recurrence of Patients with Hepatocellular Carcinoma after Curative Resection. *J Cancer* 8 (8): 1338-1346.
279. DÍAz-Zaragoza, M., R. HernÁNdez-ÁVila, R. Viedma-RodrÍGuez, D. Arenas-Aranda, and P. Ostoa-Saloma. 2015. Natural and adaptive IgM antibodies in the recognition of tumor-associated antigens of breast cancer (Review). In *Oncol Rep* 34: (3): 1106-1114.
280. Woof, J. M., and M. W. Russell. 2011. Structure and function relationships in IgA. *Mucosal Immunol* 4 (6): 590-597.
281. Pabst, O. 2012. New concepts in the generation and functions of IgA. *Nat Rev Immunol* 12 (12): 821-832.
282. Chen, K., and A. Cerutti. 2011. The Function and Regulation of Immunoglobulin D. *Curr Opin Immunol* 23 (3): 345-352.
283. Wu, L. C., and A. A. Zarrin. 2014. The production and regulation of IgE by the immune system. *Nat Rev Immunol* 14 (4): 247-259.
284. Lu, L. L., T. J. Suscovich, S. M. Fortune, and G. Alter. 2017. Beyond binding: antibody effector functions in infectious diseases. *Nature Reviews Immunology* 18 (1): 46-61.
285. Forthal, D. N. Functions of Antibodies. *Microbiol Spectr* 2 (4): 1-17.
286. Yang, D. H., L. J. Ho, and J. H. Lai. 2014. Useful biomarkers for assessment of hepatitis C virus infection-associated autoimmune disorders. *World J Gastroenterol* 20 (11): 2962-2970.
287. Narciso-Schiavon, J. L., and L. Schiavon Lde. 2015. Autoantibodies in chronic hepatitis C: A clinical perspective. *World J Hepatol* 7 (8): 1074-1085.
288. Amin, K., A. H. Rasool, A. Hattem, T. A. Al-Karboly, T. E. Taher, and J. Bystrom. 2017. Autoantibody profiles in autoimmune hepatitis and chronic hepatitis C identifies similarities in patients with severe disease. *World J Gastroenterol* 23 (8): 1345-1352.
289. Williams, M. J., A. Lawson, K. R. Neal, S. D. Ryder, and W. L. Irving. 2009. Autoantibodies in chronic hepatitis C virus infection and their association with disease profile. *J Viral Hepat* 16 (5): 325-331.

290. Himoto, T., and T. Masaki. 2012. Extrahepatic manifestations and autoantibodies in patients with hepatitis C virus infection. *Clin Dev Immunol* 2012: 871401.
291. Gilman, A. J., A. K. Le, C. Zhao, J. Hoang, L. A. Yasukawa, S. C. Weber, J. M. Vierling, and M. H. Nguyen. 2018. Autoantibodies in chronic hepatitis C virus infection: impact on clinical outcomes and extrahepatic manifestations. In *BMJ Open Gastroenterol* 5 (1): e000203.
292. Shiku, H., T. Takahashi, L. A. Resnick, H. F. Oettgen, and L. J. Old. 1977. Cell surface antigens of human malignant melanoma. III. Recognition of autoantibodies with unusual characteristics. *J Exp Med* 145 (3): 784-789.
293. Van der Bruggen, P., C. Traversari, P. Chomez, C. Lurquin, E. De Plaen, B. J. Van den Eynde, A. Knuth, and T. Boon. 2007. A gene encoding an antigen recognized by cytolytic T lymphocytes on a human melanoma. *J Immunol* 178 (5): 2617-2621.
294. Wang, K., X. Xu, Y. Nie, L. Dai, P. Wang, and J. Zhang. 2009. Identification of tumor-associated antigens by using SEREX in hepatocellular carcinoma. *Cancer Lett* 281 (2): 144-150.
295. Sioud, M., M. Hansen, and A. Dybwad. 2000. Profiling the immune responses in patient sera with peptide and cDNA display libraries. *Int J Mol Med* 6 (2): 123-128.
296. Zhang, Z., L. Xu, and Z. Wang. 2011. Screening serum biomarkers for early primary hepatocellular carcinoma using a phage display technique. *J Clin Lab Anal* 25 (6): 402-408.
297. Klade, C. S., T. Voss, E. Krystek, H. Ahorn, K. Zatloukal, K. Pummer, and G. R. Adolf. 2001. Identification of tumor antigens in renal cell carcinoma by serological proteome analysis. *Proteomics* 1 (7): 890-898.
298. Looi, K. S., E. S. Nakayasu, R. A. Diaz, E. M. Tan, I. C. Almeida, and J. Y. Zhang. 2008. Using proteomic approach to identify tumor-associated antigens as markers in hepatocellular carcinoma. *J Proteome Res* 7 (9): 4004-4012.
299. Joos, T. O., M. Schrenk, P. Hopfl, K. Kroger, U. Chowdhury, D. Stoll, D. Schorner, M. Durr, K. Herick, S. Rupp, K. Sohn, and H. Hammerle. 2000. A microarray enzyme-linked immunosorbent assay for autoimmune diagnostics. In *Electrophoresis*, Germany 21 (13): 2641-2650.
300. Robinson, W. H., C. DiGennaro, W. Hueber, B. B. Haab, M. Kamachi, E. J. Dean, S. Fournel, D. Fong, M. C. Genovese, H. E. de Vegvar, K. Skriner, D. L. Hirschberg, R. I. Morris, S. Muller, G. J. Pruijn, W. J. van Venrooij, J. S. Smolen, P. O. Brown, L. Steinman, and P. J. Utz. 2002. Autoantigen microarrays for multiplex characterization of autoantibody responses. *Nat Med* 8 (3): 295-301.
301. Chan, S. M., and P. J. Utz. 2005. The challenge of analyzing the proteome in humans with autoimmune diseases. In *Ann N Y Acad Sci*, United States. 1062: (1): 61-68.
302. Anderson, K. S., and J. LaBaer. 2005. The sentinel within: exploiting the immune system for cancer biomarkers. *Journal of Proteome Research* 4 (4): 1123-1133.
303. Raza, A., and G. K. Sood. 2014. Hepatocellular carcinoma review: Current treatment, and evidence-based medicine. *World J Gastroenterol* 20 (15): 4115-4127.

304. Harper, M. E., and A. Dugaiczyk. 1983. Linkage of the evolutionarily-related serum albumin and alpha-fetoprotein genes within q11-22 of human chromosome 4. *Am J Hum Genet* 35 (4): 565-572.
305. Seregni, E., C. Botti, and E. Bombardieri. 1995. Biochemical characteristics and clinical applications of alpha-fetoprotein isoforms. *Anticancer Res* 15 (4): 1491-1499.
306. Baig, J. A., J. M. Alam, S. R. Mahmood, M. Baig, R. Shaheen, I. Sultana, and A. Waheed. 2009. Hepatocellular carcinoma (HCC) and diagnostic significance of A-fetoprotein (AFP). *J Ayub Med Coll Abbottabad* 21 (1): 72-75.
307. Tangkijvanich, P., N. Anukulkarnkusol, P. Suwangool, S. Lertmaharit, O. Hanvivatvong, P. Kullavanijaya, and Y. Poovorawan. 2000. Clinical characteristics and prognosis of hepatocellular carcinoma: analysis based on serum alpha-fetoprotein levels. *J Clin Gastroenterol* 31 (4): 302-308.
308. Schütte, K., C. Schulz, and P. Malfertheiner. 2018. Hepatocellular Carcinoma: Current Concepts in Diagnosis, Staging and Treatment. *Gastrointestinal Tumors* 1 (2): 84-92.
309. Giorgio, A., G. Ferraioli, L. Tarantino, G. de Stefano, V. Scala, F. Scarano, C. Coppola, and L. Del Viscovo. 2004. Contrast-enhanced sonographic appearance of hepatocellular carcinoma in patients with cirrhosis: comparison with contrast-enhanced helical CT appearance. In *AJR Am J Roentgenol*, United States. 183 (5): 1319-1326.
310. Wang, Z., J. Tang, L. An, W. Wang, Y. Luo, J. Li, and J. Xu. 2007. Contrast-enhanced ultrasonography for assessment of tumor vascularity in hepatocellular carcinoma. In *J Ultrasound Med*, United States. 26 (6): 757-762.
311. Hamper, U. M., M. R. DeJong, C. I. Caskey, and S. Sheth. 1997. Power Doppler imaging: clinical experience and correlation with color Doppler US and other imaging modalities. *Radiographics* 17 (2): 499-513.
312. Xu, H. X., L. Liu, M. D. Lu, H. P. Li, G. J. Liu, and J. P. Li. 2003. Three-dimensional power Doppler imaging in depicting vascularity in hepatocellular carcinoma. *J Ultrasound Med* 22 (11): 1147-1154.
313. Claudon, M., D. Cosgrove, T. Albrecht, L. Bolondi, M. Bosio, F. Calliada, J. M. Correas, K. Darge, C. Dietrich, M. D'Onofrio, D. H. Evans, C. Filice, L. Greiner, K. Jager, N. Jong, E. Leen, R. Lencioni, D. Lindsell, A. Martegani, S. Meairs, C. Nolsoe, F. Piscaglia, P. Ricci, G. Seidel, B. Skjoldbye, L. Solbiati, L. Thorelius, F. Tranquart, H. P. Weskott, and T. Whittingham. 2008. Guidelines and good clinical practice recommendations for contrast enhanced ultrasound (CEUS) - update 2008. *Ultraschall Med* 29 (1): 28-44.
314. Bruix, J., and M. Sherman. 2011. Management of hepatocellular carcinoma: an update. *Hepatology (Baltimore, Md.)* 53 (3): 1020-1022.
315. European Association for the Study of Liver., European Organisation for Research and Treament of Cancer. 2012. EASL-EORTC clinical practice guidelines: management of hepatocellular carcinoma. *J Hepatol* 56 (4): 908-943.
316. Siegelman, E. S., and E. K. Outwater. 1998. MR imaging techniques of the liver. *Radiol Clin North Am* 36 (2): 263-286.
317. Outwater, E. K., R. Blasbalg, E. S. Siegelman, and M. Vala. 1998. Detection of lipid in abdominal tissues with opposed-phase gradient-echo images at 1.5 T: techniques and diagnostic importance. *Radiographics* 18 (6): 1465-1480.
318. Ito, K., D. G. Mitchell, T. Gabata, H. W. Hann, P. N. Kim, T. Fujita, H. Awaya, K. Honjo, and N. Matsunaga. 1999. Hepatocellular carcinoma: association with

increased iron deposition in the cirrhotic liver at MR imaging. *Radiology* 212 (1): 235-240.
319. Materne, R., A. M. Smith, F. Peeters, J. P. Dehoux, A. Keyeux, Y. Horsmans, and B. E. Van Beers. 2002. Assessment of hepatic perfusion parameters with dynamic MRI. In *Magn Reson Med*. United States. 47 (1): 135-142.
320. Song, D. S., and S. H. Bae. 2012. Changes of guidelines diagnosing hepatocellular carcinoma during the last ten-year period. *Clin Mol Hepatol* 18 (3): 258-267.
321. Scarsbrook, A. F., A. Ganeshan, J. Statham, R. V. Thakker, A. Weaver, D. Talbot, P. Boardman, K. M. Bradley, F. V. Gleeson, and R. R. Phillips. 2007. Anatomic and functional imaging of metastatic carcinoid tumors. In *Radiographics*. Rsna, 2007., United States 27 (2): 455-477.
322. Wudel, L. J., Jr., D. Delbeke, D. Morris, M. Rice, M. K. Washington, Y. Shyr, C. W. Pinson, and W. C. Chapman. 2003. The role of [18F]fluorodeoxyglucose positron emission tomography imaging in the evaluation of hepatocellular carcinoma. *Am Surg* 69 (2): 117-124.
323. Khan, M. A., C. S. Combs, E. M. Brunt, V. J. Lowe, M. K. Wolverson, H. Solomon, B. T. Collins, and A. M. Di Bisceglie. 2000. Positron emission tomography scanning in the evaluation of hepatocellular carcinoma. In *Journal of hepatology*, Denmark. 32 (5): 792-797.
324. Ho, C. L., S. C. Yu, and D. W. Yeung. 2003. 11C-acetate PET imaging in hepatocellular carcinoma and other liver masses. *J Nucl Med* 44 (2): 213-221.
325. Finn, R. S. 2016. The Role of Liver Biopsy in hepatocellular carcinoma. *Gastroenterol Hepatol (N Y)* 12 (10): 628-630.
326. Chang, M. H. 2003. Decreasing incidence of hepatocellular carcinoma among children following universal hepatitis B immunization. *Liver Int* 23 (5): 309-314.
327. Lernout, T., G. Hendrickx, A. Vorsters, L. Mosina, N. Emiroglu, and P. Van Damme. 2014. A cohesive European policy for hepatitis B vaccination, are we there yet? *Clin Microbiol Infect* 20 (Suppl 5): 19-24.
328. Kao, J. H. 2015. Hepatitis B vaccination and prevention of hepatocellular carcinoma. *Best Pract Res Clin Gastroenterol* 29 (6): 907-917.
329. Kew, M. C. 2010. Prevention of hepatocellular carcinoma. In *Annals of Hepatology*, Mexico. 120-132.
330. Schütte, K., F. Balbisi, and P. Malfertheiner. 2016. Prevention of hepatocellular carcinoma. In *Gastrointest Tumors* 3 (10): 37-43.
331. Su, T. H., and J. H. Kao. 2015. Improving clinical outcomes of chronic hepatitis B virus infection. *Expert Rev Gastroenterol Hepatol* 9 (2): 141-154.
332. Fan, J. G., and G. C. Farrell. 2009. Prevention of hepatocellular carcinoma in nonviral-related liver diseases. *J Gastroenterol Hepatol* 24 (4): 712-719.
333. Vilar-Gomez, E., Y. Martinez-Perez, L. Calzadilla-Bertot, A. Torres-Gonzalez, B. Gra-Oramas, L. Gonzalez-Fabian, S. L. Friedman, M. Diago, and M. Romero-Gomez. 2015. Weight Loss Through Lifestyle Modification Significantly Reduces Features of Nonalcoholic Steatohepatitis. *Gastroenterology* 149 (2): 367-378.
334. Singh, S., P. P. Singh, A. G. Singh, M. H. Murad, and W. Sanchez. 2013. Anti-diabetic medications and the risk of hepatocellular cancer: a systematic review and meta-analysis. *Am J Gastroenterol* 108 (6): 881-891.
335. Yu, S. Z. 1995. Primary prevention of hepatocellular carcinoma. *Journal of Gastroenterology and Hepatology* 10 (6): 674-682.

336. Breinholt, V., M. Schimerlik, R. Dashwood, and G. Bailey. 1995. Mechanisms of chlorophyllin anticarcinogenesis against aflatoxin B1: complex formation with the carcinogen. *Chem Res Toxicol* 8 (4): 506-514.
337. Kamat, J. P., K. K. Boloor, and T. P. Devasagayam. 2000. Chlorophyllin as an effective antioxidant against membrane damage in vitro and ex vivo. In *Biochim Biophys Acta*, Netherlands. 1487 (2-3): 113-127.
338. Okuno, M., S. Kojima, and H. Moriwaki. 2001. Chemoprevention of hepatocellular carcinoma: concept, progress and perspectives. In *Journal of Gastroenterology and Hepatology*, Australia 16 (12): 1329-1335.
339. Muto, Y., H. Moriwaki, and A. Saito. 1999. Prevention of second primary tumors by an acyclic retinoid in patients with hepatocellular carcinoma. *N Engl J Med* 340 (13): 1046-1047.
340. Sudakin, D. L. 2003. Dietary aflatoxin exposure and chemoprevention of cancer: a clinical review. *J Toxicol Clin Toxicol* 41 (2): 195-204.
341. Morel, F., O. Fardel, D. J. Meyer, S. Langouet, K. S. Gilmore, B. Meunier, C. P. Tu, T. W. Kensler, B. Ketterer, and A. Guillouzo. 1993. Preferential increase of glutathione S-transferase class alpha transcripts in cultured human hepatocytes by phenobarbital, 3-methylcholanthrene, and dithiolethiones. *Cancer Research* 53 (2): 231-234.
342. Niederau, C., R. Fischer, A. Purschel, W. Stremmel, D. Haussinger, and G. Strohmeyer. 1996. Long-term survival in patients with hereditary hemochromatosis. In *Gastroenterology*, United States. 110 (4): 1107-1119.
343. Bishayee, A., R. J. Thoppil, A. Waghray, J. A. Kruse, N. A. Novotny, and A. S. Darvesh. 2012. Dietary Phytochemicals in the Chemoprevention and Treatment of Hepatocellular Carcinoma: In Vivo Evidence, Molecular Targets, and Clinical Relevance. *Curr Cancer Drug Targets* 12 (9): 1191-1123.
344. Singh, S., P. P. Singh, L. R. Roberts, and W. Sanchez. 2014. Chemopreventive strategies in hepatocellular carcinoma. *Nat Rev Gastroenterol Hepatol* 11 (1): 45-54.
345. Bishayee, A., R. J. Thoppil, A. Waghray, J. A. Kruse, N. A. Novotny, and A. S. Darvesh. 2012. Dietary phytochemicals in the chemoprevention and treatment of hepatocellular carcinoma: in vivo evidence, molecular targets, and clinical relevance. *Curr Cancer Drug Targets* 12 (9): 1191-1232.
346. Camma, C., M. Giunta, P. Andreone, and A. Craxi. 2001. Interferon and prevention of hepatocellular carcinoma in viral cirrhosis: an evidence-based approach. In *Journal of Hepatology*, Denmark 34 (4): 593-602.
347. Huang, J. F., M. L. Yeh, M. L. Yu, C. Y. Dai, C. F. Huang, C. I. Huang, P. C. Tsai, P. C. Lin, Y. L. Chen, W. T. Chang, N. J. Hou, Z. Y. Lin, S. C. Chen, and W. L. Chuang. 2015. The tertiary prevention of hepatocellular carcinoma in chronic hepatitis C patients. *J Gastroenterol Hepatol* 30 (12): 1768-1774.
348. Lu, T., W. K. Seto, R. X. Zhu, C. L. Lai, and M. F. Yuen. 2013. Prevention of hepatocellular carcinoma in chronic viral hepatitis B and C infection. *World J Gastroenterol* 19 (47): 8887-8894.
349. Llovet, J. M., C. Bru, and J. Bruix. 1999. Prognosis of hepatocellular carcinoma: the BCLC staging classification. *Semin Liver Dis* 19 (3): 329-338.
350. Kinoshita, A., H. Onoda, N. Fushiya, K. Koike, H. Nishino, and H. Tajiri. 2015. Staging systems for hepatocellular carcinoma: Current status and future perspectives. *World J Hepatol* 7 (3): 406-424.

351. Saleh, D., M. Muhammad, B. A. A., and K. Tawfik. 2017. Current and Future Treatment of Hepatocellular Carcinoma: An Updated Comprehensive Review. *J Clin Transl Hepatol* 6 (1): 69-78.
352. Finn, R. S. 2013. Emerging targeted strategies in advanced hepatocellular carcinoma. *Semin Liver Dis* 33 (Suppl 1): S11-19.
353. Cucchetti, A., A. Vitale, M. Cescon, M. Gambato, L. Maroni, M. Ravaioli, G. Ercolani, P. Burra, U. Cillo, and A. D. Pinna. 2014. Can liver transplantation provide the statistical cure? *Liver Transpl* 20 (2): 210-217.
354. Sala, M., J. M. Llovet, R. Vilana, L. Bianchi, M. Sole, C. Ayuso, C. Bru, and J. Bruix. 2004. Initial response to percutaneous ablation predicts survival in patients with hepatocellular carcinoma. *Hepatology (Baltimore, Md.)* 40 (6): 1352-1360.
355. Villanueva, A., P. Newell, and Y. Hoshida. 2010. Inherited hepatocellular carcinoma. *Best Practice & Research. Clinical Gastroenterology* 24 (5): 725-734.
356. Hasegawa, K., M. Makuuchi, T. Takayama, N. Kokudo, S. Arii, M. Okazaki, K. Okita, M. Omata, M. Kudo, M. Kojiro, Y. Nakanuma, K. Takayasu, M. Monden, Y. Matsuyama, and I. Ikai. 2008. Surgical resection vs. percutaneous ablation for hepatocellular carcinoma: a preliminary report of the Japanese nationwide survey. *Journal of Hepatology* 49 (4): 589-594.
357. Sacco, R., G. Tapete, N. Simonetti, R. Sellitri, V. Natali, S. Melissari, G. Cabibbo, L. Biscaglia, G. Bresci, and L. Giacomelli. 2017. Transarterial chemoembolization for the treatment of hepatocellular carcinoma: a review. In *J Hepatocell Carcinoma* 4: 105-110.
358. Kudo, M., O. Matsui, N. Izumi, H. Iijima, M. Kadoya, Y. Imai, T. Okusaka, S. Miyayama, K. Tsuchiya, K. Ueshima, A. Hiraoka, M. Ikeda, S. Ogasawara, T. Yamashita, T. Minami, and K. Yamakado. 2014. JSH Consensus-Based Clinical Practice Guidelines for the Management of Hepatocellular Carcinoma: 2014 Update by the Liver Cancer Study Group of Japan. *Liver Cancer* 3 (3-4): 458-468.
359. Sangro, B., C. L. Maini, G. M. Ettorre, R. Cianni, R. Golfieri, D. Gasparini, S. Ezziddin, P. M. Paprottka, F. Fiore, M. Van Buskirk, J. I. Bilbao, R. Salvatori, E. Giampalma, O. Geatti, K. Wilhelm, R. T. Hoffmann, F. Izzo, M. Inarrairaegui, C. Urigo, A. Cappelli, A. Vit, H. Ahmadzadehfar, T. F. Jakobs, R. Sciuto, G. Pizzi, and S. Lastoria. 2018. Radioembolisation in patients with hepatocellular carcinoma that have previously received liver-directed therapies. *Eur J Nucl Med Mol Imaging* 45 (10): 1721-1730.
360. Nojiri, K., K. Sugimoto, K. Shiraki, M. Tameda, Y. Inagaki, S. Ogura, C. Kasai, S. Kusagawa, M. Yoneda, N. Yamamoto, Y. Takei, T. Nobori, and M. Ito. 2013. Sorafenib and TRAIL have synergistic effect on hepatocellular carcinoma. *Int J Oncol* 42 (1): 101-108.
361. Daher, S., M. Massarwa, A. A. Benson, and T. Khoury. 2018. Current and Future Treatment of Hepatocellular Carcinoma: An Updated Comprehensive Review. In *J Clin Transl Hepatol* 6 (1): 69-78.
362. Wu, Y. X., J. H. Yang, and H. Saitsu. 2016. Bortezomib-resistance is associated with increased levels of proteasome subunits and apoptosis-avoidance. *Oncotarget* 7 (47): 77622-77634.
363. Augello, G., M. Modica, A. Azzolina, R. Puleio, G. Cassata, M. R. Emma, C. Di Sano, A. Cusimano, G. Montalto, and M. Cervello. 2018. Preclinical

evaluation of antitumor activity of the proteasome inhibitor MLN2238 (ixazomib) in hepatocellular carcinoma cells. *Cell Death Dis* 9 (2): 28.

364. Bishayee, A., and A. S. Darvesh. 2012. Angiogenesis in hepatocellular carcinoma: a potential target for chemoprevention and therapy. *Curr Cancer Drug Targets* 12 (9): 1095-1118.
365. Sangro, B., C. Gomez-Martin, M. de la Mata, M. Inarrairaegui, E. Garralda, P. Barrera, J. I. Riezu-Boj, E. Larrea, C. Alfaro, P. Sarobe, J. J. Lasarte, J. L. Perez-Gracia, I. Melero, and J. Prieto. 2013. A clinical trial of CTLA-4 blockade with tremelimumab in patients with hepatocellular carcinoma and chronic hepatitis C. *J Hepatol* 59 (1): 81-88.
366. Glokler, J., and P. Angenendt. 2003. Protein and antibody microarray technology. *J Chromatogr B Analyt Technol Biomed Life Sci* 797 (1-2): 229-240.
367. Akada, J., S. Kamei, A. Ito, M. Ito, T. Kitagawa, H. Furumoto, Y. Kato, M. Tamesa, M. Takashima, M. Shirai, H. Yamano, M. Oka, Y. Kuramitsu, and K. Nakamura. 2013. A new type of protein chip to detect hepatocellular carcinoma-related autoimmune antibodies in the sera of hepatitis C virus-positive patients. *Proteome Sci* 11 (1): 33.
368. Zhong L, Z. W., Zer C, Ge K, Gao X, Kernestine KH. 2010. Protein Microarray. BMC biotechnology 10: 12 .
369. Yeste, A., and F. J. Quintana. 2013. Antigen microarrays for the study of autoimmune diseases. *Clin Chem* 59 (7): 1036-1044.
370. Papp, K., and J. Prechl. 2012. The use of antigen microarrays in antibody profiling. *Methods Mol Biol* 815: 175-185.
371. Mendoza, L. G., P. McQuary, A. Mongan, R. Gangadharan, S. Brignac, and M. Eggers. 1999. High-throughput microarray-based enzyme-linked immunosorbent assay (ELISA). *Biotechniques* 27 (4): 778-788.
372. Sobek. J., A. C., Schlapbach. R. 2018. Quality Considerations and Selection of Surface Chemistry for Glass-Based DNA, Peptide, Antibody, Carbohydrate, and Small Molecule Microarrays | SpringerLink. *Microarrays. Methods in Molecular Biology* 382: 17-31.
373. Bussow, K., D. Cahill, W. Nietfeld, D. Bancroft, E. Scherzinger, H. Lehrach, and G. Walter. 1998. A method for global protein expression and antibody screening on high-density filters of an arrayed cDNA library. *Nucleic Acids Res* 26 (21): 5007-5008.
374. Haab, B. B., M. J. Dunham, and P. O. Brown. 2001. Protein microarrays for highly parallel detection and quantitation of specific proteins and antibodies in complex solutions. *Genome Biol* 2 (2): Research0004.
375. MacBeath, G., and S. L. Schreiber. 2000. Printing proteins as microarrays for high-throughput function determination. *Science* 289 (5485): 1760-1763.
376. Arenkov, P., A. Kukhtin, A. Gemmell, S. Voloshchuk, V. Chupeeva, and A. Mirzabekov. 2000. Protein microchips: use for immunoassay and enzymatic reactions. *Anal Biochem* 278 (2): 123-131.
377. Afanassiev, V., V. Hanemann, and S. Wölfl. 2000. Preparation of DNA and protein micro arrays on glass slides coated with an agarose film. In *Nucleic Acids Res* 28 (12): e66.
378. Kersten, B., A. Possling, F. Blaesing, E. Mirgorodskaya, J. Gobom, and H. Seitz. 2004. Protein microarray technology and ultraviolet crosslinking combined with mass spectrometry for the analysis of protein-DNA interactions. *Anal Biochem* 331 (2): 303-313.

379. Angenendt, P., J. Glokler, D. Murphy, H. Lehrach, and D. J. Cahill. 2002. Toward optimized antibody microarrays: a comparison of current microarray support materials. *Anal Biochem* 309 (2): 253-260.
380. Angenendt, P. 2005. Progress in protein and antibody microarray technology. *Drug Discovery Today* 10 (7): 503-511.
381. Espina, V., E. C. Woodhouse, J. Wulfkuhle, H. D. Asmussen, E. F. Petricoin, 3rd, and L. A. Liotta. 2004. Protein microarray detection strategies: focus on direct detection technologies. *J Immunol Methods* 290 (1-2): 121-133.
382. Varnum, S. M., R. L. Woodbury, and R. C. Zangar. 2004. A protein microarray ELISA for screening biological fluids. *Methods Mol Biol* 264: 161-172.
383. Kattah, M. G., P. J. Utz, and I. Balboni. 2008. Protein microarrays address the elephant in the room. In *Clin Chem*, United States 54 (6): 937-939.
384. Wellhausen, R., and H. Seitz. 2012. Facing current quantification challenges in protein microarrays. *J Biomed Biotechnol* 2012: 831347.
385. Wu, P., and D. W. Grainger. 2006. Comparison of hydroxylated print additives on antibody microarray performance. *Journal of proteome research* 5 (11): 2956-2965.
386. Preininger, C., J. Dayteg, R. 2005. Optimizing processing parameters for signal enhancement of oligonucleotide and protein arrays on ARChip Epoxy. *Bioelectrochemistry* 67 (2): 155–162.
387. Servoss, S. L., R. Gonzalez, S. Varnum, and R. C. Zangar. 2009. High-throughput analysis of serum antigens using sandwich ELISAs on microarrays. *Methods in molecular biology (Clifton, N.J.)* 520: 143-150.
388. Selvarajah, S., O. H. Negm, M. R. Hamed, C. Tubby, I. Todd, P. J. Tighe, T. Harrison, and L. C. Fairclough. 2014. Development and validation of protein microarray technology for simultaneous inflammatory mediator detection in human sera. *Mediators Inflamm* 2014: 820304.
389. Grace Bio-Labs, G. 2013. Immunoassays: Protein Arrays vs. ELISA and Westerns.https://gracebio.com/immunoassays-protein-arrays-vs-elisa-and-westerns/.
390. Gheath Alatrash, J. J. M. 2013. Immune Biology of Allogeneic Hematopoietic stem cell transplantation. In *chapter 7-Tumour-associated antigens*, *ScienceDirect*. 143-164.
391. Balboni, I., S. M. Chan, M. Kattah, J. D. Tenenbaum, A. J. Butte, and P. J. Utz. 2006. Multiplexed protein array platforms for analysis of autoimmune diseases. *Annu Rev Immunol* 24: 391-418.
392. Wang, K . 2009. Immunogenicity of Ra1A and its tissue-specific expression in hepatocellular carcinoma. - *Inter J Immuno Pathol Pharmacol* 22 (3): 735-743.
393. Wang, K., Y. Chen, S. Liu, S. Qiu, S. Gao, X. Huang, J. Zhang, X. Peng, W. Qiani, and J. Y. Zhang. 2009. Immunogenicity of Ra1A and its tissue-specific expression in hepatocellular carcinoma. *Int J Immunopathol Pharmacol* 22 (3): 735-743.
394. Xu, H., N. Gu, Z. B. Liu, M. Zheng, F. Xiong, S. Y. Wang, N. Li, and J. Lu. 2012. NY-ESO-1 expression in hepatocellular carcinoma: A potential new marker for early recurrence after surgery. In *Oncol Lett* 3 (1): 39-44.
395. Vigneron, N. 2015. Human Tumor Antigens and Cancer Immunotherapy. *Biomed Res Int* 2015: 948501.
396. Koziol, J. A., H. Imai, L. Dai, J. Y. Zhang, and E. M. Tan. 2018. Early detection of hepatocellular carcinoma using autoantibody profiles from a panel of tumor-associated antigens. *Cancer Immunol Immunother* 67 (5): 835-841.

397. Nomura, F., K. Sogawa, K. Noda, M. Seimiya, K. Matsushita, T. Miura, T. Tomonaga, H. Yoshitomi, F. Imazeki, H. Takizawa, K. Mogushi, M. Miyazaki, and O. Yokosuka. 2012. Serum anti-Ku86 is a potential biomarker for early detection of hepatitis C virus-related hepatocellular carcinoma. *Biochem Biophys Res Commun* 421 (4): 837-843.
398. Liu, H., J. Zhang, S. Wang, Z. Pang, Z. Wang, W. Zhou, and M. Wu. 2012. Screening of autoantibodies as potential biomarkers for hepatocellular carcinoma by using T7 phase display system. *Cancer Epidemiol* 36 (1): 82-88.
399. Chen, Y., Y. Zhou, S. Qiu, K. Wang, S. Liu, X. X. Peng, J. Li, E. M. Tan, and J. Y. Zhang. 2010. Autoantibodies to tumor-associated antigens combined with abnormal alpha-fetoprotein enhance immunodiagnosis of hepatocellular carcinoma. *Cancer Lett* 289 (1): 32-39.
400. Looi, K. S., E. S. Nakayasu, R. A. de Diaz, E. M. Tan, I. C. Almeida, and J. Y. Zhang. 2008. Using Proteomic Approach to Identify Tumor-Associated Antigens as Markers in Hepatocellular Carcinoma. *J Proteome Res* 7 (9): 4004-4012.
401. Li, L., S. H. Chen, C. H. Yu, Y. M. Li, and S. Q. Wang. 2008. Identification of hepatocellular-carcinoma-associated antigens and autoantibodies by serological proteome analysis combined with protein microarray. *J Proteome Res* 7 (2): 611-620.
402. Chen, X., S. Fu, F. Chen, H. Chen, and Z. Chen. 2008. Identification of tumor-associated antigens in human hepatocellular carcinoma by autoantibodies. *Oncol Rep* 20 (4): 979-985.
403. Akere, A., and J. A. Otegbayo. 2007. Evaluation of the pattern and prognostic implications of anti-p53 in hepatocellular carcinoma. *Singapore Med J* 48 (1): 41-44.
404. Zhou, S. F., X. X. Xie, Y. H. Bin, L. Lan, F. Chen, and G. R. Luo. 2006. Identification of HCC-22-5 tumor-associated antigen and antibody response in patients. *Clin Chim Acta* 366 (1-2): 274-280.
405. Takashima, M., Y. Kuramitsu, Y. Yokoyama, N. Iizuka, T. Harada, M. Fujimoto, I. Sakaida, K. Okita, M. Oka, and K. Nakamura. 2006. Proteomic analysis of autoantibodies in patients with hepatocellular carcinoma. *Proteomics* 6 (13): 3894-3900.
406. Looi, K., R. Megliorino, F. D. Shi, X. X. Peng, Y. Chen, and J. Y. Zhang. 2006. Humoral immune response to p16, a cyclin-dependent kinase inhibitor in human malignancies. *Oncol Rep* 16 (5): 1105-1110.
407. Yagihashi, A., K. Asanuma, D. Kobayashi, N. Tsuji, T. Torigoe, N. Sato, and N. Watanabe. 2005. Autoantibodies to survivin in patients with chronic hepatitis and hepatocellular carcinoma. *Autoimmunity* 38 (6): 445-448.
408. Su, Y., H. Qian, J. Zhang, S. Wang, P. Shi, and X. Peng. 2005. The diversity expression of p62 in digestive system cancers. *Clin Immunol* 116 (2): 118-123.
409. Himoto, T., S. Kuriyama, J. Y. Zhang, E. K. Chan, M. Nishioka, and E. M. Tan. 2005. Significance of autoantibodies against insulin-like growth factor II mRNA-binding proteins in patients with hepatocellular carcinoma. *Int J Oncol* 26 (2): 311-317.
410. Raedle, J., G. Oremek, M. Truschnowitsch, M. Lorenz, W. K. Roth, W. F. Caspary, and S. Zeuzem. 1998. Clinical evaluation of autoantibodies to p53 protein in patients with chronic liver disease and hepatocellular carcinoma. *Eur J Cancer* 34 (8): 1198-1203.

411. Covini, G., E. K. Chan, M. Nishioka, S. A. Morshed, S. I. Reed, and E. M. Tan. 1997. Immune response to cyclin B1 in hepatocellular carcinoma. *Hepatology* 25 (1): 75-80.
412. He, Y., K. Wang, and N. Yan. 2014. The recombinant expression systems for structure determination of eukaryotic membrane proteins. In *Protein Cell*. 5 (9): 658-672.
413. Khan, K. H. 2013. Gene Expression in Mammalian Cells and its Applications. *Adv Pharm Bull* 3 (2): 257-263.
414. Zhu, J. 2012. Mammalian cell protein expression for biopharmaceutical production. *Biotechnol Adv* 30 (5): 1158-1170.
415. Arnold L. Demiah, P. V. 2009. Production of recombinant proteins by microbes and higher organisms. *Biotechnol Adv* 27 (3): 297–306.
416. Brodel, A. K., A. Sonnabend, and S. Kubick. 2014. Cell-free protein expression based on extracts from CHO cells. *Biotechnol Bioeng* 111 (1): 25-36.
417. Walsh, G. 2010. Post-translational modifications of protein biopharmaceuticals. *Drug Discov Today* 15 (17-18): 773-780.
418. Imataka, H., and S. Mikami. 2009. [Advantages of human cell-derived cell-free protein synthesis systems]. *Seikagaku* 81 (4): 303-307.
419. Sunley, K., and M. Butler. 2010. Strategies for the enhancement of recombinant protein production from mammalian cells by growth arrest. *Biotechnol Adv* 28 (3): 385-394.
420. Sahdev, S., S. K. Khattar, and K. S. Saini. 2008. Production of active eukaryotic proteins through bacterial expression systems: a review of the existing biotechnology strategies. *Mol Cell Biochem* 307 (1-2): 249-264.
421. Bandaranayake, A. D. 2014. Recent advances in mammalian protein production. *FEBS* 588 (2): 253-260.
422. Li, B., H. Y. Wu, X. P. Qian, Y. Li, and W. F. Chen. 2003. Expression, purification and serological analysis of hepatocellular carcinoma associated antigen HCA587 in insect cells. *World J Gastroenterol* 9 (4): 678-682.
423. Kobayashi, T., S. Mikami, S. Yokoyama, and H. Imataka. 2007. An improved cell-free system for picornavirus synthesis. *J Virol Methods* 142 (1-2): 182-188.
424. Nielsen, K. H. 2014. Protein expression-yeast. *Methods Enzymol* 536: 133-147.
425. Kim, T. K., and J. H. Eberwine. 2010. Mammalian cell transfection: the present and the future. In *Anal Bioanal Chem*. 397 (8): 3173-3178.
426. Hartley, J. L. 2012. Why proteins in mammalian cells? *Methods Mol Biol* 801: 1-12.
427. Recillas-Targa, F. 2006. Multiple strategies for gene transfer, expression, knockdown, and chromatin influence in mammalian cell lines and transgenic animals. *Mol Biotechnol* 34 (3): 337-354.
428. Glover, D. J., H. J. Lipps, and D. A. Jans. 2005. Towards safe, non-viral therapeutic gene expression in humans. *Nat Rev Genet* 6 (4): 299-310.
429. Wurm, F. M. 2004. Production of recombinant protein therapeutics in cultivated mammalian cells. *Nat Biotechnol* 22 (11): 1393-1398.
430. Holmen, S. L., M. W. Vanbrocklin, R. R. Eversole, S. R. Stapleton, and L. C. Ginsberg. 1995. Efficient lipid-mediated transfection of DNA into primary rat hepatocytes. *In Vitro Cell Dev Biol Anim* 31 (5): 347-351.
431. Tlaxca, J. L., C. R. Anderson, A. L. Klibanov, B. Lowrey, J. A. Hossack, J. S. Alexander, M. B. Lawrence, and J. J. Rychak. 2010. Analysis of in vitro transfection by sonoporation using cationic and neutral microbubbles. *Ultrasound Med Biol* 36 (11): 1907-1918.

432. Dobson, J. 2006. Gene therapy progress and prospects: magnetic nanoparticle-based gene delivery. *Gene Ther* 13 (4): 283-287.
433. Yao, C. P., Z. X. Zhang, R. Rahmanzadeh, and G. Huettmann. 2008. Laser-based gene transfection and gene therapy. *IEEE Trans Nanobioscience* 7 (2): 111-119.
434. O'Brien, J. A., and S. C. R. Lummis. 2006. Biolistic transfection of neuronal cultures using a hand-held gene gun. *Nature Protocols* 1 (2): 977.
435. Mehier-Humbert, S., and R. H. Guy. 2005. Physical methods for gene transfer: improving the kinetics of gene delivery into cells. *Adv Drug Deliv Rev* 57 (5): 733-753.
436. Walsh, G. 2010. Biopharmaceutical benchmarks 2010. *Nat Biotechnol* 28 (6): 917-924.
437. Ohana, R. F., and R. Hurst. 2015. Purification of Recombinant Proteins from Cultured Mammalian Cells by HaloTag Technology. *Curr Protoc Mol Biol* 110: 10.31.11-15.
438. Liu, H. F., J. Ma, C. Winter, and R. Bayer. 2010. Recovery and purification process development for monoclonal antibody production. *MAbs* 2 (5): 480-499.
439. Hage, D. S. 1999. Affinity chromatography: a review of clinical applications. *Clin Chem* 45 (5): 593-615.
440. Terpe, K. 2003. Overview of tag protein fusions: from molecular and biochemical fundamentals to commercial systems. *Appl Microbiol Biotechnol* 60 (5): 523-533.
441. Raines, R. T., M. McCormick, T. R. Van Oosbree, and R. C. Mierendorf. 2000. The S.Tag fusion system for protein purification. *Methods Enzymol* 326: 362-376.
442. Einhauer, A., and A. Jungbauer. 2001. The FLAG peptide, a versatile fusion tag for the purification of recombinant proteins. *J Biochem Biophys Methods* 49 (1-3): 455-465.
443. Einhauer, A., and A. Jungbauer. 2001. The FLAG™ peptide, a versatile fusion tag for the purification of recombinant proteins. *Journal of Biochemical and Biophysical Methods* 49 (1-3): 455-465.
444. Arnau, J., C. Lauritzen, G. E. Petersen, and J. Pedersen. 2006. Current strategies for the use of affinity tags and tag removal for the purification of recombinant proteins. *Protein Expr Purif* 48 (1): 1-13.
445. Chapman, C. J., A. Murray, J. E. McElveen, U. Sahin, U. Luxemburger, O. Tureci, R. Wiewrodt, A. C. Barnes, and J. F. Robertson. 2008. Autoantibodies in lung cancer: possibilities for early detection and subsequent cure. *Thorax* 63 (3): 228-233.
446. Zhao, X., G. Li, and S. Liang. 2013. Several affinity tags commonly used in chromatographic purification. *J Anal Methods Chem* 2013 (1): 581093.
447. Demain, A. L., and P. Vaishnav. 2009. Production of recombinant proteins by microbes and higher organisms. *Biotechnol Adv* 27 (3): 297-306.
448. Palomares, L. A., S. Estrada-Mondaca, and O. T. Ramirez. 2004. Production of recombinant proteins: challenges and solutions. *Methods Mol Biol* 267: 15-52.
449. Wingfield, P. T. 2015. Overview of the Purification of Recombinant Proteins. *Curr Protoc Protein Sci* 80: 6.1.1-6.1.35.
450. Pina, A. S., C. R. Lowe, and A. C. Roque. 2014. Challenges and opportunities in the purification of recombinant tagged proteins. *Biotechnol Adv* 32 (2): 366-381.

451. Bandaranayake, A. D., and S. C. Almo. 2014. Recent advances in mammalian protein production. *FEBS Lett* 588 (2): 253-260.
452. Yallop, C. A., and I. Svendsen. 2001. The effects of G418 on the growth and metabolism of recombinant mammalian cell lines. In *Cytotechnology*. 35 (2): 101-114.
453. Sousa, M. M., K. W. Steen, L. Hagen, and G. Slupphaug. 2011. Antibody cross-linking and target elution protocols used for immunoprecipitation significantly modulate signal-to noise ratio in downstream 2D-PAGE analysis. *Proteome Sci* 4 (9): 45.
454. Antrobus, R., and G. H. Borner. 2011. Improved elution conditions for native co-immunoprecipitation. *PLoS One* 6 (3): e18218.
455. Ying, X., S. Han, C. He, C. Zhou, Y. Dong, M. Cai, X. Sui, C. Ma, X. Sun, Y. Zhang, W. Gou, C. Mason, and Q. Zhu. 2017. Autoantibodies against glucose-regulated protein 78 as serological biomarkers in metastatic and recurrent hepatocellular carcinoma. In *Oncotarget*. 8 (15): 24828-24839.
456. Zhu, H., H. Luo, M. Yan, X. Zuo, and Q. Z. Li. 2015. Autoantigen Microarray for High-throughput Autoantibody Profiling in Systemic Lupus Erythematosus. In *Genomics Proteomics Bioinformatics*. 13 (4): 210-218.
457. Reymond Sutandy, F., J. Qian, C. S. Chen, and H. Zhu. 2013. Overview of Protein Microarrays. *Curr Protoc Protein Sci* Chapter 27: Unit-27.1.
458. Ayoglu, B., J. M. Schwenk, and P. Nilsson. 2016. Antigen arrays for profiling autoantibody repertoires. *Bioanalysis* 8 (10): 1105-1126.
459. Hu, C., W. Huang, H. Chen, G. Song, P. Li, Q. Shan, X. Zhang, F. Zhang, H. Zhu, L. Wu, and Y. Li. 2015. Autoantibody profiling on human proteome microarray for biomarker discovery in cerebrospinal fluid and sera of neuropsychiatric lupus. *PLoS One* 10 (5): e0126643.
460. Rosenberg, J. M.2015. Protein Microarrays: A New Tool for the Study of Autoantibodies in Immunodeficiency. *Frontiers in Immunology* 6: 138.
461. Gonzalez, A. G., M. A. Herrador, and A. G. Asuero. 2010. Intra-laboratory assessment of method accuracy (trueness and precision) by using validation standards. *Talanta* 82 (5): 1995-1998.
462. Ferlay, J. 2010. Estimates of worldwide burden of cancer in 2008: GLOBOCAN 2008. *International Journal of Cancer* 127 (12): 2893-2917.
463. Trad, D., N. Bibani, M. Sabbah, H. Elloumi, D. Gargouri, A. Ouakaa, and J. Kharrat. 2017. Known, new and emerging risk factors of hepatocellular carcinoma (review). *La Presse Médicale* 46 (11): 1000-1007.
464. Plentz, R. R., and N. P. Malek. 2015. Early Detection of Hepatocellular Carcinoma: How to Screen and Follow up Patients with Liver Cirrhosis According to the GERMAN S3 Guideline? In *Diagnostics (Basel)* 5(4): 497-503.
465. Tsuchiya, N., Y. Sawada, I. Endo, K. Saito, Y. Uemura, and T. Nakatsura. 2015. Biomarkers for the early diagnosis of hepatocellular carcinoma. *World J Gastroenterol* 21 (37): 10573-10583.
466. Zhang, H., J. Xia, K. Wang, and J. Zhang. 2015. Serum autoantibodies in the early detection of esophageal cancer: a systematic review. *Tumour Biol* 36 (1): 95-109.
467. Xia, J., J. Shi, P. Wang, C. Song, K. Wang, J. Zhang, and H. Ye. 2016. Tumour-Associated Autoantibodies as Diagnostic Biomarkers for Breast Cancer: A Systematic Review and Meta-Analysis. *Scand J Immunol* 83 (6): 393-408.

468. Koziol, J. A., H. Imai, L. Dai, J. Y. Zhang, and E. M. Tan. 2018. Early detection of hepatocellular carcinoma using autoantibody profiles from a panel of tumor-associated antigens. *Cancer Immunol Immunother* 67 (5): 835-841.
469. Middleton, C. H., W. Irving, J. F. R. Robertson, A. Murray, C. B. Parsy-Kowalska, I. K. Macdonald, J. McElveen, J. Allen, G. F. Healey, B. J. Thomson, S. J. Ryder, S. Holdenrieder, and C. J. Chapman. 2014. Serum Autoantibody Measurement for the Detection of Hepatocellular Carcinoma. In *PLoS One* 9 (18): E103867.
470. Brenier-Pinchart, M. P., H. Fricker-Hidalgo, C. Dard, and H. Pelloux. 2017. Impact of heat-inactivation on anti-Toxoplasma IgM antibody levels. *Clin Chem Lab Med* 55 (12): e291-e293.
471. Graur, F., L. Furcea, E. Mois, A. Biliuta, A. T. Rozs, V. Negrean, and N. Al Hajjar. 2016. Analysis of p53 Protein Expression in Hepatocellular Carcinoma. *J Gastrointestin Liver Dis* 25 (3): 345-349.
472. Lv, X., G. Ye, X. Zhang, and T. Huang. 2017. p16 Methylation was associated with the development, age, hepatic viruses infection of hepatocellular carcinoma, and p16 expression had a poor survival: A systematic meta-analysis (PRISMA). *Medicine (Baltimore)* 96 (38): e8106.
473. Lee, Y. R., and S. Y. Park. 2015. P53 expression in hepatocellular carcinoma: influence on the radiotherapeutic response of the hepatocellular carcinoma. *Clin Mol Hepatol* 21 (3): 230-231.
474. Zhan, P., and Y. N. Ji. 2014. Prognostic significance of TP53 expression for patients with hepatocellular carcinoma: a meta-analysis. In *Hepatobiliary Surg Nutr*. 3(1): 11-17.
475. Yi, S. W., J. S. Choi, J. J. Yi, Y. H. Lee, and K. J. Han. 2018. Risk factors for hepatocellular carcinoma by age, sex, and liver disorder status: A prospective cohort study in Korea. *Cancer* 124 (13): 2748-2757.
476. Ying, X. 2014. Serum anti-osteopontin autoantibody as a novel diagnostic and prognostic biomarker in patients with hepatocellular carcinoma. *Oncology Reports* 32 (4): 1550-1556.
477. Liu, W., B. Peng, Y. Lu, W. Xu, W. Qian, and J. Y. Zhang. 2011. Autoantibodies to tumor-associated antigens as biomarkers in cancer immunodiagnosis. *Autoimmun Rev* 10 (6): 331-335.
478. Jorge Moscat, M. K., Maria Diaz-Meco. 2016. p62 in Cancer: Signaling Adaptor Beyond Autophagy: Cell. *Cell* 167 (3): 606-609.
479. Enomoto, H., H. Nakamura, W. Liu, and S. Nishiguchi. 2015. Hepatoma-Derived Growth Factor: Its Possible Involvement in the Progression of Hepatocellular Carcinoma. In *Int J Mol Sci* 16(6): 14086-14097.
480. Sui, G. 2018. Study of the correlation between H-ras mutation and primary hepatocellular carcinoma. *Oncology Letters* 4 (4): 779-782.
481. Himoto, T., and M. Nishioka. 2013. Autoantibodies in liver disease: important clues for the diagnosis, disease activity and prognosis. In *Auto Immun Highlights* 4 (2): 39-53.
482. Forner, A., M. Reig, and J. Bruix. 2018. Hepatocellular carcinoma. *Lancet* 391 (10127): 1301-1314.
483. Worland, T., B. Harrison, L. Delmenico, and D. Dowling. 2018. Hepatocellular Carcinoma Screening Utilising Serum Alpha-Fetoprotein Measurement and Abdominal Ultrasound Is More Effective than Ultrasound Alone in Patients with Non-viral Cirrhosis. *J Gastrointest Cancer* 49 (4): 476-480.

484. Zekri, A. R. N., A. Youssef, Y. M. Bakr, R. M. Gabr, O. S. Ahmed, M. H. Elberry, A. M. Mayla, M. Abouelhoda, and A. A. Bahnassy. 2016. Early detection of hepatocellular carcinoma co-occurring with hepatitis C virus infection: A mathematical model. *World J Gastroenterol* 22 (16): 4168-4182.
485. Moran-Mirabal, J. M., C. P. Tan, R. N. Orth, E. O. Williams, H. G. Craighead, and D. M. Lin. 2007. Controlling Microarray Spot Morphology with Polymer Lift-off Arrays. *Anal Chem* 79 (3): 1109-1114.
486. Mujawar, L. H. 2014. Influence of the relative humidity on the morphology of inkjet printed spots of IgG on a non-porous substrate.*RSC* 4 (37): 19380.
487. Campbell, C. T., Y. Zhang, and J. C. Gildersleeve. 2010. Current Protocols in Chemical Biology Construction and Use of Glycan Microarrays. *Curr Protoc Chem Biol* 2 (1): 37-53.
488. Rosenberg, J. M., and P. J. Utz. 2015. Protein Microarrays: A New Tool for the Study of Autoantibodies in Immunodeficiency. *Front Immunol* 7 (6): 138
489. Sauer, U. 2017. Analytical Protein Microarrays: Advancements Towards Clinical Applications. *Sensors (Basel)* 17 (2): E256.
490. Wood, B. A., R. M. Troyer, J. A. Terwee, and S. Vandewoude. 2012. Microsphere immunoassay for the detection of cytokines in domestic cat (Felis catus) plasma: elevated IL-12/23 in acute feline immunodeficiency virus infections. *Vet Immunol Immunopathol* 145 (3-4): 604-610.
491. Lucas, J. L., E. A. Tacheny, A. Ferris, M. Galusha, A. K. Srivastava, A. Ganguly, P. M. Williams, M. C. Sachs, M. Thurin, J. V. Tricoli, W. Ricker, and J. C. Gildersleeve. 2017. Development and validation of a Luminex assay for detection of a predictive biomarker for PROSTVAC-VF therapy. *PLoS One* 12 (8): e0182739.
492. Turhal, N. S., B. SavaŞ, Ö. ÇOŞKun, E. BaŞ, B. Karabulut, D. Nart, T. Korkmaz, D. Yavuzer, G. Demir, G. DoĞUsoy, and M. ArtaÇ. 2015. Prevalence of K-Ras mutations in hepatocellular carcinoma: A Turkish Oncology Group pilot study. In *Mol Clin Oncol* 3(6): 1275-1279.
493. Blanchard, P., L. Quero, V. Pacault, M.-H. Schlageter, V. Baruch-Hennequin, and C. Hennequin. 2012. Prognostic significance of anti-p53 and anti-KRas circulating antibodies in esophageal cancer patients treated with chemoradiotherapy. *BMC Cancer* 12 (1): 119.
494. Karnoub, A. E., and R. A. Weinberg. 2008. Ras oncogenes: split personalities. *Nat Rev Mol Cell Biol* 9 (7): 517-531.
495. Lin, Y. W., C. F. Li, H. Y. Chen, C. Y. Yen, L. C. Lin, C. C. Huang, H. Y. Huang, P. C. Wu, C. H. Chen, S. C. Chen, and M. H. Tai. 2012. The expression and prognostic significance of hepatoma-derived growth factor in oral cancer. *Oral Oncol* 48 (7): 629-635.
496. Jiang, C. G., Q. Chen, L. Wu, G. Wang, and J. Ma. 2018. The innovative regularity and role of p16 methylation in blood during HCC development. In *J Cancer* 19 (11): 1925-1931.
497. Ezzeldin, M., E. Borrego-Diaz, M. Taha, T. Esfandyari, A. L. Wise, W. Peng, A. Rouyanian, A. Asvadi Kermani, M. Soleimani, E. Patrad, K. Lialyte, K. Wang, S. Williamson, B. Abdulkarim, M. Olyaee, and F. Farassati. 2014. RalA signaling pathway as a therapeutic target in hepatocellular carcinoma (HCC). *Mol Oncol* 8 (5): 1043-1053.
498. Xiang, X., H. Qin, X. You, Y. Wang, L. Qi, L. Ma, B. Xiang, J. Zhong, and L. Li. 2017. Expression of P62 in hepatocellular carcinoma involving hepatitis B virus infection and aflatoxin B1 exposure. In *Cancer Med* 6 (10): 2357-2369.

499. Kunst, C., M. Haderer, S. Heckel, S. Schlosser, and M. Müller. 2016. The p53 family in hepatocellular carcinoma. *Tranlational Cancer Research* 5 (6): 632-638.
500. Zhen, C., L. Chen, Q. Zhao, B. Liang, Y. X. Gu, Z. F. Bai, K. Wang, X. Xu, Q. Y. Han, D. F. Fang, S. X. Wang, T. Zhou, Q. Xia, W. L. Gong, N. Wang, H. Y. Li, B. F. Jin, and J. H. Man. 2013. Gankyrin promotes breast cancer cell metastasis by regulating Rac1 activity. *Oncogene* 32 (29): 3452-3460.
501. Zamani, P., M. Matbou Riahi, A. A. Momtazi-Borojeni, and K. Jamialahmadi. 2017. Gankyrin: a novel promising therapeutic target for hepatocellular carcinoma. *Artif Cells Nanomed Biotechnol* 46 (7): 1302-1313.
502. Gerace, E., and D. Moazed. 2015. Affinity Pull-Down of Proteins Using Anti-FLAG M2 Agarose Beads. *Methods Enzymol* 559 (1): 99-110.
503. Morlacchi, S., F. Sciandra, M. G. Bigotti, M. Bozzi, W. Hübner, A. Galtieri, B. Giardina, and A. Brancaccio. 2012. Insertion of a myc-tag within α-dystroglycan domains improves its biochemical and microscopic detection. In *BMC Biochem*. 14 (1): 13.
504. Boellner, S., and K. F. Becker. 2015. Reverse Phase Protein Arrays-Quantitative Assessment of Multiple Biomarkers in Biopsies for Clinical Use. *Microarrays (Basel)* 4 (2): 98-114.
505. Liu, Y., C. M. Li, L. Yu, and P. Chen. 2007. Optimization of printing buffer for protein microarrays based on aldehyde-modified glass slides. *Front Biosci* 12: 3768-3773.
506. Wang, T., M. Liu, S. J. Zheng, D. D. Bian, J. Y. Zhang, J. Yao, Q. F. Zheng, A. M. Shi, W. H. Li, L. Li, Y. Chen, J. H. Wang, Z. P. Duan, and L. Dong. 2017. Tumor-associated autoantibodies are useful biomarkers in immunodiagnosis of α-fetoprotein-negative hepatocellular carcinoma. *World J Gastroenterol* 23 (19): 3496-3504.

APPENDIX

Standard deviation of IgG responses to *Candida* and Tetanus on three different days (intra assay) before extrapolation from IgG standard dilutions curves. (Reference to Figure 50).

Antigen	Samples	Day 1	Day 2	Day 3
Candida	Purified IgG 1	34.70	32.06	48.7.29
	Purified IgG 2	17.56	11.73	26.29
	Purified IgG 3	6.73	9.26	8.62
	Purified IgG 4	59.82	41.63	102.40
	Purified IgG 5	5.50	6.52	4.06
	Serum 1	152.60	61.08	45.81
	Serum 2	15.20	6.16	27.78
	Serum 3	14.18	8.16	8.24
	Serum 4	46.62	36.08	18.33
	Serum 5	8.50	3.26	6.90
Tetanus	Purified IgG 1	442.90	345.40	120.70
	Purified IgG 2	35.68	10.98	18.12
	Purified IgG 3	59.59	61.14	109.9
	Purified IgG 4	157.80	80.85	87.67
	Purified IgG 5	60.69	43.22	17.47
	Serum 1	366.50	257.80	156.90
	Serum 2	39.05	7.49	62.64
	Serum 3	155.50	63.73	125.5
	Serum 4	156.30	46.10	163.4
	Serum 5	210.50	67.17	37.30

Standard deviation of IgG responses to *Candida* and Tetanus across three days (inter-assay) before extrapolation from IgG standard dilutions curves. (Reference to Figure 50).

Samples	*Candida*	Tetanus
Purified IgG 1	452.20	3310
Purified IgG 2	64.23	110.50
Purified IgG 3	75.23	437.70
Purified IgG 4	700.90	136.80
Purified IgG 5	5.79	653.10
Serum 1	1416	3968
Serum 2	363.80	1792
Serum 3	247.30	1882
Serum 4	1439	4068
Serum 5	71.04	3838

Standard deviation of IgG standard dilutions curves probed with purified IgG from serum and serum samples. (Reference to Figure 51).

	DAY 1	DAY 2	DAY 3
IgG 1	677.40	186.20	150.60
IgG 2	440.60	302.10	791.10
IgG 3	235.60	332.90	397.20
IgG 4	291.10	81.77	213.80
IgG 5	316.70	310.90	778.80
Serum 1	321.90	379.30	321.70
Serum 2	440.60	96.17	165.60
Serum 3	235.60	332.90	247.60
Serum 4	291.10	81.77	312.60
Serum 5	316.70	310.80	265.40

Standard deviation of IgG responses to *Candida* and Tetanus on three different days (intra assay) after extrapolation from IgG standard dilutions curves. (Reference to Figure 52).

Antigen	Samples	Day 1	Day 2	Day 3
Candida	Purified IgG 1	0.163	0.014	0.069
	Purified IgG 2	0.039	0.042	0.045
	Purified IgG 3	0.026	0.031	0.014
	Purified IgG 4	0.235	0.186	0.186
	Purified IgG 5	0.075	0.022	0.007
	Serum 1	0.560	0.250	0.079
	Serum 2	0.030	0.038	0.068
	Serum 3	0.5659	0.028	0.146
	Serum 4	0.1849	0.166	0.038
	Serum 5	0.021	0.011	0.013
Tetanus	Purified IgG 1	3.615	2.571	0.218
	Purified IgG 2	0.085	0.041	0.031
	Purified IgG 3	0.268	0.237	0.191
	Purified IgG 4	0.760	0.440	0.170
	Purified IgG 5	0.178	0.169	0.031
	Serum 1	1.760	1.878	0.349
	Serum 2	0.772	0.050	0.167
	Serum 3	0.842	0.294	0.248
	Serum 4	1.050	0.348	0.413
	Serum 5	0.756	0.313	0.077

Standard deviation of IgG responses to *Candida* and Tetanus across three days (inter-assay) after extrapolation from IgG standard dilutions curves. (Reference to Figure 52).

Samples	*Candida*	*Tetanus*
Purified IgG 1	1.146	11.39
Purified IgG 2	0.290	1.067
Purified IgG 3	0.185	1.956
Purified IgG 4	0.512	2.312
Purified IgG 5	0.078	0.852
Serum 1	0.817	2.515
Serum 2	1.037	1.041
Serum 3	0.218	2.037
Serum 4	1.823	1.611
Serum 5	0.284	4.574

Standard deviation of anti-TAA IgG responses to HCC TAAs when printed in three microtiter volumes (5 µl, 10 µl, 20 µl). (Reference to Figure 59).

5 µl	**Block 1**	**Block 2**	**Block 3**	**Block 4**	**Block 5**	**Block 6**	**Block 7**
AFP	1992	1146	140.7	1030	1357	654.6	366.4
Gankyrin	2875	1918	1855	2280	1528	2259	1297
GRP78	1959	1694	935.7	1208	1123	845.6	715.7
P62	295.9	184.3	267.3	246.9	251.8	370.7	192.2
APCN	1183	442.3	356.1	285.6	733.9	109.1	110.4
10 µl	**Block 1**	**Block 2**	**Block 3**	**Block 4**	**Block 5**	**Block 6**	**Block 7**
AFP	1776	750.5	846.1	1082	932.7	642.6	470.3
Gankyrin	1756	500.8	1414	1412	1338	949.4	829.2
GRP78	450.7	510.3	631.9	432.3	376.4	561.7	636.6
P62	251.4	85.68	106.7	150.7	84.43	68.58	56.51
APCN	728.2	211.8	322.8	310.6	339.1	116.8	203.5
20 µl	**Block 1**	**Block 2**	**Block 3**	**Block 4**	**Block 5**	**Block 6**	**Block 7**
AFP	1593	613.1	1877	2679	669.8	1100	525.5
Gankyrin	3712	2795	1917	2607	1094	1678	985.2

GRP78	1409	1098	746.9	871.9	772.8	987.3	1095
P62	578.8	283.1	301.8	296.8	531.1	239.1	331.1
APCN	847.9	444.7	330.8	408.3	598.1	416.4	665.7

Standard deviation of anti-TAA IgG responses to HCC TAAs when probed with different dilutions of primary (monoclonal mouse anti-His_6) and secondary (anti-mouse) antibodies. (Reference to Figure 70).

A. Anti-mouse antibody (1:10000 in antibody diluent)

Anti-His_6 mouse antibody dilution in 5% BSA	**1:2000**	**1:5000**	**1:7000**	**1:10000**
IMP1	2505	3782	4375	1724
GRP78	2255	1875	2499	1526
Gankyrin	2334	3790	2617	2217
AFP	613.3	2985	1848	1226

B. Anti-mouse antibody (1:20000 in antibody diluent)

Anti-His_6 mouse antibody dilution in 5% BSA	**1:2000**	**1:5000**	**1:7000**	**1:10000**
IMP1	3110	3572	977.7	2237
GRP78	526.8	1046	2114	1526
Gankyrin	2745	3014	3641	1754
AFP	2065	2162	2438	1338

C. Anti-mouse antibody (1:30000 in antibody diluent)

Anti-His_6 mouse antibody dilution in 5% BSA	**1:2000**	**1:5000**	**1:7000**	**1:10000**
IMP1	2586	1172	4819	3113
GRP78	2991	1762	1116	678.4
Gankyrin	3323	2625	655.3	2654
AFP	1169	973.4	2094	934.6

Standard deviation of HCC anti-TAA IgG responses to ten HCC Tumour-Associated Antigens on day 1 (intra-assay). (Reference to Figure 73).

TAAs	Block 1	Block 2	Block 3	Block 4	Block 5
P62	952.40	716.60	1017	929.40	821.60
AFP	955.40	811.50	1202	958.30	930.70
HRAS	1528	1082	1057	866.10	940.80
Gankyrin	760.30	842.30	724.60	541.10	837.70
APCN	897.40	880.40	666.50	1067	643.80
GRP78	783.20	823.20	859.90	443.10	737.50
HDGF	877.60	1045	714.60	1028	1015
KRAS	1235	789.90	757	1335	975.80
RALA	554.70	822	505.60	550.50	400.10
IMP1	922.70	928.80	984.70	958.60	689.70

Standard deviation of HCC anti-TAA IgG responses to ten HCC Tumour-Associated Antigens on day 2 (intra-assay). (Reference to Figure 73).

TAAs	Block 1	Block 2	Block 3	Block 4	Block 5
P62	667.80	674.50	516.50	539.30	876.40
AFP	686.40	1066	671.70	820	528.10
HRAS	545.20	909.80	794	623.70	865.40
Gankyrin	956.70	1021	1088	907.80	799.80
APCN	924.50	830.20	891.80	617	965.40
GRP78	790.70	559.70	799.40	1083	1104
HDGF	914.30	985.90	890.80	1123	781.40
KRAS	1026	868.50	772.60	788	6029
RALA	800.60	933.10	351.20	602.90	441.40
IMP1	854.40	575.50	832.10	793.90	1003

Standard deviation of HCC anti-TAA IgG responses to ten HCC Tumour-Associated Antigens on day 3 (intra-assay). (Reference to Figure 73).

TAAs	Block 1	Block 2	Block 3	Block 4	Block 5
P62	588.50	682.80	783.80	691.60	798.60
AFP	972	469.20	848.40	1541	873.60
HRAS	820.20	877.200	1598	874.60	579
Gankyrin	1238	1487	1066	807.70	1549
APCN	1163	520.50	291.80	1403	775.10
GRP78	1485	490.40	1255	970.50	1078
HDGF	1024	806.70	988.50	823.70	851.90
KRAS	520.50	778	537.20	865.40	1360
RALA	798.70	704.40	509.60	463.90	877.80
IMP1	624.10	879.10	1093	1261	868.90

Standard deviation of HCC anti-TAA IgG responses before interpolation with IgG standard curve on day 1 (intra-assay). (Reference to Figure 76).

TAAs	Sample 1	Sample 2	Sample 3	Sample 4	Sample 5	Sample 6	Sample 7
AFP	238	33.58	23.08	33.08	27.52	203	34.80
Gankyrin	236.70	283.10	52.94	86.78	70.25	380.80	72.12
APCN	29.20	32.85	32.20	74.20	202.70	106.40	27.92
GRP78	116.80	50.74	51.24	51.49	19.23	278.25	39.40
HDGF	14.97	23.54	30.34	27.32	14.77	22.15	25.68
KRAS	24.20	26.43	35.53	41.34	27.16	37.05	43.74
RALA	23.86	44.92	61.70	19.62	29.83	32.29	31.13
IMP1	26.45	39.29	32.40	39.97	254.40	36.24	15.71
P62	32.63	27.66	27.50	23.65	8.75	29.16	7.25
HRAS	77.35	48.30	33.34	46.64	144.10	43.78	12.30

Standard deviation of HCC anti-TAA IgG responses before interpolation with IgG standard curve on day 2 (intra-assay). (Reference to Figure 76).

TAAs	Sample 1	Sample 2	Sample 3	Sample 4	Sample 5	Sample 6	Sample 7
AFP	411.90	50.96	46.67	30.78	23.15	320.80	31.30
Gankyrin	276.8	253.70	204.20	33.63	14.51	316.90	30.57
APCN	80.30	22.52	25.08	26.36	143.40	142	28.58
GRP78	324	21.20	26.52	34.06	26.05	198.70	23.80
HDGF	15.86	30.93	21.56	21.71	20.67	27.27	31.25
KRAS	21.75	26.43	18.69	31.91	16.65	30.92	26.52
RALA	23.86	32.29	26.54	19.62	29.83	38.40	31.13
IMP1	26.23	15.76	18.11	29.84	247.30	32.56	19.76
P62	47.68	39.53	10.62	21.04	23.59	30.69	29.27
HRAS	30.24	65.38	18.58	22.39	151.60	31.88	12.30

Standard deviation of HCC anti-TAA IgG responses before interpolation with IgG standard curve on day 3 (intra-assay). (Reference to Figure 76).

TAAs	Sample 1	Sample 2	Sample 3	Sample 4	Sample 5	Sample 6	Sample 7
AFP	280.10	20.77	49.50	18.66	13.70	337.20	41.12
Gankyrin	356.90	349.30	26.17	69.01	34.71	728.80	29.25
APCN	29.13	29.63	23.08	23.70	295.10	30.55	24.52
GRP78	329.50	49.42	35.92	29.90	29.59	328.10	32.75
HDGF	29.31	32.75	13.33	23.72	29.70	18.36	26.05
KRAS	31.18	18.63	22.39	30.65	31.82	25.53	23.60
RALA	34.19	23.99	11.93	17.96	10.32	25.53	42.10
IMP1	31.10	28.52	15.93	11.15	88.11	24.94	6.51
P62	25.16	22.01	34.64	24.12	21.33	29.47	10.22
HRAS	30.41	29.16	32.13	27.11	152.50	33.73	11.46

Standard deviation of HCC anti-TAA IgG responses after interpolation with IgG standard curve on day 1 (intra-assay). (Reference to Figure 77).

TAAs	Sample 1	Sample 2	Sample 3	Sample 4	Sample 5	Sample 6	Sample 7
AFP	0.070	0.013	0.005	0.008	0.010	0.058	0.012
Gankyrin	0.134	0.134	0.013	0.026	0.026	0.148	0.026
APCN	0.009	0.009	0.013	0.010	0.085	0.030	0.009
GRP78	0.014	0.014	0.012	0.005	0.007	0.094	0.014
HDGF	0.005	0.005	0.007	0.007	0.010	0.006	0.040
KRAS	0.010	0.010	0.008	0.001	0.010	0.010	0.015
RALA	0.009	0.009	0.015	0.031	0.105	0.009	0.010
IMP1	0.006	0.006	0.008	0.004	0.003	0.009	0.005
P62	0.011	0.011	0.007	0.007	0.008	0.008	0.003
HRAS	0.020	0.02	0.008	0.004	0.012	0.012	0.004

Standard deviation of HCC anti-TAA IgG responses after interpolation with IgG standard curve on day 2 (intra-assay). (Reference to Figure 77).

TAAs	Sample 1	Sample 2	Sample 3	Sample 4	Sample 5	Sample 6	Sample 7
AFP	0.083	0.020	0.010	0.009	0.009	0.090	0.011
Gankyrin	0.173	0.129	0.060	0.010	0.010	0.134	0.011
APCN	0.020	0.040	0.006	0.008	0.062	0.040	0.010
GRP78	0.114	0.009	0.006	0.010	0.009	0.070	0.008
HDGF	0.005	0.012	0.005	0.008	0.007	0.007	0.010
KRAS	0.010	0.010	0.005	0.003	0.006	0.008	0.009
RALA	0.012	0.013	0.006	0.003	0.109	0.008	0.010
IMP1	0.013	0.006	0.004	0.030	0.106	0.009	0.006
P62	0.006	0.016	0.003	0.006	0.009	0.008	0.010
HRAS	0.015	0.030	0.005	0.006	0.065	0.009	0.004

Standard deviation of HCC anti-TAA IgG responses after interpolation with IgG standard curve on day 3 (intra-assay). (Reference to Figure 77).

TAAs	Sample 1	Sample 2	Sample 3	Sample 4	Sample 5	Sample 6	Sample 7
AFP	0.076	0.005	0.002	0.008	0.001	0.104	0.001
Gankyrin	0.012	0.093	0.006	0.030	0.011	0.317	0.010
APCN	0.007	0.007	0.002	0.009	0.003	0.009	0.001
GRP78	0.024	0.011	0.003	0.012	0.003	0.124	0.001
HDGF	0.002	0.008	0.003	0.001	0.005	0.005	0.003
KRAS	0.002	0.004	0.003	0.0003	0.009	0.006	0.015
RALA	0.009	0.005	0.003	0.010	0.010	0.007	0.016
IMP1	0.008	0.006	0.004	0.002	0.033	0.007	0.009
P62	0.006	0.005	0.005	0.005	0.009	0.008	0.010
HRAS	0.008	0.007	0.001	0.001	0.060	0.009	0.004

Standard deviation of HCC anti-TAA IgG responses before interpolation with IgG standard curve across three different days (inter-assay). (Figure 78).

TAAs	Sample 1	Sample 2	Sample 3	Sample 4	Sample 5	Sample 6	Sample 7
AFP	702.80	116.80	77.67	71.60	80.91	693.90	173.70
Gankyrin	725.4	894.70	309.70	168.80	83.91	914.70	91.21
APCN	131.70	61.85	81.60	125.70	708.80	718.10	77.55
GRP78	704.90	72.21	86.28	56.46	58.94	923.50	79.07
HDGF	49.29	70.03	48.68	69.30	49.42	97.82	80.10
KRAS	65.05	53.50	99.55	67.01	62.56	151.80	64.50
RALA	112	78.89	108.70	61	66.87	84.46	61.83
IMP1	96.29	68.11	47.42	87.90	729.30	84.72	45.41
P62	88.83	74.43	62.54	82.99	52.16	84.26	47.30
HRAS	166.3	102.60	56.68	114.40	519.50	72.05	45.50

Standard deviation of HCC anti-TAA IgG responses after interpolation with IgG standard curve across three different days (inter-assay). (Reference to Figure 78).

TAAs	Sample 1	Sample 2	Sample 3	Sample 4	Sample 5	Sample 6	Sample 7
AFP	0.301	0.060	0.030	0.015	0.036	0.154	0.067
Gankyrin	0.351	0.196	0.150	0.073	0.097	0.381	0.105
APCN	0.016	0.008	0.027	0.027	0.235	0.165	0.016
GRP78	0.020	0.024	0.015	0.028	0.014	0.260	0.312
HDGF	0.005	0.009	0.136	0.015	0.010	0.040	0.003
KRAS	0.353	0.014	0.010	0.009	0.200	0.022	0.022
RALA	0.040	0.018	0.009	0.007	0.037	0.040	0.020
IMP1	0.032	0.027	0.015	0.010	0.230	0.036	0.040
P62	0.020	0.024	0.011	0.009	0.021	0.052	0.018
HRAS	0.034	0.056	0.018	0.014	0.240	0.071	0.017